Thesis submitted for the degree of

Doctor of Philosophy

in the

University of Oxford.

INVESTIGATION OF THE POTENTIAL OF Pb/Pb RADIOMETRIC DATING FOR THE DIRECT AGE DETERMINATION OF CARBONATES.

Jonathan Russell

University College

and

Department of Earth Sciences,

University of Oxford.

Trinity, 1992.

ISOCHRONIC

Although it yields the date you lacked,
(Or any other date in fact),
Don't ever base a paper on
The single-datum monochron.

The duochron is perfect for
The dumb, the novice and the raw,
Because even the utterly inept
Can find the slope and intercept.

The scatterchron or errorchron
Defines a sort of polygon.
Just choose an age, fudge a bit,
And somewhere there's a perfect fit.

The isochron is rather rare,
But if you choose your points with care,
Rejecting those that don't fall on
The line - Behold!! An isochron!!

attributed to R.Miller

INVESTIGATION OF THE POTENTIAL OF Pb/Pb RADIOMETRIC DATING FOR THE DIRECT AGE DETERMINATION OF CARBONATES.

J. Russell

University College and Department of Earth Sciences,
University of Oxford.

Submitted for the degree of Doctor of Philosophy,
Trinity Term, 1992.

ABSTRACT

Recent studies have demonstrated the potentially robust nature of U-Pb and Pb/Pb systematics within certain sedimentary and metamorphic carbonates (e.g. Moorbath et al., 1987; Jahn, 1988; Jahn et al., 1990; DeWolf & Halliday, 1991). During the course of this work, the Pb/Pb dating technique has been applied successfully to the direct dating of Proterozoic stromatolitic carbonates from Western Australia and India, Silurian stromatoporoidal carbonates from Sweden and Archaean marbles from India, permitting the direct age determination of depositional/early diagenetic, late diagenetic and metamorphic events. Results indicate that large variations in μ value ($^{238}U/^{204}Pb$) and virtually homogeneous initial Pb isotopic compositions are a recurrent feature of sedimentary and metamorphic carbonates.

Authigenic marine carbonates may incorporate U and Pb through a variety of geochemical mechanisms;

- organic complexing;
- crystal lattice substitution;
- adsorption onto particulate oxyhydroxides and
- early diagenetic reduction.

Since modern and ancient carbonates have U and Pb concentrations of the order of ppm, whereas dissolved U and Pb in the oceans occur at 3.2 ppb and 0.003 ppb, preconcentration within the water column must be an important factor in the establishment of appropriate geochemical conditions. The rapid scavenging of Pb, compared to rates of U fixation under suboxic conditions, means that depositional μ values seldom approach the sea water figure of c.80,000.

Owing to the largely independent geochemical behaviour of U and Pb, early diagenetic, late diagenetic and metamorphic recrystallisation may either partially disturb Pb/Pb and U-Pb systematics or effect complete resetting of radiometric ages. Consequently, results from geochronological studies should be interpreted only after due consideration of all available geological information.

The extensive distribution of metamorphic and sedimentary carbonates throughout the geological record, coupled with the apparent robustness of Pb/Pb systematics, means that this technique can offer an effective means of event dating, stratigraphic correlation and time scale calibration, particularly in the Precambrian where independent age constraints are limited. In addition, the identification of late diagenetic recrystallisation ages offers exciting potential for constraining the diagenetic histories of sedimentary basins.

List of Contents

List of Tables

Chapter 2:

Chapter 3:

Chapter 4:

Chapter 5:

Chapter 6:

Appendix A:

Appendix B:

List of Figures

Chapter 1:

Chapter 2:

Chapter 3:

Chapter 4:

Chapter 5:

Chapter 6:

Appendix A:

Acknowledgements

I would like to take this opportunity to thank the many people, whose help and assistance over the last few years have made the completion of this thesis possible. Firstly, I wish to express my gratitude to **Dr. Martin Whitehouse, Professor Stephen Moorbath** and **Dr. Paul Taylor** who, in various guises at various times, have provided invaluable ideas, encouragement, practical assistance and sterling supervision. I am indebted to each of them.

The **British Petroleum Exploration Operating Company Limited** generously provided all necessary financial support, covering academic costs, fieldwork expenditure and my personal subsistence over a three and a half year period. I would like to thank them for their interest in this exciting, new branch of isotope geology and for their proficiency in dealing with logistical matters concerning the project. In particular, **Dr. Dominic Emery** and **Professor Max Coleman**, my two B.P. links, deserve special thanks for their oracular supervision and help in establishing academic contacts.

I am grateful to **Professor Moorbath** for access to chemical and analytical facilities in the Oxford Age Laboratory; to **Dr. John Arden** and **Roy Goodwin** for instruction and assistance in the chemical preparation of samples; to **Steve Wyatt** for frequently coming to the aid of an isotope geochemist in distress; to my fellow geochemistry D.Phil students, **Dr. Ed Thorogood**, **Dr. Marcio Pimentel** and **Dr. Charlie Jones**, for useful discussion and helping to keep things in perspective when results were not forthcoming; and to **Dr. Richard Corfield** and **Julie Cartlidge** for access to stable isotope analytical facilities.

A large number of people have assisted in the provision and collection of sample materials and the subsequent discussion and interpretation of analytical results.

- With regard to the Western Australian Proterozoic stromatolites, I would like to thank the **Geological Survey of Western Australia** (**GSWA**) and its Director, **Dr. Philip Playford**, for providing sample materials, reprints and permission to reproduce GSWA diagrams and data; **Kath Grey**, whose extensive knowledge of Western Australian Precambrian stromatolites and comments have been invaluable; **Alan Thorne** and **Ian Williams** for discussion of the Nabberu, Bangemall, Yeneena and Savory Basin results; and **Professor Bill Schopf** for sample materials, stimulating

discussion and an invaluable reference text (Earth's Earliest Biosphere – Schopf, 1983).

- I wish to thank **Dr. B. Krishna Rao** for the provision of Indian Archaean marble samples; **Dr. Brian Chadwick** for discussion of results and the provision of elusive Indian references and **Dr. Clark Friend** for access to unpublished results.

- **Dr. Dhiraj Banerjee** kindly provided the Indian Proterozoic stromatolites and numerous reprints.

- I am most grateful to the **University of Lund** for permission to use the field station 'Allekvia' during fieldwork on Gotland and to **Dr. Lennart Jeppsson** for discussion of results. **Fredrik Jerre** and **Mats Arup** were perfect hosts during my stay and **Sâra Gabe** was an able field assistant. **Dr. Steve Kershaw** assisted with the classification of stromatoporoids.

- **Professor Andrew Knoll**, **Dr. Keene Swett**, **Dr. Martin Brasier** and **Phil Powell** provided additional carbonate and phosphorite samples, although the results are not included in this work.

Elaine Scott, **Gavin Wall**, **Dr. Will Featherstone**, **Louis Moresi**, **Sarah Crampton**, **Pam Sansom** and the rest of the post-graduate community at Oxford have been a continual source of solace during the traumas of thesis writing and job-hunting and **Simon Davey** has been the instigator of numerous valuable discussions, usually over a bottle of wine and occasionally about geology! I would especially like to thank **Dr. David Bell** for all of his help and encouragement over the last seven years.

Finally, and most importantly, I would like to express my immense gratitude to my parents, **Paul and Kath Russell**, for ultimately making this work possible through their help, advice, understanding and support over the years and to my fiancée, **Sâra Gabe**, for her encouragement and uncanny ability to provide pleasant distractions at opportune moments. This thesis is dedicated to them.

INVESTIGATION OF THE POTENTIAL OF Pb/Pb RADIOMETRIC DATING FOR THE DIRECT AGE DETERMINATION OF CARBONATES.

J. Russell

University College and Department of Earth Sciences,
University of Oxford.

Submitted for the degree of Doctor of Philosophy,
Trinity Term, 1992.

EXTENDED ABSTRACT

The lack of reliable radiometric methods for determining directly the age of sediments has been a long-standing problem in the earth sciences. Although Rb-Sr and K-Ar studies on authigenic components of fine grained clastic sediments have met with limited success (e.g. Clauer, 1981), both systems tend to yield dates that are younger than the inferred depositional age owing to loss of radiogenic Ar and mobility of Rb during burial metamorphism. As a consequence, sediment ages have been constrained characteristically by indirect reference to underlying basement rocks, intrusives and/or interstratal volcanics of known age.

Moorbath et al. (1987) first demonstrated that it was possible to apply the Pb/Pb method to the direct age determination of carbonates when they obtained a date of 2839 ± 33 Ma (2σ) for a stromatolitic limestone from Zimbabwe - a result which they interpreted as close to the age of deposition. If it were possible to demonstrate that the Pb/Pb and U-Pb methods of radiometric dating could be applied to a wide range of carbonates (limestones, macrofossils, cements, marbles), the extensive distribution of such materials throughout the geological record could see the techniques become effective as tools for stratigraphic correlation, the construction of event stratigraphies and time scale calibration, particularly in the Precambrian where independent age constraints are limited and a functional biostratigraphy lacking. A number of recent studies have obtained credible age data from limestones (Smith et al., 1991; DeWolf & Halliday, 1991), stromatolites (Cuvellier, 1989; Jahn et al., 1990), corals (Smith & Farquhar, 1989) and marbles (Taylor & Kalsbeek, 1990) using Pb/Pb and U-Pb techniques.

A number of carbonate sample materials have been investigated from a wide age range (Late Archaean to Silurian) to permit a meaningful assessment of the potential of direct Pb/Pb carbonate dating. Standard analytical procedures were adapted to permit the efficient extraction and isotopic analysis of sub-microgramme quantities of Pb and U from the HCl-soluble fractions of whole-rock carbonate samples without significant contribution from contaminant blank (<1%).

A suite of marbles was analysed from the Late Archaean Lower Chitradurga Group (Dharwar Supergroup, India). Seventeen isotopic analyses from five different samples give a Pb/Pb errorchron (MSWD 50.1) that corresponds to a date of 2639 ± 32 Ma (**Figure 0.3.1**). Petrographic studies on the marbles, which were collected over a distance of some 60 km, indicate that all sedimentary features have been obliterated by pervasive, low temperature amphibolite facies metamorphism and the date is interpreted, therefore, as the age of metamorphic recrystallisation. As such, it provides a minimum constraint on the depositional age of the precursor sediments. Marbles from inferred equivalent deposits in the Sandur Schist Belt to the east (high temperature amphibolite grade) yield a Pb/Pb date of 2475 ± 65 Ma and suggest that the elevated thermal gradients in the region had maintained U-Pb open system conditions for c.150 Ma before blocking temperatures for U-Pb systematics were finally reached. These observations are consistent with independent radiometric data from the late tectonic Chitradurga and Closepet Granites (Taylor et al., 1984; Friend, pers. comm. 1992). Average model μ_1 values of 7.88 and 8.48, respectively, imply that the Chitradurga and Sandur marbles had significantly different sources and this raises questions about the stratigraphic equivalence of their progenitors. Incomplete Pb isotopic homogenisation of non-carbonate components during metamorphism resulted in the generation of a spurious isochron date of 2219 ± 140 Ma for Sandur residue data (rotated palaeoisochron). This figure has no age significance. Carbonate Pb isotopic ratios, on the other hand, became homogenised during metamorphism, resulting in the generation of a reliable Pb/Pb isochron. Carbonate-residue disequilibrium in marbles and other calcareous materials is an intriguing phenomenon that merits further investigation.

A series of Proterozoic stromatolitic carbonates were analysed from Western Australia and the Aravalli-Delhi orogenic belt, Peninsular India. Geological Survey of Western Australia (GSWA) samples 88032 (*Pilbaria perplexa*) and 46207 (*Asperia ashburtonia*) both come from the Duck Creek Dolomite of the Wyloo Group (Ashburton Basin) and have an inferred age of between 2.2-1.6 Ga. Nine analyses of GSWA 88032 define a Pb/Pb errorchron date of 1717 ± 64 Ma and nine analyses of GSWA

46207 an isochron date of 1741 ± 53 Ma. Both results are in statistical agreement and indicate that a date of c.1.73 Ga is geologically significant. GSWA workers believe that deposition of the formation occurred around 1.89 Ga (based on the occurrence of similar stromatolite taxa in the more tightly-constrained sediments of the Rocknest Formation, Wopmay Orogen, Canada) and so petrographic evidence for carbonate recrystallisation and disruption of primary stromatolitic fabrics is interpreted as the age of late diagenetic recrystallisation, possibly related to fluid activity from the greenschist facies metamorphism that can be seen to affect rocks in the vicinity.

GSWA 46589 (*Yandilla meekatharrensis*) and GSWA 84767 (?*Pilbaria deverella*) both come from the Yelma Formation of the Earaheedy Group (Nabberu Basin) which has an inferred age of between 1.8-1.6 Ga. Sixteen analyses of GSWA 46589 define an errorchron date of 2008 ± 68 Ma and six analyses of GSWA 84767 a concordant date of 1946 ± 71 Ma. Both are significantly older than the depositional age inferred from independent data. However, evidence to support a depositional/early diagenetic age of c.2.0 Ga exists;

- no similar stromatolitic taxa are found anywhere in the world in rocks younger than 1.8 Ga;
- microfossils from the Earaheedy Group carbonates show a distinct similarity with those from the 2.0 Ga Gunflint Chert of Canada;
- petrographic observations do not suggest extensive disruptive recrystallisation of original sedimentary fabrics and
- stromatolites from the underlying Glengarry Group yield a Pb/Pb isochron date of 2258 ± 180 Ma.

It is concluded that sediments of the Earaheedy Group were deposited around 2.0 Ga.

Many stromatolites, although demonstrating excellent preservation of primary sedimentary fabrics, have failed to produce meaningful radiometric results. This may result from a failure to homogenise Pb isotopic ratios at (re-)crystallisation, a particularly limited variation in U/Pb ratios or subsequent disturbance of closed system conditions. Nevertheless, additional results for carbonate stromatolites from the Kimberley and Bangemall Basins have permitted a re-evaluation of the inter-basinal correlation of Proterozoic deposits from Western Australia.

In light of reliable independent age constraints and petrographic evidence for recrystallisation, a Pb/Pb date of 1202 ± 87 Ma for phosphatic stromatolites from

the Proterozoic Aravalli Supergroup, Peninsular India, is interpreted as the age of metamorphic recrystallisation, associated with the Delhi Orogeny (?1.7-1.1 Ga). A depositional/early diagenetic age of 1627 ± 46 Ma for stromatolites from undeformed Upper Vindhyan Supergroup stromatolites (previous constraints >1.4-?0.7 Ga) indicates that Vindhyan deposits should be now correlated with the Aravalli and Delhi Supergroups, rather then the Marwar Supergroup as was previously inferred. The lack of deformation implies that Upper Vindhyan rocks were not affected by the Aravalli and Delhi Orogenies and therefore must have been emplaced by movement along the Great Boundary Fault at sometime < 1100 Ma. An imprecise Pb/Pb date of 471 ± 270 Ma for stromatolites from the Marwar Supergroup, which unconformably overlies the Delhi Supergroup, strongly suggests that correlation with the Vindhyan Basin is no longer valid and that the sediments are more likely to be broadly equivalent to the Cambrian rocks of the Salt Range.

Well preserved Silurian macrofossils from the Swedish island of Gotland were analysed to test whether the Pb/Pb (and U-Pb) technique could be applied to Phanerozoic carbonates. Analyses of stromatoporoidal carbonates from the lower Middle Klinteberg Beds (*ludensis* biozone, Wenlock-Ludlow boundary) define a Pb/Pb errorchron date of 432 ± 15 Ma, within error of the inferred boundary age (420 Ma - McKerrow, pers. comm. 1992). This date is interpreted as the age of deposition/early diagenesis. Unfortunately, the slow rate of change of the radiogenic $^{207}Pb/^{204}Pb$ ratio during the Phanerozoic means that even the extremely large range of Pb isotope ratios documented for these sponges ($^{206}Pb/^{204}Pb$ from 18.7 to 81.9) is incapable of producing a level of precision that can be used for purposes of Phanerozoic time scale calibration. U-Pb analyses on the same stromatoporoids indicate that Quaternary weathering resulted in isotopic disturbance. Selected analyses of one particular hand specimen define a ^{238}U-^{206}Pb date of 435 ± 9 Ma, concordant with the Pb/Pb date, and suggest that the effects of weathering may have been localised. A second Pb/Pb date of 326 ± 11 Ma for stromatoporoids from the stratigraphically lower Middle Wenlock Slite Formation (*rigidus* & *lundgreni* biozones) is interpreted as the age of late diagenetic recrystallisation due to interaction with fluids channelled along sub-surface north-south faults. Klinteberg samples remained unaffected by this recrystallisation event because the two horizons are stratigraphically separated by a sequence of largely impermeable shales (Upper Slite and Mulde Formations). Systematic variations of U and Pb concentrations and Pb isotope ratios allow an insight into the behaviour of U and Pb under conditions of deposition/diagenesis.

A broad geochemical model is proposed to explain why carbonates should make suitable materials for dating by Pb/Pb and U-Pb methods. Authigenic marine carbonates may incorporate U and Pb through a variety of geochemical mechanisms;

- organic complexing;
- crystal lattice substitution;
- adsorption onto particulate oxyhydroxides and
- early diagenetic reduction.

Since modern and ancient carbonates have U and Pb concentrations of the order of ppm, whereas dissolved U and Pb in the oceans occur at 3.2 ppb and 0.003 ppb, preconcentration within the water column must be an important geochemical factor. Organic complexing is considered to be of paramount importance. The rapid scavenging of Pb, compared to rates of U fixation under suboxic conditions, means that depositional μ values, however, seldom approach the sea water figure of c.80,000.

It is proposed that carbonates which are deposited from seawater by chemical precipitation, possess an intimate association with organic material and have low clastic contents should be suitable for U-Pb and Pb/Pb studies. Indeed, biogenic carbonates that correspond to these criteria (stromatolites, stromatoporoids, corals and sponges) have produced credible geochronological information. Owing to the largely independent geochemical behaviour of U and Pb, early diagenetic, late diagenetic and metamorphic recrystallisation may either partially disturb Pb/Pb and U-Pb systematics or effect complete resetting of radiometric ages. Consequently, results from geochronological studies should be interpreted only after due consideration of all available geological information (petrography, cathodoluminescence, stable isotopes, independent age constraints, tectonic and diagenetic histories).

The extensive distribution of metamorphic and sedimentary carbonates throughout the geological record, coupled with the apparent robustness of Pb/Pb systematics, means that the Pb/Pb method can offer an effective means of event dating, stratigraphic correlation and even time scale calibration, particularly in the Precambrian where independent age constraints are limited. Continued development of the U-Pb method applied to Phanerozoic carbonates may yet provide chronometric information of a precision useful for time scale calibration ($\pm$ 1 Ma). In addition, the identification of late diagenetic recrystallisation ages offers exciting potential for constraining the diagenetic histories of sedimentary basins. Sedimentary and metamorphic carbonates should now be considered credible sources of age information for both Precambrian and Phanerozoic sequences.

Chapter 1:

INTRODUCTION TO TIME SCALES AND THE DATING OF SEDIMENTS

1.1: INTRODUCTION

While the radiometric dating of igneous and metamorphic rocks has for many years been a matter of routine (see reference lists in Faure, 1986), the direct dating of sediments has remained a notorious problem in the earth sciences. The majority of sediments make unsuitable sample materials because of low concentrations of radioactive parent elements, an abundance of inherited detrital components and/or potential for diagenetic alteration resulting in isotopic disturbance, but recent attempts to radiometrically date chemical and authigenic sediments with low clastic contents and simple post-depositional histories have demonstrated considerable promise.

This work sets out to investigate the potential of the Pb/Pb method of radiometric dating for the direct age determination of carbonates through studies on selected Archaean marbles, Precambrian stromatolites and Phanerozoic macrofossils. The

project was funded by British Petroleum Exploration Operating Co. Ltd. and isotopic investigations were carried out under the supervision of Professor S.Moorbath, Dr. M.Whitehouse and Dr. P.Taylor at the Age Laboratory, Department of Earth Sciences, University of Oxford.

1.2: TIME SCALES

In 1911 Arthur Holmes wrote with remarkable vision that, "*data will be collected from which it will be possible to graduate the geological column with an ever increasingly accurate time scale*". As the number of reliable dates for well defined stratigraphic horizons and the precision of those dates has increased, it has been possible for the geological community to reach close agreement and even consensus on the chronometric position of key geological boundaries.

This is particularly true of the Phanerozoic, where high precision geochronology, detailed stratigraphic correlation and biostratigraphic zonation have reduced disagreement over the age of epoch boundaries to characteristically less than 5 Ma (Harland et al., 1989; McKerrow, pers. comm. 1992). Differences between published time scales arise because of; (i) uncertainties in the chrononstratigraphic position of dated horizons, (ii) variations in the quality and reliability of age data, (iii) erroneous geological interpretation of dates and (iv) variations in the statistical combination of data used to produce the final time scale. Biostratigraphic criteria, as well as defining the major chronostratigraphic boundaries, are used to further dissect the Phanerozoic time scale into increasingly smaller divisions, for example ammonite and graptolite biozones. Ultimately, calibration of the Phanerozoic time scale is constrained by the accuracy with which global chronostratigraphic horizons can be dated and so if direct Pb/Pb or U-Pb dating of carbonates is to be of use in the Phanerozoic, it must be able to produce reliable dates of an accuracy and precision approaching that available from other methods, such as Rb-Sr on biotite and U-Pb on zircon.

Horizons that are both chronometrically and chronostratigraphically defined and which can therefore be used as absolute reference levels for time scales are extremely rare in the Precambrian and consequently there is no universally accepted formal subdivision for this eon. To exemplify this point, the published time scales of Stockwell (1964), Goldich (1968), James (1972; 1979), Harland (1978), Salop (1977), Sims (1980), Frarey (1981) and Harland et al. (1989) each have largely independent

nomenclatures and numerical time divisions.

While local Precambrian chronostratigraphies have been successfully erected from field studies, inter-basinal and inter-continental correlations remain, at best, tentative. Existing age data is usually restricted to sporadic studies on basement metamorphic rocks and igneous intrusions while the interleaving undated sedimentary basins may be many tens of kilometres thick. Biostratigraphy is of limited use since genuine microfossils have been identified from very few localities of restricted geographical and temporal distribution (Schopf, 1983).

The accuracy of any Precambrian time scale is constrained by the limited number of reliable radiometric dates for Precambrian rocks and the difficulty in correlating local chronostratigraphic boundaries on a regional or global scale. Thus the ability to reliably date unmetamorphosed sedimentary sequences by absolute means, especially those containing microfossils, actually provides the potential for global stratigraphic correlation and consequently could prove a very powerful correlative tool. Pb/Pb dating of Precambrian carbonates can yield direct dates for sediments where only bracketing basement and igneous intrusion ages exist. Further research into the early geobiologic and geotectonic evolution of the earth, coupled with the refinement of local Precambrian stratigraphies and the publication of many more geochronologic studies, should see the development and acceptance of a Precambrian time scale with divisions based on well dated and constrained, geologically significant events, as is the case for the Phanerozoic, rather than on empirical boundaries.

1.3: THE DATING OF ANCIENT SEDIMENTS

1.3.1: *INTRODUCTION*

Attempts to date ancient sedimentary rocks may be split conveniently into two approaches. The indirect approach seeks to constrain a sediment's age by reference to associated rocks and events of known age or to relative chemo-, magneto- or biostratigraphic divisions. The direct approach seeks to determine an absolute numerical value, typically by the application of appropriate radioactive decay schemes.

1.3.2: *INDIRECT METHODS OF DATING SEDIMENTS*

Age Bracketing

The simplest application of indirect dating is the construction of a basic lithostratigraphy from field observations. A logical progression of this approach is to constrain the age of a sediment or sedimentary sequence by reference to lithostratigraphically older and younger rocks whose age is reliably known. Typically, underlying basement rocks and intrusive igneous events are used, but greater precision may be possible where suitable intercalated volcanics are present within a sequence (Kowallis et al., 1989).

Indirect dating is commonly used in the literature to constrain the age of Archaean and Proterozoic sediments. The precision is obviously dependent upon the volume and quality of age data available for related non-sedimentary rocks. For example, the deposition of microfossiliferous stromatolites preserved in cherts from the Towers Formation of the Warrawoona Group, Pilbara Block, Western Australia (Lowe, 1980; Hickman, 1980) has been indirectly constrained to between 3450 and 2900 Ma, by reference to;

- a U-Pb date of 3452 ± 16 Ma for zircons separated from dacitic lavas, 1.5 km below the stromatolites (Pidgeon, 1978)
- a 3050 ± 180 Ma Rb-Sr date for granites intrusive into the entire sequence (Compston & Arriens, 1968).

The proximity of the cherts to the dacitic lavas suggests that the depositional age is likely to be nearer 3450 Ma than 3050 Ma and other age data for the area (Hamilton et al., 1981; De Laeter & Blockley, 1972 and Oversby, 1976) are consistent with this interpretation.

Where ages for related rocks are unavailable, syngenetic galena Pb model ages may give a broad indication of sediment age. At their oldest, such minerals are contemporaneous with their host rocks but if diagenetic galenas are misidentified as syngenetic, erroneous age conclusions may be drawn. Careful field observation and petrographic work are therefore vital for correct model age interpretation. The assumptions implicit in the calculation of Pb model ages mean that the values are less reliable than those calculated from true isochrons and consequently they should be checked for consistency with other relevant age data, where available.

Biostratigraphy

By tracing the evolution of fossil lineages through the geological record, noting the points at which particular fossils appear and subsequently disappear and then relating these observations to the host strata it is possible to construct a biostratigraphic zonation that permits fossiliferous strata to be located within a chronostratigraphic scale. This has been successfully applied to Mesozoic ammonites and in particular to those of the Middle to Upper Cretaceous (Hancock, 1991). During this time, ammonite evolution occurred at a rapid pace and for the Middle Cenomanian to Middle Maastrichtian alone over 60 ammonite zones are recognised, each characterised by a particular ammonite species identifiable in the stratigraphic record. Once chronometric tie-points have been satisfactorily established, allowing chronostratigraphic horizons to be located precisely within a numerical time scale, appropriate portions of biostratigraphic scales may be used to subdivide the period of time between tie-points. Assumptions pertaining to constancy of rates of evolution are implicit in this approach.

Chemostratigraphy

For portions of the geological record where the sedimentary record is nearly complete, it is also possible to use chemostratigraphy to define chronostratigraphic scales. Strontium, oxygen, calcium, carbon and sulphur isotopes are briefly considered.

While the residence time of strontium in the open oceans of the world is in the order of 10^6 years it only takes 10^3 years to completely mix those oceans (Taylor & McLennan, 1985) and so the strontium input becomes rapidly isotopically homogenised. Strontium is principally removed from the open oceans by authigenic co-precipitation with calcium carbonate, typically in the form of limestones and so, barring significant alteration through diagenesis, dolomitisation, metasomatism or metamorphism, the isotopic composition of strontium in ancient open marine limestones preserves a record of the changing strontium isotopic composition of the world's ocean system through time and may be used to construct a chemostratigraphic scale. Burke et al. (1982) analysed nearly eight hundred samples of marine carbonate and constructed such a graph showing the variation of $^{87}Sr/^{86}Sr$ throughout Phanerozoic time (**Figure 1.3.1**). Individual $^{87}Sr/^{86}Sr$ values do not uniquely define a particular chronostratigraphic horizon since the graph has numerous points of inflexion but for portions that are approximately linear, such as the Lower to Middle

Jurassic (Jones, 1991), Upper Cretaceous (McArthur et al., 1992) or Middle to Upper Tertiary, the chemostratigraphy may be used to identify uniquely particular chronostratigraphic horizons.

Figure 1.3.1: Variation of the $^{87}Sr/^{86}Sr$ ratio of marine carbonates in Phanerozoic time, after Burke et al. (1982)

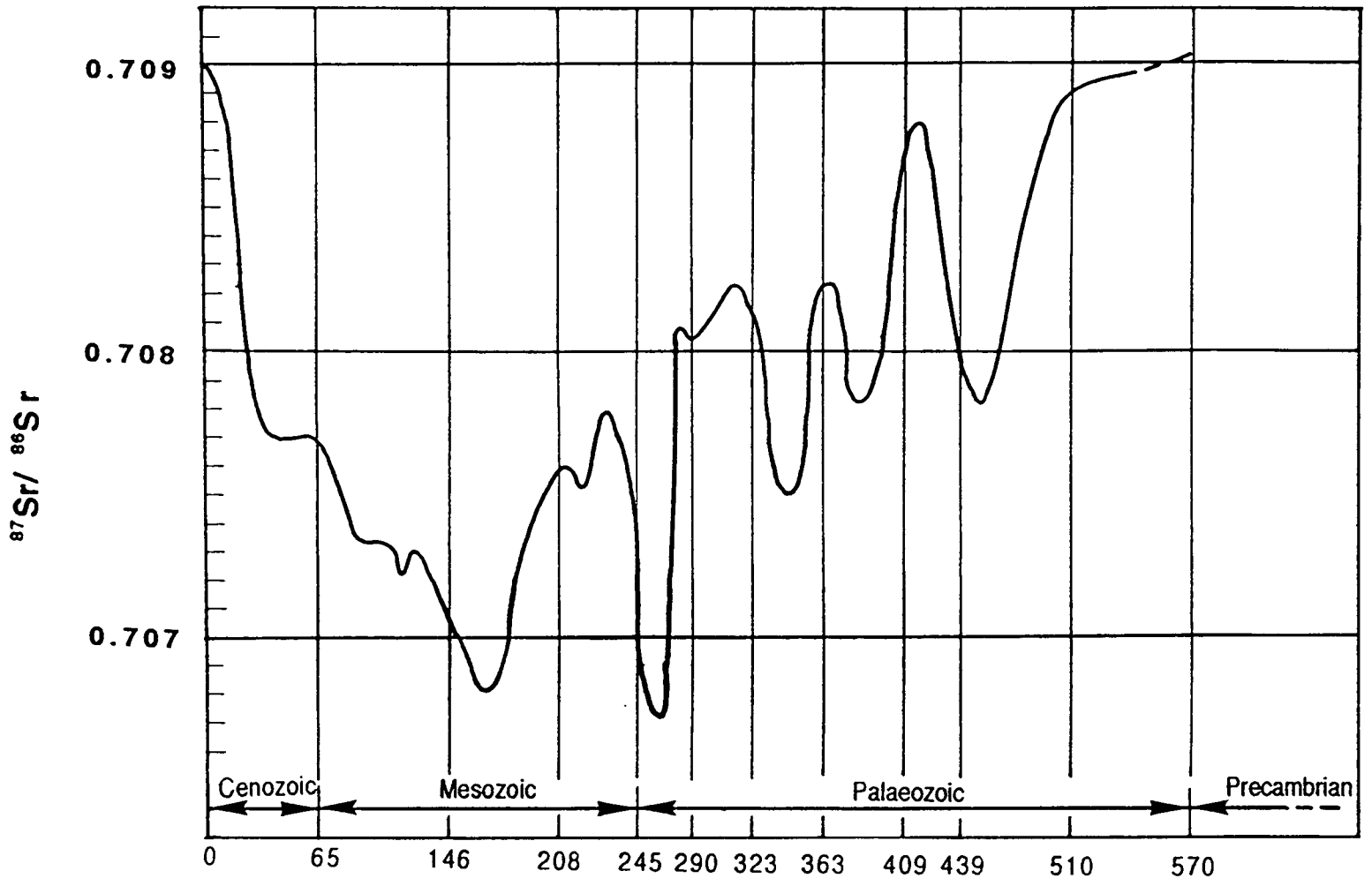

McArthur et al. (1992) gave an impressive example of the global potential of strontium isotope correlations when they compared the $^{87}Sr/^{86}Sr$ ratios of open marine macrofossiliferous carbonate material from Campanian-Maastrichtian boundary sections at Kronsmoor in Germany, the Western Interior of the United States and the English Chalk, as illustrated in **Figure 1.3.2**. Integrated $^{87}Sr/^{86}Sr$ ratios of 0.707723 ± 0.000009 from Kronsmoor and 0.707730 ± 0.000022 from the English Chalk are in good statistical agreement and demonstrate the validity of both the method of strontium isotope stratigraphy and the assumptions implicit in it. Extrapolating an $^{87}Sr/^{86}Sr$ ratio of 0.707723 ± 0.000009, the authors were able to locate the Campanian-Maastrichtian boundary within the Western Interior section and found that it lay within the *jenseni* biozone.

Figure 1.3.2: Sr isotope curves and related geochronological data for macrofossiliferous carbonates from Campanian-Maastrichtian boundary sections

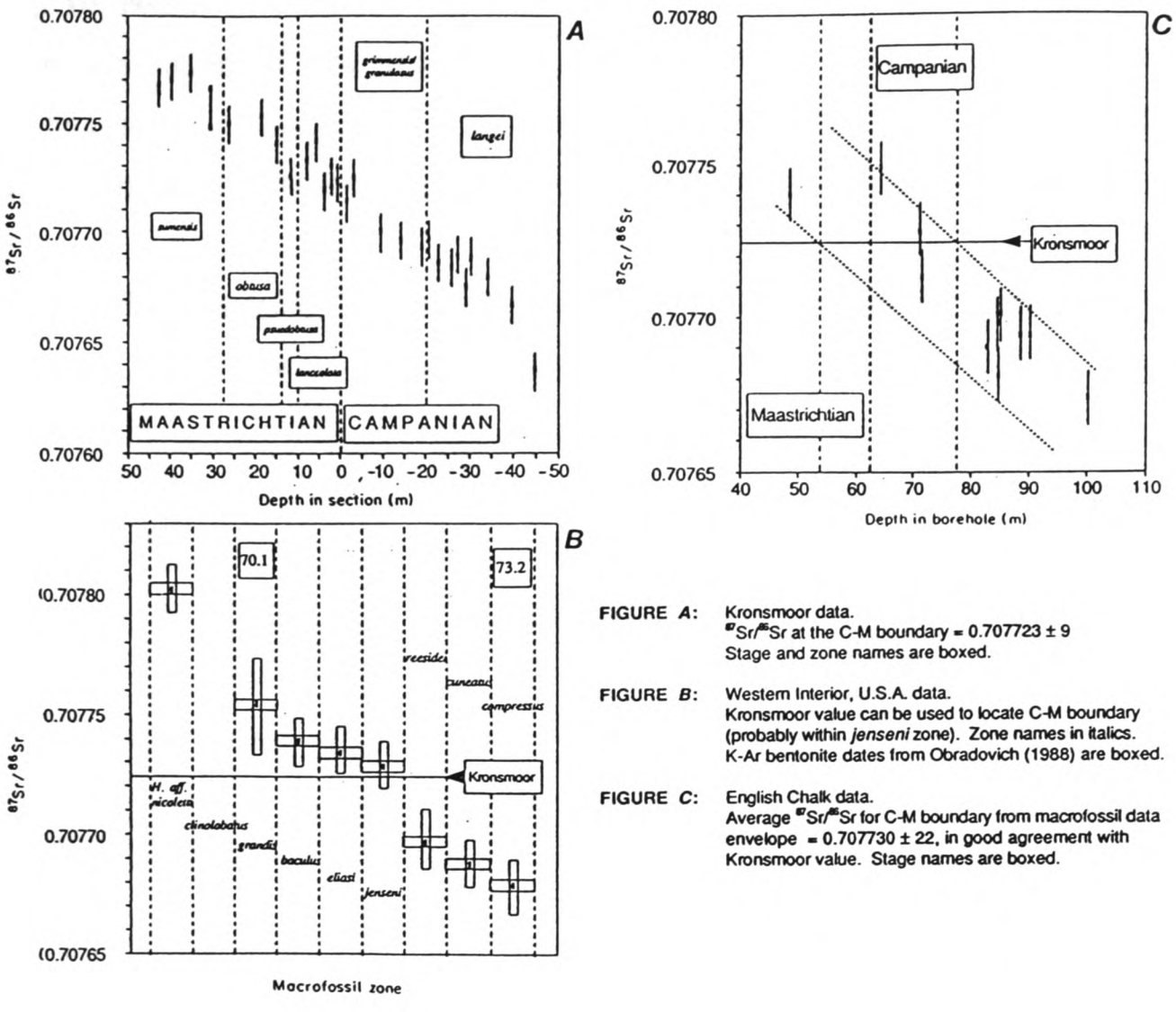

FIGURE *A*: Kronsmoor data.
$^{87}Sr/^{86}Sr$ at the C-M boundary = 0.707723 ± 9
Stage and zone names are boxed.

FIGURE *B*: Western Interior, U.S.A. data.
Kronsmoor value can be used to locate C-M boundary (probably within *jenseni* zone). Zone names in italics.
K-Ar bentonite dates from Obradovich (1988) are boxed.

FIGURE *C*: English Chalk data.
Average $^{87}Sr/^{86}Sr$ for C-M boundary from macrofossil data envelope = 0.707730 ± 22, in good agreement with Kronsmoor value. Stage names are boxed.

Oxygen isotope signatures of sedimentary carbonates and sulphates are influenced by latitude, climate, certain organism-specific vital effects (Kahn & Williams, 1981) and are relatively easily altered by diagenetic processes common at the earth's surface, the sediment-water interface and within the sedimentary pile, making them of limited use for chronostratigraphic purposes when applied to the ancient geological record. It should be noted that in the Cenozoic, however, episodes of glaciation have been monitored and timed from measurements of the oxygen isotopic composition of pelagic and benthonic foraminifera (Emiliani & Shackleton, 1974; Woodruff et al., 1981).

Russell et al. (1978) demonstrated that calcium isotopic variation in nature is significant but only occurs within a narrow range of magnitude c.2.5‰ for $\delta^{40}Ca$. Unfortunately, isotopic fractionation caused by analytical equipment has a magnitude of up to 3‰, larger than the observed natural variation (Russell & Papanastassiou, 1978) and until such fractionation can be quantified or eliminated, chemostratigraphic applications are limited.

Carbon isotopes are fractionated during inorganic exchange reactions such

as the precipitation of calcium carbonate and the biogenic fixation of CO_2, HCO_3^-, CO and CH_4, resulting in relative enrichment of ^{13}C in oxidised carbonate carbon and of ^{12}C in reduced organic carbon which has more negative $\delta^{13}C$ values as a result. Preservation of the isotopic variation of these two principal varieties of carbon in the sedimentary record, typically as carbonates and kerogens, provides a potential means of chronostratigraphic correlation.

Figure 1.3.3: The variation of isotopic composition of carbonate and organic carbon as a function of time, after Schopf (1983)

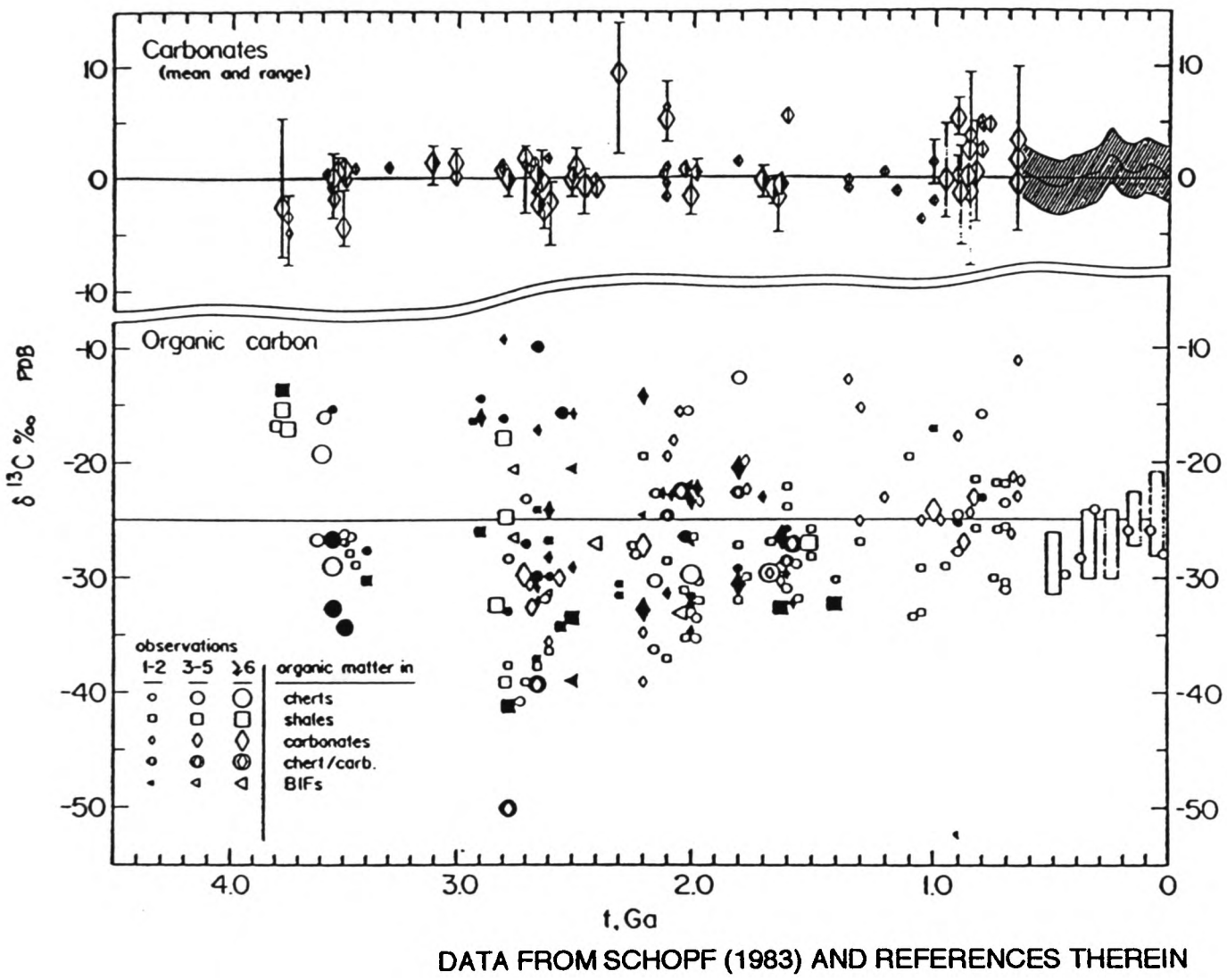

Although the $\delta^{13}C$ of marine carbonates has been close to zero throughout that portion of the geological record for which sedimentary carbonates are preserved (< 3600 Ma), secular variations have been described for the Phanerozoic by Veizer et al. (1980) that are mirrored by variations in $\delta^{13}C$ for organic carbon from kerogens, a consequence of the fact that total carbon in the exogenic and endogenic terrestrial systems is constant and therefore $\delta^{13}C_{carbonate} - \delta^{13}C_{organic}$ is constant. Primary oscillations apparently extend back into the Precambrian but the comparatively small number of data points for which acceptable stratigraphic and chronometric resolution are available makes the definition of distinct trends particularly difficult (see **Figure 1.3.3**). In addition, alteration of primary depositional signals by diagenesis, dehydrogenation or graphitisation can cause positive or negative $\delta^{13}C$ shifts depend-

ing on the process and the carbon type affected (Hoefs & Hay, 1976). Effects are more noticeable with the organic carbon signal, explaining the excess scatter of $\delta^{13}C_{organic}$ in the Precambrian, when compared with the $\delta^{13}C_{carbonate}$ signal.

In the Phanerozoic, carbon isotope chemostratigraphy applied to well preserved marine carbonate sections, may provide moderately high correlation potential for particular horizons/events. An example is the use of the dual positive $\delta^{13}C_{carbonate}$ excursions of +7‰ and +3‰ detected by Tucker (1986) for the Moroccan Precambrian-Cambrian boundary section for broad chronometric and chronostratigraphic correlation with other boundary sections in China, India, Siberia, Iran and Newfoundland (Cowie & Brasier, 1989). The magnitude of the spikes may vary between sections in response to local conditions of deposition and secondary modification, but their chronostratigraphic location provides the potential for global correlation. The ease of $\delta^{13}C$ primary signal modification means that absolute values have only limited correlative potential but trends of $\delta^{13}C$ can be used to correlate particular global events between sections around the world.

The principle cause for natural sulphur isotopic variation is the reduction of sulphate ions by anaerobic bacteria in sediments, such as *Desulfovibrio desulfuricans*, which produce H_2S relatively enriched in ^{32}S (and thus sulphides with similar isotopic compositions) and leave sulphates relatively enriched in ^{34}S. Since the isotopic composition of sulphur in gypsum is not significantly fractionated from that of the precipitating brine (Thode & Monster, 1965), the observed variation of marine sulphate $\delta^{34}S$ during the Late Proterozoic and Phanerozoic (Claypool et al., 1980) (**Figure 1.3.4**) records the changing sulphur isotopic composition of marine waters. Schidlowski et al. (1977) and Claypool et al. (1980) have proposed integrated models to explain these reported variations. Unfortunately, similar trends are not observed in the Archaean, Lower Proterozoic and Middle Proterozoic (older than c.900 Ma) since sulphates are uncommon, difficult to constrain chronostratigraphically and may have suffered substantial alteration. If care were taken to analyse pristine samples of marine sulphate from well constrained horizons of Late Proterozoic age or younger, portions of the $\delta^{34}S$ curve that have rapid rates of change could be used for local correlation but the global potential is limited by the general susceptibility of marginal marine environments to local variations in sulphur flux.

Figure 1.3.4: Variation of $\delta^{34}S$ of marine sulphate minerals through geological time, after Claypool et al. (1980)

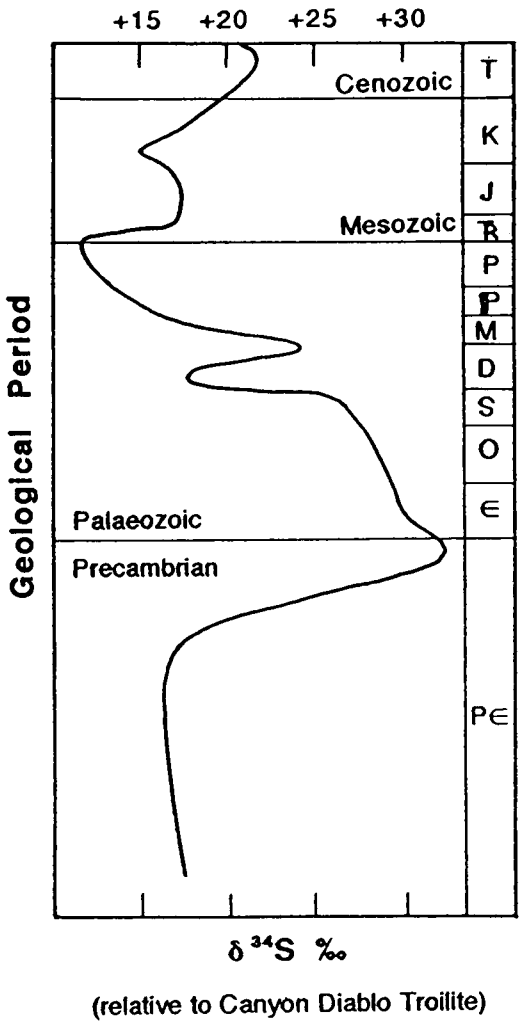

If one selects appropriate intervals where chemostratigraphic variables change rapidly without inflexion and for which reliable chronometric and chronostratigraphic tie-points exist, then by assuming a constant depositional rate the chemostratigraphy may be used to subdivide the chronometric time scale. For example, Obradovich & Cobban (1975) and Obradovich (1988) published K-Ar radiometric dates for bentonites from the Western Interior of the United States that can be tied in with both the ammonite biostratigraphy and Sr isotope chemostratigraphy (see **Figure 1.3.2**). A figure of 70.1 ± 0.7 Ma for a bentonite from the *Baculites grandis* zone, four zones beneath the Campanian-Maastrichtian boundary, and a second date of 73.2 ± 0.7 Ma for the *Baculites compressus* zone, three zones above the boundary, indicate that the period between the two horizons (five zones and two nominal half-zones) has a duration of between 0.28 Ma and 0.75 Ma. This allows the computation of the mean rate of increase of $^{87}Sr/^{86}Sr$ across the Campanian-Maastrichtian boundary (0.000025 Ma^{-1}), assuming sedimentation rates were approximately constant. In turn, this may be used to derive ages for sediments containing unaltered macrofossils of known Sr isotopic composition from horizons located chronostratigraphically between the two dated bentonites.

1.3.3: *DIRECT METHODS OF DATING SEDIMENTS*

The literature contains a number of examples of the application of radioactive decay schemes to the problem of direct dating of sediments. These studies have met with varying degrees of success. Direct dating of depositional events in sediments involves the application of one or more of the dating methods to authigenic components which precipitated at the time of deposition and have subsequently remained closed systems with respect to the elements concerned. This rules out the majority of detrital clastic sediments but chemical sediments, and carbonates in particular, could be suitable as sample materials if post-depositional disturbances have been minimal. It might also prove possible to obtain direct dates for diagenetic events in sediments if recrystallisation is capable of effecting isotopic rehomogenisation and the resetting of radiometric ages.

K-Ar and K-Ca Studies

As far back as the 1950s Lipson (1958) and Goldich et al. (1959) attempted to date sediments using the K-Ar decay scheme and more recently Odin (1982) has continued with and refined the methodology. Unfortunately, very few authigenic phases in sediments contain sufficient K to be of use and many that do are unable to quantitatively retain radiogenic ^{40}Ar. Certain smectite group clay minerals and glauconite (a term used to describe a range of authigenic K-Fe aluminosilicates with high Fe^{3+}/Fe^{2+} ratios; Burst, 1958) are the notable exceptions but even with these minerals one must be aware of the potential for contaminant detrital inclusions to produce spuriously old dates and for diagenetic or metamorphic alteration to cause partial daughter loss and result in dates which are anomalously young with respect to the true depositional age (Perry, 1974; Aronson & Hower, 1976). Clauer (1981) emphasised the importance of considering all available geological data in the interpretation of the age significance of any numerical dates obtained.

Although some evolved glauconites containing > 7% K_2O have produced dates that are reconcilable with biostratigraphic age, K-Ar dating of this mineral group is generally considered to provide a minimum age for deposition, reflecting burial metamorphism or structural deformation rather than any depositional event *per se* . The potential for widespread application is limited because glauconite is of restricted geological occurrence in the Phanerozoic (with the notable exception of the Cretaceous greensands) and but a rare constituent of Precambrian sediments.

The branched decay of ^{40}K leads to the formation of stable ^{40}Ca by β^- decay in addition to ^{40}Ar from electron capture. Early attempts to apply the K-Ca method to evaporites by Polevaya et al. (1958), Wilhelm & Ackermann (1972) and Heumann et al. (1979) met with considerable success and results tended to be more accurate than those obtained from K-Ar studies on the same materials owing to the retentivity of ^{40}Ca. Future studies on authigenic K-bearing minerals such as glauconite, sylvite, langbeinite and potassium feldspar have excellent potential if uncertainty due to instrumental mass fractionation can be eliminated.

Rb-Sr Studies

In the application of Rb-Sr dating to sediments, care must be taken to distinguish between authigenic components that may yield dates reflecting depositional age (Odin, 1982) (e.g. glauconite, certain clay minerals and potassium feldspars, sylvite and carnallite) and detrital minerals that tend to produce spurious dates reflecting the general age of the source area. Evaporitic minerals are unsuitable for Rb-Sr age determinations because of their high solubility.

Moorbath (1969) obtained Rb-Sr dates of 915 ± 24 Ma for siltstones from the Lower Torridonian of Stoer and 744 ± 17 Ma for the Applecross Formation of the Upper Torridonian (corrected for the revised decay constants), in good agreement with independent constraints and interpreted them as, "*the time of diagenesis of the sediments, closely following deposition and compaction*". Clauer (1981) obtained Rb-Sr dates for Upper Proterozoic sediments from Mauritania of between 998 ± 34 Ma and 595 ± 45 Ma that decreased in agreement with both lithostratigraphy and stromatolite biostratigraphy and he concluded that they had an approximate stratigraphic significance. K-Ar dates on the same samples, however, were discordant and fell into two groups around 620 ± 50 Ma and 450 ± 20 Ma which Clauer considered to indicate two distinct later geological events related to episodes of indirect tectonism and glaciation (Deynoux et al., 1978).

Gorokhov et al. (1981) published Rb-Sr whole rock and fine fraction (< 2μm) dates for Middle Proterozoic sediments and metasediments of the Ovruch Mountain Range, northwestern Ukraine. The Ovruch Group unconformably overlies the Pugachevian Group which is intruded by the granitic Korosten Complex dated at between 1680 ± 24 Ma and 1730 Ma (Rb-Sr whole rock - Gorokhov, 1964; zircon ages - Vinogradov et al., 1957; Komlev & Gorokhov, 1962; Scherbak, 1978). A whole rock date of 1587 ± 74 Ma and a fine fraction date of 1574 ± 31 Ma for sediments from the

Pugachevian Group are interpreted as the age metamorphic recrystallisation, whereas a whole rock date of 1385 ± 112 Ma and a fine fraction date of 1389 ± 74 Ma for sediments from the Ovruch Group are considered to be indicative of the depositional age. This interpretation is reinforced by the high initial $^{87}Sr/^{86}Sr$ ratios of Ovruch sediments which are consistent with derivation from the erosion of an underlying granitic terrain. K-Ar age data for the Pugachevian Group fall between 1450-1490 Ma (Ivantishin et al., 1962; Filippov et al., 1961) and for the Ovruch Group between 1220-1390 Ma (Scherbak, 1978), confirming that for fine grained sediments Rb-Sr ages tend to be nearer the true depositional value than those calculated from K-Ar data, which may represent the end of regional or burial metamorphism.

In the interpretation of Rb-Sr sediment dates one must consider the relative contributions of 'old' signals from detrital phases, 'depositional' signals from resistant authigenic components and 'young' signals from post-depositional recrystallisation events such as diagenesis, burial metamorphism and structural deformation. Clauer (1979; 1982) and Bonhomme (1982) discovered that the separation of differing size fractions of fine grained sediments could aid date interpretation. In particular, they found that analysing authigenic/diagenetic illites with grain diameters < 2 μm produced Rb-Sr dates that tended to correspond to early diagenetic or even depositional ages, while K-Ar dates for the same materials reflected the end of diagenesis or burial metamorphism. Clauer (1981) summarised that, "*a) results should be interpreted with care and coherence, b) the application of isotopic dating to sediments should not be systematically rejected, even if uncertainties remain, because it requires a different approach from classical geochronology*" and, "*the geochronology of sedimentary Precambrian sequences should always be integrated in large-scale studies*".

Sm-Nd Studies

Although there are no authigenic sedimentary minerals which contain sufficient elemental concentrations and Sm/Nd variation to be dated directly by the Sm-Nd method, the fact that the two elements are chemically similar means that Sm/Nd ratios do not become significantly fractionated during chemical weathering, transport, sedimentation or diagenesis and hence calculated Nd model ages may reflect the age of the sediment source and be of use in provenance studies (e.g. O'Nions et al., 1983; Thorogood, 1991). Model ages for sediments over 2000 Ma approximate to the inferred age of sedimentation (O'Nions et al., 1983; Goldstein et al., 1984; Allègre & Rousseau, 1984) and can be used to reinforce results from other

isotopic investigations, whereas younger sediments have model ages that exceed their stratigraphic age by as much as 1500 Ma, reflecting the extent and nature of reworking of relatively old crustal material.

Pb/Pb Studies

The Pb isotopic investigation of sediments started over thirty years ago when Chow & Patterson (1959) analysed the isotopic composition of manganese nodules and Wampler & Kulp (1962) determined Pb model ages for ancient marbles from Southern Rhodesia that were equal to or older than ages for known metamorphic episodes in the region. The authors concluded that the model ages represented minimum ages for sedimentation, although they were probably more closely related to the last phase of metamorphism and stated that,"*under suitable conditions the isotopic composition of lead in carbonate rocks may give valuable information on the geologic history of an area*".

Despite this early indication that Pb isotopes had potential for the direct dating of carbonate sediments, much of the subsequent work concentrated on their use in characterising source areas of recent clastic-dominated sediments (Chow, 1965; Hart & Tilton, 1966; Doe et al., 1966), where variable, largely inherited Pb isotopic ratios reflected basement age rather than the effects of *in situ* decay of U. Doe (1970a) listed all published data on the Pb isotopic composition of Phanerozoic sediments (after the work of Patterson, 1953; Engel & Patterson, 1957; Cobb & Kulp, 1961; Chow & Patterson, 1962a; Chow, 1965; 1968; Doe et al., 1966; Hart & Tilton, 1966; Muffler & Doe, 1968; Tatsumoto & Snavely, 1969) and later that year addressed the potential of U-Th-Pb systematics for the direct dating of sedimentary rocks for the first time (Doe, 1970b). The author concluded that sediment Pb/Pb isochrons more closely reflected average source age than the age of sedimentation.

A decade passed before the first report of direct carbonate dating was published by Moorbath & Taylor (1985) who indicated that a preliminary Pb/Pb errorchron[1] corresponding to a date of c.2800 Ma had been obtained for a limestone from Zimbabwe. Two years later, Moorbath et al. (1987) published full details of the 2839 ± 33 Ma Pb/Pb errorchron date (MSWD[2] 75) for the Mushandike stromatolitic limestone

---

[1] errorchron refers to a regression for which the mean square of weighted deviates is greater than 2.5 and the probability that data scatter is solely attributable to analytical causes is less than c.15%

[2] mean square of weighted deviates, essentially proportional to the ratio of observed data scatter to data scatter predicted by the assigned errors

(see **Figure 1.3.5**)(Orpen & Wilson, 1981) which had been obtained from the analysis of twenty-one separate 0.5 g whole rock fragments from a single stromatolite core plug (25 cm long by 2.5 cm diameter) collected from a low-strain enclave in an area of otherwise complexly-deformed sediments and amphibolites along the northern margin of the Masvingo greenstone belt. The remarkably large range of Pb isotopic compositions ($^{206}Pb/^{204}Pb$ from 31.468-140.499) exceeded that found in the majority of igneous and metamorphic rocks and a particularly high model μ_1 value of 12.4, (late Archaean igneous rocks in the vicinity had values between 7.8-8.5) was interpreted as the result of a," *short-lived high μ stage of Pb isotope evolution immediately before the closure of the Mushandike stromatolitic limestone U-Pb systems*". Moorbath et al. (1987) interpreted the geological significance of the date as "*close to the age of deposition of the Mushandike stromatolitic limestone, although resetting due to a low-pressure, andalusite-forming metamorphic event cannot be ruled out*" .

Unpublished results (Moorbath, pers. comm. 1991) for five HCl-soluble analyses from a second adjacent core gave a concordant isochron (MSWD 2.1) corresponding to a date of 2875 ± 73 Ma (**Figure 1.3.5**) and seven single samples from seven other separate drill cores produced a combined date of c.2850 Ma. Although disequilibrium was detected between the lead in the HCl-soluble fractions and that in the silicate residues, it was not possible to extract subsets of data that defined significantly different dates and evidently the centimetre-size domains sampled had remained essentially closed systems with respect to both U and Pb for some 2850 Ma.

Moorbath et al. (1987) concluded by stating that, "*We regard the Pb/Pb technique as extremely promising for the direct dating of time of deposition of ancient stromatolitic limestones as well as other sedimentary horizons intercalated with, or bracketed by, limestone beds. If the great ranges in U/Pb and corresponding Pb isotope ratios between adjacent small domains turn out to be a common feature of sedimentary carbonates, it may be possible to extend the applicability of the Pb/Pb dating method to limestones through most of the Proterozoic*". **The current work, which commenced in October 1988, seeks to investigate this proposal and, in addition, to extend the studies to include Phanerozoic carbonates and macrofossils and metamorphosed carbonates.**

Figure 1.3.5: Pb/Pb age data for the Mushandike stromatolitic limestone, Zimbabwe, after Moorbath et al. (1987)

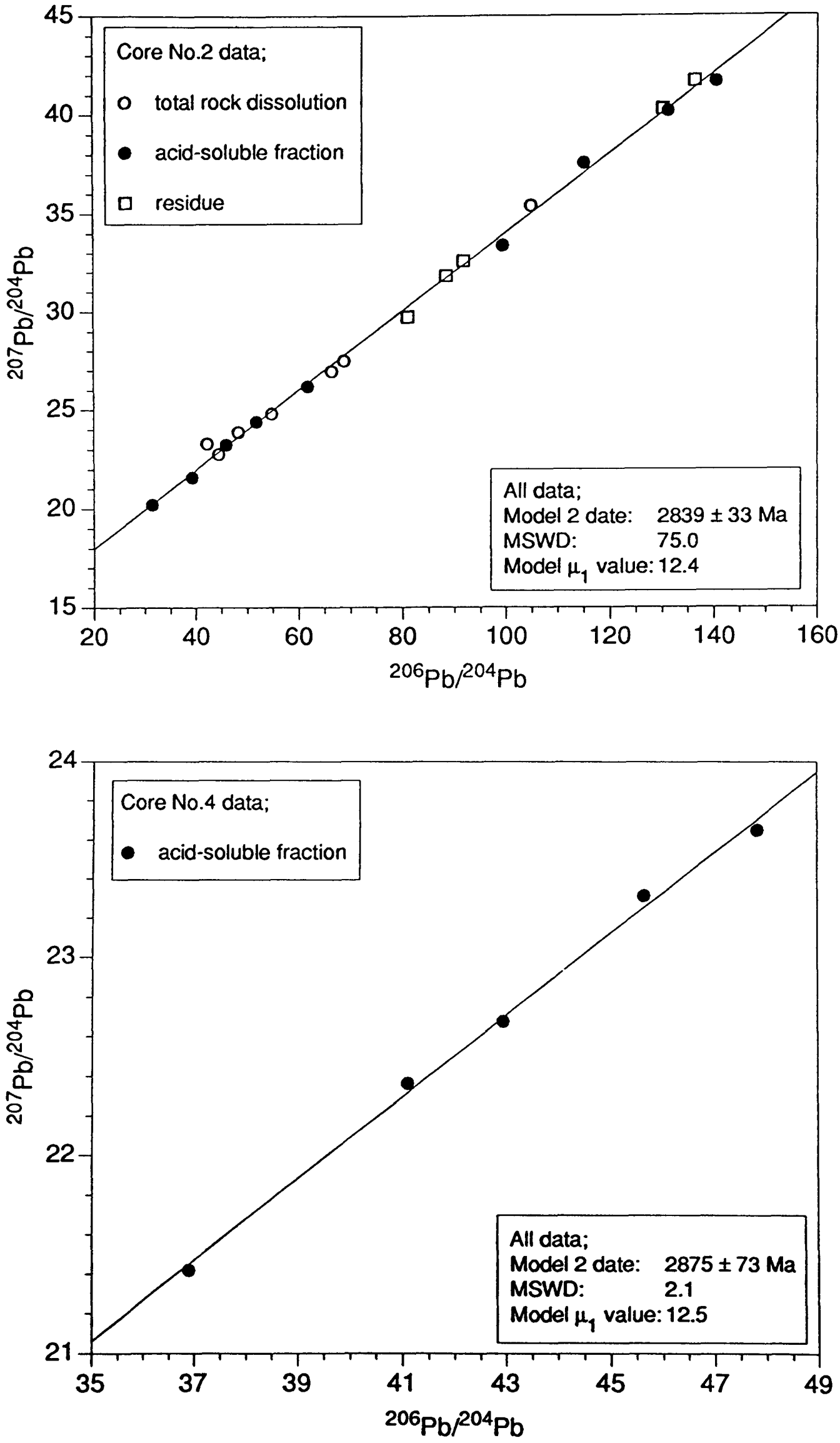

Since 1987 there has been much interest in the potential of direct dating of carbonate materials and a number of papers and abstracts have been published on the Pb/Pb dating of sedimentary carbonates (Jahn & Cuvellier, 1989; Cuvellier, 1989; Jahn et al., 1990; Russell, 1991); U-Pb dating of sedimentary carbonates (Smith & Farquhar, 1989; Smith et al., 1991; DeWolf & Halliday, 1991); Pb/Pb dating of marbles (Jahn, 1988; Taylor & Kalsbeek, 1990) and Pb/Pb dating of igneous carbonatites (Andersen & Taylor, 1987). In addition, Parnell & Swainbank (1990) demonstrated that Pb/Pb dating could be applied to the dating of hydrocarbon migration through studies on solidified uraniferous bitumens.

Jahn et al. (1990) reported a date of 2557 ± 49 Ma for the stromatolitic Transvaal Dolomite (Schmidtsdrif Formation, Ventersdorp Supergroup, South Africa) from an eleven point Pb/Pb errorchron (MSWD 10) (**Figure 1.3.6**). The carbonate showed no evidence of large scale recrystallisation and the authors interpreted the date as the age of dolomitisation, fitting in with the majority of other published age constraints for the Supergroup. The stromatolitic dolomite exhibited a more limited range of Pb isotopic composition than the Mushandike stromatolite ($^{206}Pb/^{204}Pb$ between 15.575-22.750 cf. 31.468-140.499) and a model μ_1 value (7.72 cf. 12.4) characteristic of Pb sourced from juvenile mantle-derived rocks (MORB mantle has a μ_1 value of c.7.9).

Cuvellier (1989) reported dates for stromatolitic dolomites from the Changcheng Group of China in an unpublished thesis from the University of Rennes that were in general agreement with published geochronological information for the Sinian System. A date of 1428^{+106}_{-114} Ma (MSWD 9.22) with a model μ_1 value of 8.42 for the Gaoyuzhuang Formation (**Figure 1.3.7**) was interpreted as the age of syn-depositional dolomitisation, supporting a date of 1434 ± 50 Ma for stratiform galenas from the same formation (Kweiyang Institute of Geochemistry, 1977). A more precise date of 1489 ± 15 Ma (MSWD 5) for the Tuanshanzi Formation (also **Figure 1.3.7**), lower in the succession, had a slightly lower model μ_1 value of 8.23 and was interpreted as the age of a dolomitisation event that followed deposition by some 100-150 Ma to conform with a U-Pb zircon date of c.1600 Ma from an overlying trachyte (Lu, unpublished data). Model μ_1 values for both dolomites suggest derivation of Pb from essentially juvenile, mantle-derived protoliths and imply that the Mushandike stromatolite may indeed have undergone significant diagenetic/metamorphic transformation.

Figure 1.3.6: Pb/Pb errorchron for the Transvaal Dolomite, Schmidtsdrif Formation, South Africa, after Jahn et al. (1990)

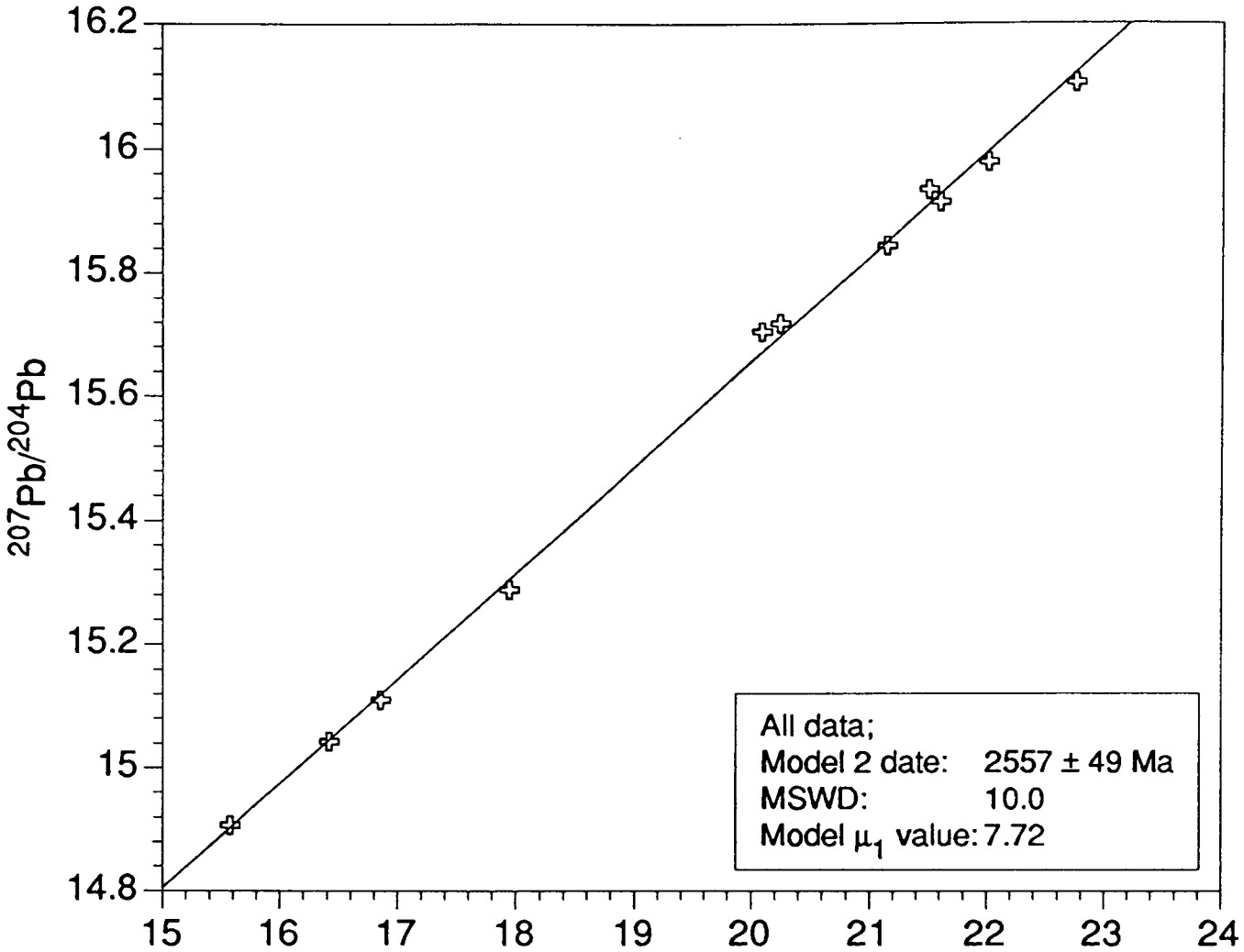

Jahn (1988) and Taylor & Kalsbeek (1990) showed that the same Pb/Pb technique could be applied effectively to marbles. The geological interpretation of Pb/Pb dates is somewhat simpler than for sedimentary carbonates since the marbles have clearly undergone metamorphic recrystallisation and this process is known to reset radiometric ages for other metamorphic rock types (Faure, 1986). At present, insufficient data exists for the concept of 'blocking temperatures' to be investigated and so dates are generally interpreted as representing the age of 'metamorphic recrystallisation'.

Jahn (1988) dated a previously unrecognised Jurassic thermal event affecting Permian carbonates (Jahn et al., 1984; Burke et al., 1982) collected over a wide area from the Tananao Schist Belt of Taiwan, when he obtained a seventeen point Pb/Pb errorchron date of 166 ± 33 Ma (MSWD 6.6, model μ_1 value 8.34) (**Figure 1.3.8**). Taylor & Kalsbeek (1990) obtained isochron dates of 1881 ± 20 Ma (MSWD 1.73, model μ_1 value 8.28) and 1845 ± 23 Ma (MSWD 1.12, model μ_1 value 8.24) for marbles of the Rinkian and Nagssugtoqidian mobile belts of West Greenland (**Figure 1.3.9**), concordant with independent metamorphic Rb-Sr and Pb/Pb studies in the vicinity that gave a weighted mean of 1880 ± 50 Ma (Kalsbeek et al., 1984). However, a third date of 1773 ± 22 Ma (MSWD 3.96, model μ_1 value 9.51) for marbles from the

Figure 1.3.7: Pb/Pb age data for stromatolitic dolomites from the Changcheng Group, China, after Cuvellier (1989)

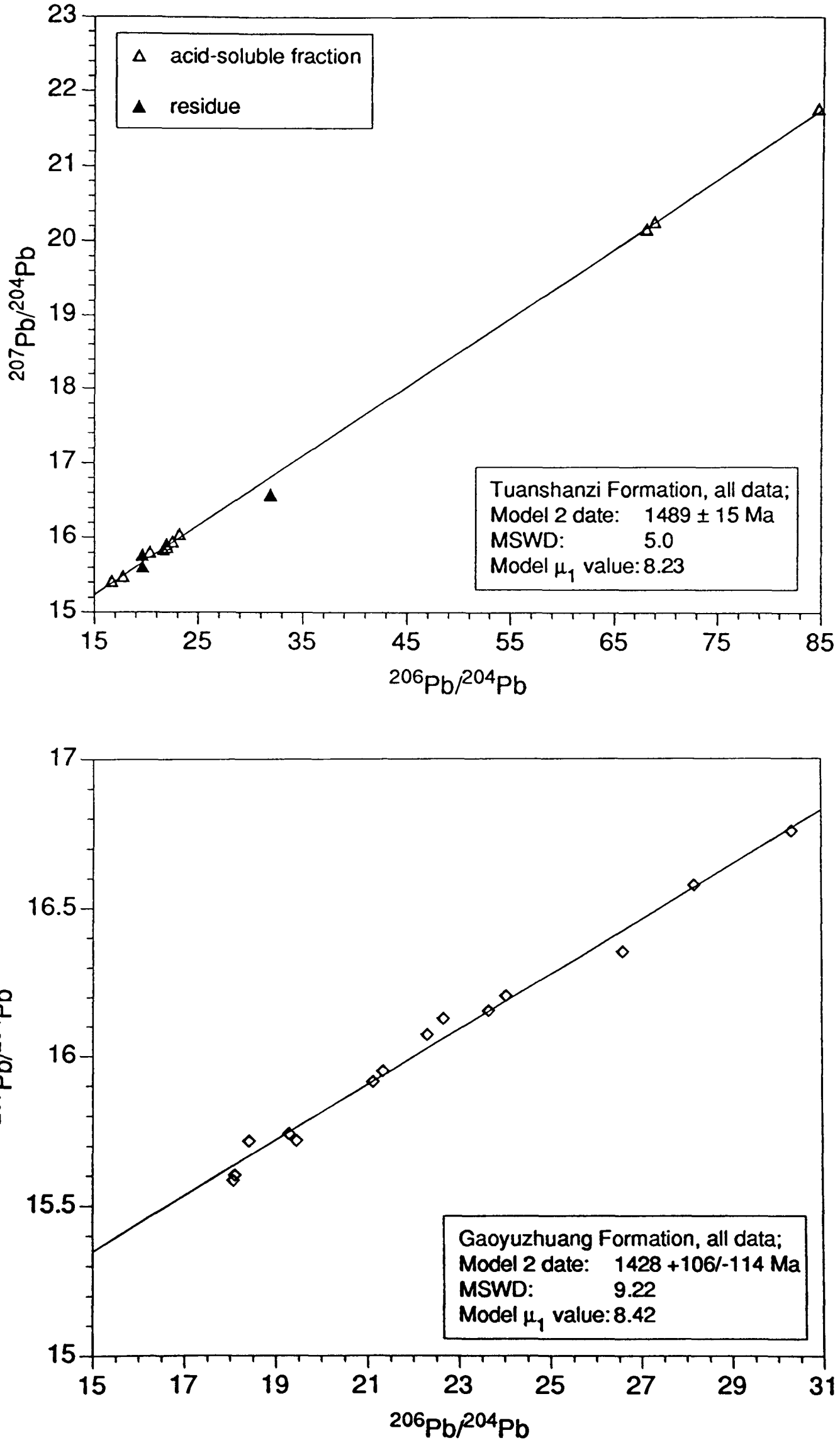

Ammassalik mobile belt to the southeast (**Figure 1.3.9**) was at odds with a U-Pb zircon date of 1886 ± 2 Ma for late tectonic intrusives (Hansen & Kalsbeek, 1989) and an Rb-Sr whole rock date of 1871 ± 50 Ma for associated metapelites (Kalsbeek & Taylor, 1989). The authors interpreted this anomalously young date as the age of a separate metamorphic event, the higher model μ_1 value implying an evolved pre-metamorphic crustal history, but they acknowledged that further investigation was required.

Figure 1.3.8: Pb/Pb errorchron for Tananao Schist Belt marbles, Taiwan, after Jahn et al. (1988)

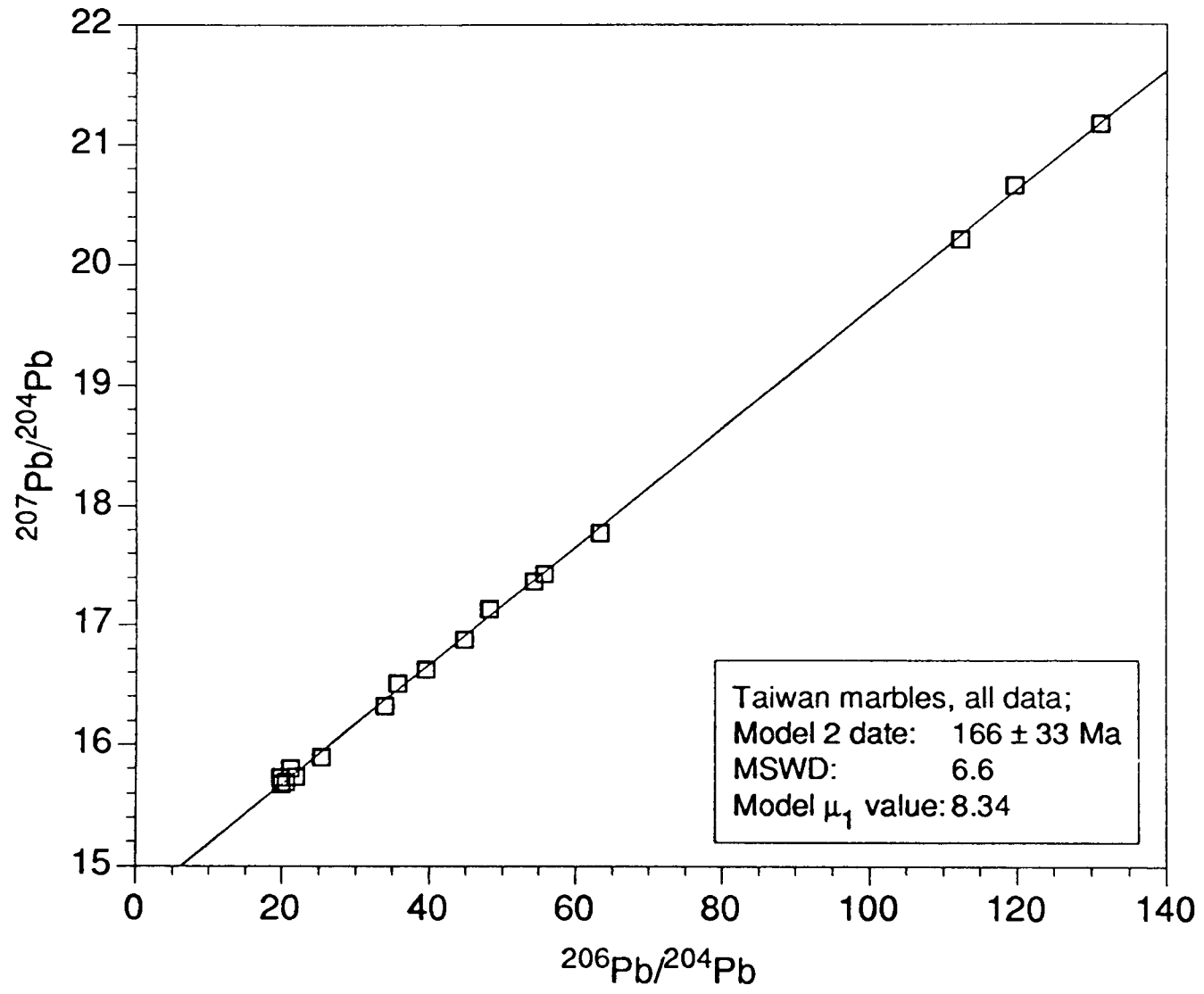

Andersen & Taylor (1987) demonstrated a further application of carbonate Pb/Pb dating when they obtained a date of 540 ± 14 Ma for the Fen carbonatite complex, southeast Norway, from an eighteen point errorchron (MSWD 3.63, model μ_1 value 8.15). The date was interpreted as the, "*age of emplacement of the intrusion*", with the elevated initial Pb isotopic composition and model μ_1 value suggestive of partial crustal contamination. Positive correlation between apatite content and $^{206}Pb/^{204}Pb$ ratios suggested that variable *in situ* μ_2 values ($^{238}U/^{204}Pb$) were most likely attributable to the fractionation of apatite. The cause of μ value variation in sedimentary carbonates has not yet been satisfactorily explained.

Figure 1.3.9: Pb/Pb age data for Greenland Proterozoic marbles, after Taylor & Kalsbeek (1990)

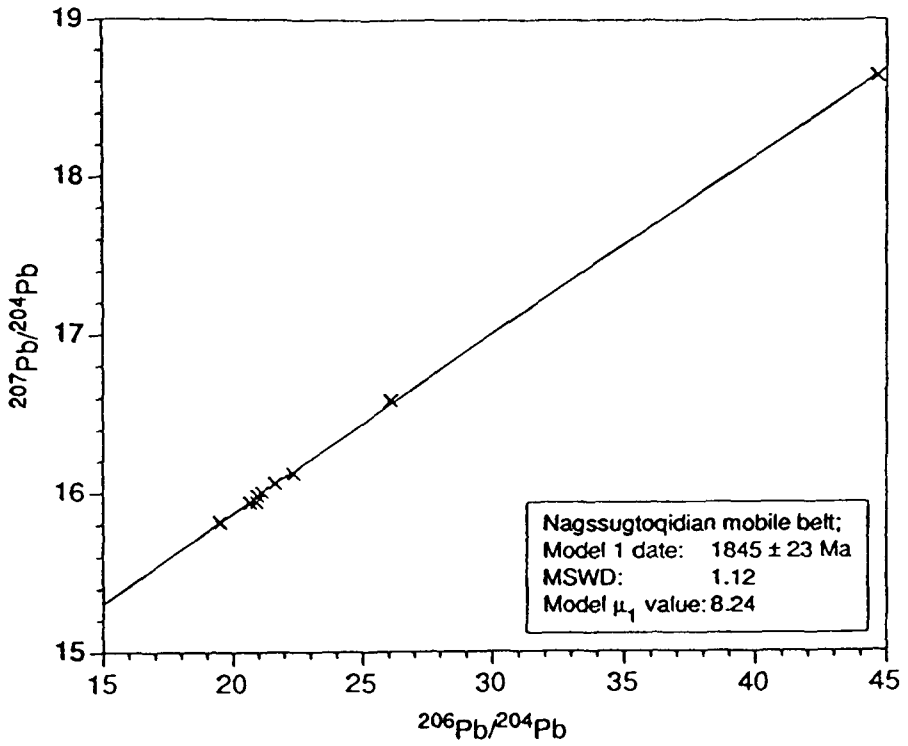

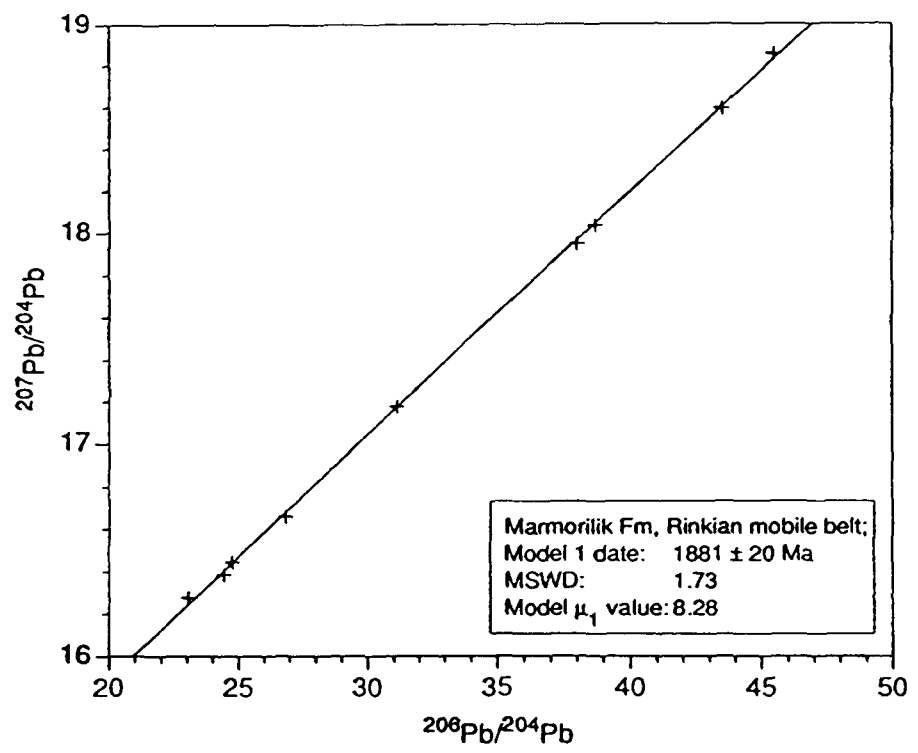

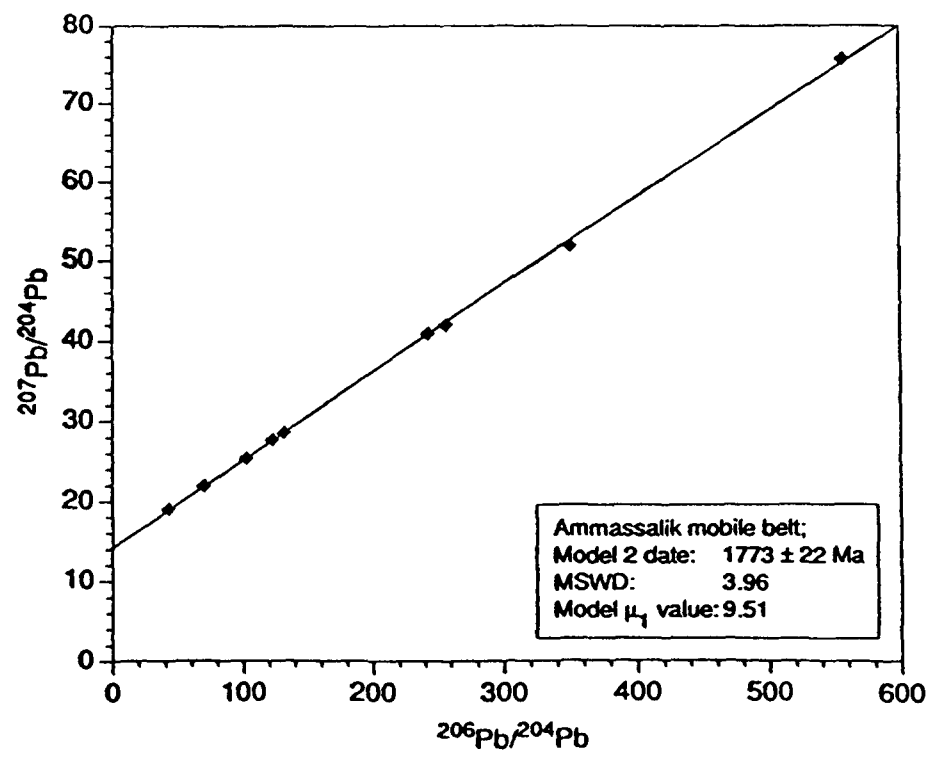

U-Pb Studies

A logical progression of the application of Pb/Pb studies was to investigate whether the U-Pb isotopic method of dating could be applied to carbonates. Theoretically, this method is capable of far greater precision, particularly for younger rocks. Although U-Pb dating requires the determination of absolute elemental concentrations and closed system conditions may be easily disturbed by loss/gain of U or Pb, work by geochronologists at Toronto has demonstrated successfully that geologically useful dates can be obtained.

Smith & Farquhar (1989) obtained a ^{238}U-^{206}Pb errorchron date of 376 ± 10 Ma (MSWD 4.7) for nine analyses of *Heliophyllum* rugose corals from the Givetian Hungry Hollow Formation of Western Ontario, Canada (**Figure 1.3.10**). The corals had evidently maintained closed U-Pb system conditions since c.380 Ma despite the mobility of U and, to a lesser extent, Pb under oxidising near-surface conditions (Rosholt et al., 1973; Oversby, 1976). Within error, the date agreed well with the inferred boundary ages for Givetian strata from Harland et al. (1989) (377.4 Ma and 380.8 Ma) and was interpreted as the age of diagenesis, occurring soon after deposition. Although the corresponding ^{235}U-^{207}Pb date of 427 ± 57 Ma was concordant (the imprecision being attributed to a lack of radiogenic ^{207}Pb), the Pb/Pb data exhibited a significant degree of scatter (**Figure 1.3.10**) and this was attributed to low in *situ* μ_2 values (0.2-22.1), a lack of radiogenic Pb (maximum 2.7%) and analytical difficulties in measuring the resulting limited Pb isotopic range.

DeWolf & Halliday (1991) published U-Pb data for Upper Ordovician limestones from New York State which palaeomagnetic evidence suggested had been disturbed in the late Palaeozoic. The ^{238}U-^{206}Pb date of 454 ± 8 Ma (MSWD 12.8) which they obtained (**Figure 1.3.11**) was in excellent agreement with Ar-Ar and U-Pb zircon dates of 454 ± 6 Ma and 457 ± 1 Ma for an underlying bentonitic horizon and they concluded that any remagnetising fluids had not interacted with the carbonate, which had remained essentially undisturbed since deposition. The authors suggested that the method had a potential precision of ± 1 Ma and therefore could be of use in Palaeozoic time scale calibration.

Figure 1.3.10: ^{238}U-^{206}Pb and Pb/Pb data for *Heliophyllum* corals from the Givetian of Ontario, Canada, after Smith & Farquhar (1989)

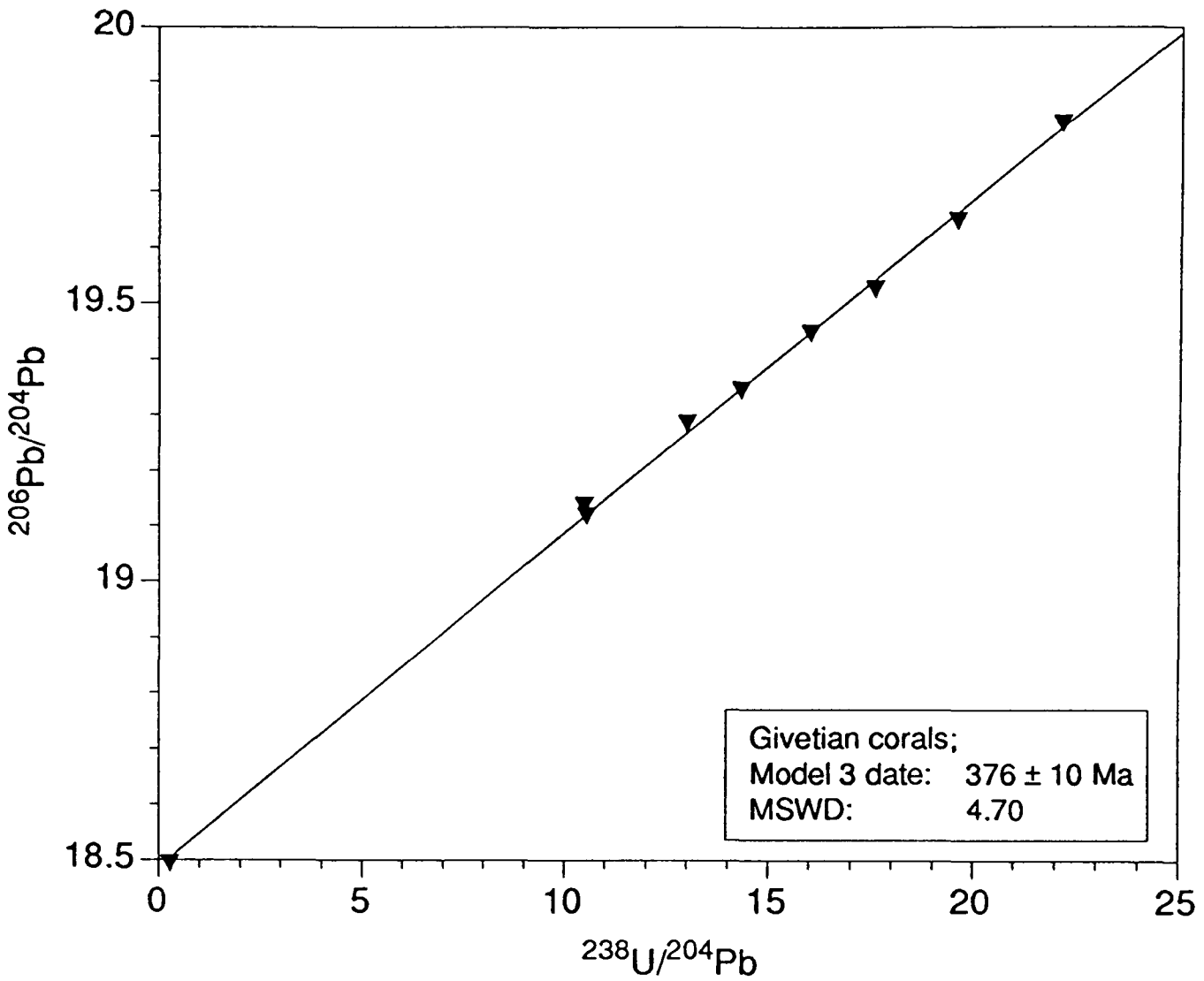

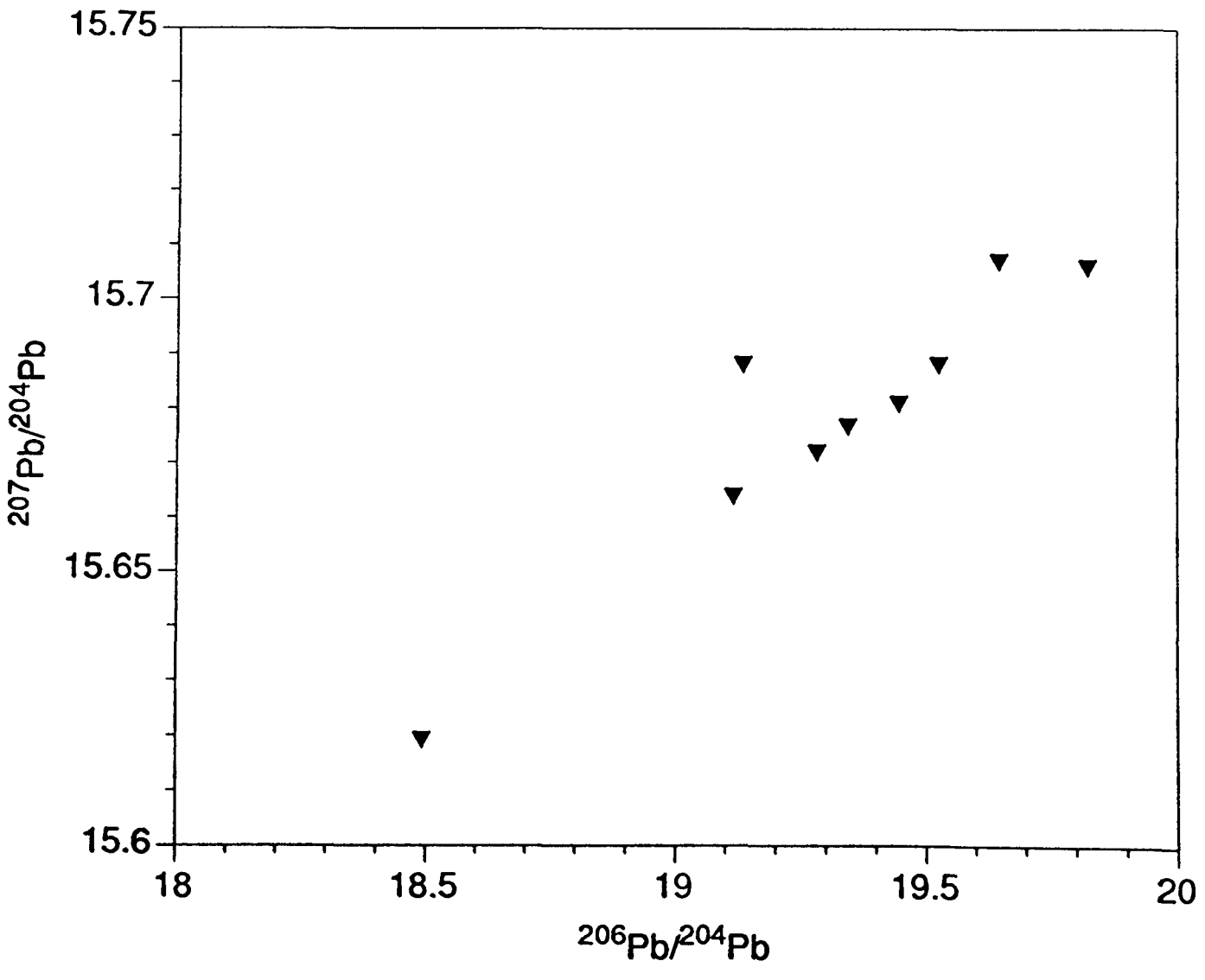

Figure 1.3.11: ^{238}U-^{206}Pb data for a remagnetised Upper Ordovician limestone, New York State, after DeWolf & Halliday (1991)

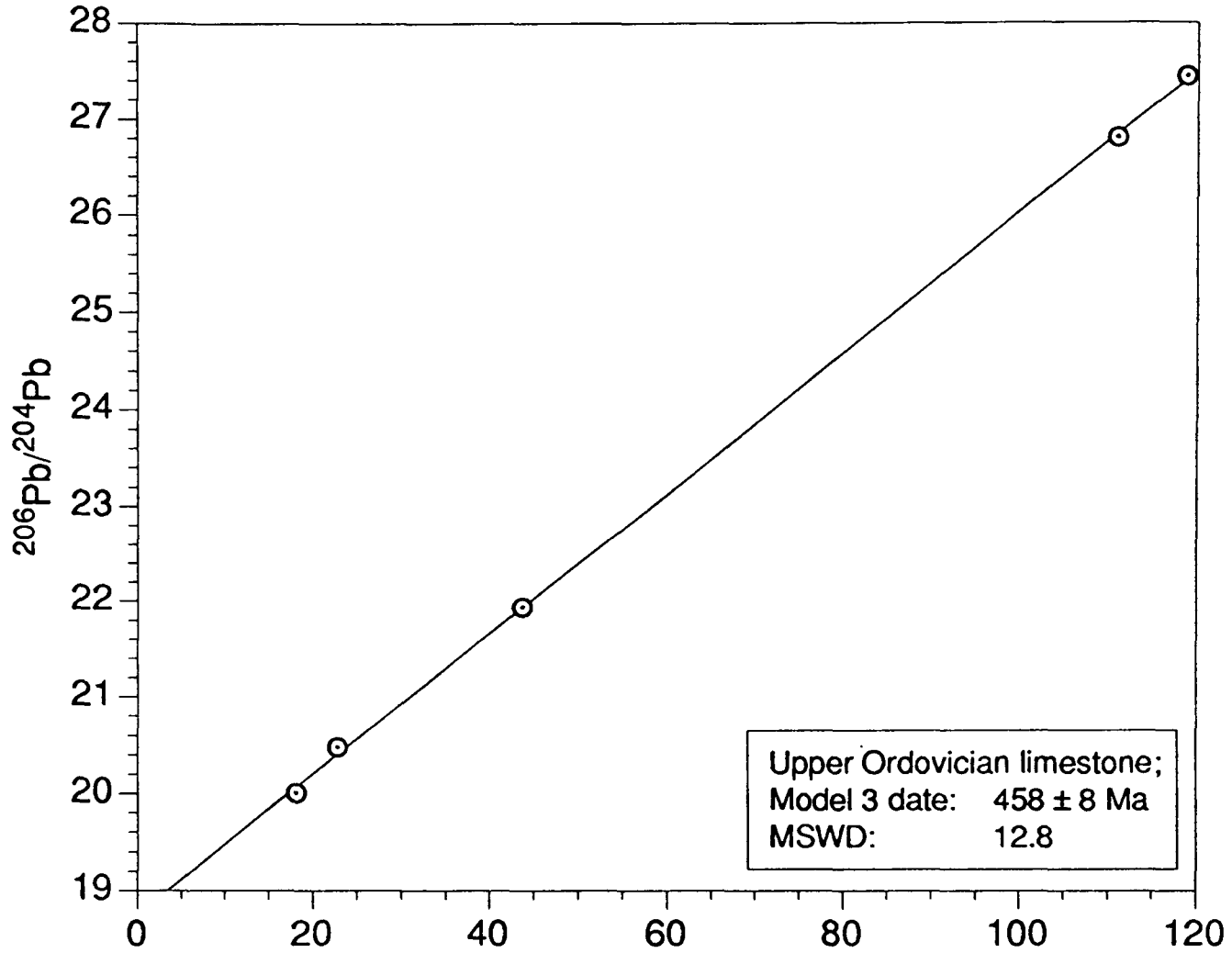

In a study of Ordovician carbonates from the Lucas Formation, Ontario, Smith et al. (1991) reported apparent $^{206}Pb^*/^{238}U$ and $^{207}Pb^*/^{235}U$ dates for six carbonates based on U and Pb concentration data and an inferred 400 Ma initial Pb isotopic composition (Stacey & Kramers, 1975). Results varied from 231.5 ± 1.4 Ma to 244.9 ± 1.6 Ma, at odds with the chronostratigraphic age. In addition, dates of 238.2 ± 1.1 Ma and 45 Ma were calculated for separate luminescent phases within a recrystallised spar-rich carbonate. The dates were interpreted as indicating separate episodes of late diagenetic recrystallisation (c.235 Ma and 45 Ma) and the authors pointed out that this was, "*consistent with the idea of recurrent fluid activity along fracture zones in subsurface sediments in the Michigan Basin*". The *in situ* μ_2 values (up to 62000) were orders of magnitude higher than had been previously noted for any carbonate material and reflect significant U enrichment during diagenetic recrystallisation, with U concentrations reaching 7 ppm. The potential of U-Pb systematics for dating episodes of carbonate diagenesis offers intriguing possibilities for the constraint of sediment deformational histories.

1.4: SUMMARY

The accuracy of time scale calibration is governed ultimately by the volume of reliable chronometric ages for well defined chronostratigraphic horizons. The Phanerozoic geochronologic time scale is reasonably well constrained, with disagreement over the chronometric location of the majority of epoch boundaries being typically ≤ 5 Ma. Indeed, recent Ar/Ar and U-Pb zircon studies on volcanic ash bands have produced error bars of < 1 Ma and the portions of the Phanerozoic time scale that are most accurately defined are those for which such dated interstratal volcanics exist. Available Phanerozoic bio- and chemostratigraphies permit further non-quantitative subdivision based on assumptions concerning the constancy of evolutionary and depositional rates.

The Precambrian geochronological time scale, however, is extremely poorly defined because of the cratonic nature of most lithostratigraphies, the lack of a functional biostratigraphy and the small number of reliable dates available. Consequently, time divisions have been arbitrarily located. The direct dating of Precambrian sediments potentially has far greater precision (< 50 Ma) than is available from indirect constraints such as basement and intrusive ages. Consequently, in the absence of a functional biostratigraphy the direct age determination of Precambrian sediments holds the key to both inter-continental correlation and the development of a global chronometric time scale.

The direct dating of carbonates by Pb/Pb and U-Pb methods clearly has extensive applications in the earth sciences since appropriate carbonate sample materials are both temporally and geographically widespread:-

- as sedimentary limestones, both marine and lacustrine, they are frequently constituents of extensive sedimentary basins for which chronometric age data may be both limited and imprecise;
- as metamorphically recrystallised marbles they occur throughout the major deformational belts of the world;
- they also occur as part of the essential mineralogy of evolved igneous associations such as carbonatites;
- as macrofossils they record the evolution of the early life on earth (stromatolites) and constitute the vast majority of the preserved fossil record throughout the Late Precambrian and Phanerozoic and
- as cements they are often significant constituents of sedimentary, igneous and metamorphic carbonate and non-carbonate rock types and reflect episodes of

secondary alteration/recrystallisation in response to the activity of carbonate rich fluids.

In the Precambrian, it is possible that reliable Pb/Pb dating of stromatolitic carbonates could be used not only to trace rates of early evolution on the planet but also to date and correlate chronostratigraphic horizons within and between continents and thereby erect an integrated time scale. The potential precision of the method may approach 1% of the regressed date and as such permit greater resolution than is available from indirect constraints. The dating of marbles can contribute to the understanding of the timing of major tectonic episodes.

In the Phanerozoic, the precision of the Pb/Pb method is limited by slow evolution of the radiogenic $^{207}Pb/^{204}Pb$ ratio but the large ranges in Pb isotope composition frequently demonstrated by sedimentary, igneous and diagenetic carbonates mean that geologically useful precision is attainable. Phanerozoic time scale calibration is principally accomplished through the isotopic study of interstratal volcanic horizons, where precision of < 1 Ma is possible, but continued development of direct U-Pb carbonate dating may soon rival this approach. In addition, the potential of both Pb/Pb and U-Pb systematics for dating episodes of carbonate diagenesis offers exciting possibilities for constraining sediment deformational histories.

In the following chapters, this work undertakes to further investigate the potential of direct Pb/Pb carbonate dating by applying the technique to stromatolites from reasonably well constrained Precambrian chronostratigraphies in Australia (**Chapter 2**) and India (**Chapter 4**), to untried Phanerozoic carbonate macrofossils (**Chapter 5**) and to Archaean marbles (**Chapter 3**), with a view to the development of a broad geochemical model explaining the general suitability of carbonates for radiometric dating using Pb/Pb and U-Pb systematics (**Chapter 6**).

Chapter 2:

WESTERN AUSTRALIAN PROTEROZOIC STROMATOLITES

2.1: INTRODUCTION

The geology of Western Australia, illustrated in **Figure 2.1.1**, comprises stable Archaean cratons, Proterozoic orogenies and sedimentary basins ranging in age from Early Proterozoic to Cenozoic. The current status of knowledge concerning broad geological relationships in the state is summarised in the 1:2500000 geological map of Western Australia compiled by Myers & Hocking (1988). From this work it is evident that while the age and lithostratigraphy of most Phanerozoic basins are well defined, the same is not true of their Precambrian counterparts. Field mapping by the Geological Survey of Western Australia (GSWA) has established basic working lithostratigraphies for most of the Precambrian basins but chronometric constraints are conspicuously limited. Age constraints for sedimentary sequences tend to be based on the small number of reliable dates for basement rocks and intrusive magmatics, rare glauconite Rb-Sr and K-Ar studies and broad Pb model ages.

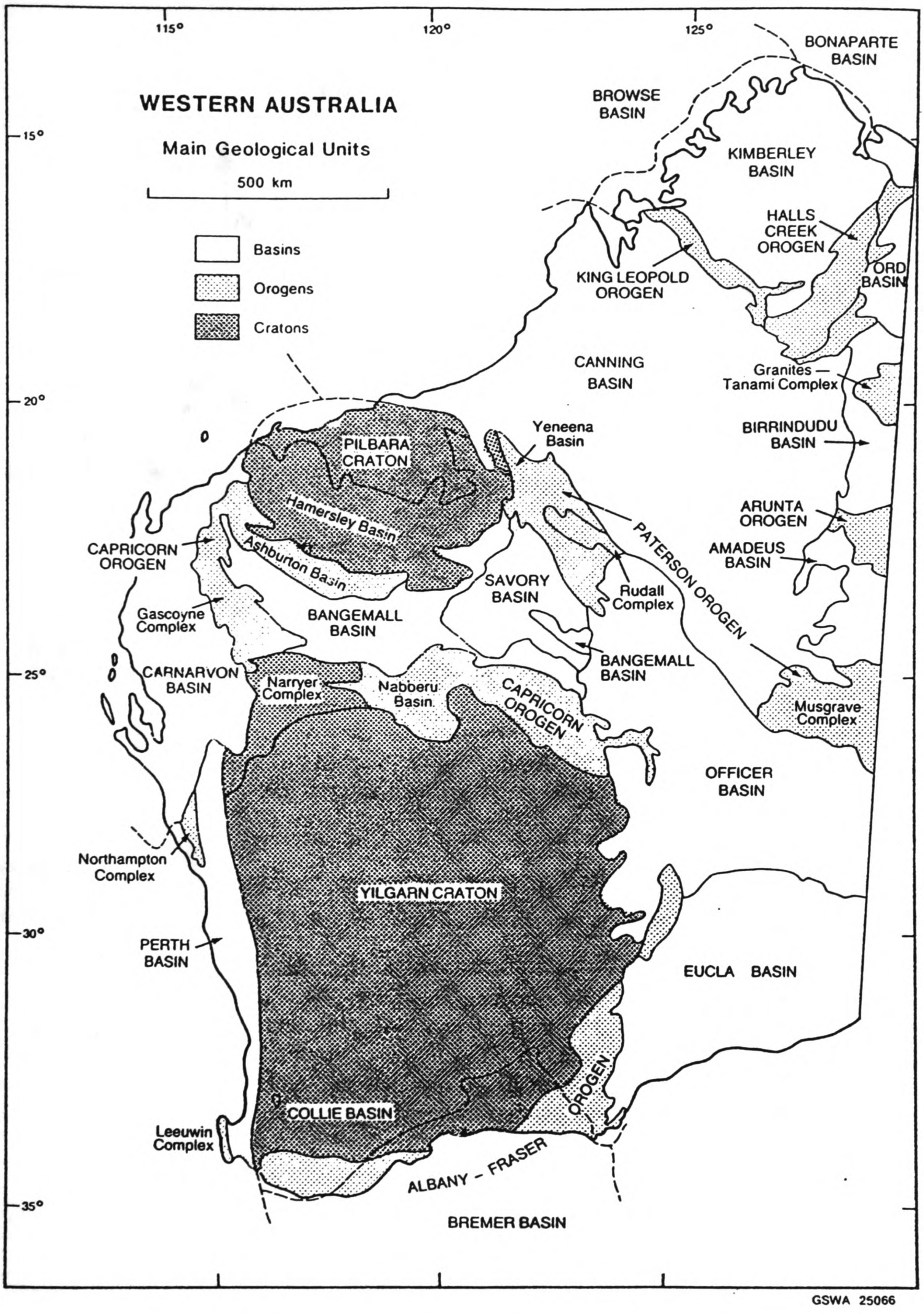

Figure 2.1.1: The main geological units of Western Australia

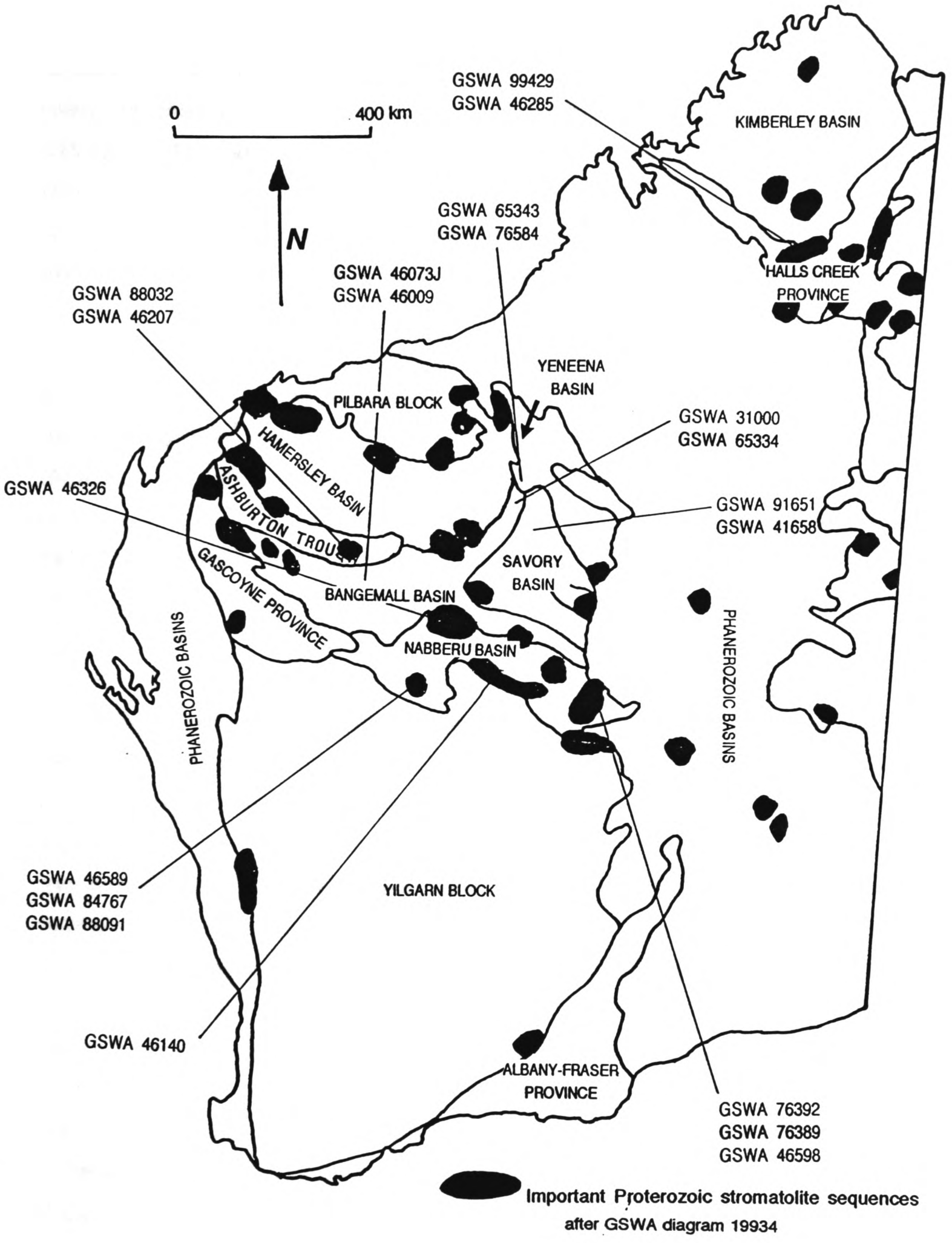

Figure 2.1.2: The basinal distribution of Western Australian stromatolites investigated in this study

Intra-basinal lithostratigraphic correlation is at best uncertain and so the ability to directly date stromatolitic carbonates, abundant in at least one formation of most Precambrian basins, is potentially a powerful correlative tool and one that could be used to help calibrate the Precambrian time scale. In addition, direct dating of stromatolitic limestones would allow the establishment of a temporal framework for palaeontological observations, permitting further critical comment to be made on the validity of stromatolite chronostratigraphy and the potential of microfossils as correlative indicators for the Proterozoic.

The subdivision and correlation of strata using stromatolites was developed by Russian workers (Semikhatov, 1976) but elsewhere reservations exist because of uncertainty over the importance of environment in influencing stromatolite form (Monty, 1977; Walter, 1977). Distinguishing environmental controls from gross evolutionary morphological change is vital in the erection of a functional biostratigraphy which will only occur once more refined systematic descriptions are published at the form/specific level and the volume of reliable, precise radiometric age constraints increases.

Chapter 2 applies the Pb/Pb method to the direct dating of stromatolites from Proterozoic basins in the state of Western Australia with a view to commenting on potential inter-basinal stratigraphic correlations. Studies are based upon the Pb isotopic investigation of twenty carbonate stromatolite hand specimens, representative of six separate basins, whose distribution is illustrated in **Figure 2.1.2**. Sample preparation and analysis followed the procedures outlined in **Appendix B**. Initially, two or three preliminary reconnaissance analyses were performed per specimen to provide an indication of the Pb isotopic composition and range before suitable samples (those with radiogenic compositions and a significant isotopic range) were selected for more detailed investigation. Stromatolite samples were kindly provided by the GSWA, whose help and logistical support throughout this work is gratefully acknowledged. Dr. P.Playford, Director of the Survey, and K.Grey receive special thanks.

2.2: ASHBURTON BASIN (CAPRICORN OROGEN)

2.2.1: *INTRODUCTION*

The Ashburton Basin outcrops over an area of some 30 000 km^2 on the southern

margin of the Pilbara Craton (see **Figure 2.1.1**). It forms the northern part of the Capricorn Orogen, a major belt of orogenically deformed and metamorphosed supracrustals, magmatic rocks and high grade metamorphic complexes that formed in response to relative convergence of the Pilbara and Yilgarn Cratons in the late Early to Middle Proterozoic. The basin has a stratigraphic thickness in excess of 12 km and metamorphism has locally reached upper greenschist facies.

2.2.2: *STRATIGRAPHY*

The Ashburton Basin unconformably overlies the Hamersley Basin on the southern margin of the Pilbara Craton and is itself unconformably overlain by the Mount Minnie, Blair and Bresnahan Basins. These are in turn unconformably overlain by the Bangemall Basin to the south and the Carnarvon Basin to the west. To the southwest, Ashburton rocks grade into the Gascoyne Complex with increased metamorphic grade and magmatism.

Figure 2.2.1: Stratigraphy of the Ashburton Basin, after Thorne & Seymour (1991)

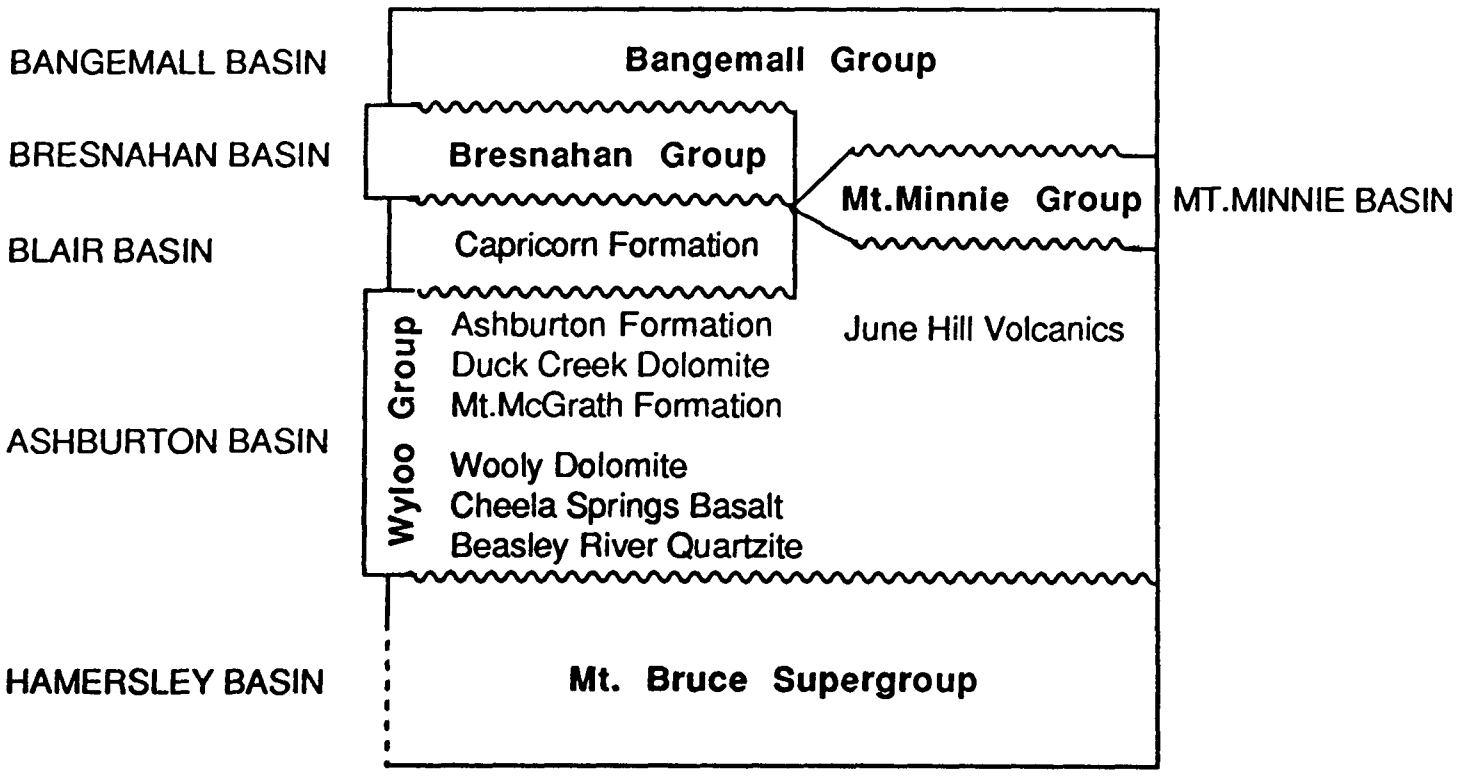

Although the Wyloo Group is the sole lithostratigraphic unit of the Ashburton Basin, the stratigraphy has received considerable revision since the early work of MacLeod et al. (1963) and the recent scheme of Thorne & Seymour (1991) was adopted for this study (see **Figure 2.2.1**). Bunting (1986) and a number of other workers have suggested that the Wyloo Group correlates with the Glengarry Group

of the Nabberu Basin, another constituent of the Capricorn Orogen outcropping to the north of the Yilgarn Craton and separated from the Ashburton Basin by the younger Bangemall Basin and the Gascoyne Complex. Given the lack of age data such a correlation has to be treated as speculative.

Two stromatolitic carbonates were analysed from the Duck Creek Dolomite of the Wyloo Group, Ashburton Basin. GSWA 88032 was collected from a site 2 km south of Duck Creek Gorge and GSWA 46207 from a separate locality, 8 km to the southwest as indicated in **Figure 2.2.2**.

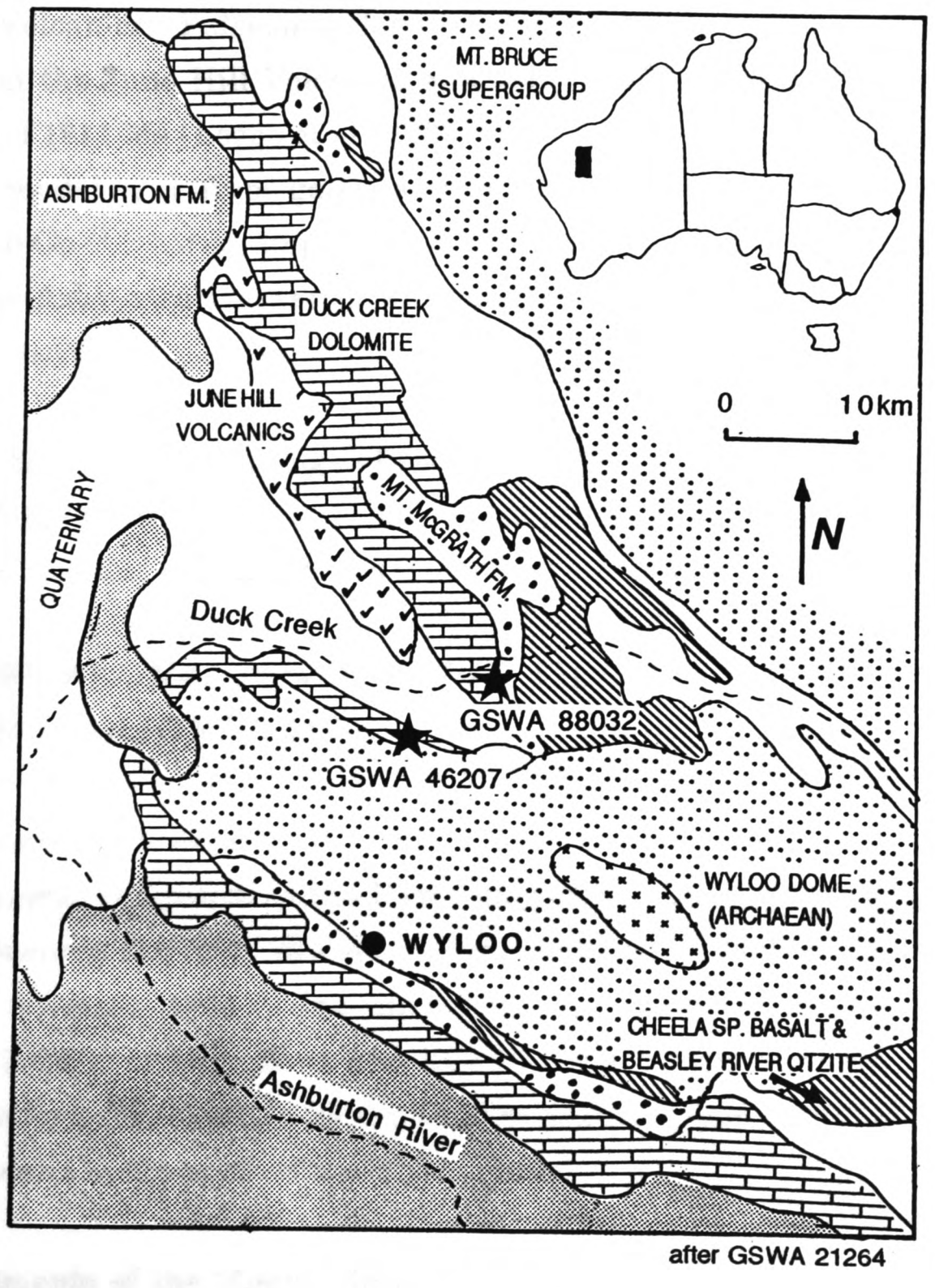

Figure 2.2.2: Localities for stromatolite samples from the Ashburton Basin, Western Australia

2.2.3: *AGE CONSTRAINTS*

The age of the Wyloo Group is poorly known. Clasts of Woongarra Volcanics from the underlying Hamersley Basin have been identified in the basal conglomerate of the Beasley River Quartzite and dated by U-Pb zircon studies at 2470 ± 30 Ma (Compston et al., 1981), providing a maximum age limit. The minimum limit is established from the inferred age of 1.6-1.1 Ga for the overlying Bangemall Group of the Bangemall Basin (Muhling & Brakel, 1985; Richards et al., in prep.).

Other dating studies have concentrated on the Ashburton Formation and the June Hill Volcanics. Pidgeon & Horwitz (1991) obtained a U-Pb date of 1843 Ma for zircons from the June Hill Volcanics and early Rb-Sr work on the same formation gave dates of 1811 Ma (Leggo et al., 1965) and 1977 ± 165 Ma[3] (Compston & Arriens, 1968). Pb model ages from galenas within the Ashburton Formation fall in the region of 2.0 Ga (Richards, unpublished data) and the Boolaloo Granodiorite, intrusive into the Ashburton Formation was dated by Rb-Sr mineral isochron at 1680 Ma by Leggo et al. (1965).

On this evidence, the age of the Wyloo Group and the Ashburton Basin is between 2500 and 1680 Ma, although the upper limit is probably nearer 1800 Ma. Gee (1980) concluded that the Wyloo Group had a probable age of about 2000 Ma.

2.2.4: *FORMATIONAL PETROGRAPHY, SEDIMENTOLOGY AND PALAEONTOLOGY*

Deposits of the basal Beasley River Quartzite (220-360 m thick), which unconformably overlie sediments of the Hamersley Basin, are representative of a former tidally influenced fan-delta system on the southwest margin of the Pilbara craton (Thorne & Seymour, 1991). The unconformably overlying Cheela Springs Basalt comprises 2000 m of basic flows and sills with associated marginal marine clastics that are conformably overlain by the shallow marine stromatolitic carbonates of the Wooly Dolomite to the south of the Wyloo Dome.

Sediments of the Mount McGrath Formation (0-1200 m), unconformable on both the lower Wyloo Group and the Hamersley Basin, record a marine regression in response to tectonic uplift and erosion. Coarse siliclastic detrital material was

---

[3] the Rb-Sr dates and all subsequent references to pre-1977 Rb-Sr dates have been recalculated using the revised decay constant for ^{87}Rb (1.42×10^{-11} a^{-1}) published by Steiger & Jäger (1977)

deposited in braided deltas in the north, while carbonates and mudstones further south indicate a shallow marine environment. Detrital supply gradually waned and waters deepened slightly towards the end of the formation.

The Duck Creek Dolomite (1000 m) was deposited conformably on the Mount McGrath Formation and consists of frequently stromatolitic bedded dolomite which is locally intensely silicified. The formational petrography has been described by Horwitz (1981; 1982) and Seymour et al. (1988), its sedimentology by Thorne (1985) and its palaeontology by a number of authors including Grey (1982; 1985), Hofmann & Schopf (1983), Knoll & Barghoorn (1976) and Walter (1972).

Two major facies associations were recognised within the Duck Creek Dolomite by Thorne & Seymour (1991). The outer shelf, slope and basin association with thinly bedded dolomite (0.01-0.15 m) and local conglomerates dominated during deposition of the Early and Late Duck Creek Dolomite when deeper water conditions prevailed over much of the basin. A generally low energy environment with limited terrigenous input is inferred from the dolomitic lamination, allowing conglomerates to be interpreted as submarine mass-flow deposits resulting from slope-failure and resedimentation. Chloritic mudstone became a prominent constituent towards the summit as terrigenous input increased. The second inner shelf association comprises a number of facies; offshore barrier, subtidal lagoon, intertidal shelf and supratidal and was most prominent during the Middle Duck Creek Dolomite when maximum progradation of the carbonate shelf occurred. Repeated shallowing-upward cycles are taken to indicate the delicate balance that existed between regression and transgression along the barred carbonate shoreline (Thorne, 1985) as the possible result of local tectonic subsidence, regional tectonism or glaciation. Disrupted domical stromatolites and irregularly replaced fenestrae in supratidal deposits are interpreted as relict evaporite structures.

The stromatolite *Pilbaria perplexa* Walter 1972 (GSWA 88032), collected from the type locality 2 km south of Duck Creek Gorge (WYL 027; see **Figure 2.2.2**), is associated with the subtidal lagoonal facies of the inner shelf association (Thorne & Seymour, 1991) when periods of emergence were rare. It occurs as small columnar forms measuring 0.02-0.05 m across and up to 0.25 m high that exhibit irregular branching and link to form continuous tabular biostromes with large niches and pockets. Broadly similar forms are noted from the Yelma and Frere Formations of the Earaheedy Group by Grey (1985) (inferred age 1.7 Ga - Richards & Gee, 1985); the Rocknest Formation, Epworth Group, northern Canada by Semikhatov (1978)

(1.9 Ga - Hoffman & Bowring, 1984) and the Schmidtsdrif Formation, Transvaal Group, South Africa by Bertrand-Sarfati & Eriksson (1977) (dated at 2.56 Ga - Jahn et al., 1990). Larger columnar forms that branch less frequently (*Pilbaria* cf. *perplexa* Walter 1972) and smaller domal stromatolites are also associated with this facies in the shallower water, higher energy conditions of the low intertidal environment.

Asperia ashburtonia Grey 1985 (GSWA 46207) was collected from the type locality some 5 km north of Paulsen mine (WYL 029 see **Figure 2.2.2**). It occurs in high intertidal to supratidal facies as small branching, subparallel to divergent columnar forms that aggregate to form broad domal stromatolitic structures with relief of up to 0.3 m (Thorne & Seymour, 1991). Walls are not developed and the laminae tend to be flat to gently convex with a distinctly banded microstructure that can be traced between adjacent columns. *Asperia ashburtonia* most probably grew in laterally restricted pools under subaerial conditions liable to seasonal submergence (Grey, 1984). Largely similar biohermal forms with microdigitate morphologies and banded microstructures (e.g. *Asperia aspera* Semikhatov 1978) have been documented from formations between 1.2 and 2.6 Ga in Canada, Western Australia, China, South Africa and Russia.

Depositional environment appears to have strongly influenced stromatolite form and this explains the wide temporal and geographical distribution of pilbariform and asperiform stromatolites in the geological record, a view discussed by Monty (1977). The limited availability of accurate radiometric age constraints for stromatolitic formations coupled with the poor taxonomic diagnosis, systematic description and sedimentological analysis of stromatolites means that it is not yet possible to distinguish the effects of ecological similarities from any gross evolutionary change in stromatolite morphology and so age ranges for most stromatolites can only be broadly constrained. Consequently, the routine application of stromatolite biostratigraphy is not yet possible.

The Duck Creek Dolomite is one of the few documented Proterozoic deposits that preserve a microfossil assemblage (Knoll & Barghoorn, 1976; Knoll et al., 1978). Although microfossils are rarely found in stromatolitic carbonate deposits because of the destructive nature of diagenetic recrystallisation (Hoffman, 1975), they are frequently preserved where early diagenetic silica permineralisation took place, such as within chert bands in the carbonate. Microfossils of coccoid form (*Huroniospora* sp., ?*Leptoteichos golubicii*), septate filamentous form (*Ferrimonilis* sp., *Gunflintia* sp., *Rhicnonema* sp.), tubular unbranched form (*Siphonophycus*

sp.) and more bizarre form (*Kakabekia* sp., *Eoastrion* sp.) are all found in the Duck Creek Dolomite (Schopf, 1983). Most tend to be very large generic representatives and may be indicative of Early Proterozoic gigantism (Schopf, 1983).

There is a distinct generic similarity between the Duck Creek Dolomite flora and that preserved in the Gunflint Chert of Canada which has an inferred age of 1.8-2.1 Ga (Schopf, 1983) (only *Ferrimonilis* sp., *Rhicnonema* sp. and *Siphonophycus* sp. have not been documented in the Gunflint Chert). There is also a strong similarity between the Duck Creek Dolomite flora and those of certain other Early Proterozoic North American formations with inferred ages of approximately 1.85 to 2.0 Ga. The Tyler Formation (1.6-2.5 Ga - Schopf, 1983) contains *Animikiea* sp., *Eoastrion* sp., *Gunflintia* sp., *Huroniospora* sp. and *Kakabekia* sp.. The Sokonoma Formation (1.8-2.5 Ga - Schopf, 1983) contains *Animikiea* sp., *Eoastrion* sp., *Gunflintia* sp. and *Huroniospora* sp.. In addition, *Gunflintia* sp. is also found in the Pokegama Formation (1.8-2.1 Ga - Schopf, 1983); *Huroniospora* sp. in the Pokegama and Kasegalik (1.76 ± 0.037-2.5 Ga - Schopf, 1983) Formations; *Leptoteichos* sp. in the Kasegalik and McLeary (1.76 ± 0.037-2.5 Ga - Schopf, 1983) Formations and *Rhicnonema* sp. in the Kasegalik Formation.

Within Australia, the Frere Formation (poorly constrained - Schopf, 1983) contains *Eoastrion* sp., *Gunflintia* sp., *Huroniospora* sp. and *Kakabekia* sp.; the Amelia Dolomite (1.65-1.67 Ga - Plumb et al., 1981; Schopf, 1983) *Gunflintia* sp. and *Huroniospora* sp.; the H.Y.C. Pyritic Shale (1.65-1.67 Ga - Plumb et al., 1981; Schopf, 1983) *Eoastrion* sp., *Ferrimonilis* sp., *Gunflintia* sp. and *Huroniospora* sp.; the Cooley Dolomite (around 1.6 Ga - Schopf, 1983) *Eoastrion* sp. and *Huroniospora* sp.; the Balbirini Dolomite (around 1.6 Ga - Schopf, 1983) *Gunflintia* sp., *Huroniospora* sp. and *Siphonophycus* sp.; the Bungle Bungle Dolomite (around 1.6 Ga - Plumb et al., 1981; Schopf, 1983) *Leptoteichos* sp. and *Rhicnonema* sp. and the Paradise Creek Formation (around 1.6 Ga - Schopf, 1983) *Eoastrion* sp. and probably *Gunflintia* sp. and *Huroniospora* sp..

Even allowing for the fact that formational ages are poorly constrained, the Australian deposits above are significantly younger than the inferred 1.89 Ga age for the Duck Creek Dolomite (Grey, pers. comm. 1991) and the majority of North American deposits. The apparently large age ranges of many of the microfossil genera and uncertainties over the importance of environmentally forced morphological convergence make them unsuitable for precise biostratigraphic or chronostratigraphic correlation at present. As the number of positive identifications of

Proterozoic microfossils increases and their recognition and description at the specific level becomes refined, integration of Precambrian biostratigraphy and radiometric chronostratigraphy should allow the identification of 'zone microfossils' and thereby facilitate correlation of suitably fossiliferous deposits within and between continents. Micropalaeontology thus has greater potential for stratigraphic purposes than the study of stromatolite morphology.

The June Hill Volcanics (120 m) are a series of mafic lavas, tuffs and agglomerates interbedded with felsic volcanics and sediments that locally overlie the Duck Creek Dolomite. They are succeeded by the very thick, dominantly clastic Ashburton Formation (5-12 km) which marks the last episode of deposition in the Ashburton Basin. Three major facies associations were recognised by Thorne & Seymour (1991) which suggested deposition took place in a deep-sea submarine-fan complex.

Two major episodes of deformation have affected the Ashburton Basin. The earliest (syn-Wyloo Group) formed part of the northern Opthalmia Fold Belt and resulted in upright to steeply inclined, north-facing buckle-type folds (Tyler & Thorne, 1990), interpreted as a consequence of basement instability and north-south crustal shortening. The latter (post-Wyloo but pre-Bresnahan Group) produced the Ashburton Fold Belt which principally affected rocks in the south of the basin. It occurred in two stages; the first pre-Capricorn Formation stage (D_1) produced large-scale folds and low grade regional metamorphism due to overthrusting from the southwest; the second post-Capricorn Formation pre-Bresnahan Group stage (D_2) produced the most obvious folding and faulting in the belt as the result of a major dextral-wrenching event affecting the Pilbara Craton and associated supracrustals.

Two principal episodes of mineralisation are also documented (syn-D_2 Ashburton Fold Belt and post-Bresnahan Group) and these have produced economic accumulations of Au, Cu, Pb, Ag, Fe and U, principally in WNW, NNW and NE trending faults, shears and quartz veins associated with the Duck Creek Dolomite and Ashburton Formation. Pb model ages from galena samples within the Duck Creek Dolomite have been obtained by Leggo et al. (1965) for the Silent Sisters mine (1700 ± 150 Ma) and Richards (unpublished data) for the Aerial mines (1550 Ma), providing possible constraints on the age of mineralisation. Ewers & Ferguson (1985) suggested that the secondarily enriched U deposits of the Bresnahan Group may have resulted from neutralisation of U- and F-bearing acid solutions by wall-rock reactions along the host fault planes.

2.2.5: *RESULTS*

Pb isotopic results for stromatolites GSWA 88032 and 46207 from the Duck Creek Dolomite are presented in **Table 2a** and illustrated in **Figure 2.2.3**. Each set of analyses independently demonstrates a large, co-linear range of radiogenic Pb isotopic compositions when plotted on a Pb/Pb diagram (except for analysis 88032I), with the implication that at isotopic closure, large variations in U/Pb ratios existed over centimetre-size domains and that closed system conditions were maintained thereafter.

Table 2a: Pb isotopic compositions of carbonate stromatolites from the Duck Creek Dolomite, Wyloo Group, Ashburton Basin (GSWA 88032, 46207)

SAMPLE	CORRECTED RATIOS *		
	$^{206}Pb/^{204}Pb$	$^{207}Pb/^{204}Pb$	$^{208}Pb/^{204}Pb$
88032	48.567 ± 0.092	19.100 ± 0.050	39.566 ± 0.104
88032 I	53.222 ± 0.064	20.117 ± 0.028	39.161 ± 0.052
88032 a	57.943 ± 0.068	20.106 ± 0.028	42.261 ± 0.064
88032 b	59.138 ± 0.060	20.221 ± 0.024	45.207 ± 0.056
88032 c	63.098 ± 0.064	20.640 ± 0.026	41.410 ± 0.052
88032 d	62.131 ± 0.062	20.512 ± 0.024	42.093 ± 0.052
88032 e	65.710 ± 0.070	20.912 ± 0.026	44.286 ± 0.056
88032 f	64.228 ± 0.072	20.766 ± 0.028	42.236 ± 0.060
88032 g	61.333 ± 0.062	20.445 ± 0.026	41.430 ± 0.052
88032 h	66.807 ± 0.066	21.038 ± 0.026	42.076 ± 0.052
46207	47.280 ± 0.048	18.921 ± 0.022	36.549 ± 0.044
46207 a	50.974 ± 0.052	19.298 ± 0.024	36.828 ± 0.046
46207 b	48.339 ± 0.048	19.036 ± 0.024	36.553 ± 0.046
46207 c	43.001 ± 0.042	18.437 ± 0.022	36.277 ± 0.044
46207 d	45.104 ± 0.046	18.681 ± 0.022	36.350 ± 0.046
46207 e	43.167 ± 0.042	18.492 ± 0.022	36.113 ± 0.044
46207 I	48.403 ± 0.056	19.026 ± 0.030	36.664 ± 0.060
46207 II	52.544 ± 0.054	19.487 ± 0.024	36.325 ± 0.044
46207 III	52.380 ± 0.052	19.445 ± 0.024	36.935 ± 0.046

* Corrected for mass fractionation of 0.130% ± 0.012 ($2\sigma_{mean}$) amu^{-1} [4]
Errors are $2\sigma_{mean}$ for corrected ratios

[4] see calculation of mass fractionation correction in **Appendix A.3.1**

Figure 2.2.3: Pb isotopic data for carbonate stromatolites from the Duck Creek Dolomite, Wyloo Group, Ashburton Basin (GSWA 88032, 46207)

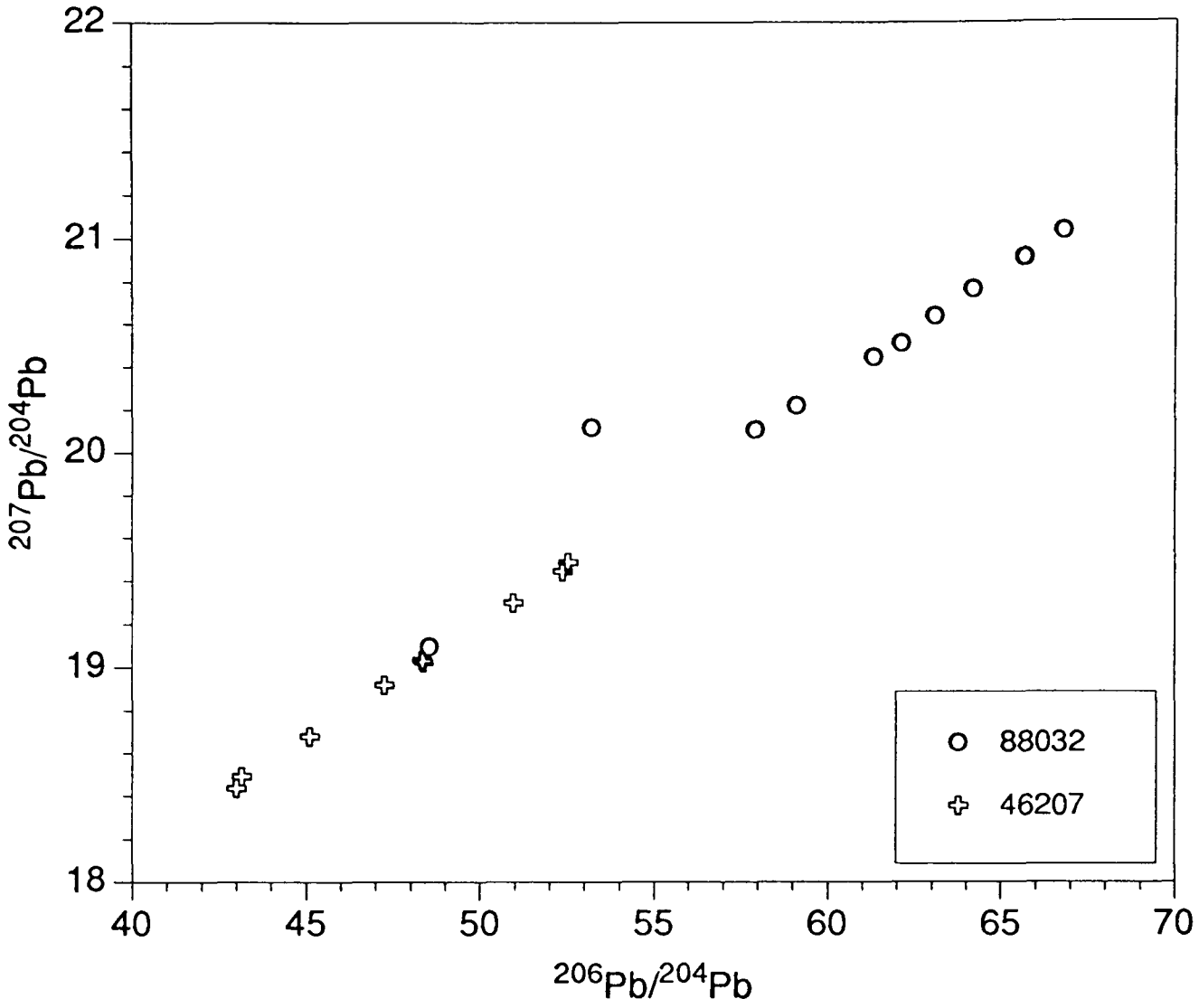

Nine of the ten analyses of separate fragments of *Pilbaria perplexa*, GSWA 88032, define a well fitted Pb/Pb errorchron whose slope corresponds to a date of 1717 ± 64 Ma using a Model 2 Yorkfit[5], with an MSWD of 4.88 and a model μ_1 value[6] of 8.73 ± 0.30 (**Figure 2.2.4**). Point 88032I was omitted because it lay off the line defined by the other analyses, possibly due to the inclusion of some secondary, isotopically distinct mineral phase within the analysed fragment. Unfortunately, it is not possible to quantify this suggestion further since the analytical procedure is destructive and original sample material non-recoverable.

In thin section, the observed 2-3 mm, light to dark grey, discontinuous lamination exhibited by GSWA 88032 is seen to be a function of bimodal carbonate grain size. Darker laminae are composed of a saccharoidal mosaic of fine grained carbonate crystals, while the lighter lenses comprise coarser, bladed carbonate frequently associated with secondary, colourless dolomite rhombs and patchy microc-

---

5 calculated using the Isoplot version 2.11 package of Ludwig (1990), see **Appendix A** for details

6 assuming single stage growth with parameters T = 4.57 x 10^9 a, $^{206}Pb/^{204}Pb$ = 9.307 and $^{207}Pb/^{204}Pb$ = 10.294 (Tatsumoto et al., 1973). See treatment in **Appendix A.6**

rystalline quartz, probably formed in solution vugs. Rare opaque phases occur within the carbonate and late deformation is indicated by stylolite formation with associated iron oxide staining and cross-cutting quartz stringers.

Figure 2.2.4: Pb isotopic data for GSWA 88032, Duck Creek Dolomite, Wyloo Group, Ashburton Basin

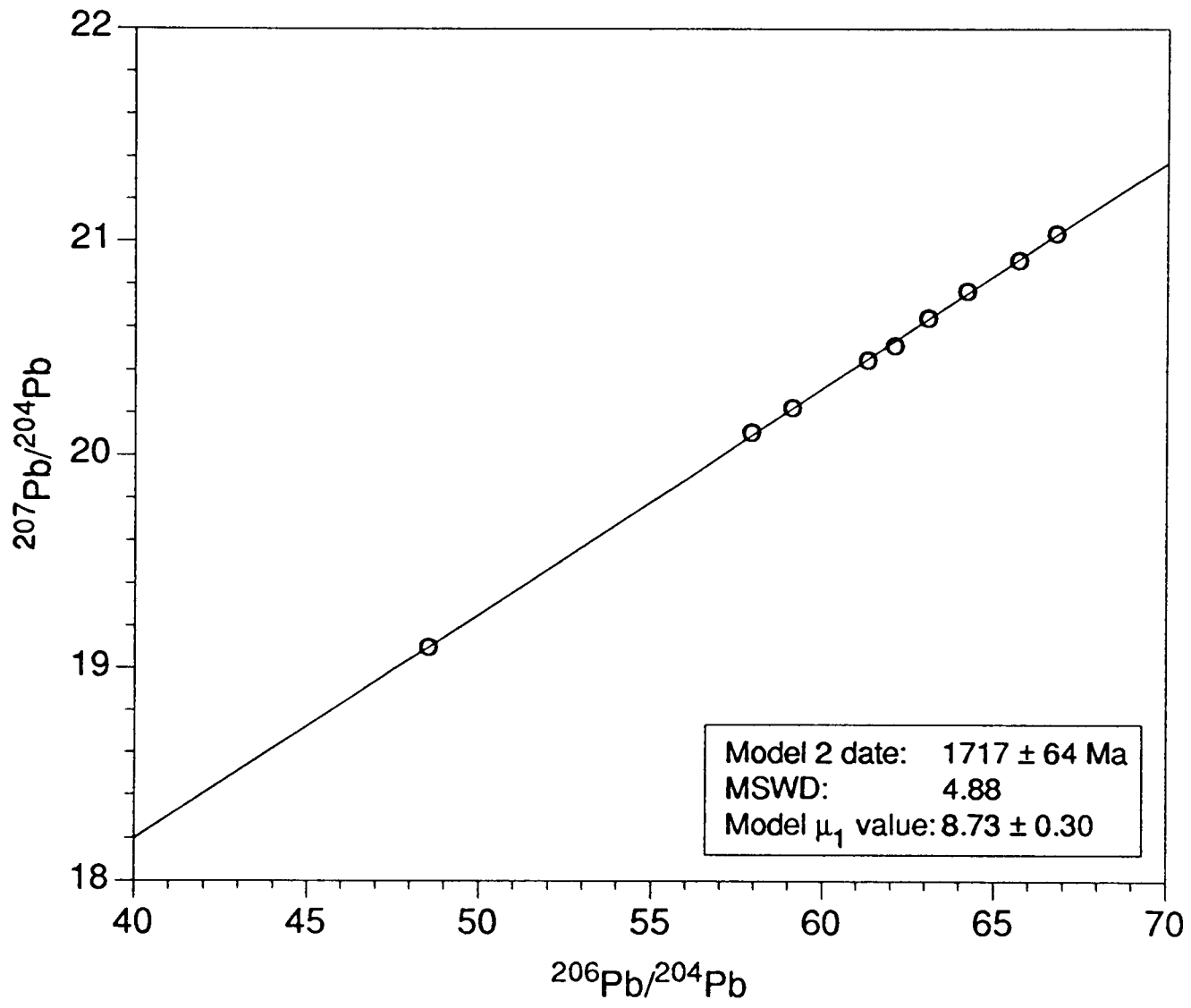

Nine analyses of GSWA 46207, *Asperia ashburtonia*, define a Pb/Pb isochron date of 1741 ± 53 Ma (MSWD 2.13, model μ_1 value 8.53 ± 0.17) (see **Figure 2.2.5**). The Pb isotopic ratios tend to be lower than those for GSWA 88032, indicating lower *in situ* μ_2 values ($^{238}U/^{204}Pb$) at the point of isotopic closure.

Thin sections were unavailable for this particular stromatolite, but Grey (1984) described the holotype as having a poorly preserved, banded microstructure with well defined light and dark microlaminae, approximately 250 μm thick, grouped into macrolaminae up to 3 mm in thickness, whose colour was a function of that of the constituent microlaminae. Extensive recrystallisation and dolomitisation, coupled with frequent secondary silicification, had altered much of the original stromatolitic fabric, making determination of the original microstructure impossible.

Figure 2.2.5: Pb isotopic data for GSWA 46207, Duck Creek Dolomite, Wyloo Group, Ashburton Basin

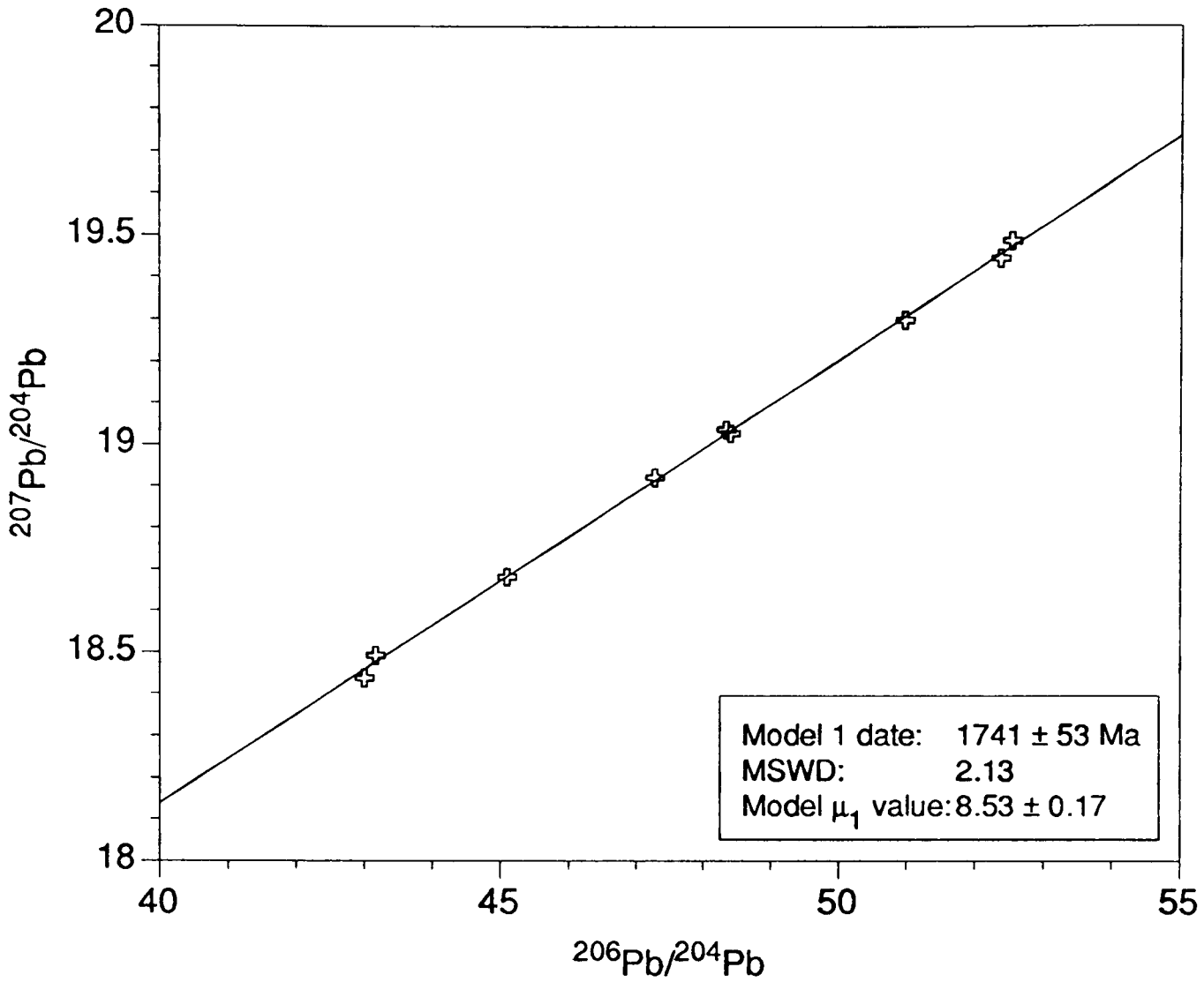

Figure 2.2.6: Stable isotopic data for GSWA 88032 and 46207, Duck Creek Dolomite, Wyloo Group, Ashburton Basin

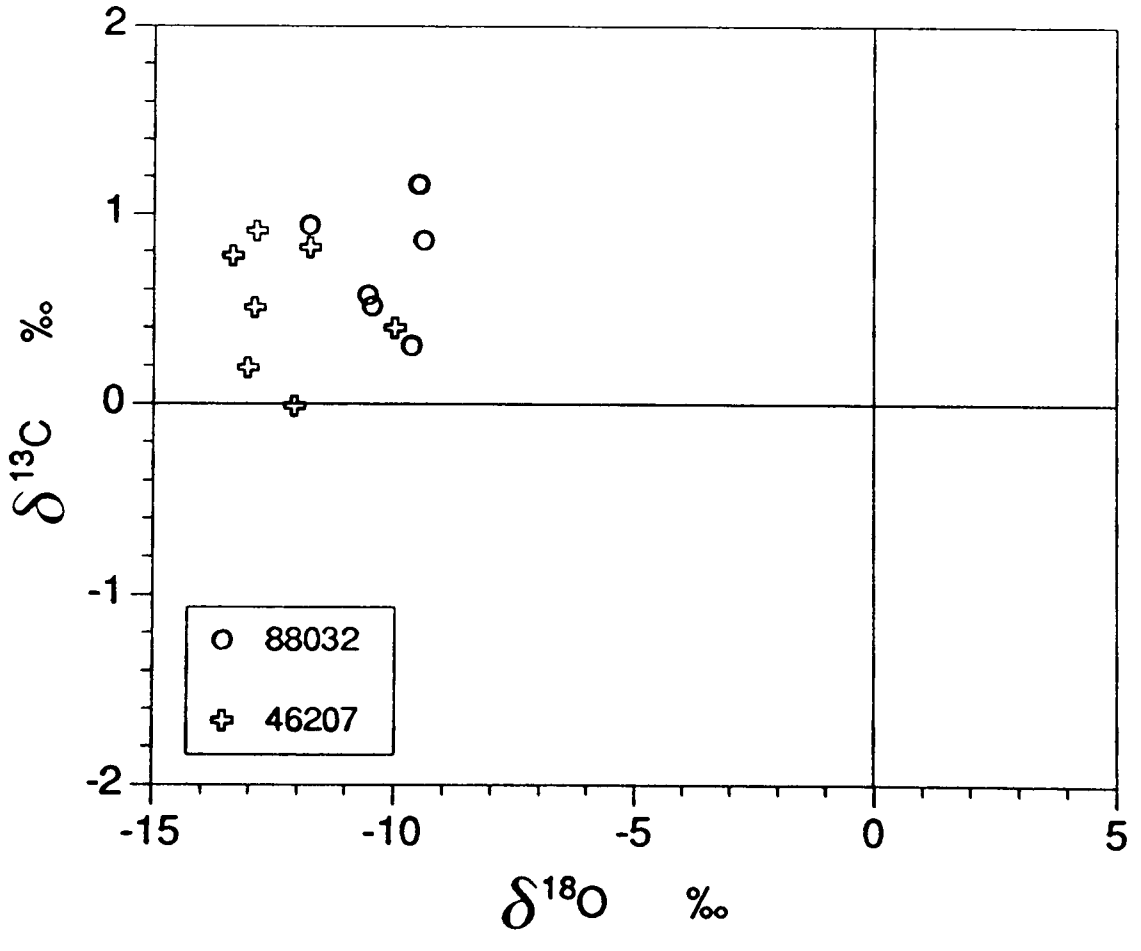

Stable isotope data for GSWA 88032 and 46207 are presented in **Figure 2.2.6**. Analyses of both samples cluster with $\delta^{13}C$ values of between -0.01 and 1.16‰ and light $\delta^{18}O$ values of between -9.40 and -13.36‰. Samples of GSWA 46207 tend to have slightly lighter oxygen isotopic compositions. The low positive $\delta^{13}C$ and negative $\delta^{18}O$ values are consistent with an interpretation in terms of deposition in a marine intertidal to supratidal environment and subsequent subjection to dolomitisation under mixing zone conditions. However, late recrystallisation involving a medium with light to very light $\delta^{18}O$ values and near-marine $\delta^{13}C$ values, such as might be encountered during burial metamorphism, can not be ruled out.

2.2.6: *DISCUSSION*

Stable isotopic results may be reconciled with the sample petrography. Preservation of lamination in both stromatolites suggests that the carbonates have not suffered extensive deformation since deposition, but saccharoidal textures indicate that original microstructures have been modified and recrystallised. Dolomitisation is documented in each sample. Secondary silicification and stylolitisation post-date carbonate recrystallisation but do not appear to have had a significant effect on gross sample morphology.

Pb/Pb dates for GSWA 88032 and 46207 are concordant within error, implying that the value has geological significance. Systematic errors may be discounted since the stromatolites are taxonomically distinct and were collected from separate localities more than 8 km apart (Grey, pers. comm. 1991). Combination of the two data sets (excluding 88032I) produces an eighteen point errorchron whose gradient corresponds to a date of 1778 ± 27 Ma (MSWD 5.53, model μ_1 value 8.43 ± 0.11). This approach may be justified in that the individual dates, the combined date and all model μ_1 values fall within error of one another. The combination technique could prove useful for other stratigraphically equivalent sample sets where data for individual stromatolites is limited either in volume or isotopic range.

The Pb/Pb stromatolite date for the Duck Creek Dolomite falls within the broad age constraints for the Wyloo Group (2.5-1.68 Ga) but is considerably younger than the inferred depositional age for the formation of 1.89 Ga used by the GSWA. This value is based on dates from correlated stromatolitic carbonates in the Rocknest Formation, Wopmay Orogen, northern Canada (Grotzinger, 1988; 1989; Grey, pers. comm. 1991). Microfossil evidence would also tend to suggest that a depositional

age of greater than 1.85 Ga was likely, although the data from other Australian deposits is ambiguous. In addition, the 1843 Ma date for zircons from the stratigraphically higher June Hill Volcanics (Pidgeon & Horwitz, 1991) is inconsistent with the interpretation of the isotopic results as a depositional age.

The Duck Creek Dolomite has been locally metamorphosed to prehnite-pumpellyite facies and pumpellyite-actinolite facies, representative of burial depths of between 4 and 5 km (Schopf, 1983). It is proposed that the 1.72-1.78 Ga dates represent the age of carbonate recrystallisation driven by syn-D_2 (post-Capricorn Formation, pre-Bresnahan Group) burial metamorphism and therefore provide a minimum age for deposition of the Ashburton Basin. The recrystallisation event could not have been sufficiently intense to obliterate the stromatolitic fabric and lamination. Pb model ages for galena samples from the Duck Creek Dolomite that are associated with the syn-D_2 mineralisation event give similar dates of 1700 ± 150 Ma (Leggo et al., 1965).

The general questions of the origin of U and Pb in carbonate stromatolites and the possible geological means of isotopic resetting are addressed in **Chapter 6**.

2.3: NABBERU BASIN (CAPRICORN OROGEN)

2.3.1: *INTRODUCTION*

The Nabberu Basin comprises a series of lithostratigraphic units deposited on the northern margin of the Yilgarn Craton during the Early Proterozoic (see **Figure 2.1.1**). The basin forms the southern part of the Capricorn Orogen, represented further north by the Gascoyne Complex and Ashburton Basin (section **2.2**), and consists of unmetamorphosed platform sequences, locally metamorphosed and deformed sediments and basement dome inliers.

2.3.2: *STRATIGRAPHY*

The Nabberu Basin unconformably overlies Archaean rocks of the Yilgarn Craton in the south and the Narryer Complex in the west and is itself unconformably overlain by the Late Proterozoic Bangemall Basin to the north and the Phanerozoic Officer Basin to the east. The stratigraphic succession consists of four unconformable units; the basal Glengarry Group, the Padbury Group, the Earaheedy Group and

the local Scorpion Group at the top of the basin (see **Figure 2.3.1**). Detailed descriptions are given in Gee (1990). Archaean basement domal inliers outcrop within the basin and a late, tectonically unrelated structure, the Teague ring structure, intrudes the Earaheedy Group in the east (see **Figure 2.3.2**).

Figure 2.3.1: Stratigraphy of the Nabberu Basin, after Gee (1990)

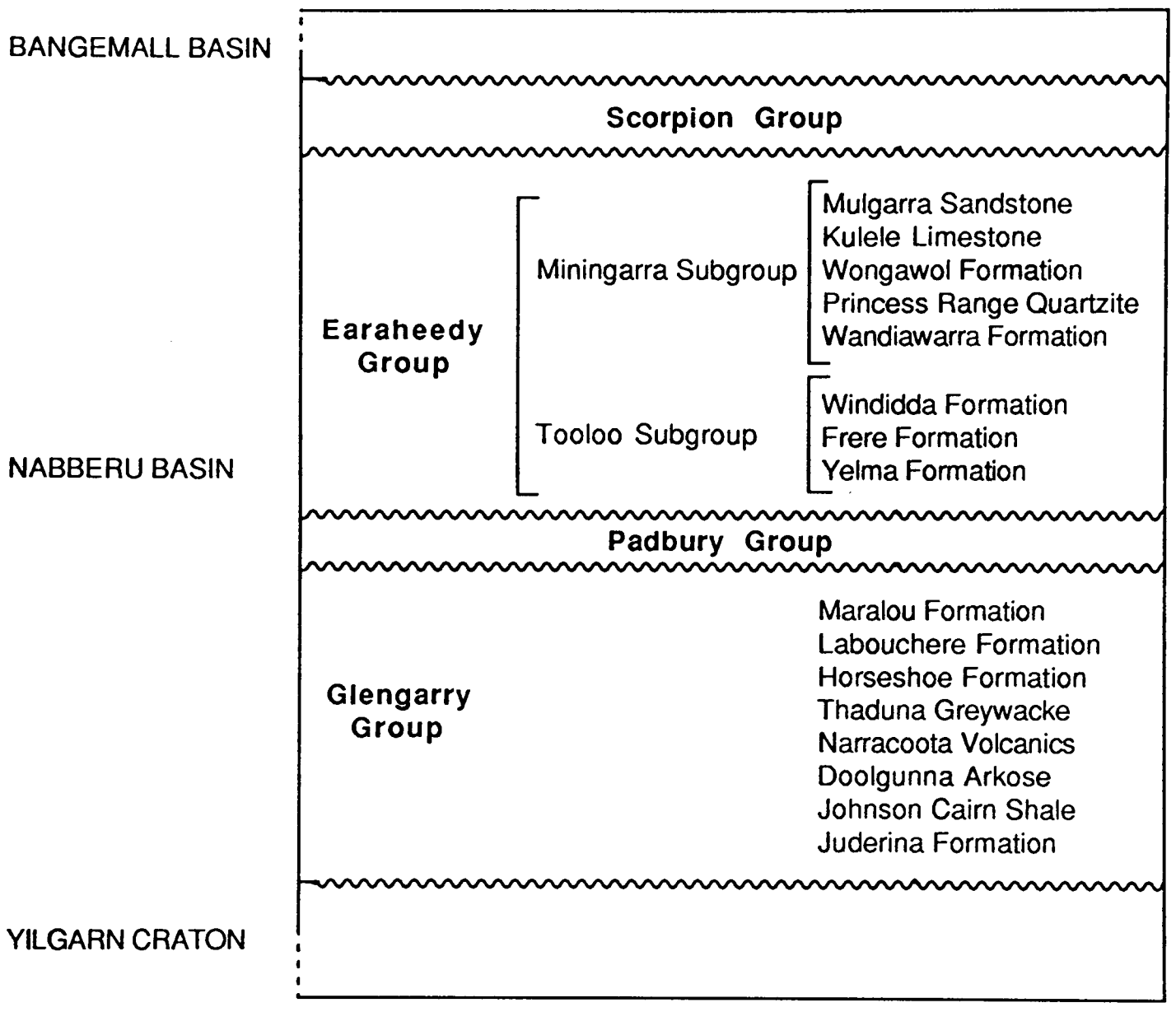

From tectonic considerations, Thorne (pers. comm. 1991) and a number of other workers consider that the Glengarry Group and possibly the Earaheedy Group may have been deposited around the same time as the Wyloo Group of the Ashburton Basin. Reliable radiometric dates are required for confirmation.

Stromatolitic carbonates were available from the Juderina Formation of the Glengarry Group (GSWA 88091) and the Yelma (GSWA 46589, 84767), Frere (GSWA 76392, 76389, 46326) and Windidda (GSWA 46598, 46140) Formations of the Earaheedy Group (see **Figure 2.3.2**).

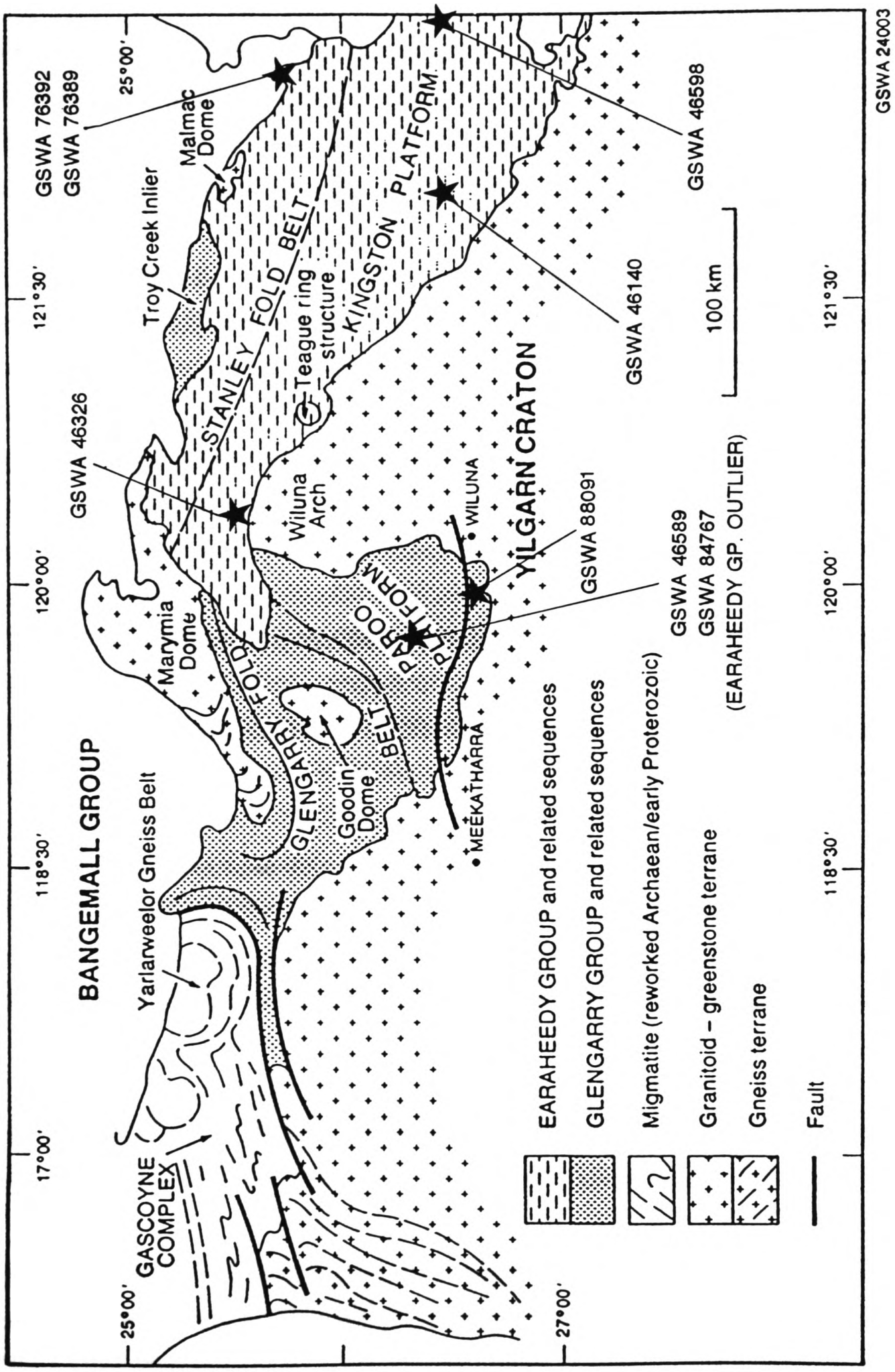

Figure 2.3.2: Localities for stromatolite samples from the Nabberu Basin, Western Australia

2.3.3: *AGE CONSTRAINTS*

The age of the Nabberu Basin is very poorly constrained (Bunting, 1986). The youngest granitoids of the Yilgarn Craton have been dated at 2461 ± 92 Ma (Williams et al., 1978) and 2573 ± 52 Ma (Stuckless et al., 1981) using the Rb-Sr method and thus the basin has a maximum age of c.2.5 Ga. A minimum limit for the basin is provided by the 1630 Ma Rb-Sr date for syenites from the Teague ring structure which intrudes the Earaheedy Group (Bunting et al., 1980). The unconformably overlying Bangemall Basin has an inferred age of between 1.6 and 1.1 Ga (Muhling & Brakel, 1985; Richards et al., in prep.). Additional published age data is summarised below;

- galenas from the Thaduna Greywacke, Glengarry Group, have given Pb model ages of 1.8 Ga (Richards, unpublished data);
- diagenetic galenas from the Yelma Formation have given Pb model ages of around 1.7 Ga (Richards & Gee, 1985);
- detrital glauconites from the Yelma Formation gave Rb-Sr dates of 1556-1674 Ma and K-Ar dates of 1670-1710 Ma (Preiss et al., 1975);
- glauconite from the Windidda Formation gave K-Ar dates of 1685 ± 35 Ma (Horwitz, 1975).

The potential ease with which K-Ar and Rb-Sr glauconite dates may be reset (Clauer, 1981) and the inaccuracies associated with galena Pb model ages mean that the age of the Nabberu Basin can only be confidently stated as Early Proterozoic, although Gee (1990) quantifies this as between 2.0 and 1.6 Ga, tending towards the latter.

2.3.4: *FORMATIONAL PETROGRAPHY, SEDIMENTOLOGY AND PALAEONTOLOGY*

Deposits of the Glengarry Group outcrop in the west of the Nabberu Basin and record a shallow marine transgression across the emergent Yilgarn Craton (Juderina Formation, Johnson Cairn Shale - c.500 m), followed by an oceanic rift facies (Doolgunna Arkose, Narracoota Volcanics, Thaduna Greywacke - up to 16 km) a basin-fill facies (Horseshoe Formation, Labouchere Formation - 3 km) and a final shale-carbonate shelf facies (Maralou Formation).

GSWA 88091, a non-determined stromatolite form with small branching columns of 2-3 cm relief, comes from the basal Juderina Formation, where a super-

mature, cross-bedded quartz sandstone is overlain by shallow water shales and fossiliferous chert/carbonate layers. Pseudomorphs of gypsum and anhydrite in the cherts indicate that locally sabkha-type conditions were developed. The stromatolites are often completely silicified and carbonate examples such as GSWA 88091 are rare. Although several stromatolites have been reported from the Glengarry Group, none have been formally described.

The Padbury Group (conglomerates, shales, banded iron formations and dolomites) unconformably succeeds Glengarry Group sediments in the west of the basin. Gee (1990) suggested that it was intermediate in age between the Glengarry Group in the west and the Earaheedy Group sediments which unconformably overlie them to the east, but this is somewhat interpretative since the Padbury Group only outcrops as synclinal keels within folded Glengarry Group sediments.

The Earaheedy Group is only exposed in the east of the basin and comprises 6 km of marine platform sediments (clastics, carbonates and cherty iron formations) in two major transgressive-regressive cycles. Throughout deposition of the group, the deepest portion of the basin lay to the north. The Yelma Formation comprises 1500 m of sandstone, siltstone and shale in the north, but in the south it is just 150 m thick with glauconitic sandstone passing into a shallow water shale deposit with a lagoonal to intertidal carbonate member containing the stromatolites *Yandilla meekatharrensis* Grey 1985 (GSWA 46589, collected from the type locality GLG 001) and *?Pilbaria deverella* Grey 1985 (GSWA 84767).

Yandilla meekatharrensis forms large (> 5 cm) upwardly-expanding (turbinate) columns with irregular margins, poorly developed walls and vermiform microstructure that are fan-shaped in cross section. It occurs in upward shallowing sequences in association with *Yelma digitata* and *Pilbaria deverella*, probably indicating deposition in a lagoonal environment (Grey, 1985). The stromatolite has also been found in the overlying Frere Formation. *Pilbaria deverella* has the columnar branching form containing large niches and pockets that is characteristic of all pilbariform stromatolites.

A transgressive pulse from the northeast saw facies belts retreat to the southwest during deposition of the Frere Formation and extensive marine shelf conditions were established over much of the eastern Nabberu Basin, leading to the formation of cherts, shales and iron formations with local stromatolitic carbonates being limited to the southern margin. The iron formations are granular, cherty and

locally oolitic and bear a striking resemblance to those around Lake Superior, Canada which have an inferred age of 2.0 Ga. The stromatolites *Yandilla meekatharrensis* (GSWA 76392, 76389) and *Yelma digitata* Grey 1984 (GSWA 46326) were analysed from this formation. Their association with *Pilbaria deverella* in upward-shallowing sequences is distinctly similar to those sequences containing pilbariform and asperiform stromatolites from the Wyloo Group, Ashburton Basin and this has led a number of workers to suggest that deposition of the two groups may have been approximately synchronous at around 1.89 Ga (Thorne, pers. comm. 1991; Grey, pers. comm. 1992).

Yelma digitata is an asperiform stromatolite, that is it exhibits a microdigitate morphology with a banded microstructure. Indeed, Grey (pers. comm. 1992) suggests that upon taxonomic review, *Yelma digitata* may shortly be re-assigned to *Asperia*. It occurs as stratiform columnar and branching columnar stromatolites with small columns that subdivide into multifurcate branches (2-5 mm across) towards their summit. Laminae tend to be continuous, of relatively constant thickness and occur at the same level in adjacent columns. Grey & Thorne (1985) suggested that the laminated fabrics in asperiform stromatolites may be indicative of periodic precipitation under alternating submergent and emergent conditions, possibly due to seasonal control.

A moderately varied microfossil assemblage has been documented from the Frere Formation. Schopf (1983) listed occurrences of coccoid forms (*Huroniospora* spp.), septate filamentous forms (*Gunflintia minuta* Barghoorn), tubular unbranched forms (*Animikiea* sp.) and more bizarre forms (cf. *Archaeorestis schreiberensis* Barghoorn, *Eoastrion bifurcatum* Barghoorn, *Eoastrion simplex* Barghoorn, ?*Eomichrystridium barghoornii* Deflandre, *Kakabekia umbellata* Barghoorn), described in more detail by Walter (1972) and Walter et al. (1976).

There is a distinct floral similarity with rocks of the Gunflint Chert where *Animikiea* sp., *Archaeorestis schreiberensis* Barghoorn, *Eoastrion bifurcatum* Barghoorn, *Eoastrion simplex* Barghoorn, *Eomichrystridium barghoornii* Deflandre, *Gunflintia minuta* Barghoorn, *Huroniospora* spp. and *Kakabekia umbellata* Barghoorn are all found. No Frere flora have as yet been found in Precambrian rocks from either Europe or Africa, but in North America; the Tyler Formation (1.6-2.5 Ga - Schopf, 1983) contains *Animikiea* sp., *Eoastrion* sp., *Gunflintia* sp., *Huroniospora* sp. and *Kakabekia* sp.; the Sokonoma Formation (1.8-2.5 Ga - Schopf, 1983) contains *Animikiea* sp., *Eoastrion* sp., *Gunflintia* sp. and *Huroniospora* sp.

and the Kasegalik Formation (1.76 ± 0.037-2.5 Ga - Schopf, 1983) contains *Huroniospora* sp.. Of the younger, microfossiliferous Australian formations; the Duck Creek Dolomite contains *Eoastrion* sp., *Gunflintia* sp., *Huroniospora* sp. and *Kakabekia* sp.; the Amelia Dolomite (1.65-1.67 Ga - Plumb et al., 1981; Schopf, 1983) *Gunflintia* sp. and *Huroniospora* sp.; the H.Y.C. Pyritic Shale (1.65-1.67 Ga - Plumb et al., 1981; Schopf, 1983) *Animikiea* sp., *Eoastrion* sp., *Gunflintia* sp. and *Huroniospora* sp.; the Cooley Dolomite (around 1.6 Ga - Schopf, 1983) *Eoastrion* sp. and *Huroniospora* sp.; the Balbirini Dolomite (around 1.6 Ga - Schopf, 1983) *Gunflintia* sp., *Huroniospora* sp. and the Paradise Creek Formation (around 1.6 Ga - Schopf, 1983) *Eoastrion* sp., *Gunflintia* sp. and *Huroniospora* sp..

These observations reinforce earlier statements that the small number of microfossiliferous Proterozoic localities coupled with the fact that few publications give positive specific identifications (including systematic description) limits the usefulness of micropalaeontology for biostratigraphic correlation at the present time. The genera *Eoastrion*, *Gunflintia*, and *Huroniospora* appear to have been long-lived (?>2.2 to <1.6 Ga), widespread and possibly environmentally influenced. *Archaeorestis schreiberensis* Barghoorn and *Eomichrystridium barghoornii* Deflandre, on the other hand, are only found in the Frere Formation and the Gunflint Chert. It could be that they represent potential zone microfossils and indicate correlation of the two formations or the two localities may merely be a sample of a much wider distribution. The question will only be resolved by continued palaeontologic and radiometric studies.

Marine regression extended the shallow water facies belts to the north once more during the deposition of the Windidda Formation and lagoonal stromatolitic carbonates became abundant in the south while mudstones were deposited in the basin centre. *Windidda granulosa* (GSWA 46598) and *Carnegia wongawolensis* Grey 1984 (GSWA 46140) are representative of the stromatolites found.

Windidda granulosa is a moderately large stromatolite with a granular microstructure that exhibits wide, divergent, multifurcate branching near the base that develops into smooth straight columns (up to 20 cm in diameter) with multilaminate wall structures (Grey, 1984). Thin dark laminae occur only near the column margins. *Carnegia wongawolensis* is a considerably smaller form that comprises closely spaced, sinuous divergent branches up to 2 cm in diameter that regularly coalesce, forming larger structures. Laminae are convex, irregular and have wavy, lenticular profiles.

The following limited flora have been described from the Windidda Formation by Schopf (1983); unstudied coccoid microfossils, septate filamentous forms (*Archaeotrichion* sp.) and tubular unbranched forms (*Eomycetopsis* sp.). Other than in the Windidda Formation, *Eomycetopsis* is known from the Amelia Dolomite, H.Y.C. Pyritic Shale, Balbirini Dolomite and Bungle Bungle Dolomite and *Archaeotrichion* from the Bungle Bungle Dolomite but neither are reported from the extensively studied Gunflint Chert, the Duck Creek Dolomite or the Frere Formation (which immediately underlies the Windidda Formation), suggesting that it is biostratigraphically distinct from them. These three formations have at least four genera in common (*Eoastrion* sp., *Gunflintia* sp., *Huroniospora* sp. and *Kakabekia* sp.) and are inferred to be approximately stratigraphically equivalent.

A second rapid transgression reworked carbonate shoals to form conglomerates which were deposited as a part of the Wandiawarra Formation along with glauconitic sandstones and extensive, laminated micaceous shales. The ensuing slow regression produced the quartzose Princess Range Quartzite, the Wongawol Formation, the stromatolitic Kulele Limestone and the Mulgarra Sandstone. The Kulele Limestone contains smaller scale cycles indicating that short-term emergence/slow submergence was superimposed on the larger scale regression.

The Glengarry Group and the Earaheedy Group have separate structural styles related to relative movements of the Pilbara and Yilgarn Cratons. The pre-Earaheedy Group Glengarry Fold Belt (see **Figure 2.3.2**) is a complex structural unit resulting from a combination of east-west crustal fracture, dextral compressional shear and basement domal uplift. Multi-generation folds, faults and metamorphism are characteristic. The Stanley Fold Belt, which affects deposits of the eastern Earaheedy Group is much simpler and forms an asymmetrical synclinorium upon which minor fold structures are superimposed. The Teague ring structure has no obvious structural relationship to either belt and post-dates both phases of deformation.

2.3.5: *RESULTS*

Eight analyses of GSWA 88091 from the Juderina Formation (**Table 2b**) exhibit notably less radiogenic Pb isotopic compositions than either of the stromatolites from the Ashburton Basin (maximum $^{206}Pb/^{204}Pb$ of 19.299) and have a limited isotopic range ($^{206}Pb/^{204}Pb$ from 18.127 to 19.299), implying a more restricted variation in μ_2 values at the time of isotopic closure. The entire sample set defines a poor errorchron whose slope corresponds to a date of 2313 ± 460 Ma (MSWD 4.30, model μ_1 value 8.39 ± 0.07), but by omitting two analyses (88091i and 88091v) the MSWD reduces to just 0.47 and the resultant isochron defines a more precise date of 2258 ± 180 Ma (model μ_1 value 8.38 ± 0.03) (**Figure 2.3.3**). Since omission of these two points does not significantly alter the model μ_1 value and both dates are within error, the more precise value is adopted.

Table 2b: Pb isotopic compositions of carbonate stromatolites from the Juderina Formation, Glengarry Group, Nabberu Basin (GSWA 88091)

SAMPLE	CORRECTED RATIOS *		
	$^{206}Pb/^{204}Pb$	$^{207}Pb/^{204}Pb$	$^{208}Pb/^{204}Pb$
88091 i **	18.659 ± 0.018	15.843 ± 0.020	37.153 ± 0.048
88091 ii	18.692 ± 0.020	15.806 ± 0.020	37.019 ± 0.046
88091 iii	19.069 ± 0.020	15.873 ± 0.020	37.020 ± 0.046
88091 iv	19.202 ± 0.020	15.891 ± 0.020	37.087 ± 0.046
88091 v	18.844 ± 0.018	15.874 ± 0.020	37.056 ± 0.046
88091 vi	18.278 ± 0.018	15.756 ± 0.020	36.845 ± 0.046
88091 vii	18.127 ± 0.018	15.740 ± 0.020	36.775 ± 0.046
88091 viii	19.299 ± 0.020	15.902 ± 0.020	36.983 ± 0.046

* Corrected for mass fractionation of 0.130% ± 0.012 ($2\sigma_{mean}$) amu^{-1}
Errors are $2\sigma_{mean}$ for corrected ratios
** Pb concentration: 5.755 ± 0.025 ppm

In thin section, GSWA 88091 comprises buff carbonate with a well defined millimetre-scale irregular lamination, which varies in thickness laterally and is predominantly a function of carbonate grain size (the darker laminae comprising finer grained material). Small amounts of detrital, subrounded quartz and feldspar, often exhibiting strained extinction and subgrain formation, are found in the coarser laminae. The recrystallised carbonate crystals form mutual boundary angles of approximately 120°, implying that during recrystallisation there was no strongly oriented stress field. Although recrystallisation has destroyed any microstructural

detail, the gross morphological characteristics of the stromatolite remain intact. Incomplete secondary silicification is found to be concentrated around solution vugs in the coarser laminae and occasionally extends parallel to the lamination. Late, cross-cutting haematitic stylolites occur approximately perpendicular to the lamination.

Figure 2.3.3: Pb isotopic data for GSWA 88091, Juderina Formation, Glengarry Group, Nabberu Basin

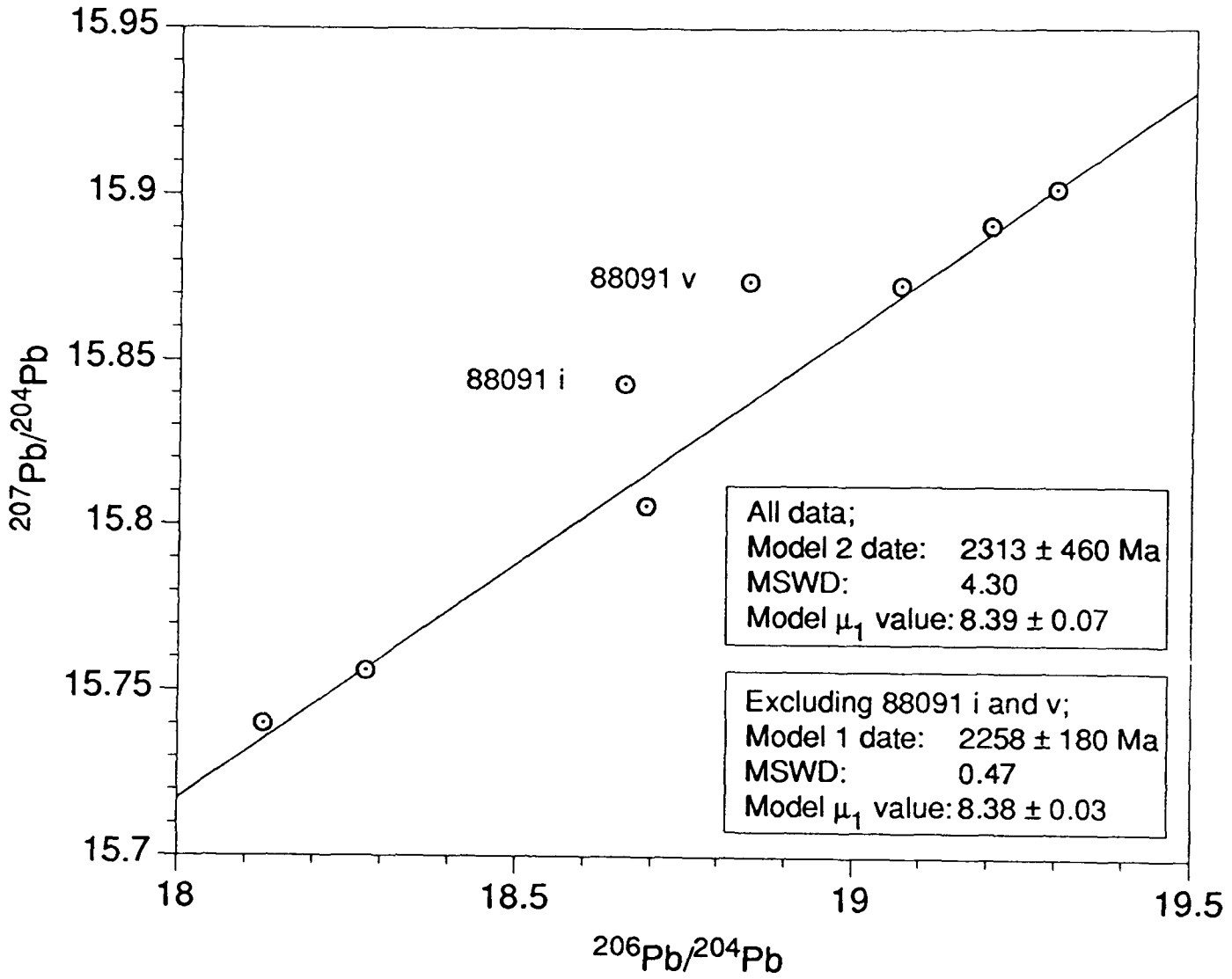

Stable isotopic analyses of GSWA 88091 have $\delta^{13}C$ values of 9.28, 9.36 and 9.00‰ and $\delta^{18}O$ values of -5.58, -5.39 and -4.93‰ respectively. Although the oxygen values are not unusual for open marine carbonate, the $\delta^{13}C$ values are atypically heavy and might indicate deposition in a restricted marine environment and/or the involvement of CO_2-reducing methanogenic bacteria during anoxic diagenesis, producing isotopically light methane and relatively heavy carbonate. Such heavy carbonate $\delta^{13}C$ values imply that the carbonate recrystallisation observed in thin section was diagenetically rather than metamorphically controlled.

Table 2c: Pb isotopic compositions of carbonate stromatolites from the Yelma Formation, Earaheedy Group, Nabberu Basin (GSWA 46589, 84767)

SAMPLE	CORRECTED RATIOS *		
	$^{206}Pb/^{204}Pb$	$^{207}Pb/^{204}Pb$	$^{208}Pb/^{204}Pb$
46589 I	34.119 ± 0.038	17.855 ± 0.024	38.783 ± 0.054
46589 II	31.488 ± 0.034	17.498 ± 0.022	38.026 ± 0.050
46589 III	36.466 ± 0.036	18.091 ± 0.022	38.048 ± 0.048
46589 IV	28.183 ± 0.042	17.123 ± 0.030	37.917 ± 0.080
46589 V	32.622 ± 0.034	17.618 ± 0.022	37.993 ± 0.048
46589 VI	36.502 ± 0.044	18.070 ± 0.030	38.260 ± 0.082
46589 VII	34.990 ± 0.034	17.946 ± 0.022	38.176 ± 0.048
46589 VIII	27.096 ± 0.028	16.976 ± 0.022	37.916 ± 0.048
46589 A	36.882 ± 0.046	18.234 ± 0.026	38.903 ± 0.068
46589 B	38.657 ± 0.044	18.474 ± 0.026	38.581 ± 0.060
46589 C	31.910 ± 0.038	17.554 ± 0.024	38.334 ± 0.050
46589 D	31.459 ± 0.032	17.479 ± 0.022	38.419 ± 0.048
46589 E	34.375 ± 0.034	17.841 ± 0.022	37.819 ± 0.046
46589 F	39.843 ± 0.042	18.532 ± 0.024	38.780 ± 0.050
46589 G	32.257 ± 0.032	17.588 ± 0.022	38.301 ± 0.048
46589 H**	44.147 ± 0.044	19.039 ± 0.022	38.933 ± 0.048
84767	169.299 ± 0.234	33.103 ± 0.048	37.852 ± 0.058
84767 I	224.423 ± 0.254	39.674 ± 0.052	37.223 ± 0.050
84767 II	166.243 ± 0.194	32.780 ± 0.044	37.418 ± 0.050
84767 III	199.550 ± 0.226	36.865 ± 0.048	36.950 ± 0.048
84767 IV	177.402 ± 0.190	34.121 ± 0.044	37.684 ± 0.048
84767 V	190.192 ± 0.202	35.523 ± 0.044	37.632 ± 0.048

* Corrected for mass fractionation of 0.130% ± 0.012 ($2\sigma_{mean}$) amu^{-1}
Errors are $2\sigma_{mean}$ for corrected ratios
** Pb concentration: 2.023 ± 0.006 ppm

Results for GSWA 46589 and 84767 are presented in **Table 2c**, **Figure 2.3.4** and **Figure 2.3.5**. **Sixteen analyses of GSWA 46589, all from a single hand specimen, define a Pb/Pb errorchron with a large range in Pb isotopic compositions whose slope is proportional to a date of 2008 ± 68 Ma (MSWD 11.1, model μ_1 value 8.62 ± 0.15). It is not possible to extract substantially different subsets of data.**

Figure 2.3.4: Pb isotopic data for GSWA 46589, Yelma Formation, Earaheedy Group, Nabberu Basin

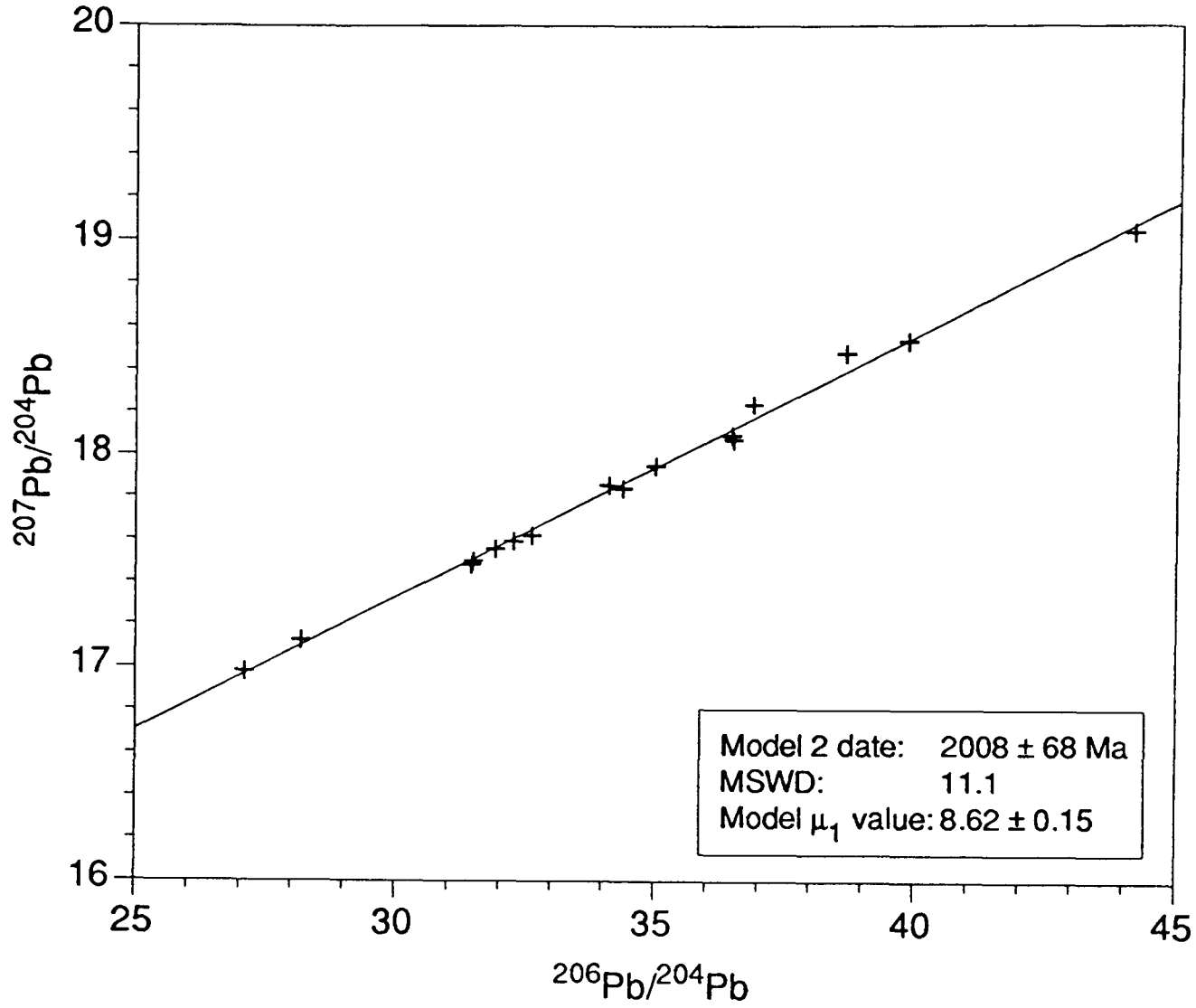

In thin section the stromatolite shows a weakly developed lamination on a scale of 3-5 mm that is locally obscured by carbonate recrystallisation. Carbonate grains tend to be equant and variably stained by secondary iron oxides, giving the overall hand specimen a buff coloration, but most of the original microstructural detail has been lost due to recrystallisation. Extremely rare, well rounded clastic quartz fragments are found within the carbonate.

Six analyses of GSWA 84767 (**Figure 2.3.5**) produced the most radiogenic Pb isotopic compositions observed in any of the stromatolites analysed and also the largest isotopic range. They define an errorchron corresponding to a date of 1946 ± 71 Ma with an MSWD of 40.9 and a particularly low model μ_1 value of 7.16 ± 1.59. Within error the date is concordant with that for the stratigraphically equivalent GSWA 46589.

Figure 2.3.5: Pb isotopic data for GSWA 84767, Yelma Formation, Earaheedy Group, Nabberu Basin

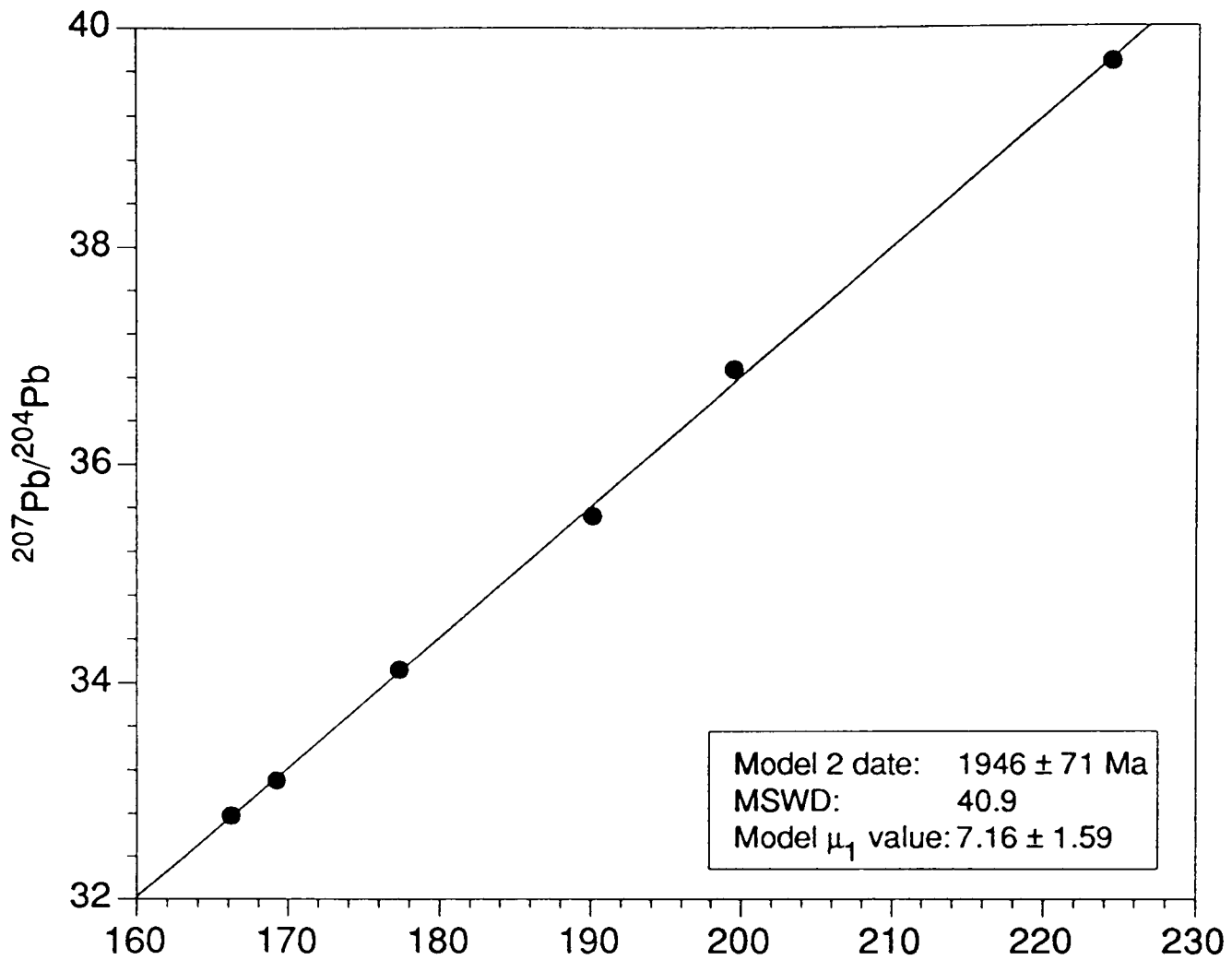

In thin section it is not possible to distinguish any lamination and the carbonate grains are mostly elongate and irregular in shape, with a maximum length of 1.5 mm. Irregular grain boundaries and the lack of lamination are taken as evidence of strong recrystallisation. Minimal secondary staining by iron oxides is also noted.

It is evident that both GSWA 46589 and 84767 exhibited considerable variation in U/Pb ratios at their respective points of isotopic closure. The *in situ* μ_2 values varied from 32.96-79.62 for GSWA 46589 and 431.54-596.65 for GSWA 84767. When attempting to model U and Pb fixation in carbonate stromatolites (**Chapter 6**), the reason for large variations in μ_2 values (and consequent Pb isotopic compositions), both between samples and within individual stromatolites, needs to be explained.

Stable isotopic data for the Yelma Formation stromatolites are given in **Figure 2.3.6**. Two separate clusters of points are identified, suggesting that the stromatolites had slightly differing diagenetic histories. However, each cluster has low positive $\delta^{13}C$ and negative $\delta^{18}O$ values, consistent with a lagoonal to supratidal marine origin and subsequent marine diagenetic recrystallisation.

Figure 2.3.6: Stable isotopic data for GSWA 46589 and 84767, Yelma Formation, Earaheedy Group, Nabberu Basin

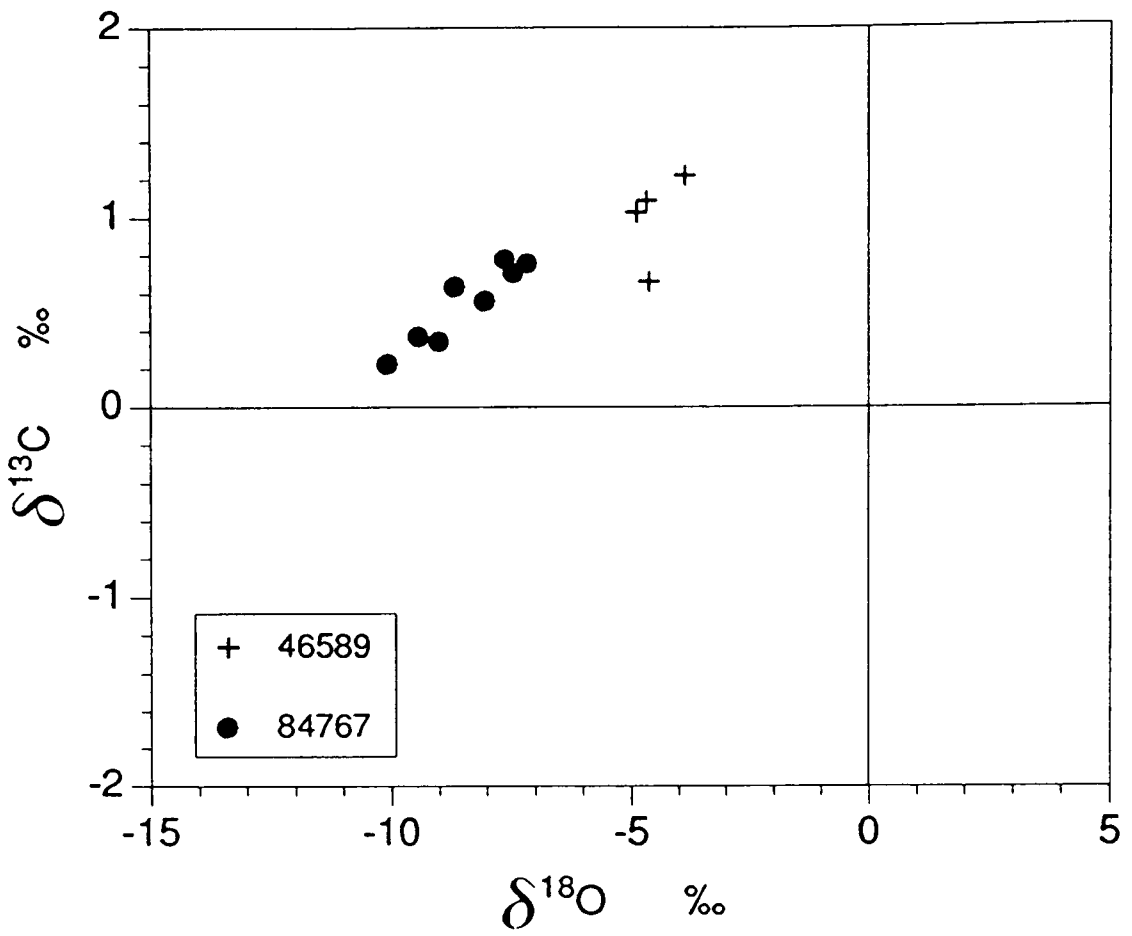

If one attempts to combine the two sets of Pb isotope data, the resultant 'errorchron' regression yields a date of 1865 ± 9 Ma (MSWD 44.9, model μ_1 value 8.90 ± 0.09). This value, however, has no true age significance and serves to highlight the potentially dangerous conclusions that may be drawn if strictly independent sets of data are erroneously combined. Since the two data sets have distinct isotopic ranges, their combination effectively produces a two point errorchron but the significant difference in model μ_1 values (8.62 ± 0.15 and 7.16 ± 1.59) means that the gradient of this line does not reflect the true isotopic age. The combination technique should only be considered where individual sample sets have very similar model μ_1 values and the combined date is concordant with individual regressions. If it is to be used where the volume of data is particularly limited, one has to be realistic in drawing conclusions.

Pb isotopic data for stromatolites from the Frere Formation are tabulated in **Table 2d** and presented graphically in **Figure 2.3.7**. Considering the comparative success of dating stromatolites from other Proterozoic formations in Western Australia by the Pb/Pb method, the results are disappointing. Analyses have less radiogenic Pb isotopic compositions than previously encountered, a much smaller isotopic range ($^{206}Pb/^{204}Pb$ from 16.2-18.2), variable precision and exhibit scatter. Consequently, it is not possible to fit a line to the data either by considering individual

data sets or by combination.

GSWA 76392 and GSWA 76389 are classified as *Yandilla meekatharrensis* but they do not exhibit the same isotopic characteristics as GSWA 46589 from the Yelma Formation. One must assume either that the closed system conditions have been upset by diagenetic recrystallisation, that suitable conditions for U and Pb fixation were not originally established or that initial Pb showed significant variation in isotopic composition.

Table 2d: Pb isotopic compositions of carbonate stromatolites from the Frere Formation, Earaheedy Group, Nabberu Basin (GSWA 76392, 76389 & 46326)

SAMPLE	CORRECTED RATIOS *		
	$^{206}Pb/^{204}Pb$	$^{207}Pb/^{204}Pb$	$^{208}Pb/^{204}Pb$
76392	17.693 ± 0.038	15.599 ± 0.044	41.521 ± 0.120
76392 a	17.654 ± 0.046	15.720 ± 0.048	40.564 ± 0.142
76392 d	17.704 ± 0.086	15.661 ± 0.074	40.591 ± 0.232
76392 e	17.671 ± 0.070	15.624 ± 0.076	40.446 ± 0.236
76392 f	18.025 ± 0.020	15.653 ± 0.020	42.009 ± 0.054
76392 g	17.783 ± 0.076	15.781 ± 0.076	41.433 ± 0.314
76389	17.681 ± 0.110	15.715 ± 0.106	41.589 ± 0.232
76389 a	16.195 ± 0.016	15.459 ± 0.018	35.933 ± 0.044
76389 b	17.788 ± 0.018	15.618 ± 0.020	41.356 ± 0.054
76389 d	17.647 ± 0.022	15.627 ± 0.022	41.059 ± 0.056
76389 e	18.167 ± 0.018	15.637 ± 0.020	42.344 ± 0.052
76389 h	17.571 ± 0.038	15.624 ± 0.052	40.492 ± 0.130
46326 A	17.712 ± 0.020	15.892 ± 0.024	38.569 ± 0.074

* Corrected for mass fractionation of 0.130% ± 0.012 ($2\sigma_{mean}$) amu^{-1}
Errors are $2\sigma_{mean}$ for corrected ratios

In thin section GSWA 76389 is clearly laminated, the discontinuous, irregular laminae corresponding to variations in carbonate grain size. Gross sedimentary fabric is well preserved, even though the carbonate has undergone recrystallisation. Rare, disseminated quartz clasts occur and late haematitic staining is noted, particularly associated with the coarser grained carbonate.

Figure 2.3.7: Pb isotopic data for carbonate stromatolites from the Frere Formation, Earaheedy Group, Nabberu Basin

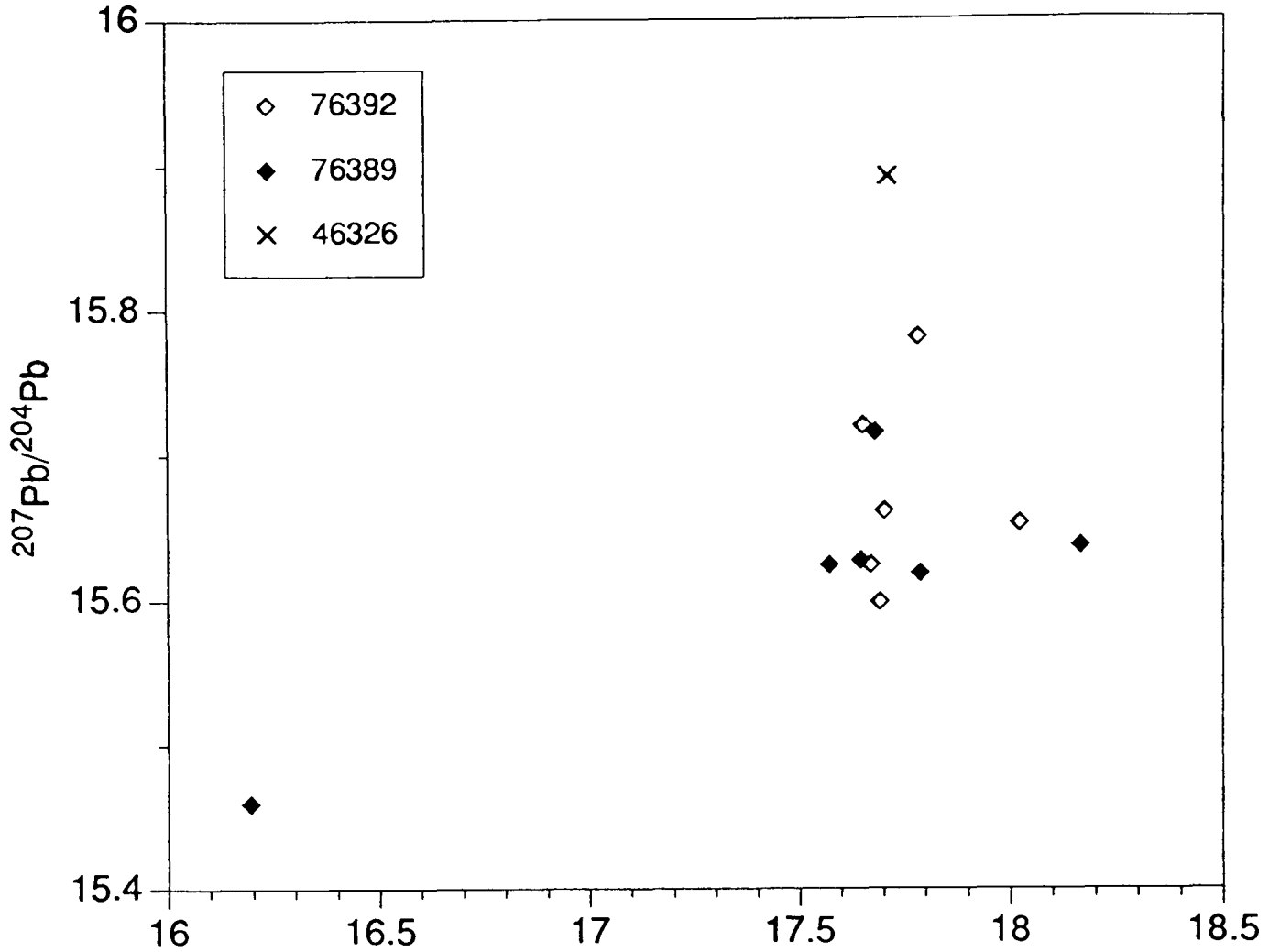

GSWA 76392 has a more poorly preserved 3 mm lamination that also shows evidence of recrystallisation. Isolated sub-angular to sub-rounded quartz fragments are associated with the carbonate. The coarser carbonate grains have bedding-parallel, non-determined organic remains that occur along stylolitic stringers from which coarse, bladed carbonate crystals radiate.

Stable isotopic data for the Frere Formation are both limited and unequivocal. $\delta^{13}C$ analyses of 76392 and 76389 gave values of -0.30 and -0.35‰, while respective $\delta^{18}O$ values were -10.10 and -9.56‰. Oxygen values are lighter than those for the specimen of *Yandilla meekatharrensis* from the Yelma Formation which average around -5‰ (GSWA 46589, **Figure 2.3.6**) and this may indicate that meteoric ground-waters have been involved in carbonate diagenesis. Pb and more importantly U are highly soluble in such waters under oxidising conditions (note that haematite is observed in thin section) and early U loss may be the reason for the modern unradiogenic Pb isotopic compositions and limited isotopic range. Slight metamorphism could also produce similar oxygen isotopic signatures.

The limited Pb isotopic data for Windidda Formation stromatolites are pre-

sented in **Table 2e**. Preliminary results were unradiogenic and exhibited little isotopic variation and consequently investigation of the Windidda Formation was terminated.

Table 2e: Pb isotopic compositions of carbonate stromatolites from the Windidda Formation, Earaheedy Group, Nabberu Basin (GSWA 46598, 46140)

SAMPLE	CORRECTED RATIOS *		
	$^{206}Pb/^{204}Pb$	$^{207}Pb/^{204}Pb$	$^{208}Pb/^{204}Pb$
46598	17.959 ± 0.044	15.665 ± 0.076	37.512 ± 0.230
46598 a	17.944 ± 0.036	15.738 ± 0.038	37.688 ± 0.140
46598 b	18.003 ± 0.022	15.705 ± 0.024	37.714 ± 0.074
46140 ii	16.760 ± 0.80	15.534 ± 0.072	36.716 ± 0.244

* Corrected for mass fractionation of 0.130% ± 0.012 ($2\sigma_{mean}$) amu^{-1}
Errors are $2\sigma_{mean}$ for corrected ratios

2.3.6: *DISCUSSION*

Taking into account the heavy carbon isotopic composition of GSWA 88091, the 2258 ± 180 Ma date (model μ_1 value 8.38 ± 0.03) for the Juderina Formation of the Glengarry Group is interpreted as the age of early anoxic diagenetic recrystallisation. This figure approximates to the age of deposition within the limits of the quoted 2σ errors. Such an interpretation does not contradict any of the reliable, independent age constraints since it falls between the c.2.5 Ga ages for the youngest Yilgarn granitoids (Williams et al., 1978; Stuckless et al., 1981) and the 1630 Ma date for the crypto-explosive emplacement of quartz syenite in the Teague Ring Structure (Bunting et al., 1980). The value is, however, somewhat older than the inferred age of 2.0-1.6 Ga for the Glengarry Group currently used by the GSWA. Consequently, the correlation of Glengarry Group sediments with the Ashburton Basin by Bunting (1986) should be considered no longer valid.

Concordant dates for carbonate stromatolites from the Yelma Formation of the overlying Earaheedy Group (GSWA 46589 - 2008 ± 68 Ma, model μ_1 value 8.62 ± 0.15; GSWA 84767 - 1946 ± 71 Ma, model μ_1 value 7.16 ± 1.59) imply that an age of c.2.0 Ga is geologically significant and this too is consistent with available age constraints for the Earaheedy Group (2.5-1.63 Ga). No evidence of metamorphism is documented for these particular samples and in light of the stable isotopic data

(see **Figure 2.3.6**), the date is interpreted as the age of early diagenetic carbonate recrystallisation, approximating to the depositional age of the sediments.

Although the GSWA currently assume the depositional age of the Earaheedy Group to be 1.8-1.6 Ga (Grey, pers. comm. 1991), there is now supporting evidence for an older, 2.0 Ga age;

- Pb isotopic data collected in this work suggest that the underlying Glengarry Group has a depositional age of c.2.3 Ga, not 2.0-1.8 Ga as previously thought,
- granular, cherty, oolitic iron formations in the Frere Formation bear a striking resemblance to iron formations around Lake Superior in Canada which have an inferred age of 2.0 Ga,
- no similar stromatolite taxa are known from rocks aged between 1.6-1.8 Ga elsewhere in the world but similar forms are documented within the Gunflint Chert of Canada which also has an inferred age of 2.0 Ga,
- the microfossil assemblage from the overlying Frere Formation (but not the Windidda Formation) has distinct similarities with that of the florally rich Gunflint Chert and this would allow taxonomic consideration in an evolutionary rather than environmental framework.

Stromatolites from the Frere and Windidda Formations exhibited either too much data scatter or insufficient isotopic variation to yield useful age information. This may be attributed to the fact that suitable conditions for U and Pb fixation may never have been established, initial Pb may have had a heterogeneous isotopic composition or closed system conditions may have been disturbed by diagenetic recrystallisation/burial metamorphism with resultant U mobilisation under oxidising conditions.

Pb/Pb dates for stromatolites from the Juderina and Yelma Formations are chronometrically consistent and indicate that deposition of the Glengarry Group occurred between c.2.4-2.0 Ga and deposition of the Earaheedy Group between 2.0-1.63 Ga. From this evidence it is probable that the Yelma and Frere Formations of the Earaheedy Group in the Nabberu Basin correlate with parts of the Wyloo Group in the Ashburton Basin (see section **2.2**) and the Gunflint Chert of Canada. Similarities in stromatolite forms in upward-shallowing cycles exposed in the Earaheedy and Wyloo Groups may therefore be attributed to evolutionary mechanisms rather than environmental convergence. In possessing a distinct microfossil assemblage to the Yelma Formation, the Windidda Formation (and overlying Miningarra Subgroup and Scorpion Group) are inferred to be significantly younger than 2.0 Ga.

2.4: KIMBERLEY BASIN

2.4.1: *INTRODUCTION*

The Kimberley Basin outcrops over an area of 160 000 km^2 on the northern coast of Western Australia (see **Figure 2.1.1**) and its southern margins are located within the King Leopold and Halls Creek orogenic belts (**Figure 2.4.2**). The basinal succession is predominantly sedimentary, although a very thick dolerite sill intrudes the lowermost groups.

2.4.2: *STRATIGRAPHY*

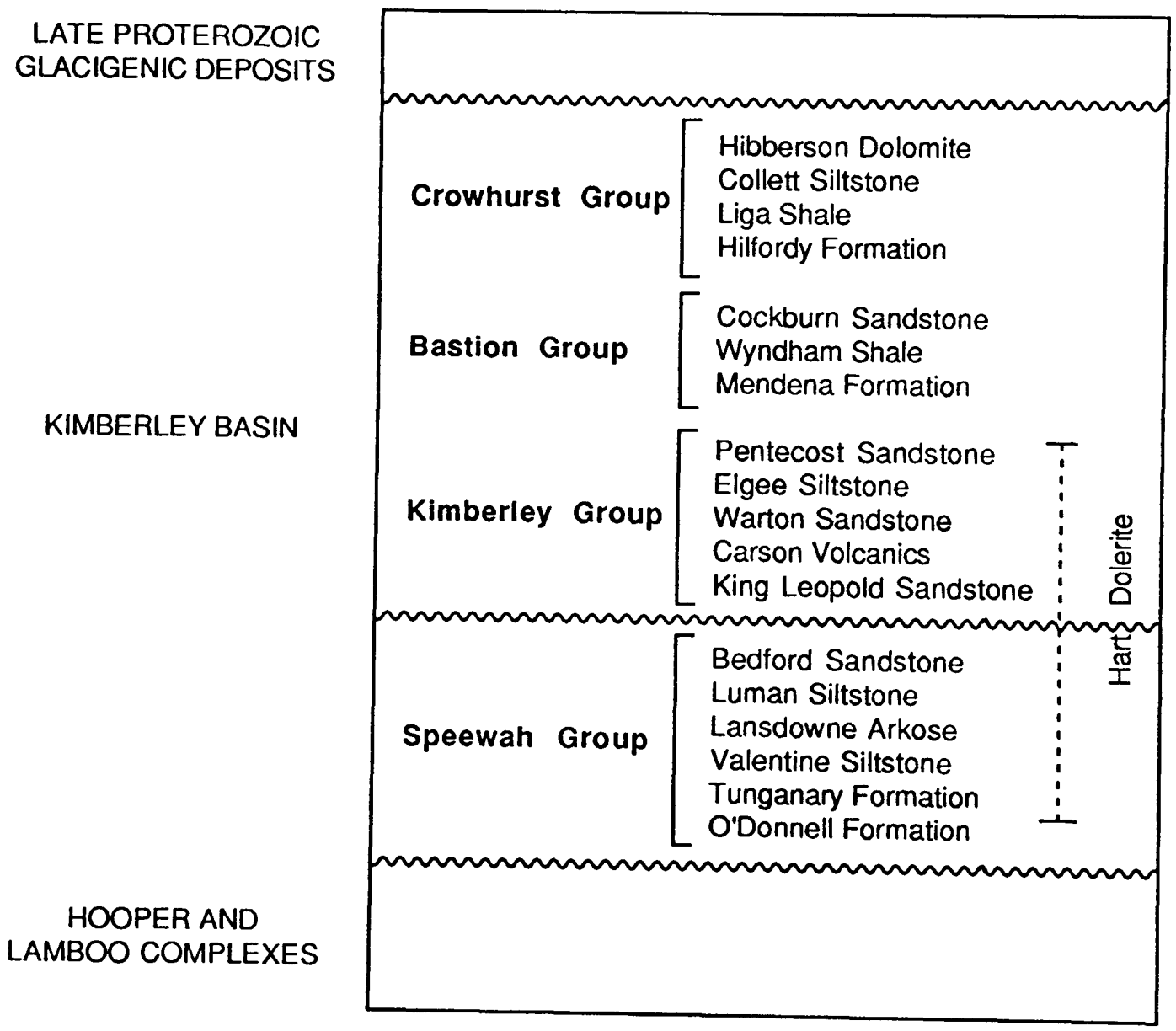

Figure 2.4.1: Stratigraphy of the Kimberley Basin, after Griffin & Grey (1990) with amendments from Griffin et al. (in press)

The sediments of the Kimberley Basin unconformably overlie the late Early Proterozoic rocks of the Hooper and Lamboo Complexes (Gellatly et al., 1975; Griffin

& Myers, 1988a,b) in the south and are themselves unconformably overlain by the inferred Middle Proterozoic Colombo Sandstone and Late Proterozoic glacigene sequences.

The basin comprises four lithostratigraphic units; the basal Speewah Group, the unconformably overlying Kimberley Group, the Bastion Group and the local Crowhurst Group. A brief description of the constituent formations may be found in Griffin & Grey (1990). The extensive Hart Dolerite sill intrudes both the Speewah and Kimberley Group (**Figure 2.4.1**). The basin is geographically separated from other Early Proterozoic deposits in Western Australia by the predominantly Mesozoic Canning Basin and consequently attempts at inter-basinal correlation have not been made.

Stromatolitic carbonates were analysed from the Teronis Member of the Elgee Siltstone, Kimberley Group (GSWA 46285) and the Hibberson Dolomite of the Crowhurst Group (GSWA 99429). Their localities are illustrated in **Figure 2.4.2** overleaf.

2.4.3: *AGE CONSTRAINTS*

The age of the lowermost groups of the Kimberley Basin is well constrained when compared to other Proterozoic deposits in the region. The Lennard Granite at the summit of the Hooper Complex has been dated by the Rb-Sr method at 1840 ± 50 Ma (Bofinger, 1967; Page, 1976) and this provides a maximum age for the basin. The Hart Dolerite intrudes most formations up to and including the Pentecost Sandstone (the topmost formation of the Kimberley Group) and has been dated at 1762 ± 15 Ma by Bofinger (1967) using the Rb-Sr method, as reported in Page et al. (1984), and at c.1.8 Ga by recent, unpublished U-Pb work on zircons extracted from granophyric portions (Page, unpublished data). Thus the Speewah and Kimberley Groups were deposited between 1.89 and 1.75 Ga.

The age of the Bastion and Crowhurst Groups is more poorly constrained but must be younger than the 1.8 Ga ages for the Hart Dolerite and older than both the unconformably overlying Colombo Sandstone which is believed to correlate with the Middle Proterozoic Mount Parker Sandstone of the Birrindudu Basin (Plumb et al., 1981) and Late Proterozoic glacigene sequences which have equivalents in eastern Australia dated at 750 Ma and 670 Ma (Coats & Preiss, 1980).

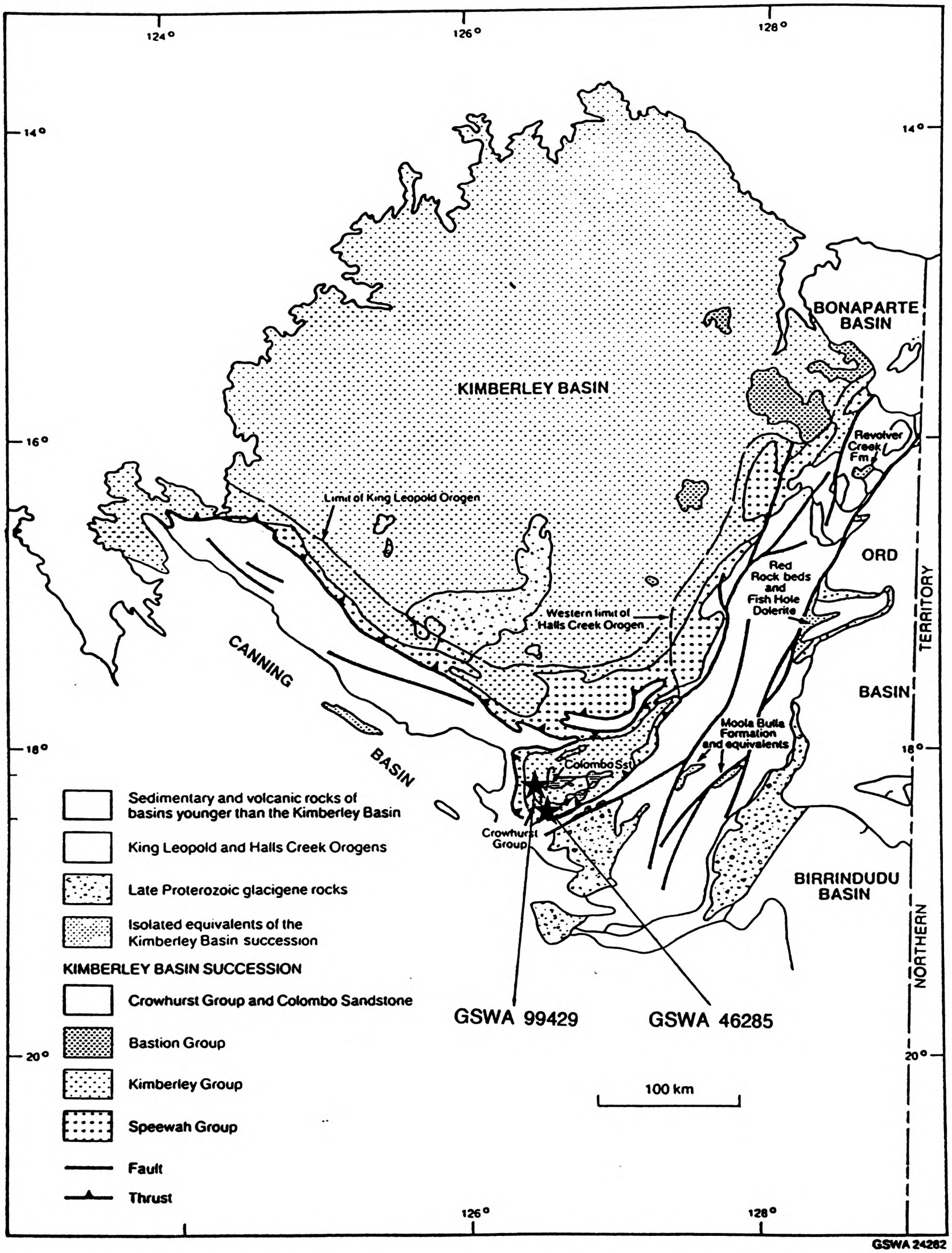

Figure 2.4.2: Localities for stromatolite samples from the Kimberley Basin, Western Australia

2.4.4: *FORMATIONAL PETROGRAPHY AND SEDIMENTOLOGY*

The sediments of the Speewah Group are approximately 1 km thick and record a broad transgressive-regressive cycle. Fluvial sandstones of the lower O'Donnell Formation grade into interfingering shallow marine and fluvial deposits of the upper O'Donnell Formation, the shallow marine Tunganary Formation (which exhibits ripple marks and cross bedding) and ultimately the deeper water deposits of the Valentine Siltstone. Regressive, shallower water conditions are indicated by the cross bedded and ripple marked Lansdowne Arkose and Luman Siltstone before a return to fluvial conditions in the Bedford Sandstone (Plumb et al., 1985).

The Kimberley Group (up to 4 km) unconformably overlies the Speewah Group and commences with a basal conglomerate that is succeeded by the mature, shallow water, cross bedded sandstone and siltstone deposits of the King Leopold Sandstone. Tholeiitic volcanics are interbedded with slightly deeper water sediments in the overlying Carson Volcanics before a return to shallower conditions is demonstrated in both the Warton Sandstone and the intertidal, stromatolitic dolomites of the basal Elgee Siltstone. The massive siltstones of the middle and upper Elgee Siltstone and the glauconitic, cross bedded Pentecost Sandstone reflect slightly deeper marine conditions. The stromatolite *?Kussoidella* form indet. Semikhatov 1978 (GSWA 46285) is typical of the Teronis Member at the base of the Elgee Siltstone. In general deposition occurred in a broad, semi-enclosed shallow marine basin with sediment supply principally from the west (Griffin & Grey, 1990).

The c.1.8 Ga Hart Dolerite is a massive composite sill of tholeiitic dolerite with less extensive granophyric units that intrude formations of the Kimberley Basin as stratigraphically high as the Pentecost Sandstone (Gellatly et al., 1975).

The Bastion Group (1.4 km) conformably overlies the Kimberley Group (Dow et al., 1964) and consists of purple and green shales with minor sandstone and dolomite, overlain by a massive quartz sandstone (Cockburn Sandstone). Ripple marks indicate shallow water marine conditions throughout with fluctuations in supply of terrigenous detritus and minor variations in sea level causing lithological changes. The localised Crowhurst Group (150 m) is considered by Plumb et al. (1981) to be equivalent to the Bastion Group and conformably overlies the Kimberley Group. A regressive marine sequence of glauconitic sandstones and siltstones (Hilfordy Formation, Liga Shale, lower Collett Siltstone) grade upwards into increasingly dolomitic sediments (upper Collett Siltstone) and ultimately the stroma-

tolitic, oolitic Hibberson Dolomite which was deposited under intertidal conditions. GSWA 99429, a non-identified stromatolitic form comes from this formation.

Two post-Kimberley Group periods of deformation produced basin and dome interference structures and faulting around the Kimberley plateau. Deformation of the overlying Late Proterozoic glacigene sequences has been caused principally by reactivation of these structures (Gellatly et al., 1975).

2.4.5: *RESULTS*

Pb isotopic results for GSWA 46285 from the Teronis Member of the Elgee Siltstone, Earaheedy Group are given in **Table 2f** and illustrated in **Figure 2.4.3**. For two of the carbonate stromatolite samples, the HCl-insoluble residues were retained after carbonate dissolution and independently analysed after attack by HF.

Results define a poor errorchron whose slope corresponds to a date of 2133 ± 440 Ma (MSWD 6.63, model μ_1 value 7.94 ± 0.34) (**Figure 2.4.3**), just within error of the inferred depositional age of c.1.8 Ga although the limited isotopic range and scatter mean that the date is too poorly constrained to be of stratigraphic use. However, it is interesting to note that the residue analyses show non-systematic behaviour with respect to their corresponding carbonate analyses. Their combination with the carbonate data set considerably enhances the Pb isotopic range. If residues (principally silicates and organics) and carbonate were in equilibrium at isotopic closure, by independently analysing their Pb isotopic compositions and subsequently combining the results, it might be possible to obtain increased precision on any dates obtained.

In thin section GSWA 46285 comprises small, laminated stromatolitic domes, 1 cm high, that are associated with clastic rich, laminated sediments. The inter-domal areas consist of carbonate-cemented quartz grainstone to quartz packestone, with rare altered mica flakes. The stromatolites pass upwards into clastic rich laminated carbonate sediments with disseminated iron oxide. Late cross-cutting carbonate veins also occur.

Table 2f: Pb isotopic compositions of carbonate stromatolites from the Kimberley Basin (GSWA 99429, 46285)

SAMPLE	CORRECTED RATIOS *		
	$^{206}Pb/^{204}Pb$	$^{207}Pb/^{204}Pb$	$^{208}Pb/^{204}Pb$
	Crowhurst Group, Hibberson Dolomite		
99429 r	20.183 ± 0.020	15.845 ± 0.020	38.675 ± 0.046
99429 ra	19.082 ± 0.018	15.726 ± 0.020	37.995 ± 0.046
99429 rb	20.231 ± 0.020	15.850 ± 0.018	39.219 ± 0.046
99429 rbR	22.348 ± 0.028	16.084 ± 0.024	40.328 ± 0.064
99429 rc	20.760 ± 0.020	15.896 ± 0.020	38.220 ± 0.046
99429 rd	20.383 ± 0.020	15.881 ± 0.020	39.074 ± 0.048
99429 rdR	22.232 ± 0.036	16.067 ± 0.028	39.968 ± 0.078
99429 g	25.760 ± 0.026	16.367 ± 0.020	41.781 ± 0.052
99429 ga	24.870 ± 0.024	16.277 ± 0.020	40.938 ± 0.050
99429 gb	22.964 ± 0.024	16.099 ± 0.020	39.230 ± 0.048
99429 gc	23.605 ± 0.024	16.160 ± 0.020	40.235 ± 0.050
99429 gcR	23.787 ± 0.024	16.160 ± 0.020	41.027 ± 0.052
99429 gd	23.335 ± 0.024	16.167 ± 0.020	40.243 ± 0.050
	Kimberley Group, Elgee Siltstone		
46285	23.178 ± 0.024	16.167 ± 0.020	45.335 ± 0.056
46285 A	23.352 ± 0.024	16.214 ± 0.020	44.809 ± 0.056
46285 AR	19.862 ± 0.026	15.737 ± 0.026	41.180 ± 0.090
46285 B	22.093 ± 0.022	16.060 ± 0.020	45.615 ± 0.056
46285 BR	22.540 ± 0.032	16.052 ± 0.034	46.966 ± 0.132

* Corrected for mass fractionation of 0.130% ± 0.012 ($2\sigma_{mean}$) amu^{-1}
Errors are $2\sigma_{mean}$ for corrected ratios
R Indicates isotopic analysis of HCl-insoluble residue of relevant sample

Pb isotopic data for GSWA 99429, a non-determined stromatolite form from the Hibberson Dolomite is illustrated in **Figure 2.4.4**. Carbonate and residue samples were analysed from two distinct portions of the stromatolite; a buff to red coloured, fine grained, weakly laminated carbonate and a coarser, laminated/oolitic grey carbonate. It is evident from **Figure 2.4.4** that the grey portion of the sample has consistently more radiogenic Pb isotopic compositions than the more massive red portion and that residue analyses from the red portion are distinctly more radiogenic than the corresponding carbonate analyses.

Figure 2.4.3: Pb isotopic data for carbonate stromatolites from the Elgee Siltstone, Kimberley Group, Kimberley Basin (GSWA 46285)

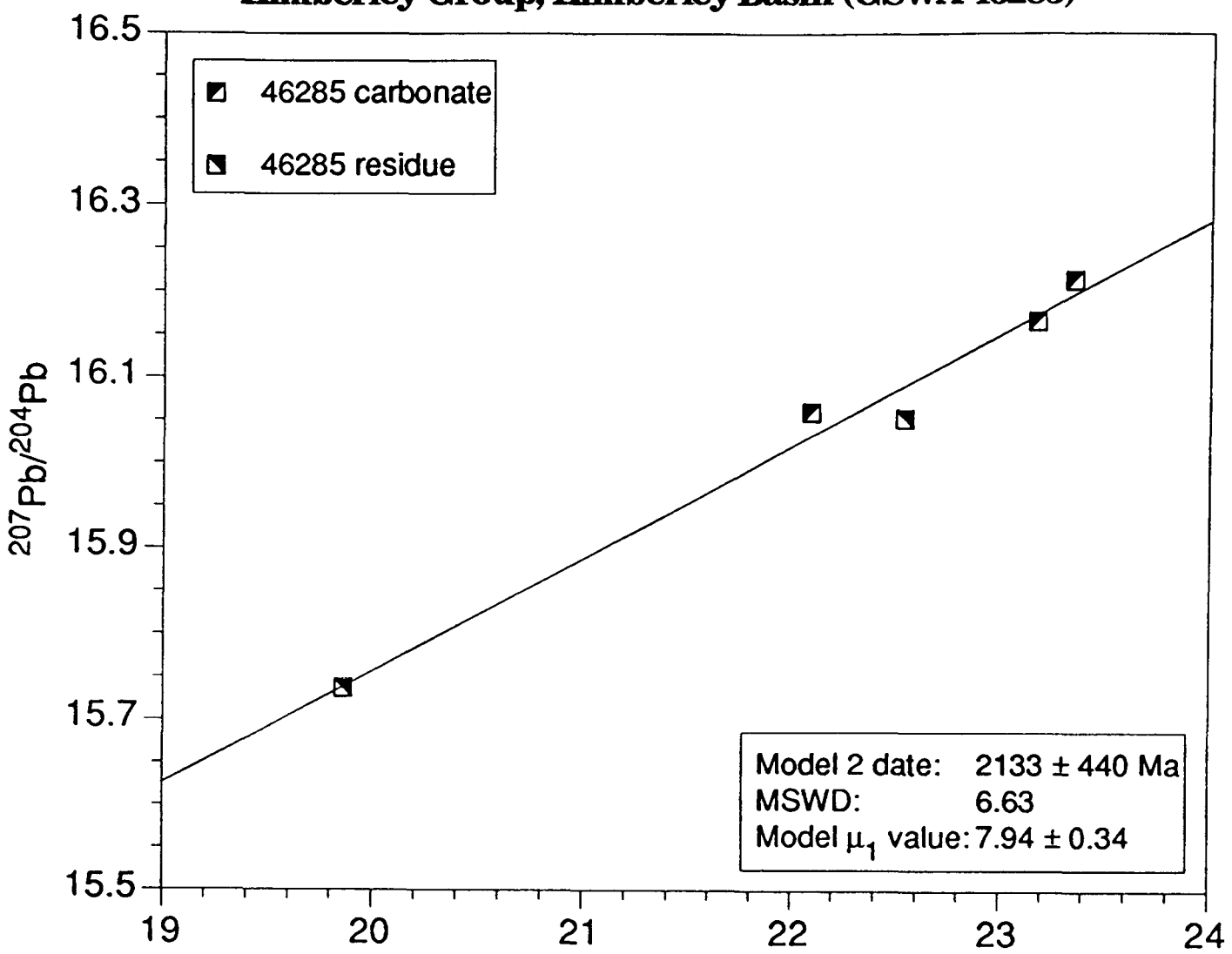

Figure 2.4.4: Pb isotopic data for carbonate stromatolites from the Hibberson Dolomite, Crowhurst Group, Kimberley Basin (GSWA 99429)

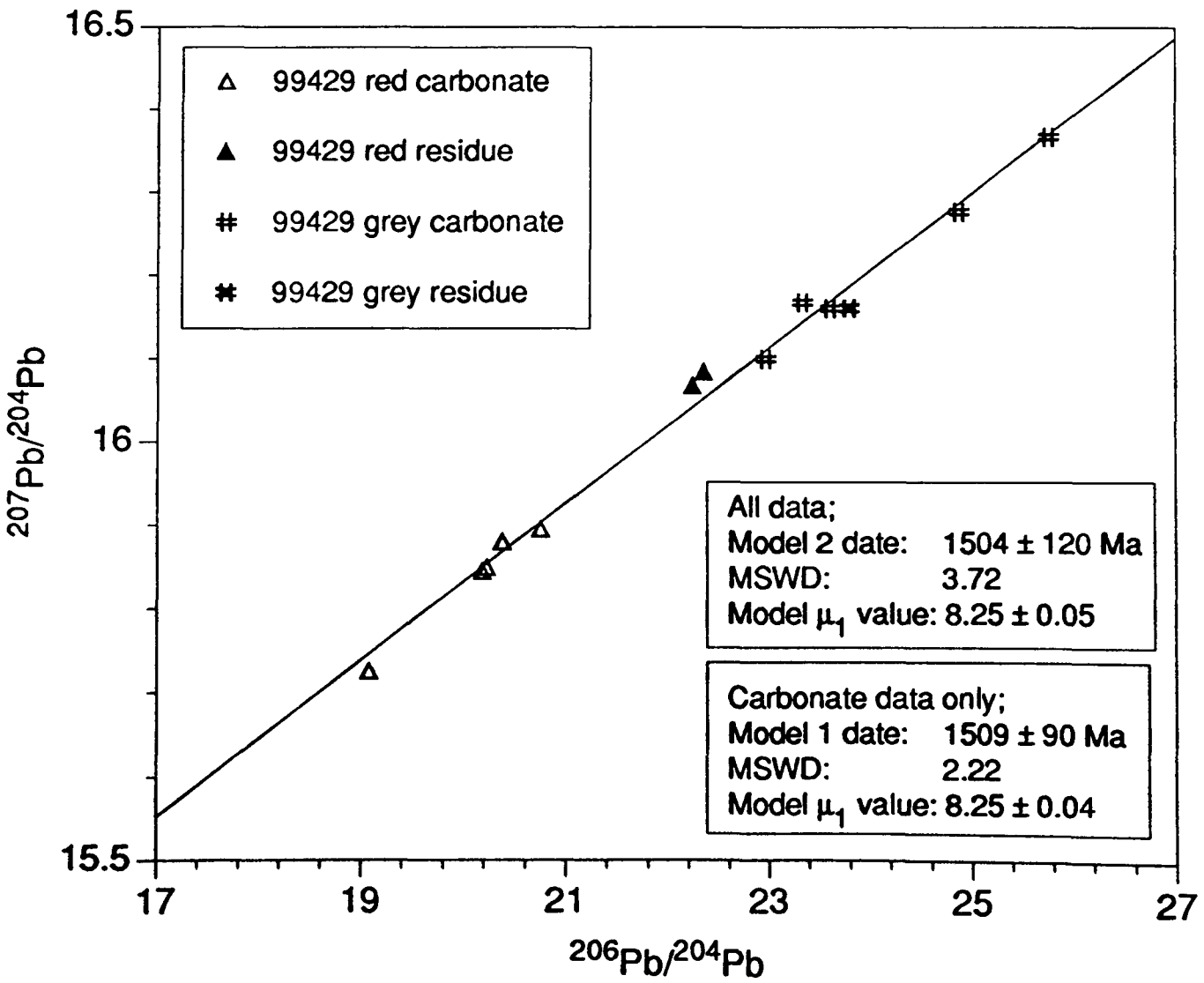

In thin section, the buff-red portion comprises very fine grained carbonate with a saccharoidal texture, variably stained by iron oxide. Variation in colour intensity picks out a poor lamination that also corresponds to minor variations in grain size. A distinct, possibly erosive boundary separates this portion from the grey carbonate which alternates between oolitic and laminated fabrics on a scale of 2-5 mm and is locally cross bedded. The ooliths are sub-circular and have cores of sparite and rare quartz, surrounded by finer grained carbonate that is clearly recrystallised. Well laminated carbonate sediment separates oolitic regions, with the lamination picked out again by variation in carbonate grain size. Rare clastic quartz crystals are observed throughout the thin section. Late, unrelated carbonate veins occur perpendicular to the lamination, disrupting the sedimentary fabric.

The carbonate analyses define a ten point Pb/Pb isochron whose slope corresponds to a date of 1509 ± 90 Ma (MSWD 2.22, model μ_1 value 8.25 ± 0.04). If the residue data is included, this value alters to 1504 ± 120 Ma (MSWD 3.72, model μ_1 value 8.25 ± 0.05). The dates are chronometrically consistent with c.1.8 Ga ages for the Hart Dolerite which intrudes formations underlying the Hibberson Dolomite.

One must also consider the data for the buff-red and grey portions independently (**Figure 2.4.5** and **Figure 2.4.6**) since the 1.5 Ga date might be the result of combination of strictly independent sets of data. All available GSWA 99429 red data define a seven point Pb/Pb isochron date of 1772 ± 120 Ma (MSWD 0.93, model μ_1 value 8.19 ± 0.04) while GSWA 99429 red carbonate data alone define a five point isochron date of 1726 ± 240 Ma (MSWD 1.46, model μ_1 value 8.20± 0.06) (**Figure 2.4.5**). Both values are somewhat older than that for the combined data set and lie closer to the 1762 ± 15 Ma age of the Hart Dolerite (Bofinger, 1967). It is evident that inclusion of the residue data merely increases the isotopic range and reduces the errors without significantly altering the magnitude of the date or model μ_1 value.

All GSWA 99429 grey data (**Figure 2.4.6**) define a six point Pb/Pb errorchron date of 1490 ± 430 Ma (MSWD 4.07, model μ_1 value 8.25 ± 0.25), while exclusion of the sole residue analysis gives a date of 1456 ± 460 Ma (MSWD 3.26, model μ_1 value 8.28 ± 0.26). Again, whether the residue analysis is included or not the regressed date and model μ_1 value remain very similar, suggesting that both carbonate and residue were in equilibrium at isotopic closure. Although the limited isotopic range and data scatter result in large errors, it should be noted that the absolute values of both dates are similar to the 1.5 Ga value for the combined GSWA 99429 data set.

Figure 2.4.5: Pb isotopic data for GSWA 99429 red, Hibberson Dolomite, Crowhurst Group, Kimberley Basin

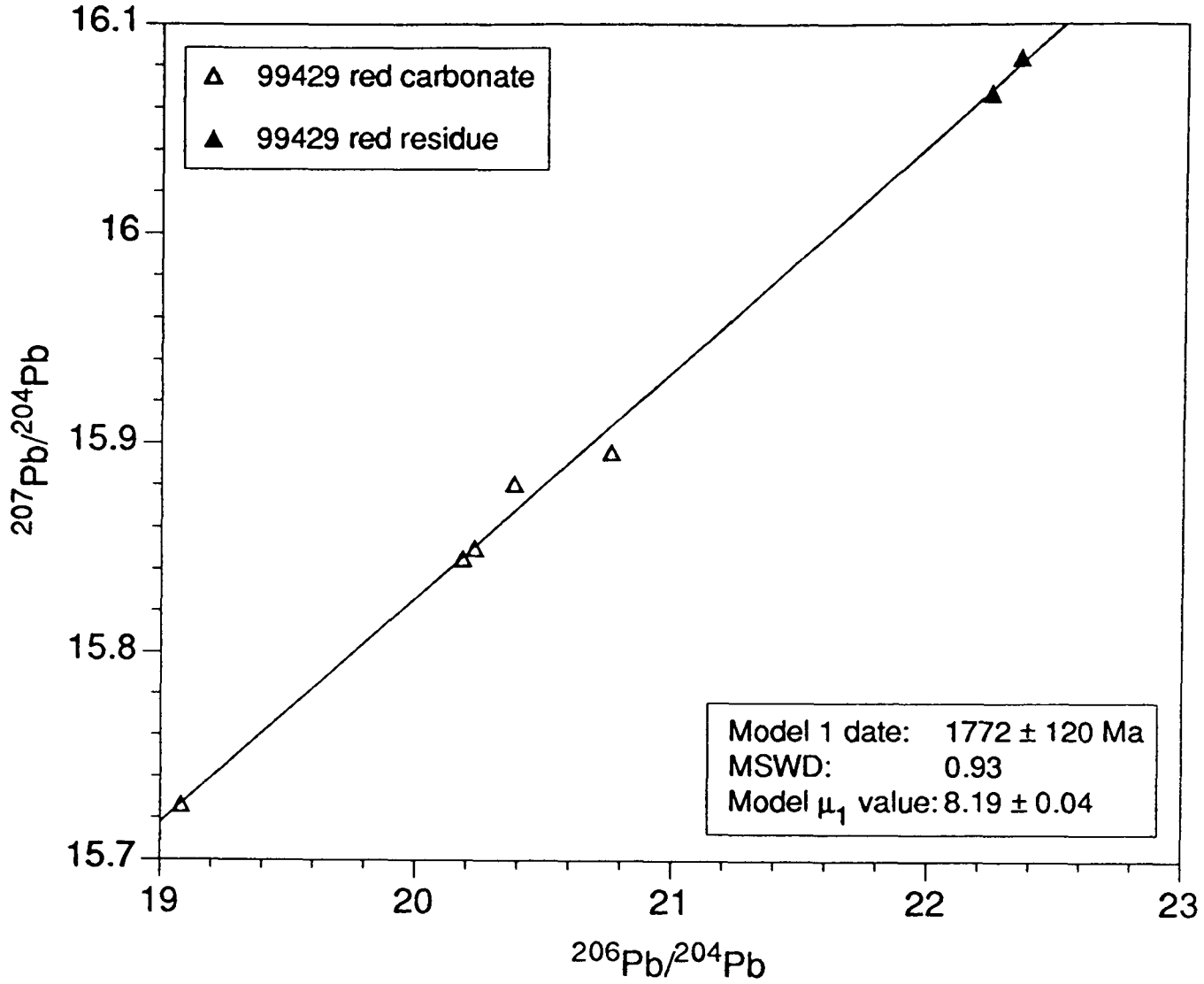

Figure 2.4.6: Pb isotopic data for GSWA 99429 grey, Hibberson Dolomite, Crowhurst Group, Kimberley Basin

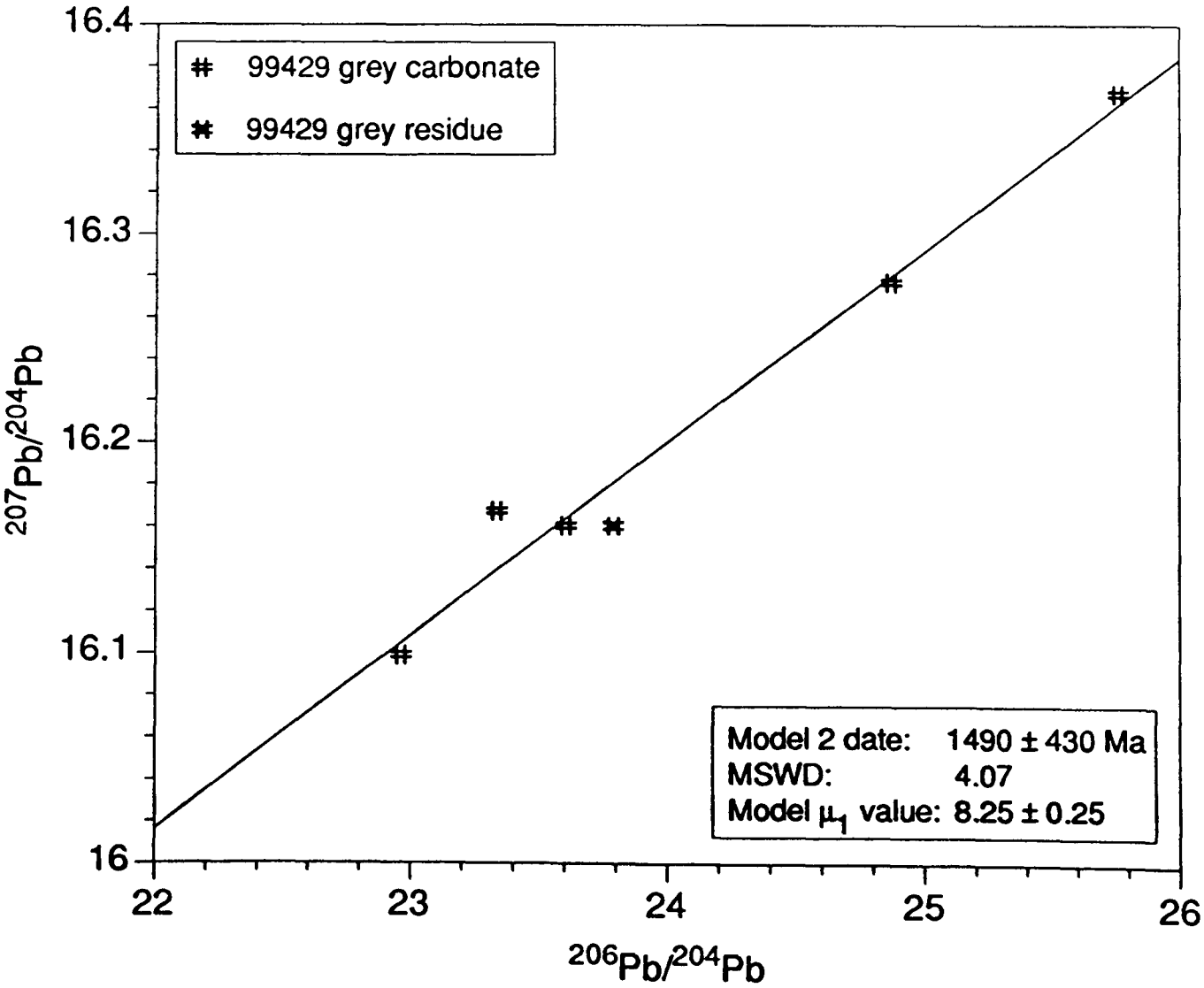

Stable isotopic data are illustrated in **Figure 2.4.7**. $\delta^{13}C$ values cluster around -1 to -1.5‰ and $\delta^{18}O$ values around -7‰, from which it may be deduced that the two components of GSWA 99429 have had very similar diagenetic histories. The data suggest that meteoric waters and/or slight burial metamorphism may have been involved during carbonate recrystallisation, although the preservation of ooliths in thin section augurs against a significant role for the latter.

Figure 2.4.7: Stable isotopic data for GSWA 99429, Hibberson Dolomite, Kimberley Group, Kimberley Basin

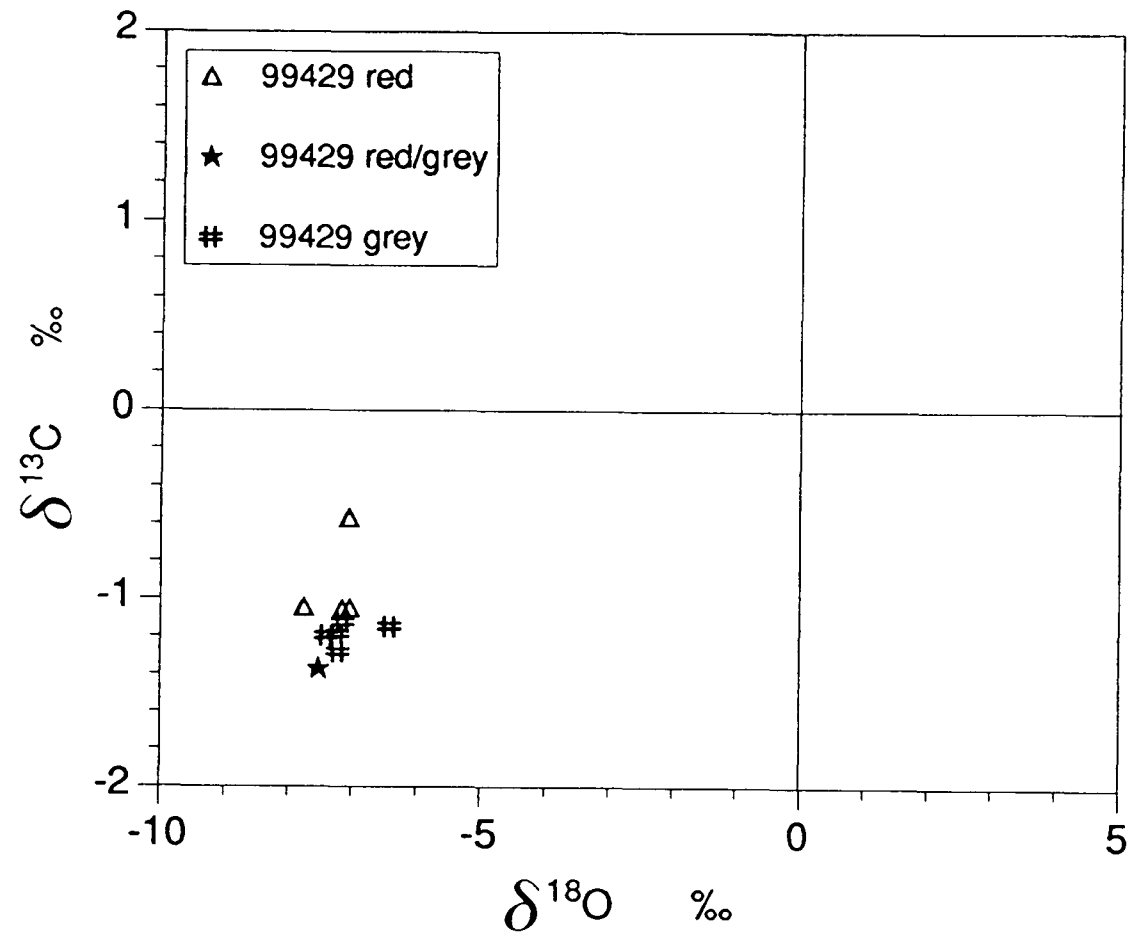

2.4.6: *DISCUSSION*

It is unclear which of the above dates is/are geologically significant, but if one considers the stable isotopic data illustrated in **Figure 2.4.7**, the compositional similarity of red and grey analyses supports a common diagenetic history for both portions of GSWA 99429 and suggests that the combined date of 1509 ± 90 Ma is geologically significant. It is interpreted as the age of diagenetic recrystallisation involving meteoric groundwaters and as such provides a minimum age for deposition of the Kimberley Basin.

Age data for the Kimberley Basin imply that the Speewah and Kimberley Groups (> 1.8 Ga) correlate with parts of the Ashburton Basin and Earaheedy Group of the Nabberu Basin. The Bastion and Crowhurst Groups are aged between 1.5-1.8 Ga and are younger than the Ashburton Basin (> 1.8 Ga) and much, if not

all of the Nabberu Basin (?1.63-2.3 Ga).

2.5: BANGEMALL BASIN

2.5.1: *INTRODUCTION*

The Bangemall Basin outcrops over an irregular area of some 87 000 km^2 between the Archaean Pilbara and Yilgarn Cratons (see **Figure 2.1.1**) and comprises seven lithological units of dominantly clastic sediments with extensive intrusive basaltic sills and dykes. The oldest part of the basin obscures Capricorn Orogen structures in the west, while to the east, younger facies are identified beneath the unconformable Savory Basin cover.

2.5.2: *STRATIGRAPHY*

The Bangemall Basin unconformably overlies rocks of the Capricorn Orogen, the Narryer Complex and the Hamersley Basin and is unconformably overlain by the Late Proterozoic Savory and Yeneena Basins and the Phanerozoic Officer Basin. The seven constituent lithostratigraphic units (see **Figure 2.5.1** and **Figure 2.5.2**) young from east to west and two distinct age groups have been proposed, although the exact correlation between formations of the older Edmund and Scorpion Subgroups and the younger Mucalana, Collier, Manganese and Kharban Subgroups (plus the Cornelia Sandstone) has not been finalised.

Stromatolitic carbonates were available from the Irregully Formation (GSWA 46073J) and the Cheyne Springs Formation (GSWA 46009) of the Edmund Subgroup and the Stag Arrow Formation of the younger Manganese Subgroup (GSWA 65334, 31000), as indicated in **Figure 2.5.2**.

Figure 2.5.1: Stratigraphy of the Bangemall Basin, after Williams (1990a)

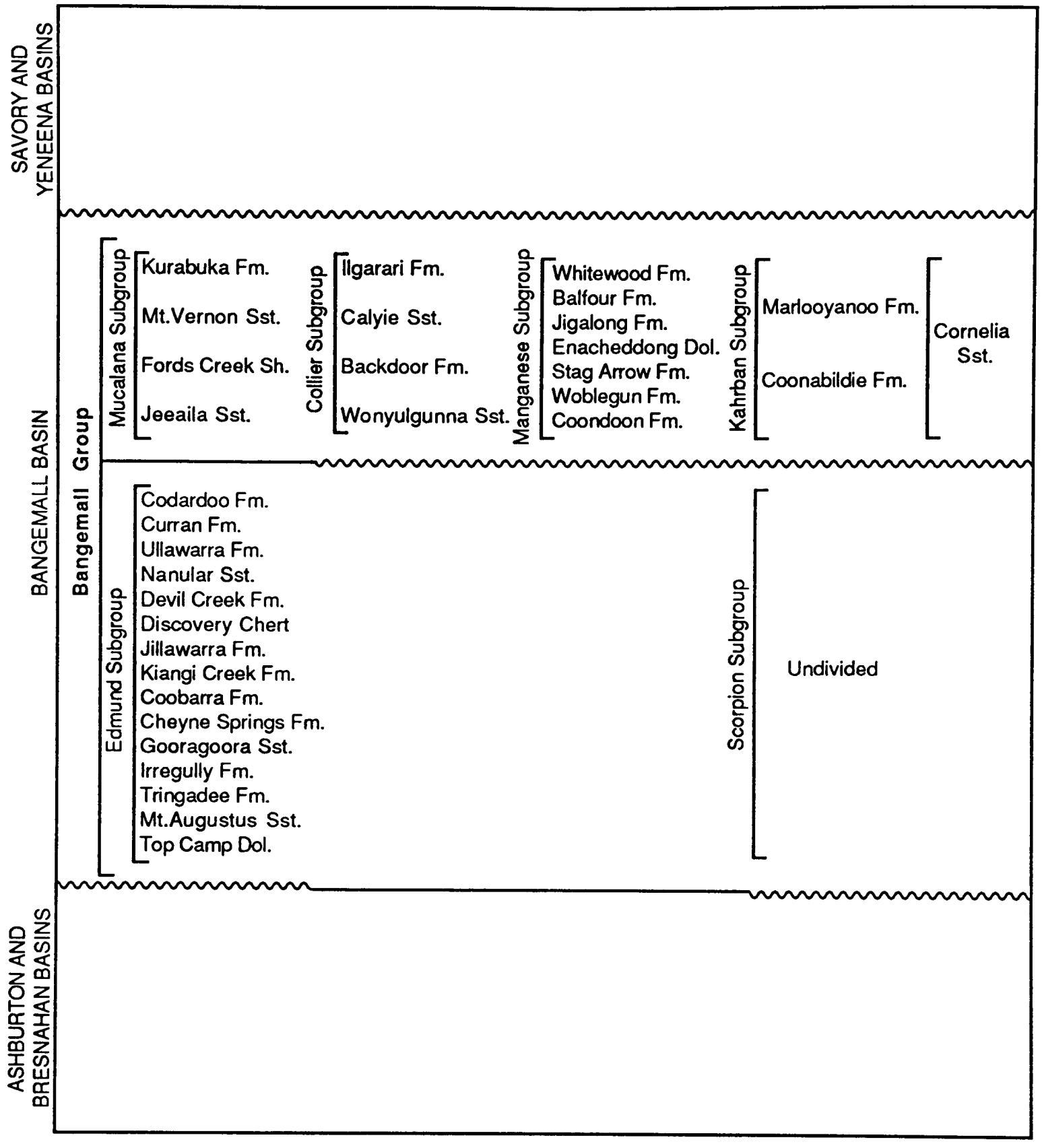

2.5.3: *AGE CONSTRAINTS*

Several age determinations have been made on deposits of the Bangemall Basin, but the results are by no means unequivocal. With reference to the older units;

- Richards et al. (in prep.) obtained Pb model ages of 1.5-1.6 Ga for syngenetic galenas from rocks equivalent to the Irregully and Tringadee Formations of the Edmund Subgroup;
- Gee et al. (1976) published an Rb-Sr date of 1098 ± 42 Ma for an altered rhyolite

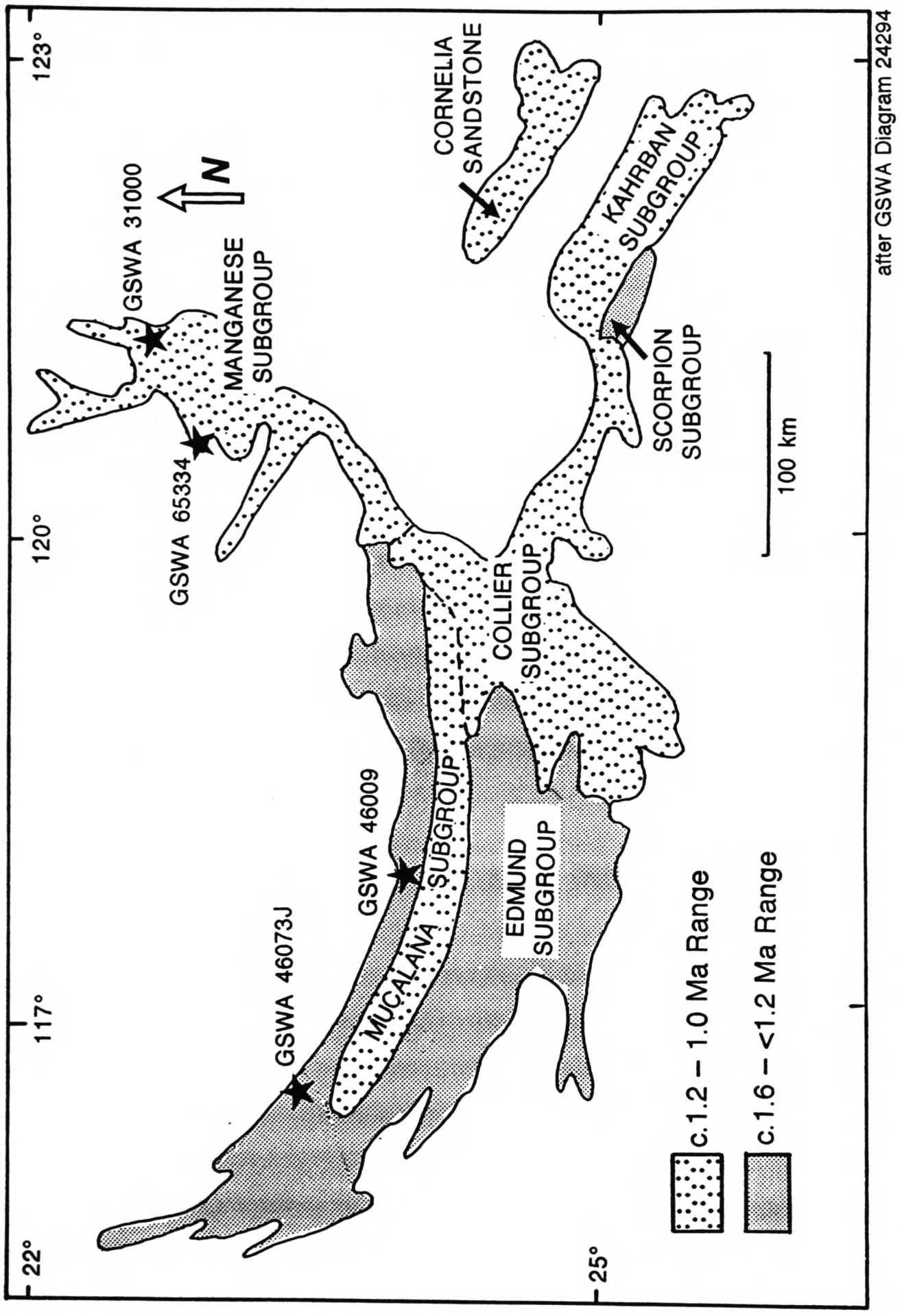

Figure 2.5.2: Localities for stromatolite samples from the Bangemall Basin, Western Australia

from the base of the Coobarra Formation and

• Compston & Arriens (1968) obtained an Rb-Sr date of 1080 ± 80 Ma for black shales from the Curran Formation and poorly constrained values of around 1080 Ma for felsic rocks from the Jillawarra Formation (both recalculated using the revised decay constants in Steiger & Jäger, 1977).

With reference to the younger lithostratigraphic units;

• Richards et al. (in prep.) obtained Pb model ages of 1.11 Ga for galenas from the Fords Creek Shale in the Mucalana Subgroup;

• Goode & Hall (1981) obtained a K-Ar date of 1.05 Ga for glauconites from the Coondoon Formation of the Manganese Subgroup and

• preliminary glauconite Rb-Sr data for the Stag Arrow Formation have yielded a date of 1.33 Ga (Williams, pers. comm. 1991).

From this information Williams (1990a) concluded that the Edmund and Scorpion Subgroups had a depositional age of between 1.6 and 1.2 Ga and that the Mucalana, Collier, Manganese and Kharban Subgroups and the Cornelia Sandstone inlier were between 1.2 and 1.0 Ga old. The recent glauconite Rb-Sr date, however, suggests that the boundary between the two age groups may be nearer 1.35 Ga (Grey, pers. comm. 1991).

2.5.4: *FORMATIONAL PETROGRAPHY AND SEDIMENTOLOGY*

The Edmund Subgroup is the dominant lithostratigraphic unit in the west of the Bangemall Basin (see **Figure 2.5.2**). It is subdivided into fifteen formations (12 km thick) and is correlated with the undivided Scorpion Subgroup (10 km thick) that is found in the east (see **Figure 2.5.1**). Vogt & Stumpfl (1987) and Boddington (1987) claimed to recognise separate western and eastern divisions of the Edmund Subgroup but the area requires extensive remapping before substantiation of this proposal is possible.

The units immediately above the basal, shallow water Top Camp Dolomite are restricted and indicate alluvial fan deposition from locally eroded horsts (Mt. Augustus Sandstone, Tringadee Formation). The Irregully Formation was deposited under lagoonal conditions, is largely dolomitic and contains abundant stromatolites such as *Colonella* form indet. (GSWA 46073J), a large, unbranched, stromatolite with club-shaped columns up to 15 cm across that is indicative of moderate depth, quiet water conditions.

An open marine shelf sequence subsequently transgressed the lagoon (Kiangi Creek Formation, Jillawarra Formation), although the Cheyne Springs Formation marks a short term return to shallow water carbonate environments with the stromatolite *Conophyton* form indet. (GSWA 46009) common (Grey, pers. comm. 1992). This new form of *Conophyton* is thought to be restricted to the period from 1600 to 1000 Ma and occurs as large conical forms, again indicative of moderate water depth and quiet conditions. The Discovery Chert was deposited at the maximum extent of the transgression before a rapid regressive phase deposited the stromatolitic Devil Creek Formation under similar conditions to those of the Irregully and Cheyne Springs Formations. Renewed slow transgression resulted in the deposition of the barrier-bar sediments of the Nanular Sandstone (Muhling & Brakel, 1985) and the turbiditic facies of the Ullawarra, Curran and Coodardoo Formations.

The younger Mucalana, Collier, Manganese and Kharban Subgroups and the Cornelia Sandstone are all correlated with one another at the subgroup level. Certain direct correlations are also possible at the formation level. Stromatolites were available from the Manganese Subgroup which outcrops in a northeast-trending zone on the southeast margin of the Pilbara Craton. Its basal units, the Coondoon Formation and the Woblegun Formation are laterally equivalent, the former reflecting shallow marine transgression over karstified Hamersley Basin sediments, while the latter is more typical of a stable marine shelf environment with deposition of shale, siltstone, fine glauconitic sandstone and minor chert. The succeeding Stag Arrow Formation was deposited in shallow water shelf conditions and comprises a wide variety of deposits including local stromatolitic dolomites. GSWA 65334 and 31000 are both non-determined stromatolite forms from the Stag Arrow Formation which is directly correlated with the Backdoor Formation of the Collier Subgroup and the Fords Creek Shale of the Mucalana Subgroup. Regression resulted in deposition of the local Enacheddong Dolomite before slight deepening culminated in the coarse alluvial fan deposits of the topmost Whitewood Formation.

Extension between the stable Ashburton Basin platform and the Gascoyne Complex initiated Bangemall Basin development via block faulting (Williams, 1990a). Western sediments have been deformed by the post-depositional Edmund Fold Belt which exhibits open to tight folds with steeply dipping axial planar surfaces. Late compression resulted in an additional amount of easterly thrusting. The structure of the eastern subgroups is less clear. While the Collier Subgroup and Cornelia Sandstone have a similar structural style to the Edmund Fold Belt, although trends

are more variable, the Manganese Subgroup is cut in the north by listric growth faults that also affect the Pilbara Craton and in the south by steep reverse and sinistral strike-slip faults associated with Savory Basin inversion

2.5.5: *RESULTS*

Results for stromatolites from the Edmund Subgroup of the Bangemall Group are detailed in **Table 2g** and illustrated in **Figure 2.5.3**. The ten analyses of *Colonella* (GSWA 46073J) exhibit unradiogenic Pb isotopic compositions and very limited isotopic variation ($^{206}Pb/^{204}Pb$ from 18.369 to 18.963). Together they define a poor Pb/Pb isochron date of 2309 ± 640 Ma with an MSWD of 2.23 and a model μ_1 value of 8.33 ± 0.10. Combining GSWA 46009 and GSWA 46073J data, on the basis that they are both from the same subgroup, a more precise date of 1436 ± 230 Ma is obtained with an MSWD of 3.28 and a model μ_1 value of 8.41 ± 0.03.

Table 2g: Pb isotopic compositions of carbonate stromatolites from the Edmund Subgroup, Bangemall Basin (GSWA 46073J, 46009)

SAMPLE	CORRECTED RATIOS *		
	$^{206}Pb/^{204}Pb$	$^{207}Pb/^{204}Pb$	$^{208}Pb/^{204}Pb$
	Bangemall Group, Edmund Subgroup, Irregully Formation		
46073J i	18.417 ± 0.030	15.741 ± 0.030	37.445 ± 0.082
46073J ii	19.012 ± 0.022	15.857 ± 0.022	37.743 ± 0.052
46073J A	18.979 ± 0.020	15.816 ± 0.022	37.629 ± 0.064
46073J a	18.640 ± 0.024	15.802 ± 0.022	37.660 ± 0.062
46073J b °	18.574 ± 0.018	15.765 ± 0.020	37.522 ± 0.046
46073J c	18.650 ± 0.018	15.783 ± 0.020	37.485 ± 0.048
46073J d	18.773 ± 0.018	15.802 ± 0.020	37.688 ± 0.048
46073J e	19.012 ± 0.036	15.825 ± 0.034	37.764 ± 0.084
46073J g	18.500 ± 0.018	15.770 ± 0.020	37.448 ± 0.046
46073J h	18.631 ± 0.018	15.767 ± 0.020	37.450 ± 0.046
	Bangemall Group, Edmund Subgroup, Cheyne Springs Formation		
46009	21.659 ± 0.044	16.063 ± 0.040	38.545 ± 0.120
46009 a	21.554 ± 0.022	16.027 ± 0.020	38.348 ± 0.048

* Corrected for mass fractionation of 0.130% ± 0.012 ($2\sigma_{mean}$) amu^{-1}
Errors are $2\sigma_{mean}$ for corrected ratios

° Pb concentration: 3.382 ± 0.020 ppm

Figure 2.5.3: Pb isotopic data for carbonate stromatolites from the Edmund Subgroup, Bangemall Group, Bangemall Basin (GSWA 46073J, 46009)

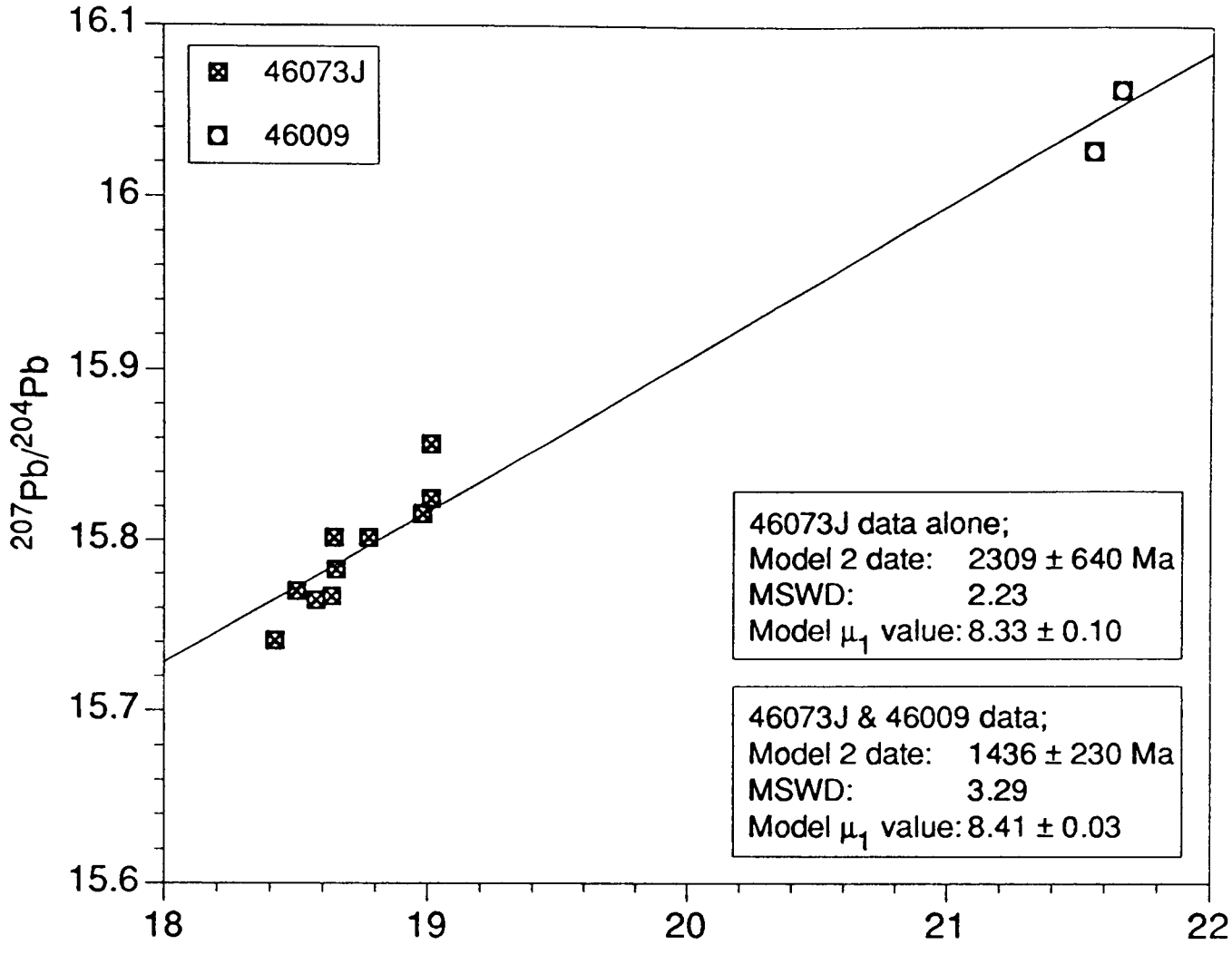

Although the combined date of 1436 ± 230 Ma is consistent with 1.6-1.2 Ga age constraints for the Edmund Subgroup, it is clear that GSWA 46073J analyses lie along a different slope to that of the combined data set, which in effect may be compared to a spurious 'two-point' isochron. The fact that there is a probable sequence break between the Irregully and Cheyne Springs Formations (Grey, pers. comm. 1992) and the limited stable isotopic data available (illustrated in **Figure 2.5.4**) suggest that the two formations have had differing diagenetic histories.

In thin section GSWA 46073J exhibits a well preserved, fine scale (2 mm) lamination that is picked out by minor size variations in fine grained, saccharoidal, recrystallised carbonate. Negative $\delta^{13}C$ values suggest that meteoric waters or burial metamorphism were involved during recrystallisation, but since the rare quartz grains that exist show no evidence of strain effects, subgrain formation or dynamic recrystallisation, it is probable that metamorphism did not play an important role. Fresh, late haematite occurs throughout the stromatolite indicating the presence of oxidising conditions during diagenesis.

Figure 2.5.4: Stable isotopic data for GSWA 46073J and 46009, Edmund Subgroup, Bangemall Group, Bangemall Basin

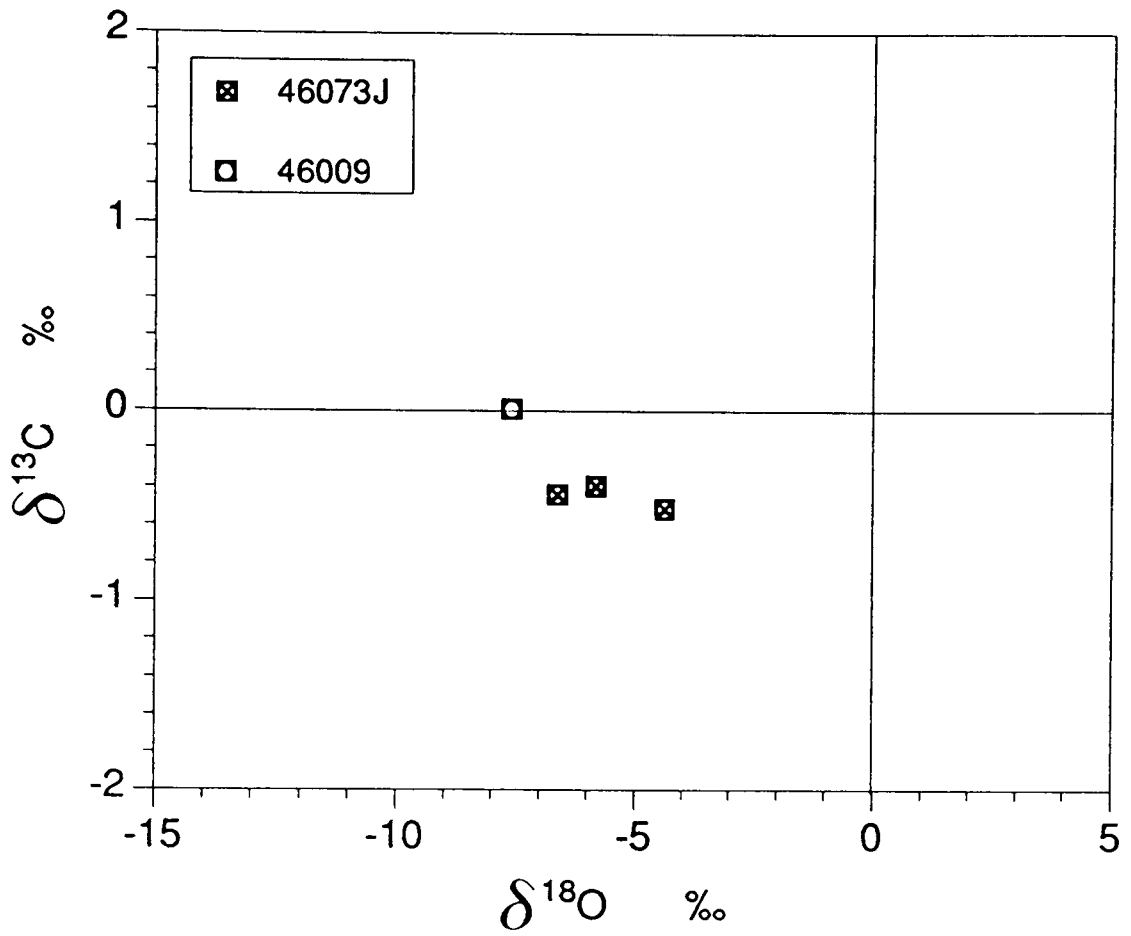

The problems associated with interpretation of dates from combined data sets with small isotopic ranges in the absence of independent age control are self-evident. Nevertheless, it is interesting to note that the combined date of 1436 ± 230 Ma for the Edmund Subgroup is consistent with the inferred depositional age, even though the errors are too large for the date to be of stratigraphic use. This probably results from the fact that the two stromatolites possessed similar μ_1 values and initial Pb isotopic ratios at approximately the same time of isotopic closure (i.e. within error of the date).

Results for stromatolites from the same Stag Arrow Formation of the younger Manganese Subgroup (GSWA 31000, 65334) are listed in **Table 2h** and illustrated in **Figure 2.5.5**. The Pb isotopic composition of analyses from both stromatolites are more radiogenic than those for the Edmund Subgroup and also exhibit a much larger isotopic range ($^{206}Pb/^{204}Pb$ from 19.288 to 24.084 for GSWA 31000 and 26.943 to 33.808 for 65334). Potential causes for the variation of Pb isotope ratios within individual samples and between samples are discussed in **Chapter 6**.

Table 2h: Pb isotopic compositions of carbonate stromatolites from the Manganese Subgroup, Bangemall Basin (GSWA 31000, 65334)

SAMPLE	CORRECTED RATIOS *		
	$^{206}Pb/^{204}Pb$	$^{207}Pb/^{204}Pb$	$^{208}Pb/^{204}Pb$
	Bangemall Group, Manganese Subgroup, Stag Arrow Formation		
31000	24.147 ± 0.036	16.323 ± 0.034	38.203 ± 0.082
31000 a	23.302 ± 0.024	16.168 ± 0.020	38.202 ± 0.048
31000 b	20.734 ± 0.020	15.939 ± 0.020	38.224 ± 0.046
31000 c	19.338 ± 0.020	15.800 ± 0.020	39.944 ± 0.048
65334	30.649 ± 0.044	16.782 ± 0.030	50.402 ± 0.108
65334 A	31.847 ± 0.034	16.848 ± 0.022	50.676 ± 0.068
65334 B	33.896 ± 0.036	17.033 ± 0.022	51.234 ± 0.066
65334 C	29.675 ± 0.044	16.754 ± 0.028	50.234 ± 0.088
65334 F	27.675 ± 0.048	16.522 ± 0.032	50.918 ± 0.206
65334 G	27.013 ± 0.042	16.517 ± 0.026	51.034 ± 0.116
65334 H	30.960 ± 0.048	16.875 ± 0.036	50.155 ± 0.114

* Corrected for mass fractionation of 0.130% ± 0.012 ($2\sigma_{mean}$) amu^{-1}
Errors are $2\sigma_{mean}$ for corrected ratios

Seven analyses of GSWA 65334 define a poor Pb/Pb errorchron whose slope corresponds to a date of 1171 ± 450 Ma (MSWD 8.37, model μ_1 value 8.53 ± 0.40). Four analyses of GSWA 31000 define a similarly poor Pb/Pb errorchron corresponding to a date of 1705 ± 670 Ma (MSWD 8.35, model μ_1 value 8.27 ± 0.32) (**Figure 2.5.5**).

In thin section GSWA 65334 consists of buff carbonate exhibiting a weak lamination, but much sedimentary detail has been destroyed by carbonate recrystallisation. Quartz occurs as rare, detrital clasts within the stromatolitic structure and as microcrystalline quartz in solution cavities. The development of late haematite has locally caused intense staining. GSWA 31000 shows a broad, domal, laminated fabric (2-3 mm), with a discontinuous lamination picked out by red, iron-stained micrite lenses between areas of colourless, equant calcite that contain rare subangular, detrital quartz. Recrystallisation has again obscured much of the microstructural detail while preserving the sedimentary fabric intact.

The two stromatolites have similar stable isotopic compositions (see **Figure 2.5.6**) with $\delta^{18}O$ values around -5‰ and $\delta^{13}C$ values between -0.4 and -1‰. Such figures, although not conclusive, are consistent with diagenetic recrystallisation of

Figure 2.5.5: Pb isotopic data for carbonate stromatolites from the Stag Arrow Formation, Manganese Subgroup, Bangemall Basin (GSWA 31000, 65334)

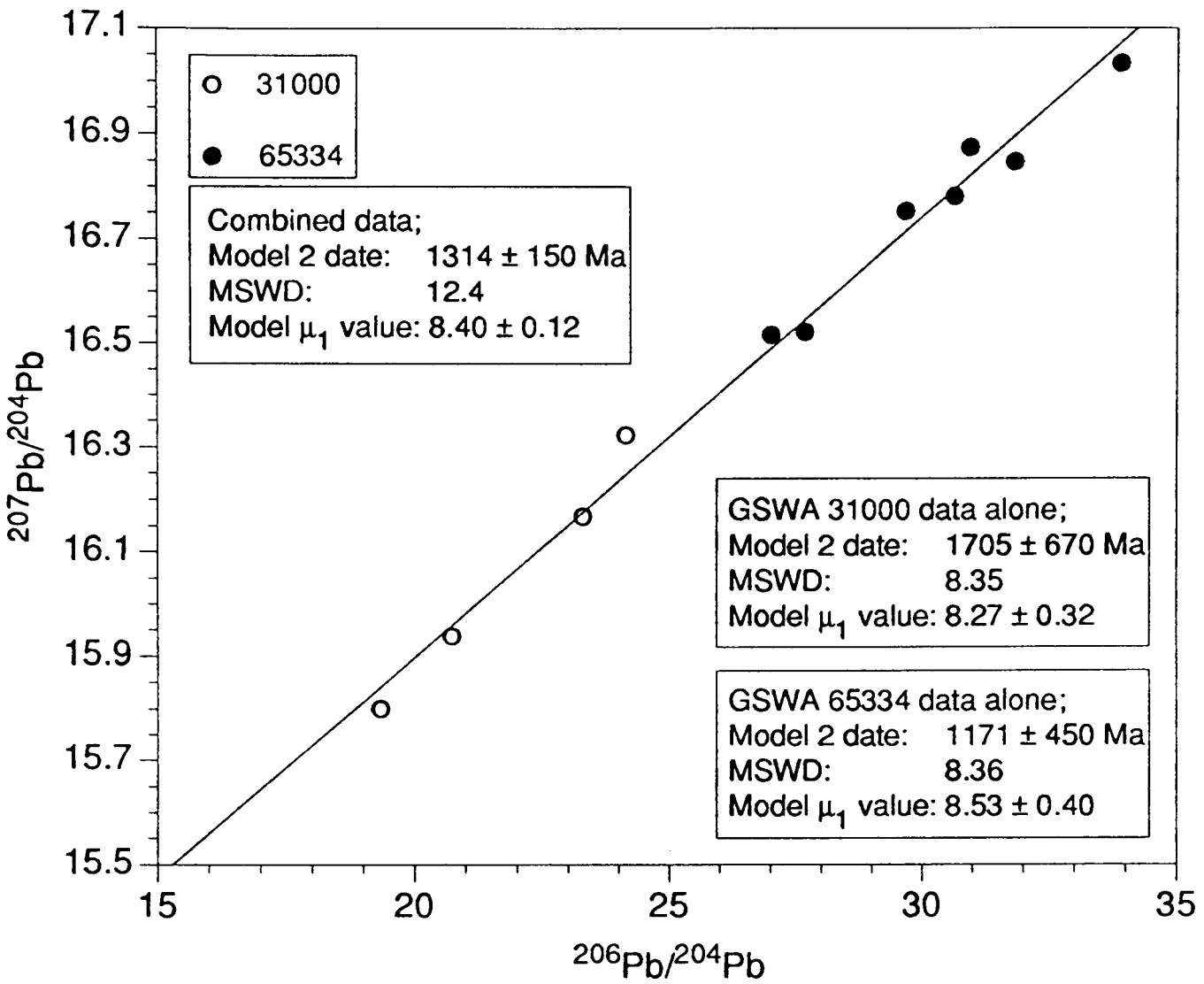

Figure 2.5.6: Stable isotopic data for GSWA 31000 and 65334, Stag Arrow Formation, Manganese Subgroup, Bangemall Group, Bangemall Basin

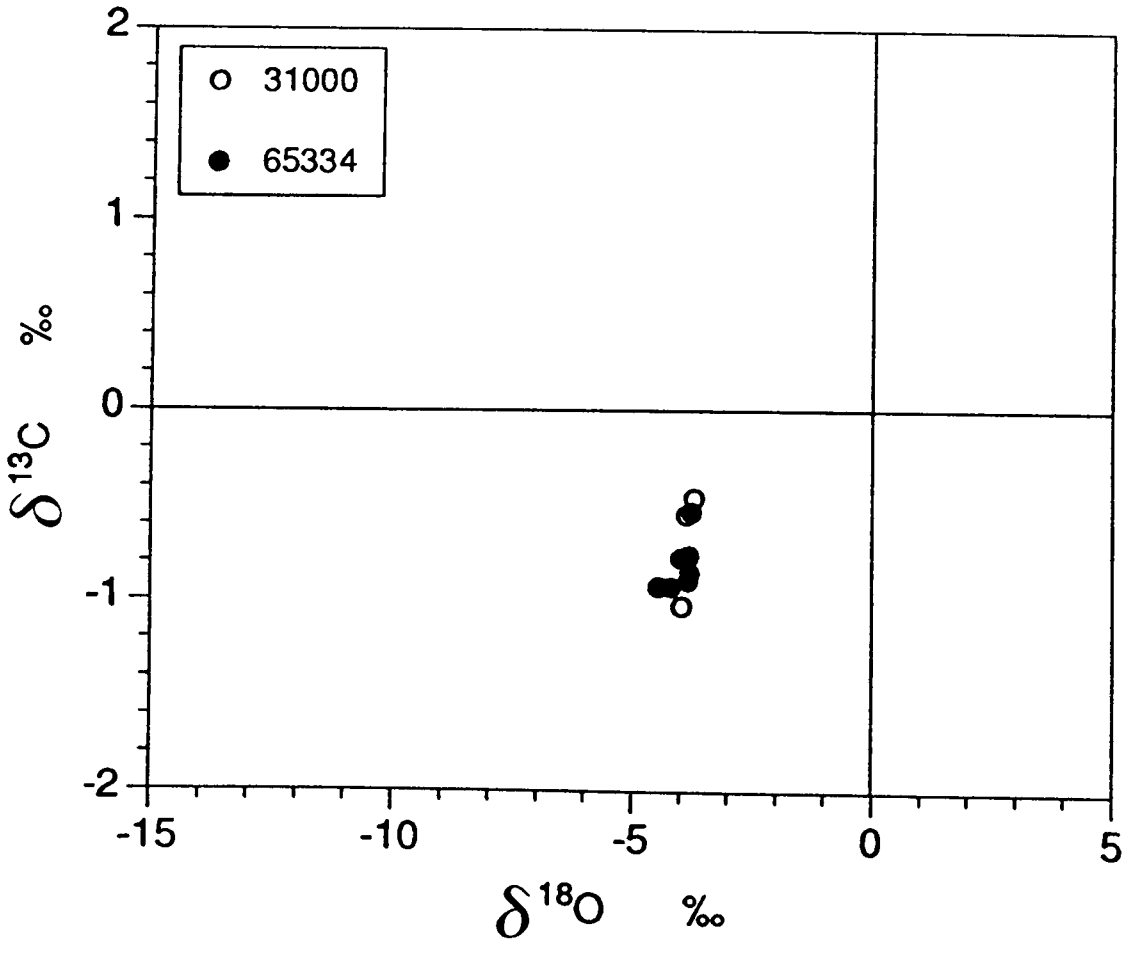

primary marine carbonate under meteorically influenced conditions. The similarity in composition suggests that the two samples were subject to similar diagenetic histories.

Independently, these two results are of little use because of excess data scatter and limited Pb isotopic ranges, but combination of all available data (justifiable since the dates and model μ_1 values of the individual fits were consistent within error and the samples were collected from localities less than 1 km apart) yields a Pb/Pb errorchron corresponding to a date of 1314 ± 150 Ma with an MSWD of 12.4 and a model μ_1 value of 8.40 ± 0.12. This date is interpreted as the age of diagenetic recrystallisation based on the similarity of stable isotopic composition of the two samples (see **Figure 2.5.6**).

2.5.6: *DISCUSSION*

The inferred age of the Edmund Subgroup is 1.6-1.2 Ga and although individual regressions for 46073J and 46009 are poorly defined and imprecise, it is intriguing that the combined date of 1436 ± 230 Ma is consistent with these constraints. In the absence of independent age control, careful and realistic interpretation of dates is essential where data sets with limited isotopic ranges are combined. Useful age data may still result if samples possess similar μ_1 values and initial Pb isotopic ratios and have experienced similar geological histories (with particular reference to recrystallisation events).

The inferred age of the Manganese Subgroup is 1.2-1.0 Ga, although recent unpublished Rb-Sr glauconite data suggest that the base may be nearer 1.35 Ga (Williams, pers. comm. 1991). The combined date of 1314 ± 150 Ma, interpreted as the age of diagenetic recrystallisation, suggests that a 1.35 Ga date for the base may indeed be valid, but it is unable to resolve the question beyond doubt.

Combination of all available Bangemall Group data (**Figure 2.5.7**) produces a Pb/Pb errorchron date of 1304 ± 66 Ma, with an MSWD of 7.79 and a model μ_1 value of 8.41 ± 0.03. Considering the wide stratigraphic and geographic distribution of samples, it is unlikely that this date can be reconciled with any distinct geological event unless basin-wide recrystallisation is invoked. Since the Edmund Subgroup samples and Manganese Subgroup samples come from separate tectonic belts with differing structural styles this is most improbable and consequently the date is interpreted as the average age of the Bangemall Group, resulting from broad

Figure 2.5.7: Pb isotopic data for carbonate stromatolites from the Bangemall Group, Bangemall Basin (GSWA 31000, 65334, 46073J, 46009)

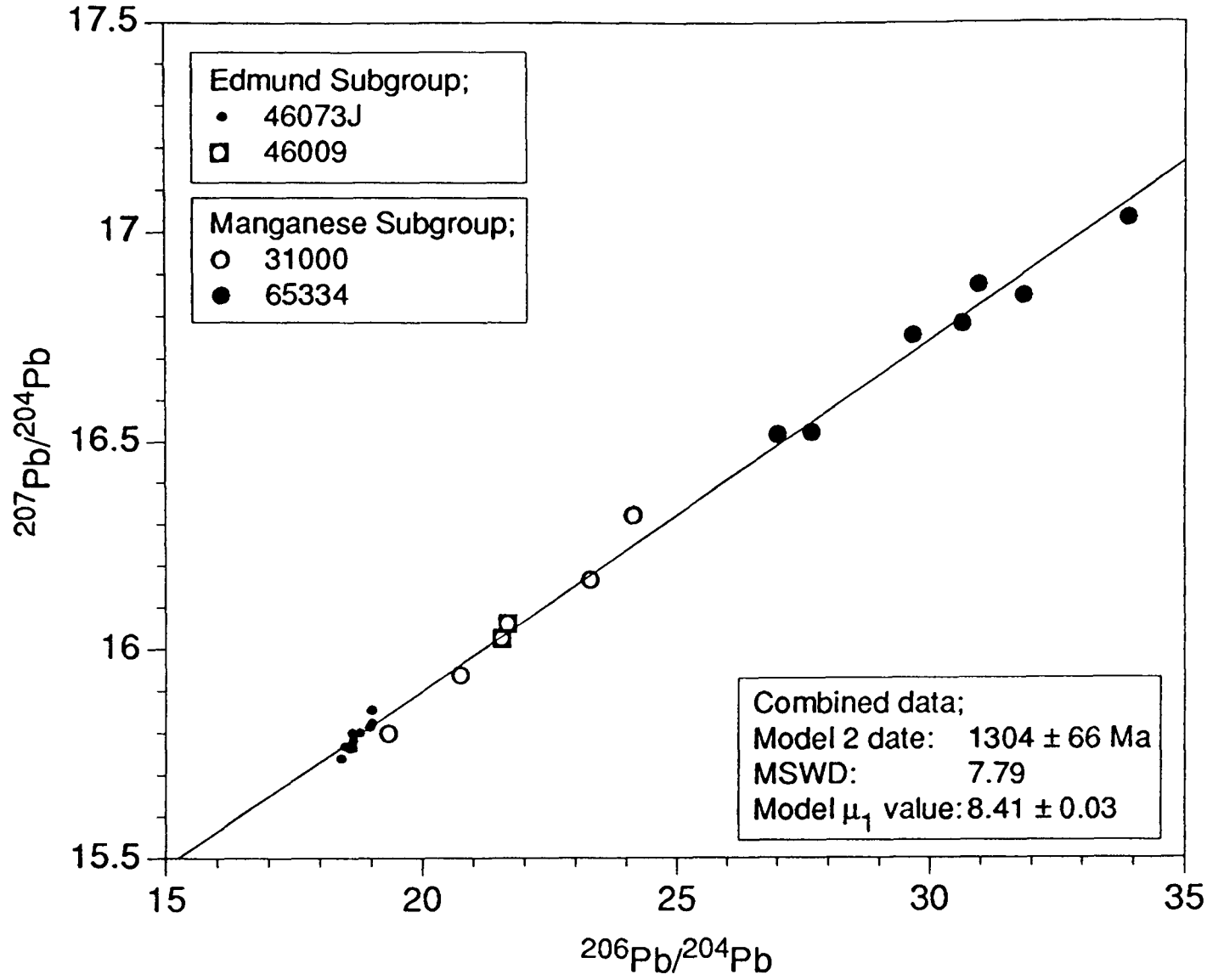

similarities in age, model μ_1 value and initial Pb isotopic ratio of the four stromatolitic samples. The combined date is concordant with independent constraints and confirms the basin to be Middle Proterozoic in age.

2.6: YENEENA BASIN (PATERSON OROGEN)

2.6.1: *INTRODUCTION*

The Yeneena Basin consists of a sequence of low grade metasediments grouped into one lithostratigraphic unit, the Yeneena Group, that forms the northwestern outcrop (36000 km^2) of the Paterson Orogen along with the Rudall Complex and Karara Sandstone (see **Figure 2.1.1**). It is separated from the remainder of the Paterson Orogen to the southeast (Musgrave Complex) by the Phanerozoic Canning and Officer Basins.

2.6.2: *STRATIGRAPHY*

The metasediments of the Yeneena Basin unconformably overlie deposits of the Archaean/Early Proterozoic Hamersley Basin in the west, the Manganese Subgroup of the Bangemall Basin in the southwest and the Rudall Complex in the southeast. In turn, they are unconformably overlain by the Late Proterozoic Savory Basin in the southwest, the Phanerozoic Officer Basin in the southeast and the Phanerozoic Canning Basin in the northeast.

Three zones are recognised from the west, central and northeastern regions of the basin and they are separated from each other by broad sand-covered areas with minimal exposure. Only the Isdell Formation is recognised from all three zones and the available carbonate stromatolites (GSWA 65343 and 76584) come from this unit or its lateral equivalents (see **Figure 2.6.1** and **Figure 2.6.2**).

Figure 2.6.1: Stratigraphy of the Yeneena Basin, after Williams (1990c)

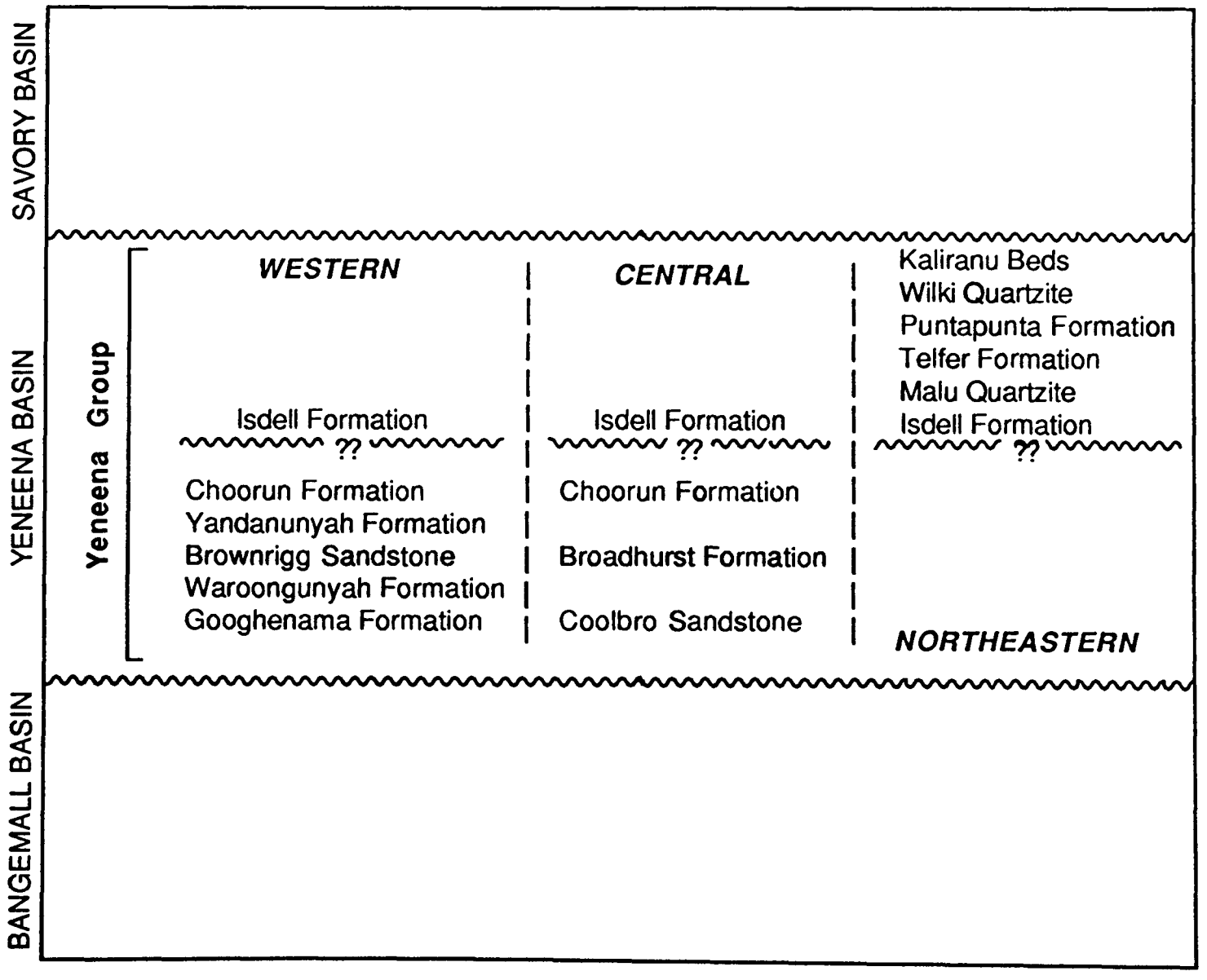

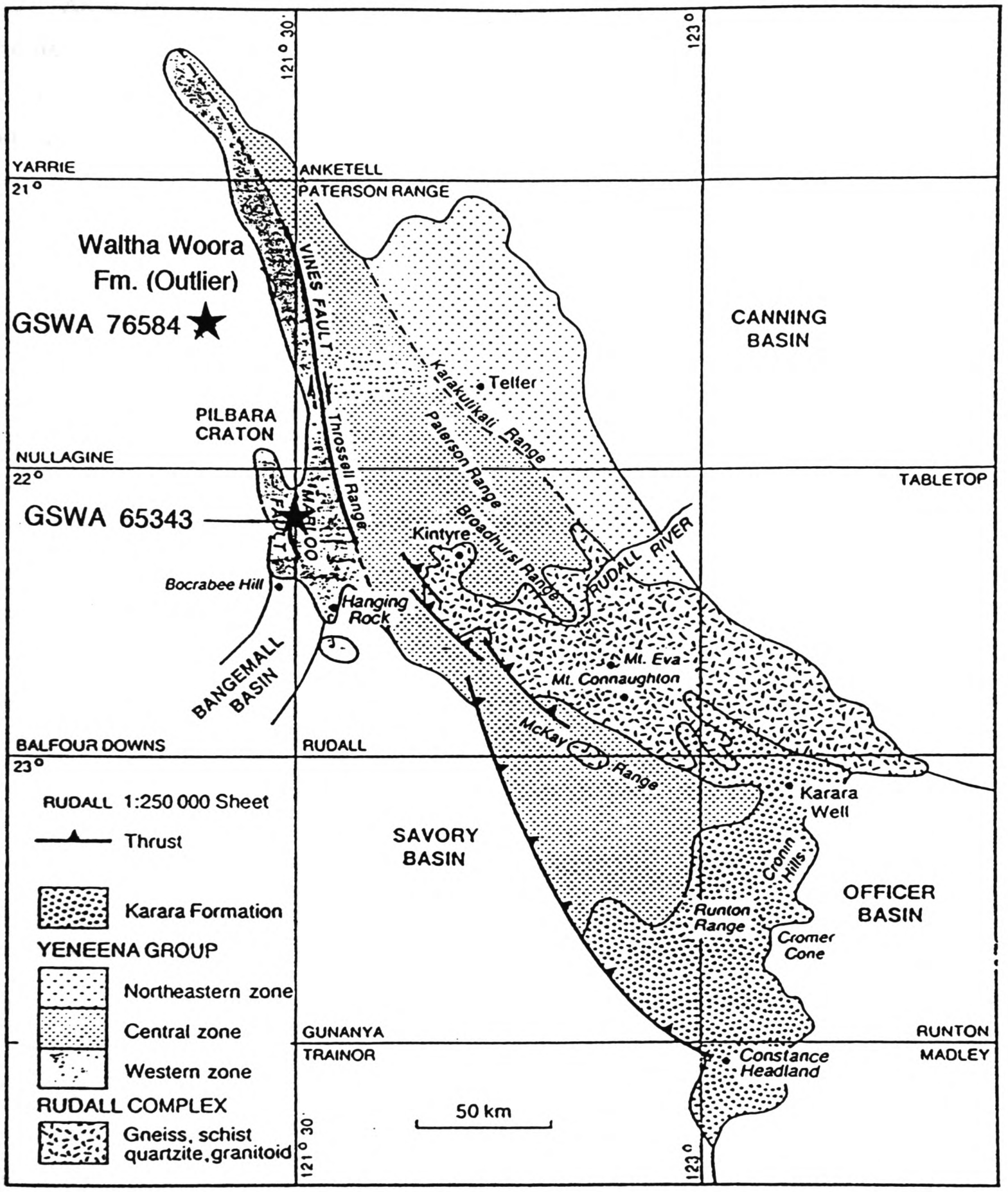

Figure 2.6.2: Localities for stromatolite samples from the Yeneena Basin, Western Australia

2.6.3: *AGE CONSTRAINTS*

As is the case for most Proterozoic sedimentary basins in Western Australia, the depositional age of the Yeneena Basin is poorly constrained. Chin & de Laeter (1981) published an Rb-Sr date of 1333 ± 44 Ma (initial $^{87}Sr/^{86}Sr$ ratio of 0.7869) for retrograded gneisses from the Rudall Complex and a date of 1132 ± 21 Ma for pegmatitic veins post-dating gneiss deformation. The authors suggested that the former represented the age of metamorphism of the Rudall Complex and that the latter corresponded to the age of deformation of Yeneena Group sediments. In addition, Yeneena sediments unconformably overlie deposits of the Manganese Subgroup in the Bangemall Basin which has an inferred age of 1.2-1.0 Ga (see section **2.5**), apparently constraining deposition to between 1.2 and 1.1 Ga. However, Pb model ages for supposedly syngenetic galenas from the Broadhurst Formation have values between 750 and 900 Ma and dolerite sills that intrude the sediments of the central zone have yielded poor 700-750 Ma Rb-Sr isochrons. Moreover, the Yeneena Group is unconformably overlain by the Savory Basin which contains glacigene sequences similar to those in the Amadeus Basin dated at 750 and 690 Ma and the late tectonic Mount Crofton Granite, whose intrusion marked the culmination of the Paterson Orogen, has been dated at 688 ± 32 Ma by Goellnicht et al. (1988). Consequently, the balance of evidence suggests that the Yeneena Group has a somewhat larger depositional age range of between ?1200 and 750 Ma.

2.6.4: *FORMATIONAL PETROGRAPHY AND SEDIMENTOLOGY*

In the western zone of the Yeneena Basin the sedimentary sequence remains unmetamorphosed and six formations are recognised, reflecting a cyclicity of conditions between shallow water deposition of terrigenous clastics (Googhenama, Brownrigg Sandstone and Choorun Formations) and carbonates (Waroongunyah, Yandanunyah and Isdell Formations). The general environment of deposition is considered to be a shallow marine stable shelf (Williams, 1990c).

The Isdell Formation is the only formation to be recognised in all three zones and it contains small non-determined, branching-columnar, carbonate stromatolites (GSWA 65343) that have been correlated with similar forms in the outlying Waltha Woora Formation (GSWA 76584) 70 km to the north (see **Figure 2.6.2**) (Grey, unpublished data). The available samples are typical of the western zone and have had simple structural and metamorphic histories.

Below the Isdell Formation in the central zone, three formations are recognised; the basal fluvial Coolbro Sandstone; the shallow marine Broadhurst Formation, which has both clastic and carbonate components with extensive Cu, Pb, Zn and Au mineralisation and the unstable shelf sediments of the Choorun Formation (Chin et al., 1980). Deposits of the central zone show variable, low grade regional metamorphism that tends to decrease in grade upsection and westwards.

In the northeastern zone, the Isdell Formation is the lowest exposed member of the Yeneena Group and is succeeded by alternating clastic (Malu Quartzite, Wilki Quartzite) and carbonate-rich shelf deposits (Puntapunta and Kaliranu Formations). The Telfer Formation is transitional and hosts significant Au accumulations. The overall sequence preserves the marine deposits of a slowly subsiding shallow basin and the low grade regional metamorphism is locally overprinted by high temperature contact metamorphism from intrusive granitoids.

The structural styles of the three zones are distinct; sediments of the western zone are broadly folded and faulted, with a general easterly dip; those of the central zone show numerous long, parallel, tight asymmetrical folds with gently plunging axes trending in a northwesterly direction and those of the northeastern zone demonstrate abundant 'dome-and-basin' structures as a result of short folds with double-plunging axes arranged *en echelon*.

2.6.5: *RESULTS*

Pb isotopic results for Yeneena Group stromatolites are listed in **Table 2i** and presented graphically in **Figure 2.6.3**. Analyses of GSWA 65343 show little Pb isotopic variation and are of little use for age determination. Similarly, analyses of HCl-soluble components of GSWA 76584 demonstrate little isotopic variation, but if one considers the analyses of HCl-insoluble residues in addition, the range is considerably enhanced and the complete 76584 data set defines a Pb/Pb isochron date of 988 ± 120 Ma with an MSWD of 1.74, and a model μ_1 value of 8.23 ± 0.06. The residue analyses were considerably less radiogenic than the corresponding carbonate analyses.

Table 2i: Pb isotopic compositions of carbonate stromatolites from the Yeneena Group, Yeneena Basin (GSWA 65343, 76584)

SAMPLE	CORRECTED RATIOS *		
	$^{206}Pb/^{204}Pb$	$^{207}Pb/^{204}Pb$	$^{208}Pb/^{204}Pb$
	Yeneena Group, Isdell Formation		
65343	20.522 ± 0.030	15.939 ± 0.040	41.241 ± 0.228
65343 a	20.708 ± 0.022	15.904 ± 0.020	41.462 ± 0.052
65343 b	21.263 ± 0.020	16.012 ± 0.024	42.311 ± 0.066
65343 d	20.947 ± 0.024	15.910 ± 0.030	41.819 ± 0.090
65343 e	21.272 ± 0.018	15.933 ± 0.046	42.270 ± 0.106
65343 f	20.957 ± 0.018	15.948 ± 0.028	41.867 ± 0.070
65343 g	20.937 ± 0.018	15.972 ± 0.022	41.904 ± 0.062
65343 h	21.164 ± 0.036	15.981 ± 0.024	42.387 ± 0.060
	Yeneena Group, Waltha Woora Formation (outlier)		
76584	27.685 ± 0.044	16.308 ± 0.020	52.263 ± 0.064
76584 A	26.368 ± 0.022	16.236 ± 0.020	51.694 ± 0.064
76584 AR	20.574 ± 0.022	15.794 ± 0.024	41.264 ± 0.074
76584 B	26.346 ± 0.022	16.231 ± 0.020	52.331 ± 0.064
76584 BR	20.698 ± 0.022	15.830 ± 0.020	41.549 ± 0.054
76584 C	26.079 ± 0.022	16.224 ± 0.020	51.419 ± 0.064
76584 D	26.373 ± 0.022	16.231 ± 0.022	51.141 ± 0.068
76584 E	26.451 ± 0.022	16.235 ± 0.020	51.660 ± 0.064

* Corrected for mass fractionation of 0.130% ± 0.012 ($2\sigma_{mean}$) amu^{-1}
Errors are $2\sigma_{mean}$ for corrected ratios
R Indicates isotopic analysis of HCl-insoluble residue of relevant sample

Thin sections were unavailable for GSWA 65334, but 76584 shows small, red-brown, laminated stromatolite columns, approximately 4 cm x 1 cm with a 1 mm lamination. Inter-columnar areas are composed of carbonate-cemented quartz packestone of somewhat lighter colour due to less intense haematitic staining from late, cross-cutting, iron oxide-rich stylolites. Despite the microstructure being obscured by carbonate recrystallisation, the sedimentary textures and fabric are well preserved, suggesting that any metamorphic activity in the region was extremely limited.

Figure 2.6.3: Pb isotopic data for carbonate stromatolites from the Yeneena Group, Yeneena Basin (GSWA 76584, 65343)

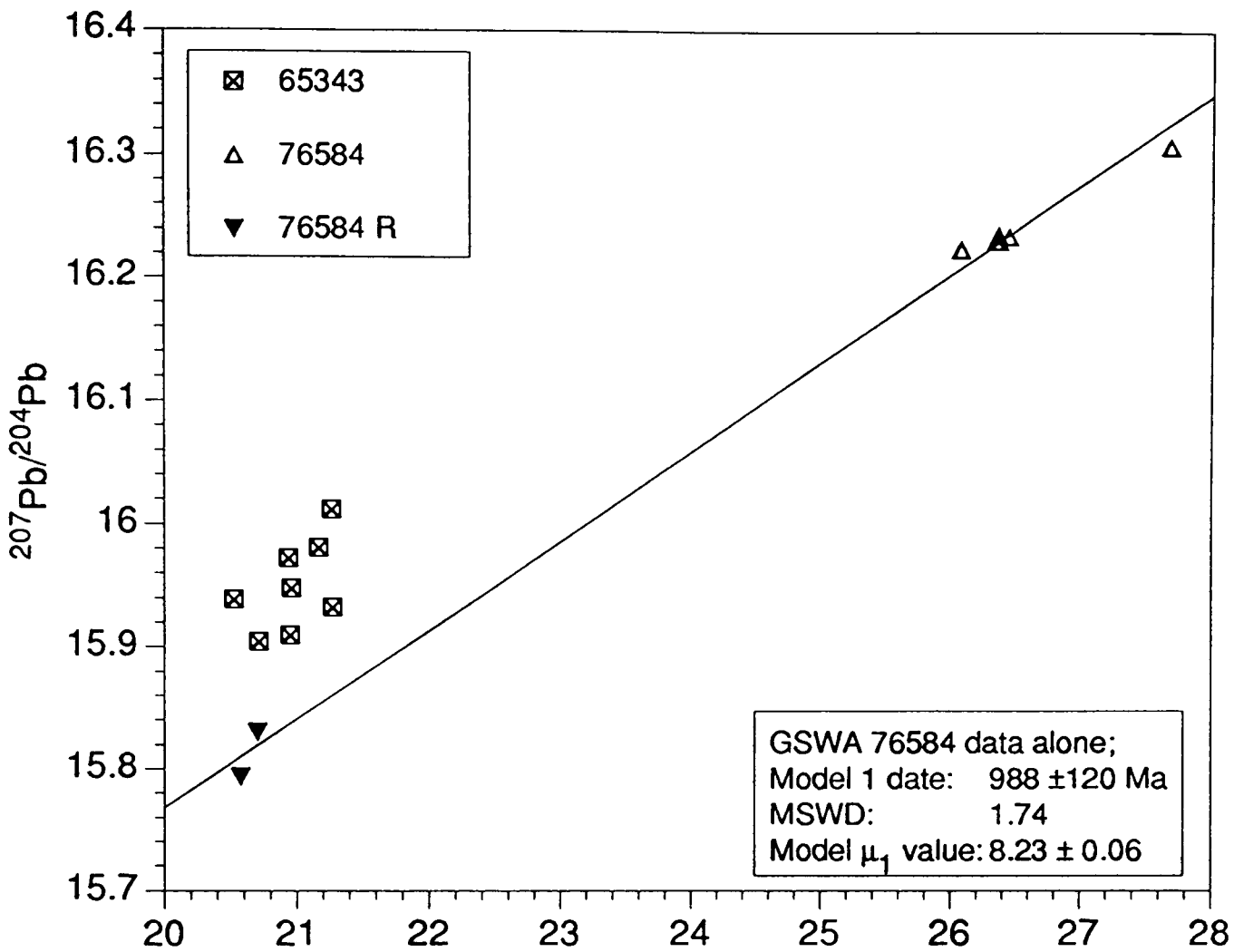

Stable isotopic data for the two samples are both limited and variable. Specimen 76584 returned $\delta^{13}C$ compositions of -0.66 and -2.46‰ and $\delta^{18}O$ values of -5.43 and -4.14‰ respectively, while 65343 had more negative $\delta^{13}C$ compositions of -3.70 and -3.80‰ and $\delta^{18}O$ values of -6.51 and -14.66‰.

2.6.6: *DISCUSSION*

The Yeneena Group has a depositional age range of ?1200-750 Ma. A date of 988 ± 120 Ma for GSWA 76584 from the Isdell Formation is consistent with these constraints and interpreted as the age of diagenetic recrystallisation from the petrographic and stable isotopic evidence. The figure approximates to the depositional age within the scale of the quoted errors and these conclusions therefore imply that the 1132 ± 21 Ma date of Chin & de Laeter (1981) for pegmatites cutting the Rudall Complex does not correspond to the age of deformation of Yeneena Group sediments.

GSWA 76584 carbonate and residue were apparently part of the same system at isotopic closure (shown by the fact that they plot along the same isochron) and combination of the two data subsets enhances the isotopic range and precision of

the regressed date. The fact that the residue analyses were less radiogenic than the corresponding carbonate analyses, while GSWA 99429 red residue analyses were distinctly more radiogenic (see section **2.4.5**) is an intriguing problem which is addressed in section **2.8** and again in **Chapter 6**.

GSWA 65334 either possessed very little variation of *in situ* μ values at isotopic closure or suffered significant U loss through diagenesis producing an extremely limited Pb isotopic range with significant data scatter from which age data could not be obtained. Variable negative $\delta^{18}O$ and negative $\delta^{13}C$ compositions imply that the latter was more likely.

2.7: SAVORY BASIN

2.7.1: *INTRODUCTION*

The Savory Basin outcrops over an area of 33000 km^2 to the southeast of the Archaean Pilbara Craton. The sole lithostratigraphic unit is the Savory Group, a sequence of shallow water marine, fluvial and glacigene deposits that unconformably overlies the Paterson Orogen to the northeast and Bangemall Basin to the west (see **Figure 2.1.1**).

2.7.2: *STRATIGRAPHY*

The sediments of the Savory Basin unconformably overlie deposits of the Middle Proterozoic Bangemall Basin to the northwest, west and south (Manganese, Collier and Kharban Subgroups respectively), the Bangemall inlier of Cornelia Sandstone and the Paterson Orogen deposits of the Yeneena Basin to the northeast. In turn, they are unconformably overlain by the Phanerozoic Officer Basin to the east.

The Savory Group is divided into western and eastern zones that are separated by large areas of non-exposure (**Figure 2.7.1**). Consequently, the two zones have developed independent stratigraphies and it is difficult to correlate between them. Carbonate stromatolites were available from the Boondawari Formation of the western zone (GSWA 91651) and the Skates Hills Formation of the eastern zone (GSWA 41658) (see **Figure 2.7.2**).

Figure 2.7.1: Stratigraphy of the Savory Basin, after Williams (1990b)

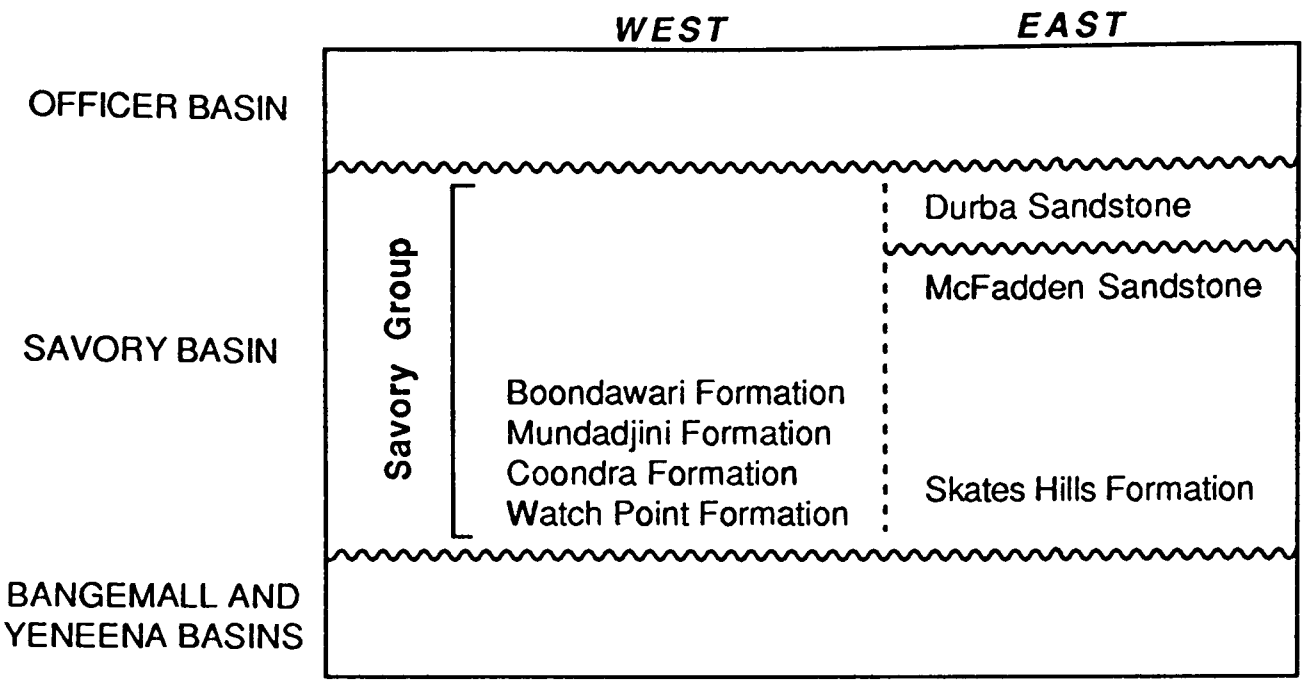

2.7.3: *AGE CONSTRAINTS*

Very few direct age determinations are available for the Savory Group but since the basin unconformably overlies the Yeneena Group its age is probably younger than c.800 Ma, that is Late Proterozoic. Indeed, the Skates Hills Formation has been biostratigraphically correlated with the 815-825 Ma Loves Creek Member of the Bitter Springs Formation in the Amadeus Basin from stromatolite evidence (Williams, 1992; Grey, pers. comm. 1992). Unpublished data for a dolerite intrusion in the Boondawari Formation give an Rb-Sr date of 640 Ma (Williams, pers. comm. 1991) and the same formation has been compared with a glacigenic sequence in the Amadeus Basin, central Australia dated around 670 Ma. From this limited evidence, Williams (1992) proposed that the Savory Basin had an age range of 890-610 Ma.

2.7.4: *FORMATIONAL PETROGRAPHY AND SEDIMENTOLOGY*

The four formations of the western Savory Basin represent shallow water marine and deltaic deposits. Interbedded shale and siltstone of the Watch Point Formation occurs with fine grained sandstone in a coarsening-upward sequence typical of distal turbidites. These deposits are succeeded by the high energy conglomeratic debris flow deposits of the basal Coondra Formation and the deltaic, medium grained sandstone and channelised conglomerates of the upper Coondra Formation. The Mundadjini Formation contains pseudomorphs of halite and gypsum in fine grained sandstone that also exhibits abundant ripple marks. Associated dolomite lends weight to interpretation as a nearshore, shallow marine to tidal-flat,

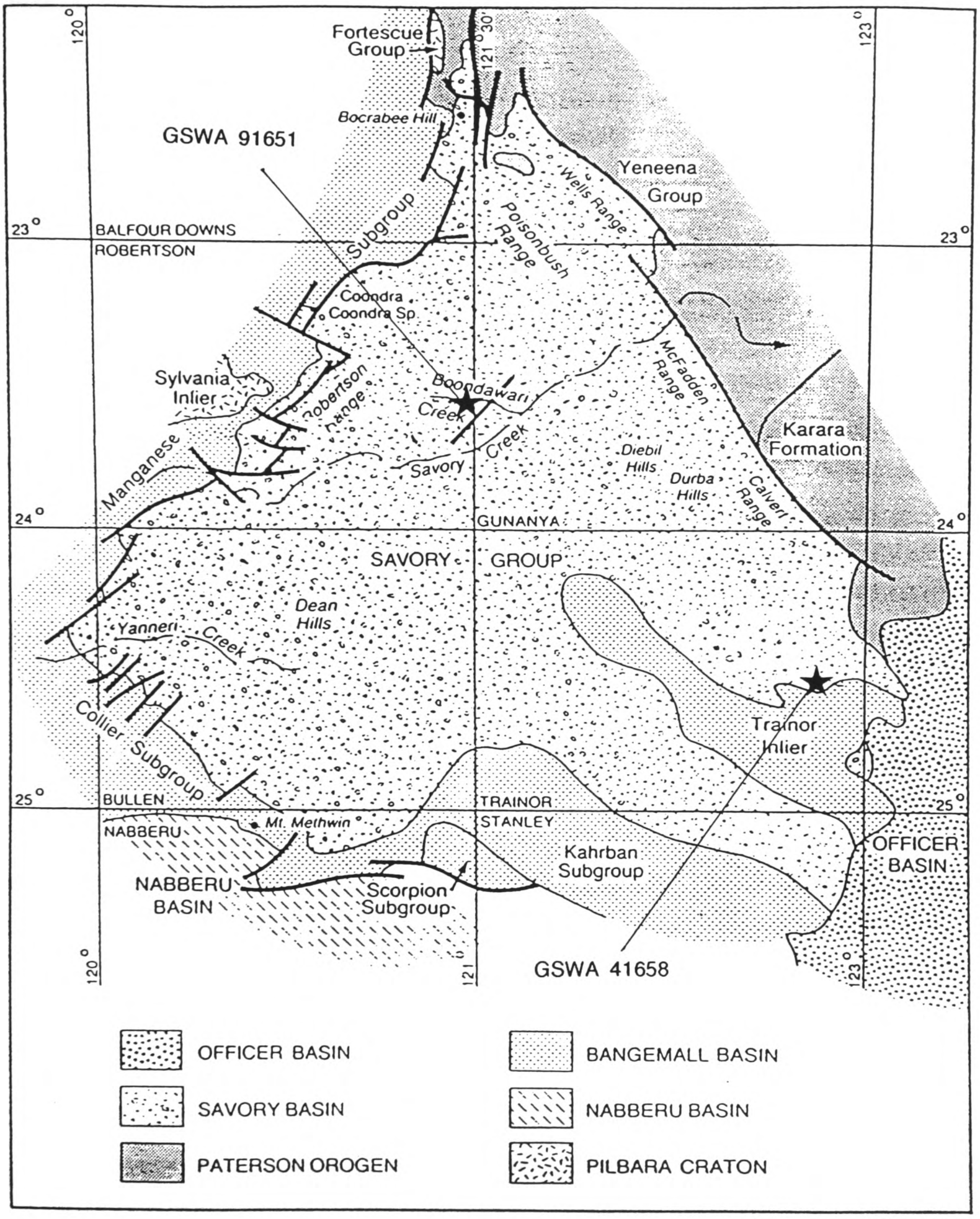

Figure 2.7.2: Localities for stromatolite samples from the Savory Basin, Western Australia

lagoonal and evaporitic sequence. Deposition of the Boondawari Formation marked a distinct environmental change with coarse glacigenic diamictite horizons interbedded with sandstone, shale and dolomite containing stromatolites of undetermined form (GSWA 91651).

The basal formation of the eastern Savory Basin is the Skates Hills Formation, a shallow water clastic sequence of conglomerate, sandstone siltstone and shale that is capped by a stromatolitic dolomite containing *Acaciella* cf. *australica* Walter 1972 (GSWA 41658). The stromatolite occurs as small, straight, regularly spaced, dolomitic columnar forms, 10-25 mm across and generally lacking wall development. Bridging and branching are locally common. Microlaminae are variable in regularity and thickness but tend to be continuous across columns. The Mundadjini Formation of the western Savory Basin and the Bitter Springs Formation of the Amadeus Basin are inferred to be equivalent. The overlying McFadden Sandstone is interpreted by Goode & Hall (1981) as representing a prograding delta-front advancing into a shallow marine basin and consists of cross bedded quartz sandstone with minor conglomerate, siltstone and shale. It is unconformably overlain by the Durba Sandstone, a quartz sandstone probably derived from erosion of the McFadden Sandstone.

In general, the Savory Group dips gently away from the basin margins which are mostly faulted. 'Dome-and-basin' interference structures resulted from interaction of southwest and northwest-trending open folds. Faulting within the basin has a dominantly northeastern trend, whereas marginal faulting is more complex with listric growth faults possibly being reactivated in the Robertson Fault System as thrusts displacing Savory Group sediments onto the northwestern foreland.

2.7.5: *RESULTS*

Limited results for stromatolites from the Savory Group are listed in **Table 2j** and plotted in **Figure 2.7.3** overleaf. Although just one Pb isotopic analysis was available for GSWA 91651, the four carbonate analyses and one residue analysis for GSWA 41658 define a poor Pb/Pb errorchron whose slope corresponds to a date of 1058 ± 470 Ma with an MSWD of 7.73 and a model μ_1 value of 8.17 ± 0.26). Again, it should be noted that the residue analysis was distinctly less radiogenic than the corresponding carbonate analysis and its inclusion served to increase the Pb isotopic range.

Table 2j: Pb isotopic compositions of carbonate stromatolites from the Savory Group, Savory Basin (GSWA 41658, 91651)

SAMPLE	CORRECTED RATIOS *		
	$^{206}Pb/^{204}Pb$	$^{207}Pb/^{204}Pb$	$^{208}Pb/^{204}Pb$
	Savory Group, Skates Hills Formation		
41658 A	27.952 ± 0.028	16.306 ± 0.020	46.042 ± 0.122
41658 AR	19.948 ± 0.034	15.733 ± 0.044	37.866 ± 0.286
41658 B	27.606 ± 0.040	16.298 ± 0.026	45.823 ± 0.164
41658 D	26.508 ± 0.040	16.281 ± 0.030	45.441 ± 0.244
41658 F	27.034 ± 0.036	16.259 ± 0.028	44.585 ± 0.220
	Savory Group, Boondawari Formation		
91651	19.015 ± 0.018	15.765 ± 0.020	39.222 ± 0.124

* Corrected for mass fractionation of 0.130% ± 0.012 ($2\sigma_{mean}$) amu^{-1}
Errors are $2\sigma_{mean}$ for corrected ratios

Figure 2.7.3: Pb isotopic data for carbonate stromatolites from the Savory Group, Savory Basin (GSWA 91651, 41658)

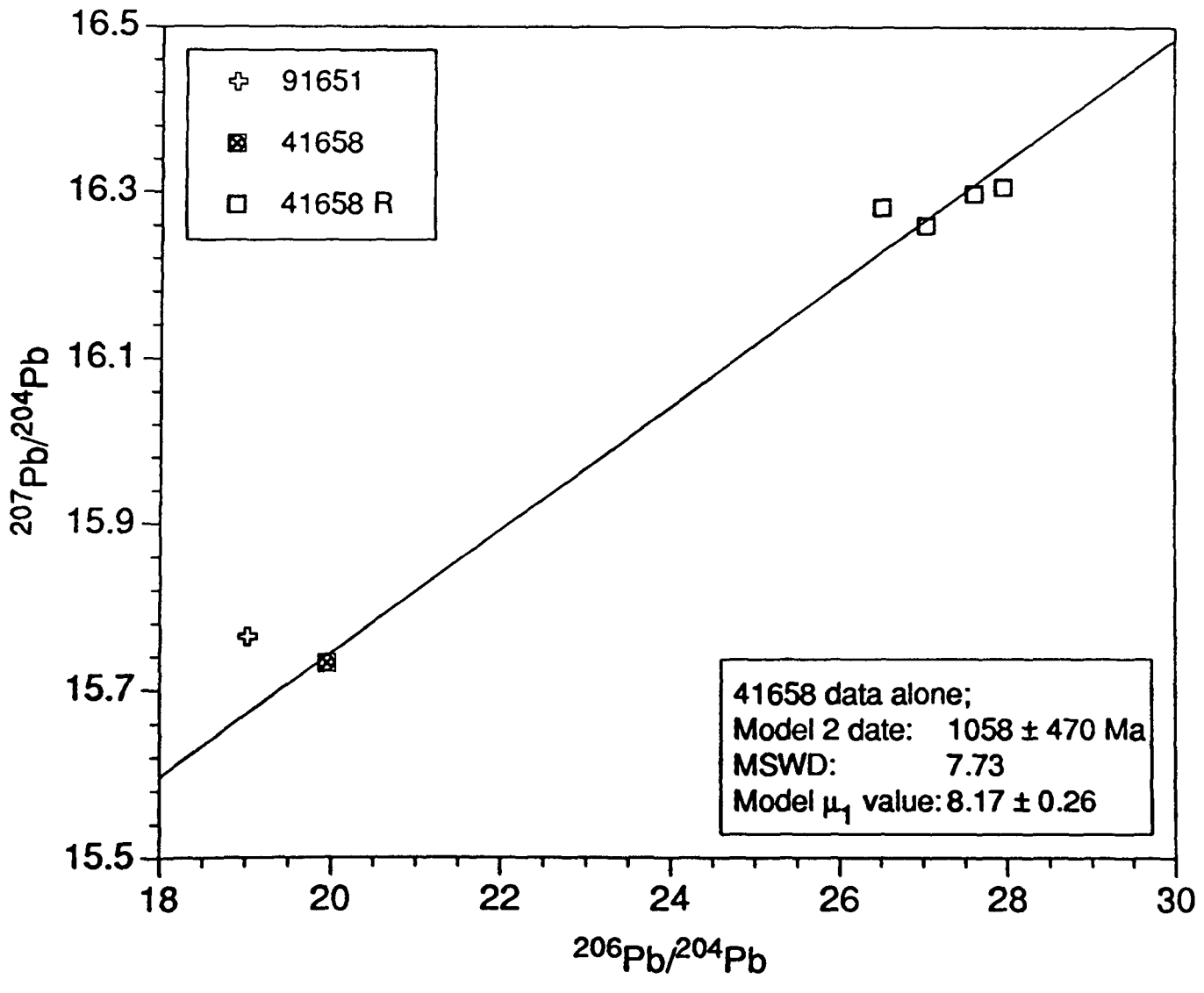

2.7.6: *DISCUSSION*

Although the date of 1058 ± 470 Ma is consistent with the inferred depositional age of the Savory Basin (890-610 Ma), the very large errors mean that it has limited chronostratigraphic value. Further work would be required to more accurately constrain the date before the question of its geological significance could be addressed, but it is reassuring to observe that the date is of the correct magnitude.

2.8: CONCLUSIONS

In this study the Pb/Pb method has been applied successfully to the direct dating of a number of Precambrian carbonate stromatolites from Western Australia. Where useful age data have been obtained, the precision of the Pb/Pb date characteristically represents a significant improvement on existing age constraints from published geochronological studies for related rocks. Revised depositional age ranges for lithostratigraphic groups and basins are presented in **Figure 2.8.1**, alongside the previously inferred depositional ages (largely after Myers & Hocking, 1988, who based their values on selected radiometric data plus local biostratigraphic, tectonic and other qualitative considerations) and indirect geochronologic constraints from published dates for associated rocks.

The combined date of 1778 ± 27 Ma (model μ_1 value 8.43 ± 0.11) for stromatolites from the Duck Creek Dolomite of the Wyloo Group is consistent with individual regressions of GSWA 88032 and 46207 data, but younger than the inferred depositional age range for both the formation (?2.0-1.89 Ga) and the basin (?2.5-1.843 Ga) (see section **2.2**). This date is interpreted as the age of metamorphically induced recrystallisation and represents a new minimum depositional age for the Ashburton Basin.

A major revision of the depositional age and therefore inter-basinal correlation of the Nabberu Basin is proposed. Deposition of the Glengarry Group was inferred to have occurred between 2.0-1.8 Ga and the Earaheedy Group between 1.8-1.6 Ga, although published radiometric data only constrain the age of the Nabberu Basin to between 2.5-1.63 Ga (see section **2.3**). Concordant Pb/Pb dates of 2008 ± 68 Ma (model μ_1 value 8.62 ± 0.15) and 1946 ± 71 Ma (model μ_1 value 7.16 ± 1.59) for GSWA 46589 and 84767 from the Yelma Formation of the Earaheedy Group are interpreted as early diagenetic and imply that deposition of the group commenced nearer 2.0 Ga.

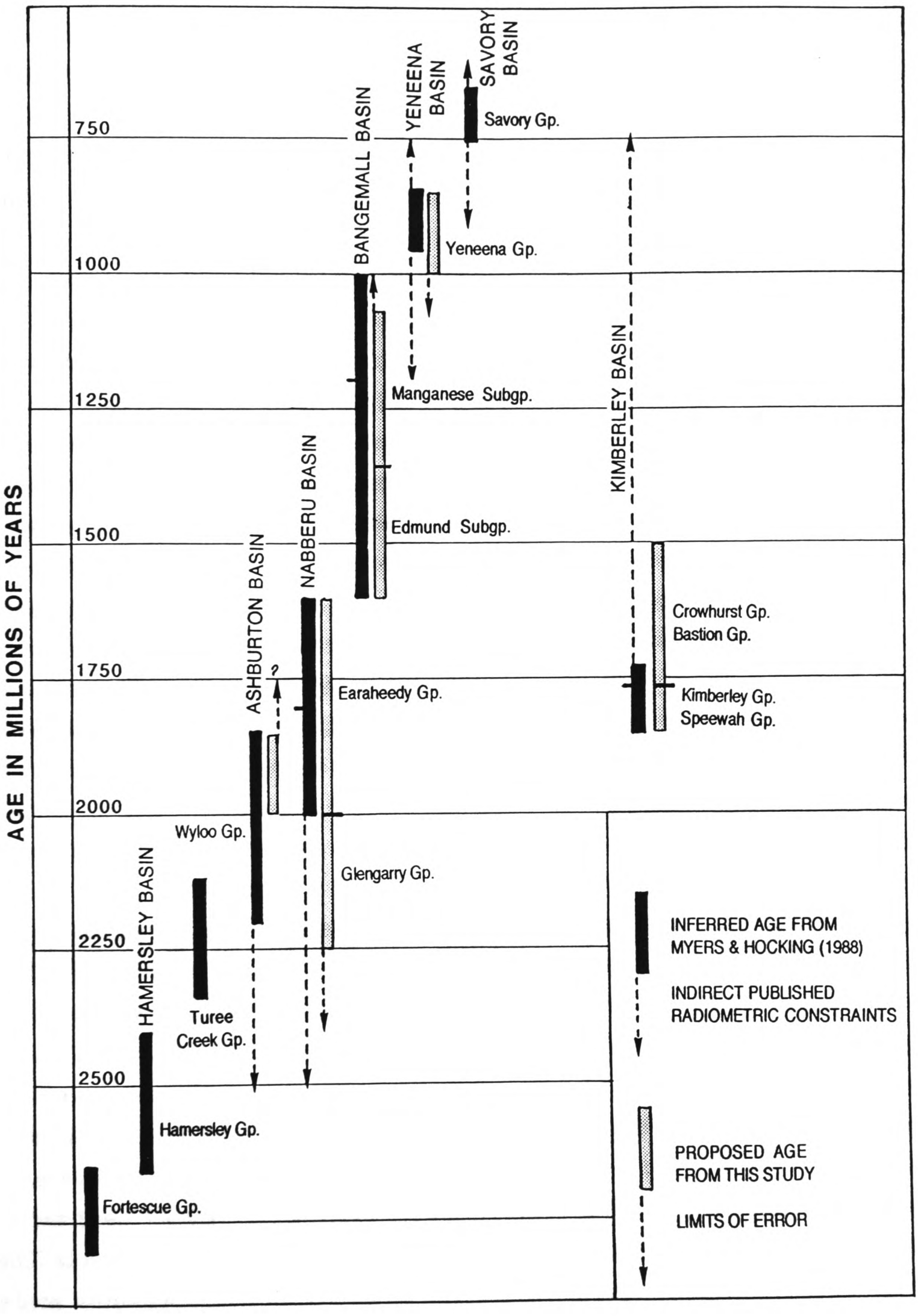

Figure 2.8.1: Proposed depositional ages for selected Precambrian lithostratigraphic units from Western Australia

An early diagenetic age of 2258 ± 180 Ma (model μ_1 value 8.38 ± 0.03) for GSWA 88091 from the basal Glengarry Group is stratigraphically consistent with the new Earaheedy Group data and implies that Glengarry deposition may have commenced as early as 2.4 Ga. If the inferred 2.0 Ga maximum age for the Ashburton Basin is correct, much of the Earaheedy Group may be correlated with the Ashburton Basin, while the Glengarry Group is somewhat older.

While bracketing ages for the entire Kimberley Basin are imprecise (1.84-0.67 Ga), the basal Speewah and Kimberley Groups are more tightly constrained to between 1.84-1.76 Ga (see section **2.4**). An imprecise Pb/Pb date of 2133 ± 440 Ma (model μ_1 value 7.94 ± 0.34) for GSWA 46285 from the Kimberley Group is within error consistent with these values but further data are required. The Bastion and Crowhurst Groups are younger than 1.76 Ga but their minimum age is poorly constrained. A date of 1509 ± 90 Ma (model μ_1 value 8.25 ± 0.04) for all available data from carbonate stromatolite GSWA 99429 (uppermost Hibberson Dolomite) is interpreted as the age of diagenetic recrystallisation and therefore provides a minimum age for deposition of the Kimberley Basin. Consequently, the Speewah and Kimberley Groups are correlated with parts of the Wyloo Group in the Ashburton Basin (?Duck Creek Dolomite) and possibly the Miningarra Subgroup of the Earaheedy Group, Nabberu Basin but they are distinctly younger than the Glengarry Group of the Nabberu Basin. The Bastion and Crowhurst Groups may correlate with the youngest Earaheedy Group sediments, but this is not certain.

The Bangemall Basin is divided into older units inferred to be between 1.6-1.2 Ga and younger units inferred to be between 1.2-1.0 Ga (see section **2.5**). All available data from the younger Manganese Subgroup (GSWA 65334 and 31000) yield a Pb/Pb date of 1314 ± 150 Ma (model μ_1 value 8.40 ± 0.12) which is interpreted as the age of early diagenetic recrystallisation. Coupled with an unpublished Rb-Sr glauconite date of 1.331 Ga for the Manganese Subgroup (Williams, pers. comm. 1991), this suggests that the boundary between the two age groups should be placed at c.1.35 Ga rather than 1.2 Ga. All available data from the older Edmund Subgroup (GSWA 46073J and 46009) define a tenuous date of 1436 ± 230 Ma (model μ_1 value 8.41 ± 0.03), which although based on a restricted sample set, is reassuringly consistent with independent constraints. All of the available Bangemall Basin data from both age groups define an average value for the basin of 1304 ± 66 Ma (model μ_1 value 8.41 ± 0.03), confirming the deposits as Middle Proterozoic. The older Bangemall Basin lithostratigraphic units are younger than the Nabberu Basin but may correlate with the Crowhurst Group of the Kimberley Basin.

A diagenetic recrystallisation age of 988 ± 120 Ma (model μ_1 value 8.23 ± 0.06) for GSWA 76584 from the Isdell Formation is consistent with poorly defined age constraints for the Yeneena Basin (?1.2-0.75 Ga) (see section **2.6**). Yeneena sediments unconformably overlie the Bangemall Basin.

Unfortunately, it was not possible to improve the 0.89-0.61 Ga constraints for the Savory Basin from the limited Pb isotopic data available for GSWA 41658 and 91651 (see section **2.7**). An imprecise date of 1058 ± 470 Ma (model μ_1 value 8.17 ± 0.26) for GSWA 41658 is within error of these figures but requires further analytical results to be of stratigraphic value.

These results are a clear indication that Pb/Pb techniques may be used for the direct age determination of ancient stromatolitic carbonates. Pb/Pb age constraints for basins and lithostratigraphic groups are broadly consistent with inferred depositional ages and in many cases permit greater resolution. The resultant potential for Precambrian time scale calibration is self-evident. The chronometric regional correlation of basins, groups and even formations that direct dating permits should allow a critical assessment of the validity of Precambrian stromatolite and microfossil biostratigraphies to be made. Preliminary data from Western Australia suggest that micropalaeontology will prove to be the more reliable as the number of dated microfossiliferous localities increases. Stromatolite form may be used for purposes of relative correlation, but environmental sensitivity means that inferred chronometric constraints could be highly suspect.

Combination of data from the same stratigraphic horizon, formation, group or even basin frequently serves to enhance both the Pb isotopic range and precision of the regressed date. For such an approach to be justified, the model μ_1 values and dates for individual sample set regressions and the total data set should be within error. Pb isotopic ranges were also enhanced in the cases of GSWA 46285, 99429 and 41658 by the inclusion of HCl-insoluble residue analyses which tended to have isotopic compositions distinct from the carbonate data, although systematic carbonate-residue behaviour was not observed. Potential causes for this phenomenon are discussed in **Chapter 6**.

Model μ_1 values have been quoted for all data regressions. Full derivation of the model μ_1 value is given in **Appendix A.6**, but it can be thought of as the $^{238}U/^{204}Pb$ ratio of a source region normalised for U decay to the present day. In the case of

igneous or metamorphic rocks the concept of a source region is clear and definable but for sediments, and carbonates in particular, the source of elemental U and Pb is uncertain and it may be that some combination of detrital, authigenic, early and late diagenetic processes operates to produce an average $^{238}U/^{204}Pb$ value (see discussion in **Chapter 6**). Consequently, absolute model μ_1 values for carbonate stromatolites can not be used in any quantitative fashion. Where values differ significantly, one may infer distinct geological histories, as is the case for GSWA 46285 and 99429 from the Kimberley Basin (model μ_1 values of 7.94 ± 0.34 and 8.25 ± 0.04 respectively, see section **2.4**), but since model μ_1 values for Western Australian carbonate stromatolites generally fall in the 8.2-8.7 range, more detailed conclusions are not possible.

The reason why many carbonate stromatolites make highly suitable sample materials for Pb/Pb dating has not yet been satisfactorily explained in the literature. For many stromatolites, measured radiogenic Pb isotopic compositions coupled with large compositional ranges signify that high, variable *in situ* μ values (μ_2 values) must have existed on a sub-centimetre scale at the point of isotopic closure. This might be explained by variable U concentrations, Pb concentrations or both. For other stromatolites, unradiogenic Pb isotopic compositions and extremely limited compositional ranges may signify similar low *in situ* μ_2 values or reflect later geochemical disturbance and homogenisation. A general geochemical model is proposed and discussed in **Chapter 6**.

It is evident from studies of Western Australian stromatolites that the identification of stromatolitic samples which show promise for Pb isotopic dating is not possible using standard petrographic or stable isotopic techniques. The majority of rapid analytical techniques (S.E.M., I.C.P., cathodoluminescence and proton probe) are also unsuitable because of the low elemental concentrations involved (usually < 5 ppm Pb for most stromatolites). Consequently, full Pb isotopic analysis seems to be the most effective means of determining a particular sample's dating potential. Two or three analyses of each specimen will provide an indication of both the Pb isotopic composition and any isotopic variation, permitting the selection of promising samples (those with significant colinear isotopic variation) for continued investigation.

Chapter 3:

INDIAN ARCHAEAN CARBONATES

3.1: INTRODUCTION

The Dharwar Supergroup, a system of late Archaean volcanosedimentary basins, is well exposed in the state of Karnataka, southern Peninsular India. Petrologic evidence and way-up criteria indicate that deposition occurred on a sialic basement of Archaean Peninsular Gneiss (tonalitic to granitic polyphase gneisses and charnockites) and older Sargur Group supracrustals (quartzites, aluminous metasediments, banded iron formations, amphibolites and ultramafic schists; Naqvi et al., 1978) in an intracratonic or continental margin setting (Chadwick et al., in press).

The Karnataka Craton is subdivided on the basis of metamorphic grade. The southern region, a high grade granulite facies terrain, is separated from the northern region with its greenschist to lower amphibolite facies rocks by an E-W prograde transition that cuts the dominant N-S structural trend (see **Figure 3.1.1**).

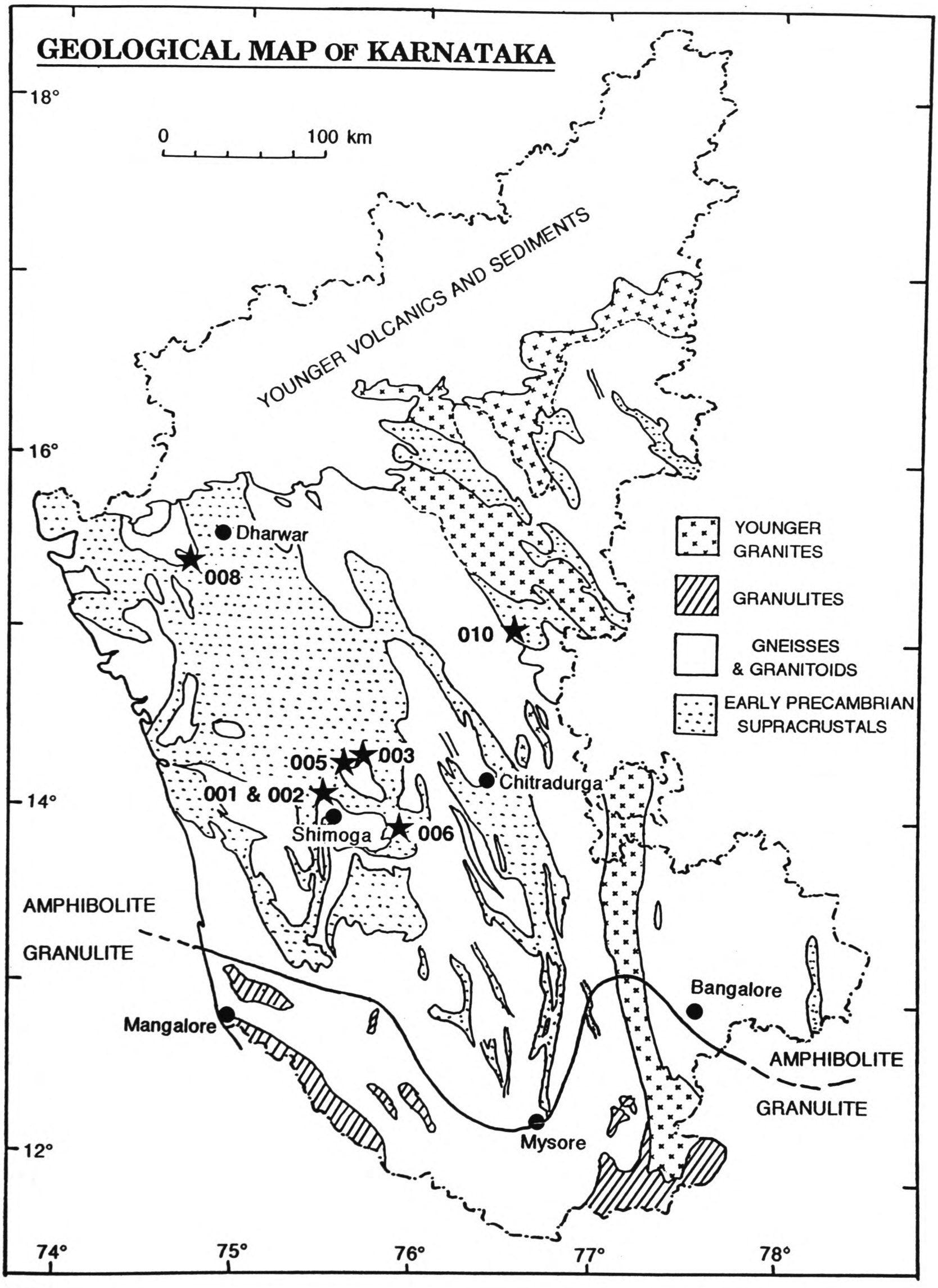

Figure 3.1.1: Geological map of Karnataka, western India, including localities for carbonate samples

The northern region is further subdivided. Low temperature mineral assemblages (chlorite, biotite, garnet and green amphibole with rare chloritoid and kyanite) characterise the late Archaean supracrustals west of the mylonitic belt that forms the eastern boundary of the Chitradurga Schist Belt (Chadwick et al., in press) (see **Figure 3.1.1**), while high temperature assemblages (andalusite, sillimanite and cordierite) dominate the restricted Late Archaean supracrustal outcrops to the east.

The Peninsular Gneiss basement in the west contains abundant epidote, chlorite and carbonate, indicating the involvement of CO_2-rich fluids in a low temperature retrogressive event. In the east, basement gneisses show evidence for partial melting and intrusion by Late Archaean granites, for example the enigmatic Closepet Granite which is exposed in a N-S tract that echoes the strike of the supracrustal associations (Chadwick et al., in press).

The Sargur supracrustals are older than the tonalitic-granitic association that forms much of the Peninsular Gneiss but evidence for their internal stratigraphy, age and original basement is lacking. Medium to high grade metamorphism of the Sargur supracrustals occurred during intrusion of the polyphase Peninsular Gneiss and this was followed by cooling, uplift and erosion leading to the unconformable deposition of Dharwar Supergroup supracrustals.

A second lower grade metamorphism affected the deformed Dharwar deposits in central Karnataka and caused partial retrogression of pre-Dharwar metamorphic assemblages in Sargur deposits (Drury & Holt, 1980). Elsewhere in Peninsular India, high grade Late Archaean metamorphism was occurring at this time. Evidence for the post-Archaean metamorphic history found in high grade terrains elsewhere in India has not been documented thus far in the low grade rocks of Karnataka. Proterozoic dolerite dykes intrude the low grade deposits of central Karnataka, which themselves form the basement to the Proterozoic basins of Cuddapah in the east and Kaladgi-Bhima in the northwest.

Chapter 3 investigates the application of direct Pb/Pb dating to Late Archaean marbles from the Dharwar Supergroup. In collaboration with Dr.B.Chadwick of the University of Exeter and Dr.B.Krishna Rao of the University of Mysore, whose assistance is gratefully acknowledged, a suite of seven carbonate samples was analysed from inferred equivalent stratigraphic horizons within the Chitradurga and Sandur Schist Belts, Karnataka. Sample localities are given in **Figure 3.1.1**.

3.2: STRATIGRAPHY OF THE DHARWAR SUPERGROUP

The Dharwar Supergroup outcrops within the low grade metamorphic terrain of Karnataka State and comprises the basal Bababudan Group, the overlying Lower Chitradurga Group and the topmost Upper Chitradurga Group (Swami Nath et al., 1976), as illustrated in **Figure 3.2.1**. Way-up criteria within the volcanosedimentary succession indicate that there has been no significant tectonic disruption of the sequence.

The Bababudan Group is up to 7500 m thick and consists in the main of carbonate bearing metavolcanics interbedded with orthoquartzites, phyllites and banded ferruginous cherts that unconformably overlie basement granodiorite of the Peninsular Gneiss. The unconformity is marked by the Kartikere Conglomerate which was sourced from the west (Fareeddudin et al., 1988). Pillow structures indicate that some of the precursor basalts originated by subaqueous eruption and the interpretation of a marine setting is reinforced by wave and current ripples, cross bedding and water escape structures found in interbedded orthoquartzites. Limited occurrences of acid volcanics are found at Bababudan and northeast of the Honnali Dome.

The Lower Chitradurga Group comprises shallow marine and alluvial facies that suggest a gradual northwards shift of depocentre with time and indicate a generally unstable depositional environment. Typical deposits are polymict conglomerates, cross bedded and ripple marked orthoquartzites, phyllites showing lamination and evidence for soft sediment deformation, cherty laminated limestones, sandy limestones and local Fe-Mn rich cherts. The sequence is capped by a major basic to acid volcanic complex of which the acidic portion (Daginkatte Formation) has a relatively homogeneous composition and grain size (Taylor et al., 1984; Chadwick et al., 1991) and is interpreted as a pyroclastic ash flow deposit.

The analysed carbonate samples all come from the Lower Chitradurga Group or its inferred equivalents in the high temperature, low grade terrain to the east of the mylonitic zone which forms the eastern boundary of the Chitradurga Schist Belt (see **Figure 3.1.1**).

- KR003 and KR005 come from two separate localities 12 km apart in the Aleshpur Formation, as defined by Chadwick et al. (1990; 1991), northwest of the Honnali Dome.

- KR006 was collected from the Kur Gudda Formation, southeast of the Honnali Dome.
- KR001 and KR002 come from the same locality near Kumsi, southwest of the Honnali Dome. This area has not been directly correlated with the formations defined by Chadwick et al. (1990; 1991) but is inferred to be of Lower Chitradurga Group age. Stromatolitic carbonates from this region have been described by Vasudev et al. (1989).
- KR008 comes from the North Kanara region some 160 km to the northwest of the Honnali Dome and is inferred to be equivalent to the Lower Chitradurga Group from broad stratigraphic and petrological similarities.
- KR010 was collected from the Sandur Schist Belt which lies to the east of the main Chitradurga Schist Belt (Roy & Biswas, 1979; 1983), within the high temperature zone of the low grade metamorphic terrain. Stromatolitic carbonates from relatively undeformed rocks in this area have been described by Murthy & Krishna Reddy (1984).

Figure 3.2.1: Stratigraphy of the Dharwar Supergroup around the Honnali Dome, after Chadwick et al. (1991)

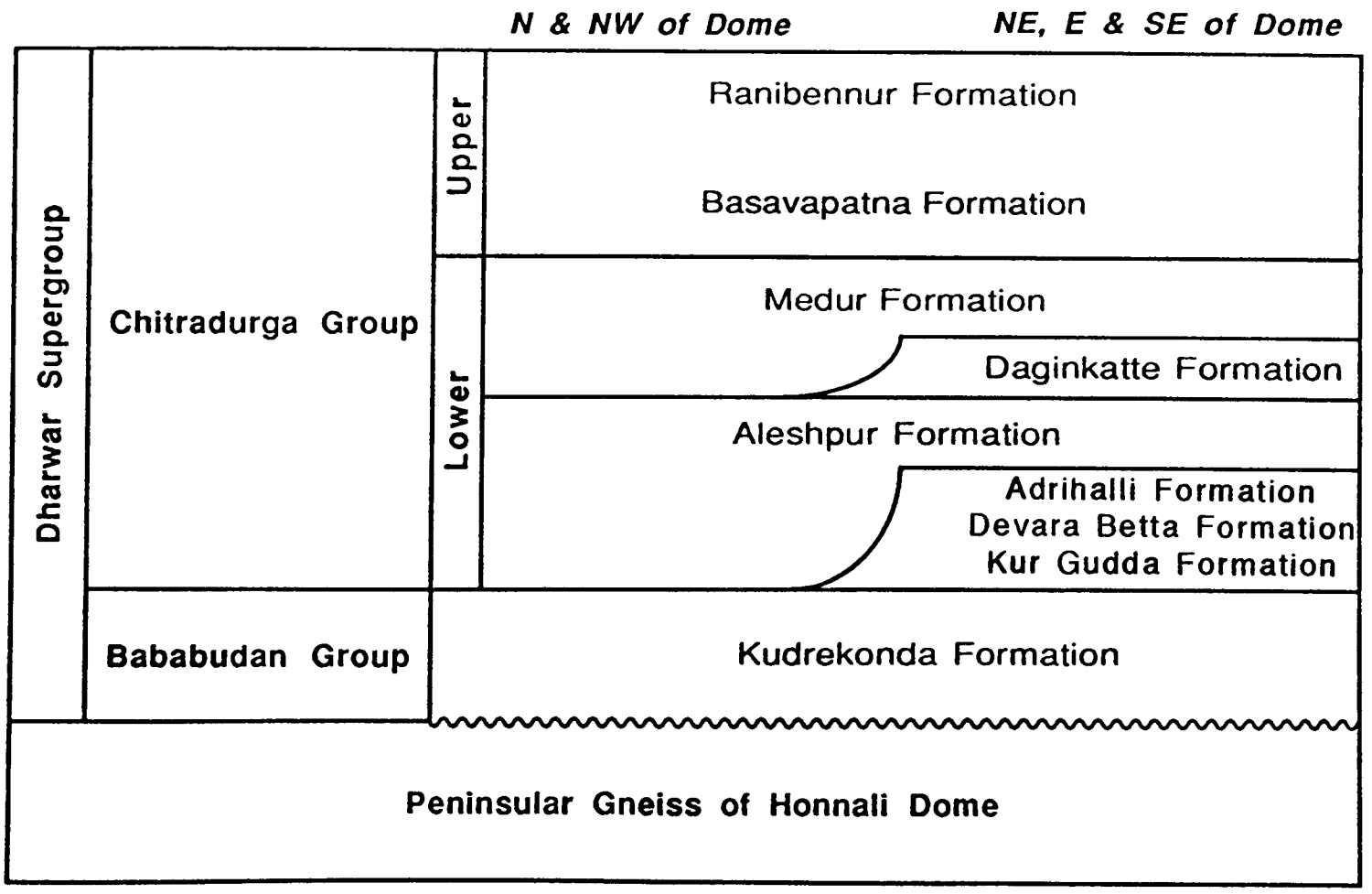

The Upper Chitradurga Group has a more uniform lithological character, indicative of an increasingly more stable depositional environment and commences

with the extensive, thin (50 m) Fe-rich cherts and phyllites of the Basavapatna Formation. Poor exposure limits observation of the Ranibennur Formation but local outcrops indicate that fine greywackes with interbedded Fe-rich cherts and acid volcanics dominate, suggesting an environmental comparison with the Daginkatte Formation.

Chadwick et al. (in press) define a three stage tectonostratigraphic model for the evolution of the Dharwar repository;

- Stage 1 - a passive continental margin or intracratonic rift setting sited on ancient sialic basement for the shallow marine and volcanic deposits of the Bababudan Group, followed by
- Stage 2 - a transpressive active continental margin or microcontinental arc setting for the alluvial and shallow marine sediments and volcanics of the Lower Chitradurga Group, culminating with
- Stage 3 - a similar setting, but with more quiescent conditions, producing more uniform sedimentation in the Upper Chitradurga Group.

The structure of the Dharwar Supergroup is dominated by steep to vertical faults and variably oriented, open to tight folds (Chadwick et al., 1991). Cover deformation occurred in a heterogeneous ductile fashion and contrasts with the typically cataclastic basement deformation, although ductile deformation is found along narrow mylonitic basement sutures. Major CO_2-rich fluid activity during basement deformation is indicated by abundant secondary carbonate and evidence of retrograde metamorphism in basement rocks.

3.3: AGE CONSTRAINTS

The age of the Peninsular Gneiss and that of the late Archaean granitoids which intrude the Dharwar Supergroup have been the subject of a number of recent isotopic investigations. These studies have enabled the age of the Dharwar Supergroup to be indirectly constrained but direct dating of this supracrustal association has until now proven problematic.

The basement of Peninsular Gneisses (which constitutes both granodiorites and polyphase gneisses) have yielded Pb/Pb whole rock, Rb-Sr whole rock and U-Pb zircon ages of between 3400-2950 Ma, as detailed in Taylor et al. (1984), Gupta et al. (1988), and Friend & Nutman (1991). The Chitradurga Granite, which intrudes

Dharwar Supergroup rocks of the Chitradurga Schist Belt, has been dated by Taylor et al. (1984) at 2605 ± 18 Ma by the Pb/Pb method (model μ_1 value 7.68). Recent U-Pb studies by Friend & Nutman (1991) on zircons separated from the late tectonic Closepet Granite gave a crystallisation age of 2513 ± 5 Ma, although unpublished Rb-Sr studies on the same 'intrusion' (Friend, pers. comm. 1992) indicate that the granite should be divided into distinct northern and southern portions, separated by an ENE-WSW boundary that passes along the northern margin of the Sandur Schist Belt. These unpublished studies dated the northern portion at 2433 ± 54 Ma (MSWD 0.36, $^{87}Sr/^{86}Sr_i$ 0.7046 ± 0.006, Sr < 110 ppm) and the southern portion at 2517 ± 36 Ma (MSWD 3.13, $^{87}Sr/^{86}Sr_i$ 0.70208 ± 0.00042, Sr > 180 ppm). Additional geochronological information has been published by, amongst others, Venkatasubramanian & Narayanaswamy (1974a; 1974b; 1974c), Venkatasubramanian (1975), Grew & Manton (1984), Buhl (1987), Buhl et al. (1987) and Taylor et al. (1988).

These data constrain the depositional age of the Dharwar Supergroup west of the mylonitic zone to between 2950-2600 Ma and east of the mylonitic zone to between 2950-2500 Ma. This is at odds with a whole rock Pb/Pb date of 2565 ± 28 Ma for acid volcanics from the Daginkatte Formation at the top of the Lower Chitradurga Group to the west of the mylonite belt (Taylor et al., 1984). The authors interpreted this poorly fitted isochron as the result of open system behaviour that also produced a particularly high K_2O content (5.70-9.58%) for the pyroclastic ash flow deposit. Taylor et al. (1988) obtained significantly older Sm/Nd model ages of 2990 and 3060 Ma for these same volcanics, indicating a significant crustal contribution to the volcanics and reinforcing evidence for a sialic basement during deposition of the Dharwar Supergroup.

3.4: RESULTS

Pb isotopic results for carbonates from the Lower Chitradurga Group west of the mylonitic zone are detailed in **Table 3a**. The first three digits indicate the sample number and these are followed by an analysis identifier. Although individual samples exhibit limited isotopic ranges, the combination of results from all samples, on the basis of their inferred stratigraphic equivalence, produces an age-related linear array on a Pb/Pb diagram (see **Figure 3.4.1**). Results for correlated carbonates from the Sandur Schist Belt east of the mylonitic zone are detailed in **Table 3c** and clearly define a separate array (see **Figure 3.4.1**), implying that the two areas have had distinct geological histories and must be considered independently.

Table 3a: Pb isotopic composition of carbonates from the Lower Chitradurga Group, western Karnataka

SAMPLE	CORRECTED RATIOS *		
	$^{206}Pb/^{204}Pb$	$^{207}Pb/^{204}Pb$	$^{208}Pb/^{204}Pb$
001 X1	14.998 ± 0.016	14.867 ± 0.018	35.509 ± 0.044
001 X2	16.114 ± 0.016	15.076 ± 0.018	34.154 ± 0.042
001 200	16.229 ± 0.016	15.149 ± 0.018	35.713 ± 0.044
001 205	16.081 ± 0.016	15.119 ± 0.018	33.890 ± 0.042
002 120	15.601 ± 0.016	15.050 ± 0.018	35.244 ± 0.044
002 212	16.091 ± 0.016	15.146 ± 0.018	35.169 ± 0.044
002 213	15.220 ± 0.016	15.006 ± 0.018	34.954 ± 0.044
002 218	15.804 ± 0.016	15.074 ± 0.018	34.801 ± 0.042
002 215	15.077 ± 0.016	14.964 ± 0.018	34.518 ± 0.042
003 227	13.700 ± 0.014	14.577 ± 0.018	33.462 ± 0.042
003 228	13.585 ± 0.014	14.583 ± 0.018	33.500 ± 0.040
003 230	13.534 ± 0.014	14.551 ± 0.018	33.415 ± 0.040
005 241	13.985 ± 0.014	14.673 ± 0.018	33.724 ± 0.042
006	33.740 ± 0.034	18.262 ± 0.022	34.105 ± 0.042
006 A	34.150 ± 0.034	18.304 ± 0.022	34.076 ± 0.042
006 B	35.648 ± 0.036	18.545 ± 0.022	34.095 ± 0.042
006 C	35.029 ± 0.036	18.476 ± 0.022	34.132 ± 0.042
008	20.121 ± 0.020	15.820 ± 0.020	35.053 ± 0.042
008 515	19.649 ± 0.020	15.752 ± 0.020	34.056 ± 0.042
008 X1	17.422 ± 0.018	15.425 ± 0.018	34.433 ± 0.042
008 524	17.860 ± 0.018	15.519 ± 0.018	34.053 ± 0.042

* Corrected for mass fractionation of 0.130 % ± 0.012 ($2\sigma_{mean}$) amu^{-1}
Errors are $2\sigma_{mean}$ for corrected ratios

Results for Chitradurga Schist Belt carbonates are shown in more detail in **Figure 3.4.2**, where analyses of the six separate samples define a twenty-one point Pb/Pb errorchron date of 2639 ± 32 Ma (MSWD 50.1, model μ_1 value 7.79 ± 0.03). The poor fit of the errorchron is most probably attributable to slight variations in the initial Pb isotopic ratios and μ_1 values of samples that were collected from widely separated localities. Since individual sample sets and combinations thereof demonstrate only limited isotopic ranges (see **Table 3a**), the dates they define have

Figure 3.4.1: Pb isotopic data for Chitradurga Schist Belt carbonates and their inferred equivalents from the Sandur Schist Belt, Karnataka, India

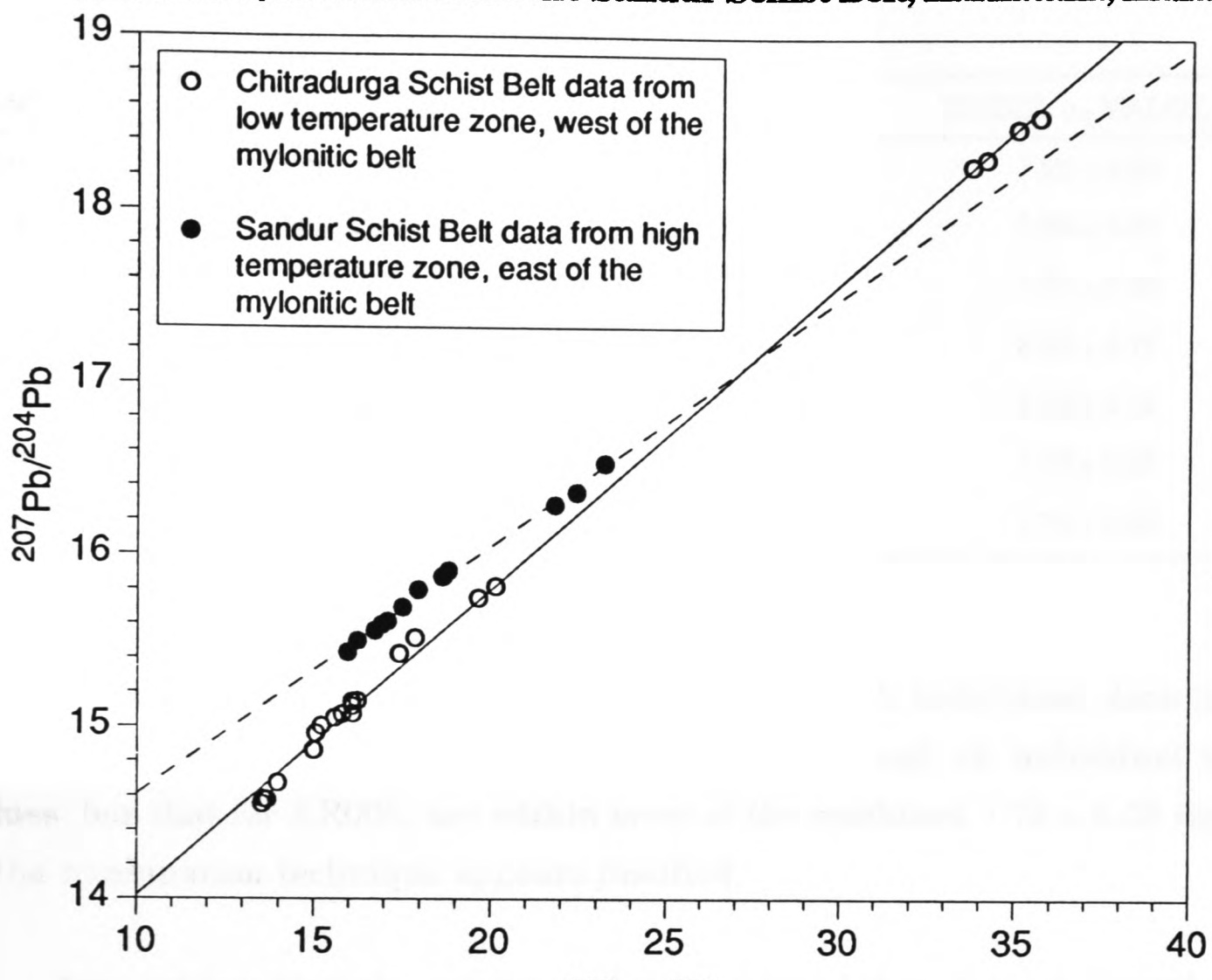

Figure 3.4.2: Pb isotopic data for Lower Chitradurga Group carbonates from the Chitradurga Schist Belt, Karnataka, India

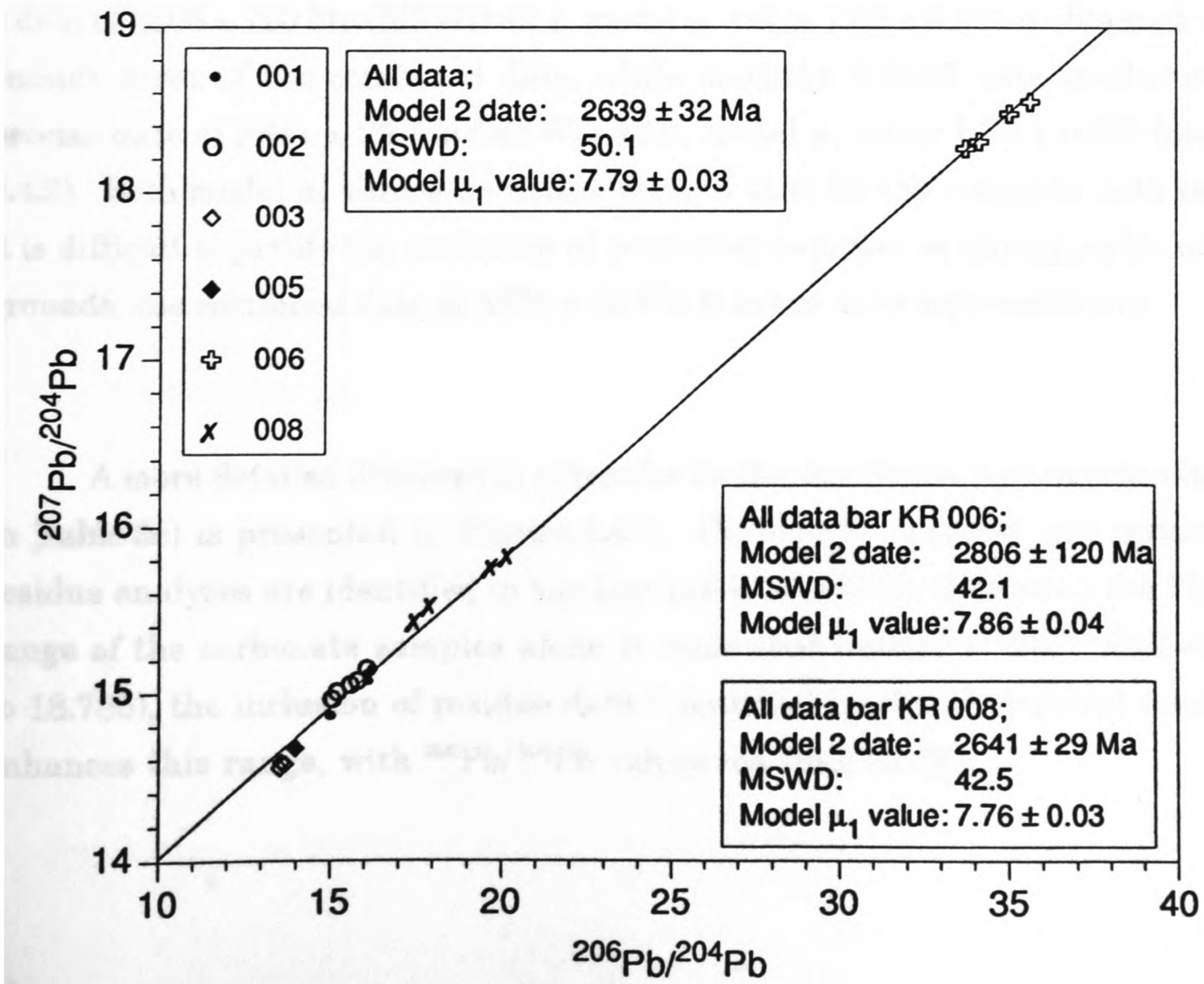

Table 3b: Errorchron fits, MSWD and model μ_1 values for data subsets from Chitradurga Schist Belt carbonates

SAMPLE	DATE (Ma)	MSWD	MODEL μ_1 VALUE
KR001	2992 ± 890	13.7	7.92 ± 0.69
KR002	2519 ± 530	2.83	7.83 ± 0.23
KR001 & 002	2742 ± 550	20.5	7.87 ± 0.28
KR003 & 005	3269 ± 1300	6.06	8.40 ± 6.77
KR006	2429 ± 590	4.62	8.50 ± 2.14
KR008	2249 ± 370	3.73	7.99 ± 0.08
ALL DATA	2639 ± 32	50.1	7.79 ± 0.03

stratigraphically unacceptable error bars. Since each individual date is within error of the combined 2639 ± 32 Ma date (**Table 3b**) and all individual model μ_1 values, bar that for KR008, are within error of the combined 7.79 ± 0.03 figure, use of the combination technique appears justified.

It is evident that the precision of the combined date depends heavily on four analyses of KR006 and that the KR008 data appears to define a slightly younger date with a higher model μ_1 value. By omitting all KR006 analyses from the regression, a date of 2806 ± 120 Ma (MSWD 42.1, model μ_1 value 7.86 ± 0.04) is obtained, only just outside error of the combined date, while omitting KR008 data produces a more precise date of 2641 ± 29 Ma (MSWD 42.5, model μ_1 value 7.76 ± 0.03) (see **Figure 3.4.2**). Both model μ_1 values lie within error of that for the complete data set. Since it is difficult to justify the exclusion of particular samples on stratigraphic or isotopic grounds, the combined date of 2639 ± 32 Ma is taken to be representative.

A more detailed illustration of results for Sandur Schist Belt samples (tabulated in **Table 3c**) is presented in **Figure 3.4.3**. Carbonate analyses and corresponding residue analyses are identified in the key and it is evident that while the Pb isotopic range of the carbonate samples alone is somewhat limited ($^{206}Pb/^{204}Pb$ from 16.710 to 18.785), the inclusion of residue data (identified by closed symbols) considerably enhances this range, with $^{206}Pb/^{204}Pb$ values reaching 23.221.

Table 3c: Pb isotopic composition of carbonates from the Sandur Schist Belt, eastern Karnataka

SAMPLE	CORRECTED RATIOS *		
	$^{206}Pb/^{204}Pb$	$^{207}Pb/^{204}Pb$	$^{208}Pb/^{204}Pb$
010 X3	17.081 ± 0.016	15.614 ± 0.018	36.208 ± 0.044
010 X3A	17.497 ± 0.018	15.694 ± 0.020	37.014 ± 0.046
010 X3AR	22.416 ± 0.022	16.360 ± 0.020	39.091 ± 0.048
010 X2	15.956 ± 0.024	15.433 ± 0.026	35.415 ± 0.092
010 X2A	16.232 ± 0.016	15.501 ± 0.020	35.726 ± 0.044
010 X2AR	16.909 ± 0.022	15.595 ± 0.028	36.288 ± 0.078
010 X2B	16.710 ± 0.016	15.559 ± 0.020	35.935 ± 0.044
010 X2BR	17.957 ± 0.030	15.799 ± 0.072	36.720 ± 0.130
010 X1	18.627 ± 0.048	15.875 ± 0.050	38.612 ± 0.154
010 X1A	18.675 ± 0.018	15.876 ± 0.020	38.527 ± 0.046
010 X1AR	21.802 ± 0.022	16.291 ± 0.020	39.100 ± 0.050
010 X1B	18.785 ± 0.018	15.908 ± 0.020	38.575 ± 0.048
010 X1BR	23.221 ± 0.134	16.530 ± 0.110	39.988 ± 0.272

* Corrected for mass fractionation of 0.130% ± 0.012 ($2\sigma_{mean}$) amu^{-1}
Errors are $2\sigma_{mean}$ for corrected ratios

R Indicates residue of corresponding carbonate sample

The combined data set defines a thirteen point Pb/Pb errorchron whose slope corresponds to a date of 2285 ± 83 Ma (MSWD 5.10, model μ_1 value 8.47 ± 0.01), significantly younger than the inferred equivalents from the Chitradurga Schist Belt to the west and with a significantly higher model μ_1 value (8.47 ± 0.01 cf. 7.79 ± 0.03). The Pb isotopic compositions of HCl-insoluble residues are consistently more radiogenic than those for the corresponding carbonate analyses and in addition, define a distinctly shallower slope. Since these residue analyses have a profound effect on the regressed date, one should independently consider the carbonate and residue data.

Carbonate data alone define a seven point Pb/Pb isochron (MSWD 1.16) whose slope corresponds to a date of 2475 ± 65 Ma with a model μ_1 value of 8.50 ± 0.01, while residue data alone define a five point isochron (MSWD 1.81) corresponding to a date of 2219 ± 140 Ma with a model μ_1 value of 8.46 ± 0.07. Omitting KR010 X1BR and KR010 X2BR increases the precision of this date to 2227 ± 64 Ma without significantly altering the MSWD or model μ_1 value (1.93 and 8.45 ± 0.03 respectively).

Figure 3.4.3: Pb isotopic data for carbonates and HCl-insoluble residues from the Sandur Schist Belt, eastern Karnataka, India

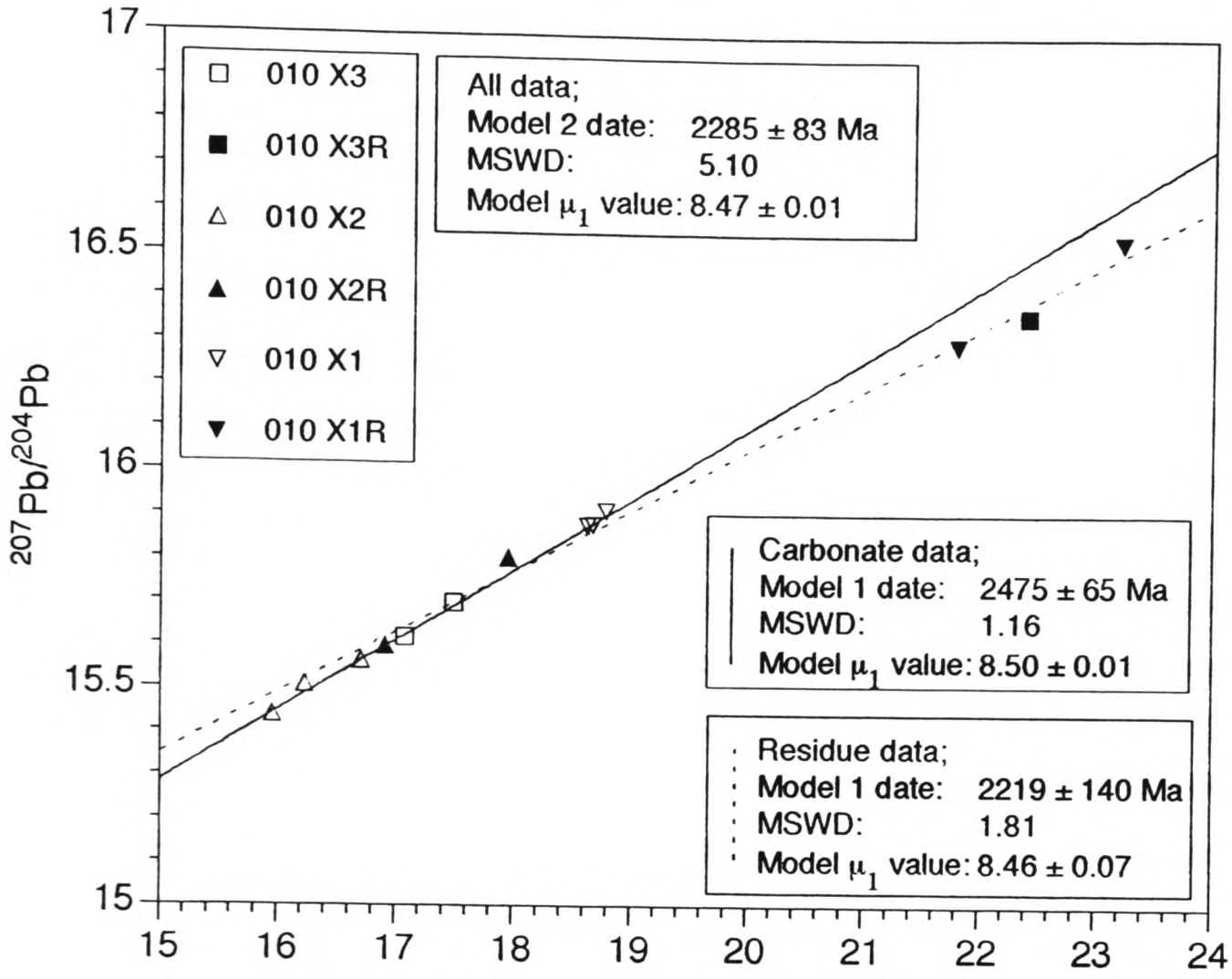

3.5: DISCUSSION

For the low temperature western zone, the carbonate date of 2639 ± 32 Ma (MSWD 50.1, model μ_1 value 7.79 ± 0.03) is consistent with the 2605 ± 18 Ma date (model μ_1 value 7.68) of Taylor et al. (1984) for the Chitradurga Granite. Both model μ_1 values are similar to those for typical Archaean mantle sources (7.5-8; Moorbath & Taylor, 1981), suggesting that the U and Pb may have been sourced from juvenile, mantle-derived crust. This is supported by a high initial $^{87}Sr/^{86}Sr$ value for the Chitradurga Granite (0.706 ± 0.004; Venkatasubramanian & Narayanaswamy, 1974a) which implies that Sr in the granite was not derived directly from the upper mantle but had a more evolved, probably crustal source.

Available hand specimens and thin sections indicate that the samples consist dominantly of medium to coarse grained calcite and dolomite with distinct granoblastic metamorphic textures and hence the date is interpreted as the age of isotopic closure in response to metamorphic recrystallisation of precursor carbonate and/or siliceous carbonate rocks. It is proposed that this event corresponds to the low

temperature, amphibolite grade retrogression which resulted in the formation of abundant epidote, chlorite and carbonate in the Peninsular Gneiss basement from the action of CO_2-rich fluids. Given the similarity of the dates, it is not possible to resolve this recrystallisation and intrusion of the post-tectonic Chitradurga Granite into the Dharwar Supergroup as two separate events. From extrapolation of the errors, the granite intrusion must have occurred less than 50 Ma after metamorphism but it is possible that the two events may have been contemporaneous.

While individual samples exhibit limited ranges of Pb isotopic composition, the combination of data from samples with the same inferred stratigraphic position but significantly differing μ_2 values (see **Table 3d**), considerably enhances the isotopic range and also the precision of the date. In the cases of KR001, KR002, KR003 and KR005, metamorphism resulted in U loss and concomitant lowering of μ_2 values compared to the model μ_1 value of 7.79 ± 0.03. Conversely, KR008 was subject to moderate U enrichment and KR006 significant enrichment, with μ_2 values up to 43.98, perhaps reflecting amplification of primary local source U/Pb heterogeneity during amphibolite facies metamorphism.

Table 3d: Calculated μ_2 values for Lower Chitradurga Group carbonates, assuming parameters; t = 2639 ± 32 Ma, μ_1 = 7.79 ± 0.03 and $^{206}Pb/^{204}Pb_i$ = 13.402

SAMPLE	$^{206}Pb/^{204}Pb$ RANGE	μ_2 RANGE
KR001	14.998 - 16.229	3.16 - 5.59
KR002	15.077 - 16.091	3.31 - 5.32
KR003	13.534 - 13.700	0.26 - 0.59
KR005	13.985	1.15
KR006	33.740 - 35.648	40.2 - 43.98
KR008	17.422 - 20.121	7.95 - 13.28

Interpretation of data for Sandur Schist Belt carbonates from the high temperature zone of the low metamorphic grade region is more problematic because of the discordance noted between carbonate and residue data. The combined date of 2285 ± 83 Ma (MSWD 5.10, model μ_1 value 8.47 ± 0.01) is considered to have no true age significance since it merely averages isotopically independent, but similar, carbonate and residue data sets.

The carbonate data alone define a well fitted 2475 ± 65 Ma isochron (MSWD

1.16, model μ_1 value 8.50 ± 0.01) (see **Figure 3.4.3**), significantly younger than the age of metacarbonates in the low temperature zone and with a significantly higher model μ_1 value (8.50 ± 0.01 cf. 7.79 ± 0.03). Within error, the date is consistent with available Rb-Sr and U-Pb zircon ages for the Closepet Granite, (2433 ± 54 Ma, 2517 ± 36 Ma and 2513 ± 5 Ma - Friend & Nutman, 1991; Friend, pers. comm. 1992) and is interpreted as the age of metamorphism of siliceous carbonate parental rocks during the same event that resulted in the intrusion of the late tectonic Closepet granitic rocks.

The 150 Ma discrepancy between the youngest event recorded in the low temperature zone to the west (c.2600 Ma) and the youngest event in the high temperature zone to the east (c.2450 Ma) could indicate that the elevated thermal gradient which existed in the high temperature zone during amphibolite grade metamorphism maintained U-Pb open system conditions for a substantial period of time (c.150 Ma) before the blocking temperature for U-Pb systematics was finally reached. Alternatively, one might consider the possibility that the 2475 ± 65 Ma carbonate isochron dates a separate metamorphic event in the east, which overprinted the earlier 2600 Ma event.

The particularly high single-stage model μ_1 value of 8.50 ± 0.01 for the carbonate data suggests that prior to metamorphism, significant source U enrichment (or Pb depletion) occurred compared with typical values for marbles from the west of Karnataka (model μ_1 value 7.79 ± 0.03) and Archaean mantle sources (model μ_1 values of 7.5-8) and . Calculated μ_2 values for the Sandur carbonates vary from 3.97 to 10.01 implying that the metamorphism resulted in inconsistent U-Pb behaviour, with U loss/Pb gain dominant in KR010 X3 and KR010 X2, but U gain/Pb loss dominant in KR010 X1.

For the Sandur carbonates to have formed in response to metamorphism of extant 2600 Ma marbles of similar character to those found in the Chitradurga Belt would have required a short-lived (< c.150 Ma), high μ_2 stage (μ_2 16.60) of isotopic evolution between 2639 Ma and 2475 Ma, before metamorphism caused lowering of μ_3 values (μ_2 values in the two-stage evolution) to between 3.97 and 10.01. Evidence to substantiate such a proposal is lacking and consequently an evolution involving one metamorphic event with varying thermal gradients is invoked to explain the difference in metamorphic ages between low and high temperature zones. The c.2500 Ma ages for eastern late tectonic granites, compared with values of c.2600 Ma in the west, are consistent with the idea of an elevated thermal gradient in the east.

Residue data from the high temperature zone define an isochron date of 2219 ± 140 Ma (MSWD 1.81, model μ_1 value 8.46 ± 0.07) (see **Figure 3.4.3**) which is significantly younger than both the corresponding carbonate metamorphic age of 2475 ± 65 Ma (MSWD 1.16, model μ_1 value 8.50 ± 0.010) and the carbonate metamorphic age from the western, low temperature zone (2639 ± 32 Ma, MSWD 50.1, model μ_1 value 7.79 ± 0.03). It also post-dates ages for both sets of late tectonic granitic intrusions (c.2600 Ma and c.2500 Ma). By omitting two points, the precision of the residue date may be improved to 2227 ± 64 Ma without significantly altering either the MSWD or model μ_1 value (1.93 and 8.45 ± 0.03 respectively).

It should be noted that not only do the residue analyses define a separate isochron, but they are also consistently more radiogenic than their carbonate fractions. This phenomenon may be explained by considering the crystallographic structures of the constituent minerals. Trigonal calcite and dolomite, the dominant carbonate minerals in the marbles, commonly permit isomorphic substitution of Mg^{2+}, Mn^{2+} and Fe^{2+} for Ca^{2+} since they all have similar chemical properties and ionic radii which are less than that of Ca^{2+} (c.1.0Å). At the trace element level, Sr^{2+} and Pb^{2+} may also reside in the trigonal structure but the straining effect of their larger ionic radii (>1.1Å) limits the potential for substitution. Sr^{2+} and Pb^{2+} more commonly substitute for Ca^{2+} in the less symmetrical orthorhombic structure of aragonite (end-member $SrCO_3$ is stable as strontianite and $PbCO_3$ as cerussite) but under amphibolite facies conditions, primary aragonite is stabilised as other trigonal carbonate minerals. Incompatibles with high valencies, such as U^{4+} and Th^{4+}, do not substitute readily within either the trigonal or orthorhombic carbonate structures. More probably they are either adsorbed onto grain boundaries, associated with reducing microenvironments produced by local organic concentrations (U^{4+}) or scavenged by particulate matter (Th^{4+}). With silicates such as mica, amphibole, clinopyroxene and accessory minerals (e.g. zircon, sphene and apatite), however, U and Th are more easily accommodated in the crystal structures. In addition, U is particularly mobile under oxidising conditions in fluid media. Hence, it is possible that much of the U originally associated with sedimentary phases could become mobilised by metamorphism and be taken up by recrystallising silicate and accessory phases, resulting in elevated μ_2 values and explaining the more radiogenic uranogenic Pb isotopic compositions observed today. Conversely, post-depositional redistribution of Th is controlled by physical processes (see discussion in **6.6**).

The documented discordance of carbonate and residue data from the same rock requires careful interpretation. It signifies that syn- to post-metamorphic

isotopic disturbance must have selectively and systematically affected certain lithic components. Although spurious Pb/Pb isochrons are a recognised feature of a number of metamorphic terrains, mainly in response to U disturbance in systems where Pb isotopic homogenisation is incomplete (Moorbath & Taylor, 1985; Whitehouse, 1989), discordance between lithic components on the scale of a single hand specimen has not been previously reported.

Whitehouse (1989) proposed two principal types of U-Pb fractionation behaviour in metamorphic rocks (see **Figure 3.5.1**);

- type I, where complete Pb isotopic homogenisation occurs and reliable isochrons are generated, and
- type II, where Pb isotopic homogenisation is incomplete or absent.

Figure 3.5.1: Models for U-Pb isotopic behaviour during metamorphism, after Whitehouse (1989)

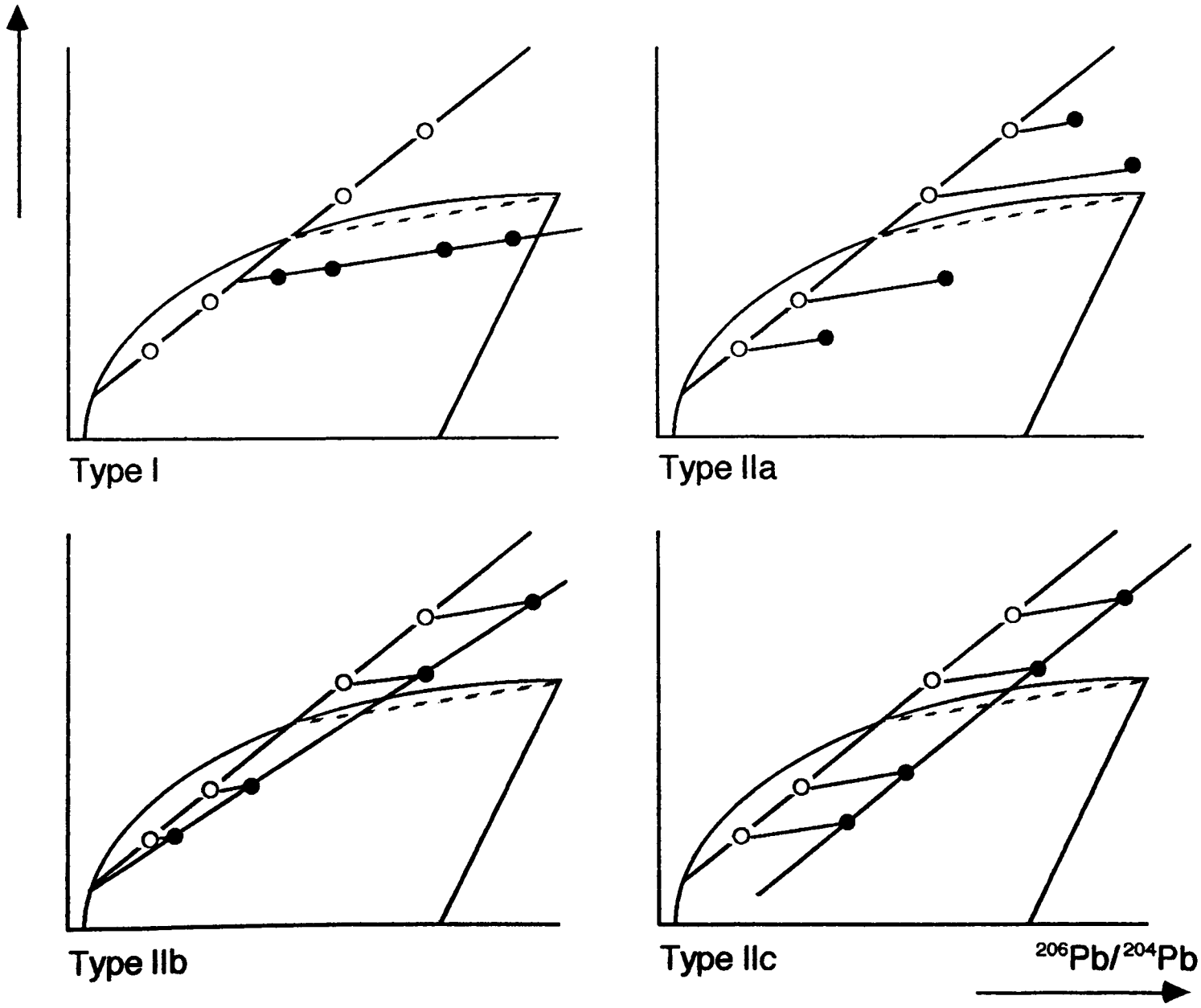

He further divided type II behaviour into IIa, IIb and IIc models, depending on the relationship between the post-t_2 and pre-t_2 μ values (his μ_3 and μ_2 values

respectively for multi-stage Pb isotopic evolution), where t_2 is the age of the fractionating metamorphic event, t_1-t_2 the period of pre-metamorphic crustal residence and t_0-t_1 mantle residence. With type IIa behaviour, post-metamorphic μ_3 values are variable and unrelated to pre-metamorphic μ_2 values; with type IIb behaviour, $\mu_3 = k\mu_2$ and with type IIc behaviour, $\mu_3 = k$, where k is a constant. Each model type has predictable consequences for the behaviour of uranogenic Pb isotopes. Reliable isochrons are only generated under type I conditions or under type IIa conditions where very high μ_3 values exist and the effect of incomplete Pb isotopic homogenisation at metamorphism is minimised.

In the case of the Sandur rocks, it is suggested that the carbonate data corresponds to type I behaviour. Metamorphism at c.2.5 Ga (t_2) caused homogenisation of Pb isotope ratios and the variation in μ values that existed (μ_3) resulted in subsequent isochron generation. Behaviour of the residue data is somewhat more complicated. To yield a date younger than the age of metamorphism, one must envisage a general type IIb scenario where incomplete non-carbonate Pb isotopic homogenisation at metamorphism and a proportional (or inverse proportional) relationship between μ_3 and μ_2 values produces rotation of the palaeoisochron. With conventional type IIb behaviour, however, the apparent age of the rotated palaeoisochron becomes asymptotic to the age of metamorphism, t_2, for large μ_3 values (Whitehouse, 1989) and so it is not possible to explain an underaged palaeoisochron by this model.

A new model, termed here type IId, is proposed to explain the underaged rotated palaeoisochron observed for Sandur residue data (see **Figure 3.5.2**). Type IId behaviour involves incomplete Pb isotopic homogenisation at t_2 with U/Pb fractionation according to the rule $\mu_3 = k/\mu_2$, where k is a constant. The effect of this type of behaviour is to rotate the palaeoisochron around a certain Pb isotopic composition (which in the case of the Sandur data corresponds to the intersection of the t_2 present-day carbonate isochron with the rotated residue palaeoisochron) to produce a present-day isotopic array whose slope corresponds to a date somewhat younger than t_2. Such a date has no geological age significance.

In geological terms, type IId behaviour requires the least radiogenic pre-metamorphic samples to generate the highest μ_3 values on metamorphism and *vice versa*, that is the least radiogenic samples must preferentially uptake U, discriminate against Pb, or both. The relative mobility of U under normal metamorphic conditions strongly suggests that it is the behaviour of U, rather than of Pb, that

would prove the controlling factor.

Figure 3.5.2: Proposed type IId model to explain underaged, rotated palaeoisochrons (condition $\mu_3 = k/\mu_2$)

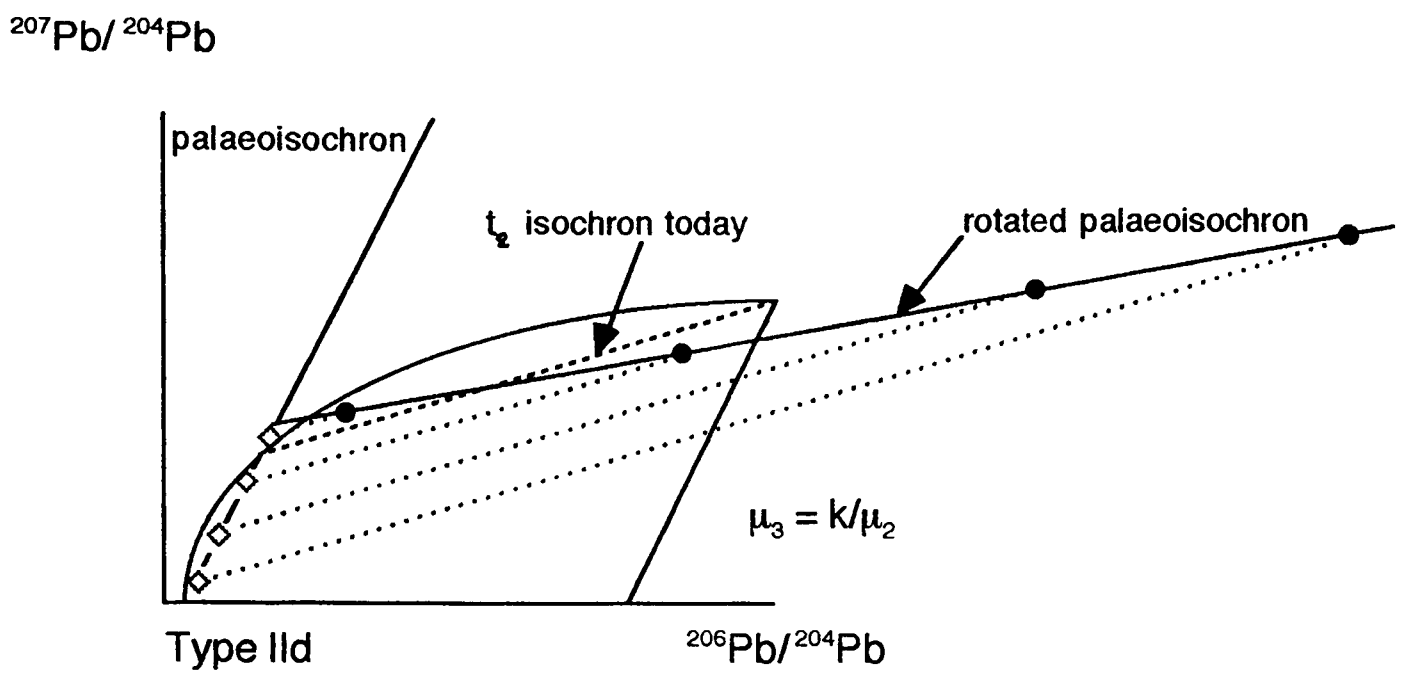

Using the above models, the Sandur data could be interpreted in the following manner:-

- Between t_1 and t_2 Pb isotopic heterogeneity existed within the siliceous carbonates that formed the precursors to the Sandur marbles (t_2 represents the date of metamorphism, 2475 ± 65 Ma, but t_1 is not defined since the rocks may have had a complex evolution prior to t_2).
- At t_2, metamorphism resulted in homogenisation of carbonate Pb isotopic ratios and significant loss of non-structurally bound U. The carbonates retained a proportion of uranium such that variable post-metamorphic μ values (μ_3 for this model) of between 3.97 and 10.01 existed and subsequent parental U decay produced a present-day, type I t_2 isochron.
- Metamorphism at t_2, however, failed to homogenise non-carbonate Pb isotopic ratios (type II behaviour) and U mobilised from carbonate recrystallisation was preferentially accommodated in silicate and accessory minerals, raising their post-metamorphic μ values above those for the coexistent carbonate and resulting in the development of more radiogenic present-day Pb isotopic compositions.
- For the residue data to define a date younger than that of the t_2 isochron, type IId behaviour is invoked, where $\mu_3 = k/\mu_2$. The least radiogenic pre-metamorphic non-carbonate material must have preferentially incorporated U (or discriminated against Pb) and generated the highest post-metamorphic μ_3 values. Such a date has no true geological significance. Incorporation of U into the non-carbonate materials must have been inversely proportional to their μ_2 value. It is suggested

that metamorphic recrystallisation of non-carbonate materials resulted in the incorporation of significant amounts of U released during carbonate recrystallisation. Low μ_2 materials, initially relatively deficient in U, must have preferentially accommodated U on recrystallisation and therefore generated relatively high μ_3 values, when compared to materials possessing initially high μ_2 values. If the carbonate plus residue formed a closed system throughout recrystallisation, the total amount of U would be finite and U uptake would have to be buffered. Consequently, a point would be reached when no further U was available for incorporation into silicate and accessory minerals, resulting in the cessation of μ_3 development and leaving the low μ_2 materials with relatively high μ_3 values and the high μ_2 materials with relatively low μ_3 values, in other words $\mu_3 = k/\mu_2$.

This scenario may be compared with type IIb behaviour, where an unlimited U source (open system conditions) would allow the high μ_2 materials to continue to uptake U and ultimately generate the highest μ_3 values so that $\mu_3 = k\mu_2$. In such a case, at high μ_3 values the rotated palaeoisochron becomes asymptotic to the present-day t_2 isochron. Underaging only appears possible with type IId behaviour, that is buffered U uptake resulting from finite U supply.

3.6: CONCLUSIONS

The successful application of direct Pb/Pb dating to marbles has clearly demonstrated that the low and high temperature zones of amphibolite grade metamorphism in Karnataka have differing sources and metamorphic histories. In the west, low temperature Chitradurga Schist Belt carbonates were regionally metamorphosed at 2639 ± 32 Ma (see **Figure 3.4.2**, MSWD 50.1, model μ_1 value 7.79 ± 0.03), around the same time that the late tectonic Chitradurga Granite was intruded. Reliable model μ_1 values for Lower Chitradurga Group marbles average 7.88, suggesting a mantle-derived, juvenile crustal source. The 2565 ± 28 Ma date for acid volcanic rocks from the Daginkatte Formation must be anomalously young, as previously suggested by Taylor et al. (1984) and so it is concluded that the Dharwar Supergroup in the vicinity of the Chitradurga Schist Belt was deposited at some time between 2950 and 2600 Ma.

As a consequence of the elevated thermal gradient in the east, metamorphism of the Sandur Schist belt continued until blocking temperatures for U and Pb were finally reached at 2475 ± 65 Ma (see **Figure 3.4.3**, MSWD 1.16, model μ_1 value 8.50 ±

0.01), around the same time as the intrusion of the late tectonic Closepet Granite. Disequilibrium between carbonate and non-carbonate components during metamorphism resulted in incomplete Pb isotopic homogenisation for the latter and preferential U uptake according to the model $\mu_3 = k/\mu_2$ (type IId behaviour, as proposed in this study). Consequently, Pb isotopic compositions for HCl-insoluble residues are consistently more radiogenic than those for corresponding carbonate analyses.

Although average model μ_1 values are higher in the east than the west (8.48 cf. 7.88), implying a more evolved crustal source, it is not possible from this evidence to comment on the potential stratigraphic equivalence of the respective precursor rocks. While radiometric constraints place deposition of the Sandur carbonate precursors between 2950 Ma and 2475 Ma, a range of 2950-2600 Ma is more probable. Neither the anomalously young residue date of 2219 ± 140 Ma (see **Figure 3.4.3**, MSWD 1.81, model μ_1 value 8.46 ± 0.07), nor the combined date of 2285 ± 83 Ma (see **Figure 3.4.3**, MSWD 5.10, model μ_1 value of 8.47 ± 0.01) have any real geological significance.

Chapter 4:

INDIAN PROTEROZOIC STROMATOLITES

4.1: INTRODUCTION

The Aravalli-Delhi orogenic belt outcrops in the northwest Indian states of Rajasthan, Gujarat and Haryana and runs 700 km NNE-SSW from Delhi to Palanpur, the width of outcrop varying between 30 and 200 km (see **Figure 4.1.1**). It comprises a system of Proterozoic volcanosedimentary basins, the Aravalli and Delhi Supergroups, deposited unconformably upon the peneplained Banded Gneiss Complex basement.

To the west, the Aravalli-Delhi belt is overlain by the Upper Proterozoic to Lower Cambrian Marwar Supergroup, while to the east, separated from the main belt by outcrop of the Banded Gneiss Complex, the Bhilwara Supergroup contains sediments equivalent to the Aravalli Supergroup. Deposits of the Vindhyan Supergroup, whose age is very poorly constrained, are faulted against Bhilwara deposits along the northeast-southwest trending Great Boundary Fault. The late Cretaceous

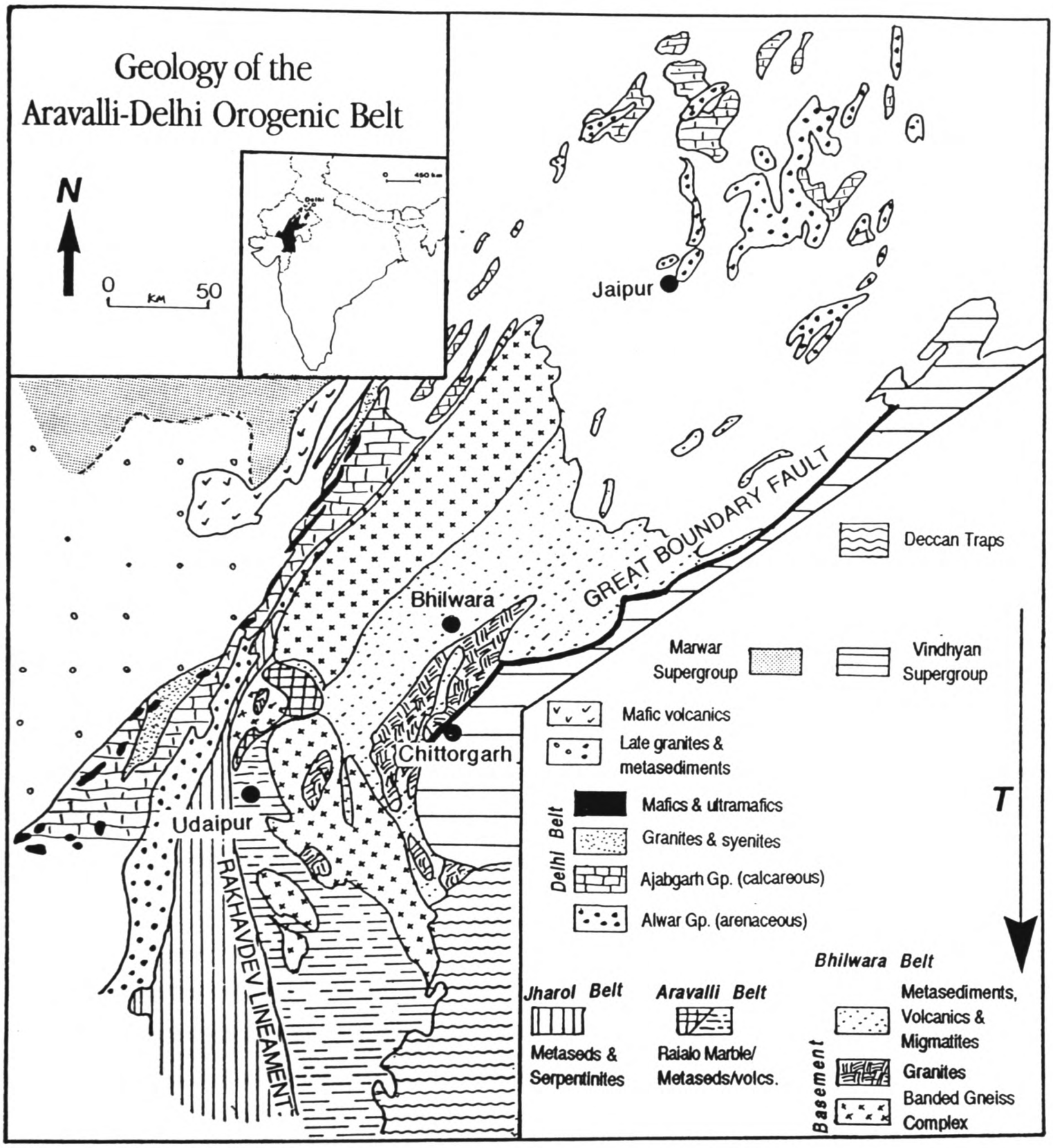

Figure 4.1.1: Geology of the Aravalli-Delhi orogenic belt and surrounding area, after Deb et al. (1989) and Sugden et al. (in press), with inferred correlations

Deccan Traps unconformably overlie Aravalli and Vindhyan Supergroup sediments in the south of the region.

Stromatolitic carbonate samples were analysed from phosphatic deposits within the Aravalli Supergroup around Udaipur; from Lower Vindhyan sediments of the Son Valley and inferred equivalents in the Chandi Formation of the Raipur Group (Chattisgarh Supergroup) and the Bhagwanpura Limestone around Chittorgarh; and from limestones of the Upper Vindhyan and inferred equivalents in the Marwar (Trans-Aravallis) Supergroup of the Jodhpur district, Rajasthan. Hand specimens and logistical support were kindly provided by Dr. D.M.Banerjee of the University of Delhi, India.

4.2: STRATIGRAPHY OF THE ARAVALLI-DELHI OROGENIC BELT REGION

The stratigraphy of the Aravalli-Delhi orogenic belt was first described by Heron (1935; 1953) and all subsequent work, for example that of Raja Rao (1976) and Gupta et al. (1980), has built on his astute proposal that evolution of the region took place in three orogenic episodes, represented by the Banded Gneiss Complex, the Aravalli Supergroup and the Delhi Supergroup. **Figure 4.2.1** illustrates the broad stratigraphic relationships that are believed to hold within the region. There is a degree of uncertainty associated with several of the correlations due in the main to a general lack of reliable age data for deposits in the area.

The Banded Gneiss Complex consists predominantly of gneisses that exhibit granulite facies metamorphism northwest of Bhilwara and lower grade amphibolite facies metamorphism east of Udaipur (Sen, 1970). In addition, enclaves of weakly metamorphosed sediments exist, possibly equivalent to Aravalli deposits, and the complex contains a number of granites that probably include pre-Aravalli, post-Aravalli and post-Delhi components (Crawford, 1970). Consequently, Roy (1987) proposed that the single unit status of the Banded Gneiss Complex was difficult to maintain and that pre-Aravalli rocks should be termed the Mewar Gneiss and considered independent of other components.

Figure 4.2.1: Regional stratigraphy of the Aravalli-Delhi orogenic belt, after Heron (1953), Roy (1987), Deb et al. (1989) and Banerjee et al. (1992)

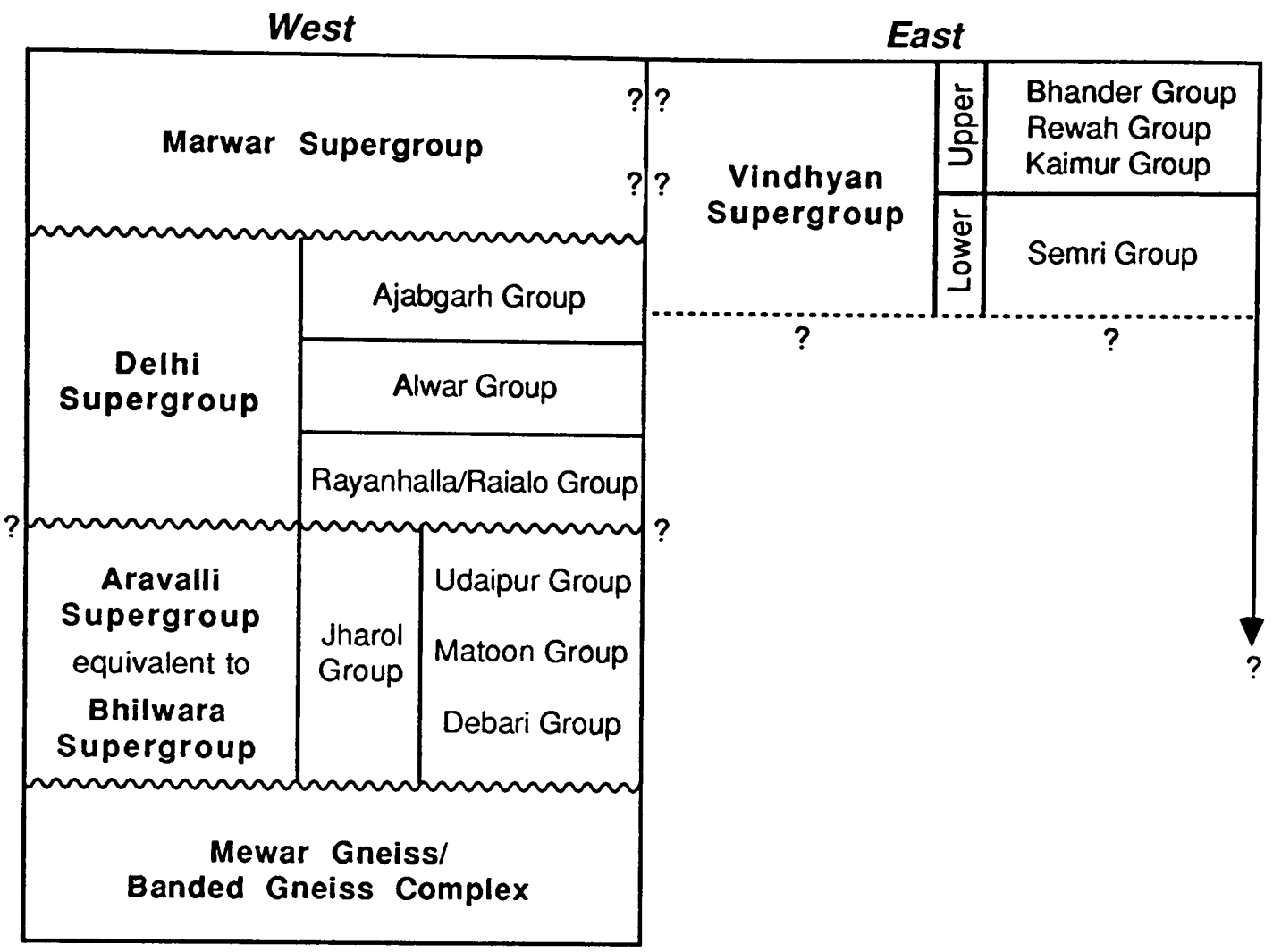

The Mewar Gneiss forms the peneplained basement to both Aravalli sediments in the west and Bhilwara deposits in the east. Roy et al. (1980) and Roy & Paliwal (1981) detail localities at which a profound unconformable relationship may be observed. The basement suffered polyphase folding and metamorphism (M1) of constituent biotite-hornblende gneisses, granitic rocks, amphibolites, aluminous paragneisses, quartzites, marbles and pegmatites prior to deposition of the Aravalli pile and basal Aravalli conglomerates are found to contain boulders of Mewar origin. North of Nathdwara, basement foliation and Aravalli schistosity become sub-parallel and this has led to uncertainty in establishing local basement-cover relationships (Sen, 1970; 1983). In fact, this geometry resulted from the transposition of basement foliation during post-Aravalli tectonic deformation and the true relationship between Mewar Gneiss and Aravalli sediments is an unconformable one (Heron, 1953; Roy & Paliwal, 1981; Roy, 1987). M1 metamorphism culminated in intrusion of the late-synkinematic Untala and Gingla Granites around 3000 Ma (actually dated at 2950 ± 150 Ma by Choudhary et al., 1984), while later M2 metamorphism resulted in the synkinematic emplacement of the Darwal Granite with the first deformation of the Aravalli pile around 1900 Ma.

The Aravalli Supergroup outcrops in a wedge-shaped belt in the region around and to the south of Udaipur. It comprises variably metamorphosed volcanics and shelf sediments that gradually thin to the north and are succeeded by the Raialo carbonates (Naha & Halyburton, 1977a; Roy & Paliwal, 1981; Roy et al., 1984) which Singh (1982) and Roy (1987) considered to be the basal unit of the Delhi Supergroup. Roy (1987) noted lithological differences between these dolomitic carbonates and dolomite-free Raialo marble outliers that are associated with basement gneisses and proposed that the former be renamed the Rayanhalla Group to avoid confusion. This interpretation is not yet accepted universally, however, and the correlation and precise stratigraphic position of the 'Raialo' carbonates remains controversial.

Aravalli sedimentation began in the east with the unconformable deposition of a linear belt of locally conglomeratic quartzite on peneplained gneissic basement, although the unconformity is frequently obscured by 0.5-3.0 km of tholeiitic to andesitic greenschists and amphibolites (Roy & Paliwal, 1981). As the detrital supply waned, a carbonate dominated association was deposited in the warm, shallow marine shelf environment (Banerjee, 1971b). Rapid facies changes between dolomitic carbonate, Fe-dolomite, Mn-dolomite, phyllitic dolomite, carbonaceous phyllite and orthoquartzite signify the importance of sea-floor topography in determining facies geometry (supratidal, intertidal, tidal, shelf, bank or shoal) and hence the nature of sedimentation (Roy & Paliwal, 1981). Ripple marks, parallel laminations, syneresis cracks and cross bedding were noted by Banerjee et al. (1986) and confirm the shallow water conditions.

A notable feature of the carbonate association is the occurrence of stromatolitic dolomite and phosphate in a limited region around Udaipur City. The stromatolites include both columnar and stratiform varieties and have been studied by many authors including Muktinath & Sant (1967), Raja Rao et al. (1968), Muktinath et al. (1969), Banerjee (1971a; 1971b), Chauhan (1979; 1980), Paliwal (1980) and Banerjee et al. (1980). *Minjaria* sp., *Minjaria calceolota*, *Collenia* sp., *Collenia baicalica*, *Collenia columnaris*, *Collenia symmetrica*, *Collenia kussiensis*, *Linella avis*, *Baicalia prima* and *Kussiella kussiensis* have all been described from occurrences in Aravalli phosphorite deposits. Their presence indicates shallow intertidal to supratidal marine conditions and their distribution (see **Figure 4.2.2**) reflects the distribution of palaeohighs on the Aravalli shelf seafloor. In addition, Banerjee (1983) reported filamentous organisms of cyanobacterial affinity from the Dakan Kotra phosphorite deposit.

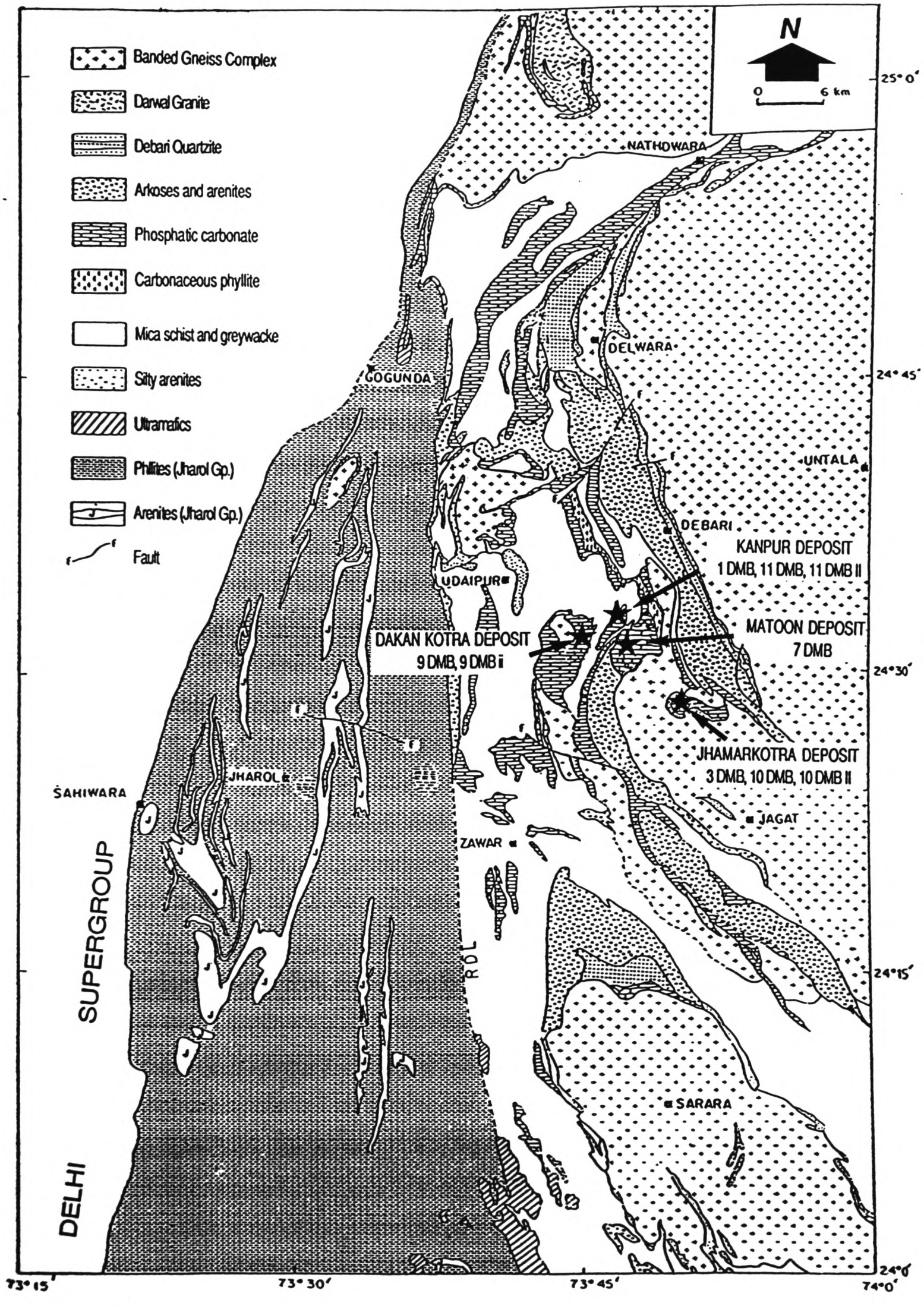

Figure 4.2.2: Geology of the Udaipur region with localities for stromatolitic phosphorite deposits from the Aravalli Supergroup, after Heron (1953) and Banerjee & Bhattacharya (1989)

The nature of the phosphate has been investigated by Banerjee (1971a), Banerjee et al. (1980) and Banerjee et al. (1986), and a broader overview of Proterozoic phosphorites in the Indian subcontinent has been presented by Banerjee (1986). The frequent association of phosphate with stromatolitic carbonate, while inter-columnar areas remain non-phosphatic, suggests that biogenic activity was important in phosphate generation - whether by primary phosphate fixation (Azad & Borchardt, 1970) or by subsequent oxidation and replacement of bacterially reduced hypophosphites (Banerjee et al., 1980). The fact that pseudomorphs of phosphate (principally carbonate fluorapatite) after carbonate and other minerals are not observed makes a replacement origin seem unlikely but conversely, the similarity of $\delta^{13}C$ values for carbonate carbon and structurally bound carbon in carbonate fluorapatite (see **Table 4h**) implies that replacement is more likely than primary fixation (Banerjee et al., 1986). The origin of phosphate in restricted shallow water environments remains enigmatic.

Banerjee et al. (1980) proposed that the Aravalli phosphorites formed in a restricted shallow marine environment, with submarine escarpments restricting shelf-basin interchange and producing oxygen-deficient, phosphate-rich shelf waters, particularly in the vicinity of stromatolite columns where circulation would have been even more restricted. The authors argued that the associated high algal productivity would cause localised CO_2 depletion around basement highs such as Kanpur and Jhamarkotra, raising the water pH and resulting in deposition of phosphate and carbonate from saturated waters (Banerjee, 1971a).

Phosphatic stromatolite samples were analysed from the Kanpur (1, 5 and 11 DMB), Jhamarkotra (3 and 10 DMB), Matoon (7 DMB) and Dakan Kotra (9 DMB) Deposits of the carbonate association, southeast of Udaipur (see **Figure 4.2.2**). All four deposits probably occupy the same stratigraphic position within the Matoon Group (formerly referred to as the Matoon Formation) (Banerjee, pers. comm. 1992), although this view is contested by Roy and co-workers who place the phosphorites much lower in the Aravalli succession (see discussion in Banerjee & Bhattacharya, 1989). Local heterogeneity of water chemistry between restricted palaeodepressions on the Aravalli sea-floor resulted in variation of the character and average composition of phosphate (ostensibly carbonate fluorapatite) between deposits (see Banerjee et al., 1980). The occurrence of late sparite and strained or recrystallised quartz crystals in many stromatolites has been attributed to the lower greenschist facies metamorphic activity documented elsewhere in the Udaipur region (Banerjee et al., 1980).

The carbonate association is succeeded by a thick rhythmic association of greywackes and phyllites, similar to deposits found in deeper parts of the Aravalli Basin to the west (Jharol Group). These fine grained clastics are indicative of an increased supply of terrigenous detritus and a contraction of the shelf environment to the east. The greywackes contain omnidirectional palaeocurrent indicators (Banerjee & Bhattacharya, 1989) which suggest that in addition to the passive continental margin formed by the Banded Gneiss Complex/Mewar Gneiss in the east, a strandplain landmass existed to the west, separating the shelf from deeper parts of the basin and creating the restricted circulation required for phosphate accumulation. This strandplain provided the source for the principally volcaniclastic greywackes. Roy & Paliwal (1981) suggested that the conglomerate-arkose-orthoquartzite deposits of Debari, found only in the east of the region may be shallower water equivalents of this association.

Aravalli Supergroup sedimentation was brought to a close by the deposition of a thick quartzite-silty arenite association (Udaipur Group). A basal polymict lenticular conglomerate is overlain by a thick orthoquartzite, frequently exhibiting cross bedding, and then by siltstones with fining upward sequences, characteristic of fluviatile origin (Allen, 1965; Pettijohn, 1975).

Throughout Aravalli times, a thick rhythmic sequence of greywackes and phyllites was deposited in the deeper parts of the basin to the west (Jharol Group; Gupta et al., 1980). These deposits are unconformably overlain by the Delhi Supergroup to the west and are bounded in the east by the Rakhavdev lineament, a north-south zone of serpentinites and amphibolites formed by the collision of the Aravalli continental margin with the landmass that formerly lay to the west.

Aravalli deposits (and associated Jharol Group sediments) record the sedimentation history of a passive continental margin, shelf-basin transition and contain evidence for the destruction of a landmass that originally lay to the west (Deb et al., 1989). The geometry of sediment bodies reflects irregularities in sea-floor topography and the nature and disposition of continental relief on both the passive continental margin and the offshore strandplain. The metamorphic grade is generally low (lower greenschist facies), although it does increase to the west, attaining a maximum of upper amphibolite facies in the Rajpura-Dariba Mines region.

A similar volcanosedimentary deposit of low metamorphic grade, the

Bhilwara Belt, outcrops to the east of the Banded Gneiss Complex/Mewar Gneiss and was thought by some to be older than the Aravalli Supergroup (Raja Rao, 1976). However, Roy et al. (1981) demonstrated their broad stratigraphic equivalence from structural and stratigraphic studies and this was subsequently confirmed by Deb et al. (1989) using Pb model ages from syngenetic stratiform galenas. To the north, metamorphic grades attain granulite facies where late tectonic movements associated with continental collision have thrust Banded Gneiss Complex/Mewar Gneiss over Bhilwara sediments.

The Delhi Supergroup outcrops in the west of the region and unconformably overlies the Jharol Group, Aravalli Supergroup and Banded Gneiss Complex/Mewar Gneiss (see **Figure 4.1.1**). It comprises the basal metacarbonates of the Rayanhalla Group (formerly Raialo Group or Series, see above); the overlying Alwar Group, a sequence of coarse clastics deposited under shallow water conditions; and the upper Ajabgarh Group of deeper water carbonate and pelitic shelf deposits. Contemporaneous volcanic activity is indicated by the extensive preservation of pillow structures throughout the Delhi Supergroup.

Deformation of the Aravalli-Delhi rocks has been studied by a number of authors, including Naha & Chaudhuri (1968), Naha & Halyburton (1974; 1977a; 1977b), Roy et al. (1971; 1980; 1981; 1985), Roy & Jain (1974), Sharma (1978), Mukhopadhyay & Gosh (1980), Ray (1983), Naha et al. (1984), Roy & Das (1985) and Mohanty & Naha (1986). Three main episodes of folding affected the Aravalli Supergroup (AF_1, AF_2 and AF_3), upon which the effects of later flat-lying, small scale folds were superimposed (Roy, 1973; Naha & Halyburton, 1974; Roy, 1987). AF_1 folding produced east-west plunging reclined and inclined folds with a penetrative schistosity, later refolded by variably oriented, open to tight AF_2 structures and again by subvertical AF_3 folds with east-west strikes. Intermittent development of ductile shear zones along basement-cover contacts allowed cover rocks to deform independently of the basement (Roy et al., 1985). Three episodes of folding are also recognised in the Delhi Supergroup (DF_1, DF_2 and DF_3). DF_1 and DF_2 occurred in close conjunction, initially producing recumbent isoclinal geometries, subsequently modified by upright DF_2 folds (Roday, 1979; Banerjee & Mitra, 1977). DF_3 structures form broad, open folds at high angles to the earlier structures.

Roy (1987) proposed that the geological evolution of the region should be considered within the framework of four major tectonic, magmatic and metamorphic events occurring at c.3000 Ma (the Mewar Gneiss Orogeny, M1), c.2000 Ma (the

Aravalli Orogeny, M2), c.1450 Ma (the Delhi Orogeny, M3) and 750-850 Ma (post-Delhi anorogenesis). Aravalli metamorphism (M2) is associated with AF_1 folding and shear zone formation and resulted in highly variable lowest greenschist to amphibolite grade rocks, with local development of granulite facies. In the vicinity of Udaipur, however, accommodation of deformation along mylonitic shear zones means that rocks are largely unaffected, allowing the stratigraphy to be confidently established. DF_1 and DF_2 episodes are inferred to be equivalent to AF_2 deformation and broadly contemporaneous with M3 lowest greenschist to amphibolite facies Delhi metamorphism, although Roy & Das (1985) suggest that M3 recrystallisation outlasted tectonic deformation. DF_3 and AF_3 folding are related to post-Delhi deformation and may have been accentuated by more recent Himalayan collisions. Local post-Delhi thermal metamorphism (M4) overprints M3 signals in the Delhi Supergroup, but is not obviously related to DF_3.

The Vindhyan Supergroup, inferred to be of Upper Proterozoic age, outcrops over an area of some 60000 km^2 and is faulted against the Aravalli-equivalent Bhilwara Belt along the northeast-southwest trending Great Boundary Fault. It is unconformably overlain in the south by the Deccan Traps. Owing to the lack of reliable age data, the precise stratigraphic position of the Vindhyan deposits is still controversial. While Deb et al. (1989) describe the deposits as post-orogenic molasse, formed from the collision of the Aravalli continental margin with a Delhi island arc (i.e. post-Delhi age as illustrated in **Figure 4.2.1**), they also acknowledge that the limited age data (see section **4.3**) equally allow them to be interpreted as equivalents of the Aravalli Supergroup, the Delhi Supergroup, or both as first proposed by Tugarinov et al. (1965).

The Lower Vindhyan Semri Group and its inferred regional equivalents reflect variable conditions of sedimentation. The total thickness varies between 20 and 4000 m and consists of shallow marine carbonates interbedded with glauconitic sandstones, shales and silicified pyroclastics, in addition to local conglomerates and abundant volcanics. Marked lateral facies variations are a notable feature of the deposits which accumulated in two separate basins, the first in Rajasthan and the second further east, near Rewa. Stromatolitic carbonates were analysed from the condensed Semri Group section in the Son Valley, near Chitrakut (12 DMB) (Auden, 1933; Singh & Pal, 1970); from basal Lower Vindhyan rocks of the Bhagwanpura Limestone Formation in the Chittorgarh region (2 DMB) (Prasad, 1975); and from the equivalent Chandi Formation of the Raipur Group in the Chattisgarh Basin, eastern Peninsular India (13, 18 and 20 DMB) (Jairaman & Banerjee, 1980;

Murti, 1987; Dutt, 1963).

The stromatolites *Gymnosolen* sp., *Inzeria* sp., *Baicalia* sp., *Tungussia* sp. and *Cryptozoon occidentale* have all been described from the Chattisgarh Basin by Schnitzer (1977), Srivastava (1977) and Jairaman & Banerjee (1980). They occur principally as columnar forms composed of micrite with disseminated spar and exhibit distinct variations in colour from black to buff to red. *Kussiella kussiensis*, *Colonella lodhwarensis* and *Collenia symmetrica* were recorded from the condensed Chitrakut section by Kumar (1976).

Upper Vindhyan sediments are largely undeformed and of more uniform character than the Lower Vindhyan (Wadia, 1966). Although a transgressive unconformable relationship is prominent in the north of the region, where it is marked by a coarse conglomerate, it becomes less apparent further south and in the vicinity of the Son Valley and around Chittorgarh a conformable transition has been demonstrated. The Upper Vindhyan is divided into the basal Kaimur Group (maximum 400 m), the Rewa Group (60-450 m) and the topmost Bhander Group (180-900 m), the latter two containing diamondiferous conglomerates. Whereas the Kaimur, Rewa and upper Bhander Groups consist of alternating shales and sandstones with local development of conglomerates, the lower Bhander Group is largely calcareous and contains the stromatolitic Bhander Limestone. Stromatolitic carbonates were analysed from the Nagod Limestone Formation of the Upper Vindhyan Bhander Limestone, south of the Panna Semaria-Salaiya area (8 and 21 DMB).

The Marwar Supergroup, named by Khan (1971), outcrops in the northwest of the region around Jodhpur (see **Figure 4.1.1**) and unconformably overlies the Delhi Supergroup. The exact stratigraphic correlations are unknown but most authors have correlated the Marwar Supergroup with the type Vindhyan sequence of the Son Valley, for example Banerjee & Jyotsna Chopra (1986) and Soni et al. (1987). Consequently, publications frequently refer to the Marwar deposits as the 'Trans-Aravallis Vindhyans'. However, Barman (1980) studied stromatolites from the area (*Collenia pseudocolumnaris*, *Colleniella* and *Cryptozoon occidentale*) and proposed that the Marwar rocks had no affinity with those of the type Vindhyan section but correlated with Cambrian rocks of the Salt Range in the Punjab. Accordingly, Awasthi & Prakash (1981) gave the age range of the Marwar Supergroup as Upper Proterozoic to Cambrian. Stromatolitic limestones were analysed from the Bilara carbonates of the Marwar Supergroup (14 DMB and 14 DMB II).

4.3: AGE CONSTRAINTS

As with many Precambrian sequences, there is lack of reliable age data for the Aravalli-Delhi orogenic belt, the Vindhyan and Marwar Supergroups and even the Banded Gneiss Complex/Mewar Gneiss, reinforcing the potential that direct dating of carbonates holds for the resolution of geochronological dilemmas in ancient carbonate-bearing sequences.

Limited age data for the Banded Gneiss Complex suggest a multiphase body consisting of gneissic components as old as 3500 Ma (Sm-Nd - MacDougall et al., 1983; Pb/Pb - Vinogradov et al., 1964). Younger components include;

- amphibolite facies gneisses and synorogenic granites in the south which have been dated at 2950 ± 150 Ma and are believed to have formed due to M1 metamorphism of evolved, highly fractionated metasediments and metamorphics/intrusives (Choudhary et al., 1984);
- the Berach Granite in the east which has been dated at 2600 ± 150 Ma (Choudhary et al., 1984; Crawford, 1970), although Roy (1987) and Banerjee & Bhattacharya (1989) express doubts over the geological interpretation of this value; and
- northern granitic components as young as 1900 Ma (Choudhary et al., 1984), believed to have been emplaced with AF_1 deformation of Aravalli sediments (syn-M2).

The age range of the Banded Gneiss Complex is therefore 3500-1900 Ma, although the lower limit probably includes a period of Aravalli-Bhilwara sedimentation. The Mewar Gneiss, that is pre-Aravalli basement, can be constrained to between 3500-?2600 Ma if the Berach Granite is considered its youngest dated component.

Deb et al. (1989) studied syngenetic stratiform galena deposits and obtained grouped Pb model ages of c.1700 Ma for the Aravalli Supergroup and c.1800 Ma for the Bhilwara Supergroup using a '*Proterozoic model*' of common Pb isotopic evolution developed by R.I.Thorpe[6]. Using the more traditional model of Stacey & Kramers (1975)[7], these values equate to respective ages of c.1665 Ma and c.1750 Ma and compare well with a Pb model age of 1700 Ma published by Chernyshev et al. (1980) for the Bhilwara deposits, reinforcing the suggestion that the two Supergroups are broadly age equivalent.

---

6 Parameters for 'Proterozoic model' of Thorpe from Deb et al. (1989) are;
$T_o = 3810$ Ma; $^{206}Pb/^{204}Pb_i = 10.844$; $^{207}Pb/^{204}Pb_i = 12.632$; $^{208}Pb/^{204}Pb_i = 31.100$.

7 Parameters for model of Stacey & Kramers (1975) are;
$T_o = 3700$ Ma; $^{206}Pb/^{204}Pb_i = 11.152$; $^{207}Pb/^{204}Pb_i = 12.998$; $^{208}Pb/^{204}Pb_i = 31.230$.

Upper and lower age limits for Aravalli-Bhilwara sedimentation are extremely poorly defined and Banerjee (1986) noted that, "*in correlation terms, the geological, palaeontological, sedimentological, environmental and radiometric data are often at odds*". An imprecise Rb-Sr isochron of 1985 ± 300 Ma for a post-Aravalli, pre-Delhi granite (Crawford, 1970) suggests that 1700 Ma is a suitable minimum limit for deposition of the Aravalli pile, while Nd model ages of 2600-2300 Ma for underlying metavolcanics (MacDougall et al., 1984) imply that a figure of around 2600 Ma may be an appropriate maximum limit. Naha et al. (1967) suggested that the Darwal Granite represented the granitisation product of Aravalli metasediments, emplaced during AF_1 folding and contemporaneous M2 metamorphism, thereby inferring that the 1900 ± 80 Ma Rb-Sr date for the intrusion (Choudhary et al., 1984) represented a minimum age for Aravalli sedimentation. This appears improbable in light of the syngenetic galena Pb model age data of Deb et al. (1989) which would suggest a value of c.1700-1600 Ma was more appropriate for the end of Aravalli sedimentation. Poorly defined fission track ages of 1400 Ma for garnets and epidotes from the Bhilwara Supergroup (Nand Lal et al., 1976) are believed to represent metamorphic cooling ages, probably associated with M3 metamorphism.

Hence the depositional age range of the Aravalli and Bhilwara Supergroups is inferred to be between 2600-1700 Ma. It is suggested that the 1900 ± 80 Ma date for the Darwal granite may represent an intrusive episode during a much longer Aravalli Orogeny. Estimates of the age of the Matoon Deposit of the Aravalli Supergroup by Salops (1968) and Keller et al. (1960) using stromatolite biostratigraphic correlation varied from Middle Riphean (1000-1850 Ma) to Upper Riphean (600-620 Ma) and failed to provide unequivocal ages for the sediments.

Granites intruding the Alwar Group of the Delhi Supergroup give Rb-Sr ages of 1565 ± 100 Ma (Choudhary et al., 1984) and Pb model ages for syngenetic stratiform galena deposits from the upper Ajabgarh Group fall in the region of 1100 Ma (Deb et al., 1989) (c.1000 Ma using parameters from Stacey & Kramers, 1975), implying that deposition of the Delhi Supergroup occurred between 1650-?1100 Ma. This range is in good agreement with the proposal of Roy & Paliwal (1981) that the Delhi Orogeny occurred between 1660-1200 Ma. However, Gopalan et al. (1979) dated the Khetri granite, considered by Roy & Das (1985) to have been emplaced synkinematically with DF_1 and DF_2 folding, at 1480 ± 40 Ma prompting Roy (1987) to conclude that this date corresponded to the end of the Delhi Orogeny and placed a minimum constraint on Delhi sedimentation. This date is considerably

older than 1.1 Ga Pb model ages for syngenetic galenas from the Delhi Supergroup (Deb et al., 1989) and since the tectonic interpretation of the Khetri Granite remains questionable, it is surmised that the Delhi Supergroup was deposited at some time between 1650-1100 Ma. Precise Pb/Pb dating of the Rayanhalla Group carbonates would provide more accurate constraints for the onset of Delhi sedimentation.

The age of the Vindhyan Supergroup, which lies in faulted contact with the Bhilwara Supergroup, is extremely poorly constrained and as a result the rocks have in the past been correlated with the Cambrian of the Salt Range (Fox, 1928 - quoted in Soni et al., 1987), the Marwar Supergroup (Gupta et al., 1980), the Delhi Supergroup (Tugarinov et al., 1965) and even the Aravalli Supergroup (Deb et al., 1989). Phlogopite micas separated from the Majhgawan kimberlite, which intrudes the Kaimur Group of the Upper Vindhyan, have been dated at 1140 ± 12 Ma (Crawford & Compston, 1970) and 1130 ± 20 Ma (Grantham, 1969 - quoted in Soni et al., 1987). K-Ar glauconite studies on sandstones from the Lower Vindhyan Semri Group have given dates of c.1400 Ma (Vinogradov et al., 1964), while similar studies by the same authors on sandstones from the Kaimur Group yielded dates of 910 ± 39 Ma and 940 Ma, at odds with values for the Majhgawan kimberlite. Since glauconite K-Ar dates are considered to provide only minimum ages for sedimentation because of diagenetic Ar loss (Clauer, 1981), one can only infer minimum ages of 1100 Ma for the Kaimur Group and 1400 Ma for the Semri Group. Banerjee (pers, comm. 1991) estimated a minimum age of 700-950 Ma for the Bhander Group, giving the Vindhyan Supergroup a possible depositional age range of >1400-?700 Ma and explaining why the rocks have in the past been correlated with Marwar, Delhi and even Aravalli deposits. Kumar (1982) compared the stromatolite forms from Chitrakut with those of the Lower Riphean Burzyan of southern Ural which has an inferred age of greater than 1260 Ma.

Palaeomagnetic studies on the equivalent Chattisgarh sequence by Verma et al. (1977) suggested that the stromatolitic Raipur Group had a probable age of 1250-1300 Ma. This range was based on the relative location of the Raipur magnetic pole between those for the Rewa and Cuddapah Sandstones, which have probable ages of 800-900 Ma (Crawford, 1969) and 1220-1600 Ma (Crawford & Compston, 1973) respectively. K-Ar studies on authigenic glauconites from sandstones of the underlying Chandarpur Group by Kreuzer et al. (1977) yielded dates of 700-750 Ma, reiterating the problems associated with the interpretation of glauconite geochronology.

The age of the Marwar Supergroup (Trans-Aravallis Vindhyans) is not well

established, but is generally accepted to be between Upper Proterozoic and Lower Cambrian (Awasthi & Prakash, 1981). In the past, Marwar rocks have been correlated with the type Vindhyan section of the Son Valley (see above for age constraints) and the Cambrian Salt Range deposits. This controversy is discussed further in section **4.4**.

4.4: RESULTS

Pb isotopic results for stromatolitic carbonates from four phosphorite deposits within the Aravalli Supergroup are detailed in **Tables 4a**, **4b**, **4c** and **4d**. Results for four separate Kanpur Deposit samples (1 DMB, 11 DMB, 11 DMB II Phos and 11 DMB II Non-Phos) are provided in **Table 4a** and presented graphically in **Figure 4.4.1**. In addition, results are given for two galena samples collected from diagenetic veins cross-cutting stromatolites of the Badgaon Deposit, which is equivalent to the Kanpur Deposit (Banerjee, pers. comm. 1992).

The eleven 11 DMB analyses exhibit a large colinear range in Pb isotopic ratios ($^{206}Pb/^{204}Pb$ 16.663-73.563) that defines a Pb/Pb errorchron date of 1159 ± 140 Ma, with an MSWD of 42.0 and a model μ_1 value of 8.46 ± 0.29. None of the other Kanpur samples exhibit such large isotopic ranges individually, but all analyses lie along approximately the same line that is defined by the 11 DMB data alone (see **Figure 4.4.1**). Combining all of the stromatolite data from the Kanpur Deposit produces a more precise seventeen point errorchron, corresponding to a date of 1161 ± 78 Ma (MSWD 46.1, model μ_1 value 8.46 ± 0.12).

Calculated Pb model ages for the two galena samples from the Badgaon Deposit yield figures of 1048 Ma (model μ_1 value 10.6) and 1056 Ma (model μ_1 value 10.6) respectively, using the two stage model of Stacey & Kramers (1975) (see footnote [7] for parameters). These model ages are consistent with the geological observation that the samples were collected from veins that cross-cut Kanpur-equivalent Badgaon stromatolites (dated at 1161 ± 78 Ma).

Table 4a: Pb isotopic compositions of carbonates from the Kanpur Deposit, Aravalli Supergroup, Udaipur, Rajasthan

SAMPLE	CORRECTED RATIOS *		
	$^{206}Pb/^{204}Pb$	$^{207}Pb/^{204}Pb$	$^{208}Pb/^{204}Pb$
1 DMB	18.478 ± 0.116	15.825 ± 0.114	37.919 ± 0.270
1 DMB I	18.367 ± 0.104	15.680 ± 0.094	37.623 ± 0.244
11 DMB	47.148 ± 0.054	18.137 ± 0.024	37.725 ± 0.052
11 DMB I	26.161 ± 0.136	16.501 ± 0.082	37.622 ± 0.238
11 DMB II	16.663 ± 0.088	15.475 ± 0.078	36.175 ± 0.212
11 DMB a	73.563 ± 0.642	20.102 ± 0.160	37.500 ±.0.352
11 DMB b	56.853 ± 0.058	18.677 ± 0.022	37.756 ± 0.046
11 DMB c	42.398 ± 0.042	17.812 ± 0.022	37.674 ± 0.046
11 DMB d	45.711 ± 0.146	18.014 ± 0.062	37.907 ± 0.134
11 DMB e	39.978 ± 0.048	17.521 ± 0.026	37.673 ± 0.054
11 DMB f	50.707 ± 0.168	18.194 ± 0.072	37.627 ± 0.198
11 DMB g	55.178 ± 0.054	18.612 ± 0.022	37.649 ± 0.046
11 DMB h	41.786 ± 0.080	17.678 ± 0.038	37.577 ± 0.102
11 DMB II Phos	25.807 ± 0.026	16.469 ± 0.020	37.661 ± 0.046
11 DMB II Phos a	27.649 ± 0.028	16.573 ± 0.020	37.656 ± 0.046
11 DMB II Non-Phos	18.361 ± 0.018	15.785 ± 0.020	37.677 ± 0.046
11 DMB II Non-Phos a	18.496 ± 0.018	15.770 ± 0.020	37.760 ± 0.046
Galena I	17.496 ± 0.018	15.721 ± 0.020	37.240 ± 0.046
Galena II	17.504 ± 0.018	15.730 ± 0.020	37.271 ± 0.048

* Corrected for mass fractionation of 0.130 % ± 0.012 ($2\sigma_{mean}$) amu^{-1}
Errors are $2\sigma_{mean}$ for corrected ratios

Results for three separate stromatolitic samples from the Jhamarkotra Deposit (3 DMB, 10 DMB and 10 DMB II) are given in **Table 4b** and presented graphically in **Figure 4.4.2**. 10 DMB and 10 DMB II were collected from the same locality. 3 DMB data alone exhibit a significant degree of scatter and while 10 DMB data have only a limited Pb isotopic range, combination of 10 DMB and 10 DMB II data produces a five point Pb/Pb errorchron corresponding to a date of 1350 ± 120 Ma with an MSWD of 3.26 and a model μ_1 value of 7.88 ± 0.19. The entire Jhamarkotra data set defines a more precise ten point errorchron date of 1316 ± 87 Ma (MSWD 62.8, model μ_1 value 7.89 ± 0.19), within error of the 10 DMB date.

Figure 4.4.1: Pb isotopic data for Kanpur Deposit stromatolites, Aravalli Supergroup, India

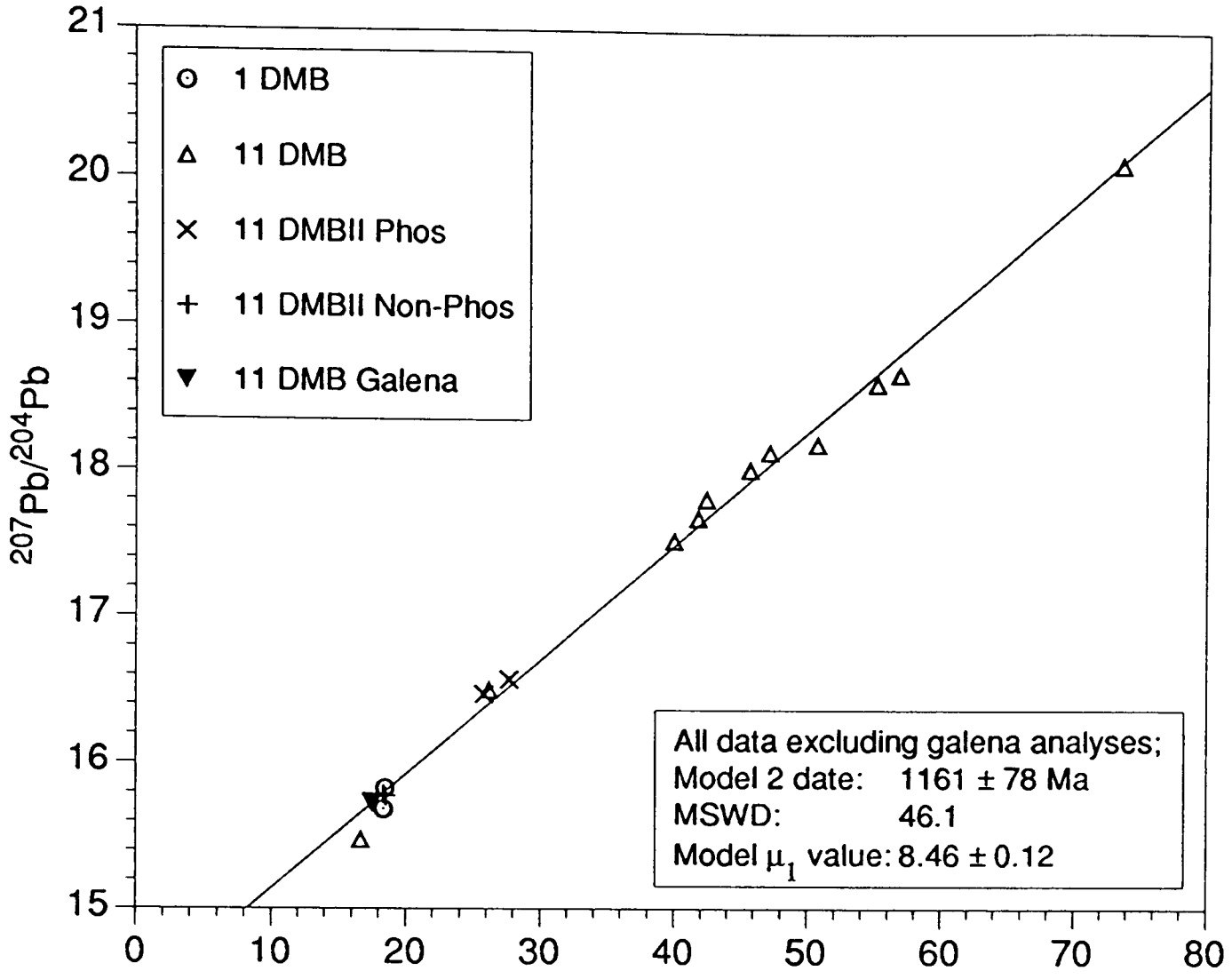

Table 4b: Pb isotopic compositions of carbonates from the Jhamarkotra Deposit, Aravalli Supergroup, Udaipur, Rajasthan

SAMPLE	CORRECTED RATIOS *		
	$^{206}Pb/^{204}Pb$	$^{207}Pb/^{204}Pb$	$^{208}Pb/^{204}Pb$
3 DMB	53.701 ± 0.054	18.381 ± 0.022	37.815 ± 0.046
3 DMB a	57.130 ± 0.058	18.870 ± 0.022	37.862 ± 0.046
3 DMB b	53.520 ± 0.054	18.422 ± 0.022	37.732 ± 0.046
3 DMB c	55.119 ± 0.054	18.501 ± 0.022	37.800 ± 0.046
10 DMB	21.643 ± 0.100	15.802 ± 0.076	36.998 ±.0.262
10 DMB I	21.923 ± 0.200	15.684 ± 0.146	36.421 ± 0.382
10 DMB X	22.686 ± 0.022	15.887 ± 0.020	36.988 ± 0.046
10 DMB Y	22.202 ± 0.026	15.822 ± 0.022	37.009 ± 0.052
10 DMB II	59.115 ± 0.060	19.041 ± 0.024	37.683 ± 0.046
10 DMB II D	47.280 ± 0.382	17.892 ± 0.126	37.334 ± 0.282

* Corrected for mass fractionation of 0.130 % ± 0.012 ($2\sigma_{mean}$) amu^{-1}
Errors are $2\sigma_{mean}$ for corrected ratios

Figure 4.4.2: Pb isotopic data for Jhamarkotra Deposit stromatolites, Aravalli Supergroup, India

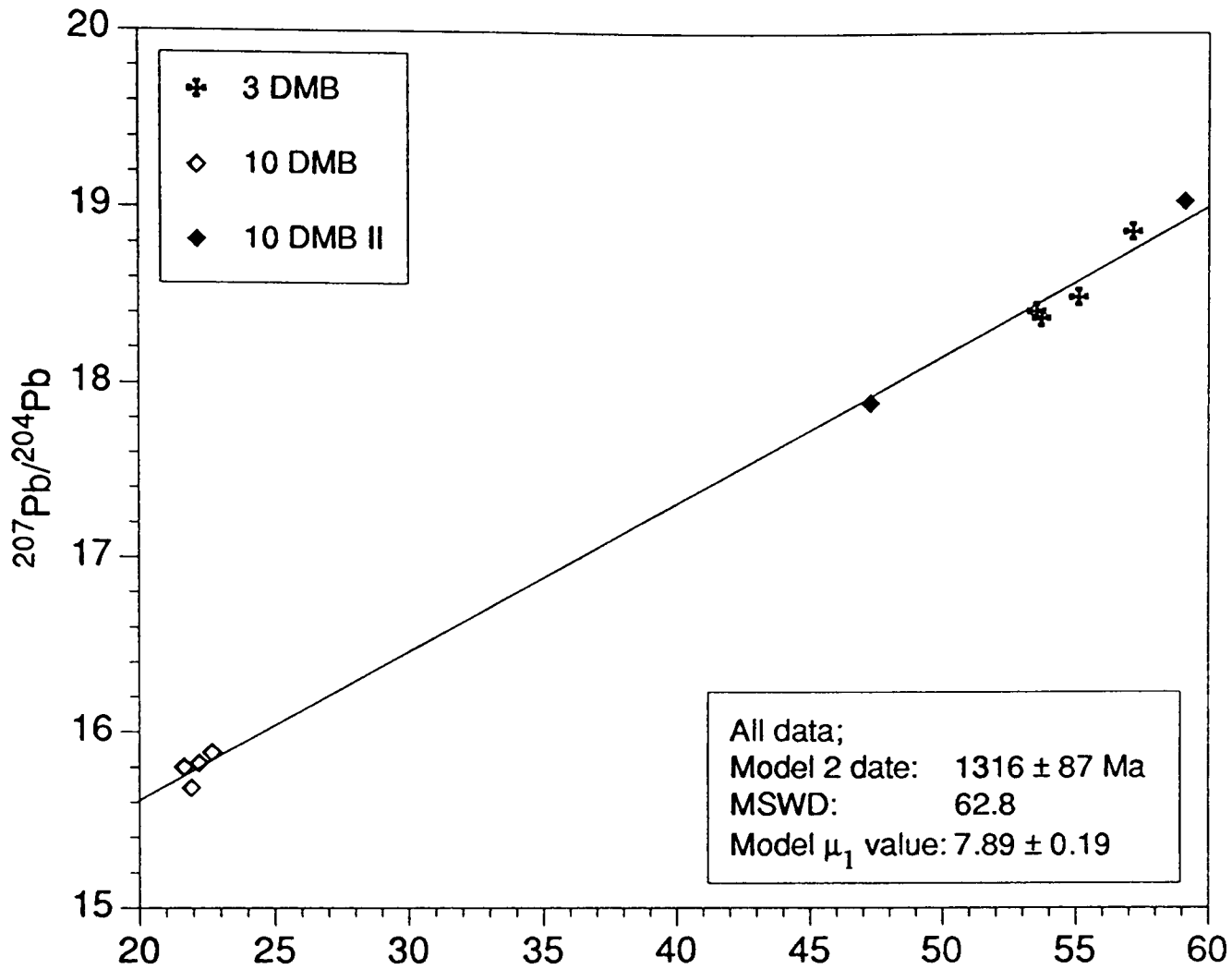

The Jhamarkotra date of 1316 ± 87 Ma and the Kanpur date of 1161 ± 78 Ma are just within error of one another but the respective model μ_1 values of 7.89 ± 0.19 and 8.46 ± 0.12 indicate that the Pb in the stromatolites originated from significantly different sources.

Pb isotopic results for the one stromatolite analysed from the Matoon Deposit (7 DMB) are given in **Table 4c** and presented graphically in **Figure 4.4.3**. In addition, the results are given for the one HCl-insoluble residue that was analysed (7 DMB BR). Although the Pb isotopic ratios exhibited by 7 DMB samples are moderately radiogenic, the relatively limited range ($^{206}Pb/^{204}Pb$ 30.861-35.474), degree of scatter and small number of data points conspire to produce an imprecise errorchron date of 1712 ± 340 Ma (MSWD 3.48, model μ_1 value 8.24 ± 0.59). Petrographic observations indicate that 7 DMB comprises small, dark grey columnar stromatolite sections with moderately well defined, slightly chaotic lamination. The mineralogy is dominated by recrystallised dolomitic carbonate with minor quartz, white mica and phosphate apparently replacing carbonate. It should be noted that for 7 DMB B, the HCl-insoluble residue has a more radiogenic Pb isotopic composition than the corresponding HCl-soluble carbonate fraction.

Table 4c: Pb isotopic compositions of carbonates from the Matoon Deposit, Aravalli Supergroup, Udaipur, Rajasthan

SAMPLE	CORRECTED RATIOS *		
	$^{206}Pb/^{204}Pb$	$^{207}Pb/^{204}Pb$	$^{208}Pb/^{204}Pb$
7 DMB	30.861 ± 0.032	16.976 ± 0.020	36.934 ± 0.046
7 DMB A	34.123 ± 0.034	17.319 ± 0.022	36.843 ± 0.046
7 DMB B	34.711 ± 0.108	17.372 ± 0.058	36.906 ± 0.120
7 DMB BR	35.474 ± 0.048	17.472 ± 0.028	36.960 ±.0.058
7 DMB C	33.134 ± 0.036	17.254 ± 0.024	36.832 ± 0.056

* Corrected for mass fractionation of 0.130 % ± 0.012 ($2\sigma_{mean}$) amu^{-1}
Errors are $2\sigma_{mean}$ for corrected ratios
R Indicates residue of corresponding carbonate sample

Figure 4.4.3: Pb isotopic data for Matoon Deposit stromatolites, Aravalli Supergroup, India

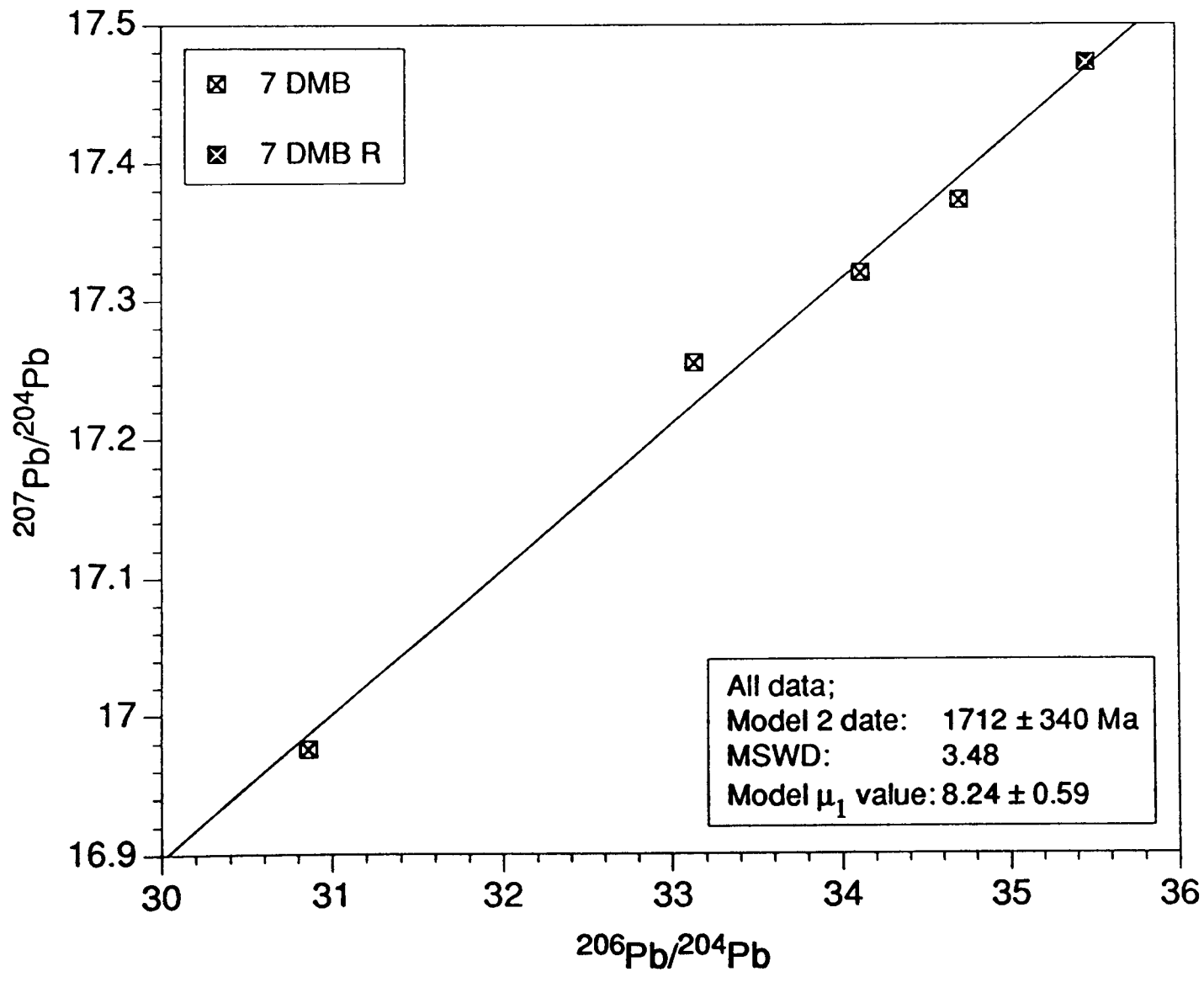

The large errors on both date and model μ_1 value make quantitative comparisons with results for the Kanpur and Jhamarkotra deposits difficult, but if one considers all Aravalli Supergroup data together (see **Figure 4.4.5**), the Matoon data does appear to define a slightly steeper slope (and therefore an older age). It should

be recognised though, that this may be merely a consequence of the limited number of data points and the small isotopic range.

Pb isotopic results for carbonate stromatolites from the fourth deposit at Dakan Kotra (9 DMB and 9 DMB ii) are given in **Table 4d**, illustrated in **Figure 4.4.4** and again as part of the complete Aravalli Supergroup data set in **Figure 4.4.5**. In addition, results are given for the analysis of one HCl-insoluble residue (9 DMB ii DR).

Table 4d: Pb isotopic compositions of carbonates from the Dakan Kotra Deposit, Aravalli Supergroup, Udaipur, Rajasthan

SAMPLE	CORRECTED RATIOS *		
	$^{206}Pb/^{204}Pb$	$^{207}Pb/^{204}Pb$	$^{208}Pb/^{204}Pb$
9 DMB II	56.773 ± 0.060	18.956 ± 0.024	37.770 ± 0.048
9 DMB a	39.197 ± 0.040	17.535 ± 0.022	37.594 ± 0.046
9 DMB b	39.610 ± 0.040	17.613 ± 0.022	37.652 ± 0.046
9 DMB c	44.366 ± 0.044	17.992 ± 0.022	37.727 ±.0.046
9 DMB d	53.131 ± 0.054	18.566 ± 0.022	37.780 ± 0.046
9 DMB ii	44.575 ± 0.044	17.922 ± 0.022	37.885 ± 0.046
9 DMB ii a	37.615 ± 0.038	17.296 ± 0.022	37.720 ± 0.046
9 DMB ii b	32.398 ± 0.032	16.917 ± 0.020	37.529 ±.0.046
9 DMB ii c	40.138 ± 0.040	17.416 ± 0.022	37.806 ± 0.046
9 DMB ii A	37.383 ± 0.038	17.300 ± 0.022	37.705 ± 0.046
9 DMB ii B	51.255 ± 0.058	18.329 ± 0.024	38.119 ± 0.050
9 DMB ii C	33.636 ± 0.038	17.053 ± 0.022	37.702 ± 0.050
9 DMB ii D	42.124 ± 0.044	17.634 ± 0.022	37.890 ±.0.046
9 DMB ii DR	46.803 ± 0.048	17.949 ± 0.022	37.903 ± 0.046

* Corrected for mass fractionation of 0.130 % ± 0.012 ($2\sigma_{mean}$) amu^{-1}
Errors are $2\sigma_{mean}$ for corrected ratios
R Indicates residue of corresponding carbonate sample

9 DMB data exhibits a more radiogenic isotopic range and a slightly higher absolute value of model μ_1 than 9 DMB ii data and defines an imprecise errorchron date of 1123 ± 270 Ma (MSWD 31.1, model μ_1 value 8.76 ± 0.55). 9 DMB ii data defines a date of 1059 ± 190 Ma (MSWD 30.7, model μ_1 value 8.61 ± 0.29) including the one residue analysis and 1089 ± 210 Ma (MSWD 31.8, model μ_1 value 8.58 ± 0.32) excluding

this point. All of the dates are within error of one another, implying geological significance, although the scale of the errors limits the chronostratigraphic potential of the dates. The residue data (9 DMB ii DR) is more radiogenic than the corresponding carbonate analysis ($^{206}Pb/^{204}Pb$ 46.803 cf. 42.124), implying higher *in situ* μ_2 values. Stromatolite 9 DMB ii comprises black to grey, heavily phosphatic dolomite with irregular stromatolitic lamination picked out by recrystallised carbonate lenses. Phosphate, quartz and chloritised mica constitute the principal residue components.

Figure 4.4.4: Pb isotopic data for Dakan Kotra Deposit stromatolites, Aravalli Supergroup, India

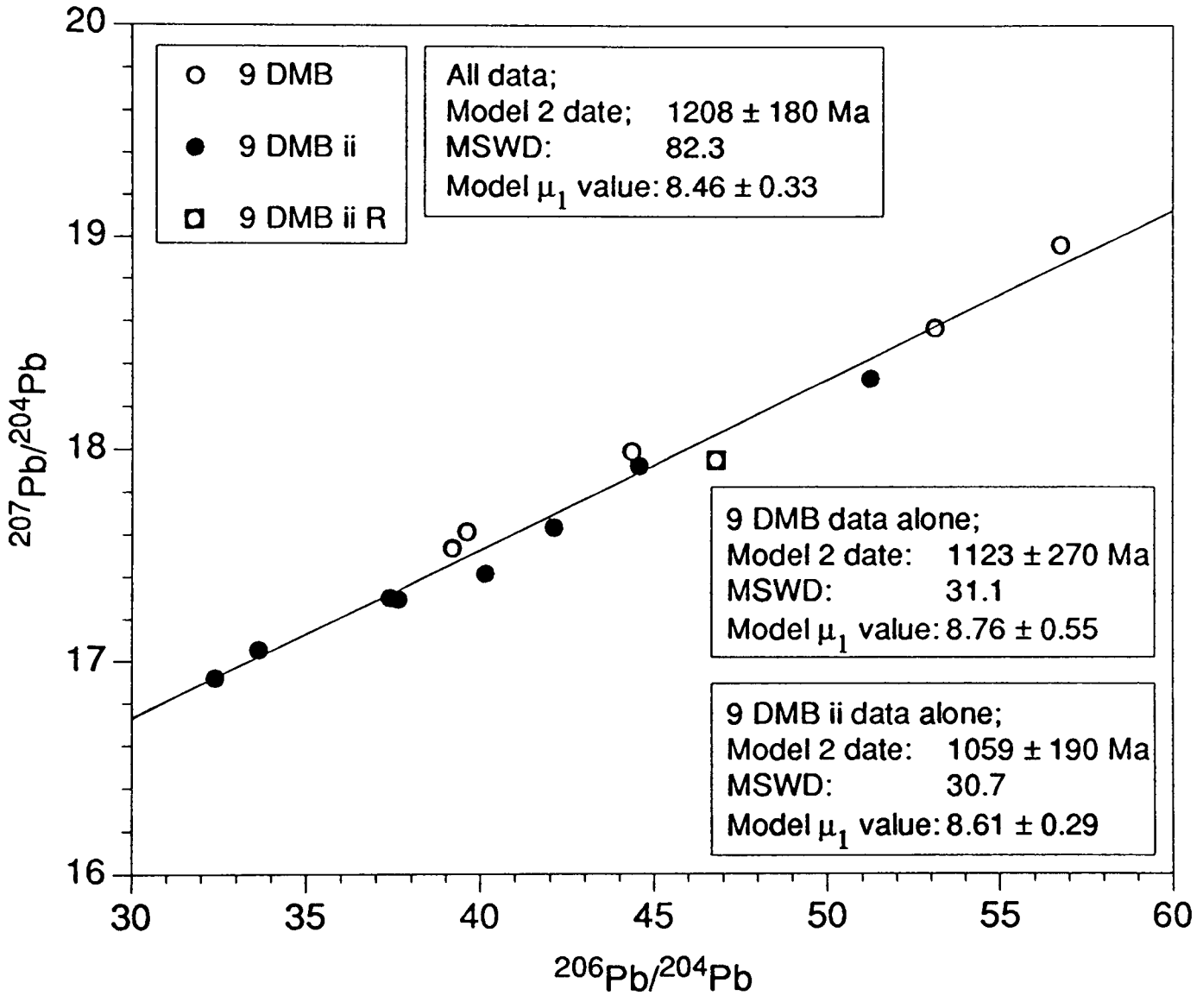

The model μ_1 values of the separate fits lie within error, justifying combination of the entire sample set to produce an increased Pb isotopic range. The combined errorchron date of 1208 ± 180 Ma (MSWD 82.3, model μ_1 value 8.46 ± 0.33) is consistent with other dates for the Dakan Kotra Deposit, but the large increase in MSWD suggests that 9 DMB and 9 DMB ii data may be strictly independent. While the combination of data increases the Pb isotopic range, it also increases the overall scatter and consequently does not result in a significant improvement in precision. The combined date remains of the correct magnitude, however, because we are considering data from stratigraphically correlated rocks of the same inferred age with similar μ_1 values.

Figure 4.4.5: All Pb isotopic data for the Aravalli Supergroup, India

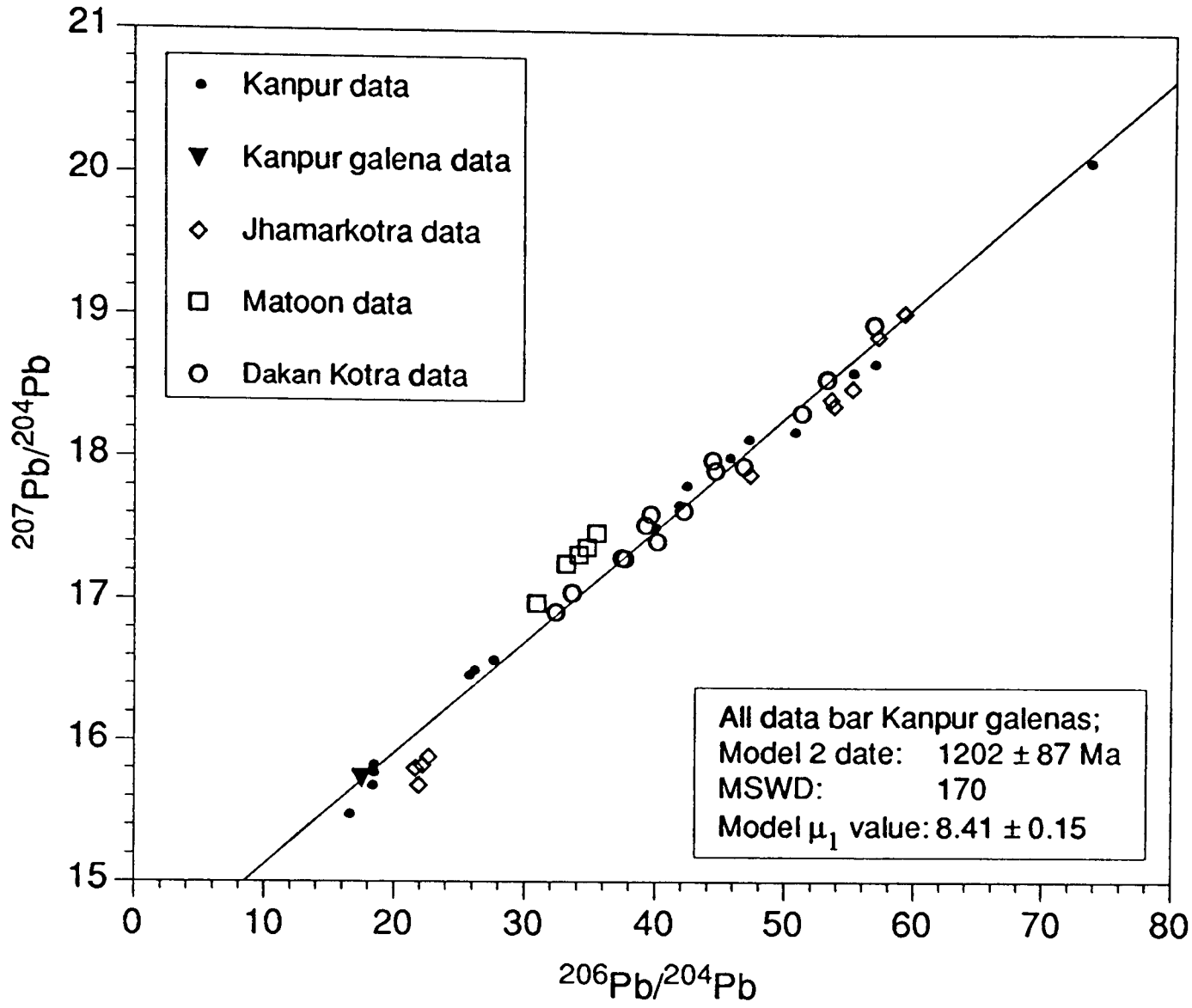

Data from all four deposits (including the diagenetic Badgaon Deposit galenas) are plotted in **Figure 4.4.5** and define a broad linear array. Regression of the total data set (excluding galena analyses) produces a Pb/Pb errorchron whose slope corresponds to a date of 1202 ± 87 Ma, with a model μ_1 value of 8.41 ± 0.15. The extremely high MSWD of 170 is mainly due to the scatter produced by variations in μ values and dates between deposits but also partly results from scatter within individual data sets. Since the combined date is within error of the dates for the Kanpur, Jhamarkotra and Dakan Kotra Deposits (see **Table 4e**) and because the date for the Matoon Deposit is based on a small number of analyses with only a limited Pb isotopic range, the combined figure of 1202 ± 87 Ma is taken to be representative of the Aravalli Supergroup.

Table 4e: Comparison of regressed data for individual phosphorite deposits and combined Aravalli Supergroup data

DATA SET	DATE (Ma)	MSWD	MODEL μ_1
Kanpur Deposit	1161 ± 78	46.1	8.46 ± 0.12
Jhamarkotra Deposit	1316 ± 87	62.8	7.89 ± 0.19
Matoon Deposit	1712 ± 340	3.48	8.24 ± 0.59
Dakan Kotra Deposit	1208 ± 180	82.3	8.46 ± 0.33
Aravalli Supergroup	1202 ± 87	170	8.41 ± 0.15

Pb isotopic data for inferred Lower Vindhyan stromatolites of the Bhagwanpura Limestone Formation, Chittorgarh (Prasad, 1975) (2 DMB); the condensed basal Lower Vindhyan section in the Son Valley, near Chitrakut (Auden, 1933; Singh & Pal, 1970) (12 DMB); and the equivalent Chandi Formation of the Raipur Group in the Chattisgarh Basin (Jairaman & Banerjee, 1980; Murti, 1987; Dutt, 1963) (13,18 and 20 DMB) are detailed in **Table 4f** and illustrated in **Figure 4.4.6**.

Table 4f: Pb isotopic compositions of carbonates from the Lower Vindhyan Supergroup and its inferred equivalents

SAMPLE	CORRECTED RATIOS *		
	$^{206}Pb/^{204}Pb$	$^{207}Pb/^{204}Pb$	$^{208}Pb/^{204}Pb$
Bhagwanpura Limestone Formation, Chittorgarh, Vindhyan Basin			
2 DMB	21.696 ± 0.022	16.159 ± 0.020	40.286 ± 0.050
Semri Group, Chitrakut, Son Valley, Vindhyan Basin			
12 DMB	20.785 ± 0.022	16.078 ± 0.020	38.000 ±.0.048
Chandi Formation, Raipur Group, Chattisgarh Basin			
13 DMB I	18.704 ± 0.018	15.768 ± 0.020	40.480 ±.0.050
18 DMB	18.363 ± 0.018	15.713 ± 0.020	40.601 ± 0.050
18 DMB II	18.254 ± 0.018	15.714 ± 0.020	39.683 ±.0.048
20 DMB	19.059 ± 0.028	15.797 ± 0.028	39.957 ± 0.074
20 DMB I	18.938 ± 0.020	15.785 ± 0.020	39.554 ± 0.050

* Corrected for mass fractionation of 0.130 % ± 0.012 ($2\sigma_{mean}$) amu^{-1}
Errors are $2\sigma_{mean}$ for corrected ratios

Figure 4.4.6: Pb isotopic data for Lower Vindhyan stromatolites and inferred equivalents, Vindhyan Supergroup, India

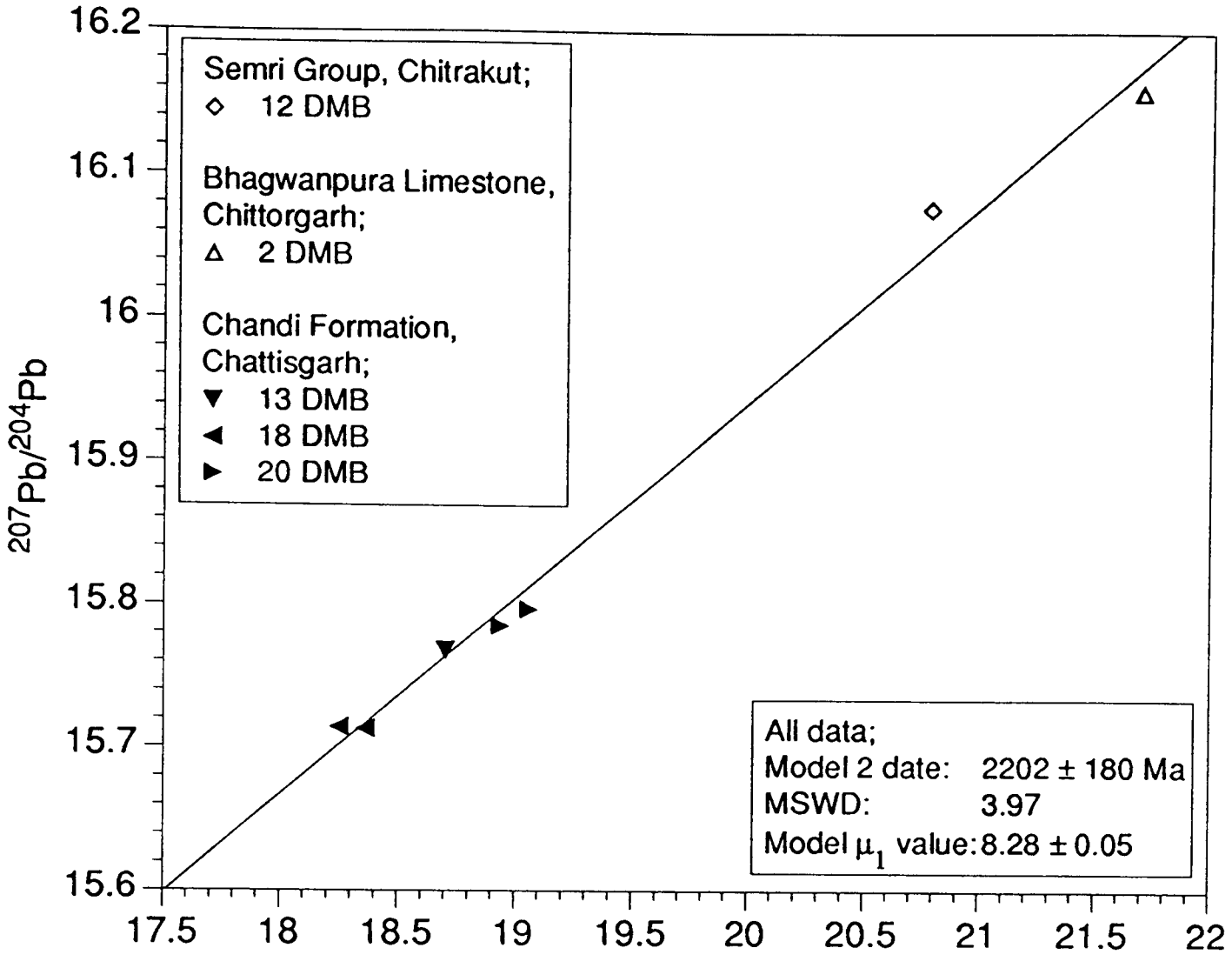

All seven analyses define a well fitted Pb/Pb isochron whose slope corresponds to a date of 2202 ± 180 Ma (MSWD 3.97, model μ_1 value 8.28 ± 0.05) (see **Figure 4.4.6**). However, this isochron fit may be a fortuitous consequence of the limited data set since the stratigraphic correlation of the Bhagwanpura Limestone Formation and the Chandi Formation (Raipur Group) with the condensed basal Vindhyan section of the Son Valley has not been demonstrated unequivocally. The former was previously correlated with the Raialo carbonates (Heron, 1936) but has been subsequently equated to the basal part of the Lower Vindhyan Group (Raja Rao & Mahajan, 1965; Prasad, 1975), while the Raipur Limestone of the Chandi Formation (Srivastava, 1977; Jairaman & Banerjee, 1980) outcrops in Madhya Pradesh, some 800 km SE of Chittorgarh and its correlation with the Lower Vindhyan rests on the pioneering work of King (1885). If one merely considers data from the Chattisgarh Basin, the five analyses define an isochron date of 1839 ± 430 Ma (MSWD 0.74, model μ_1 value 8.32 ± 0.04), within error of the combined data set, but until positive evidence for correlation exists, it should be acknowledged that both dates might not directly relate to the true geological age of the Lower Vindhyan.

Data for Upper Vindhyan limestones of the Bhander Group (8 and 21 DMB)

and for possible equivalents from the Marwar Supergroup (14 DMB and 14 DMB II) are detailed in **Table 4g** and illustrated graphically in **Figure 4.4.7**. Results for analyses of HCl-insoluble residues of 8 DMB and 14 DMB II are included.

Table 4g: Pb isotopic compositions of carbonates from the Upper Vindhyan Supergroup and inferred equivalents from the Marwar Supergroup

SAMPLE	CORRECTED RATIOS *		
	$^{206}Pb/^{204}Pb$	$^{207}Pb/^{204}Pb$	$^{208}Pb/^{204}Pb$
Upper Vindhyan Limestone, Maihar, Madhya Pradesh			
8 DMB	37.616 ± 0.038	17.652 ± 0.022	68.623 ± 0.086
8 DMB a	33.095 ± 0.034	17.228 ± 0.022	68.900 ± 0.086
8 DMB b	33.004 ± 0.034	17.192 ± 0.022	62.957 ± 0.078
8 DMB c	30.650 ± 0.030	16.939 ± 0.020	63.589 ± 0.078
8 DMB d	33.579 ± 0.034	17.214 ± 0.020	63.974 ± 0.078
8 DMB A	30.689 ± 0.030	16.998 ± 0.020	56.230 ± 0.068
8 DMB B	34.722 ± 0.062	17.340 ± 0.038	62.084 ± 0.146
8 DMB BR	25.517 ± 0.064	16.340 ± 0.056	43.811 ± 0.116
8 DMB C	35.887 ± 0.036	17.499 ± 0.022	59.425 ± 0.074
8 DMB D	35.892 ± 0.038	17.481 ± 0.022	67.604 ± 0.086
21 DMB	18.390 ± 0.018	15.742 ± 0.020	38.800 ± 0.048
21 DMB A	18.484 ± 0.018	15.763 ± 0.020	39.037 ± 0.048
Marwar Supergroup, Bilara, Western Rajasthan			
14 DMB	145.976 ± 0.228	22.954 ± 0.044	38.431 ± 0.080
14 DMB b	173.086 ± 0.276	24.537 ± 0.040	38.510 ± 0.070
14 DMB c	166.816 ± 0.244	24.198 ± 0.040	38.563 ± 0.066
14 DMB e	185.338 ± 0.494	25.342 ± 0.078	38.452 ± 0.176
14 DMB II	112.858 ± 0.124	21.378 ± 0.028	38.017 ± 0.048
14 DMB II a	130.380 ± 0.174	22.454 ± 0.032	38.200 ± 0.058
14 DMB II A	158.059 ± 0.262	24.203 ± 0.040	38.436 ± 0.066
14 DMB II B	147.012 ± 0.194	23.351 ± 0.034	38.392 ± 0.056
14 DMB II D	117.577 ± 0.552	21.895 ± 0.088	38.037 ± 0.190
14 DMB II DR	102.091 ± 0.222	20.347 ± 0.046	37.997 ± 0.086

* Corrected for mass fractionation of 0.130 % ± 0.012 ($2\sigma_{mean}$) amu^{-1}
Errors are $2\sigma_{mean}$ for corrected ratios
R Indicates residue of corresponding carbonate sample

The data illustrated in **Figure 4.4.7** clearly demonstrate that the Marwar analyses are independent of those for the Upper Vindhyan and strongly suggest

that the two are not equivalent. All Upper Vindhyan data define a twelve point Pb/Pb errorchron which corresponds to a date of 1627 ± 76 Ma with an MSWD of 7.25 and a model μ_1 value of 8.33 ± 0.10. Excluding the sole residue analysis (8 DMB BR) adjusts the date to 1602 ± 47 Ma (MSWD 5.82, model μ_1 value 8.38 ± 0.06). Considering 8 DMB data alone gives a ten point errorchron date of 1751 ± 130 Ma (MSWD 8.46, model μ_1 value 8.12 ± 0.23) including the residue analysis and a nine point date of 1609 ± 170 Ma (MSWD 7.23, model μ_1 value 8.37 ± 0.27) excluding this analysis. It is worth noting that the residue of 8 DMB is considerably less radiogenic than the HCl-soluble fraction ($^{206}Pb/^{204}Pb$ 25.517 cf. 34.722). All Upper Vindhyan regressions give dates that are within error of one another and have very similar model μ_1 values. Since it is not possible to extract significantly different subsets of data, it is concluded that the combined date of 1627 ± 76 Ma is representative of the Upper Vindhyan.

Figure 4.4.7: Pb isotopic data for inferred Upper Vindhyan stromatolites, Vindhyan Supergroup, India

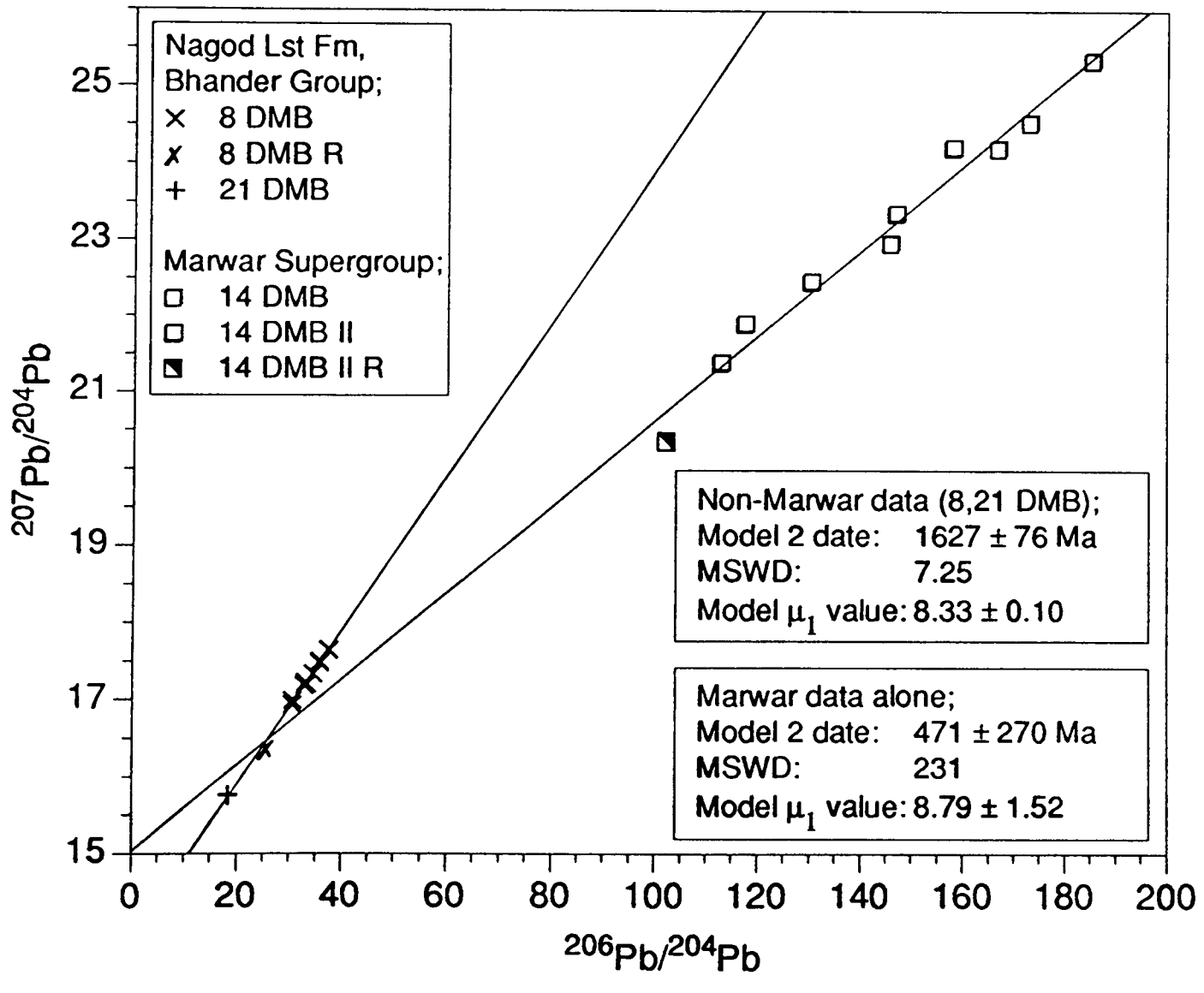

Results for two stromatolite samples (14 DMB and 14 DMB II) from the Marwar Supergroup are also given in **Table 4g** and **Figure 4.4.7**. In the past, these rocks have been correlated with both Vindhyan and Cambrian deposits on the basis of stromatolite morphology (see section 4.2). Analyses have significantly more

radiogenic Pb isotopic ratios than Upper Vindhyan data and fall along a much shallower, albeit poorly defined slope, that signifies a much younger date. All ten analyses define a date of 471 ± 270 Ma (MSWD 231, model μ_1 value 8.79 ± 1.52) and all carbonate data a date of 319 ± 280 Ma (MSWD 162, model μ_1 value 9.68 ± 1.47). Alone, analyses of 14 DMB define a date of 615 ± 190 Ma (MSWD 3.88, model μ_1 value 7.54 ± 1.37), while 14 DMB II data define a date of 768 ± 400 Ma (MSWD 132, model μ_1 value 7.40 ± 2.53) including the sole residue analysis and 566 ± 410 Ma (MSWD 53.5, model μ_1 value 8.64 ± 2.25) excluding it. The sole HCl-insoluble residue analysis (14 DMB II DR) has a Pb isotopic composition that is less radiogenic than the corresponding HCl-soluble carbonate analysis ($^{206}Pb/^{204}Pb$ 102.091 cf. 117.577).

The degree of data scatter and shallow gradient of the slope unfortunately result in large errors on the regressed dates despite the remarkably large range in Pb isotope ratios ($^{206}Pb/^{204}Pb$ from 102.091 to 185.338). Although this limits the usefulness of the data for purposes of absolute chronostratigraphy, all of the dates are significantly younger than those for the supposedly correlated Vindhyan deposits and this places grave doubts on their stratigraphic equivalence.

4.5: DISCUSSION

Dates obtained from Pb isotopic data for carbonates from phosphorite deposits of the Aravalli Supergroup are summarised in **Table 4e**. The combined regression date of 1202 ± 87 Ma (MSWD 170, model μ_1 value 8.41 ± 0.15) is taken to be representative of the Aravalli Supergroup, since the older value of 1712 ± 340 Ma for the Matoon Deposit (MSWD 3.48, model μ_1 value 8.24 ± 0.59) is based on only a small number of data points possessing a limited isotopic range. This combined date represents an average age for the four phosphorite deposits and masks variations in date and model μ_1 value that exist between individual deposits. For example, the Jhamarkotra Deposit has a significantly lower model μ_1 value than any of the other regressions (7.89 ± 0.19) and was probably sourced from a distinct reservoir to the Kanpur, Dakan Kotra and possibly even Matoon Deposits, yet in the combined data set the higher model μ_1 values of the other deposits mask this low value to produce an averaged figure of 8.41 ± 0.15. It is clear, however, that the regressed dates are for the most part significantly younger than the inferred 2600-1700 Ma age of Aravalli sedimentation and in fact approximate to the end of the 1660-1200 Ma 'Delhi Orogeny', as proposed by Roy & Paliwal (1981). The Aravalli dates are also a little younger

than poorly defined 1.4 Ga fission track ages reported by Nand Lal et al. (1976) for garnets and epidotes from the Bhilwara Supergroup which they believed to represent metamorphic cooling ages. These fission track ages are consistent with the culmination of the 'Delhi Orogeny', as defined by Roy (1987), at 1450 Ma and would be interpreted as M3 metamorphic cooling ages.

Banerjee et al. (1980) noted the occurrence of recrystallisation effects in carbonate and detrital quartz crystals and the relative abundance of late sparite in all phosphatic carbonate stromatolites from the Aravalli Supergroup. This observation is confirmed and reinforced by a number of petrographic thin section studies carried out in this work. It is proposed that these phenomena are related to the episode of regional lower greenschist facies metamorphism (M3) that accompanied tectonic deformations DF_1, DF_2 and AF_2, and resulted from collision of an offshore island arc with the Aravalli continental margin in late to post-Delhi times. Although metamorphic effects are subdued in the vicinity of Udaipur, fluid activity could have been sufficient to result in the observed carbonate recrystallisation and produce isotopic resetting of primary depositional signals without effecting large scale greenschist facies metamorphic recrystallisation and mineralogical reconstitution. It is proposed therefore that the combined c.1.2 Ga date for Aravalli Supergroup phosphorites corresponds to a metamorphic cooling age and approximates to the end of Aravalli-Delhi tectonic deformation (Delhi Orogeny).

Supporting evidence exists for this interpretation. HCl-insoluble residue analyses for Aravallian stromatolites (7 DMB BR and 9 DMB ii DR) both exhibit more radiogenic Pb isotopic compositions than their corresponding carbonate analyses ($^{206}Pb/^{204}Pb$ 35.474 cf. 34.711 and 46.803 cf. 42.124, respectively). The documented isotopic discordance could either be attributable to higher *in situ* μ values (μ_2 values) for detrital/authigenic non-carbonate components or to preferential relocation of mobilised carbonate U in silicate and phosphate minerals during metamorphic recrystallisation (as observed in Indian Archaean marbles, **Chapter 3**), or perhaps more realistically to some combination of both.

Published stable isotopic data for Aravalli Supergroup carbonate phosphorites (Banerjee et al., 1986; Banerjee et al., 1992) and results obtained from this study are detailed in **Table 4h**. The similarity of phosphate $\delta^{13}C_{apatite}$ and $\delta^{18}O_{apatite}$ and carbonate $\delta^{13}C$ and $\delta^{18}O$ values suggests that the phosphate probably originated from the replacement of carbonate rather than primary precipitation, as Banerjee et al. (1980) had proposed from petrographic observations. The stable isotopic data could

Table 4h: Stable isotopic data for the Aravalli Supergroup

SAMPLE	C_{total}	$C_{organic}$	CO_2 in apatite	$\delta^{13}C_{apatite}$	$\delta^{13}C_{carbonate}$	$\delta^{18}O_{apatite}$	$\delta^{18}O_{carbonate}$	$\delta^{13}C_{organic}$
	(%)	(%)	(%)			(all ‰ relative to PDB)		
Matoon Group - Kanpur Deposit								
1 DMB	—	—	—	—	-0.6	—	-6.3	—
11 DMB (a)	—	—	—	—	-0.3	—	-10.8	—
11 DMB (b)	—	—	—	—	-0.2	—	-10.8	—
11 DMB (c)	—	—	—	—	-0.4	—	-10.5	—
11 DMB (d)	—	—	—	—	+0.1	—	-11.2	—
11 DMB Phos (a)	—	—	—	—	+0.1	—	-11.8	—
11 DMB Phos (b)	—	—	—	—	+0.2	—	-11.6	—
Matoon Group - Jhamarkotra Deposit								
3 DMB (a)	—	—	—	—	±0.0	—	-10.7	—
3 DMB (b)	—	—	—	—	±0.0	—	-10.8	—
10 DMB (a)	—	—	—	—	-0.3	—	-10.4	—
10 DMB (b)	—	—	—	—	-3.3	—	-7.9	—
10 DMB II	—	—	—	—	±0.0	—	-11.4	—
Matoon Group - Matoon Deposit								
7 DMB (a)	—	—	—	—	-1.6	—	-11.2	—
7 DMB (b)	—	—	—	—	-2.1	—	-12.0	—
Matoon Group - Dakan Kotra Deposit								
9 DMB (a)	—	—	—	—	-0.4	—	-10.1	—
9 DMB (b)	—	—	—	—	-0.6	—	-10.5	—
9 DMB ii (a)	—	—	—	—	-0.3	—	-10.2	—
9 DMB ii (b)	—	—	—	—	-0.3	—	-10.4	—
2.1*	2.86	0.16	1.38	—	-1.1	—	-10.6	-14.7
2.2*	7.27	0.15	1.30	—	+0.7	—	-13.4	-15.9
2.3*	6.01	0.19	0.50	-1.0	-0.7	-10.4	-10.3	-13.7
2.4*	4.61	0.32	0.49	-0.7	-0.4	-11.6	-11.1	-14.1
2.5*	7.38	0.28	0.55	—	-0.1	—	-11.3	-13.2
2.6*	1.57	0.23	0.50	-0.4	-0.8	-11.6	-11.4	-14.5
2.7*	8.77	0.13	1.02	+0.2	+0.1	-11.6	-11.6	-13.9
2.8*	2.20	0.05	1.40	±0.0	-2.2	—	-10.8	—
2.9*	2.02	0.24	0.90	—	-1.1	—	-11.8	-21.8
2.10*	1.70	0.14	0.30	+0.2	-0.6	—	-11.8	—
2.11*	8.10	0.45	0.20	—	-0.7	—	-14.1	-11.4
2.12*	7.80	0.09	0.38	—	-1.6	—	-17.6	-17.6
Debari Gp.**	—	3.39	—	—	—	—	—	-28.3
	—	0.27	—	—	—	—	—	-8.1
	—	1.02	—	—	—	—	—	-25.2
Matoon Gp.**	—	0.43	—	—	—	—	—	-9.7
	—	0.92	—	—	—	—	—	-12.5
	—	—	—	—	—	—	—	-11.7
	—	—	—	—	—	—	—	-17.6
Jharol Gp.**	—	1.62	—	—	—	—	—	-20.2

* Data from Banerjee et al. (1986). Samples are non-specific from Aravallian phosphorite deposits of Udaipur and Madhya Pradesh

** Data from Banerjee et al. (1992). Samples are all Aravalli Supergroup carbonates
Data from this work are quoted to the same number of decimal places as in the above studies

also indicate the effects of metamorphism. Although $\delta^{13}C_{carbonate}$ values (-3.3 to +0.7‰) are consistent with a marine intertidal to supratidal origin and $\delta^{18}O_{carbonate}$ values (-17.6 to -6.3‰) are not unusual for sedimentary carbonates of this age (Banerjee et al., 1986), there is evidence for a positive excursion in $\delta^{13}C_{organic}$ values (range -8.1 to -28.3‰, average -15.8‰), compared with the well-defined norm for the fossil $\delta^{13}C_{organic}$ record of -25 to -27‰.

Banerjee et al. (1986) attributed this positive $\delta^{13}C_{organic}$ excursion to probable primary factors associated with a diffusion-limited assimilatory pathway, akin to modern cyanobacteria which also have heavy kerogen compositions. However, the authors also stated that increasing metamorphic grade could result in similarly heavy $\delta^{13}C_{organic}$ compositions in response to progressive $^{13}C/^{12}C$ exchange between kerogen and carbonate during isotopic re-equilibration (Valley & O'Neil, 1981; Arneth et al., 1985). More recently, Banerjee et al. (1992) analysed H/C values for Aravalli carbonates and phyllites in addition to total organic carbon (TOC) and $\delta^{13}C_{organic}$ values and obtained a range of 0.03-0.34. Such low absolute values are indicative of advanced thermal degradation (Hayes et al., 1983) and suggest that elevated metamorphic temperatures were indeed a contributing factor to the alteration of Aravalli sediments.

While the majority of Aravalli sediments exhibit greenschist to amphibolite facies metamorphism, the phosphorite deposits in the area around Udaipur remained largely unaffected because deformation was accommodated along basal mylonitic shear zones. Nevertheless, the evidence indicates that M3 metamorphism must still have accounted, at least in part, for the observed carbonate recrystallisation, the positive excursion in $\delta^{13}C_{organic}$ values, the low H/C ratios and the resetting of Pb/Pb carbonate systematics.

Pb model ages of c.1050 Ma for diagenetic galenas from veins cutting stromatolites of the Badgaon Deposit, equivalent to those of the Kanpur Deposit, indicate a late episode of Pb mineralisation derived from a relatively U enriched source with comparatively high μ_1 value (c.10.6). This figure is approximately equivalent to dates of 1.1 Ga for syngenetic galenas from the Delhi Supergroup (Deb et al., 1989).

Dates for both the Upper and Lower Vindhyan Supergroup are in excess of the minimum 1400 Ma K-Ar date for glauconites from the Semri Group of the Lower Vindhyan (Tugarinov et al., 1965). The Lower Vindhyan date of 2202 ± 180 Ma (MSWD 3.97, model μ_1 value 8.28 ± 0.05) (see **Figure 4.4.6**) may be spurious,

as previously stated, since it is calculated from the combination of restricted data sets of uncertain correlation. The Upper Vindhyan date of 1627 ± 76 Ma (MSWD 7.25, model μ_1 value 8.33 ± 0.10) (see **Figure 4.4.7**), however, is derived from a larger data set for which no significantly different data subsets can be defined and hence it is concluded that this value has real geological significance.

The sole Upper Vindhyan residue analysis (8 DMB BR) is considerably less radiogenic than its corresponding HCl-soluble fraction ($^{206}Pb/^{204}Pb$ 25.517 cf. 34.722). Petrographic observations reveal fine grained grey carbonate, exhibiting a sub-millimetre scale stromatolitic lamination, whose principal non-carbonate components are fine grained quartz and haematite, along with very rare white mica. The differing isotopic composition of carbonate and residue could indicate that metamorphic recrystallisation had not extensively affected the stromatolitic sediments, since one might expect metamorphically mobilised U to become preferentially sited in silicate fractions on recrystallisation, thereby increasing their *in situ* μ_2 values and resulting in more radiogenic Pb isotopic compositions than co-existing carbonate. This is in accordance with the observation of Banerjee et al. (1992) that, "*no signs of a metamorphic overprint are evident*" in the Vindhyan Basin. In the absence of evidence for a metamorphic event, the 1627 ± 76 Ma date is interpreted as the age of deposition/early diagenesis, the two being indistinguishable within the scale of the quoted errors.

Stable isotopic data for the Vindhyan Supergroup, detailed in **Table 4i**, may also be considered consistent with this interpretation. $\delta^{13}C_{carbonate}$ values range from +0.2 to +4.2‰ and are largely typical of depositional signals for shallow marine sediments (+0.4 ± 2.6‰; Schidlowski et al., 1983), although they do suggest the presence of evolved kerogens in certain samples. $\delta^{18}O_{carbonate}$ values vary from -3.1 to -10.7‰ and suggest that variable degrees of post-depositional $^{18}O/^{16}O$ exchange with isotopically light meteoric and surface waters had taken place. Banerjee et al. (1992) detailed $\delta^{13}C_{organic}$ analyses for limestones and shales from the Vindhyan Supergroup (see **Table 4i**) and found that Lower Vindhyan limestones and shales averaged -24.7‰, while Upper Vindhyan shales averaged -31.2‰. These values are typical of sedimentary organic carbon in the geological record, which averages -27 ± 7‰ (Schidlowski et al., 1983), and suggest that minimal post-depositional alteration has occurred.

Table 4i: Stable isotopic data for the Vindhyan Supergroup

SAMPLE	TOC	$\delta^{13}C_{carbonate}$	$\delta^{18}O_{carbonate}$	$\delta^{13}C_{organic}$
	(%)	(all ‰ relative to PDB)		
LOWER VINDHYAN				
Semri Group, Chitrakut, Son Valley				
12 DMB (a)	—	+0.5	-7.0	—
12 DMB (b)	—	+0.2	-6.9	—
Bhagwanpura Limestone Formation, Chittorgarh				
2 DMB (a)	—	+0.6	-6.6	—
2 DMB (b)	—	+0.7	-6.3	—
Raipur Group, Chattisgarh				
18 DMB (a)	—	+3.1	-8.5	—
18 DMB (b)	—	+2.9	-6.5	—
20 DMB (a)	—	+2.7	-10.3	—
20 DMB (b)	—	+2.6	-10.7	—
*	—	+4.0	-10.0	—
32**	0.21	—	—	-19.8
33**	1.51	—	—	-26.0
RP-3**	3.95	—	—	-25.9
RP-4**	0.21	—	—	-24.1
34**	0.89	—	—	-29.7
35**	1.28	—	—	-25.9
36**	0.27	—	—	-19.8
RP-6**	0.12	—	—	-26.0
UPPER VINDHYAN				
Kaimur Group				
I/1**	—	—	—	-23.3
I/3**	—	—	—	-32.8
I/3N**	—	—	—	-33.0
I/4**	—	—	—	-33.2
I/4N**	—	—	—	-32.9
II/8**	—	—	—	-31.9
Bhander Group				
8 DMB (a)	—	+0.6	-3.1	—
8 DMB (b)	—	+0.6	-4.5	—
21 DMB (a)	—	+4.2	-8.0	—

* Data from Banerjee (1990)
** Data from Banerjee et al. (1992)
Data from this work are quoted to the same number of decimal places as in the above studies

Thus, it appears unlikely that Deb et al. (1989) correctly described the Vindhyan deposits as post-orogenic molasse sediments formed from the collision of the Aravalli continental margin with a Delhi island arc (i.e. post-Delhi age). The new age data for the Upper Vindhyan indicates that the deposits are equivalent to the Delhi Supergroup in part, and Vindhyan sedimentation may have extended as far back as mid to late Aravalli times. Tugarinov et al. (1965) and Deb et al. (1989) have

commented on the possibility of such an interpretation.

The opinion that deposits of the Vindhyan Supergroup could be stratigraphically correlated with those of the Marwar Supergroup (hence termed the Trans-Aravallis Vindhyans), as advocated by Banerjee & Jyotsna Chopra (1986) and a number of other authors, was questioned by Barman (1980) who suggested that Marwar stromatolites bore closer affinity to fossils found in the Cambrian successions of the Salt Range. Although Pb isotopic results for the Marwar Supergroup are imprecise, they define a Pb/Pb errorchron date of 471 ± 270 Ma which is clearly significantly younger than the 1627 ± 76 Ma age for Upper Vindhyan carbonates (see **Figure 4.4.7**). High *in situ* μ_2 values of between 302 and 592 are indicated by the present-day radiogenic carbonate Pb analyses. The fact that the sole HCl-insoluble residue analysis (14 DMB II DR) has a composition that is less radiogenic than the corresponding HCl-soluble analysis ($^{206}Pb/^{204}Pb$ 102.091 c.f. 117.577) may again indicate that the stromatolite had not been subject to significant metamorphic alteration. In thin section, an alternation of quartz-rich and carbonate-rich layers defines a regular, 2-3 mm stromatolitic lamination, but sub-angular to sub-rounded grain geometries and evidence of subgrain formation in both quartz and calcite suggest that diagenetic recrystallisation has occurred.

Table 4j: Stable isotopic data for the Marwar Supergroup

SAMPLE	TOC	$\delta^{13}C_{carbonate}$	$\delta^{18}O_{carbonate}$	$\delta^{13}C_{organic}$
	(%)		(all ‰ PDB)	
14 DMB (a)	—	+0.4	+2.6	—
14 DMB (b)	—	+0.5	+5.4	—
14 DMB II (a)	—	+0.4	+3.6	—
14 DMB II (b)	—	+0.5	+5.1	—

Data from this work are quoted to the same number of decimal places as in previous studies

Limited stable isotopic data for the Marwar Supergroup are detailed in **Table 4j** and although the $\delta^{13}C$ values are typical of shallow marine carbonates, the $\delta^{18}O$ values are relatively heavy and show a positive range of between +2.6 and +5.4‰, averaging +4.2‰. It should be noted that 14 DMB and 14 DMB II analyses come from two separate stromatolites, some 30 m apart, and as such the stable isotope data can not be directly attributed to peculiar microenvironmental conditions but have to be explained in some more general context. Such heavy oxygen compositions are unusual in that carbonate sediment formed in shallow sea water tends to have

$\delta^{18}O$ values of around -0.5‰ relative to PDB (Scoffin, 1987) and in ancient rocks, post-depositional $^{18}O/^{16}O$ exchange with isotopically light meteoric and surface waters through weathering will usually lead to progressive ^{18}O depletion and more negative $\delta^{18}O$ values. This peculiar isotopic signature may be explained through a model involving early carbonate recrystallisation by ^{16}O depleted evaporitic groundwaters which formed in stromatolitic intertidal to supratidal environments without significant fractionation of the carbon isotopic signature. It is interesting to consider that the subsequent preservation of such an isotopic signal requires restricted post-recrystallisation interaction with external, ^{18}O depleted surface groundwaters.

4.6: CONCLUSIONS

Critical assessment of published age data for the Aravalli-Delhi orogenic belt within the framework of the four stage evolutionary model proposed by Roy (1987) and the inferred regional stratigraphy (illustrated in **Figure 4.2.1**), allows the geochronology of the belt to be established. Direct Pb/Pb dating of stromatolites from the Aravalli, Vindhyan and Marwar Supergroups has provided new age constraints which have been integrated to revise ages for the Delhi Orogeny, the Vindhyan Supergroup and the Marwar Supergroup and to reassess their lithostratigraphic correlations.

The minimum age range for the polyphasal Mewar Gneiss (strictly pre-Aravalli basement cf. Banded Gneiss Complex) is 3500-2600 Ma. The first major metamorphic event occurred at c.3000 Ma (M1) and resulted in the intrusion of the Untala and Gingla granites in the south (2950 ± 150 Ma, Choudhary et al., 1984). The 2600 ± 150 Ma date for the Berach granite (Choudhary et al., 1984) is the youngest for positively identified pre-Aravalli basement and may signify culmination of the Mewar Gneiss Orogeny (approximately 3000-2600 Ma).

Deposition of the Aravalli Supergroup and the equivalent Bhilwara Supergroup took place some time between 2600-1700 Ma (2.6-2.3 Ga Nd model ages for sub-Aravalli volcanics - MacDougall et al., 1984; 1.7-1.8 Ga Pb model ages for syngenetic galenas from Aravalli/Bhilwara sediments - Deb et al., 1989). Northern granitic outcrops of the Banded Gneiss Complex, such as the Amet Granites (1870 ± 200 Ma; Choudhary et al., 1984), bear a distinct similarity in age to the Darwal Granite (1900 ± 80 Ma, Choudhary et al., 1984), which some consider to have been synkinematically emplaced with first folding of the Aravalli pile (M2, AF_1) (Naha

et al., 1967). This interpretation is inconsistent with published Pb model ages and the intrusions are interpreted within the context of a longer Aravalli Orogeny (approximately 2000-1750 Ma).

Deposition of the Delhi Supergroup occurred between 1600-?1100 Ma (1565 ± 100 Ma granites intrude the Alwar Group - Choudhary et al., 1984; 1.1 Ga Pb model ages for syngenetic galenas of the upper Ajabgarh Group - Deb et al., 1989). Effects of the main Delhi Orogeny continued from c.1500-1150 Ma, and are constrained by;

- a 1480 ± 40 Ma date for the Khetri granite (Gopalan et al., 1979), considered to have been emplaced during Delhi deformation;
- 1400 Ma fission track cooling ages for garnets and epidotes from the Bhilwara Supergroup (Nand Lal et al., 1976); and
- a new 1202 ± 87 Ma Pb/Pb date for metamorphically recrystallised (M3) phosphatic stromatolites from the Matoon Group, Aravalli Supergroup (this work, see **Figure 4.4.5**).

The application of direct Pb/Pb carbonate dating to the basal Delhi Rayanhalla marbles would allow a more meaningful interpretation of the Delhi metamorphic history. It is proposed that Pb model ages of c.1050 Ma for galenas from diagenetic veins in the Aravallian Badgaon phosphorite Deposit (this work, section **4.4**) are equivalent to the late 1.1 Ga episode of base metal deposition observed in the Delhi Supergroup (Deb et al., 1989). This episode of mineralisation took place after the culmination of Delhi orogenic activity (around 1200 Ma).

Variation in the regressed dates for individual Aravallian phosphorite deposits (see **Table 4e**) may reflect variable metamorphic fluid activity in the region during the Delhi Orogeny, despite the fact that all deposits lie within 10 km of one another. Indeed, a particularly low model μ_1 value for the Jhamarkotra Deposit (7.89 cf. 8.3-8.6) implies that sources for recrystallising groundwaters were not uniform. Model μ_1 values for the other deposits are concordant within error and average 8.39, suggesting a U-Pb source of evolved character, such as the Banded Gneiss Complex which outcrops to the east. While dates for the Kanpur, Jhamarkotra and Dakan Kotra Deposits clearly indicate post-Aravalli recrystallisation, the imprecise Matoon date of 1712 + 340 Ma may correspond to earlier M2 recrystallisation during the Aravalli Orogeny (2000-1750 Ma).

Very poor age constraints were previously available for the Vindhyan Supergroup, which lies faulted against the Aravalli-equivalent Bhilwara Supergroup to the east of the Berach granite. A depositional age range of >1400-?700 Ma was

inferred. However, Pb/Pb data for stromatolites from undeformed Upper Vindhyan carbonates define a much older depositional/early diagenetic age of 1627 ± 46 Ma (this work). In light of this evidence, Vindhyan deposits should be correlated in part with the Aravalli and Delhi Supergroups, as was originally proposed by Tugarinov et al. (1965) (cf. **Figure 4.2.1**). Vindhyan sediments remained unaffected by the deformations of the Aravalli and Delhi Orogens, suggesting that movement along the Great Boundary Fault occurred later than c.1100 Ma.

No published direct age data exist for sediments of the Marwar Supergroup and consequently they have been correlated in the past with the Vindhyan Supergroup and sediments of the Cambrian Salt Range, amongst others. Pb/Pb data for stromatolites from the Bilara region give an imprecise latest Upper Proterozoic to lower Phanerozoic date of 471 ± 270 Ma (this work). While detailed chronostratigraphic observations are not possible, it is evident that the deposits, which unconformably overlie the Delhi Supergroup, do not correlate with the Vindhyan Supergroup and are more likely to be broadly equivalent to those of the Salt Range, as suggested by Barman (1980).

Figure 4.6.1: Regional stratigraphy of the Aravalli-Delhi orogenic belt, after Heron (1953), Roy (1987), Deb et al. (1989), Banerjee et al. (1992) and this work

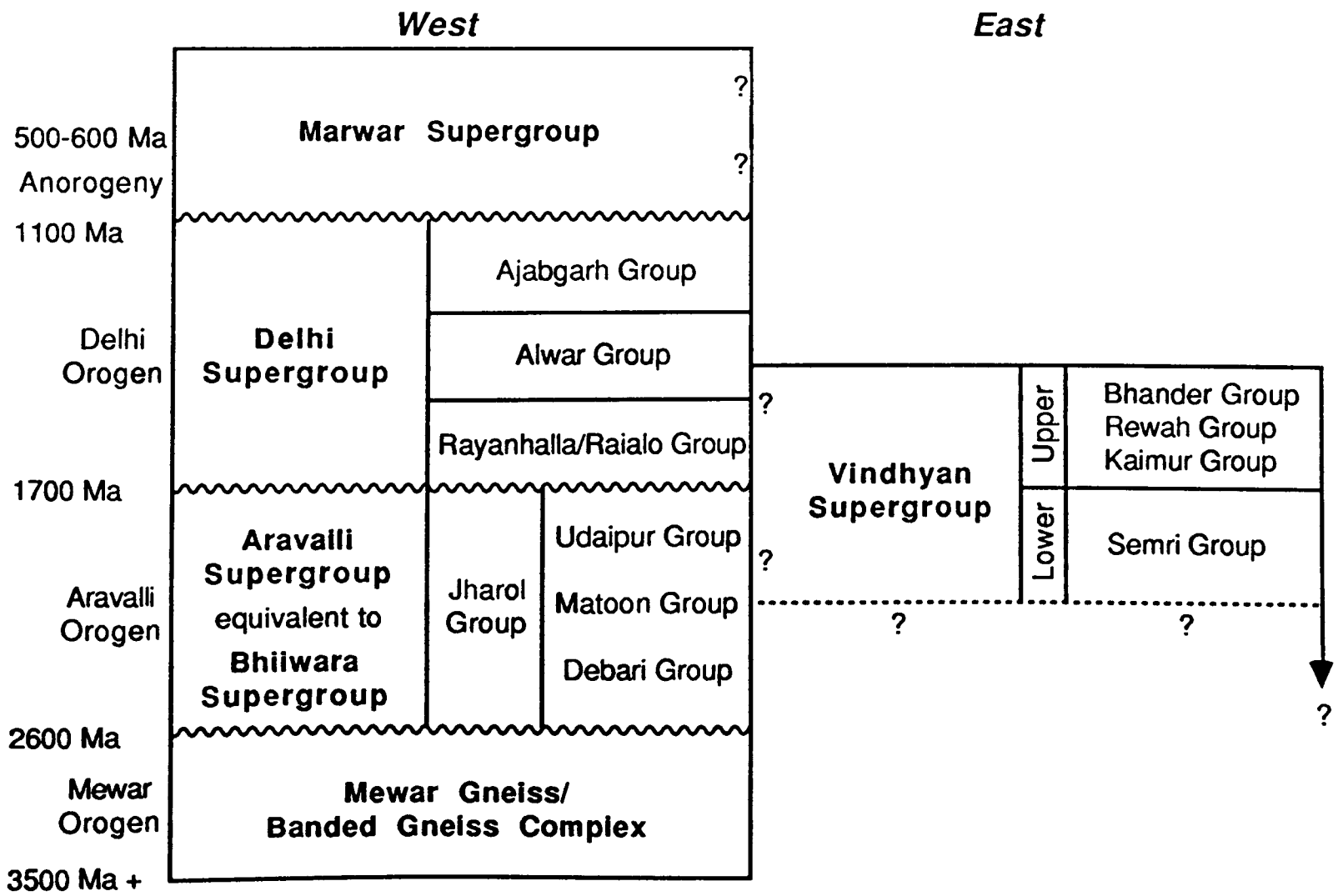

Figure 4.6.1 summarises the revised chronostratigraphy for the region of the Aravalli-Delhi orogenic belt and may be compared with **Figure 4.2.1**. An approximate indication of chronometric scale is marked along the left-hand margin. This regional stratigraphy will continue to improve as the volume of reliable age data increases.

It is clear that stromatolites (whether phosphatic or calcareous) are highly suitable organisms for direct dating by the Pb/Pb method. The technique appears most useful for Middle to Late Proterozoic and Archaean sediments, although large Pb isotopic ranges for younger materials indicate that further investigation is merited (see **Chapter 5**). Results should be realistically interpreted and then only after due consideration of all available field data, biostratigraphic correlations, petrographic work, stable isotopic information (particularly $\delta^{13}C_{organic}$) and independent age constraints. Discordance between carbonate and residue Pb isotopic compositions may be of use in detecting the effects of metamorphic recrystallisation. Most importantly, it is necessary to guard against reliance on preconceived ideas and models that may be based on limited and/or dubious data.

Chapter 5:

SILURIAN CARBONATES FROM GOTLAND, SWEDEN

5.1: INTRODUCTION

Gotland is Sweden's largest island and is situated 110 km off the east coast of the mainland, in the Baltic Sea. It measures over 137 km in length and has an area in excess of 3000 km^2. The exposed Silurian marine sequence, which ranges in age from late Llandovery to late Ludlow, is renowned for the rich fossil assemblages (Porifera, Coelenterata, Echinodermata, Brachiopoda, Bryozoa et al.) and carbonate reefs which it contains. The sedimentary record reflects the slow pulsatory regression of a relatively shallow, pericratonic, tropical carbonate sea across the stable, southerly dipping, western margin of the Russian Precambrian shield (Bassett et al., 1989). Correlated rocks are exposed in other Baltic countries (Poland, Estonia, Latvia, Lithuania) but major facies variations have resulted in inconsistent stratigraphic nomenclature for these successions.

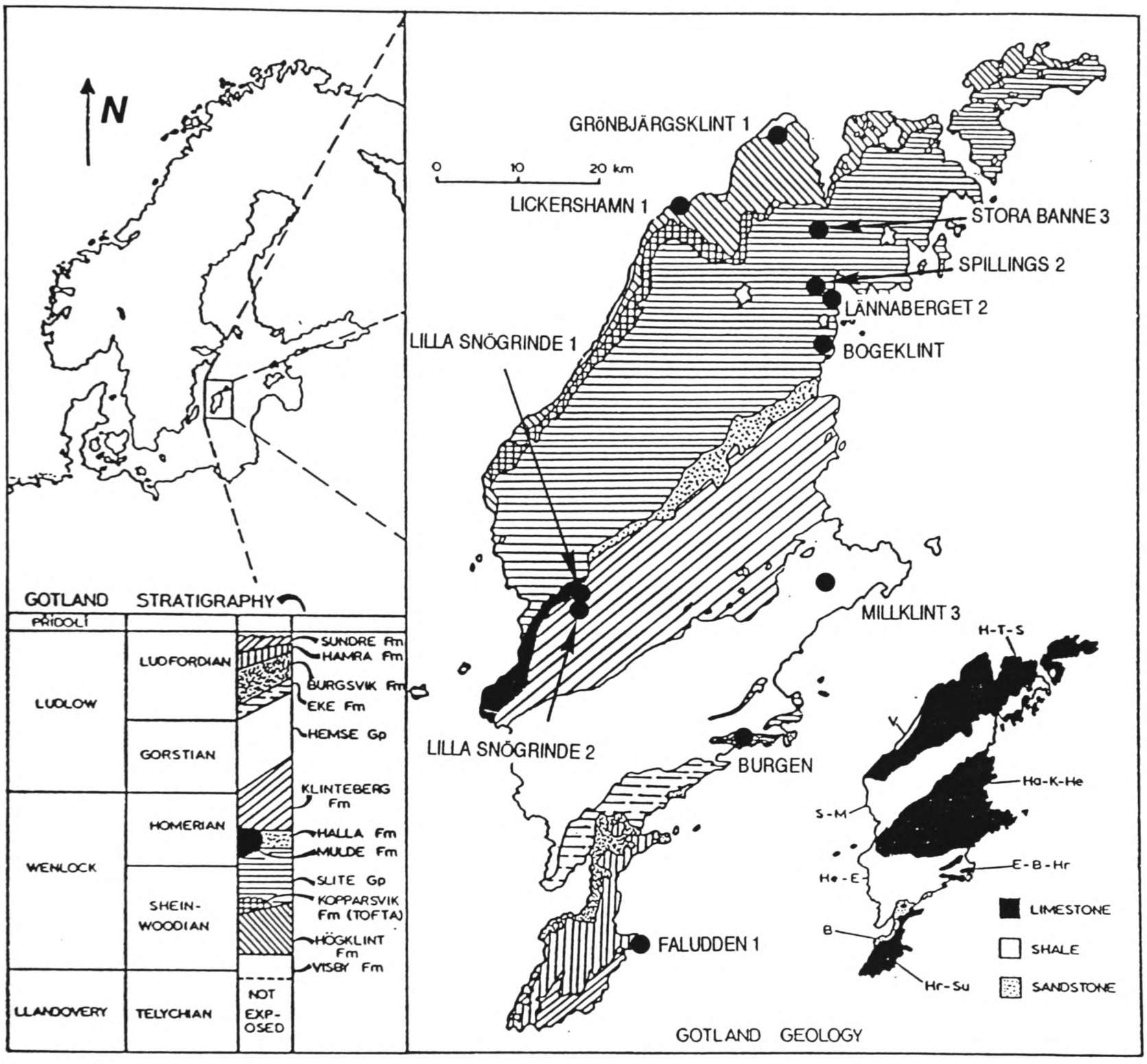

Figure 5.1.1: Geological units of the Swedish island of Gotland, including localities for carbonate samples, using the nomenclature of Frykman (1989)

Tectonic deformation of the carbonate dominated Gotland succession has been minimal and a lack of conodont colour alteration indicates that the sediments have never been subjected to elevated temperatures as a consequence of deep burial (Epstein et al., 1977; Jeppsson, 1983). Coupled with the occurrence of dated bentonite horizons within the succession (Odin et al., 1986a), this makes the Silurian rocks of Gotland ideal candidates for testing the applicability of Pb/Pb and U-Pb dating to Phanerozoic carbonates.

The rocks strike northeast-southwest and have a maximum regional dip of 2-3° to the southeast. Carbonate dominated areas form topographic highs in the northwest, centre and southeast of the island (30-80 m elevation), while the interleaving marl dominated beds form topographic lows. Biogenic carbonates (corals, stromatoporoids, crinoids) and whole rock samples were analysed from seven separate horizons within the succession (Upper Visby Formation, Högklint Formation unit b, Slite Formation unit g, lower Middle Klinteberg Formation, Hemse Formation unit e, Hamra Formation/Burgsvik Formation boundary and Lower Sundre Formation), for which sample localities are indicated in **Figure 5.1.1**. The excellent set of referenced localities for Gotland, published initially by Laufeld (1974b), facilitated easy identification of the selected horizons across the island. A current listing of these reference localities, including many new ones identified since 1974, is kept at the University of Lund's research station, east of Visby (Allekvia). The help and support of Dr. Lennart Jeppsson in arranging fieldwork is gratefully acknowledged.

5.2 THE SILURIAN OF GOTLAND

5.2.1: *INTRODUCTION*

The fossiliferous sediments of the island of Gotland have long attracted the attention of the geological community. It was in 1845 that Murchison first correlated the exposed sequence with the type Silurian rocks of the British Isles (as defined by Murchison, 1839). Improvements in the understanding of Gotland's geology owe much to the work of Hede, who refined the stratigraphy through a series of eight maps published between 1921 and 1940, and proposed the recognition of thirteen broad lithostratigraphic units, redefined as formations by Frykman (1989), and over fifty lettered sub-units which are still in use today. Previously, the Gotland lithostratigraphic units had been referred to as 'beds' (Hede, 1958) and 'groups' (Laufeld, 1974b). The broad stratigraphic relationships of the lithostratigraphic

units on the island are illustrated in **Figure 5.2.1**.

Figure 5.2.1: Stratigraphy of the Silurian succession on the island of Gotland, Sweden

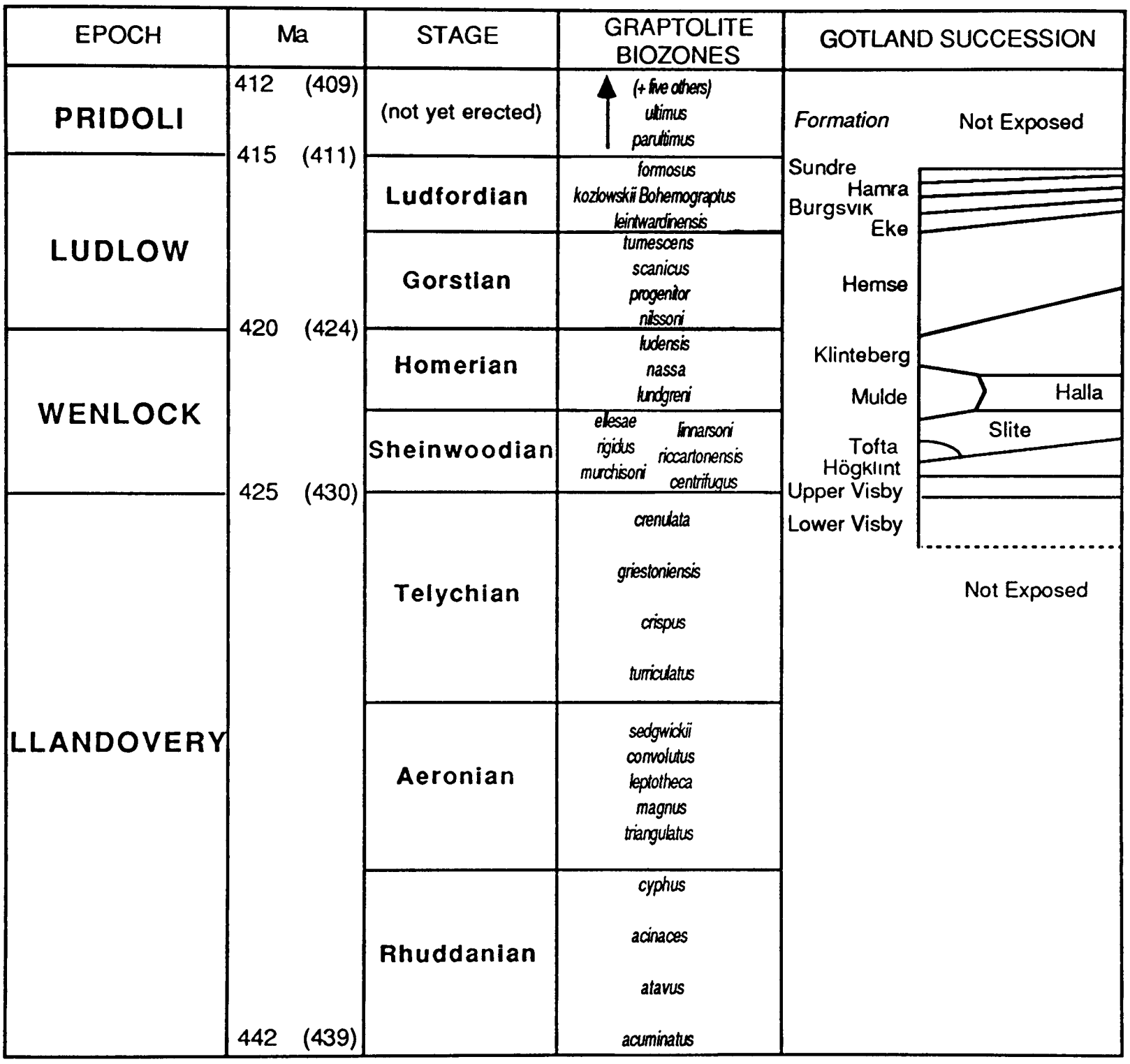

Vertical scale is chronometric and relates to values for the time scale of McKerrow (pers. comm. 1992)
Values in brackets are from the time scale of Harland et al. (1989)
Diagrammatic representation of Gotland lithostratigraphy is interpretative

Bore hole and geophysical data indicate that beneath the 500 m of exposed latest Llandovery to Late Ludlow sediments, occur 150 m of older Silurian rocks, 75-125 m of Ordovician sediments and 150-225 m of Cambrian to Precambrian sediments (Laufeld & Bassett, 1981). Deposition of this entire sequence took place on a crystalline basement, formed by the gently southward dipping Precambrian shield on the western margin of the Russian Platform (Laufeld & Bassett, 1981).

Biostratigraphic division of the sequence is based upon the abundant conodont fragments which are found in the shallow water sediments (Jeppsson, 1983 and references therein) and rarer graptolite occurrences. Correlation with the British Silurian, which is zoned on the basis of graptolite taxa from deeper water sediments, can be made confidently to within one graptolite biozone.

5.2.2: *STRATIGRAPHIC SUCCESSION*

Hede's thirteen lithostratigraphic divisions (Hede, 1921; 1925a) are recognised to be both heterogeneous and diachronous in nature (Sundquist, 1982b), but they still form the basis for stratigraphic studies and correlations on the island. Lithological units are briefly described by Laufeld & Bassett (1981). The original lettering of Hede's sub-divisions has been reinstated and somewhat refined by Laufeld (1974b) as an aid to correlation.

The Lower Visby Formation, which is exposed along the NW coast of the island, has a maximum thickness of 9 m and comprises shallow water calcareous mudstones and thin argillaceous limestones with banks of halysitid corals and pentamerid brachiopods. It lies within the *crenulata* graptolite biozone, that is topmost Llandovery. The Upper Visby Formation, which is up to 15 m thick, has a similar lithology in its lower portions (nodular argillaceous limestones interbedded with shales and mudstones) but upsection, above the Llandovery-Wenlock boundary, the limestones become thicker and bedded, corresponding to a transition from dominantly soft bottom to hard bottom conditions. The base of the Wenlock is indicated by the appearance of cyrtograptid graptolites in more argillaceous deposits, indicative of the *centrifugus* and *murchisoni* biozones. The first major bentonites are found in these sediments. Two specimens of the tabulate coral *Favosites* sp. (0907898, 0907899), collected approximately 8 m apart from the same horizon, were analysed from an Upper Visby section at Lickershamn 1. **Figure 5.1.1** locates Lickershamn 1 and the other sampled reference localities, but more detailed descriptions may be found in Laufeld (1974b).

The lower Wenlock Högklint Formation attains a maximum thickness of some 35 m and contains the first major reefal carbonates on the island. The reefs developed in a carbonate wedge facies adjacent to a shale belt and contain evidence for extremely shallow water conditions (ripple marked surfaces), synsedimentary marine cementation (pseudofibrous calcite after acicular/fibrous aragonite/high magnesian calcite primary cement) and emergence (erosion surfaces, dissolution

cavities and vadose crystal silt infills) (Watts, 1982). Inter-reefal sediments consist of crinoidal grainstones, grading offshore into argillaceous limestones and marls. A single specimen of domal stromatoporoid (1007893), measuring 20 cm in diameter and having relief of 10 cm, was analysed from a weathered outcrop of Högklint Formation unit b at Grönbjärgsklint 1, an extensive cliffed section in the north of the island. The overlying Tofta Formation (up to 8 m thick) also contains evidence for local emergence and is marked at its summit by a slight angular discordance which separates the constituent lenses of stromatoporoids, oncolites and oolites from the complex facies variations of the Slite Formation.

In the northeast of the island, the Slite Formation (up to 100 m thick) consists of several generations of reefal carbonates and inter-reefal crinoidal and bryozoan limestones, but to the southwest they pass into progressively more marly facies. The topmost 5 m consists of the Slite Siltstone, a uniform, fine grained siliclastic sourced from the west. Stromatoporoidal carbonates were analysed from widely separated unit g localities at Stora Banne 3 (1907895, unit g lower to basal part, *rigidus* biozone or older) and Spillings 2 (2307896, 2307897, unit g, *lundgreni* biozone) and specimens of the tabulate coral *Heliolites* sp. were analysed from unit g localities at Lännaberget 2 (1507892, unit g, *lundgreni* biozone) and Bogeklint 2 (1907899, unit g outlier). It is known that unit g of the Slite Formation (dominantly Sheinwoodian) contains limestone beds of varying age (Jeppsson, pers. comm. 1991) and this results in uncertainty in precise correlation between localities. This observation will be readdressed during discussion of the results in section 5.5.

The Halla Formation has a maximum thickness of 15 m and comprises coarse oolites and small unstratified carbonate mounds that pass upsection into bituminous and argillaceous limestones. Shallow water conditions are again indicated by ripple marked sediment surfaces. To the southwest, the beds thin and are replaced by the equivalent, deeper water deposits of the Mulde Formation (up to 25 m thick).

The Klinteberg Formation, which spans the Wenlock-Ludlow boundary (marked by the incoming of *nilssoni* biozone faunas), is up to 70 m thick and in the southwest contains autochthonous stromatoporoid/tabulate coral biohermal framestones with coarse inter-reefal crinoidal grainstones, packstones and rudstones. To the northeast, they pass into a complex of protected quieter water carbonate facies, containing abundant algal oncolites and bedded limestones. Hede (1958) divided the formation into six subunits in the northeast, but recognised only lower,

middle and upper units in the southwest. Frykman (1989) interpreted the southwest deposits as indicative of a shallow water, southerly dipping ramp-like setting with numerous shoals and barriers. Occasional storm activity is indicated by the presence of mud drapes on rippled surfaces. The Klinteberg Formation has been placed within the *ludensis*, *nilssoni* and ?*scanicus* graptolite biozones (topmost Wenlock to Ludlow, see **Figure 5.3.1**) by Martinsson (1967) from ostracode work and Larsson (1979) from tentaculid faunas. Jaeger (1981) reported *scanicus* faunas from the stratigraphically overlying Hemse Formation and this represents further evidence of the diachroneity of facies on Gotland.

Stromatoporoidal carbonates were analysed from localities within the lower Middle Klinteberg Formation at Lilla Snögrinde 1 and Lilla Snögrinde 2, within the southwest reefal tract of Klinteberg sedimentation. Both localities are from the upper part of the *ludensis* biozone (topmost Wenlock - Jeppsson, pers. comm. 1991) and lie extremely close to the Wenlock-Ludlow boundary. 16078913 and LS were collected from Lilla Snögrinde 2 and are both large domal forms of fresh appearance that show good preservation of internal structure and an amount of sparry calcite cementation. It was possible to split 16078913 into sequential growth zones along latilaminae, allowing a more detailed isotopic study. 16078914 and 16078916 were collected some 56 m apart from Lilla Snögrinde 1 and both exhibit strongly recrystallised textures, with no preservation of internal structure.

Lilla Snögrinde 1 comprises typical Klinteberg biohermal framestones, lithologically similar and equivalent in age to those described from Wenlock Edge by Scoffin (1971) and Riding (1981). Faunally, they are dominated by stromatoporoids and tabulate corals, with rarer colonial rugose corals (for example *Acervularia*), algae, bryozoans and brachiopods. Bioerosion is sparse and the reefs pass laterally into cross bedded crinoidal grainstones. This locality is interpreted as a high energy, very shallow water (<10 m) deposit (Frykman, 1989). Lilla Snögrinde 2 comprises rudstones and floatstones that contain *in situ* small domal stromatoporoids (Frykman, 1989) and are associated with abundant cross bedded, ripple marked crinoidal grainstones. The deposit is interpreted as a fore-reef ramp setting, closely associated with the main bioherms and skeletal sand bars. Early marine cementation is common and evidence of meteoric diagenesis (Frykman, 1984; 1985) suggests periods of Klinteberg emergence.

The Hemse Formation is a maximum of 100 m thick and shows a similar facies distribution to the Slite Formation, with stromatoporoid and bivalve rich

limestones dominant in the northeast, but graptolitic marls becoming more abundant towards the southwest. Hardgrounds are a notable feature of Hemse sedimentation. A single whole rock sample was analysed from bedded limestones of the Hemse Formation, unit e at Millklint 3 (1807899). An increase in the proportion of calcareous algae is found in the overlying argillaceous limestones and marls of the Eke Formation (maximum 15 m thick), which contain small reefs and mounds in the northeast. Cherns (1982) documented evidence for an episode of emergence and subaerial karstic erosion during Eke times. A series of 1-2 m solution basins have been carved into lithified lower Eke Formation rocks in the east of the island and are infilled with shallow marine stromatolitic sediments, overlain by shallow marine carbonates. The lithological sequence suggests emergence, erosion, subsidence and shallow water subtidal to intertidal deposition, before re-establishment of normal salinity, shallow marine conditions by Upper Ludlow times, prior to deposition of the Burgsvik Beds.

A significant northwest-derived clastic pulse is recorded in the Burgsvik Formation (50 m), where thick spore-bearing, fine grained, fluvially-influenced sandstones are found intercalated with thin shales and marls. Only locally are carbonate oolitic facies developed, marking embayments protected from clastic flushing. Syndepositional soft sediment deformation is indicated by the preservation of sags and water escape structures in the sandstones. Two samples of crinoidal stems were analysed from a Hamra/Burgsvik Formation boundary section at Burgen, in the southeast of the island (1307897).

The Hamra Formation (40 m) passes from algal limestones to argillaceous limestones to reefal limestones, both up sequence and from southwest to northeast, where outliers occur within the Burgsvik Formation. Hamra deposits are succeeded by the youngest Silurian rocks on the island, the late Ludlow Sundre Formation (10 m), which is composed of crinoidal sediments and stromatoporoidal reefs. A single stromatoporoid sample was analysed from a coastal outcrop of the Lower Sundre Formation at Faludden 1 (2107892), in the south of the island.

Silurian carbonate-marl sedimentation was frequently interrupted by the deposition of volcaniclastic bentonite beds, generally less than 10 cm thick and composed principally of clay minerals (illite-smectite and kaolinite), biotite and feldspars (Odin et al., 1986a). Unaltered biotites separated from these bentonites have proven highly suitable sample materials for K-Ar dating, owing to their potassic nature (see section **5.3** and **Table 5a**).

5.2.3: *SAMPLE PALAEONTOLOGY*

Detailed palaeontological studies for the island of Gotland have been published by Mori (1969; 1970) and Kershaw (1981; 1987; 1990) on stromatoporoids; Martinsson (1967) on ostracodes; Laufeld (1974a) on chitinozoans; Larsson (1979) on tentaculids and Jeppsson (1974; 1979; 1983) on conodonts. Pb and U isotopic analyses performed during this investigation have concentrated on biogenic stromatoporoidal carbonates. Until recently, these calcareous organisms had been the subject of much palaeontological conjecture and before they became generally accepted as a class of phylum Porifera (after Nicholson, 1886; Galloway, 1957; Lecompte, 1956; Stearn, 1980), had been variably classified as hydrozoans and cyanobacteria (Kazmierczak, 1976; Kazmierczak & Krumbein, 1983).

Stromatoporoids were most abundant during the Ordovician, Silurian and Devonian when, along with tabulate corals, they were the principal reef-builders, but related forms are also found in isolation during the Jurassic and Cretaceous. Kershaw (1987) documented numerous examples of commensal intergrowth between Silurian stromatoporoids and tabulate corals on Gotland, indicating that the two derived some mutual benefit from symbiosis. Stromatoporoids built an open, highly porous, calcareous skeleton of laminar, domal, columnar, digitate or encrusting form. The skeleton either possessed a three-dimensional framework or had a reticulate geometry that comprised structural elements both parallel and perpendicular to the growth surface (laminae and pillars), linked to form porosity galleries. The regularity of this skeletal structure was, in certain species, disrupted by the development of astrorhizae (stellate branching canals linked by vertical tubes) and surficial mamelons, inferred to have increased the efficiency of water circulation within and over the colony (Boyajian & La Barbera, 1987). Growth discontinuities parallel to the main growth surface are marked by the development of latilaminae.

As with many classes, debate still exists over the nature of primary stromatoporoid biomineralogy, although aragonite, high magnesian calcite (HMC) or some combination thereof appear the most probable candidates. For a series of samples collected from the same Devonian outcrop in New York State, Rush & Chafetz (1991) demonstrated that stromatoporoids showed better textural preservation than bivalve shells (primary aragonite), were more recrystallised than brachiopod shells (primary low magnesian calcite, LMC) and showed a very similar preservation style to pelmatozoans (primary HMC mineralogy), concluding that stromatoporoids

secreted HMC skeletons. In addition, they documented the occurrence of abundant microdolomite rhombs within the stromatoporoid skeletons, indicative of Mg expulsion during a HMC to LMC conversion (Lohmann & Meyers, 1977). Stearn & Mah (1987), however, argued for an aragonitic skeleton, based on the abundance of rhombohedral fluid inclusions within the skeletons of Silurian and Devonian stromatoporoids.

The classification of stromatoporoids (Stearn, 1980) is based on similarities in structural detail observed in thin section, rather than gross morphology, because it is known that the organisms demonstrated a significant phenotypic plasticity in response to genetic, functional and environmental controls. All forms show at least partial diagenetic recrystallisation and for this reason, detailed microstructural classifications are not possible. In many examples, the faithful preservation of major structural elements and latilaminae, even after neomorphism, suggests that 'thin-film' diagenetic processes may have been responsible for the observed recrystallisation (Kershaw, 1990; Pingitore, 1976). Structural elements are preserved as cloudy, inclusion-rich neomorphic LMC, whereas later cement phases form a mosaic of clear, columnar to equant, primary LMC. Cathodoluminescence (CL) microscopy has proved an important tool in the petrographic study of such carbonate materials because it frequently illuminates relict primary structural detail, even after diagenetic recrystallisation, and it allows diagenetic interpretation of cement stratigraphies (Frykman, 1985).

5.2.4: *GEOLOGICAL HISTORY*

Recently acquired subsurface bore-hole and geophysical data (Flodén, 1980; Winterhalter et al., 1982) have significantly improved understanding of the regional geological picture. During the Lower and Middle Llandovery, transgressive basinal sedimentation dominated the then low southerly latitude Gotland region, depositing shales and graptolitic mudstones in relatively deep waters. At this point, the shoreline lay further north. McKerrow (1979) has suggested that the transgression was in response to melting of the Gondwanan ice caps.

Regressive shallowing in the latest Llandovery/Wenlock resulted in an increase in environmental energy and a southerly transposition of the shoreline. Carbonate dominated facies were deposited in a complex shallow water mosaic as detrital input waned and the preservation of ripple marks (Cherns, 1982; Laufeld & Bassett, 1981; Frykman, 1989) indicates that the reefs were not greatly distanced

from the shoreline. The limited fine grained clastic input indicates a hinterland of low relief. Palaeomagnetic data are consistent with a southern tropical to equatorial latitude for the Baltic region during the mid-Silurian (Bassett et al., 1989).

During Wenlock and much of Ludlow times, shallow water carbonate sedimentation was dominant, although equivalent argillaceous facies became more evident to the south, offshore. Predominantly northeast-southwest ripple orientations (Bergman, 1979; Laufeld & Bassett, 1981; Frykman, 1989) indicate that the shoreline had a similar northeast-southwest trend and this shoreline prograded in a pulsatory fashion to the southeast throughout the Silurian. Ripple wavelengths of 50-80 cm, coupled with evidence of storm reworking, suggest that water depths were generally less than 10 m (Sundquist, 1982a). By the start of the Devonian, the shoreline lay completely to the southeast of the island, leaving behind a diachronous sequence of facies belts. Continental drift had carried the Baltic region into the northern tropics by the end of the Silurian (Bassett et al., 1989).

Several transgressive-regressive cycles are superimposed on this major Silurian regression, interrupting reefal deposition and producing interfingered tracts of more argillaceous sediments, for example during the early to mid-Ludlow (Hemse Beds on Gotland) (McKerrow, 1979). Broadly speaking, carbonate rocks dominate the northern, central and southern parts of Gotland and marls occur in between, indicating two main transgressive-regressive cycles within the overall regressive framework (see **Figure 5.1.1**). When studied in detail, even smaller local cycles are found to occur within individual formations. Laufeld & Jeppsson (1976) suggested that collision of the Baltoscandian margin with Laurentia, resulting in vulcanicity, flexure of the western Russian platform and broad regional tectonic warping, might have caused these transgressive-regressive cycles.

Progressive Caledonide formation and erosion are inferred to be responsible for the clastic pulses observed in the Slite and Burgsvik Formations (sourced from the north and northwest) and the tectonic disturbances that gave rise to soft sediment deformation (Laufeld & Bassett, 1981). The clastics may be considered the first indication of the impending onset of Old Red Sandstone sedimentation. Although much of the island was submerged at the end of the last glaciation, isostatic readjustment has subsequently produced uplift rates of between 0.7-2.0 mma^{-1} in the Gulf of Bothnia and Baltic Sea region, resulting in a series of raised shorelines (Jeppsson, 1982) and subjecting the sediments to the effects of Quaternary weathering.

The island of Gotland has a very simple structural style, from which one may infer a simple post-depositional deformation history. Sediments have a general northeast-southwest strike, taken to reflect the original shoreline orientation, and a regional dip of just 2-3° to the southeast. Only around and beneath reefal masses do dips exceed 5° and vary somewhat in orientation as the result of differential sediment compaction. Minor faulting is observed, particularly along the coastal cliff sections, but the downthrow of the predominantly normal faults is usually < 1 m. Organic matter within preserved conodonts shows no observable colour alteration and indicates that throughout their geological history, the sediments have never been subjected to elevated temperatures in response to deep burial. Odin et al. (1984) suggested that a maximum burial depth of a few hundred metres was appropriate for the entire Silurian succession. Gotland's location on the stable western margin of the Russian Precambrian shield provides the explanation for the island's relatively simple geological history, which is so beautifully recorded in the exposed sequence of carbonates, marls and bentonites.

5.3: AGE CONSTRAINTS

Compared with the Archaean and Proterozoic, relatively good consensus exists on Silurian time scale calibration because of the large number of geochronological studies performed on geographically dispersed, but extremely well correlated rocks (principally bentonites, volcanics, well constrained intrusives and separates of their constituent minerals). The Silurian period was the first for which international agreement was reached on the stratigraphic definition and standardisation of all four epochs and seven stages. This division is based on the graptolite succession from the Welsh Borderlands (Bassett et al., 1975) (see **Figure 5.2.1**).

McKerrow et al. (1980; 1985), McKerrow (pers. comm. 1992), Harland et al. (1982; 1989), Odin et al. (1982), Gale et al. (1980b) and Jones et al. (1981) have all published time scales for this portion of geological time by selecting published dates from the available literature pool and applying a particular statistical treatment. The most recent time scales (Harland et al., 1989; McKerrow, pers. comm. 1992) are inevitably more reliable than their predecessors because they incorporate the most recently published age data. Epoch boundary ages from these scales are summarised in **Figure 5.2.1**, while relevant radiometric data for the Silurian are detailed in **Table 5a**. All errors are quoted at the 2σ level.

Table 5a: Published dates for the Silurian period

EPOCH	STAGE	PUBLICATION	DATE (Ma)	METHOD
Early Devonian	Lochkovian	Thirlwall (1988)	413 ± 6	Rb-Sr on biotite
SILURIAN				
Pridoli		Odin et al. (1982)	399 ± 9	K-Ar on biotite
		McKerrow et al. (1985)	407 ± 6	Rb-Sr on biotite
Ludlow	Ludfordian	Odin et al. (1986b)	417 ± 10	K-Ar on biotite
		Odin et al. (1986b)	423 ± 9	K-Ar on biotite
	Gorstian	McKerrow et al. (1985)	407 ± 14	Fission track on zircon
		Ross et al. (1982)	407 ± 18	Fission track on zircon
		Gale (1985)	415 ± 10	K-Ar on biotite/sanidine
		Ross et al. (1982)	419 ± 7	K-Ar on biotite
		Wyborn et al. (1982)	421 ± 2	K-Ar on biotite
		Gale (1985)	422 ± 6	Rb-Sr whole rock/biotite
		Kunk et al. (1985)	424 ± 4	Ar-Ar on biotite
		Odin et al. (1986b)	424 ± 8	K-Ar on biotite
		Armstrong (1978)	429 ± 8	Rb-Sr whole rock
Wenlock	Homerian	Harland et al. (1964)	413 ± 32	Rb-Sr whole rock
		Ross et al. (1982)	412 ± 24	Fission track on zircon
		Ross et al. (1982)	416 ± 18	Fission track on zircon
		Odin et al. (1986a)*	427 ± 6	K-Ar on biotite
	Sheinwoodian	Ross et al. (1982)	422 ± 14	Fission track on zircon
		Odin et al. (1986a)*	430 ± 6	K-Ar on biotite
Llandovery	Telychian	Armstrong (1978)	445 ± 30	Rb-Sr whole rock
	Aeronian	Odin et al. (1982)	436 ± 5	Ar-Ar on hornblende
	Rhuddanian	Compston et al. (1991)	429 ± 4	U-Pb on zircon
		Odin et al. (1982)	431 ± 6	Ar-Ar on hornblende
		Ross et al. (1982)*	437 ± 22	Fission track on zircon
		Tucker et al. (1990)	439 ± 2	U-Pb on zircon
		Armstrong (1978)	445 ± 26	K-Ar on biotite
		Armstrong (1978)	445 ± 40	Rb-Sr on biotite
ORDOVICIAN				
Late Ashgill		Tucker et al. (1990)	446 ± 3	U-Pb on zircon

* Data from Gotland, Sweden.

Using selected data from this pool, McKerrow (pers. comm. 1992) placed the top of the Silurian at 412 Ma, the Pridoli-Ludlow boundary at 415 Ma, the Ludlow-Wenlock boundary at 420 Ma, the Wenlock-Llandovery boundary at 425 Ma and the base of the Silurian at 442 Ma. Harland et al. (1989), to whom the precise U-Pb zircon dates of Tucker et al. (1990) and Compston et al. (1991) were unavailable, placed the same boundaries at 409 Ma, 411 Ma, 424 Ma, 430 Ma and 439 Ma respectively.

Biostratigraphic graptolite and conodont zonation allows even greater qualitative control and ideally one would be able to link independent chronostratigraphic and biostratigraphic scales to produce tie-points within an integrated geological time scale. As the volume of precise age data increases (probably in response to further high precision U-Pb zircon studies), disagreement over the age of epoch and even stage boundaries will diminish and there will be less reliance on assumptions of length of stratigraphic units and biozones (themselves reliant on estimation of rates of deposition and evolution).

5.4: RESULTS

5.4.1: *LOWER MIDDLE KLINTEBERG FORMATION*

Pb/Pb Results

Four stromatoporoidal carbonates (16078913, 16078914, 16078916 and LS), exhibiting various states of diagenetic preservation, were analysed from lower Middle Klinteberg Formation localities (*ludensis* biozone, topmost Wenlock) at Lilla Snögrinde 1 and Lilla Snögrinde 2, in the west of the island (see **Figure 5.1.1**). This horizon is stratigraphically equivalent to the Klinteberg Formation unit c, as defined in the northeast of the island (Jeppsson, pers. comm. 1991). Pb isotopic data are listed in **Table 5b** and plotted in **Figure 5.4.1**.

Twenty-nine analyses of specimen 16078913 exhibit notably radiogenic Pb isotopic compositions, a large colinear range in isotopic ratios ($^{206}Pb/^{204}Pb$ 54.042-81.948) and define a Pb/Pb isochron date of 441 ± 37 Ma (MSWD 1.42, model μ_1 value 8.14 ± 0.07) (**Figure 5.4.1**). The isotopic range is truly remarkable in that it is obtained from analyses of a single fossil specimen. Five analyses of specimen LS are less radiogenic and have a more limited Pb isotopic range ($^{206}Pb/^{204}Pb$ 25.374-28.808) which defines an imprecise date of 179 ± 270 Ma (MSWD 0.957, model μ_1 value 8.21 ± 0.09), only just within error of the 16078913 date. Specimens 16078914 and 16078916 show texture destructive recrystallisation and both have very similar unradiogenic Pb isotopic compositions. 16078913 and LS were collected from Lilla Snögrinde 2 and 16078914 and 16078916 from Lilla Snögrinde 1.

Table 5b: Pb isotopic compositions of stromatoporoidal carbonates from the lower Middle Klinteberg Formation (*ludensis* biozone), Wenlock, Gotland

SAMPLE	CORRECTED RATIOS*		
	$^{206}Pb/^{204}Pb$	$^{207}Pb/^{204}Pb$	$^{208}Pb/^{204}Pb$
16078913A	68.976 ± 0.114	18.396 ± 0.032	38.247 ± 0.062
16078913B	61.220 ± 0.068	17.988 ± 0.026	38.319 ± 0.058
16078913AIII	70.648 ± 0.116	18.490 ± 0.032	38.351 ± 0.076
16078913BI	66.529 ± 0.086	18.263 ± 0.026	38.375 ± 0.066
16078913BII	60.470 ± 0.082	17.946 ± 0.026	38.356 ± 0.064
16078913BIII	63.227 ± 0.110	18.076 ± 0.044	38.310 ± 0.104
16078913a	71.660 ± 0.142	18.552 ± 0.042	38.305 ± 0.088
16078913b	63.530 ± 0.126	18.143 ± 0.036	38.467 ± 0.080
16078913c	71.726 ± 0.110	18.579 ± 0.032	38.482 ± 0.078
16078913d	81.948 ± 0.122	19.139 ± 0.030	38.468 ± 0.070
16078913e	76.536 ± 0.136	18.851 ± 0.036	38.283 ± 0.094
16078913f	66.198 ± 0.084	18.264 ± 0.026	38.497 ± 0.062
16078913g	64.158 ± 0.120	18.145 ± 0.046	38.420 ± 0.106
16078913h	66.322 ± 0.096	18.255 ± 0.030	38.440 ± 0.072
16078913i	60.036 ± 0.082	17.913 ± 0.028	38.311 ± 0.058
16078913j	67.722 ± 0.076	18.348 ± 0.024	38.297 ± 0.050
16078913k	68.244 ± 0.168	18.372 ± 0.046	38.359 ± 0.098
16078913l	69.178 ± 0.118	18.407 ± 0.034	38.285 ± 0.070
16078913Z0	54.042 ± 0.056	17.563 ± 0.022	38.847 ± 0.048
16078913Z1A	58.005 ± 0.018	17.805 ± 0.022	38.581 ± 0.048
16078913Z1B	60.032 ± 0.062	17.922 ± 0.022	38.420 ± 0.048
16078913Z2A	59.333 ± 0.062	17.878 ± 0.022	38.399 ± 0.048
16078913Z2B	62.580 ± 0.066	18.058 ± 0.022	38.387 ± 0.048
16078913Z2C	59.462 ± 0.062	17.874 ± 0.022	38.373 ± 0.048
16078913Z3A	66.559 ± 0.070	18.244 ± 0.022	38.289 ± 0.048
16078913Z3B	64.495 ± 0.068	18.161 ± 0.022	38.932 ± 0.048
16078913Z3C	65.547 ± 0.068	18.206 ± 0.022	38.373 ± 0.048
16078913Z4A	69.612 ± 0.072	18.435 ± 0.022	38.449 ± 0.048
16078913Z4B	65.506 ± 0.072	18.230 ± 0.024	38.679 ± 0.050
16078914	18.945 ± 0.020	15.688 ± 0.020	38.233 ± 0.050
16078916	18.693 ± 0.020	15.660 ± 0.020	38.171 ± 0.048
LS1L Top	28.397 ± 0.028	16.128 ± 0.020	38.143 ± 0.046
LS1L Base	26.392 ± 0.028	16.016 ± 0.020	38.216 ± 0.048
LS1S Top	28.808 ± 0.030	16.151 ± 0.020	38.182 ± 0.048
LS1S Base	25.374 ± 0.026	15.979 ± 0.020	38.111 ± 0.046
LS1S Base	25.839 ± 0.026	16.010 ± 0.020	38.153 ± 0.048

* Corrected for mass fractionation of 0.130 % ± 0.012 ($2\sigma_{mean}$) amu^{-1}
Errors are $2\sigma_{mean}$ for corrected ratios

Figure 5.4.1: Pb isotopic data for stromatoporoids from the lower Middle Klinteberg Formation (*ludensis* biozone), Wenlock, Gotland

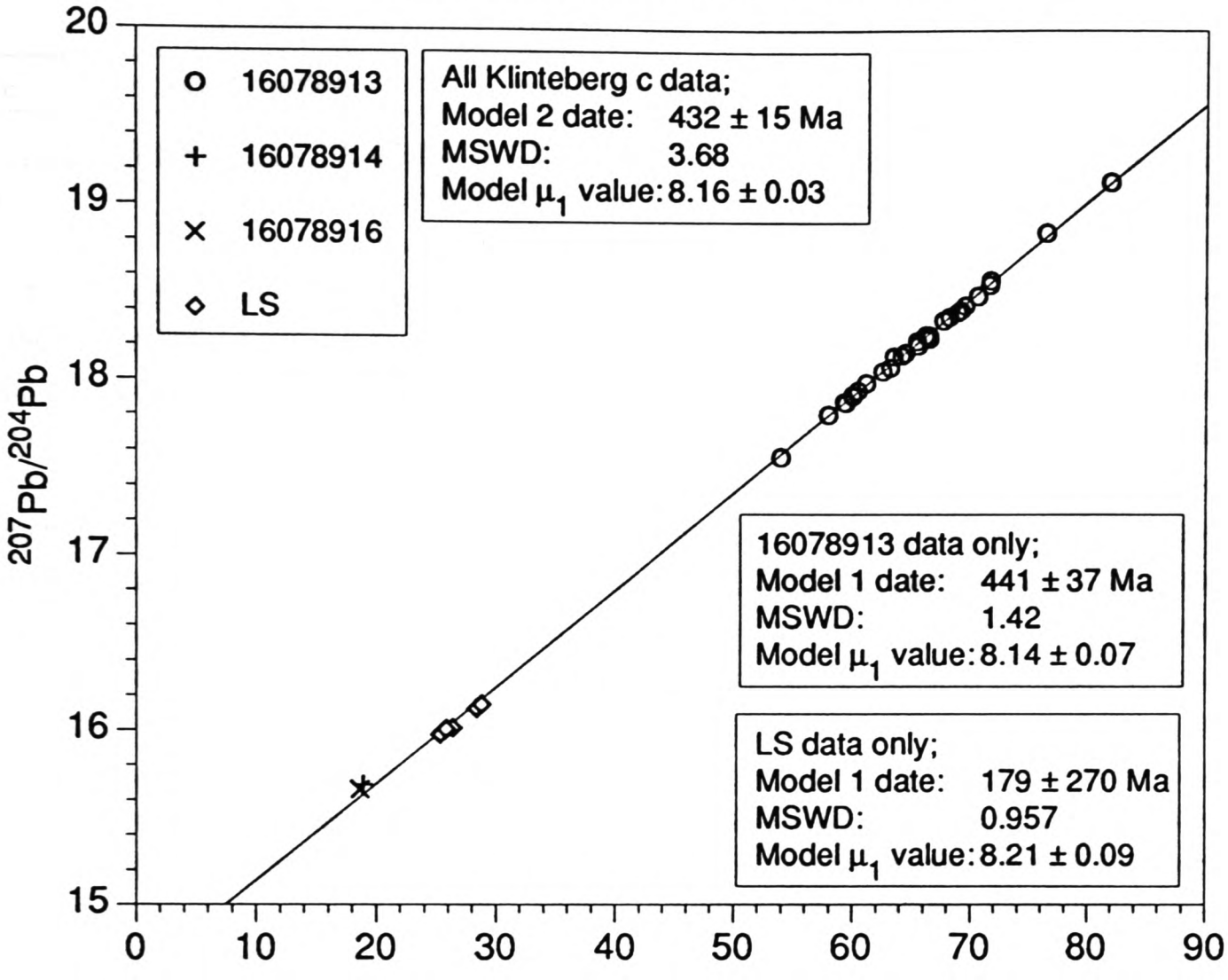

Combination of all thirty-six Pb isotopic analyses of stromatoporoids from the lower Middle Klinteberg Formation (plotted in **Figure 5.4.1**) produces a well fitted Pb/Pb errorchron, which corresponds to a date of 432 ± 15 Ma with an MSWD of 3.68 and a model μ_1 value of 8.16 ± 0.03. These values are consistent with the regressed data for 16078913 alone and suggest that this more precise combined date is representative of the stratigraphic horizon.

U-Pb Results

The U-Pb method of radiometric dating is potentially capable of yielding more precise dates for Phanerozoic materials than the Pb/Pb method, but it is also more sensitive to the natural disturbance of parent/daughter ratios. Results for U-Pb analyses of lower Middle Klinteberg stromatoporoids are detailed in **Table 5c** and illustrated in **Figure 5.4.2** and **Figure 5.4.3**.

Table 5c: U-Pb isotopic data for stromatoporoidal carbonates from the lower Middle Klinteberg Formation (*ludensis* biozone), Wenlock, Gotland

SAMPLE	CONCENTRATIONS		CORRECTED RATIOS*			
	U (ppm)	Pb (ppm)	$^{238}U/^{204}Pb$	$^{206}Pb/^{204}Pb$	$^{235}U/^{204}Pb$	$^{207}Pb/^{204}Pb$
16078913a		0.059 ± 0.000		71.660 ± 0.142		18.552 ± 0.042
16078913c		0.062 ± 0.000		71.726 ± 0.110		18.579 ± 0.032
16078913i	0.870 ± 0.020	0.150 ± 0.001	585.764 ± 9.294	60.036 ± 0.082	4.246 ± 0.068	17.913 ± 0.028
16078913j	0.915 ± 0.020	0.138 ± 0.000	715.246 ± 11.290	67.722 ± 0.076	5.185 ± 0.082	18.348 ± 0.024
16078913k	0.923 ± 0.020	0.141 ± 0.001	712.513 ± 11.312	68.244 ± 0.168	5.165 ± 0.082	18.372 ± 0.046
16078913l	0.898 ± 0.020	0.134 ± 0.000	732.629 ± 11.582	69.178 ± 0.118	5.311 ± 0.084	18.407 ± 0.034
16078913Z0	0.900 ± 0.020	0.175 ± 0.001	495.280 ± 7.814	54.042 ± 0.056	3.590 ± 0.056	17.563 ± 0.022
16078913Z1A	0.751 ± 0.020	0.129 ± 0.000	581.110 ± 9.162	58.005 ± 0.018	4.212 ± 0.066	17.805 ± 0.022
16078913Z1B	0.717 ± 0.020	0.114 ± 0.000	637.280 ± 10.050	60.032 ± 0.062	4.619 ± 0.072	17.922 ± 0.022
16078913Z2A	0.781 ± 0.020	0.122 ± 0.000	641.262 ± 10.098	59.333 ± 0.062	4.648 ± 0.074	17.878 ± 0.022
16078913Z2B	0.729 ± 0.020	0.106 ± 0.000	711.640 ± 11.204	62.580 ± 0.066	5.158 ± 0.082	18.058 ± 0.022
16078913Z2C	0.733 ± 0.020	0.107 ± 0.000	690.413 ± 10.870	59.462 ± 0.062	5.005 ± 0.078	17.874 ± 0.022
16078913Z3A	0.824 ± 0.020	0.106 ± 0.000	832.927 ± 13.136	66.559 ± 0.070	6.038 ± 0.096	18.244 ± 0.022
16078913Z3B	0.819 ± 0.020	0.104 ± 0.000	829.986 ± 13.078	64.495 ± 0.068	6.016 ± 0.094	18.161 ± 0.022
16078913Z3C	0.835 ± 0.020	0.095 ± 0.000	929.493 ± 14.640	65.547 ± 0.068	6.738 ± 0.106	18.206 ± 0.022
16078913Z4A	0.806 ± 0.020	0.084 ± 0.000	1058.468 ± 16.660	69.612 ± 0.072	7.672 ± 0.120	18.435 ± 0.022
16078913Z4B	0.741 ± 0.020	0.072 ± 0.000	1093.454 ± 17.198	65.506 ± 0.072	7.926 ± 0.124	18.230 ± 0.024
16078914	0.031 ± 0.000	0.234 ± 0.001	8.378 ± 0.134	18.945 ± 0.020	0.061 ± 0.000	15.688 ± 0.020
16078916	0.046 ± 0.000	0.597 ± 0.002	4.878 ± 0.084	18.693 ± 0.020	0.035 ± 0.000	15.660 ± 0.020

* Corrected for Pb isotopic mass fractionation of 0.130 % ± 0.012 ($2\sigma_{mean}$) amu^{-1} and U isotopic mass fractionation of 0.132 % ± 0.012 (2σ) amu^{-1}
Errors are $2\sigma_{mean}$ for concentrations and corrected ratios

Although the Pb/Pb stromatoporoid data plot along a well defined mid-Silurian isochron, it is evident from the data scatter exhibited in **Figure 5.4.2** and **Figure 5.4.3** that U-Pb closed system conditions were not maintained. Since apparent closed system conditions may be invoked for the colinear Pb/Pb data, the U-Pb disturbance must be a recent phenomenon, leaving insufficient time for the modified μ values to generate significant scatter in Pb isotopic ratios. The Pb/Pb method of radiometric dating is characteristically insensitive to recent Pb loss since the calculated date is based only on the measured radiogenic $^{207}Pb/^{206}Pb$ ratio (unlike the U-Pb method which requires determination of absolute U and Pb concentrations in addition to the Pb isotopic composition) and so provided that the lost Pb was of approximately the same isotopic composition as that remaining in the carbonate, there would be no significant effect on the calculated date.

Figure 5.4.2: ^{238}U-^{206}Pb isotopic data for stromatoporoids from the lower Middle Klinteberg Formation (*ludensis* biozone), Wenlock, Gotland

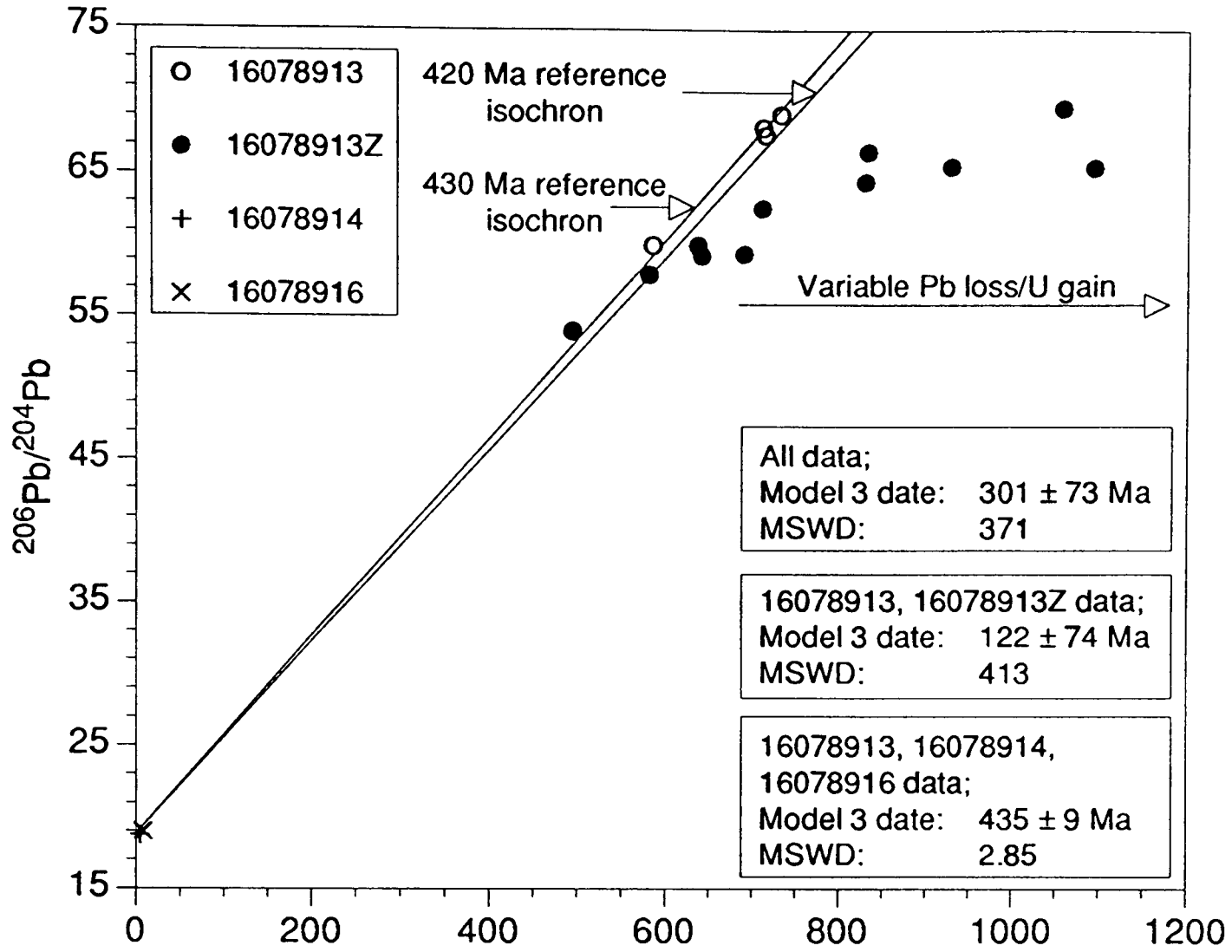

Using the Isoplot version 2.01 programme (Ludwig, 1990), the ^{238}U-^{206}Pb data for 16078913, illustrated in **Figure 5.4.2,** yield a poorly defined model 3 Yorkfit date (see **Appendix A.7**) of 122 ± 74 Ma (MSWD 413). The entire data set corresponds to a model 3 date of 301 ± 73 Ma (MSWD 371). ^{235}U-^{207}Pb analyses define model 3 dates of 139 ± 79 Ma (MSWD 435) for 16078913 samples, and 332 ± 82 Ma (MSWD 811) for the entire data set. However, none of these dates have any true geological age significance, rather they reflect the effects of recent isotopic disturbance on an original mid-Silurian isochron.

If one assumes that the least radiogenic analyses (stromatoporoids 16078914 and 16078916) approximate to the Silurian initial Pb isotopic composition of a source with μ_1 value c.8.2, it is possible to construct reference Silurian isochrons from which to interpret the isotopic disturbance. Plotting reference isochrons for 420 Ma (the date for the Wenlock-Ludlow Boundary used by McKerrow (pers. comm. 1992) and 430 Ma (the date obtained from Pb/Pb data) on **Figure 5.4.2** and **Figure 5.4.3**, it is evident that the majority of analyses plot to the right of these lines and therefore, one may conclude that Pb loss (or conceivably U gain) was responsible for the recent isotopic disturbance. More radiogenic samples had a tendency to lose more

Pb (or gain more U), explaining the general positive trend of points lying off the reference isochrons, although it should be noted that certain analyses (16078913i, j, k & l) appear not to have been subject to isotopic disturbance and consequently still plot along the reference lines. Samples 16078913i-l came from a separate piece of stromatoporoidal carbonate to 16078913Z0-Z4, while 16078914 and 16078916 were completely separate organisms.

Figure 5.4.3: ^{235}U-^{207}Pb isotopic data for stromatoporoids from the lower Middle Klinteberg Formation (*ludensis* biozone), Wenlock, Gotland

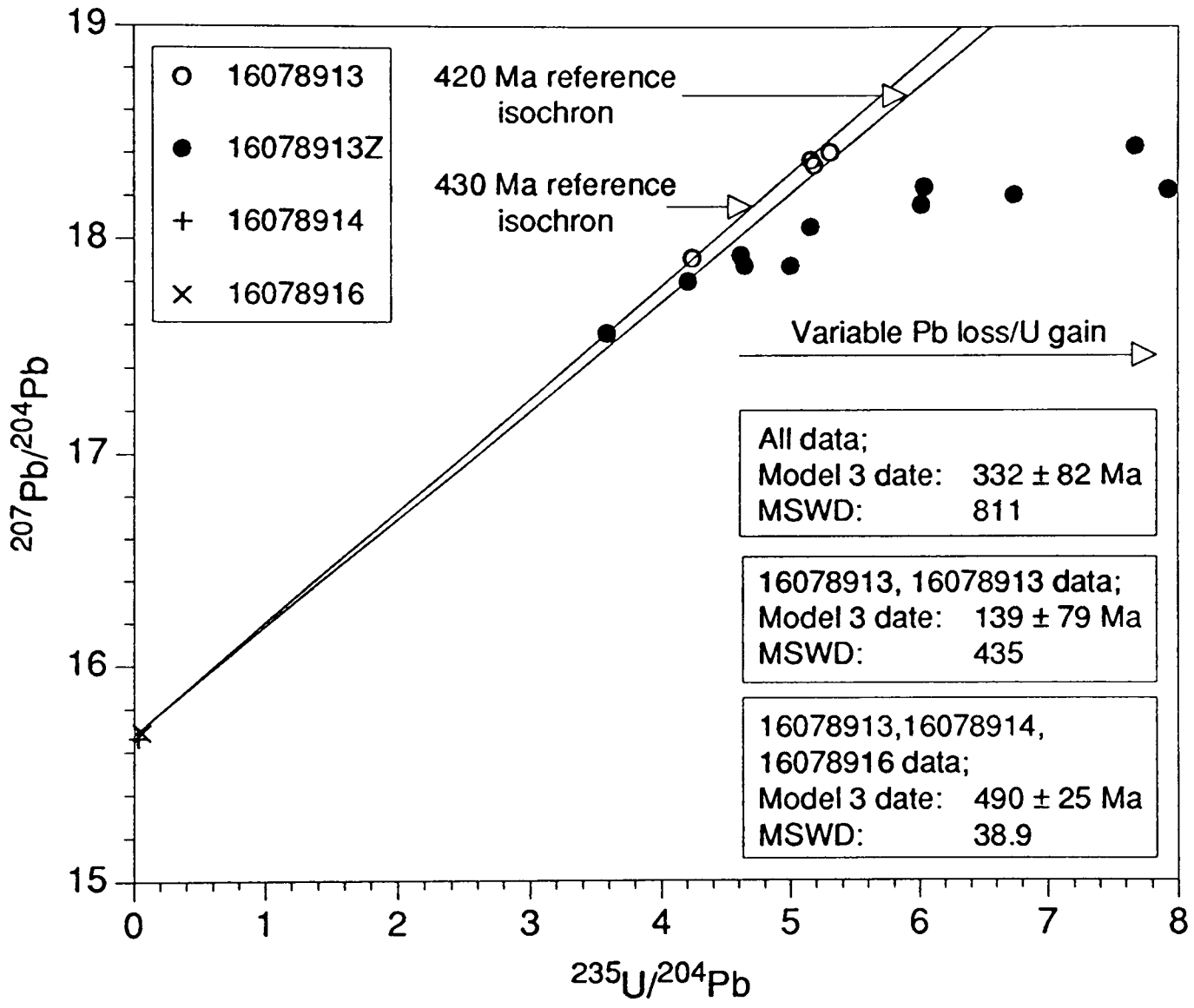

Indeed if one merely considers analyses of 16078913i, j, k, l, 16078914 and 16078916, they define a six point ^{238}U-^{206}Pb errorchron (MSWD 2.85) corresponding to a model 3 date of 435 ± 9 Ma, within error the same as that for the Pb/Pb errorchron (432 ± 15 Ma). The ^{235}U-^{207}Pb data for the same analyses show a greater degree of scatter (MSWD 38.9) and define an older, less precise date of 490 ± 25 Ma.

5.4.2: *SLITE FORMATION, UNIT g*

Pb/Pb Results

Three stromatoporoidal carbonates (1907895, 2307896 and 2307897) and two specimens of heliolitid coral (1507892 and 1907899) were analysed from Middle Wenlock Slite Formation unit g localities (*rigidus* & *lundgreni* biozones) at Lännaberget 2, Stora Banne 3, Bogeklint 2 and Spillings 2, in the NE of the island (see **Figure 5.1.1**). Pb isotopic data for the samples are listed in **Table 5d** and plotted in **Figure 5.4.4**.

Qualitatively, it is evident that each of the samples have distinct compositional ranges that plot along a well defined linear trend, implying significant variation of *in situ* μ_2 values at isotopic closure. Carbonate analyses of stromatoporoid 2307896 have very radiogenic Pb isotopic compositions and exhibit a large isotopic range ($^{206}Pb/^{204}Pb$ 49.084-80.107). Analyses of HCl-insoluble residues from the same stromatoporoid possess distinctly less radiogenic Pb isotopic compositions ($^{206}Pb/^{204}Pb$ 24.863-32.955), but plot along the same linear trend. Analyses of other stromatoporoids (2307897, 1907895) and heliolitid corals (1507892, 1907899) also plot along the same trend, but have moderate to unradiogenic Pb isotopic compositions ($^{206}Pb/^{204}Pb$ 18.536-29.667) and very limited isotopic ranges.

Data from 2307896 carbonate analyses define a sixteen point Pb/Pb isochron, corresponding to a date of 324 ± 41 Ma (MSWD 2.34, model μ_1 value 8.21 ± 0.08), too young for the specimen's Middle Silurian stratigraphic position (which approximates to an age of 423 Ma, McKerrow, pers. comm. 1992). All 2307896 data, including the residue analyses, define a more precise isochron date of 325 ± 23 Ma (MSWD 2.03, model μ_1 value 8.21 ± 0.04) (**Figure 5.4.4**). In fact, whatever combination of analyses are selected, the regressed date and model μ_1 value do not significantly alter and to demonstrate this point further, if one considers the entire data set of thirty points, an extremely well fitted isochron date of 326 ± 11 Ma is obtained, with an MSWD of 2.06 and a model μ_1 value of 8.21 ± 0.01. This value is taken as representative of the horizon and its significance is discussed in section **5.5**.

Table 5d: Pb isotopic compositions of carbonates from the Slite Formation, unit g (*rigidus* & *lundgreni* zones), Wenlock, Gotland

SAMPLE	CORRECTED RATIOS*		
	$^{206}Pb/^{204}Pb$	$^{207}Pb/^{204}Pb$	$^{208}Pb/^{204}Pb$
1507892**	24.548 ± 0.048	15.963 ± 0.036	38.765 ± 0.080
1507892A**	24.375 ± 0.028	15.956 ± 0.022	38.770 ± 0.054
1907895a°	21.434 ± 0.022	15.812 ± 0.020	38.417 ± 0.048
1907895b°	21.908 ± 0.022	15.810 ± 0.020	38.250 ± 0.048
1907895Z1°	21.736 ± 0.022	15.793 ± 0.020	38.292 ± 0.046
1907895Z1a°	21.105 ± 0.026	15.803 ± 0.022	38.464 ± 0.060
1907895Z2°	23.046 ± 0.024	15.864 ± 0.020	38.441 ± 0.048
1907899**	18.536 ± 0.018	15.628 ± 0.020	38.156 ± 0.048
1907899a**	18.546 ± 0.018	15.626 ± 0.020	38.150 ± 0.048
2307897°	28.401 ± 0.034	16.170 ± 0.022	38.592 ± 0.060
2307897a°	29.667 ± 0.030	16.222 ± 0.020	38.497 ± 0.048
2307896a°	80.107 ± 0.112	18.912 ± 0.030	38.733 ± 0.070
2307896b°	69.413 ± 0.094	18.327 ± 0.032	38.733 ± 0.068
2307896c°	65.688 ± 0.076	18.155 ± 0.034	38.660 ± 0.076
2307896Q1A°	75.169 ± 0.082	18.630 ± 0.024	38.820 ± 0.050
2307896Q1B°	76.235 ± 0.080	18.705 ± 0.024	38.881 ± 0.048
2307896Q2A°	69.545 ± 0.074	18.349 ± 0.022	38.786 ± 0.048
2307896Q2B°	67.885 ± 0.072	18.248 ± 0.022	38.773 ± 0.050
2307896Q3A°	63.725 ± 0.066	18.030 ± 0.022	38.652 ± 0.048
2307896Q3B°	55.141 ± 0.058	17.589 ± 0.022	38.659 ± 0.048
2307896Q4A°	57.521 ± 0.060	17.711 ± 0.022	38.642 ± 0.048
2307896Q4B°	73.264 ± 0.084	18.539 ± 0.024	38.760 ± 0.052
2307896Z1°	55.902 ± 0.058	17.585 ± 0.022	38.456 ± 0.048
2307896Z1 RES°	24.863 ± 0.046	15.969 ± 0.030	38.263 ± 0.076
2307896Z2A°	71.909 ± 0.074	18.453 ± 0.022	38.723 ± 0.048
2307896Z2A RES°	28.166 ± 0.150	16.199 ± 0.086	38.279 ± 0.206
2307896Z2B°	63.685 ± 0.066	18.044 ± 0.022	38.754 ± 0.048
2307896Z3°	74.606 ± 0.076	18.578 ± 0.022	38.823 ± 0.048
2307896P4°	49.084 ± 0.050	17.257 ± 0.022	38.688 ± 0.048
2307896P4 RES°	32.955 ± 0.036	16.401 ± 0.020	38.411 ± 0.050

* Corrected for mass fractionation of 0.130 % ± 0.012 ($2\sigma_{mean}$) amu^{-1}
Errors are $2\sigma_{mean}$ for corrected ratios
** Data for heliolitid corals
° Data for stromatoporoids

Figure 5.4.4: Pb isotopic data for carbonates and residues from the Slite Formation unit g (*rigidus* & *lundgreni* biozones), Wenlock, Gotland

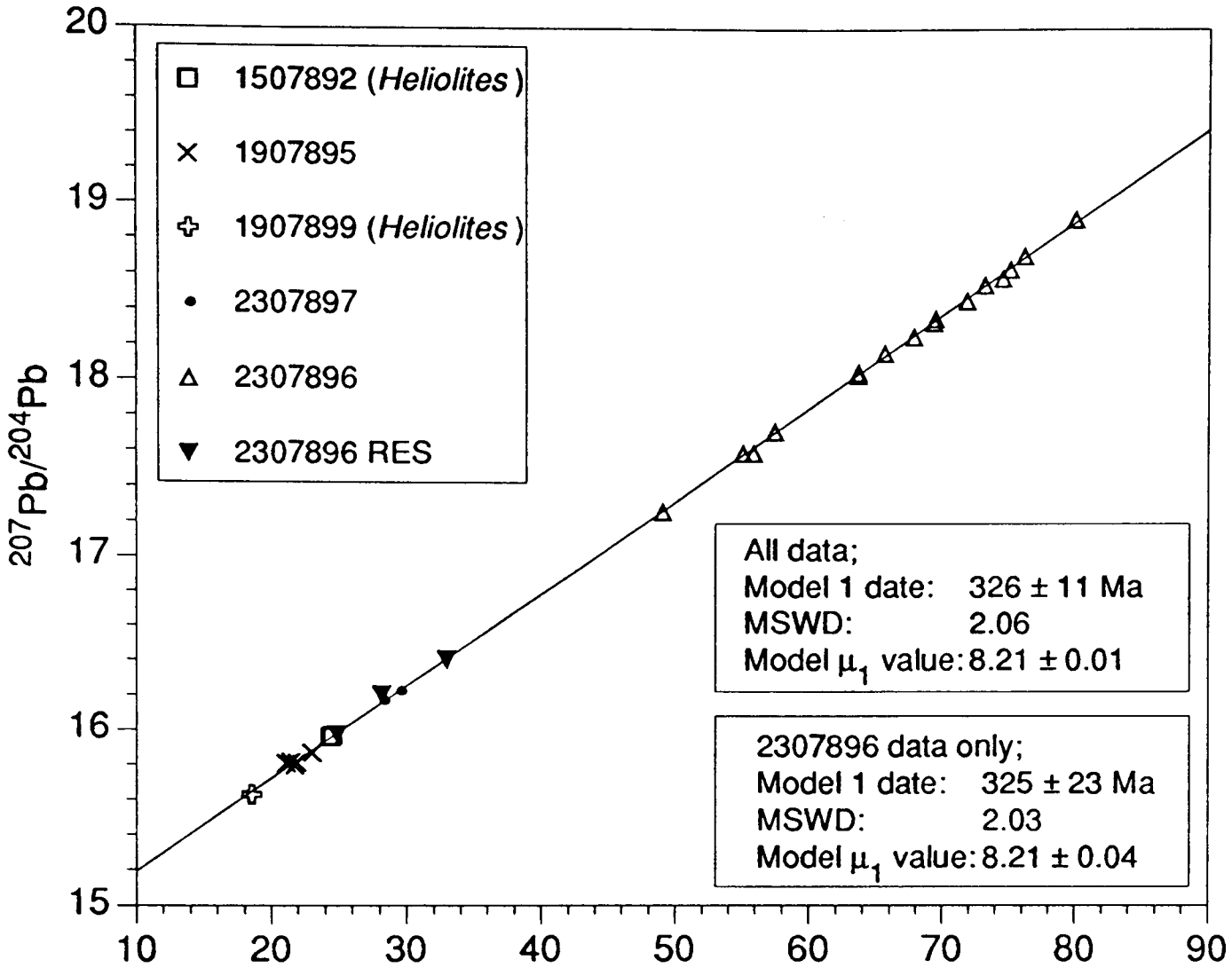

U-Pb Results

Results for U-Pb analyses of Slite Formation unit g carbonates (stromatoporoids and corals) are detailed in **Table 5e** and illustrated in **Figure 5.4.5** and **Figure 5.4.6**. While the Pb/Pb data plot along a well defined isochron, it is evident from the data scatter exhibited in **Figure 5.4.5** and **Figure 5.4.6** that U-Pb closed system conditions were not similarly maintained.

2307896 ^{238}U-^{206}Pb data define an imprecise errorchron date of 259 ± 150 Ma, the high MSWD of 281 reflecting the degree of scatter (**Figure 5.4.5**). All ^{238}U-^{206}Pb data define an errorchron date of 366 ± 88 Ma (MSWD 281). While it is clear that both dates lie within error of the Pb/Pb date (326 ± 11 Ma), unacceptably large errors on the U-Pb dates render them useless for stratigraphic purposes. Regression of ^{235}U-^{207}Pb data (**Figure 5.4.6**) yields dates of 267 ± 140 Ma (MSWD 661) for 2307896 analyses and 361 ± 74 Ma (MSWD 644) for the entire sample set, consistent with the ^{238}U-^{206}Pb information.

Table 5e: U-Pb isotopic data for carbonates from the Slite Formation, unit g (*rigidus* & *lundgreni* zones), Wenlock, Gotland

SAMPLE	CONCENTRATIONS		CORRECTED RATIOS*			
	U (ppm)	Pb (ppm)	$^{238}U/^{204}Pb$	$^{206}Pb/^{204}Pb$	$^{235}U/^{204}Pb$	$^{207}Pb/^{204}Pb$
1907895a°		0.213 ± 0.001		21.434 ± 0.022		15.812 ± 0.020
1907895b°		0.145 ± 0.001		21.908 ± 0.022		15.810 ± 0.020
1907895Z1°		0.177 ± 0.001		21.736 ± 0.022		15.793 ± 0.020
1907895Z2°	0.294 ± 0.000	0.326 ± 0.001	61.036 ± 0.964	23.046 ± 0.024	0.442 ± 0.006	15.864 ± 0.020
1907899**		0.242 ± 0.001		18.536 ± 0.018		15.628 ± 0.020
2307897°	0.261 ± 0.000	0.141 ± 0.001	134.835 ± 1.087	28.401 ± 0.034	0.977 ± 0.008	16.170 ± 0.022
2307896a°		0.087 ± 0.000		80.107 ± 0.112		18.912 ± 0.030
2307896b°	0.584 ± 0.000	0.090 ± 0.000	710.983 ± 11.204	69.413 ± 0.094	5.154 ± 0.041	18.327 ± 0.032
2307896Q1A°	0.471 ± 0.000	0.074 ± 0.000	733.516 ± 11.538	75.169 ± 0.082	5.317 ± 0.042	18.630 ± 0.024
2307896Q1B°	0.459 ± 0.000	0.069 ± 0.000	774.119 ± 12.170	76.235 ± 0.080	5.611 ± 0.044	18.705 ± 0.024
2307896Q2A°	0.478 ± 0.000	0.074 ± 0.000	707.756 ± 11.154	69.545 ± 0.074	5.130 ± 0.040	18.349 ± 0.022
2307896Q2B°	0.525 ± 0.000	0.077 ± 0.000	743.910 ± 11.718	67.885 ± 0.072	5.392 ± 0.042	18.248 ± 0.022
2307896Q3A°	0.514 ± 0.000	0.081 ± 0.000	667.525 ± 10.506	63.725 ± 0.066	4.839 ± 0.038	18.030 ± 0.022
2307896Q3B°	0.675 ± 0.020	0.101 ± 0.000	645.386 ± 10.176	55.141 ± 0.058	4.678 ± 0.037	17.589 ± 0.022
2307896Q4A°	0.614 ± 0.000	0.084 ± 0.000	719.985 ± 11.334	57.521 ± 0.060	5.219 ± 0.041	17.711 ± 0.022
2307896Q4B°	0.659 ± 0.020	0.068 ± 0.000	1094.591 ± 17.236	73.264 ± 0.084	7.934 ± 0.062	18.539 ± 0.024
2307896Z1°	0.579 ± 0.000	0.117 ± 0.000	482.151 ± 7.608	55.902 ± 0.058	3.495 ± 0.028	17.585 ± 0.022
2307896Z2A°	0.477 ± 0.000	0.076 ± 0.000	701.588 ± 11.034	71.909 ± 0.074	5.086 ± 0.040	18.453 ± 0.022
2307896Z2B°	0.662 ± 0.020	0.105 ± 0.000	662.104 ± 10.434	63.685 ± 0.066	4.799 ± 0.038	18.044 ± 0.022
2307896Z3°	0.529 ± 0.000	0.077 ± 0.000	784.492 ± 12.344	74.606 ± 0.076	5.686 ± 0.045	18.578 ± 0.022
2307896P4°	0.657 ± 0.020	0.141 ± 0.001	426.448 ± 6.728	49.084 ± 0.050	3.091 ± 0.024	17.257 ± 0.022

* Corrected for Pb isotopic mass fractionation of 0.130 % ± 0.012 ($2\sigma_{mean}$) amu^{-1} and U isotopic mass fractionation of 0.132 % ± 0.012 (2σ) amu^{-1}
Errors are $2\sigma_{mean}$ for concentrations and corrected ratios
** Data for heliolitid corals
° Data for stromatoporoids

While neither of the U-Pb decay schemes gives unequivocal age information, it is possible to model the likely cause of recent isotopic disturbance by considering the disposition of analyses relative to a 326 Ma reference isochron (the date obtained from the closed system Pb/Pb data). Assuming a model μ_1 value of 8.2, the initial $^{206}Pb/^{204}Pb$ isotopic ratio at 326 Ma would be around 17.34 (see **Figure 5.4.5**). U-Pb analyses plot, in general, to the left of this reference line, implying that the cause of recent isotopic disturbance was U loss (or theoretically Pb gain), unlike Klinteberg Formation carbonates where Pb loss (or U gain) was responsible. Very broadly speaking, more radiogenic samples were liable to greater U loss.

Figure 5.4.5: ^{238}U-^{206}Pb isotopic data for carbonates from the Slite Formation unit g (*rigidus* & *lundgreni* biozones), Wenlock, Gotland

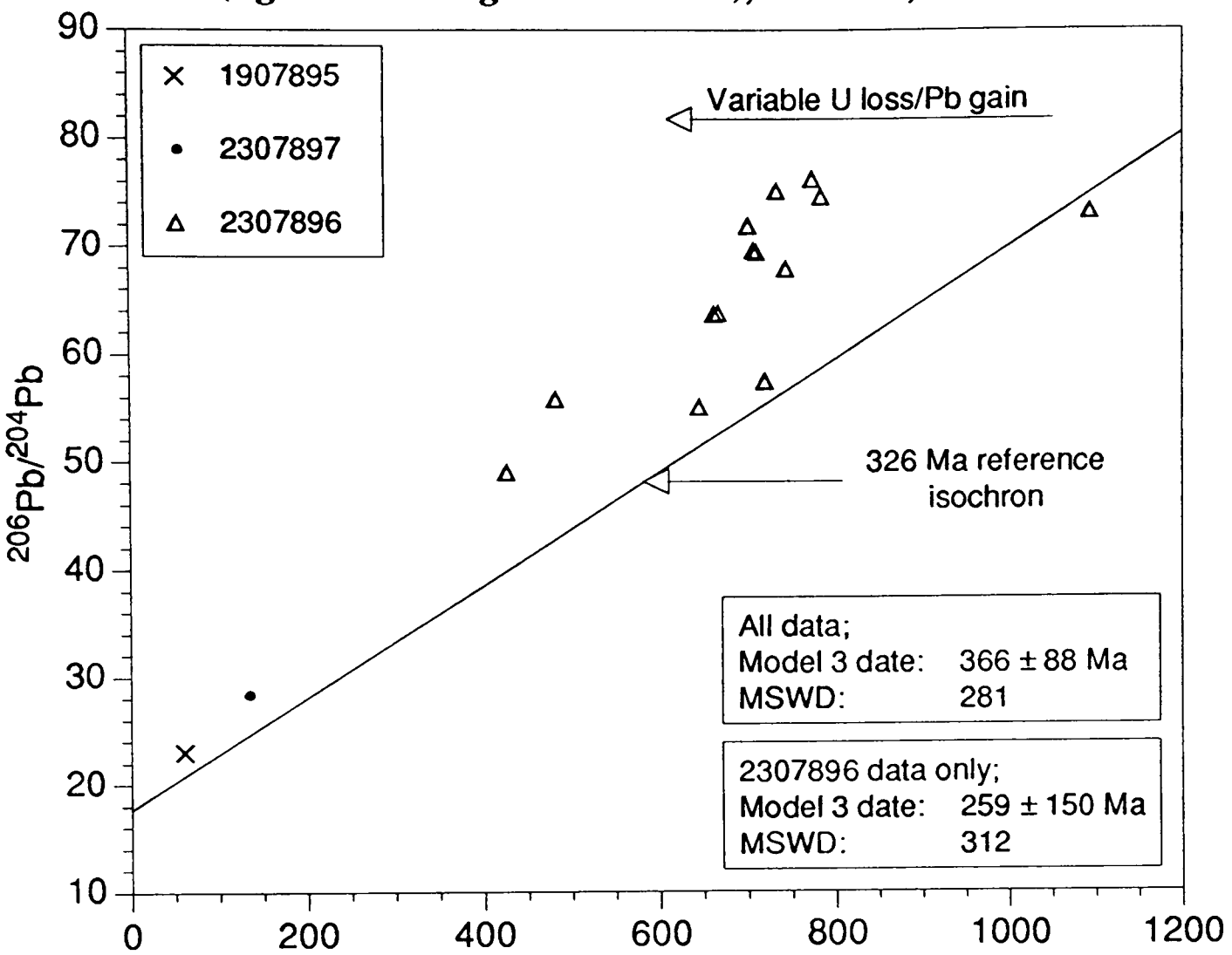

Figure 5.4.6: ^{235}U-^{207}Pb isotopic data for carbonates from the Slite Formation unit g (*rigidus* & *lundgreni* biozones), Wenlock, Gotland

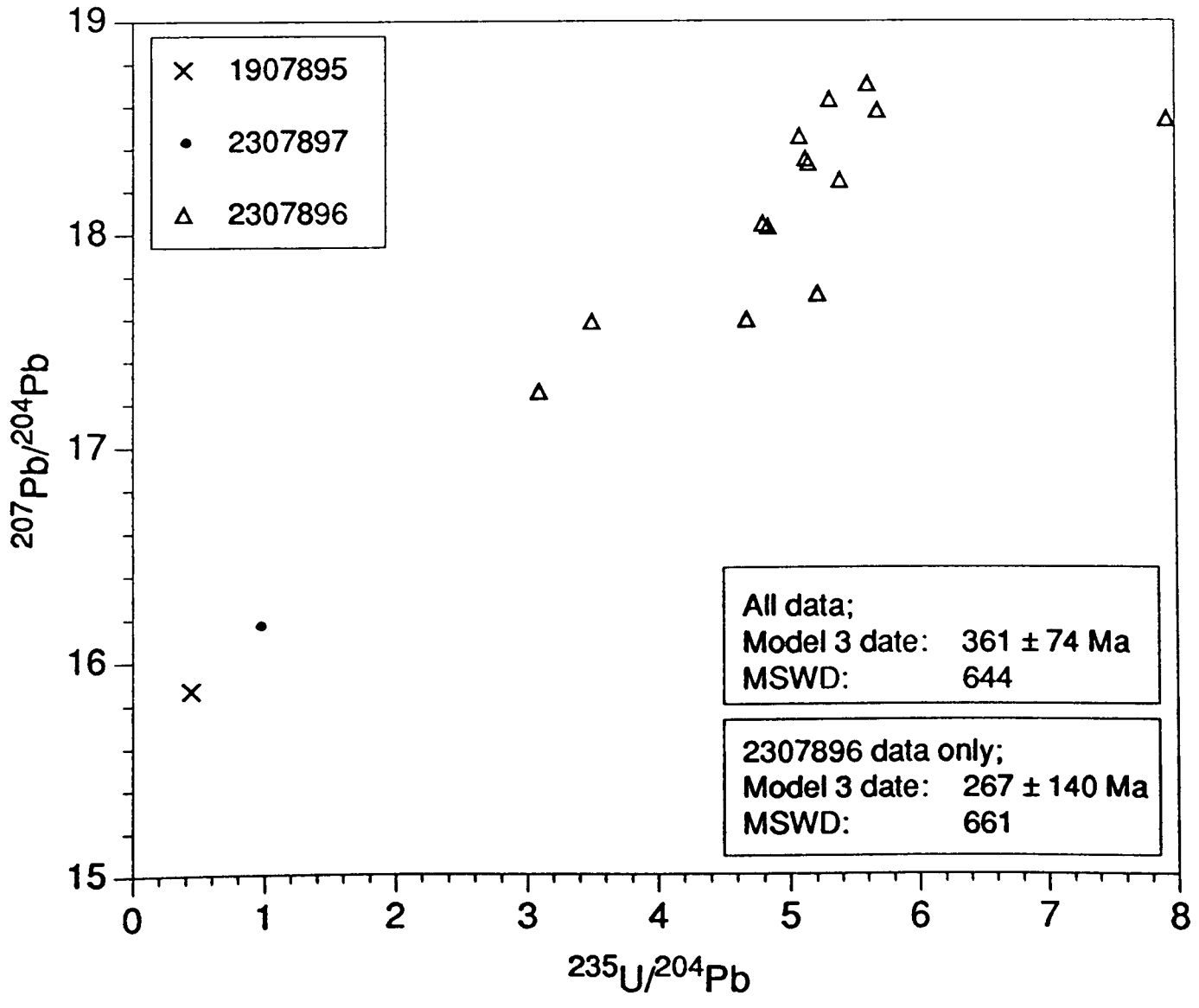

5.4.3: *OTHER FORMATIONS WITHIN THE GOTLAND SUCCESSION*

Pb/Pb Results

Limited Pb isotopic data for carbonates from other horizons within the Silurian of Gotland are detailed in **Table 5f**.

Table 5f: Pb isotopic compositions of carbonates from assorted horizons in the Silurian of Gotland

SAMPLE	CORRECTED RATIOS*		
	$^{206}Pb/^{204}Pb$	$^{207}Pb/^{204}Pb$	$^{208}Pb/^{204}Pb$
Lower Sundre Formation			
2107892a°	29.412 ± 0.040	16.200 ± 0.024	38.311 ± 0.060
2107892b°	30.315 ± 0.058	16.259 ± 0.034	38.418 ± 0.100
Hamra/Burgsvik Formation			
1307897***	18.745 ± 0.020	15.641 ± 0.020	38.316 ± 0.050
1307897c***	24.839 ± 0.064	15.935 ± 0.044	38.181 ± 0.112
Hemse Formation, unit e			
1807899^	20.062 ± 0.020	15.710 ± 0.020	38.851 ± 0.048
Högklint Formation, unit b			
1007893°	26.785 ± 0.038	16.143 ± 0.024	38.503 ± 0.064
1007893a°	30.763 ± 0.038	16.330 ± 0.026	38.321 ± 0.070
1007893b°	28.515 ± 0.046	16.258 ± 0.028	38.590 ± 0.076
1007893c°	30.431 ± 0.032	16.307 ± 0.020	38.348 ± 0.050
Visby Formation			
0907898I†	18.999 ± 0.020	15.665 ± 0.020	38.625 ± 0.048
0907898II†	18.989 ± 0.020	15.664 ± 0.018	38.595 ± 0.046
0907899I†	19.193 ± 0.020	15.713 ± 0.020	38.691 ± 0.054

* Corrected for mass fractionation of 0.130 % ± 0.012 ($2\sigma_{mean}$) amu^{-1}
Errors are $2\sigma_{mean}$ for corrected ratios
*** Crinoid data
^ Whole rock data
° Stromatoporoid data
† Favositid data

Unfortunately, insufficient data are available for isochron construction, but it is evident that stromatoporoid Pb isotopic compositions (2107892, 1007893) tend to be more radiogenic than those from coralline (0907898, 0907899), crinoidal (1307897) and whole rock samples (1807899). Indeed, considering all samples analysed from Gotland, the most radiogenic Pb isotopic compositions and the most significant Pb

isotopic ranges have been obtained from stromatoporoidal carbonates. Evidently, stromatoporoids were highly suitable organisms for the generation of large variations in U/Pb ratios at, or shortly after their deposition, and even after late diagenetic recrystallisation. In this respect they behaved in a similar fashion to the Precambrian stromatolites analysed. A broad model attempting to explain the suitability of particular carbonate materials (such as stromatoporoids and stromatolites) to Pb/Pb and U-Pb dating techniques is proposed in **Chapter 6**.

5.5: DISCUSSION

In this section, petrographic, stable isotopic and independent geological evidence are considered, with a view to obtaining meaningful interpretations for the Pb/Pb and U-Pb dates presented in section **5.4**.

5.5.1: *LOWER MIDDLE KLINTEBERG FORMATION*

Petrographic, Isotopic and Elemental Data

A significant amount of work has already been published on the palaeontology and diagenesis of the Klinteberg Formation by Mori (1970) and Frykman (1984; 1985; 1986; 1989) and this has provided a framework for reference and discussion of stromatoporoid results. Stromatoporoid 16078913, a large domal specimen collected in growth position as two pieces from Lilla Snögrinde 2, preserves a vague laminar structure in thin section, with distinct latilaminae forming planes of weakness along which the carbonate easily split. Detailed analysis of carbonate samples from successive growth zones within the organism (Z0 at the stromatoporoid/ocean interface to Z4 at the substrate) was therefore possible. Patchy preservation of structural detail indicates that imperforate, undulose laminar structures predominated, with pillars only weakly developed, suggesting classification as a Clathrodictyid, probably ?*Clathrodictyon* sp. (Kershaw, pers. comm. 1992). Structural components are preserved as cloudy, speckled carbonate, while gallery infills are clear. Neomorphic recrystallisation, however, has destroyed primary structural fabrics throughout much of the organism. Unidentified organic materials are noted, but their distribution bears little relation to gross morphological trends. Although strong diagenetic recrystallisation is evident, as described by Frykman (1984; 1985), the lack of structural deformation in well preserved areas implies that primary cementation must have been relatively early. Sparry low magnesian calcite (LMC)

crystals show elongation perpendicular to growth surfaces, while their boundaries bear no relationship to either the orientation or distribution of structural elements and frequently cut directly across them without any noticeable effect, suggesting a μm-scale thin-film process may have been operative during diagenesis (Kershaw, 1990; Pingitore, 1976). Late compressive stylolite formation parallel to latilaminae has caused local disruption of the structural fabric.

Cathodoluminescence (CL) is a particularly useful tool for the petrographic study of stromatoporoids (Kershaw, 1990), facilitating the identification of cloudy structural elements viewed in plane polarised light, and thereby aiding palaeontological classification. Under CL, 16078913 is confirmed as *Clathrodictyon* sp. and, in addition, it is possible to identify a broad cement stratigraphy. A coarse, blocky, non-luminescent clear spar cement is formed on dull luminescent cloudy structural components and is succeeded firstly by a dull luminescent LMC phase and secondly by late, dull to bright luminescent dolomite.

Frykman (1984; 1985) also documented a well defined cement stratigraphy for the Klinteberg Formation and concluded that cementation involved up to four generations of intergranular spar, in addition to fine grained internal sediment produced by emergent erosion (crystal silt of Dunham, 1969):-

Stage 1 turbid, dull luminescent epitaxial overgrowths and bladed rims with inclusions of probable microdolomite, interpreted as the closed system replacement of an early marine cement phase (Grover & Read, 1983), possibly formerly high magnesian calcite (HMC) (Lohmann & Meyers, 1977). The diagenetic replacement must have occurred prior to the deposition of stages 2, 3 and 4.

Stage 2 clear, non-luminescent spar, interpreted as having been deposited from meteoric oxidising pore waters in the form of low magnesian calcite (LMC) (Frank et al., 1982; Grover & Read, 1983). Occasional bright luminescent zones reflect periodic pore water stagnation. Stage 2 cements necessitate the presence of a local subaerially exposed recharge area, similar to that documented on Bermuda by Plummer et al. (1976), where fresh water lenses extending 10-15 m below the island's surface are found.

Stage 3 clear, bright luminescent LMC spar deposited as progressively more reducing meteoric pore waters evolved upon reburial (Frank et al., 1982; Grover & Read, 1983). Fine non-luminescent zonations indicate open system conditions with periodic reflux of oxidising waters. The association of crystal silt (characteristic of vadose diagenesis; Dunham, 1969), with

stages 3 and 4 suggests that the pore waters were sourced locally.

Stage 4 clear, subtly zoned, dull luminescent LMC spar occluding remaining porosity. This stage is usually the most abundant and is interpreted as reflecting continued reducing conditions and burial (Frank et al., 1982).

Whereas all four generations are found in biohermal framestones, inter-reefal sediments generally lack the non-luminescent spar, a feature that Frykman (1984) related to permeability differences between the two rock types. Frykman (1985) interpreted the low micrite content and the regularity and clarity of the growth zones observed in Klinteberg Formation cement stages 2, 3 and 4 as evidence of crystal growth within primary porosity and minimal subsequent diagenetic alteration of the primary LMC mineralogy. Evidence for regressive emergence exists in the Högklint, Slite and Eke Formations, but the first two could not be responsible for the Klinteberg meteoric cementation since they are stratigraphically lower in the section and it is unlikely that Eke emergence was the cause, because the formation is over 100 m higher in the section. Currently, direct evidence for emergence has not been documented for the Klinteberg Formation but continued investigations may yet reveal emergent features (such as karstification) associated with late Wenlock regression.

Diagenetically, the speckled dull luminescent skeletal components of 16078913 are interpreted as equivalent to the stage 1 cements of Frykman (1984; 1985), forming by the closed system replacement of an early, possibly synsedimentary marine cement phase. If the speckled nature of the calcite is due to the presence of microdolomite inclusions, then the precursor material was probably high magnesian calcite (HMC) (Lohmann & Meyers, 1977). The clear, non-luminescent blocky cement (equivalent to stage 2 of Frykman) was probably deposited after early cementation of the skeleton, as LMC from oxidising meteoric waters, while the clear, dull luminescent LMC cement (stage 4 of Frykman) was deposited as increasingly reducing pore waters evolved. The stage 3 cement of Frykman (1984; 1985) is not developed. Late variably luminescent dolomite, observed by Frykman (1986) at Klinteberget, but not described by Frykman (1984; 1985) for Lilla Snögrinde localities, is interpreted as having formed under mixing zone conditions after slight marine transgression.

While stromatoporoids 16078914 and 16078916 exhibit a domal structure in their outcrop at Lilla Snögrinde 1, in thin section they are seen to be completely recrystallised and preserve no primary structural detail, making classification impossible. The moderately coarse LMC spar crystals show no preferred orientation. Unfortunately, CL sections were not available but standard petrographic observations

Table 5g: Stable isotopic data for stromatoporoids from the lower Middle Klinteberg Formation (*ludensis* biozone), Wenlock, Gotland

SAMPLE	POSITION	$\delta^{13}C$‰ PDB	$\delta^{18}O$‰ PDB
16078913A1		1.74	-7.65
16078913A2		1.79	-7.25
16078913Aa		1.89	-6.66
16078913Ab		1.89	-6.65
16078913Ac		1.87	-6.80
16078913Ad		1.88	-6.71
16078913B1		1.76	-7.28
16078913B2		1.84	-7.29
16078913Ba		1.79	-7.64
16078913Bb		1.83	-7.03
16078913Bc		1.85	-7.30
16078913Bd		1.87	-7.03
16078913Z0a	outer surface - OCEAN	1.97	-5.98
16078913Z0b	inner surface	1.85	-6.60
16078913Z0c	outer surface	1.97	-6.03
16078913Z0d	inner surface	1.94	-6.51
16078913Z1a	outer surface	1.95	-5.85
16078913Z1b	centre	1.92	-6.51
16078913Z1c	inner surface	1.89	-6.92
16078913Z1d	inner surface	1.88	-6.94
16078913Z2a	outer surface	1.88	-6.97
16078913Z2b	centre	1.91	-6.85
16078913Z2c	inner surface	1.86	-6.95
16078913Z23d	inner surface	1.88	-6.91
16078913Z3a	outer surface	1.85	-6.98
16078913Z3b	centre	1.81	-7.69
16078913Z3c	inner surface	1.86	-6.96
16078913Z3d	inner surface	1.85	-6.88
16078913Z4a	outer surface	1.81	-6.90
16078913Z4b	inner surface	1.84	-6.63
16078913Z4c	coarse late spar	2.15	-7.71
16078913Z4d	coarse late spar - SUBSTRATE	2.04	-7.60
16078914A		2.96	-6.58
16078914B		2.91	-6.52
16078914a		2.81	-7.04
16078914b		2.89	-6.31
16078914c		3.01	-6.01
16078914d		3.00	-6.21
16078916A		2.87	-6.04
16078916a		2.78	-7.74
16078916b		2.95	-5.83
16078916c		2.98	-5.66
16078916d		2.94	-5.95
LSa		0.06	-7.31
LSb		0.04	-7.38
LSc		0.04	-8.02
LSd		0.10	-8.03

indicate that these samples show a greater degree of diagenetic recrystallisation than is evident at Lilla Snögrinde 2.

Stable isotopic data for stromatoporoids from the lower Middle Klinteberg Formation are detailed in **Table 5g** and plotted in **Figure 5.5.1**. All values are consistent with a shallow marine origin followed by meteoric diagenesis, despite the fact that particular samples have distinct compositional ranges.

Figure 5.5.1: Stable isotopic data for stromatoporoids from the lower Middle Klinteberg Formation (*ludensis* biozone), Wenlock, Gotland

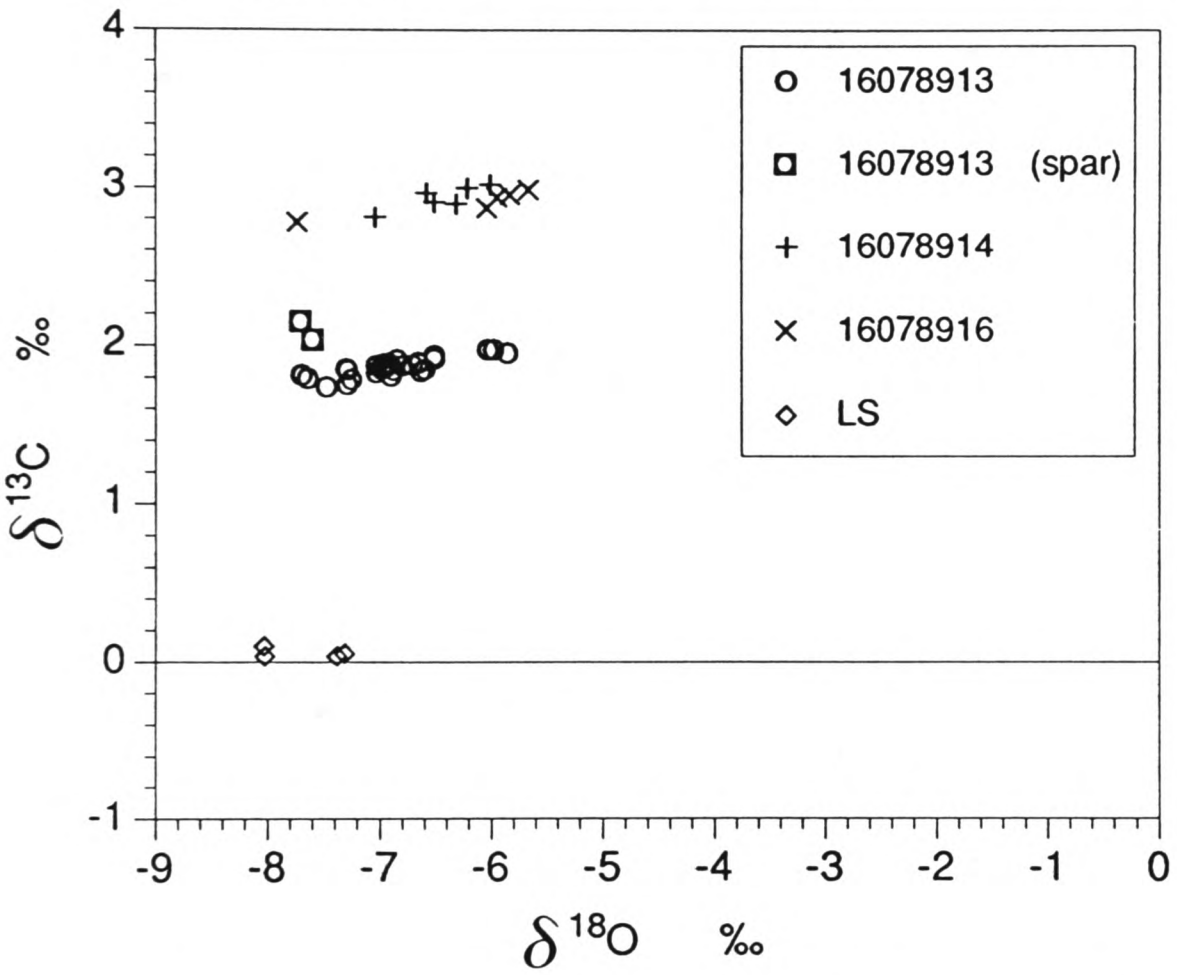

Analyses of $\delta^{13}C$ for 16078914 and 16078916 cluster around 3‰ (relative to PDB), suggesting a common isotopic history, but distinct from that experienced by 16078913 and LS, which have significantly lighter carbon isotopic compositions (around 2‰ and 0‰ respectively). Indeed, while patchy structural preservation occurs in 16078913, complete recrystallisation is noted for both 16078914 and 16078916. Late spar phases described from 16078913 have a heavier carbon isotopic composition then the remainder of the sample, implying a separate origin. All samples analysed have very similar ranges of oxygen isotopic compositions (-5.5 to -8‰), suggesting that samples may have undergone similar degrees of meteoric diagenesis and that primary carbon variations were probably the principal cause for the observed data scatter.

Figure 5.5.2: Stable isotopic data for stromatoporoid 16078913 growth zones from the lower Middle Klinteberg Formation (*ludensis* biozone), Wenlock, Gotland

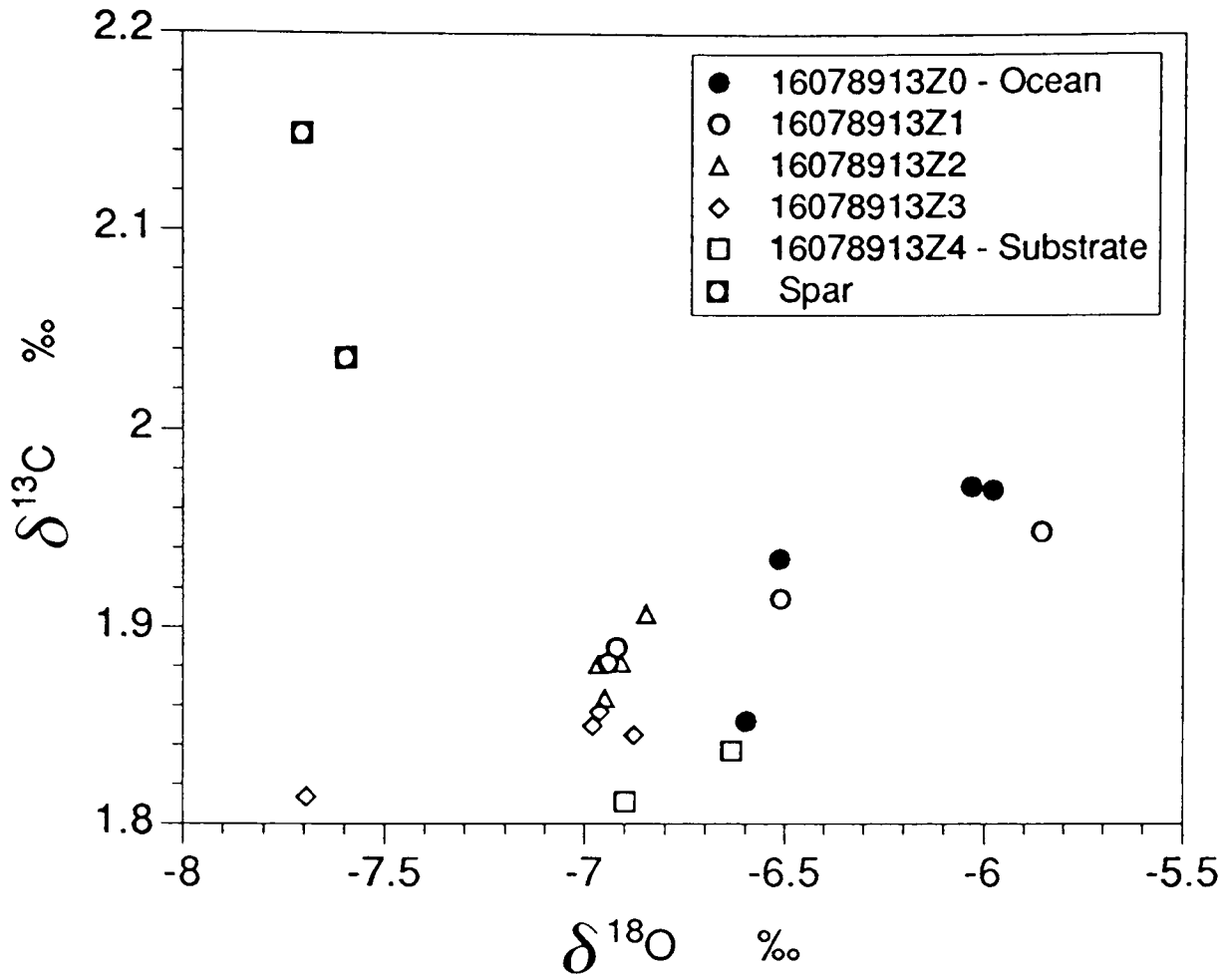

Figure 5.5.2 separates the stable isotopic data for 16078913 into the five growth zones (Z0-Z4), plus the late spar phase. Zone 4 represents the earliest formed carbonate, while zone 0 is at the stromatoporoid margin. The spar isotopic signature demonstrates this phase to be distinct from the stromatoporoidal carbonate, which shows progressively heavier carbon and oxygen isotopic compositions towards the margins.

If one also considers the variation of Pb concentration, U concentration and isotopic composition between growth zones, as illustrated in **Figure 5.5.3**, an interesting pattern begins to emerge. There is a steady increase in Pb concentration from the earliest formed carbonate (Z4, nearest the substrate) to the outermost growth zones, while the U concentration shows marked variability. The most uraniferous carbonate is associated with the outermost growth zones. The $^{206}Pb/^{204}Pb$ ratio shows a general decrease from substrate to margin, a trend echoed by the $^{207}Pb/^{204}Pb$ ratio, but the $^{208}Pb/^{204}Pb$ shows very little variation and hence it is concluded that Th was not a significant elemental contributant to stromatoporoid mineralogy. Th/Pb ratios for this sample were either close to zero, or constant (if the initial $^{208}Pb/^{204}Pb$ ratio was < c.38).

Figure 5.5.3: Concentration and isotopic composition data for 16078913 zones from the lower Middle Klinteberg Formation (*ludensis* biozone), Wenlock, Gotland

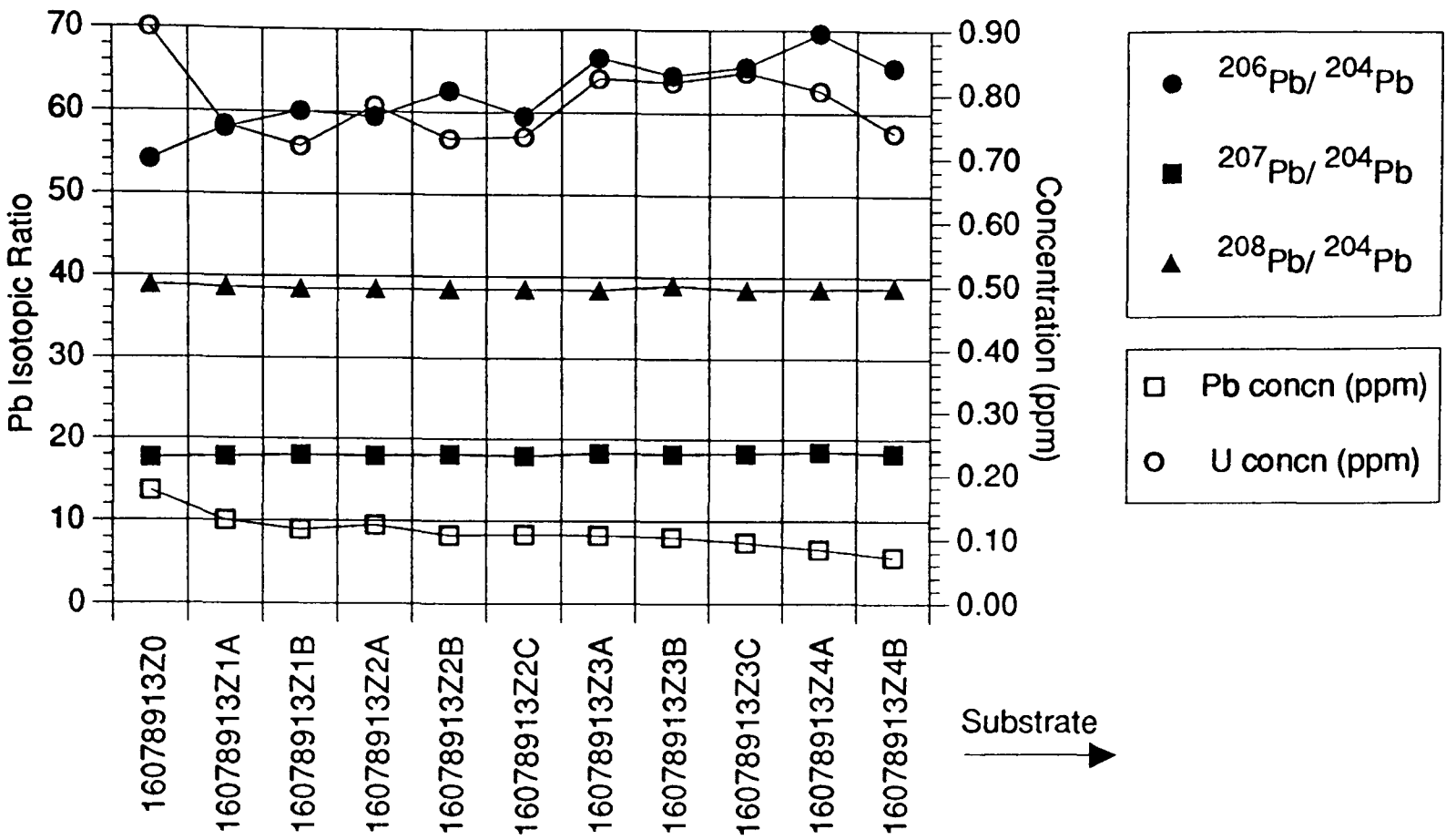

Unfortunately, the differentiation of relict depositional isotopic signatures from diagenetic ones and hence quantification of any primary biogenic isotopic/elemental fractionation is not possible, but it is clear that systematic variations in both concentration and isotopic composition do occur within the stromatoporoid and this phenomenon has to be explained in any model. From **Figure 5.4.2** and **Figure 5.4.3** it was concluded that either Pb loss or U gain was responsible for the recent isotopic disturbance experienced by the lower Middle Klinteberg carbonates. Considering the solubility of U in oxidising waters (Klinkhammer & Palmer, 1991), the well documented evidence for emergence provided by raised Quaternary shorelines on Gotland (Jeppsson, 1982) and the variability of U concentrations in **Figure 5.5.3**, modification of the primary U signal by secondary enrichment seems the more likely explanation.

Age Data and Interpretation

The Pb/Pb date of 432 ± 15 Ma for lower Middle Klinteberg Formation stromatoporoids (*ludensis* biozone) (**Figure 5.4.1**) is in good agreement with the proposed 420 Ma age of the Wenlock-Ludlow boundary (McKerrow, pers. comm. 1992). The U-Pb date of 301 ± 73 Ma (**Figure 5.4.2**) for all samples analysed from that horizon is considered to have no true age significance, rather it reflects the effects of recent isotopic disturbance due to U gain during the Quaternary. Omission of 1607891 3Z0-Z4

analyses, which all come from the same hand specimen of stromatoporoid, produces a six point ^{238}U-^{206}Pb isochron corresponding to a date of 435 ± 9 Ma, in excellent agreement with the Pb/Pb regression.

In geological terms, this c.430 Ma date is interpreted as the age of early carbonate diagenesis, probably relating to the meteoric diagenetic recrystallisation of stromatoporoids. Given the magnitude of the errors on both Pb/Pb and U-Pb dates, this value is indistinguishable from the age of deposition. In terms of accuracy, the U-Pb date of 435 ± 9 Ma is 6 Ma outside error of the inferred 420 Ma age for the Wenlock-Ludlow boundary, while the Pb/Pb date of 432 ± 15 Ma is consistent. Further U-Pb studies on appropriate stromatoporoidal samples from Lilla Snögrinde should enable an accurate date for the Wenlock-Ludlow transition to be obtained.

5.5.2: *SLITE FORMATION, UNIT g*

Petrographic, Isotopic and Elemental Data

Unlike the Klinteberg Formation, little has been published on the palaeontology or petrography of the Slite Formation and nothing on the diagenesis. Mori (1969) detailed stromatoporoids recovered from assorted Slite localities, commenting on their biostratigraphic implications and state of preservation, while Sundquist (1982b) and Laufeld et al. (1978) have published petrographic studies for parts of the Slite Formation.

Specimens 1507892 and 1907899 are both examples of the tabulate coral *Heliolites* sp.. 1507892 was collected from bedded carbonates in a small quarry at Lännaberget 2 and shows well preserved, cloudy corallite walls with porosity occlusion effected by clear LMC spar, including an early fringing phase sited on walls and tabulae. Spar crystal boundaries do not cut across either the tabulae or the walls and no clear signs of compressive deformation are evident, suggesting that lithification of carbonate sediments was relatively early (as proposed by Sundquist, 1982b). Under cathodoluminescence (CL), the corallite walls and tabulae of 1507892 are seen to be preserved as fine grained, cloudy, dull luminescent calcite, within which vestiges of length-parallel internal structure are evident. Three phases of cementation are noted;

- an initial non-luminescent, prismatic, fringing cement, preferentially sited on the concave surfaces of tabulae;
- a subsequent thick, dull luminescent, zoned LMC cement; and

•a final bright luminescent LMC cement with development of dolomite rhombs. In thin section 1907899 shows a similar preservational state to 1507892 but there is an amount of secondary iron staining in addition. Ostensibly the same cement stratigraphy is preserved, despite the fact that the two samples originate from localities some 4 km apart (Bogeklint 2 and Lännaberget 2). A non-luminescent, prismatic fringing cement, developed preferentially on one side of corallite tabulae, is succeeded by a thick, poorly zoned dull luminescent LMC generation and porosity occlusion is effected by bright luminescent calcite with associated rhombohedral dolomite.

Stromatoporoids were analysed from Stora Banne 3 (1907895) and Spillings 2 (2307896, 2307897), the locations of which are indicated on **Figure 5.1.1**. In thin section, 1907895 shows patchy preservation of a broad, open, reticulate structure with micritic chevron-type laminae, suggesting classification as ?*Ecclimadictyon* sp. (Kershaw, pers. comm. 1992). Abundant syringoporoid tabulate corals were commensally intergrown with the stromatoporoid skeletons and these are preserved as caunophore tubes within the structure. Whereas the LMC spar crystals within the stromatoporoid are elongated at 90° to the laminae, those within the caunophore tubes are of more equant habit and exhibit a broad concentric arrangement, with an early fringing cement and subsequent spar infill. CL shows that the preserved structural elements are essentially dull luminescent with bright luminescent micro-inclusions providing a speckled appearance. A thin bright luminescent band at the outer margin of the skeleton is followed by the ubiquitous blocky, non-luminescent fringing cement and thick dull luminescent calcite infill. In addition, a late bright luminescent cement is locally developed. Essentially the same cement stratigraphy is observed within both the stromatoporoid skeleton and caunophore tubes, although the dominance of each zone varies between caunophore tubes, suggesting that flow of diagenetic meteoric waters through the stromatoporoid/coral may have been variable. Rare, fine grained silicate minerals showing bright blue luminescence (principally quartz) show clearly under CL.

2307896 and 2307897 both show patchy preservation of original structural detail, again suggestive of classification as ?*Ecclimadictyon* sp. (Kershaw, pers. comm. 1992). Specimen 2307896 comprises two pieces of stromatoporoidal carbonate, both of which readily split along latilaminae allowing more detailed isotopic analysis. 2307896Q was collected in growth position, with Q1 nearest the substrate and Q4 the last growth zone. 2307896Z samples come from a fragment of the same fossil stromatoporoid but unfortunately do not directly relate to 2307896Q specimens. Pyrite

is locally developed and indicates the development of reducing conditions during diagenesis. The distribution of pyrite is not obviously related to the general growth structure of the skeleton and may be associated with a relatively late diagenetic episode. Under cathodoluminescence, the structure is seen to be preserved as dull luminescent, speckled micrite and the cement stratigraphy comprises an early, clear, non-luminescent, blocky fringing cement, followed by a generally dull luminescent amorphous phase and patchily developed dull to bright luminescent zoned dolomite. This pattern is consistent with that for other Slite Formation unit g samples.

Diagenetic interpretation of the cement stratigraphy is broadly similar to that for the Klinteberg Formation. Where preserved, the structural detail indicates that compression of the skeleton has not occurred and so early marine cementation is likely. The speckled, dull luminescent preservation of structural elements is interpreted as representing diagenetic LMC recrystallisation of early marine HMC cement, freed Mg forming microdolomite inclusions. The association of non-luminescent, LMC fringing cement with weakly zoned, dull luminescent LMC infill is interpreted as having formed in primary porosity from initially oxidising meteoric waters that progressively became more reducing as porosity occlusion progressed. Zonation resulted from slight variations in redox potential. The final development of bright luminescent calcite and dolomite rhombs may be attributable to late minor transgression, resulting in upward displacement of the mixing zone environment during progressive sediment burial (Frykman, 1986; Kaldi & Gidman, 1982; Jones et al., 1984). Alternatively, one might consider an origin in terms of distinct Mg-rich aquifers flushing the system.

Stable isotopic data for Slite Formation unit g carbonates are detailed in **Table 5h** and illustrated in **Figure 5.5.4**. Data may be grouped into two main subsets with differing $\delta^{13}C$ values; the first has $\delta^{13}C$ clustered around 1‰ and comprises 1907895 and 1907899, while the second has $\delta^{13}C$ values clustered around 0.3‰ and comprises 2307896 and 2307897. $\delta^{18}O$ values tend to lie between -6 and -8‰, suggestive of similar degrees of diagenetic alteration and implying that carbon isotopic values might reflect primary variations. Values of 1.4‰ for carbon and 0 to -4‰ for oxygen, quoted by James & Choquette (1983) for typical Silurian carbonates, reinforce the suggestion that carbon isotopic compositions may be primary and confirm the importance of meteoric fluids in diagenetic recrystallisation.

Table 5h: Stable isotopic data for carbonates from the Slite Formation unit g (*rigidus & lundgreni* biozones), Wenlock, Gotland

SAMPLE	POSITION	$\delta^{13}C$‰ PDB	$\delta^{18}O$‰ PDB
1907895Z1		1.01	-7.24
1907895Z1i		0.94	-6.99
1907895Z1ii		0.81	-7.45
1907895Z1iii		0.95	-7.10
1907895Z2a		1.04	-6.58
1907895Z2b		0.98	-6.66
1907895Z2i		0.89	-7.26
1907895Z2ii		0.86	-7.53
1907895Z2iii		0.94	-6.95
1907899		0.99	-7.19
1907899i		0.96	-7.10
1907899ii		0.96	-7.23
1907899iii		0.97	-7.15
1907899iv		0.88	-7.27
2307896Q4a	outer surface - OCEAN	0.27	-7.44
2307896Q4b	centre	0.27	-7.43
2307896Q4c	inner surface	0.29	-7.36
2307896Q4d	inner surface	0.28	-7.21
2307896Q3a	outer surface	0.30	-7.23
2307896Q3b	centre	0.32	-7.28
2307896Q3c	inner surface	0.29	-7.50
2307896Q3d	outer surface	0.30	-7.51
2307896Q2a	outer surface	0.28	-7.46
2307896Q2b	centre	0.32	-7.29
2307896Q2c	inner surface	0.33	-7.27
2307896Q2d	inner surface	0.26	-7.53
2307896Q1a	outer surface	0.45	-7.37
2307896Q1b	centre	0.35	-7.34
2307896Q1c	inner surface	0.30	-7.36
2307896Q1d	inner surface - SUBSTRATE	0.31	-7.36
2307896Z1a		0.22	-7.41
2307896Z1b		0.24	-7.20
2307896Z1c		0.27	-7.05
2307896Z2a		0.21	-7.55
2307896Z2b		0.14	-8.08
2307896Z2c		0.22	-7.47
2307896Z3a		0.22	-7.53
2307896Z3b		0.25	-7.37
2307896Z3c		0.24	-7.59
2307896Z4a		0.20	-7.64
2307896Z4b		0.21	-7.58
2307896Z4c		0.20	-7.54
2307897		0.61	-6.85
2307897a		0.27	-7.11
2307897b		0.24	-7.19
2307897c		0.25	-7.15
2307897i		0.64	-5.71
2307897ii		0.36	-6.45
2307897iii		0.20	-7.18
2307897iv		0.16	-7.30

Figure 5.5.4: Stable isotopic data for carbonates from the Slite Formation unit g (*rigidus* & *lundgreni* biozones), Wenlock, Gotland

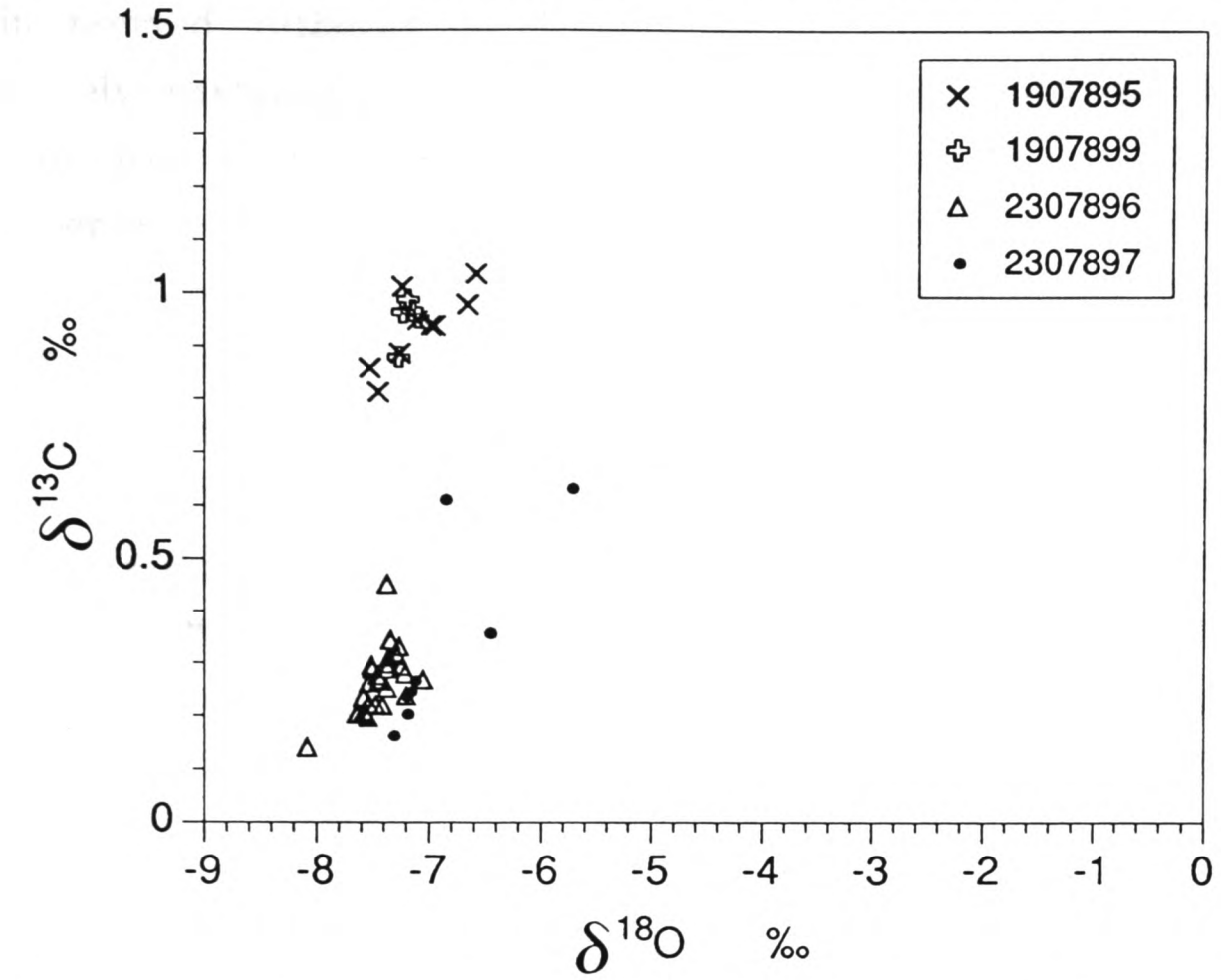

Figure 5.5.5: Stable isotopic data for stromatoporoid 2307896Q zones from the Slite Formation unit g (*rigidus* & *lundgreni* biozones), Wenlock, Gotland

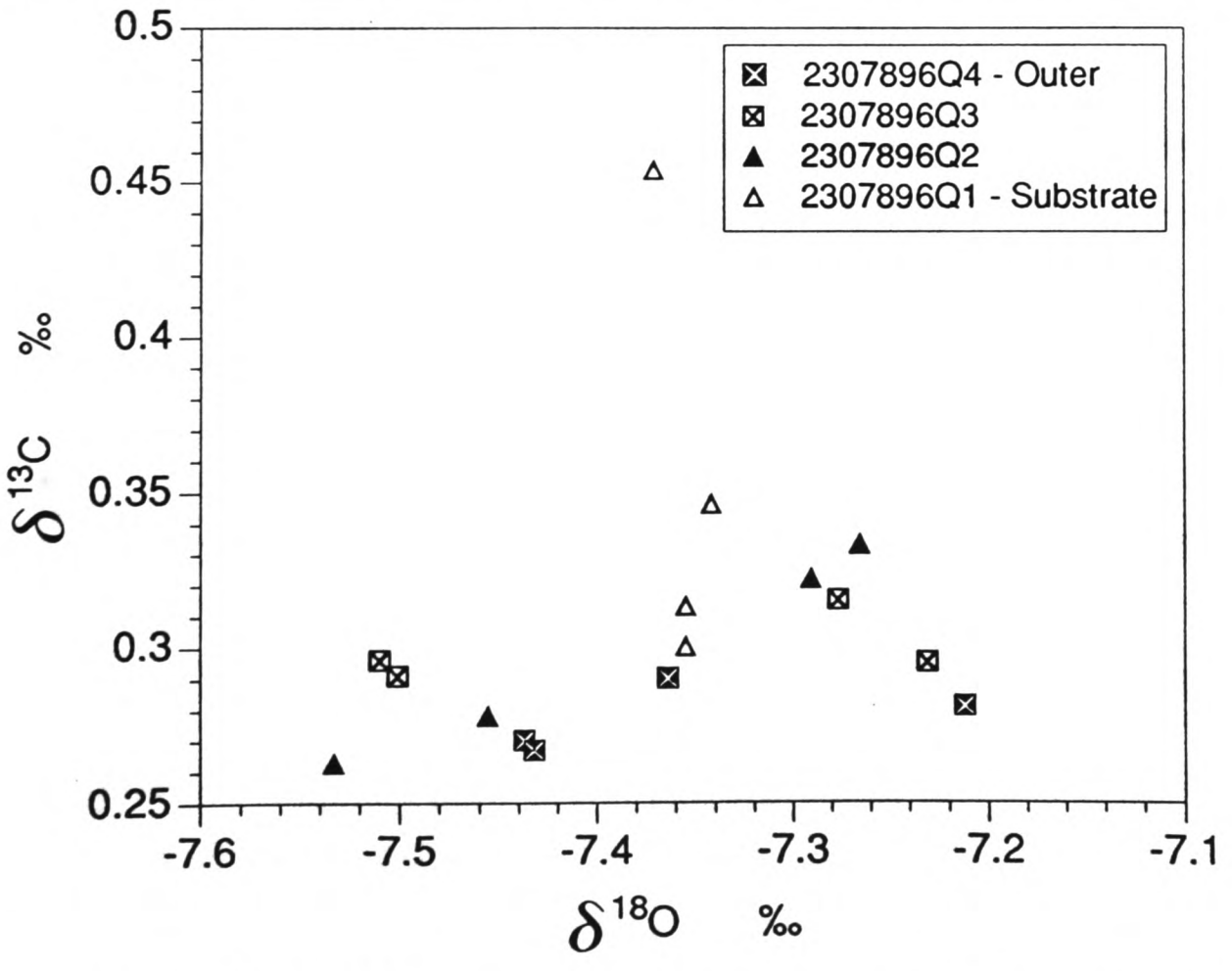

Expansion of 2307896Q zone data in **Figure 5.5.5** shows that while no clear trend in oxygen isotopic composition exists for stromatoporoidal carbonate, $\delta^{13}C$ values tend to become lighter towards the outer growth zones. This is opposite to the trend noted for stromatoporoids from the Klinteberg Formation.

Considering the variation of Pb concentration, U concentration and isotopic composition between growth zones, illustrated in **Figure 5.5.6**, systematic variations are again observed. Although the Pb concentration shows little variation, remaining approximately constant throughout the organism at around 0.8 ppm, the U concentration falls from c.0.66 ppm in the earliest formed zones to c.0.54 ppm in the outermost growth zones. This trend is opposite to that exhibited by stromatoporoid 16078913 from the Klinteberg Formation, where the Pb concentration rises from core to rim, while the U concentration is variable between 0.7 and 0.8 ppm. 2307896Q2B appears anomalously high in respect of both Pb and U concentrations. $^{206}Pb/^{204}Pb$ ratios are highest at the core and tend to decrease towards the margin (with the exception of 2307896Q4B), a trend mirrored by $^{207}Pb/^{204}Pb$ values. More interestingly, the $^{206}Pb/^{204}Pb$ ratio shows an apparent inverse relationship to the U concentration, opposite to what one might expect assuming no heterogeneity. $^{208}Pb/^{204}Pb$ values vary little from c.38, from which it may be concluded that Th/Pb (and hence Th/U) ratios were either zero (implying an initial $^{208}Pb/^{204}Pb$ ratio of c.38), in which case Th may be considered incompatible as far as stromatoporoidal carbonates were concerned, or some other constant (implying an initial $^{208}Pb/^{204}Pb$ ratio of < 38), in which case Th was uniformly accommodated within the carbonate. Considering the observed U, Pb elemental variation in stromatoporoids and the chemical similarity of U and Th, the former would appear more likely.

Figure 5.5.6: Concentration and isotopic composition data for 2307896Q zones from the Slite Formation unit g (*rigidus* & *lundgreni* biozones), Wenlock, Gotland

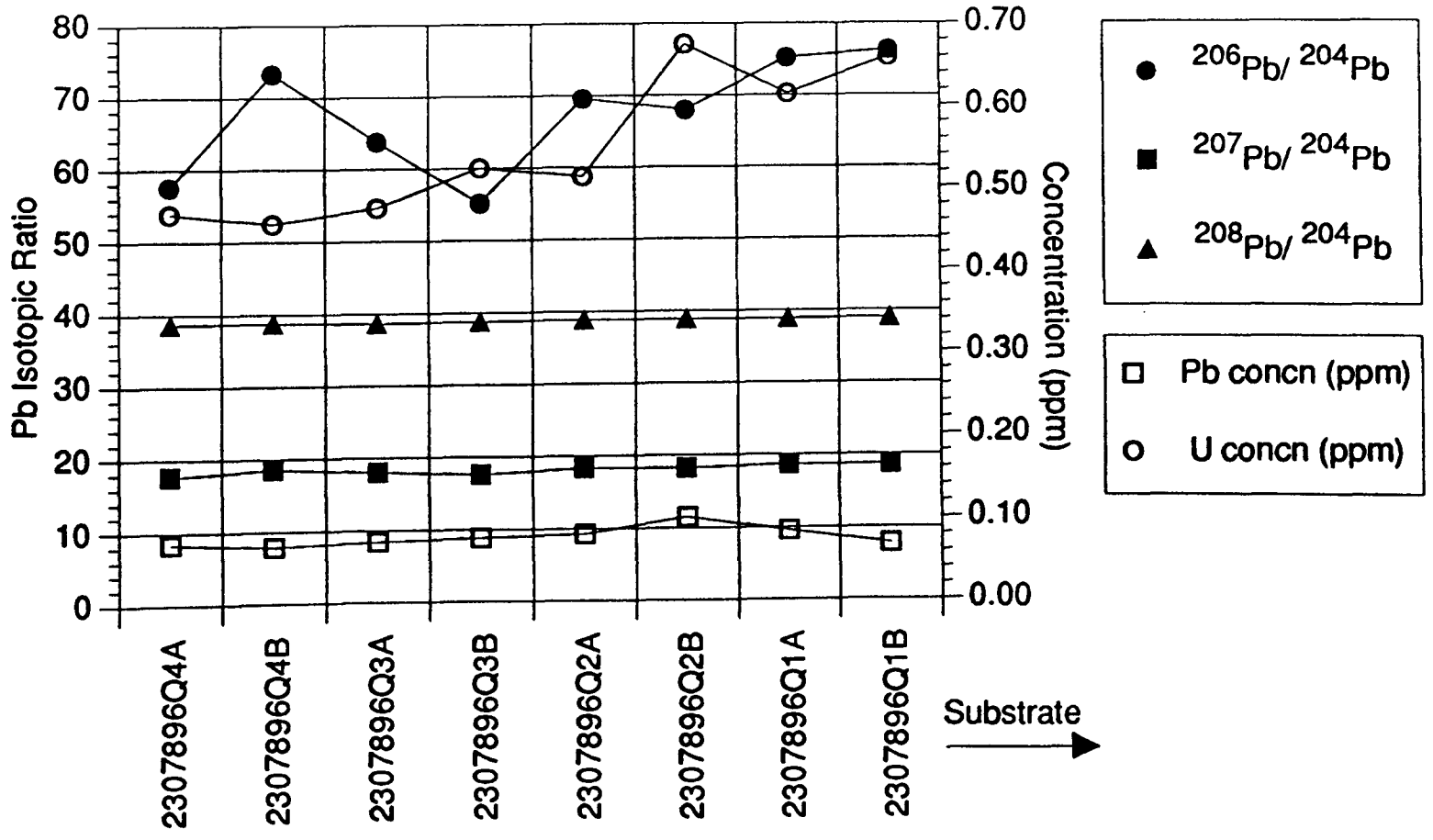

From **Figure 5.4.5** and **Figure 5.4.6**, it was implied that either Pb gain or U loss was responsible for the recent isotopic disturbance experienced by the Slite Formation carbonates. Recent Pb gain is most unlikely, since the Slite Formation Pb/Pb isochron is so well defined and any gain of Pb with a relatively modern isotopic composition would generate data scatter in excess of that observed in **Figure 5.4.4**. Consequently, it is concluded that U loss was principally responsible for the recent isotopic disturbance experienced by the carbonates. Again, considering the solubility and mobility of U in oxidising waters (Klinkhammer & Palmer, 1991) and the evidence for Quaternary emergence on Gotland (Jeppsson, 1982), this is not unreasonable. It is not possible, however, to isolate unequivocal evidence for this explanation from the concentration and isotopic composition variations.

Age Data and Interpretation

The Pb/Pb date of 326 ± 11 Ma for Slite Formation unit g stromatoporoids, residues and corals (*rigidus* & *lundgreni* biozones) (**Figure 5.4.4**) is significantly younger than the 423 Ma age for the Middle Wenlock proposed by McKerrow (pers. comm. 1992). Rather it corresponds to some Middle Namurian age (Carboniferous), although no such event has been hitherto documented on the island of Gotland. As no significant karstification of appropriate age is noted from the Gotland succession, the isotopic resetting must have been the result of some sub-surface, deep weathering event. The U-Pb date of 366 ± 88 Ma (**Figure 5.4.5**) from all available samples is less precise than the Pb/Pb date but still overlaps and is considered to reflect increased data scatter due to recent U loss during the Quaternary.

It is interesting to consider the geographical position of the sampled localities from the Slite Formation unit g, which are illustrated in **Figure 5.1.1**. Stora Banne 3, Spillings 2, Lännaberget 2 and Bogeklint 2 all lie along a distinct north-south trend that also includes the deep coastal embayment of Kappelshamnsviken on the north coast of the island, Vägumeviken further south and the east coast of the island as far as the promontory of Katthammarsvik, some 30 km to the south. In addition, the Slite Formation localities show a degree of stratigraphic variation, with some locating in the *lundgreni* biozone and others in the *rigidus* biozone, yet all lie along the same, extremely well defined Carboniferous Pb/Pb isochron. Furthermore, Klinteberg Formation rocks from the west of the island, which are c.70 m higher in the largely undisturbed stratigraphic section, yield what may be considered chron-ostratigraphically accurate ages. Not only does the isotopic resetting event affecting Slite Formation rocks appear to have been constrained to a distinct geographical

area, but also it appears to have been stratigraphically constrained, reinforcing the suggestion of sub-surface recrystallisation.

Flodén (1980) described the results of seismic soundings carried out in the Gotland area between 1964 and 1973, using velocity determinations from six key locations around the island. From his results he was able to demarcate a Jotnian fault-bounded basin to the north of the island, containing a north-south sub-Cambrian fault that aligns with Kappelshamnsviken and the north-south geographical trend previously described (see **Figure 5.5.7**). The Lärbro valley, located between the coastal inlets of Kappelshamnsviken and Vägumeviken is known to be a zone of structural disturbance (Jeppsson, pers. comm. 1992) and this suggests that effects of the deep faulting may have extended to near the surface outcrop, providing possible conduits for fluid flow.

Figure 5.5.7: Sub-Cambrian structural map and regional cross section across the Gotland region, after Flodén (1980)

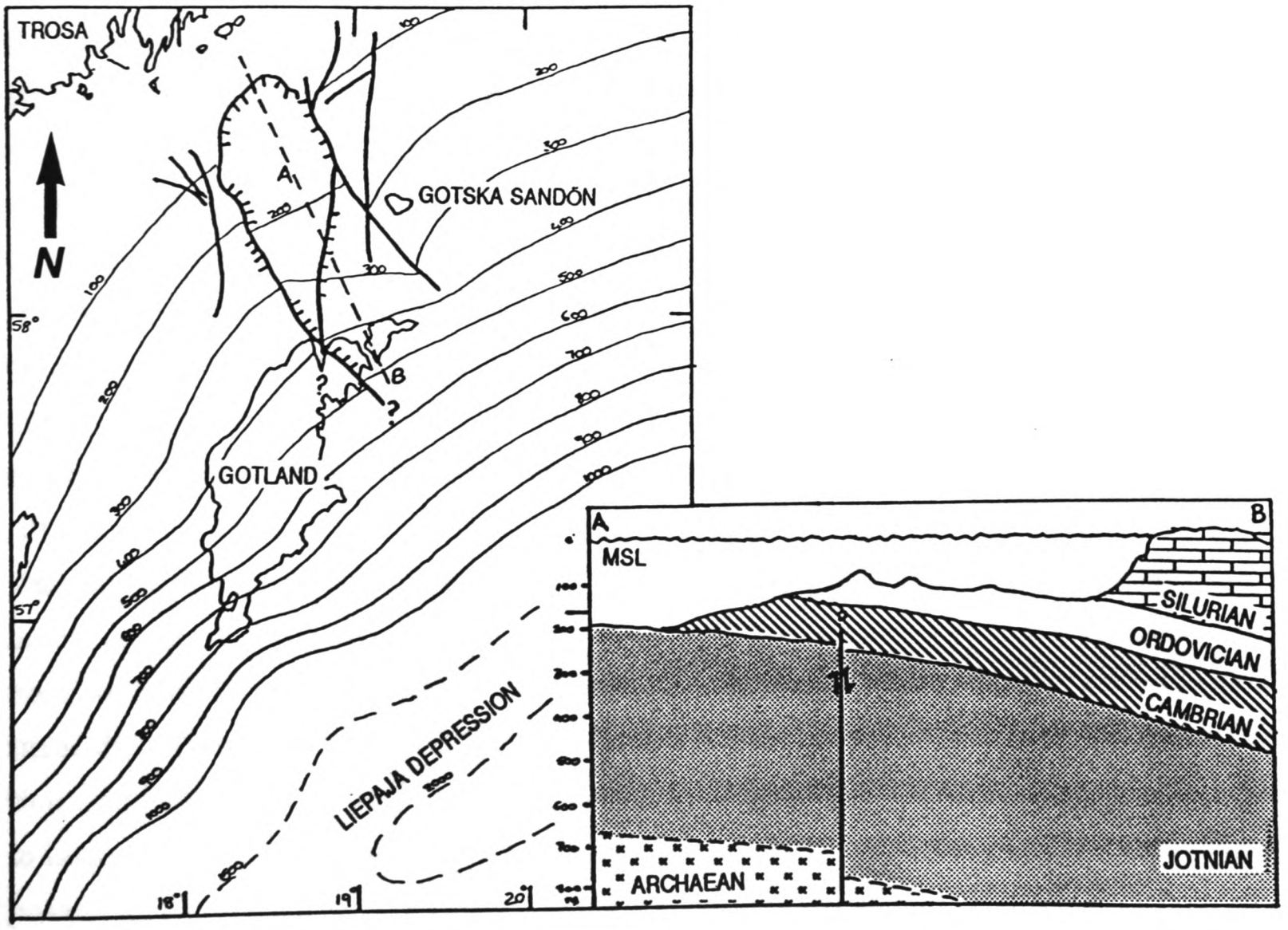

If one considers the broad petrographic variation across the island, it is possible to explain why Klinteberg Formation carbonates were unaffected by this Carboniferous event. Broadly speaking, the island is divided into five main petrographic zones (see **Figure 5.1.1**) with limestones dominating the northern (Högklint, Tofta and Lower to Middle Slite Formations), central (Halla, Klinteberg and Hemse Formations) and southern (Hamra and Sundre Formations) sections and shale dominated areas lying between (Upper Slite and Mulde Formations in the north and Hemse and Eke Formations in the south). Thus, the Slite and Klinteberg Formations, although just c.70 m apart in the stratigraphic section, are also separated by a zone of impermeable shales and mudstones which would have stratigraphically restricted fluid flow and prevented late recrystallisation of the Klinteberg Formation.

During the Carboniferous Gotland, along with the rest of Baltica, lay just north of the equator in a hot, wet climate and proceeded to move slowly north throughout the period (Scotese & McKerrow, 1990) as the western margin of Pangea began to assemble. However, little evidence exists in the geological record concerning the late Palaeozoic history of Sweden other than the occurrence of Late Carboniferous/early Permian northwest-southeast trending dykes in Skåne (southern tip of Sweden), sills in Västergötland (northeast of Gothenburg) and rift-related volcanism around Oslo in Norway. Red weathering associated with these intrusions was documented by Jeppsson & Laufeld (1986) and similar red weathering has been shown to affect rocks down to the sub-Cambrian peneplain, presumably by means of fluid percolation through faulted and jointed bedrock. The authors also commented on the frequent proximity of red weathered localities to major fault and graben systems which suggests that these structures may have acted as palaeoconduits. Although Gotland is some 300 km east of this volcanic activity, it is possible that similar Carboniferous fluid flow, directed along basement faults (such as the major north-south fault documented within the Jotnian Basin) and permeating to the near surface through carbonate-dominated lithologies along a lineament of structural disturbance (the Lärbro Valley), could have effected sub-surface recrystallisation and isotopic resetting. Unfortunately, so little is known about the post-Silurian to late glacial history of the Gotland region that further substantiation is not currently possible.

Hence, the c.330 Ma date is interpreted in geological terms as the age of late carbonate diagenetic recrystallisation during the early Late Carboniferous. Recrystallisation was the result of oxidising, ?meteorically influenced aquifers of uncertain

provenance, flowing along deep, sub-surface, north-south oriented faults, possibly during an episode of fault remobilisation connected with Hercynian/Variscan deformation. It would be interesting to investigate the geographical and stratigraphical extent of this Late Palaeozoic recrystallisation by more detailed sampling of localities in the north of the island.

5.5.3: *GENERAL DISCUSSION*

It is instructive to consider the *in situ* μ values (μ_2 values) for these carbonates and to compare them with μ values for marine and terrestrial river waters calculated from data in Chester (1990). Assuming a model μ_1 value of 8.2 (the figure from Pb/Pb regressions) and an age of 430 Ma for the Klinteberg Formation, the present day range in Pb isotopic compositions correspond to μ_2 values of 22 to 25 for the recrystallised stromatoporoids 16078914 and 16078916; 118 to 168 for LS stromatoporoids and 534 to 938 for samples of stromatoporoid 16078913. Assuming the same model μ_1 value and a 325 Ma late diagenetic age for the Slite Formation carbonates, μ_2 values are between 23 and 139 for the heliolitid corals analysed, 72 and 1214 for the stromatoporoids (614 and 1214 for 2307896) and 145 and 302 for the residues. Open marine U concentrations of 3.2 ppb and Pb concentrations of 0.003 ppb, detailed in Chester (1990), correspond to a U/Pb ratio of c.1100 and a μ value of c.80,000. U and Pb concentrations in river water are 0.24 ppb and 0.1 ppb respectively, corresponding to a U/Pb ratio of 2.4 and a much smaller μ value of around 170.

Stromatoporoids were evidently highly suitable organisms for generating the requisite elemental and isotopic variation to be good U-Pb geochronometers - that is high, variable U/Pb ratios, homogeneous initial Pb isotopic compositions and subsequent closed system conditions. In respect of their ability to sample the marine elemental signature variably, stromatoporoids appear to have been more successful than either corals, crinoids, whole rock carbonates or stromatolites, for which Moorbath et al. (1987) quoted *in situ* μ_2 values of between 20 and 113. Even so, stromatoporoid μ_2 values are still approximately two orders of magnitude lower than those that would result from *pro rata* sampling of marine elemental U and Pb signatures.

Knowledge of the mechanism of U and Pb fixation in carbonates is unfortunately limited. While Pb is known to directly substitute in the carbonate structure (particularly in primary orthorhombic carbonates, viz. cerussite) due to similarity of Pb^{2+} and Ca^{2+} ionic radii (Deer et al., 1977), U has no such natural site and is

more likely to be stabilised as organo-metallic complexes (Disnar & Trichet, 1983) due to the fixation of U under micro-reducing conditions associated with decaying organic material. Since organic material is not uniformly distributed through the stromatoporoid, this physical variation may have provided a suitable mechanism for the generation of variable U/Pb ratios. Even during diagenetic recrystallisation, when U could be lost or gained and μ values significantly altered, resilient organo-metallic complexes could still have promoted the development of variable U/Pb ratios. This suggestion is expanded in the general model proposed in **Chapter 6**.

5.6: CONCLUSIONS

Pb and U isotopic investigation of Silurian carbonates from the Swedish island of Gotland has demonstrated clearly that Pb/Pb and, in certain cases, U-Pb systematics may be applied successfully to the dating of Phanerozoic sediments, in addition to Precambrian stromatolites and marbles. Analyses of four carbonate stromatoporoids from the lower Middle Klinteberg Formation (*ludensis* graptolite biozone, Wenlock-Ludlow boundary) give a Pb/Pb date of 432 ± 15 Ma (**Figure 5.4.1**) and selected analyses a ^{238}U-^{206}Pb date of 435 ± 9 Ma (**Figure 5.4.2**). Both dates are in good agreement with the inferred Wenlock-Ludlow boundary age of 420 Ma (McKerrow, pers. comm. 1992) and are interpreted as depositional/early diagenetic ages. Other U-Pb data regressions have no age significance owing to recent isotopic disturbance (U loss) resulting from Quaternary weathering on the island. Combination of results from the four separate stromatoporoids expands the overall Pb isotopic range and thereby enhances the precision of the regressed Pb/Pb date. This sampling strategy is recommended where single organism isotopic ranges are limited or only small quantities of sample materials are available.

Analyses of three stromatoporoids and two heliolitid corals, collected from four localities within the diachronous Slite Formation unit g (*rigidus* and *lundgreni* graptolite biozones, Middle Wenlock), give a Pb/Pb date of 326 ± 11 Ma (**Figure 5.4.4**). Less precise U-Pb dates are consistent with this value, but indicate the effects of Quaternary isotopic disturbance (**Figure 5.4.5** and **Figure 5.4.6**). The 326 Ma date is approximately 100 Ma younger than the inferred stratigraphic age (423 Ma) and is interpreted as the age of late diagenetic recrystallisation during the late Carboniferous. Stratigraphically higher carbonates in the Klinteberg Formation remained unaffected by this event because diagenetic waters were probably channelled along north-south faults at depth, rising through a zone of structural distur-

bance in line with the Lärbro Valley but becoming stratigraphically constrained by the largely impermeable, shale-dominated rocks of the Upper Slite and Mulde Formations. This is the first reported chronometric control on the post-Silurian/pre-glacial geological history of the Gotland area.

Further application of Pb/Pb and U-Pb dating techniques to appropriate sample materials (stromatoporoids, corals, ?sponges) holds exciting potential for supplementing the pool of reliable age data from which the Phanerozoic time scale is constructed, particularly in the Lower Palaeozoic. In addition, it is possible to both detect and chronometrically constrain episodes of late diagenetic carbonate recrystallisation using these methods. Stromatoporoids are particularly well suited to Pb/Pb and ?U-Pb studies by virtue of their potential for large, variable *in situ* μ values. This phenomenon may relate to variable primary organic distribution within the organism, creating micro-reducing environments of differing redox potential, in which U becomes fixed to varying degrees as insoluble organo-metallic complexes.

Systematic variations in both isotopic composition (excluding thorogenic Pb, since analysed stromatoporoids had constant Th/Pb ratios, probably equal to zero) and elemental concentration were demonstrated for the two stromatoporoid samples which split along successive latilaminae (16078913Z, **Figure 5.5.3** and 2307896Q, **Figure 5.5.6**). Such variations may represent primary biogenic signals, the effects of diagenetic redistribution, or perhaps a combination of both.

Chapter 6:

GEOCHEMICAL MODEL

6.1: INTRODUCTION

In **Chapters 2, 3, 4** and **5**, the Pb/Pb method of radiometric dating has been successfully applied to the direct age determination of a variety of biogenic and metamorphic carbonate materials, ranging in age from Late Archaean to Lower Palaeozoic. Over the last five years a limited number of Pb/Pb and U-Pb dates have also been published for stromatolitic carbonates, corals, calcite cements, marbles and carbonatites (see section **1.3.3**). While it is evident that many carbonates are highly suited to geochronological study using U-Pb decay schemes, few have attempted to explain why this should be the case.

It is necessary to consider potential sources of U and Pb in carbonates, the mechanisms of elemental fixation and the subsequent susceptibility to post-depositional mobilisation before we can begin to understand why carbonates frequently develop high, variable U/Pb ratios and often maintain closed system condi-

tions for substantial periods of geological time. A considerable amount of work has been published on the geochemical behaviour of U under a variety of geological conditions because of the implications for disequilibrium dating, ore formation and nuclear waste management (for example; Degens et al., 1977; Langmuir, 1978; Broecker & Peng, 1982; Thomson et al., 1987; Wallace et al., 1988; Colley et al., 1989; Klinkhammer & Palmer, 1991). Similarly, many authors have studied the behaviour of Pb (and ^{210}Pb in particular) in the modern environment to monitor the effects of pollution from the smelting of metals and the use of leaded petrol (for example; Schaule & Patterson, 1981; Gobeil & Silverberg, 1989; Hamelin et al., 1990; Urban et al., 1990; Erel et al., 1991). **Chapter 6** attempts to apply this geochemical knowledge to develop a broad model explaining the suitability of carbonates for direct Pb/Pb and U-Pb radiometric dating.

6.2: GEOCHEMISTRY OF URANIUM

6.2.1: *URANIUM IN MARINE AND RIVER WATERS*

The behaviour of U in solution is distinctive in that unlike the majority of redox sensitive trace elements, it converts to a more insoluble form on reduction and this allows its geochemical behaviour to be relatively easily predicted. Natural U in river waters is sourced from the weathering of rocks and sediments at the earth's surface. It is transported into the marine realm as particulate matter, dissolved ionic species and/or adsorbed onto colloids.

River water has an average U concentration of 0.24 μgl^{-1} in solution and 3 ppm in the form of particulate matter, whereas marine waters average 3.2 μgl^{-1} U and marine clays have a U concentration of 2 ppm (Martin & Whitfield, 1983) (see **Table 6a**). These values compare with average figures of 3 ppm and 2 ppm for continental crust and soil (Martin & Whitfield, 1983). Lahoud et al. (1966) showed that marine carbonates had higher U concentrations than brackish carbonates, which were in turn higher than freshwater carbonates (averages of 1.06, 0.53 and 0.025 ppm respectively), in general agreement with the concentration data for river and ocean waters. In the oceanic reservoir (>pH 6), U exists mainly as soluble U^{6+} in the form of the uranyl carbonate complexes $UO_2(CO_3)_2^{2-}$, $UO_2(CO_3)_3^{4-}$ and UO_2CO_3 and also as $UO_2(HPO_4)_2^{2-}$ (Langmuir, 1978). These are probably the most important species for the uptake of U by carbonates since the charge and ionic radius discrepancy between U^{6+} and Ca^{2+} (0.8Å and 0.99Å, respectively) means that direct lattice site

substitution of hexavalent U is insignificant (Möller et al., 1976).

Table 6a: Concentrations of U, Th and Pb in marine and river waters, after Martin & Whitfield (1983)

	OCEANS		RIVERS	
	dissolved (ppb)	particulate (ppm)	dissolved (ppb)	particulate (ppm)
U	3.2	2	0.24	3
Th	0.01	10	0.1	14
Pb	0.003	200	0.1	100

The oceanic residence time of an element (ORT) is the average time an element resides in the marine reservoir prior to its removal by the sediment sink and is an indication of the reactivity of an element in the ocean system. The ORT may be defined as;

$$ORT_{element} = A/(dA/dt)$$

where A is the total amount of element in suspension/solution in sea water and dA/dt is the rate of element removal/introduction from/into the oceans under steady state conditions (Chester, 1990; Wangersky, 1986). Taylor & McLennan (1985) estimated ORT_U as 10^6 yr, Brewer (1975) as 3×10^6 yr and Martin & Whitfield (1983) as 4.9×10^5 yr. These values are two to three orders of magnitude greater than the average mixing time of the oceanic water mass (1600 yr; Chester, 1990) and so it is evident that U rapidly becomes homogenised within the oceans and the character of the lithological catchment area will not cause local perturbations in the U concentration of open marine waters (conservative behaviour of Bruland, 1980).

6.2.2: *URANIUM IN CARBONATES*

In coastal waters, trace elements may be removed either into sediments, recycled or transported into the deep oceans. As far as the dating of carbonates is concerned, we are interested in the potential mechanisms of U fixation in sediments and these all involve the reduction and desolubilisation of uranyl complexes. Lahner (1939) and Evans & Goodman (1941) were the first to determine U concentrations in

carbonates and Bell (1963) produced the first detailed study assessing potential origins of carbonate U. Theoretically, the removal of U from marine waters could be brought about by a combination of processes operating at deposition or during diagenesis, while subsequent remobilisation has the potential to modify primary concentrations.

Uranium Incorporated at Deposition

The incorporation of U into sediments during deposition may arise through some combination of;

- saturation precipitation;
- incorporation into mineral crystal lattice sites;
- incorporation into crystal defect sites;
- organic complexing and
- biospheric fixation.

The saturation precipitation of uraniferous minerals is unlikely to be important in marine waters because of low U concentrations and the oxidising nature of the majority of ocean environments. Even in anoxic basins the direct precipitation of such minerals has not been observed (Anderson, 1982; Todd et al., 1988) and no primary U minerals are known to be syngenetically deposited with carbonates (Bell, 1963).

The incorporation of trace amounts of marine U, as U^{3+}, into carbonate mineral crystal lattice sites is theoretically possible because the radius discrepancy between U^{3+} and Ca^{2+} is less than 4% and the overall valency could be stabilised by the incorporation of, for example, Na^{+} (Möller et al., 1976; Amiel et al., 1973). This process could only operate in the presence of an organic reducing agent. U^{6+} and U^{5+} exist exclusively as complexes and are not found in lattice sites. U^{4+} has a valency too large to be accommodated in carbonate lattices, despite the fact that its ionic radius (0.97Å) is very similar to that for Ca^{2+} (0.99Å), and consequently it tends to form distinct mineral phases such as uraninite (UO_2-U_3O_7). Klinkhammer & Palmer (1991) suggested that uraninite was the ultimate sink for the majority of marine U. Because of their open cell structure, orthorhombic carbonates, such as aragonite, are capable of accommodating higher concentrations of lattice-bound U than trigonal carbonates (HMC, LMC, dolomite) and U concentrations for Recent aragonitic carbonate ooids and scleractinian corals (1.5-3.5 ppm) are indeed found to be higher than HMC coralline algae, bryozoans, echinoderms and hydrozoans

(0.2-0.5 ppm) and LMC pelecypods and foraminifera (0.3-0.6 ppm) (Chung & Swart, 1990; see **Figure 6.2.1**), although it is unlikely that lattice-bound sites are entirely responsible for these U concentrations (see organic complexing below). Distribution coefficients for U into aragonite and calcite have been calculated relative to both Ca^{2+} and $UO_2(CO_3)_2^{2-}$ by Chung & Swart (1990) and Swart & Hubbard (1982). Values for aragonite of $D_{Ca^{2+}} = 0.6\text{-}1$ and $D_{UO_2(CO_3)_2^{2-}} = 0.001$, compared with $D_{Ca^{2+}} = 0.0275$ and $D_{UO_2(CO_3)_2^{2-}} = 0.00005$ for calcite, indicate that both minerals should be depleted in U with respect to marine waters (3.2 ppb) and so one must consider other possible mechanisms of U fixation and concentration.

Figure 6.2.1: Published ranges of U concentration for various modern carbonates, compiled by Chung (1988)

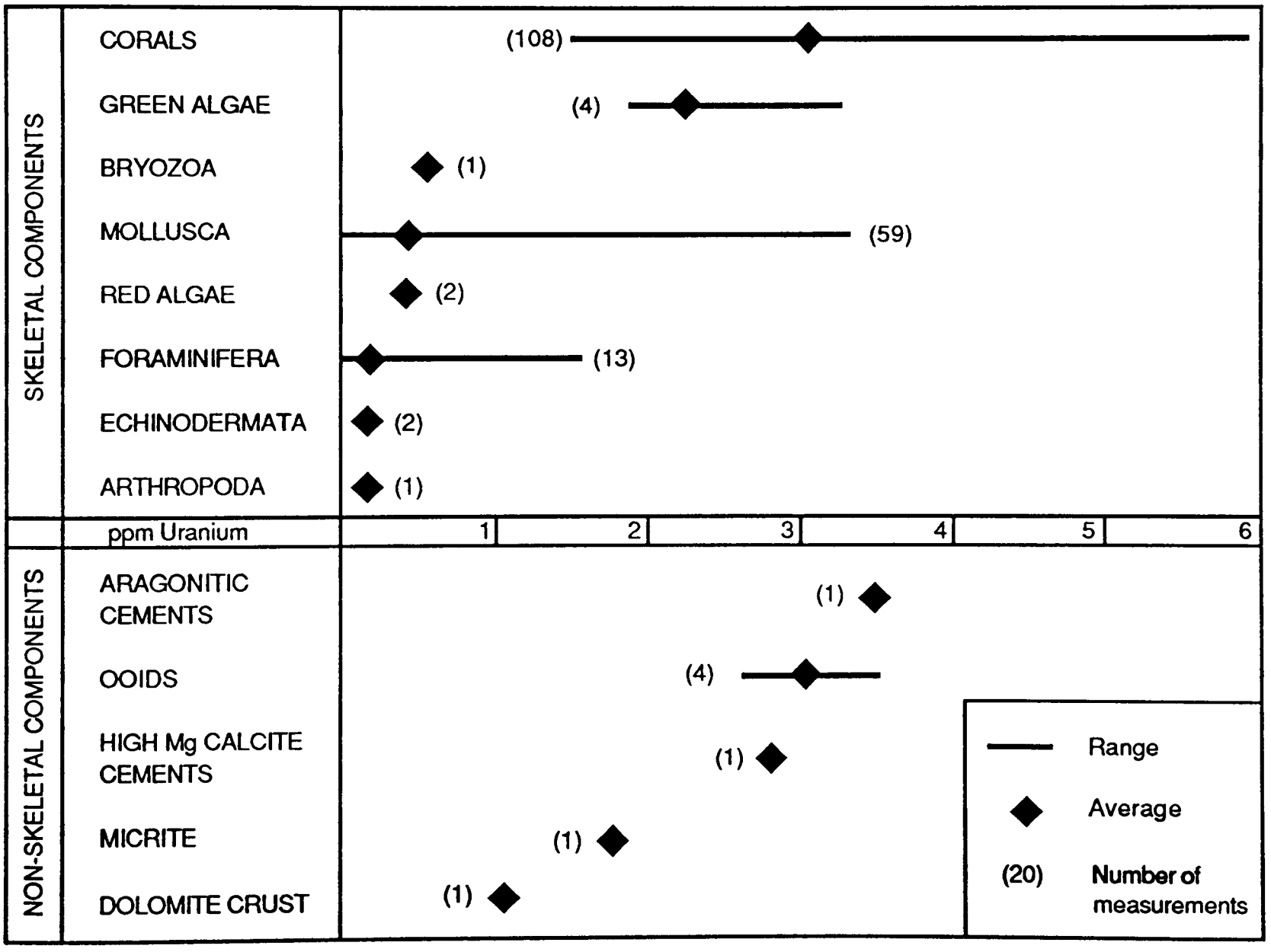

From fission track work on corals, Amiel et al. (1973) inferred that the adsorption of U onto carbonate mineral surfaces and its incorporation into crystal defect sites was of minor importance compared to the association of U with organic phases. Hsi & Langmuir (1985) noted that adsorption onto Fe-Mn oxyhydroxides could be important in effecting the removal of U from the oceans but since uranyl carbonate complexing hinders this adsorption, the process is unlikely to be important

in the carbonate saturated waters from which limestones are deposited. Primary and secondary phosphate within marine carbonate occurs principally as carbonate fluorapatite or collophane and is also capable of fixing U from seawater. Insular phosphorites tend to adsorb U^{6+} to apatite surfaces under oxidising conditions, whereas open marine apatite forms under suboxic conditions and contains dominantly U^{4+} (Roe & Burnett, 1985). In addition to surface adsorption, the open hexagonal cell structure of apatite may allow a proportion of U to be fixed in lattice-bound sites. Because marine phosphate is resilient to the effects of leaching by alkaline carbonate solutions (Roe & Burnett, 1985), an abundance of reworked detrital phosphate (for example in bone beds) may elevate the U concentration of sediments.

Dissolved organic materials are able to adsorb, complex and retain metal ions in a stable configuration and as such, have the potential to preconcentrate U in the oceans prior to deposition in the sedimentary pile. Incorporation of organic complexes within carbonates can thus supplement lattice-bound concentrations. Disnar (1981) demonstrated that Recent algal materials were capable of fixing UO_2^{2+} directly from sea water through the formation of initial oxycationic forms and subsequent robust organometallic linkages. Moreover, the author was able to show that UO_2^{2+} complexes were more stable than those formed by other divalent cations (Pb^{2+}, Mn^{2+}, Cu^{2+}, Zn^{2+}, Ni^{2+}, Co^{2+}) and concluded that this mechanism could account for the concentrations of U observed in many Precambrian algal deposits (e.g. stromatolites).

Uranium Incorporated During Early Diagenesis

U may become incorporated into sediments during early diagenesis through;

- the intermediate formation of U^{5+} complexes from uranyl complexes in suboxic, reducing pore waters and
- ultimate uraninite formation, either due to direct reduction by organic matter, indirect reduction by sulphate-reducing bacteria or continued reduction of U^{5+} complexes.

The site of early marine diagenesis, the sediment-interstitial water complex, is a zone of intense chemical, physical and biological reactions. Many of the reactions are redox related and therefore the distribution of organic carbon is vital in determining many elemental concentrations. The frequently observed association of U with sedimentary carbonaceous matter (for example coals, bitumens and kerogens) is evidence of the important role that organic materials play in the concentration of

this metal (Breger, 1974). Although most marine waters are oxidising, the sediment-water interface (Emerson & Dymond, 1984) may rapidly become suboxic to anoxic as organic matter decomposes, permitting the reduction of soluble hexavalent uranyl complexes to U^{5+}, U^{3+} and insoluble U^{4+} forms.

Klinkhammer & Palmer (1991) proposed that the principal cause of U fixation from the oceans was early diagenetic diffusion across the sediment-water interface boundary layer. As organic materials in the sediment are oxidised and cause *in situ* reduction of U^{6+} to insoluble U^{4+} in the form of uraninite (possibly via some intermediate U^{5+} complex - Kniewald & Branica, 1988), a concentration gradient becomes established in the boundary layer and marine uranyl complexes are progressively drawn into the suboxic pore waters until they themselves become reduced and fixed. The release of complexed uranyl ions from oxidised organic matter within the sediment may supplement this flux and elevate sediment U concentrations. Suitably suboxic substrates can develop less than 1 m below the sediment-water interface of oxidising oceans and have been documented by DeDeckker et al. (1988) beneath algal mats in marginal marine environments.

A correlation between U concentration and total organic concentration (TOC) has been found from studies of organic rich marine and lacustrine sediments by Klinkhammer & Palmer (1991), Andersen et al. (1989), Çagatay et al. (1990), Mo et al. (1973), Kolodny & Kaplan (1973), Baturin & Kochenov (1973), Baturin (1969), Baturin et al. (1971) and Sackett et al. (1973), although Swart (1988) did not find that this relationship held for dolomites. Despite the fact that shallow marine carbonates may not be significantly enriched in organic materials, the same mechanisms of U fixation should still apply and in this way non-lattice-bound U can become incorporated into the carbonate sedimentary record. Indeed, Swart & Hubbard (1982) found that the porous skeletons of recently deceased scleractinian corals had heterogeneous U concentrations of 5-6 ppm, higher than those for both living organisms, which average 1.5-3 ppm (and possess a homogeneous distribution), and seawater. This clear indication of early diagenetic, post-mortem U uptake was inferred to have occurred within days of death, at shallow stratal depths and the authors noted that endolithic sponges appeared particularly suited to increasing U concentrations in bioeroded specimens. The porous nature would have permitted suboxic fluids to pervade the corallite skeletons, allowing decaying organic material to fix U from solution by the mechanisms proposed above. The fact that living corals show homogeneous U concentrations, while dead corals show heterogeneity implies that U incorporation during growth may be dominated by lattice-bound and adsorptive

sites, whereas after death, redox related organic fixation becomes the dominant process and conspires to obscure depositional distributions.

Using fission track analyses, heterogeneity of U concentration was also observed for intra-skeletal portions of corals and molluscs by Schroeder et al. (1970) and Lahoud et al. (1966), with concentrations generally at the ppm level (1.9-6.8 ppm). Although data on primary U distribution in biogenic carbonates are still sparse, in light of the data from Swart & Hubbard (1982) it is possible that this heterogeneity reflects the distribution of organic material within the organisms. U profiles showed that the highest concentrations existed along external surfaces and decreased towards the innermost carbonate, reinforcing the idea of a diagenetic concentration gradient beneath the sediment surface.

The variables that are likely to determine the U content of carbonates and other sediments may be therefore summarised as;

- the degree of preconcentration of U from seawater by organic complexes;
- the distribution and concentration of organic material in the sediment;
- the extent of lattice-bound U^{3+}
- the sedimentation rate;
- the nature of any late diagenetic alteration (see below).

Uranium Incorporated During Late Diagenesis

During late diagenesis U contents within sediments may be modified by;

- introduction (or removal) via oxidising meteoric waters;

The effects of diagenesis on U distributions in carbonates have been studied by Lahoud et al. (1966), Haglund et al. (1969), Gvirtzmann et al. (1973), Chung et al. (1985), Chung & Swart (1986) and Swart (1988). The undersaturation of the majority of fluid media with respect to U and the solubility of hexavalent U in oxidising waters mean that meteoric aquifers are able to remobilise and redistribute primary and early diagenetic U in sediments. Such fluids may also introduce external U to the carbonate system. Redox reactions and the nature of the source rocks are the dominant control on elemental mobility. U-Pb isotopic systematics may be either disturbed or completely reset as a result and so careful interpretation of U-Pb and Pb/Pb isotopic data is required. If diagenesis took place relatively soon after sedimentation, that is within the age resolution of the method, it may not be possible to distinguish diagenetic ages from depositional ones.

Uranium in Metamorphic and Igneous Carbonates

A continuum of conditions exists between the diagenetic alteration of sedimentary carbonates and the formation of metamorphic carbonates (marbles) at elevated temperatures and pressures. Variation of redox conditions during metamorphism, as a function of pO_2, will control the redistribution of sedimentary/diagenetic U, in addition to any U supplied by metamorphic fluids. At the lower end of the metamorphic scale (burial metamorphism, prehnite-pumpellyite facies) there may be an inheritance of sedimentary characteristics and U distribution may continue to be organically controlled but at elevated metamorphic grade, as organic matter and U-bearing clastic phases are broken down, reconstitution of the mineral assemblage takes place and U will tend to relocate in accessory metamorphic mineral lattice sites (such as zircon, monazite and apatite). Under closed system conditions the whole rock U concentration of the marble will be a function of the U content of the sedimentary carbonate plus any U associated with detrital phases. Heterogeneous U concentrations within marbles are likely to be a function of mineralogy, the highest values being associated with accessory silicate/phosphate phases and any resilient organic compounds. Any U associated with carbonate minerals must occur either as lattice-bound U^{3+}, be located along carbonate grain boundaries/surface defect sites or be complexed with any remaining organic materials. Since marbles in high grade metamorphic terrains have complex metamorphic histories, it is realistic to expect that original sedimentary characteristics will have been lost.

Igneous carbonates (carbonatites) pass through a fluid phase prior to their intrusion and so U concentration will be a function of the nature of the parental melt and the extent of any crustal contamination. The U distribution, however, will be controlled by the mineralogy. For example, Andersen & Taylor (1988) found that the most radiogenic Pb isotopic compositions from the Fen carbonatite in Norway were obtained from apatite rich samples and suggested that apatite fractionation may have resulted in U-rich, Pb-poor cumulates, ideal for geochronological study.

6.3: GEOCHEMISTRY OF LEAD

There have been a number of recent advances in our understanding of the aqueous geochemistry of Pb, owing to the emphasis placed on monitoring levels of pollution and contamination (Settle & Patterson, 1980; Paulson et al., 1988; Hamelin

et al., 1990; Erel et al., 1991). Much of the process-based information drawn from such studies can be used to interpret results from geochronological isotopic investigations.

6.3.1: *LEAD IN MARINE AND RIVER WATERS*

Weathering of rocks at the earth's surface releases Pb which is transported via rivers towards the oceans as particulate matter, dissolved species and/or adsorbed onto colloids. Additional Pb is input from aeolian sources and as direct hydrothermal emissions within the ocean basins. River water has an average Pb concentration of 0.1 μgl^{-1} in solution and 100 ppm in the form of particulate matter, while marine waters average 0.003 μgl^{-1} Pb in solution and up to 200 ppm as particulate marine clays (Martin & Whitfield, 1983) (see **Table 6a**).

In sea water under oxidising conditions, the main species of Pb ($PbCO_3$, $Pb(CO_3)^{2-}$ and $PbCl^+$) are concentrated in the surface microlayer and fall off with depth because Pb is rapidly scavenged from the oceans. Scavenging was defined by Goldberg (1954) as the adsorptive removal of trace element metals onto particles that sink through the water column. Unlike U, Pb is a reactive trace element in ocean waters, particularly at boundary layers (e.g. river/ocean, air/sea, sediment/ocean) (Schaule & Patterson, 1981). The Pb concentration of marine waters also decreases from the central gyres to the estuarine mixing zones (Schaule & Patterson, 1981) and this reflects the fact that the majority of dissolved riverine Pb is removed by flocculation and colloid formation as river and marine waters mix in the estuarine environment.

Taylor & McLennan (1985) estimated the oceanic residence time of Pb (ORT_{Pb}) as 50 yr, Brewer (1975) as 400 yr, Martin & Whitfield (1983) as 1.1×10^3 yr and Kumar & Reddy (1985) as 10-1000 yr. Because estimates vary considerably, Wangersky (1986) proposed that ionic/complexed Pb and scavenged Pb had separate values of ORT_{Pb}. Estimates of the scavenged ORT_{Pb} generally fall in the range 47-54 yr (Balistrieri et al., 1981; Whitfield & Turner, 1987), although Jickells et al. (1984) proposed that the figure could be as low as 4 yr. The ORT_{Pb} for ionic/complexed species is an order of magnitude greater (Brewer, 1975). It is clear that both residence times are short with respect to the mean mixing time for the oceanic water mass (1600 yr - Chester, 1990) and hence the concentration and composition of Pb is heterogeneous within the oceans and largely controlled locally by source (rivers, hydrothermal and aeolian input). Pb in the oceans exhibits non-conservative behaviour (Bruland, 1980).

6.3.2: *LEAD IN CARBONATES*

Although much Pb is removed from riverine waters in estuarine environments, an amount passes into the marine realm where, like U, it is either removed into the sedimentary pile, recycled or transported into the central oceans. This study is concerned with the fixation of Pb in carbonate sediments and the subsequent susceptibility to remobilisation during diagenesis. Unfortunately, Pb does not possess the same redox-sensitive solubility characteristics as U and is difficult to monitor spatially using modern analytical techniques, so the determination of mechanisms of fixation is more problematic, particularly considering the concentrations found in carbonate rocks (characteristically much less than 10 ppm - Wedepohl, 1960; Wampler & Kulp, 1962; this study).

Lead Incorporated at Deposition

Potential mechanisms of Pb fixation operative in sediments at the time of deposition are;

- saturation precipitation;
- incorporation into carbonate lattice or defect sites;
- fixation by organic complexes;
- biogenic fixation as a poison;
- inorganic fixation by particulate scavenging.

Since Pb is undersaturated in the vast majority of marine waters under normal conditions of Eh and pH, the direct precipitation of authigenic Pb minerals from seawater is extremely uncommon. At the trace element level, Pb^{2+} may reside in the trigonal calcite/dolomite structure through substitution for Ca^{2+}, but the discrepancy in ionic radii (> 0.2Å) places strain on the crystal lattice and limits the potential for concentration. Pb^{2+} more commonly substitutes for Ca^{2+} in the less symmetrical orthorhombic structure of aragonite and indeed, end member $PbCO_3$ is stable as the mineral cerussite, but the low concentration of Pb in marine waters again limits the potential for concentration. Both aragonite and cerussite are metastable and ultimately convert to LMC in ancient carbonates. Lattice defect sites are unlikely to cause significant enhancement of carbonate Pb concentration in view of their limited availability and the low dissolved Pb concentration of seawater (0.003 ppb). Concentrations Pb in carbonates are orders of magnitude higher (up to 10 ppm; Wedepohl, 1960) and suggest that other mechanisms of fixation and

concentration are important.

The fixation of Pb as non-labile species by dissolved organic complexes at the sediment-seawater interface and within suboxic pore waters has been reported by a number of authors including Florence & Batley (1976), Duinker & Kramer (1977), Heinrichs & Mayer (1977), Tyler (1981) and Driscoll et al. (1988). Such processes limit the amount of Pb available for particulate scavenging and may serve to pre-concentrate Pb in carbonates in much the same way as is envisaged for U. The extent to which this process operates, however, is unclear. Pb may also be precon-centrated as a cumulative poison within the tissue of living organisms (Settle & Patterson, 1980).

In probability, the principal mechanism by which dissolved Pb is removed from the marine reservoir is through the formation of reactive labile species by fixation onto the surface of inorganic particulates (Krauskopf, 1956). Clays and oxyhydroxides of Fe, Mn, Al and Si are all known to rapidly and efficiently scavenge Pb from the oceans and fix it within the sedimentary pile (Lion et al., 1982; Balistrieri & Murray, 1982; 1983; 1986; Leckie et al., 1984; Trefry et al., 1985).

There is a general lack of reliable Pb concentration data for marine carbonates but what data exist, imply figures of less than 10 ppm are typical. As a selected cross section, Wedepohl (1960) reported an average figure of 9 ppm for deep sea carbonates; Jahn et al. (1990) a maximum of 1.78 ppm for Archaean stromatolites from South Africa; Moorbath et al. (1987) a maximum of 16.7 ppm for Archaean stromatolites from Zimbabwe; Smith et al. (1991) up to 0.5 ppm for calcite cements in Devonian carbonates from Ontario; Cuvellier (1989) listed concentrations of up to 2.5 ppm for Sinian stromatolites from China; and this study has determined maxi-mum Pb concentrations of 6 ppm for Proterozoic stromatolites from Western Aus-tralia and 0.6 ppm for Silurian stromatoporoids from Gotland. Inorganic particu-lates have much higher Pb concentrations than carbonates (100-200 ppm for fine grained marine clastics clays - Martin & Whitfield, 1983; White et al., 1985) and so clastic rich sediments are clearly unsuitable sample materials for U-Pb and Pb/Pb dating because the potential variation in U/Pb ratios is more limited. On balance, stromatolitic carbonates have higher Pb concentrations than both stromatoporoidal carbonates and calcite cements and this may correspond to the incorporation of particulate detritus during organism growth in intertidal to subtidal environments.

Lead Mobility During Diagenesis

The mobility of Pb during sediment diagenesis is a matter of some conjecture. While Crusius and Anderson (1991) concluded that ^{210}Pb showed no indication of mobility under the anoxic conditions experienced in dewatered turbidites from the Black Sea, Urban et al. (1990) reported significant Pb losses from peat horizons in North America. It is clear that dissolved organic matter exerts a major chemical control on Pb mobility since the two readily combine to form stable non-labile complexes (Heinrichs & Mayer, 1977; Tyler, 1981; Driscoll et al., 1988) and so redox potential must ultimately control diagenetic Pb mobility. Oxidation of organic matter through contact with freshwater can cause the liberation and loss of Pb from organic rich sediments (Gobeil & Silverberg, 1989), while the complexing and fixation of Pb from external diagenetic fluids may occur under reducing conditions. With regard to U-Pb and Pb/Pb carbonate dating, while the recent loss of Pb has no effect on Pb/Pb ages, quantitative Pb loss or gain will result in scatter on U-Pb diagrams.

The principal variables that determine the Pb content of carbonates and other sediments may be summarised as;

- the degree of preconcentration of Pb from seawater by dissolved organic matter;
- the distribution and concentration of organic material in the sediment;
- the clastic content of the sediment (since particulate matter is relatively rich in Pb);
- the character of any diagenetic fluids that impinge on the sediment.

Lead in Metamorphic and Igneous Carbonates

As is the case for U, the variation of redox conditions experienced during the transition from diagenesis to metamorphism will initially control the redistribution of sedimentary/diagenetic Pb. Resilient organometallic complexes may retain a proportion of sedimentary/early diagenetic Pb at low metamorphic grades and some Pb may substitute for Ca^{2+} in newly formed carbonate minerals but as organic matter, Pb rich clastic phases and other minerals are destabilised under conditions of elevated temperature and pressure, reconstitution of the mineral assemblage inevitably takes place. Consequently, Pb isotopic compositions will start to homogenise and Pb will tend to concentrate in metamorphic silicate mineral lattice sites (for example feldspars).

With carbonatites, Pb isotopic homogenisation is effected during magmatic

formation and the Pb concentration will be controlled by the nature of the parental melt and the extent of any crustal contamination, while the Pb distribution will be a function of the mineralogical composition of the rock. The processes involved fall within the realm of igneous geochemistry and are dominated by lattice-bound elemental sites rather than by the formation of complexes, the norm for sediments.

6.4: GEOCHEMICAL MODEL

Assimilating the data outlined in sections **6.2** and **6.3**, a broad model is proposed to explain the geochemistry of U and Pb with respect to carbonates. As with all rock types, for sample materials to be suitable for U-Pb and Pb/Pb dating high, variable U/Pb ratios and homogeneous Pb isotopic compositions must be generated at isotopic closure and closed system conditions must effectively operate thereafter.

Concentration data for U and Pb (**Table 6a**) indicate that river water has a dissolved U/Pb ratio of 2.4, while seawater has a much higher value of around 1100. These figures correspond to μ values of 170 and 80000, respectively. Both riverine and oceanic fine grained clastics have high Pb concentrations (>100 ppm). Sedimentary carbonates capable of variably sampling and concentrating dissolved U and Pb from the oceans, without the incorporation of significant amounts of clastic detrital material, therefore have the potential to generate large ranges of *in situ* μ value at deposition, ideal for geochronological study using the U-Pb and Pb/Pb techniques.

Carbonate sediments are deposited with preconcentrations of U and Pb, established authigenically within the water column through the formation of complexes with particulate or dissolved organic matter and particulate Fe-Mn oxyhydroxides. U shows a greater affinity for non-labile organic complexing, while Pb is preferentially complexed by labile inorganic Fe and Mn oxyhydroxides. Low concentrations of U and Pb may be incorporated into lattice related sites. Theoretically, both U^{3+} and Pb^{2+} can substitute for Ca^{2+} in the aragonite and, to a more limited extent, the calcite lattice but U^{3+} is stable only under reducing conditions and therefore is unlikely to be a major factor as far as primary calcium carbonate deposition is concerned (principally under oxidising conditions). Lattice-related U and Pb^{2+} (lattice sites, defect sites and surface adsorption) may be significant where detrital and organic contents are low.

Organic material may fix UO_2^{2+} directly from seawater and its presence within sedimentary carbonates creates a diagenetic environment that is inevitably subject to redox control. Oxidation of organic matter during diagenesis can create suboxic conditions within the sediment and pore water that result in the reduction of uranyl carbonate complexes to more insoluble forms, causing a decrease in pore water U concentrations. Some fixation of Pb from suboxic boundary layer waters may also occur due to complexing with dissolved organic matter, thereby limiting the potential for the formation of inorganic complexes. Thus a concentration gradient becomes established within the boundary layer and uranyl complexes are drawn down from the ocean. The flux is enhanced by U released from the decomposition of organic materials within the boundary layer and a certain amount of Pb may also be remobilised in this fashion.

Initially, uranyl complexes are probably reduced to metastable U^{5+} intermediates (Kniewald & Branica, 1988) at temperatures of 45-250°C (Meunier et al., 1990), but the ultimate sink for U from the oceans is most likely to be uraninite (Klinkhammer & Palmer, 1991), forming as temperatures extend into the 120-400°C range (Meunier et al., 1990). In low temperature diagenetic environments (<120°C) adsorption and complexing are more important processes than U mineral precipitation and so preconcentration is an important factor in determining total U concentration. The exact behaviour of Pb during early diagenesis remains unclear.

The following factors are thus important in the establishment of appropriate geochemical conditions within sedimentary carbonates;

- chemical deposition from sea water with potential for high μ values;
- intimate association with organic matter and suboxic conditions;
- a low clastic content.

Relatively speaking they all favour incorporation of U and discriminate against Pb. Biogenic carbonates (corals, stromatoporoids and stromatolites) possess each of the requisite characteristics and have been dated successfully using U-Pb and Pb/Pb techniques. Calculated *in situ* μ_2 values (a maximum of 1200 for stromatoporoids), however, are still almost two orders of magnitude lower than the μ value of seawater (80000) and this reflects the relative efficiency of Pb removal from the oceans. It would be instructive to attempt to date other carbonate materials selected using the above criteria (such as Phanerozoic sponges).

The short oceanic residence time of Pb and its highly reactive nature mean

that the Pb isotopic composition of marine sediments is particularly sensitive to the character of the erosional hinterland (external control). Uranium, on the other hand, is conservative within the oceanic regime. Rapid fixation of Pb in the coastal environment may result in minor heterogeneities in initial Pb isotopic composition, contributing to data scatter on isochron diagrams. Indeed, Bruland & Franks (1983) and White et al. (1985) documented marked variations in the Pb isotopic composition of marine sediments both between and within modern oceans, although such results may be complicated by mixing of source and anthropogenic Pb signals. Nevertheless, if large ranges in U/Pb ratios exist and the Pb isotopic heterogeneity is limited (likely because of rapid scavenging and fixation), useful age data may still be obtained. Since the processes that remove Pb from seawater (complexing, adsorption) are much more efficient in coastal regions than open oceans (Ng & Patterson, 1982; Bacon et al., 1988), it would be interesting to analyse biogenic carbonates from both recent and ancient atolls and mid-oceanic islands to see if enhanced U/Pb ratios occurred in such settings.

Model μ_1 values for sedimentary carbonates must also be controlled largely by the character of Pb input from source areas and as such will reflect the broad character of sediment catchment areas. The model μ_1 values may be subject to alteration during early diagenesis, as U and Pb are fixed in suboxic environments but should still reflect the sedimentary source region. Under conditions of late diagenesis, metamorphism or igneous activity, significant alteration of model μ_1 values is likely, depending on the nature of diagenetic system (whether open or closed), operative water/rock ratios and degree of contamination.

Modification of primary elemental and isotopic signals may occur after deposition (non-closed system) and this has implications for the interpretation of geochronological data. For isotopic ages to be reset, rehomogenisation of Pb isotopic ratios must occur without accompanying homogenisation of U/Pb ratios, although these will inevitably be modified. Since U and Pb exhibit differing geochemical behaviour, events capable of recrystallising carbonates have the potential to effect such changes;

- pressure solution and neomorphism;
- dolomitisation;
- tectonic deformation;
- metamorphic recrystallisation;
- igneous activity.

Incomplete Pb isotopic homogenisation will produce excess data scatter and age

relationships may be destroyed and/or biased, whereas U/Pb (and therefore μ value) homogenisation will result in negligible data scatter (of no use for geochronology). One should also consider the possibility that U and Pb, or their intermediate decay products (such as ^{222}Rn), become decoupled during diagenesis and/or metamorphism, producing spurious age relationships. The nature of this exploratory study does not provide a sufficiently detailed database to directly address this question, but most of the results obtained are consistent with independent age constraints and may be interpreted in simple geological terms, so any quantitative loss of intermediate daughter isotopes does not appear to have a significant effect on carbonate dates. A more directed U-Pb study on a well dated stratigraphic section (for example, the Silurian on Gotland) is required to assess the significance of intermediate daughter migration in ancient carbonates.

U-Pb data for stromatoporoids from Gotland (this work) and evidence from published fission track studies suggest that U mobility in oxidising fluids is the dominant control on post-depositional elemental and isotopic signal modification (up to the onset of metamorphism). Each recrystallisation event will tend to lower *in situ* μ_2 values for carbonates. Recent (i.e. post-Quaternary) loss of U and Pb, or gain of U will have little appreciable effect on Pb/Pb systematics, however, because any Pb lost from the system has effectively the same isotopic composition as that remaining in the sample and insufficient time remains for modified U/Pb ratios to produce significantly differing Pb isotopic compositions. U-Pb geochronology, on the other hand, requires the quantitative retention of U and Pb and so any loss/gain of U or Pb will inevitably produce excess scatter of U-Pb data and will probably destroy age relationships.

Metamorphism of sedimentary carbonates effects both large scale recrystallisation and mineral reconstitution and, depending on grade, may result in the rehomogenisation of initial Pb isotopic ratios and the resetting of isotopic ages. The point at which silicate-dominated metamorphic processes supersede the complexing and adsorption processes that are typical of sedimentary and diagenetic carbonates is uncertain, but may lie within the greenschist facies. Discordance between carbonate and silicate residue analyses noted for Archaean marbles from the Sandur Schist Belt, Karnataka (see section 3.5), indicates that carbonate Pb isotopic ratios may be more readily homogenised than silicate ratios and this discrepancy can result in the generation of spurious isochrons for silicate minerals.

6.5: SIGNIFICANCE OF RESIDUE ANALYSES

The HCl-insoluble residues of a number of carbonate samples have been investigated during this work (Western Australian stromatolites GSWA 99429, 46285, 76584 and 41658; Sandur Schist Belt Archaean marbles 010X1, 010X2 and 010X3 and Indian Proterozoic stromatolites 7 DMB, 9 DMBii, 8 DMB and 14 DMBii) and in each case marked discordance exists between the Pb isotopic composition of the carbonate and that of the residue. Carbonate dissolutions were performed using 6M HCl and any residues dissolved in concentrated HF (see **Appendix B**).

DeWolf and Halliday (1991) noted from leaching experiments that reproducible Pb isotopic ratios for a series of crinoidal grainstones were only obtained using acid strengths of less than 1M HCl. They attributed the variability obtained using strengths greater than 1M HCl to partial dissolution and leaching of residue phases. If such residue phases were to have an isotopic composition that was out of equilibrium with the carbonate, the use of 6M HCl to digest carbonate samples might result in spurious radiometric ages or excess data scatter.

For all sedimentary samples analysed, the uranogenic Pb isotopic compositions ($^{206}Pb/^{204}Pb$ and $^{207}Pb/^{204}Pb$) of both residue and carbonate plot along the same line (see **Figures 2.4.3**, **2.4.4**, **2.6.3**, **4.4.3**, **4.4.4** and **4.4.7**), indicating that both carbonate and residue acted as part of the same isotopic system and possessed similar μ_1 values at isotopic closure. Leaching of sediment residues during analytical dissolution should therefore have little effect on U-Pb or Pb/Pb dates. Similar results were obtained for 6M HCl dissolutions of the Zimbabwean Mushandike stromatolitic limestone by Moorbath et al. (1987) (see **Figure 1.3.5**). U/Pb fractionation between carbonate and residue serves to enhance the Pb isotopic range and thereby the precision on dates, where both carbonate and residue analyses are available. Where just carbonate analyses are performed, the use of strong acids during analytical dissolution may increase the Pb isotopic range by dissociating radiogenic Pb from complexes, adsorbed surface sites and interstitial grain boundaries.

It should be noted that residues from the Sandur marbles (see **Figure 3.4.3**) define a shallower slope than carbonate data because of incomplete isotopic homogenisation during metamorphism (section **3.5**) and so leaching of residues during analytical dissolution could conceivably have modified carbonate Pb isotopic compositions. However, the 2475 ± 65 Ma carbonate date is consistent with independent age constraints (2513 ± 5 Ma and 2433 ± 54 Ma for granites emplaced during meta-

morphism; see section 3.3) and so any contamination would appear not to have been significant.

Table 6b: Pb isotopic compositions of carbonates and corresponding residue analyses taken from this study and published works

SAMPLE	CORRECTED Pb ISOTOPIC COMPOSITION					
	$^{206}Pb/^{204}Pb_{CO_3}$	$^{206}Pb/^{204}Pb_{Res}$	$^{207}Pb/^{204}Pb_{CO_3}$	$^{207}Pb/^{204}Pb_{Res}$	$^{208}Pb/^{204}Pb_{CO_3}$	$^{208}Pb/^{204}Pb_{Res}$
*Western Australia, Kimberley Basin, Crowhurst Group. Stromatolite GSWA:						
99429 rb	20.321	22.348	15.850	16.084	39.219	40.328
99429 rd	20.383	22.232	15.881	16.067	39.074	39.968
99429 gc	23.605	23.787	16.160	16.160	40.235	41.027
*Western Australia, Kimberley Basin, Kimberley Group. Stromatolite GSWA:						
46285 A	23.352	19.862	16.214	15.737	44.809	41.180
46285 B	22.093	22.540	16.060	16.052	45.615	46.966
*Western Australia, Yeneena Basin, Yeneena Group. Stromatolite GSWA:						
76584 A	26.368	20.574	16.236	15.794	51.694	41.264
76584 B	26.346	20.698	16.231	15.830	52.331	41.549
*Sandur Schist Belt, India. Marble:						
010X3A	17.497	22.416	15.694	16.360	37.014	39.091
010X2A	16.232	16.909	15.501	15.595	35.726	36.288
010X2B	16.710	17.957	15.559	15.799	35.935	36.720
010X1A	18.675	21.802	15.876	16.291	38.527	39.100
010X1B	18.785	23.221	15.908	16.530	38.575	39.988
**Mushandike Stromatolitic Limestone, Zimbabwe:						
04	131.160	91.646	40.201	32.570	103.374	63.827
10	31.468	88.324	20.236	31.814	45.445	53.150
20	115.047	136.287	37.573	41.721	88.544	81.101
°Ordovician Trenton Limestone, United States:						
6.2	20.006	18.688	15.718	15.646	39.708	38.942
6.3	20.480	18.838	15.739	15.626	40.014	38.881
6.5	26.797	18.675	16.204	15.665	40.401	38.629
°°Tuanshanzi Formation Stromatolites, China:						
T1	68.055	19.688	20.158	15.609	41.434	36.702
T3	22.519	31.912	15.949	16.571	43.959	36.938
T17	16.703	19.639	15.412	15.768	36.215	37.001

* This study using 6M HCl dissolution.
** Data from Moorbath et al. (1987) using 6M HCl dissolution.
° Data from DeWolf & Halliday (1991) using 10% acetic acid dissolution.
°° Data from Cuvellier (1989) using 6M HCl dissolution.

A cross section of carbonate-residue pair Pb isotopic data are given in **Table 6a**. Although systematic differences between carbonate and residue Pb isotopic compositions are observed for some samples, this is not always the case;

- residue analyses for stromatolite GSWA 76584 from the Yeneena Basin and for the Ordovician Trenton Limestone (DeWolf & Halliday, 1991) are consistently less radiogenic than the corresponding carbonate data;
- residue analyses for stromatolite GSWA 99429 from the Kimberley Basin and for marbles from the Sandur Schist Belt are consistently more radiogenic than those for corresponding carbonates; but
- GSWA 46285, samples of Mushandike Stromatolitic Limestone (Moorbath et al., 1987) and stromatolites from the Sinian Tuanshanzi Formation (Cuvellier, 1989) show non-systematic residue-carbonate behaviour.

The mineralogical composition of the residue will be the dominant control on its isotopic composition. Silicate dominated clastic residues, low in U and rich in Pb (clays, feldspars, micas) will have less radiogenic Pb isotopic compositions than coexisting carbonate (relatively high U, low Pb) unless detrital uraniferous phases, such as apatite or zircon, are present (in which case, marked isotopic disequilibrium between residue and authigenic carbonate should be detected). Through metamorphic recrystallisation, much sedimentary/diagenetic U may become remobilised and theoretically this U will relocate in silicate minerals. Consequently, if siliceous residues have more radiogenic Pb isotopic compositions than carbonates and evidence exists for recrystallisation, this may reflect the processes of metamorphic elemental redistribution (for example, the Sandur marble data).

Non-systematic behaviour is more difficult to explain, particularly when carbonate and residue analyses all plot along the same isochron. The leaching effect of 6M HCl during analytical dissolution may cause preferential mobilisation of weakly bonded or complexed radiogenic Pb from U-rich silicates, producing radiogenic 'carbonate' analyses. Such behaviour has been documented for freshly exposed granitic rocks by Shirahata et al. (1980) and Silver et al. (1982). Where the silicate Pb is more strongly associated, residues may be more radiogenic than carbonates. Alternatively, the non-systematic behaviour might be explained by variable carbonate recrystallisation during diagenesis/metamorphism. Strongly recrystallised areas may have lost much U to residues and developed relatively unradiogenic compositions, while other areas maintained primary U concentrations. The problem remains enigmatic.

The fractionation of U and Pb between residue and carbonate during sedimentation, diagenesis and metamorphism is an interesting phenomenon that should be further investigated using sequential leaching techniques backed up by petrographic identifications and fission track studies. In this way, a more detailed understanding of the mechanisms of U and Pb fixation and mobility may result.

6.6: BRIEF COMMENT ON THORIUM AND THOROGENIC LEAD IN CARBONATES

Little mention has thus far been made of the significance of Th and thorogenic Pb, as far as carbonates are concerned. Although a full treatment is beyond the scope and aims of this study, a brief overview is presented. Marine Th shows contrasting geochemical behaviour to U under oxidising conditions and is reactive within the ocean realm (non-conservative behaviour). Dissolved Th has a concentration of 0.1 μgl^{-1} in river waters and 0.01 μgl^{-1} in marine waters, while particulate river matter averages 14 ppm Th and deep sea clays 10 ppm (Martin & Whitfield, 1983) (see **Table 6a**). Th is rapidly scavenged from the oceans as Th^{4+} adsorbed onto particulate matter (e.g. Fe-Mn oxyhydroxides) that sinks through the water column (Cochran, 1982; Nozaki et al., 1981; Bacon & Anderson, 1982). Brewer (1975) estimated the oceanic residence time of Th to be less than 100 yr, while data from Balistrieri et al. (1981) and Whitfield & Turner (1982) suggest that the deep water scavenging residence time may be as low as 22 yr.

Since Th fixation is not redox related, but controlled by inorganic particulate fixation, sedimentary carbonates that are deficient in detrital material are likely to have low Th/U ratios and to show limited correlation between uranogenic and thorogenic Pb isotopic compositions. This relationship is typical of the majority of sedimentary carbonates analysed in this study and also reported within the literature. Plots of $^{208}Pb/^{204}Pb$ vs. $^{206}Pb/^{204}Pb$ are presented for stromatolites from the Ashburton Basin, Western Australia (c.1.8 Ga), stromatolites from the Proterozoic Aravalli Supergroup (c.1.2 Ga) and the ?Cambrian Marwar Supergroup of India and stromatoporoids from the Silurian of Gotland (0.43 Ga and recrystallisation at 0.33 Ga) in **Figure 6.6.1**. In all but the case of the Upper Vindhyan Supergroup, despite large ranges in uranogenic Pb isotopic composition occurring, thorogenic Pb shows little isotopic variation and the corresponding Th/U ratios tend to be less than 0.2 (much lower than the bulk earth figure of around 4.0). Smith & Farquhar (1989) reported similarly low Th/U ratios for Ordovician corals from Ontario, while

Figure 6.6.1: Thorogenic Pb data for selected carbonates from this study

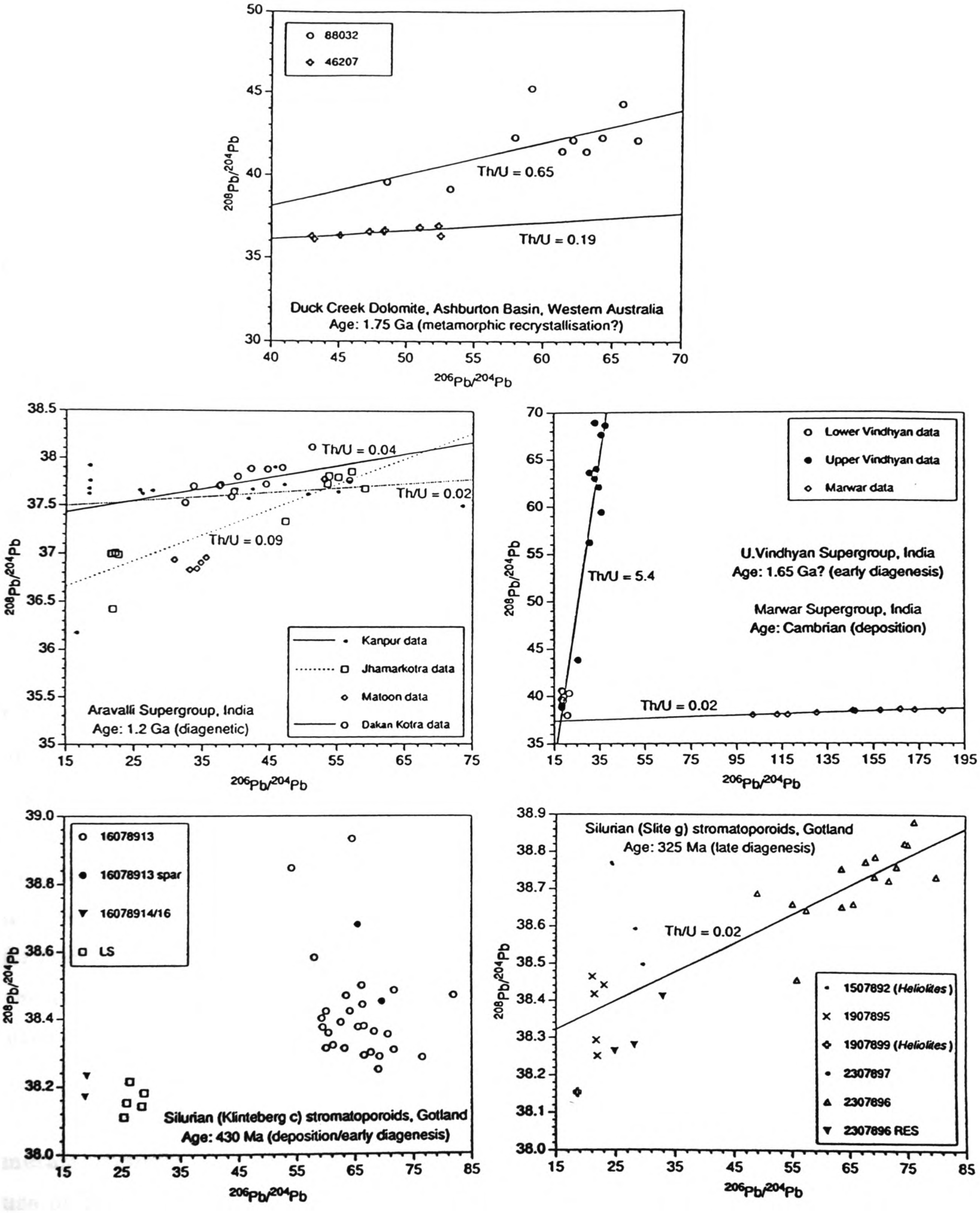

DeWolf & Halliday (1991), from limited data, reported a range of 0.5 to 2.2.

Considering the short ORT_{Th}, the concentration of Th in marine sediments will inevitably reflect the nature of the sediment hinterland. Where Th and U do correlate in sediments and Th/U ratios are enhanced, such as in the case of the Upper Vindhyan Supergroup stromatolite data (Th/U of 5.44), Th rich catchment areas are likely to be involved. Similar correlations have been reported for stromatolites from the Ventersdorp Supergroup, South Africa by Jahn et al. (1990) (Th/U of 3.94) and the Gaoyuzhuang Formation of China by Cuvellier (1989) (Th/U of 4.89). Without a thorough consideration of palaeogeography, detailed interpretation is not possible, but it is clear that Th exhibits variable behaviour with respect to sedimentary carbonates.

Diagenesis is unlikely to cause significant modification of primary Th signals because Th is not easily mobilised from particulate matter. Indeed, Santschi et al. (1983) found that Th distribution with depth in sediment columns was controlled by particle redistribution rather than diagenesis. Metamorphism, however, can cause redistribution of Th as mineral assemblages are reconstituted under conditions of elevated temperature and pressure. **Figure 6.6.2** illustrates $^{208}Pb/^{204}Pb$ vs. $^{206}Pb/^{204}Pb$ plots for Sandur Schist Belt marbles, the Mushandike Stromatolitic Limestone (Moorbath et al., 1987) and Taiwanese marbles (Jahn, 1988). Th and U are correlated in all but the Taiwanese marbles, where the signature is more typical of a sediment. Th/U ratios tend to be below the bulk earth average of 4.0, suggesting concentration of U with respect to Th in metamorphic rocks that have carbonate precursors. This is not unreasonable given the fact that U has higher primary concentrations in carbonate sediments than Th. It is interesting to note that Th/U ratios are lower for residues (6M HCl-insoluble) in both Sandur and Mushandike carbonates, whereas one might expect them to have higher ratios if Th were to become preferentially sited in silicate mineral lattice sites.

Clearly, Th behaves independently of U during deposition, diagenesis and metamorphism. Low Th concentrations in carbonates at deposition preclude the use of the Th-Pb method for direct dating but further investigation is merited to characterise the geochemical behaviour of Th in carbonates.

Figure 6.6.2: Thorogenic Pb data for selected marbles

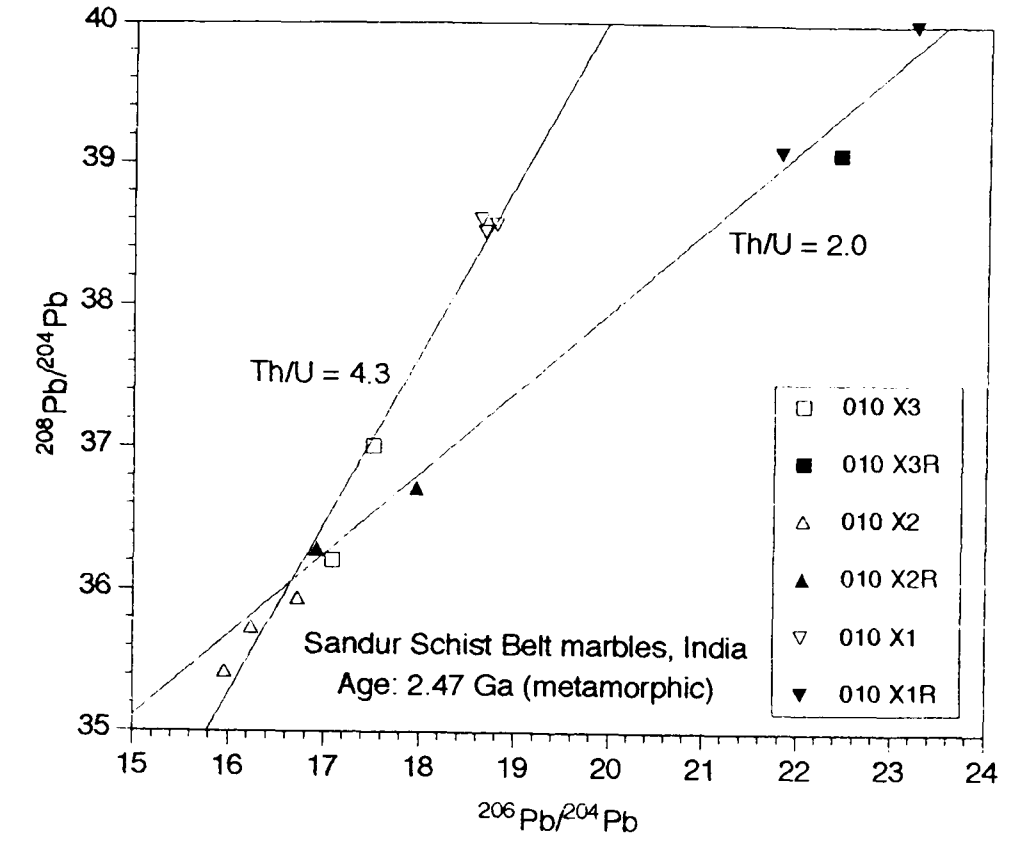

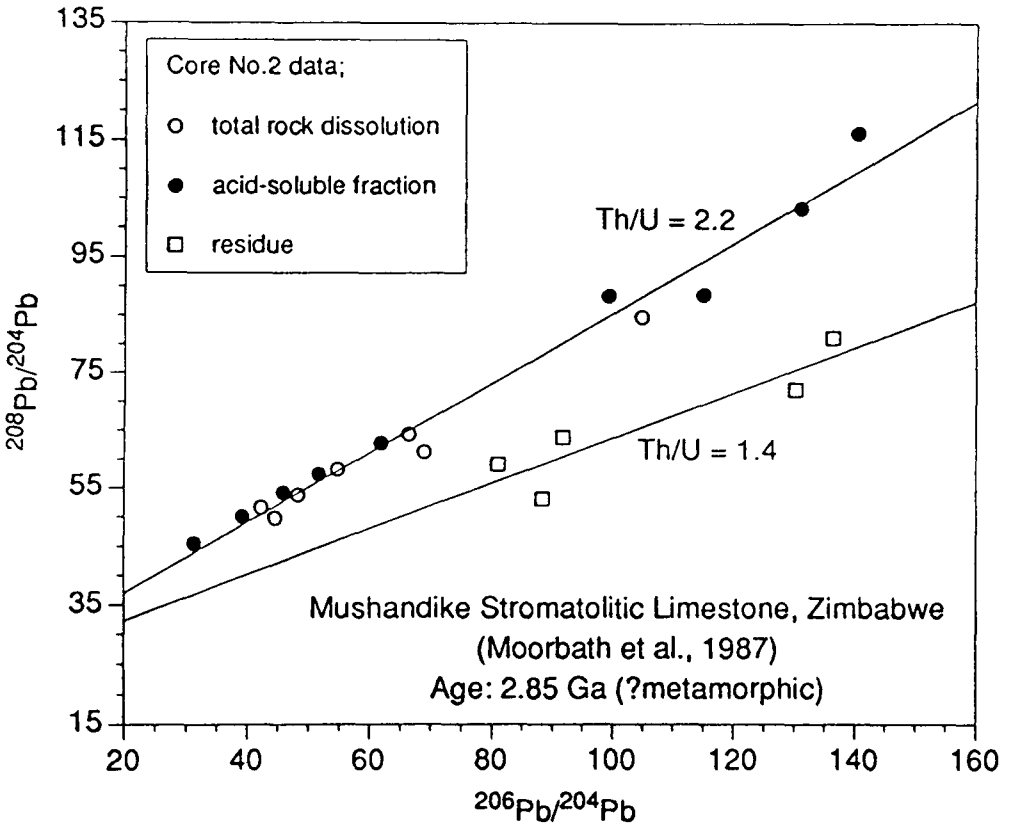

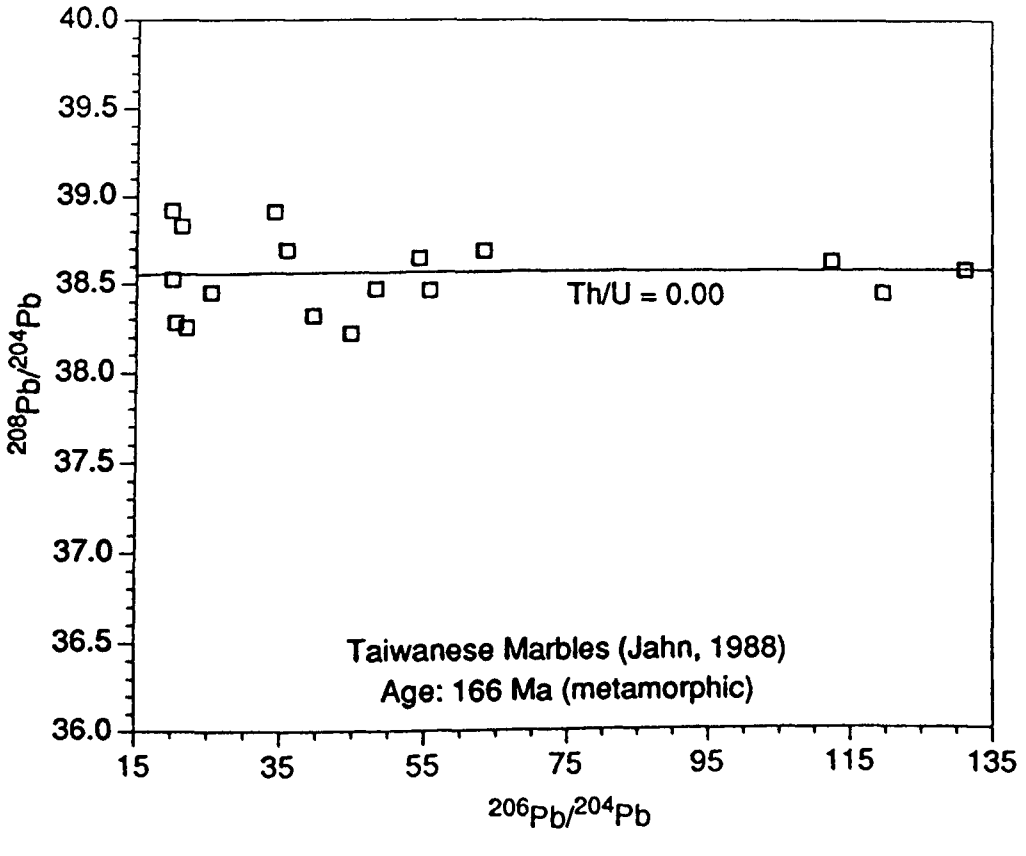

Chapter 7:

CONCLUSIONS

Analyses performed during this work using Pb/Pb and U-Pb techniques, in addition to a number of recently published studies (e.g. Jahn, 1988; Smith & Farquhar, 1989; Jahn et al., 1990; Taylor & Kalsbeek, 1990; Russell, 1991; Smith et al., 1991; DeWolf & Halliday, 1991), have demonstrated that U-Pb systems in sedimentary and metamorphic carbonates are frequently robust and as such hold considerable potential for direct dating. The ability to directly date carbonates is potentially powerful because appropriate sample materials are widely dispersed throughout the entire geological record as; marine and lacustrine limestones; macrofossils (including the earliest records of life on earth, stromatolites); cements; metamorphic marbles and even within igneous rocks as carbonatites. The potential of Pb/Pb radiometric dating for the direct age determination of carbonates has been critically assessed through its application to Proterozoic stromatolites from Western Australia, Proterozoic stromatolites from India, Archaean marbles from India and Palaeozoic

stromatoporoids from Sweden.

With regard to the Western Australian samples, chronometric information obtained from the Pb/Pb analyses of a number of Proterozoic carbonate stromatolites has permitted a re-evaluation of depositional age ranges and inter-basinal correlations within the state. A combined date of 1778 ± 27 Ma for stromatolites from the Duck Creek Dolomite (Wyloo Group, Ashburton Basin) is interpreted as the age of burial metamorphic recrystallisation and as such, represents a new minimum depositional age for the Ashburton Basin (previously indirectly constrained to between ?2.0-1.843 Ga; Myers & Hocking, 1988).

A major revision of the depositional age of the Nabberu Basin is proposed in light of depositional/early diagenetic Pb/Pb ages for stromatolites from the Glengarry and Earaheedy Groups (previous indirect constraints of 2.0-1.8 Ga and 1.8-1.6 Ga, respectively; Myers & Hocking, 1988). A date of 2258 ± 180 Ma for Glengarry stromatolites and figures of 2008 ± 68 Ma and 1946 ± 71 Ma for basal Earaheedy stromatolites suggest that deposition of the Glengarry Group took place between ?2.4-2.0 Ga and deposition of the Earaheedy Group between 2.0-?1.6 Ga. If the inferred maximum depositional age for the Ashburton Basin is correct, the Wyloo Group should now be correlated with basal parts of the Earaheedy Group, while the Glengarry Group is somewhat older.

An early diagenetic age of 1509 ± 90 Ma for stromatolites from the Hibberson Dolomite (Crowhurst Group) provides a significantly improved estimate for the minimum depositional age of the Kimberley Basin (previously > 0.67 Ga). The Speewah and Kimberley Groups are more tightly constrained by independent age data to between 1.84-1.76 Ga. Consequently, the age range of the Kimberley Basin is revised to 1.84-1.5 Ga and the older units (Speewah and Kimberley Groups) are now correlated with both the very youngest sediments of the Wyloo Group and the Miningarra Subgroup of the Earaheedy Group, while the younger Bastion and Crowhurst Groups may also correlate with younger parts of the Miningarra Subgroup.

Pb/Pb carbonate dates for stromatolites from younger subgroups of the Bangemall Basin (1314 ± 150 Ma) are in agreement with an unpublished 1.331 Ga Rb-Sr glauconite date for the Manganese Subgroup (Williams, pers. comm. 1991) and imply that the older subgroups were deposited between 1.6-1.35 Ga and the younger subgroups between 1.35-1.0 Ga. The boundary was previously placed at 1.2 Ga.

Consequently, the older Bangemall deposits (tenuously dated at 1436 ± 230 Ma in this work) may correlate with the Crowhurst Group of the Kimberley Basin but are younger than Nabberu Basin sediments.

Dates for stromatolites from the Yeneena and Savory Basins (988 ± 120 Ma and 1058 ± 470 Ma, respectively) are insufficiently precise to improve on existing estimates of depositional age (?1.2-0.75 Ga and 0.89-0.61 Ga), but are reassuringly consistent with these constraints. In the future, the ability to obtain direct radiometric dates for microfossiliferous stromatolitic deposits may enable combination of biostratigraphic and chronometric scales to produce an integrated time scale for the Proterozoic of Western Australia.

The application of Pb/Pb dating to Late Archaean/Early Proterozoic marbles from the state of Karnataka, Peninsular India, has demonstrated that the western low temperature and eastern high temperature zones of amphibolite grade metamorphism (Chitradurga Schist Belt and Sandur Schist Belt) had different sources (average model μ_1 values of 7.88 and 8.48, respectively) and experienced differing metamorphic histories. A metamorphic recrystallisation age of 2639 ± 32 Ma for the former and 2475 ± 65 Ma for the latter suggest that elevated thermal gradients in the east maintained U-Pb open system conditions for c.150 Ma before blocking temperatures were finally reached. These observations are consistent with radiometric data from the late tectonic Chitradurga and Closepet Granites (Taylor et al., 1984; Friend, pers. comm. 1992). Results from the Sandur Schist Belt indicate that disequilibrium existed between HCl-soluble and insoluble components at isotopic closure. While carbonate Pb isotopic ratios were homogenised during metamorphism, resulting in the generation of a reliable Pb/Pb isochron, incomplete homogenisation of Pb isotopic ratios in non-carbonate components, coupled with U uptake according to the model $\mu_3 = k/\mu_2$, has generated a rotated palaeoisochron that possesses no age significance.

Dates for Indian Proterozoic stromatolites from the Aravalli-Delhi orogenic belt have resulted in a revision of age constraints for the Delhi Orogeny, the Vindhyan Supergroup and the Marwar Supergroup and a reassessment of their lithostratigraphic correlations. A Pb/Pb date of 1202 ± 87 Ma for phosphatic stromatolites from the Aravalli Supergroup is interpreted as the date of metamorphic recrystallisation, associated with Delhi Orogen metamorphism (M3), while galena Pb model ages of 1.1 Ga and 1.05 Ga are inferred to correspond to late-Delhi mineralisation (Deb et al., 1989; this work). A depositional/early diagenetic age of 1627 ± 46 Ma for

stromatolites from the undeformed Upper Vindhyan Supergroup (the basin was previously constrained to between > 1.4-?0.7 Ga) indicates that Vindhyan deposits should now be correlated in part with the Aravalli and Delhi Supergroups. The lack of deformation indicates that the Upper Vindhyan rocks did not suffer the effects of either the Aravalli or Delhi Orogen and so movement along the Great Boundary Fault must have taken place later than 1100 Ma. An imprecise Pb/Pb date of 471 ± 270 Ma for stromatolites from the Marwar Supergroup, which unconformably overlies the Delhi Supergroup and was previously correlated with the Vindhyan Supergroup (Trans-Aravallis Vindhyans), strongly suggests that this correlation is no longer valid and that the Marwar deposits are more likely to be broadly equivalent to Cambrian rocks found in the Salt Range (as proposed by Barman, 1980).

Results for Silurian stromatoporoids from the Swedish island of Gotland indicate that the Pb/Pb and, in certain cases, the U-Pb method may be successfully applied to Phanerozoic carbonates. A Pb/Pb date of 432 ± 15 Ma for stromatoporoids from the Wenlock-Ludlow boundary (Klinteberg Formation) is within error of the inferred age of 420 Ma. Although recent Quaternary weathering has resulted in U mobilisation, selected U-Pb data for the same samples give a date of 435 ± 9 Ma. While these levels of precision are of limited use for time scale calibration, results indicate the validity of the method. A Pb/Pb date of 326 ± 11 Ma for stromatoporoids from the Middle Wenlock Slite Formation is interpreted as the age of late diagenetic recrystallisation in response to interaction with fluids channelled along sub-surface north-south faults in line with the Lärbro Valley. Overlying carbonates in the Klinteberg Formation remained unaffected by this recrystallisation event (whose age represents the first chronometric control on the post-Silurian pre-glacial history of the island) because they are stratigraphically separated from the Slite Formation by the largely impermeable shales of the Upper Slite and Mulde Formations. The observed systematic variations of U and Pb concentrations and Pb isotope ratios allow an insight into the behaviour of U and Pb under conditions of deposition/diagenesis.

A broad geochemical model has been proposed to explain why carbonates should be so suited to this particular method of geochronological study. Dissolved concentrations of U and Pb in seawater are 3.2 ppb and 0.003 ppb (Martin & Whitfield, 1983). These figures correspond to an extremely high μ ($^{238}U/^{204}Pb$) value of approximately 80,000. River waters have higher concentrations of dissolved Pb (0.1 ppb) and lower concentrations of dissolved U (0.24 ppb), corresponding to a much lower

μ value of 170. Particulate matter in the oceans averages 2 ppm U and 200 ppm Pb (Martin & Whitfield, 1983). Thus materials deposited authigenically from seawater, with low detrital contents (i.e. carbonates) have the potential for direct dating using U-Pb and Pb/Pb methods. In addition to any detrital content, elemental concentrations of U and Pb may become established within carbonates through a variety of mechanisms (organic complexing and preconcentration; crystal lattice substitution; surface adsorption onto particulates, particularly oxyhydroxides; and early diagenetic fixation).

Fixation of U within the sedimentary pile occurs principally during early diagenesis and is controlled by redox reactions because on reduction, soluble hexavalent U converts to insoluble tetravalent U. In addition, Disnar (1981) showed that algal material could fix UO_2^{2+} directly from seawater. Organic concentrations are therefore important in determining the U concentration of sedimentary carbonates, particularly as calculated distribution coefficients predict that lattice site related concentrations should be lower than dissolved oceanic concentrations (i.e. at the ppb level) (Chung & Swart, 1990; Swart & Hubbard, 1982), while data indicate concentrations of modern carbonates are at the ppm level (Chung, 1988). A number of authors have shown that total organic carbon and U concentration are correlated (e.g. Andersen et al., 1989; Çagatay et al., 1990; Klinkhammer & Palmer, 1991).

Conversely, Pb is fixed principally by adsorption onto the surfaces of inorganic particulate matter within the oceans (scavenging). Although the Pb isotopic composition of sediments that lack resistant uraniferous clastics is controlled by the nature of the eroded sediment hinterland and thus variable between geographical locations, large scale heterogeneity of Pb isotopic composition is unlikely in any one locality because scavenged Pb has a very short oceanic residence time (< 22 yr). Model μ_1 values of primary sediments will reflect the broad nature of the hinterland and could therefore be of use in association with palaeogeographic reconstructions as qualitative indicators of provenance.

Recrystallisation events involving oxidising fluids alter primary isotopic signatures, causing the re-solution of U (and to some extent Pb) and lowering of μ_2 values. Concomitant homogenisation of Pb isotopic ratios will reset isotopic systematics and, if some U/Pb heterogeneity is preserved, radiometric dates. However, if U/Pb ratios are also effectively homogenised, modern Pb isotopic compositions will show very little variation. If Pb isotopic ratios are not homogenised, then irrespective of U/Pb heterogeneity, excess data scatter will result. Consequently,

Pb/Pb and U-Pb dates should be interpreted within the framework of one of the following recrystallisation events;

- deposition/early diagenesis (usually indistinguishable radiometrically once error on the date is taken into consideration);
- late diagenesis; or
- metamorphic/igneous recrystallisation.

Interpretation should only be made after due consideration of all relevant geological information available (petrography; stable isotopes, particularly $\delta^{13}C_{organic}$; cathodoluminescence; independent age constraints; geotectonic evolution) and should be consistent with this data. Realistic interpretations are imperative since great reliance may come to be placed on carbonate dates, particularly in the Precambrian.

Large ranges in Pb isotope ratios over sub-centimetre size domains are a characteristic feature of many carbonates. Despite the mobility of U under diagenetic and metamorphic transformations, post-(re)crystallisation closed system conditions have, in many cases, operated for considerable periods of geological time. The Pb/Pb method has been successfully applied to a wide age range of carbonate materials (2900 Ma to 166 Ma). Pb/Pb carbonate dates for Precambrian materials may achieve a precision of ± 1% and this characteristically represents a significant improvement on former indirect constraints from dated basement rocks, intrusives and interstratal volcanics and thus is of immense chronostratigraphic and correlative potential. Moreover, the Pb/Pb method is insensitive to recent loss of U and Pb or gain of U and so may be used to investigate surface exposures of carbonates.

For samples where Pb isotopic compositions show little variation, enhanced ranges (and frequently increased precision on regressed Pb/Pb dates) may be obtained by the combination of data from separate samples. For such an approach to be justified, all samples must occupy the same inferred stratigraphic position and have model μ_1 values and individual regressed dates that are, within error, concordant (e.g. as applied to Western Australian and Indian Proterozoic stromatolites, Silurian stromatoporoids). The combination of 6M HCl-insoluble residue analyses with carbonate data can also serve to enhance the Pb isotopic range. In most of the carbonate samples studied, residue (principally silicate) and carbonate Pb isotopic data plot along the same regressed line and therefore must have had broadly similar μ_1 values at crystallisation (deposition/early diagenesis, late diagenesis, metamorphism). In the case of sedimentary carbonates this is undoubtedly related to the relatively rapid fixation of Pb in the open marine realm.

The slow rate of change of the radiogenic $^{207}Pb/^{204}Pb$ ratio during the Phanerozoic limits the precision of Pb/Pb carbonate dates and therefore their chronostratigraphic value. Nevertheless, they are useful in demonstrating the reliability of the technique and for the detection and temporal constraint of late diagenetic recrystallisation events. More precise (and accurate) constraints on sediment age can generally be obtained from K-Ar studies on bentonites and U-Pb studies on separated volcanic zircons, although rarely extremely large ranges of Pb isotope ratios (such as found for Silurian stromatoporoids) can produce meaningful chronometric information.

The U-Pb method applied to carbonates is capable of greater precision than the Pb/Pb method, particularly in the Phanerozoic (± 1 Ma; DeWolf & Halliday, 1991), and thus has potential for time scale calibration and correlation purposes. Quantitative retention of both U and Pb within the carbonate is required for successful U-Pb dating, but the ease of U mobility during diagenesis and metamorphism often means that systematics are disturbed and age relationships destroyed (or possibly reset). Carbonates from freshly exposed, non-weathered sections are essential if U-Pb dating is to be successful. In cases where U-Pb systematics have been disturbed, detailed isotopic and concentration determinations allow an insight into the mobility and behaviour of U and Pb under diagenetic/metamorphic conditions.

Since U and Pb concentrations in carbonates have been found to be generally lower than 5 ppm, quantification of potential U/Pb ratios is beyond the resolution of most standard rapid analytical techniques (S.E.M., I.C.P., proton probe). Fission track work can reliably indicate U content (Swart, 1988) but is time intensive and not always readily accessible. No obvious petrographic or stable isotopic correlation with any indicator of dating potential has been noted, other than the fact that total organic content may be proportional to U concentration (this should be investigated further), and so full Pb isotopic analysis remains the most effective means of determining a particular sample's potential for age determination. The initial analysis of two or three cleaned 1 g chips per sample (see **Appendix B**) should provide an indication of the Pb isotopic composition, potential range and concentration, allowing pre-selection of promising sample materials for more detailed analysis.

Stromatoporoids, stromatolites, corals, calcitic cements, marbles and carbonatites have all been successfully dated using direct Pb/Pb and U-Pb dating. In addition, preliminary unpublished results (this work) for a specimen of *Solenopora* from the Jurassic of Oxfordshire (Bathonian) indicate that a highly radiogenic Pb

isotopic composition ($^{206}Pb/^{204}Pb$ 119.459 ± 0.723, $2\sigma_{mean}$) has developed in a relatively short period of geological time (c.165 Ma), corresponding to an *in situ* μ_2 value of approximately 4000. Such fossil carbonate red alga could also prove highly suitable materials for U-Pb and Pb/Pb dating.

In the Precambrian, Pb/Pb carbonate geochronology holds exciting potential for both defining and refining regional and geological time scales. The ability to directly date stromatolitic carbonates has an important bearing on the calculation of rates of evolution for the earliest life on earth and allows an assessment to be made of the viability of stromatolite biostratigraphy. Preliminary results suggest that until the correct identification and systematic classification of stromatolite forms is universally agreed upon and adhered to, and the importance of environmental factors on stromatolite morphology critically assessed, it is improbable that numerical dates from comparative stromatolitic studies can be routinely used with confidence. This does not preclude valuable correlative results emerging from stromatolitic taxonomic study (Grey, pers. comm. 1992). The recent discovery of microfossiliferous Precambrian carbonates (Schopf, 1983) may result in the development of a more detailed and reliable biostratigraphic subdivision of the Precambrian and direct Pb/Pb dates for these sediments would allow the combination of biostratigraphic and chronostratigraphic scales and the development of an integrated geological time scale, currently lacking for the Precambrian. In the meantime, the availability of direct radiometric dates for sedimentary sequences (previously poorly constrained by indirect means) and metamorphic terrains permits regional correlation of formations, basins and tectonic episodes of use in intra- and intercontinental geological studies.

In the Phanerozoic, U-Pb dating of suitable carbonate materials may be of great value in calibrating the geological time scale if the potential precision of ± 1 Ma can be achieved routinely and without bias. Samples with high *in situ* μ_2 values, such as sponges (including stromatoporoids), red alga and certain calcitic cements have shown considerable promise. Abundant precise K-Ar and U-Pb zircon dates for intercalated volcanics provide an independent control from which the accuracy of carbonate results can be monitored. Pb/Pb dates are unlikely to be of use in time scale calibration because of poorer precision but may permit the identification and temporal constraint of important post-depositional events, such as hydrocarbon emplacement and late diagenetic recrystallisation, of use in characterising basin evolutionary histories.

While this study has successfully demonstrated the potential of Pb/Pb radiometric dating for the direct age determination of a variety of carbonates, it has also highlighted a number of interesting phenomena that merit further investigation.

• Detailed application of U-Pb and Pb/Pb decay schemes to appropriate lithologies from one particular well calibrated, carbonate rich stratigraphic section (such as the Silurian of Gotland) would permit a critical assessment of the precision, accuracy and consistency of carbonate dates. Results should also allow characterisation of the scale of elemental mobility during early and late diagenesis and indicate whether intermediate daughter element loss has a significant (and systematic) effect on regressed dates.

• Significant, non-systematic variations in Pb isotopic composition between 6M HCl soluble fractions and residues indicate that carbonate and residue were often not in equilibrium at isotopic closure. However, the fact that analyses generally plot along the same regressed line implies that they must have possessed distinctly similar μ_1 values, even if *in situ* μ_2 values showed considerable variation. Investigations involving different strengths of HCl and acetic acid during sample dissolution would allow the distinction of true Pb isotopic compositions for carbonate and residue components of limestones and marbles, thereby facilitating the modelling of elemental distributions within carbonates on deposition and their subsequent modification during diagenesis and metamorphism. Incomplete Pb isotopic homogenisation within non-carbonate components during metamorphism may cause the generation of rotated palaeoisochrons and spurious chronometric information. Results for Sandur Schist Belt marbles indicate that such behaviour may be complex and is little understood. A detailed programme of study within an appropriate multigrade metamorphic terrain is required to determine operative blocking temperatures and to characterise the behaviour of carbonates and silicates under conditions of elevated pressure and temperature.

• The behaviour of Th in sedimentary and metamorphic carbonates is also poorly understood. Most sedimentary carbonates have extremely low Th/U ratios, but some show a distinct correlation and may possess Th/U ratios well above the average figure for bulk earth (c.4.0). Conversely, most marbles have correlated Th and U concentrations, but others show calculated Th/U ratios of zero. It is unclear whether controls on Th or U concentration are responsible for this variation. Although the Th-Pb method is unlikely to prove an effective means of carbonate age determination because of low *in situ* Th/Pb ratios, the behaviour of Th with respect to carbonates is an intriguing problem that merits further geochemical investigation.

To conclude, Wampler & Kulp (1962) stated that, "*under suitable conditions the isotopic composition of lead in carbonate rocks may give valuable information on the geologic history of an area*". It is now clear that carbonate Pb/Pb and U-Pb systematics may be used for the direct age determination of many sedimentary, metamorphic and igneous rocks, in addition to individual carbonate macrofossils. Such materials should now be considered credible sources of age information for both Precambrian and Phanerozoic sequences.

Appendix A:

SYSTEMATICS AND ERRORS

A.1: INTRODUCTION

The theory of and principles behind the various isotopic U-Pb, Th-Pb and Pb/Pb methods of radiometric dating have been the subject of numerous studies and reviews, for example Wetherill (1956), Wasserburg (1963), Doe (1970a), Gale & Mussett (1973), and more recently Faure (1986). The reader is referred to the latter publication and the references therein for a more thorough treatment. The symbols used in this brief overview are listed in **Table Aa** and any deviation from this nomenclature is indicated in the text.

A.2: SYSTEMATIC THEORY

Naturally occurring U has three isotopes; ^{234}U, ^{235}U and ^{238}U, all of which are radioactive. Thorium exists mainly as radioactive ^{232}Th but has five other short-lived radioactive isotopes that are intermediate daughters of either ^{232}Th, ^{235}U or ^{238}U.

Ordinary Pb has four naturally occurring isotopes; ^{204}Pb, ^{206}Pb, ^{207}Pb and ^{208}Pb, of which only ^{204}Pb is not generated by any known radioactive process.

Table Aa: Key to symbols used in text

F	Mass fractionation correction (% per atomic mass unit).
M	Isotopic ratio measured from mass spectrometer, uncorrected for mass fractionation.
M*	Measured isotopic ratio corrected for mass fractionation at F% per atomic mass unit.
ΔM	Mass difference between the two isotopes constituting the ratio under consideration.
α	$^{206}Pb/^{204}Pb$ ratio, corrected for mass fractionation.
β	$^{207}Pb/^{204}Pb$ ratio, corrected for mass fractionation.
γ	$^{208}Pb/^{204}Pb$ ratio, corrected for mass fractionation.
μ	$^{238}U/^{204}Pb$ atomic ratio.
δ	$^{235}U/^{204}Pb$ atomic ratio.
κ	$^{232}Th/^{204}Pb$ atomic ratio.
NBS	Published National Bureau of Standards value for a particular ratio, uncorrected for mass fractionation.
N	Value obtained from Oxford mass spectrometer for same NBS standard ratio, uncorrected for mass fractionation.
X	Pb or U concentration of sample ($\mu g g^{-1}$ = ppm).
W	Weight of sample aliquot for isotope dilution (g).
Y	Weight of spike solution (g).
C	Concentration of spike solution ($\mu g g^{-1}$ = ppm).
T_{ik}	Atomic ratio of isotopes i and k in the spike solution, corrected for mass fractionation.
U_{ik}	Atomic ratio of isotopes i and k in the sample, corrected for mass fractionation.
M_{ik}	Atomic ratio of isotopes i and k in the spike/sample mixture, corrected for mass fractionation.
t_k	Atomic abundance of reference isotope k in the spike, as %.
u_k	Atomic abundance of reference isotope k in sample, as %.
A_t	Atomic weight of spike.
A_u	Atomic weight of sample.
σ_r	1 sigma error in 'r'

^{206}Pb is generated by the decay of ^{238}U, with ^{234}U being an intermediate daughter. ^{238}U forms 99.2743% of naturally occurring U and ^{234}U just 0.0057%. This U decay series may be summarised as;

$$^{238}_{92}U \rightarrow {}^{206}_{82}Pb + 8\,{}^{4}_{2}He + 6\,\beta^{-} + Q$$

where Q is the sum of the decay energies of the series and is equal to 47.4 MeV $atom^{-1}$ (Wetherill, 1966). The decay constant for this series, λ_1, has a value of 1.55125×10^{-10} yr^{-1} (Steiger & Jäger, 1977) and a half-life of 4.468×10^{9} yr.

^{207}Pb is generated by the decay of ^{235}U (0.7200% of natural U) via the actinium decay series, which may be summarised as;

$$^{235}_{92}U \rightarrow {}^{207}_{82}Pb + 7\,{}^{4}_{2}He + 4\,\beta^{-} + Q$$

with Q equal to 45.2 MeV $atom^{-1}$ (Wetherill, 1966). The decay constant for the actinium series, λ_2, has a value of 9.8485×10^{-10} yr^{-1} (Steiger & Jäger, 1977) and a half-life of 0.7038×10^{9} yr.

^{208}Pb is uniquely generated by the decay of ^{232}Th which comprises 100% of natural Th and this decay series may be expressed as;

$$^{232}_{90}Th \rightarrow {}^{208}_{82}Pb + 6\,{}^{4}_{2}He + 4\,\beta^{-} + Q$$

with Q equal to 39.8 MeV $atom^{-1}$ (Wetherill, 1966). The decay constant for this series, λ_3, has a value of 4.9475×10^{-11} yr^{-1} (Steiger & Jäger, 1977) and a half-life of 14.010×10^{9} yr.

In each decay series, the decay constants of the intermediate nuclides are large compared to that of the parent (i.e. their half-lives are very much shorter) and secular equilibrium is established, such that the rate of decay of the intermediate daughter nuclides is controlled by that of the parents. Providing that the system remains closed, the decay of ^{238}U to ^{206}Pb, ^{235}U to ^{207}Pb and ^{232}Th to ^{208}Pb under secular equilibrium can be treated as direct and described via basic equations.

The law of radioactive decay states that the rate of decay of a radioactive parent to its daughter isotope, D, is proportional to the number of atoms present, N;

$$-\frac{dN}{dt} \alpha N \quad (1),$$

where t is unit time and so;

$$-\frac{dN}{dt} = \lambda N \quad (2),$$

where λ is the decay constant for the particular parent isotope. Integrating this expression with respect to t, between limits such that $N = N_0$ at $t = 0$ and $N = N$ at $t = t$, gives the basic equation for all radioactive decay processes;

$$N = N_0 e^{-\lambda t} \quad (3)$$

Since the number of radiogenic daughters, D^*, produced by parental decay at any time t can be shown to be;

$$D^* = N_0 - N \quad (4),$$

simple substitution gives;

$$D^* = N_0 (1 - e^{-\lambda t}) = N (e^{\lambda t} - 1) \quad (5).$$

The total number of daughter atoms (D) at any given time is equal to the sum of those initially present at t=0 (D_0) and those that have formed from parental decay (D^*), so that;

$$D = D_0 + D^* \quad (6)$$

Substituting for D^* from (5), the basic equation for rock and mineral 'age' calculation from radioactive parent decay is obtained;

$$D = D_0 + N (e^{\lambda t} - 1) \quad (7).$$

Certain conditions must also be satisfied;

- the system must be closed with respect to both parent and daughter;
- realistic values for D_0 must be available;
- D and N must be both accurately measured and representative.

The decay constants used are those of Steiger & Jäger (1977), as detailed above.

The concept of the half-life of a radioactive parent can be defined as the time taken for half of a set number of parents to decay and so when $t = T_{1/2}$, $N = 1/2\ N_0$. Substituting in expression (3);

$$\frac{1}{2} N_0 = N_0 e^{-\lambda T_{1/2}} \quad (8)$$

from which it can be shown;

$$T_{1/2} = \frac{\ln 2}{\lambda} \quad (9).$$

Applying the three U, Th-Pb decay schemes to equation (7), expressions are obtained for each parent-daughter relationship;

$$^{206}Pb = {}^{206}Pb_0 + {}^{238}U\ (e^{\lambda_1 t} - 1) \quad (10)$$

$$^{207}Pb = {}^{207}Pb_0 + {}^{235}U\ (e^{\lambda_2 t} - 1) \quad (11)$$

$$^{208}Pb = {}^{208}Pb_0 + {}^{232}Th\ (e^{\lambda_3 t} - 1) \quad (12)$$

where ^{206}Pb, ^{207}Pb, ^{208}Pb, ^{238}U, ^{235}U and ^{232}Th are the isotopic abundances in the mineral at the time of analysis; $^{206}Pb_0$, $^{207}Pb_0$ and $^{208}Pb_0$ are the initial isotopic abundances of Pb in the rock/mineral at the time of its isotopic closure; λ_1, λ_2 and λ_3 are the decay constants of ^{238}U, ^{235}U and ^{232}Th and t is the time elapsed since the closure of the rock/mineral system to all isotopes of the U-Pb and Th-Pb decay schemes. It is possible to measure isotopic ratios more precisely than absolute abundances and so equations (10), (11) and (12) are normally divided by the isotopic abundance of ^{204}Pb in the sample. This value remains constant, since ^{204}Pb is unaffected by radioactive decay. Thus if $\alpha = {}^{206}Pb/{}^{204}Pb$, $\beta = {}^{207}Pb/{}^{204}Pb$, $\gamma = {}^{208}Pb/{}^{204}Pb$, $\mu = {}^{238}U/{}^{204}Pb$, $\delta = {}^{235}U/{}^{204}Pb$ and $\kappa = {}^{232}Th/{}^{204}Pb$, the equations may be rewritten as;

$$\alpha = \alpha_0 + \mu\ (e^{\lambda_1 t} - 1) \quad (13)$$

$$\beta = \beta_0 + \delta\ (e^{\lambda_2 t} - 1) \quad (14)$$

$$\gamma = \gamma_0 + \kappa\ (e^{\lambda_3 t} - 1) \quad (15)$$

Each equation corresponds to that of a straight line with general form $y = c' + xm'$.

Plots of μ vs. α, δ vs. β and κ vs. γ can be used to calculate the 'age' (t) and initial ratio (α_0, β_0 or γ_0) of a sample from the slope (m) and intercept (c') of the straight line defined by the isotopic composition of two or more samples which were chemically differentiated with respect to their U/Pb or Th/Pb ratio and isotopically homogenised at time t, but have subsequently remained part of the same closed system. Concentrations of U, Th and Pb are measured by isotope dilution, and are used to calculate μ, δ and κ. The Pb isotopic composition of the sample is measured directly on a mass spectrometer. Other assumptions stated above must also be satisfied. Thus, for example;

$$t_{206} = \frac{1}{\lambda_1} \ln \left(\frac{\left(\frac{^{206}Pb}{^{204}Pb}\right) - \left(\frac{^{206}Pb}{^{204}Pb}\right)_0}{\left(\frac{^{238}U}{^{204}Pb}\right)} + 1 \right) \quad (16).$$

Combining equations (13) and (14) gives;

$$\frac{(\beta - \beta_0)}{(\alpha - \alpha_0)} = \frac{^{235}U}{^{238}U} \times \frac{e^{\lambda_2 t} - 1}{e^{\lambda_1 t} - 1} \quad (17)$$

and allows one to calculate a date based on the radiogenic $^{207}Pb/^{206}Pb$ ratio, which is insensitive to recent Pb loss (that is when the Pb lost had virtually the same isotopic composition as the Pb in the mineral under analysis). Since $^{235}U/^{238}U$ has a constant value of 1/137.88 (Steiger & Jäger, 1977), there is no need to ascertain the concentration of either U or Pb in the rock/mineral, making the analytical procedure simpler. A plot of β vs. α yields a straight line for isotopically closed systems, with slope;

$$m = \frac{\left(e^{\lambda_2 t} - 1\right)}{\left(e^{\lambda_1 t} - 1\right)} \times \frac{1}{137.88} \quad (18)$$

and t, the Pb/Pb 'age', is solved for iteratively.

For a rock/mineral to be suitable for dating by the U-Pb, Th-Pb or Pb/Pb methods, it must be able to retain U and/or Th and Pb, plus the respective intermediate daughter isotopes and it must be relatively widely distributed. 'Ages' calculated from equations and (13), (14) and (18) correspond to a single-stage evolutionary model of the U-Pb system with time. Sometimes this assumption is not justified

and multistage models are required. For further details the reader is referred to Gale & Mussett (1973). The 'ages' provide information on the assumption of a closed system for the U-Pb and Pb/Pb systems;

- if the three 'ages' are the same, within analytical error, the system is termed concordant and a simple Pb history with closed system behaviour is implied;
- if the 'ages' differ, the system is termed discordant and this must be taken as evidence for one or more of the assumptions being incorrect.

The usual explanation is that the system has not remained closed and that there has been loss or gain of U, Pb or an intermediate daughter, with respect to the system as a whole, since the rock/mineral formation.

The concordia diagram, after Wetherill (1956), can be used to highlight discordant behaviour. U-Pb data is plotted as $(\alpha - \alpha_0)/\mu$ vs. $(\beta - \beta_0)/\delta$ so that there is a direct comparison of the ^{238}U-^{206}Pb and ^{235}U-^{207}Pb decay schemes for a single system.

$$\frac{\alpha - \alpha_0}{\mu} = \frac{^{206}Pb^*}{^{238}U} = e^{\lambda_1 t} - 1 \quad (19)$$

$$\frac{\beta - \beta_0}{\delta} = \frac{^{207}Pb^*}{^{235}U} = e^{\lambda_2 t} - 1 \quad (20)$$

For concordant U-Pb systems, allowing t to vary from 0 to 4.57×10^9 will produce the locus of the concordia curve. Discordant U-Pb systems will lie off the concordia curve but still may lie along a straight line termed discordia. Discordancy can be useful in determining disturbances of U-Pb systems and evaluating the history of particular samples. For further details the reader is referred to Faure (1986). The classical interpretation of discordant ages by Wetherill (1956), based on studies of zircon crystals, is one invoking episodic Pb loss or U gain, but alternative models have been proposed suggesting continuous diffusion (Tilton, 1960; Wasserburg, 1963; Wetherill, 1963), dilatant release upon uplift and erosion (Goldich & Mudrey, 1972) and release as a result of chemical weathering (Stern et al., 1966). More complex and complete disturbance of U-Pb systems, without isotopic resetting, may result in open systems for which it is very difficult to obtain useful age information.

A.3: ERROR EXPRESSIONS

If a quantity R is defined such that;

$$R = f(\tau, \upsilon, \varpi, ...),$$

the uncertainty σ_R may be calculated from the standard deviation of the mean of each variable (σ_τ, σ_υ, σ_ϖ, ...), using the expression for propagation of errors;

$$\sigma^2_R = (\partial R/\partial\tau \times \sigma_\tau)^2 + (\partial R/\partial\upsilon \times \sigma_\upsilon)^2 + (\partial R/\partial\varpi \times \sigma_\varpi)^2 + ... \quad (21).$$

A.3.1: *ERRORS IN Pb ISOTOPE RATIOS*

The error in the corrected $^{206}Pb/^{204}Pb$, $^{207}Pb/^{204}Pb$ or $^{208}Pb/^{204}Pb$ ratios, σ_{M*}, is a combination of;

- $\pm \sigma_M$ errors from mass spectrometric measurement for a given ratio;
- $\pm \sigma_F$ errors from mass fractionation correction for the same ratio;
- $\pm$ Pb blank contribution.

σ_M errors are calculated from the measured isotopic ratios and the precision of the data acquired such that, if d is the precision in ‰ for the measured ratio (M);

$$\sigma_M = d \times M \times 10^{-3} \quad (22).$$

The mass fractionation correction (F), in percent per atomic mass unit (% amu^{-1}) with respect to the ^{204}Pb reference isotope, is defined as;

$$F = [(N - NBS)/NBS] \times (100/\Delta M) \quad (23).$$

Measurements of N at Oxford have both been based on the NBS 981 standard, published NBS values for which are taken from Catanzaro et al. (1968). Between 1988 and 1991, thirty-one analyses of NBS 981 on the Oxford VG54E mass spectrometer gave the measured ratios (N) and associated errors (σ_N) summarised in **Table Ab**.

Table Ab: NBS 981 data for Oxford VG54E between 04/07/88 and 24/09/91

RATIO	$\left(\frac{^{206}Pb}{^{204}Pb}\right)$	$\left(\frac{^{207}Pb}{^{204}Pb}\right)$	$\left(\frac{^{208}Pb}{^{204}Pb}\right)$	DATE
	16.904	15.449	36.552	04/07/88
	16.902	15.441	36.539	04/07/88
	16.916	15.465	36.618	05/08/88
	16.909	15.455	16.583	16/08/88
	16.914	15.456	36.592	20/09/88
	16.897	15.441	36.520	21/01/89
	16.885	15.430	36.509	22/03/89
	16.891	15.432	36.519	27/04/89
	16.907	15.450	36.561	04/05/89
	16.880	15.417	36.519	31/07/89
	16.896	15.438	36.514	05/09/89
	16.890	15.425	36.485	11/09/89
	16.898	15.436	36.523	25/09/89
	16.895	15.439	36.526	27/09/89
	16.896	15.434	36.515	28/09/89
	16.899	15.436	36.536	01/02/90
	16.896	15.441	36.539	14/02/90
	16.904	15.442	36.543	26/02/90
	16.895	15.434	36.517	27/02/90
	16.893	15.432	36.512	23/05/90
	16.892	15.425	36.487	24/05/90
	16.885	15.427	36.509	10/01/91
	16.888	15.428	36.508	10/01/91
	16.894	15.433	36.516	26/04/91
	16.897	15.433	36.531	04/07/91
	16.881	15.422	36.486	02/09/91
	16.882	15.417	36.472	06/09/91
	16.876	15.408	36.438	16/09/91
	16.890	15.425	36.496	19/09/91
	16.884	15.418	36.476	21/09/91
	16.881	15.417	36.471	24/09/91
No. values	19	19	19	
Average, N	16.8941	15.4337	36.5197	
σ_N	0.0098	0.0126	0.0364.	

The published ratios from Catanzaro et al. (1968) (NBS) and the associated errors, σ_{NBS}, are;

$$\left(\frac{^{206}Pb}{^{204}Pb}\right) = 16.9371 \pm 0.0053$$

$$\left(\frac{^{207}Pb}{^{204}Pb}\right) = 15.4913 \pm 0.0056$$

$$\left(\frac{^{208}Pb}{^{204}Pb}\right) = 36.7213 \pm 0.0134.$$

Note that Catanzaro et al. (1968) quote errors at the 2σ level. When equation (23) is applied to these results, F can be calculated for each isotopic ratio and an average taken for the Oxford VG54E mass spectrometer during the period of study. From the $^{206}Pb/^{204}Pb$ data, a value of $\pm$ 0.127% ($\pm$ 0.0007) amu^{-1} is obtained; from the $^{207}Pb/^{204}Pb$ data, a value of $\pm$ 0.124% ($\pm$ 0.0009) amu^{-1}; and from the $^{208}Pb/^{204}Pb$ data, a value of $\pm$ 0.138% ($\pm$ 0.0011) amu^{-1}. Averaging these three figures gives a value for F of $\pm$ 0.130% ($\pm$ 0.006) amu^{-1}. All errors are quoted here at the 1σ level. Note that F is positive when the heavier isotope is the numerator of the isotopic ratio under consideration and negative when it is the denominator.

The real error in F (σ_F) is dependent on the ratio under consideration and can be derived from equation (21). It may be expressed as;

$$\sigma_F = \sqrt{\left(\frac{100}{NBS \times \Delta M}\right)^2 \times \sigma^2_N + \left(\frac{100 \times N \times \Delta M}{(\Delta M \times NBS)^2}\right)^2 \times \sigma^2_{NBS}} \qquad (24).$$

σ_F values for the isotopic ratios under consideration are given in **Table Ac**.

If M is the measured Pb isotopic ratio for the sample, M* is the same ratio corrected for mass fractionation at F% amu^{-1}, that is $\pm$ 0.130% ($\pm$ 0.006) amu^{-1}. M* can thus be expressed as;

$$M^* = M + (F \times M \times \Delta M)/100 \qquad (25).$$

The associated error, σ_{M^*}, is dependent on the ratio under consideration and may be expressed as;

$$\sigma_{M^*} = \sqrt{\left(1 + \left(\frac{F}{100} \times \Delta M\right)\right)^2 \times \sigma^2_M + \left(\frac{M}{100} \times \Delta M\right)^2 \times \sigma^2_F} \qquad (26).$$

Table Ac: σ_F values for Pb isotopic ratios from Oxford NBS 981 data

RATIO	σ_F
$^{206}Pb/^{204}Pb$	0.0329
$^{207}Pb/^{204}Pb$	0.0297
$^{208}Pb/^{204}Pb$	0.0264
$^{206}Pb/^{207}Pb$	0.1023
$^{207}Pb/^{206}Pb$	0.1000
$^{208}Pb/^{207}Pb$	0.1291
$^{208}Pb/^{206}Pb$	0.0470
$^{204}Pb/^{206}Pb$	0.0328.

σ_{M^*} is computed for each Pb isotope ratio for each sample, such that;

$$\sigma_{M^*} \text{ for } \left(\frac{^{206}Pb}{^{204}Pb}\right) = \sqrt{\left(1.0052 \times \sigma_M{}^2\right) + \left(M^2 \times 4.32964 \times 10^{-7}\right)}$$

$$\sigma_{M^*} \text{ for } \left(\frac{^{207}Pb}{^{204}Pb}\right) = \sqrt{\left(1.0078 \times \sigma_M{}^2\right) + \left(M^2 \times 7.93881 \times 10^{-7}\right)}$$

$$\sigma_{M^*} \text{ for } \left(\frac{^{208}Pb}{^{204}Pb}\right) = \sqrt{\left(1.0104 \times \sigma_M{}^2\right) + \left(M^2 \times 1.115136 \times 10^{-6}\right)}$$

$$\sigma_{M^*} \text{ for } \left(\frac{^{206}Pb}{^{207}Pb}\right) = \sqrt{\left(0.9974 \times \sigma_M{}^2\right) + \left(M^2 \times 1.046529 \times 10^{-6}\right)}$$

$$\sigma_{M^*} \text{ for } \left(\frac{^{207}Pb}{^{206}Pb}\right) = \sqrt{\left(1.0026 \times \sigma_M{}^2\right) + \left(M^2 \times 1 \times 10^{-6}\right)}$$

$$\sigma_{M^*} \text{ for } \left(\frac{^{208}Pb}{^{207}Pb}\right) = \sqrt{\left(1.0026 \times \sigma_M{}^2\right) + \left(M^2 \times 1.666681 \times 10^{-6}\right)}$$

$$\sigma_{M^*} \text{ for } \left(\frac{^{208}Pb}{^{206}Pb}\right) = \sqrt{\left(1.0052 \times \sigma_M{}^2\right) + \left(M^2 \times 2.598544 \times 10^{-6}\right)}$$

$$\sigma_{M^*} \text{ for } \left(\frac{^{204}Pb}{^{206}Pb}\right) = \sqrt{\left(0.9948 \times \sigma_M{}^2\right) + \left(M^2 \times 4.30336 \times 10^{-7}\right)}.$$

The Pb blank in the Oxford Pb laboratory (see section A.4.1) has been maintained at a level ≤ 1 ng for the entire sample preparation and analysis procedure

throughout the period of investigation and thus by analysing samples of ≥ 1 μg Pb, such that the blank contributes less than 1% of the total Pb analysed, the effects of blank may be considered negligible. σ_{M*} represents, therefore, the 1σ error on the corrected isotopic ratio and these errors, expressed as a percentage of the mass fractionation corrected ratio, may then be used in regression of the best-fit line after the methods of York (1969) and Titterington & Halliday (1979). The Isoplot version 2.11 programme of Ludwig (1990) was used for this purpose.

A.3.2: *ERRORS IN U ISOTOPE RATIOS*

The error in the corrected $^{235}U/^{238}U$ ratio, σ_{M*}, is a combination of;

- $\pm \sigma_M$ errors from mass spectrometric measurement for $^{235}U/^{238}U$;
- $\pm \sigma_F$ errors from mass fractionation correction for $^{235}U/^{238}U$;
- ± U blank contribution.

σ_M errors are calculated from the measured isotopic ratios and the precision of the data acquired, such that if d is the precision in ‰ for the measured ratio (M);

$$\sigma_M = d \times M \times 10^{-3} \quad \text{(22 from above).}$$

The mass fractionation correction, F, in percent per atomic mass unit ($\%amu^{-1}$) with respect to the ^{238}U reference isotope is defined as;

$$F = [(N - NBS)/NBS] \times (100/\Delta M) \qquad \text{(23 from above).}$$

Measurements of N at Oxford have been based on the NBS U-500 standard, published NBS values for which are taken from Garner et al. (1971). Between 1990 and 1991, eight analyses of NBS U-500 on the Oxford VG54E mass spectrometer gave the measured ratios (N) and associated errors (σ_N) detailed in **Table Ad**.

The published ratio from Garner et al. (1971), NBS, and the associated error, σ_{NBS}, is;

$$\left(\frac{^{235}U}{^{238}U}\right) = 1.0003 \pm 0.0005.$$

Note that Garner et al. (1971) quote the error at the 2σ level.

Table Ad: NBS U-500 data for Oxford VG54E between 08/05/90 and 09/05/91

RATIO	$\left(\frac{^{235}U}{^{238}U}\right)$	DATE
	0.99000	08/05/90
	0.99001	08/05/90
	0.99094	08/05/90
	0.99892	31/05/90
	0.99983	31/05/90
	1.00211	25/06/90
	1.00345	10/07/90
	0.99081	09/05/91
No values	8	
Average, N	0.99576	
σ_N	0.0055	

When equation (23) is applied to these results, a value of F for the $^{235}U/^{238}U$ ratio can be calculated for the Oxford VG54E mass spectrometer during the period of study. A figure of - 0.132% (± 0.006) amu^{-1} is obtained, the error being quoted at the 1σ level.

The real error in F, σ_F, can be derived from equation (21). It may be expressed as;

$$\sigma_F = \sqrt{\left(\frac{100}{NBS \times \Delta M}\right)^2 \times \sigma^2_N + \left(\frac{100 \times N \times \Delta M}{(\Delta M \times NBS)^2}\right)^2 \times \sigma^2_{NBS}} \qquad \text{(24 from above).}$$

It can be simply shown that for $^{235}U/^{238}U$, $\sigma_F = 0.1840$.

If M is the measured $^{235}U/^{238}U$ for the sample, M* is the same ratio corrected for mass fractionation at F% amu^{-1}, that is - 0.132% (± 0.006) amu^{-1}. M* can thus be expressed as;

$$M^* = M + (F \times M \times \Delta M)/100 \quad \text{(25 from above).}$$

The associated error, σ_{M^*}, may be expressed as;

$$\sigma_{M^*} = \sqrt{\left(1 + \left(\frac{F}{100} \times \Delta M\right)\right)^2 \times \sigma^2_M + \left(\frac{M}{100} \times \Delta M\right)^2 \times \sigma^2_F} \qquad \text{(26 from above)}$$

and therefore;

$$\sigma_{M^*} \text{ for } \left(\frac{^{235}U}{^{238}U}\right) = \sqrt{\left(0.9921 \text{ x } \sigma_M{}^2\right) + \left(M^2 \text{ x } 3.04704 \text{ x } 10^{-5}\right)}.$$

The U blank in the Oxford laboratory facilities (see section **A.4.2**) is quoted at a level of 0.039 ± 0.01 ng for the complete procedure (Gale et al., 1980a) and thus by analysing samples with ≥ 5 ng U, such that the blank contributes less than 1% of the total U analysed, the effects of blank on the isotopic signal may be considered negligible. σ_{M^*} therefore represents the 1σ error on the corrected isotopic ratio and this error, expressed as a percentage of the mass fractionation corrected ratio, may then be used, as before, in the regression of the best-fit line after the methods of York (1969) and Titterington & Halliday (1979). The Isoplot version 2.11 programme of Ludwig (1990) was used for this purpose.

A.4: Pb AND U CONCENTRATIONS AND BLANKS

The isotope dilution equation (27) forms the basis for the calculation of Pb and U concentrations and also for the determination of Pb and U blanks.

$$X = \frac{Y}{W} \text{ x } C \text{ x } \frac{t_k}{A_t} \text{ x } \frac{A_u}{u_k} \text{ x } \left(\frac{T_{ik} - M_{ik}}{M_{ik} - U_{ik}}\right) \qquad (27).$$

This may be more simply expressed as;

$$X = \frac{Y}{W} \text{ x } C \text{ x } N \text{ x } \left(\frac{T_{ik} - M_{ik}}{M_{ik} - U_{ik}}\right) \qquad (28),$$

where $N = t_k A_u / A_t u_k$ and the other symbols are as previously defined.

A.4.1: *Pb CONCENTRATIONS AND BLANKS*

Masses of the Pb isotopes are taken from Wapstra & Bos (1977).

^{204}Pb:- 203.973037 atomic mass units
^{206}Pb:- 205.974455
^{207}Pb:- 206.975885
^{208}Pb:- 207.976641.

The atomic weight of Pb in the sample, A_u can be calculated from the expression;

$$A_u = \frac{\sum M^*_{ij} A_i}{\sum M^*_{ij}} \qquad (29),$$

where j is the reference isotope ^{204}Pb for isotope composition (IC) runs, i represents the isotopes ^{208}Pb, ^{207}Pb, ^{206}Pb and ^{204}Pb in turn, M* is the ratio i/j from the mass spectrometer (corrected for mass fractionation) and A_i represents the atomic masses of the four Pb isotopes in turn. Hence;

$$A_u = \frac{\left(\frac{^{208}Pb}{^{204}Pb}\right)^* \text{x } 207.976641 + \left(\frac{^{207}Pb}{^{204}Pb}\right)^* \text{x } 206.975885 + \left(\frac{^{206}Pb}{^{204}Pb}\right)^* \text{x } 205.974455 + 203.973037}{\left(\frac{^{208}Pb}{^{204}Pb}\right)^* + \left(\frac{^{207}Pb}{^{204}Pb}\right)^* + \left(\frac{^{206}Pb}{^{204}Pb}\right)^* + 1}$$

Taking ^{206}Pb as the reference isotope k for concentration calculations, u_k, the percent atomic abundance of k in the sample is given by;

$$u_k = \frac{\left(\frac{^{206}Pb}{^{204}Pb}\right)^*}{\left(\frac{^{208}Pb}{^{204}Pb}\right)^* + \left(\frac{^{207}Pb}{^{204}Pb}\right)^* + \left(\frac{^{206}Pb}{^{204}Pb}\right)^* + 1} \text{ x } 100$$

U_{ik} is the $\left(\frac{^{207}Pb}{^{206}Pb}\right)^*$ of the sample, corrected for mass fractionation.

M_{ik} is the $\left(\frac{^{207}Pb}{^{206}Pb}\right)^*$ of the sample/spike mixture, corrected for mass fractionation.

Details of the Pb spike solution used in Oxford, considering ^{206}Pb as the reference isotope (k) (April 1985 calibration), are;

- Atomic weight, A_t; 206.9757292
- Concentration, C; $10.26 \pm 0.005\ (1\sigma)$
- Atomic ratio T_{ik} corrected for mass fractionation at ± 0.130% amu^{-1} and the associated error, $\sigma_{T_{ik}}$;

$$\left(\frac{^{207}Pb}{^{206}Pb}\right)^* = 462.40837 \pm 0.4529\ (1\sigma)$$

$$\left(\frac{^{208}Pb}{^{206}Pb}\right)^* = 0.96409 \pm 0.00122\ (1\sigma)$$

$$\left(\frac{^{204}Pb}{^{206}Pb}\right)^* = 0.01188 \pm 0.00028\ (1\sigma)$$

- Percentage atomic abundance of isotope k in the spike, t_k; 0.21535.

Y and W have to be input from the measured weights of spike solution and isotope dilution (ID) sample aliquot.

Contaminant Pb blank was assumed to have the following composition after Gale et al. (1980a);

$$\left(\frac{^{206}Pb}{^{204}Pb}\right) = 18.40, \left(\frac{^{207}Pb}{^{204}Pb}\right) = 15.62, \left(\frac{^{208}Pb}{^{204}Pb}\right) = 38.60.$$

To obtain the Pb blank in μg Pb, using ^{206}Pb as the reference isotope (k), the following values have to be entered into equation (27) along with the spike information detailed above;

- A_u = 207.2095175
- u_k = 24.99321
- $U_{ik} = \left(\frac{^{207}Pb}{^{206}Pb}\right)$ of blank = 0.8489
- M_{ik} is the $\left(\frac{^{207}Pb}{^{206}Pb}\right)^*$ of the blank/spike mixture corrected for mass fractionation.
- Y has to be input from the weight of spike solution and W is negligible.

Data concerning the contaminant Pb blank in the Oxford Pb Isotope Laboratory between 1988 and 1991 is summarised in **Table Ae**. The procedure developed for Pb separation at Oxford involves four main stages;

a) - sample dissolution
b) - pass through large FEP column (2.25 cm^3 resin volume)
c) - 2 passes through small FEP column (0.3 cm^3 resin volume)
d) - sample loading

and where appropriate these have been specified in the table.

Table Ae: Pb blanks for the period 20/11/88 to 02/09/91

DATE	BLANK TYPE	BLANK (ng Pb)
20/11/88	small column (2 passes)	0.14328
20/11/88	small column (1 pass)	0.05564
20/01/89	small column (1 pass)	0.02475
20/01/89	large column (1 pass)	0.70650
26/01/89	small column (1 pass)	0.04519
26/01/89	small column (2 passes)	0.09112
26/01/89	large column (1 pass)	0.37453
10/04/89	Loading	0.00585
30/04/90	Total procedure	1.01202
30/04/90	Total procedure	0.67092
10/06/91	Total procedure	0.44537
10/06/91	Total procedure	0.39579
28/08/91	Total procedure	0.97658
02/09/91	Sample dissolution	0.12225

The average procedural Pb blank from 5 measurements is therefore 0.70 ± 0.30 ng. The assumed composition has been stated previously. Since the combined total procedure Pb blank is reproducibly ≤ 1 ng, for samples of ≥ 1 μg Pb, where the blank contributes ≤ 1% of the total Pb, the blank may be considered negligible.

A.4.2: *U CONCENTRATIONS AND BLANKS*

Masses of the U isotopes are taken from Wapstra & Bos (1977);

^{234}U:- 234.0409474 atomic mass units
^{235}U:- 235.043925247
(^{236}U:- 236.045562941)
^{238}U:- 238.050785782.

Taking ^{238}U as the reference isotope (k), u_k, the percentage atomic abundance of isotope k in the sample is; 99.2747.
The percentage atomic abundance of ^{235}U is; 0.7196.
The atomic weight of natural U in the sample is constant under normal conditions at the earth's surface, and A_u = 238.029.

The isotopic ratios relative to ^{238}U from the terrestrial abundances quoted by Barnes et al. (1972) are;

$$\left(\frac{^{234}U}{^{238}U}\right) = 0.000055001 \pm 0.0000002518\,(1\sigma)$$

$$U_{ik} = \left(\frac{^{235}U}{^{238}U}\right) = 0.007253 \pm 0.00000368\,(1\sigma).$$

Details of the U spike solution used in Oxford, considering ^{238}U as the reference isotope (k) (1976 calibration) are;

- Atomic weight, A_t; 235.049
- Concentration, C; $8.154 \pm 0.001\,(1\sigma)$
- Atomic ratio T_{ik} and associated error, $\sigma_{T_{ik}}$; $\left(\frac{^{235}U}{^{238}U}\right)^* = 539.8 \pm 2.0\,(1\sigma)$

  $\left(\frac{^{234}U}{^{238}U}\right)^* = 1.150 \pm 0.005\,(1\sigma)$

  $\left(\frac{^{236}U}{^{238}U}\right)^* = 1.040 \pm 0.004\,(1\sigma)$
- Percentage atomic abundance of isotope k in the spike, t_k; 0.1842.

The tri-*n*-butyl phosphate method of Arden & Gale (1974a) was used for U separation and the quoted blank for the complete procedure was 0.047 ng U for a sample size of 1-2 g. Gale et al. (1980a), using the same method and laboratory facilities, reported a procedural blank of 0.039 ± 0.01 ng U for the same order of sample size. U work undertaken in this study has also used the same tri-*n*-butyl phosphate method, laboratory facilities and similar sample weights so that the reported blanks could be quoted. For samples containing ≥ 5 ng U, where the blank contributes ≤ 1% of the total U, it may be considered a negligible source of error.

A.4.3: *ERRORS IN Pb AND U CONCENTRATIONS*

The error in the concentration (σ_X) can be calculated from expression (30), itself derived from expression (21) and equation (28);

$$\sigma_X^2 = \left[\left(\frac{X}{W}\right)^2 x\,\sigma_W^2\right] + \left[\left(\frac{X}{C}\right)^2 x\,\sigma_C^2\right] + \left[\left(\frac{X}{N}\right)^2 x\,\sigma_N^2\right] + \left[\left(\frac{X}{T_{ik} - M_{ik}}\right)^2 x\,\sigma_{T_{ik}}^2\right] +$$

$$\left[\left(\frac{X}{T_{ik} - M_{ik}} x \frac{U_{ik} - T_{ik}}{M_{ik} - U_{ik}}\right)^2 x\,\sigma_{M_{ik}}^2\right] + \left[\left(\frac{X}{M_{ik} - U_{ik}}\right)^2 x\,\sigma_{U_{ik}}^2\right] + \left[\left(\frac{X}{Y}\right)^2 x\,\sigma_Y^2\right] + \ldots.$$

σ^2_N is given by the following expression;

$$\sigma^2_N = \left(\frac{t_k}{A_t}\right)^2 x \left[\sigma^{2}_{\frac{A_u}{u_k}} + \left(N^2 x \sigma^{2}_{\frac{A_t}{t_k}}\right)\right] \qquad (31).$$

For Pb, ^{206}Pb is considered the reference isotope (k). Measurements of ID aliquot weight (Y) and spike solution weight (W) are taken to be accurate and therefore the associated errors are zero. C, σ_C, T_{ik}, $\sigma_{T_{ik}}$, M_{ik}, $\sigma_{M_{ik}}$, U_{ik}, $\sigma_{U_{ik}}$, N, t_k, A_t, u_k and A_u are all as previously defined. Hence;

$$\sigma^{2}_{\frac{A_u}{u_k}} = \left[\left(206.975885\sigma_a\right)^2 + \left(207.976641\sigma_b\right)^2 + \left(203.973037\sigma_c\right)^2\right] x\ 10^{-4}$$

$$\sigma^{2}_{\frac{A_t}{t_k}} = \left[\left(206.975885\sigma_{a'}\right)^2 + \left(207.976641\sigma_{b'}\right)^2 + \left(203.973037\sigma_{c'}\right)^2\right] x\ 10^{-4}$$

where a = ^{207}Pb/^{206}Pb for the sample, corrected for mass fractionation and a'=^{207}Pb/^{206}Pb for the spike, similarly corrected. b, c and b', c' refer to the corrected ^{208}Pb/^{206}Pb and ^{204}Pb/^{206}Pb ratios of the sample and spike respectively.

For U, ^{238}U is considered the reference isotope. The measurements of ID aliquot weight (Y) and spike solution weight (W) are again taken to be accurate and therefore the associated errors are zero. C, σ_C, T_{ik}, $\sigma_{T_{ik}}$, M_{ik}, $\sigma_{M_{ik}}$, U_{ik}, $\sigma_{U_{ik}}$, N, t_k, A_t, u_k and A_u are all as previously defined for U and;

$$\sigma^{2}_{\frac{A_u}{u_k}} = \left[\left(\ 234.0409474\sigma_d\ \right)^2 + \left(\ 235.043925247\sigma_e\ \right)^2\right] x\ 10^{-4}$$

$$\sigma^{2}_{\frac{A_t}{t_k}} = \left[\left(234.0409474\sigma_{d'}\right)^2 + \left(235.043925247\sigma_{e'}\right)^2 + \left(236.045562941\sigma_f\right)^2\right] x\ 10^{-4}$$

where d and d' are the mass fractionation corrected ^{234}U/^{238}U ratios for the sample and spike respectively, e and e' the ^{235}U/^{238}U ratios and f the ^{236}U/^{238}U ratio for the spike. ^{236}U is not a significant constituent of natural U.

A.5: μ VALUES, δ VALUES AND ASSOCIATED ERRORS

The μ value is defined as the atomic ratio ^{238}U/^{204}Pb. If α, β and γ are the measured ^{206}Pb/^{204}Pb, ^{207}Pb/^{204}Pb and ^{208}Pb/^{204}Pb ratios for the sample, corrected for mass fractionation, and X_U and X_{Pb} are the U and Pb concentrations, the μ value can be expressed, using ^{238}U and ^{204}Pb as reference isotopes, in the following manner;

$$\mu = \frac{\left(\frac{u_k}{A_u} \text{ x } X\right)_{\text{uranium}}}{\left(\frac{u_k}{A_u} \text{ x } X\right)_{\text{lead}}}$$

$$= \frac{99.2747}{238.029 \text{ x } 100} \text{x} \frac{X_U}{X_{Pb}} \text{x} \left[(203.973037) + (205.974455\alpha) + (206.975885\beta) + (207.976641\gamma)\right] \quad (32).$$

If σ_α, σ_β and σ_γ are the errors in α, β and γ and H is the term in square brackets in expression (32), the following expression for σ_μ (33) can be derived from expression (21), such that;

$$\sigma^2_\mu = \left(\frac{99.2747 \text{ x } H}{238.029 \text{ x } 100 \text{ x } X_{Pb}}\right)^2 \sigma^2_{X_U} + \left(\frac{99.2747 \text{ x } H \text{ x } X_U}{238.029 \text{ x } 100 \text{ x } (X_{Pb})^2}\right)^2 \sigma^2_{X_{Pb}}$$
$$+ \left[\left(\frac{99.2747 \text{ x } X_U}{238.029 \text{ x } 100 \text{ x } X_{Pb}}\right)^2 \text{x} \left((205.974455\sigma_\alpha)^2 + (206.975885\sigma_\beta)^2 + (207.976641\sigma_\gamma)^2\right)\right].$$

The δ value is defined as the atomic ratio $^{235}U/^{204}Pb$ and using ^{235}U and ^{204}Pb as reference isotopes with other nomenclature the same;

$$\delta = \frac{\left(\frac{u_k}{A_u} \text{ x } X\right)_{\text{uranium}}}{\left(\frac{u_k}{A_u} \text{ x } X\right)_{\text{lead}}}$$

$$= \frac{0.7196}{238.029 \text{ x } 100} \text{x} \frac{X_U}{X_{Pb}} \text{x} \left[(203.973037) + (205.974455\alpha) + (206.975885\beta) + (207.976641\gamma)\right] \quad (34)$$

The associated error (σ_δ) can be calculated from the following expression (35);

$$\sigma^2_\delta = \left(\frac{0.7196 \text{ x } H}{238.029 \text{ x } 100 \text{ x } X_{Pb}}\right)^2 \sigma^2_{X_U} + \left(\frac{0.7196 \text{ x } H \text{ x } X_U}{238.029 \text{ x } 100 \text{ x } (X_{Pb})^2}\right)^2 \sigma^2_{X_{Pb}}$$
$$+ \left[\left(\frac{0.7196 \text{ x } X_U}{238.029 \text{ x } 100 \text{ x } X_{Pb}}\right)^2 \text{x} \left((205.974455\sigma_\alpha)^2 + (206.975885\sigma_\beta)^2 + (207.976641\sigma_\gamma)^2\right)\right].$$

A.6: MODEL μ_1 VALUES AND ASSOCIATED ERRORS

The calculation of model μ_1 values and their associated errors is based on the formulae presented in Ludwig (1980) and the treatment given by Eglington & Harmer (1989). The model μ_1 value may be thought of as the $^{238}U/^{204}Pb$ ratio of a source

normalised for U decay to the present day. It is calculated by simultaneously considering the t Ma isochron obtained from the regressed isotope data with the geochron at t Ma and solving for model μ_1 as shown in **Figure A.6.1**.

Figure A.6.1: Calculation of model μ_1 value

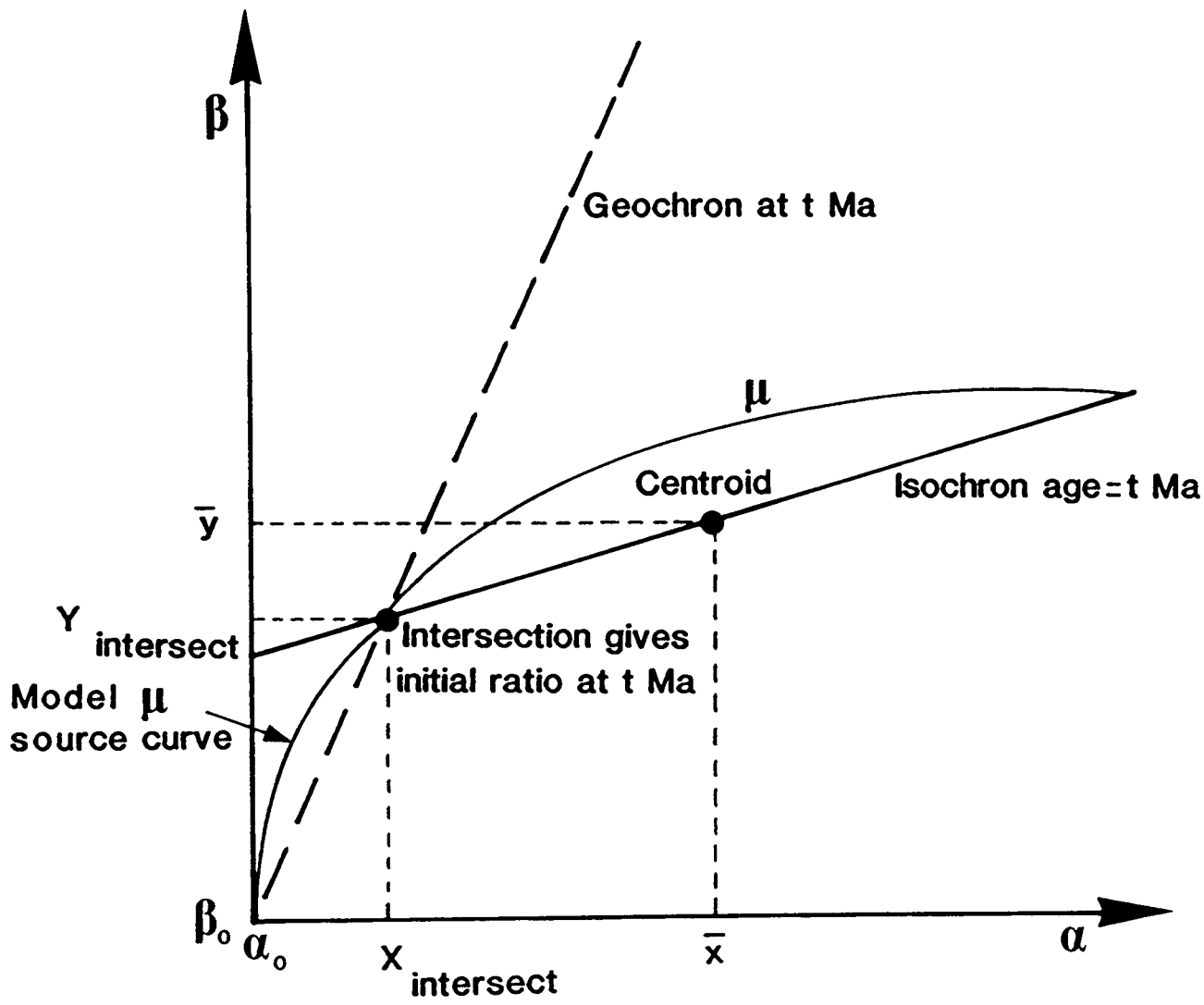

The Pb/Pb diagram has coordinates with y-axis $^{207}Pb/^{204}Pb$ (β) and x-axis $^{206}Pb/^{204}Pb$ (α). μ value curve coordinates can be represented as;

$$x = \alpha_o + \mu\left(e^{\lambda_1 T} - e^{\lambda_1 t}\right) = f_x(\mu) \qquad (36)$$

$$y = \beta_o + \frac{\mu}{137.88}\left(e^{\lambda_2 T} - e^{\lambda_2 t}\right) = f_y(\mu) \qquad (37)$$

where;

λ_1 = decay constant for ^{238}U

λ_2 = decay constant for ^{235}U

T = initial age of source

t = isochron/errorchron age

α_o, β_o = initial $^{206}Pb/^{204}Pb$ and $^{207}Pb/^{204}Pb$ ratios at T.

The gradient of the geochron at t Ma (m) is obtained by simple differentiation;

$$m = \frac{\partial f_y(\mu)}{\partial f_x(\mu)} = \frac{\left(e^{\lambda_2 T} - e^{\lambda_2 t} \right)}{137.88\left(e^{\lambda_1 T} - e^{\lambda_1 t} \right)} \quad (38)$$

enabling the equation of the geochron at t Ma to be written as;

$$f_y(\mu) = m\ f_x(\mu) + c.$$

The β-intercept, c, of the geochron at t Ma is given by;

$$c = \beta_o + \frac{\mu\left(e^{\lambda_2 T} - e^{\lambda_2 t} \right)}{137.88} - m\left[\alpha_o + \mu\left(e^{\lambda_1 T} - e^{\lambda_1 t} \right) \right] \quad (39).$$

The best-fit line for the isochron may be represented as $y = m'x + c'$, for which the gradient (m') and β-intercept (c') are obtained from the Isoplot data regression. The isochron and geochron intersect where;

$$m' x_{intercept} + c' = m x_{intercept} + c$$

and so;

$$x_{intercept} = (c' - c) / (m - m') \quad (40).$$

This represents the initial $^{206}Pb/^{204}Pb$ ratio of the source at time t and may be substituted into equation (36) as x to calculate model μ_1. Note that this calculation will depend on the model chosen for Pb evolution. The standard single-stage model infers $T = 4.57 \times 10^9$ yr, $\alpha_o = 9.307$ and $\beta_o = 10.294$ (Tatsumoto et al., 1973), while the most common two-stage model, that of Stacey & Kramers (1975), infers $T = 3.7 \times 10^9$ yr, $\alpha_o = 11.152$ and $\beta_o = 12.998$. The single-stage model has been used throughout this study unless otherwise stated. Alternatively, one may make an initial estimate of model μ_1, derive expressions for m and c to give a value for $x_{intercept}$ as above and then calculate a new value for model μ_1, repeating the iteration until successive estimates of model μ_1 fall within the required precision.

If $\bar{x}$ and $\bar{y}$ are the coordinates of the centroid of the best-fit line ($y = m'x + c'$), and $\sigma_{m'}$ and $\sigma_{c'}$ are the 1σ errors in the slope and y-intercept, the errors on the model μ_1 value are calculated from the intersection of the error envelope for the isochron

with the calculated model μ_1 source curve. Errors in model μ_1 value and age are usually quoted at the 2σ level (95% confidence limits). m and c are as previously defined for the geochron.

Ludwig (1980) showed that for an error estimate μ_a, an improved estimate (μ_b) may be calculated in the following manner;

$$m = \frac{\partial f_y(\mu_a)}{\partial f_x(\mu_a)}$$

$$m = \frac{\left(e^{\lambda_2 T} - e^{\lambda_2 t}\right)}{137.88\left(e^{\lambda_1 T} - e^{\lambda_1 t}\right)} \qquad \text{(38 above)}$$

$$f_y(\mu) = m\ f_x(\mu) + c$$

$$c = \beta_o + \frac{\mu_a\left(e^{\lambda_2 T} - e^{\lambda_2 t}\right)}{137.88} - m\left[\alpha_o + \mu_a\left(e^{\lambda_1 T} - e^{\lambda_1 t}\right)\right] \qquad \text{(39 above)}$$

$$D = 2\left[(c - c')(m - m') + \bar{x}\,\sigma_{m'}{}^2\right] \qquad (41)$$

$$E = (m - m')^2 - \sigma_{m'}{}^2 \qquad (42)$$

$$V = (c - c')^2 - \sigma_{c'}{}^2 \qquad (43)$$

$$x \text{ of } \mu_b = \frac{-D \pm \sqrt{D^2 - 4EV}}{2E} \qquad (44)$$

Hence, μ_b may be calculated by substituting for x in expression (36). Entering the new μ_b value in expression (39), with m as before, allows iterative solution of a more precise estimate of model μ_1 error by following steps (41), (42), (43) and (44). This iterative procedure can proceed until the required level of precision is achieved.

A.7: YORKFITS OF DATA

The term 'Yorkfit' refers to a linear data regression following the algorithm developed by York (1969), where each point is weighted according to both its x-error and y-error and the x-y error correlation is also taken into consideration In this study, Yorkfits were performed using the Isoplot package of Ludwig (1990) (version 2.11) which, in addition to York's original algorithm, contains modified treatments

for use with differing data types and excess data scatter (termed models). All models use the decay constants published in Steiger & Jäger (1977).

Model 1 Yorkfits use the original algorithm of York (1969) and assume that the data scatter from a straight line is solely attributable to the assigned errors (calculated using equations in **A.3**). This approach has been used where the MSWD of the regressed data is less than 2.5, that is for isochrons rather than errorchrons (MSWD > 2.5). Errors on model 1 dates are quoted at the 2σ level (95% confidence limits) and calculated using the maximum likelihood method of Titterington & Halliday (1979). Since Pb/Pb and U-Pb errors are always highly correlated, a value of 0.9 has been used for the model 1 correlation coefficient.

Model 2 Yorkfits assign equal weights and zero error correlation to each point. Although this approach is seldom realistic, it avoids weighting points according to analytical errors when some other geological cause of scatter is involved. This approach has been used where the MSWD of the regressed data is greater than 2.5 (errorchrons) and, in fact, the majority of Pb/Pb dates in this study are from model 2 Yorkfits. Errors are quoted at the 2σ level (95% confidence limits).

Model 3 Yorkfits assume data scatter is part due to assigned errors and part due to an unknown, normally-distributed variation in initial isotopic ratio. This approach has been used for U-Pb data where excess data scatter (MSWD > 2.5) suggests that initial ratio variation may have been a significant factor. All errors are quoted at the 2σ level.

Appendix B:

ANALYTICAL METHODS

B.1: INTRODUCTION

U and Pb chemical separations were performed in an overpressured clean room off the main Age Laboratory, Department of Earth Sciences, Oxford. Extensive precautions were taken to minimise contamination during the entire analytical procedure of sampling, sample preparation, chemical separation of elements, filament loading and mass spectrometric isotope ratio determination.

The clean room has a unidirectional air flow system so that incoming air is always drawn from within the main department building and cleaned via a series of coarse particulate, fine particulate and activated charcoal filters. Air is subsequently ejected from the overpressured clean room through a double door system into the main Age Laboratory. Evaporation work was performed in PFA Teflon® evaporation vessels beneath 250W bulbs mounted within a fume cabinet. A HNO_3-H_2O scrubbing system was used to further purify the air passed over the samples during

evaporation. Clean terylene labcoats, overshoes and, where necessary, caps and plastic disposable gloves were worn during geochemical work.

B.2: CONSUMABLES AND EQUIPMENT

B.2.1: *REAGENTS*

Pure and ultra-pure reagents were used during sample preparation, elemental separations and filament loading. HBr was first prepared by triple sub-boiling distillation in quartz vessels, after methods described by Mattinson (1972) and Kuehner et al. (1972), and then further purified to an ultra-pure state using a two-bottle Teflon® still comprising perfluoroalkali (PFA) bottles with polytetrafluoroethylene (PTFE) necks. HCl and H_2O were each prepared in two states of purification; as pure reagents using triple sub-boiling distillation in quartz vessels and as ultra-pure reagents after further purification in a two-bottle Teflon® still, as above. HNO_3 was prepared by triple sub-boiling distillation in quartz vessels and HF in a two-bottle Teflon® still alone. Reagent molarity was adjusted by combination of pure or ultra-pure acid with H_2O of the equivalent purity. 'Aqua Regia' is a 3:1 mixture of HCl:HNO_3 in their most concentrated states.

Pb contamination of the reagents was determined by isotope dilution and the results are shown in **Table Ba**, along with values obtained by Abranches (1977) and Arden & Gale (1974b) for Oxford reagents. Since carbonate samples analysed in this work contained significantly higher concentrations of Pb and U than the meteoritic materials analysed in the other studies, it was not necessary to repeat the extremely low levels of contamination produced during their work.

Total procedural Pb and U blanks were 0.70 ± 0.60 ng and 0.039 ± 0.020 ng respectively, the errors representing $2\sigma_{mean}$. Throughout this work, the analytical Pb and U blank contamination was ≤ 1% of the Pb and U extracted from the sample and therefore its contribution was assumed negligible.

Table Ba: Comparison of calculated reagent Pb blanks with previous values for Oxford studies

REAGENT	QUANTITY	Pb CONTAMINATION			
	(ml)	(ng)	($ngml^{-1}$)		
		A	A	B	C
H_2O - pure	10	0.12	0.012	—	—
H_2O - ultra-pure	10	0.089	0.0089	0.0032	<0.0071
HCl -pure	10	0.34	0.034	—	—
HCl - ultra-pure	10	0.053	0.0053	0.0046	<0.022
HBr - ultra-pure	10	0.36	0.036	—	—
HNO_3 - pure	10	0.98	0.098	0.0059	<0.0082

A - this study; B - Abranches (1977); C - Arden & Gale (1974b)

B.2.2: *SAMPLE BEAKERS AND COLUMNS*

Sample dissolutions were performed in cleaned, 15 ml PFA Teflon® screw-top beakers. Similar 7 ml vials were used during chemical separation of U and Pb. All beakers were number-stamped for identification purposes. Before their initial use, and after each subsequent use, the PFA Teflon® beakers were wiped out with acetone and tissues, then immersed in concentrated AnalaR® HNO_3 and heated to 60°C for 24 hours. Next they were rinsed in distilled, de-ionised water, transferred to concentrated AnalaR® HCl, heated to 60°C for a further 24 hours and finally rinsed with pure H_2O. The quoted Pb impurity limit for both AnalaR® HCl and HNO_3 is 0.05 ppm. As a final cleaning step, 5 ml of ultra-pure 6M HCl was placed in each beaker, the screw-top fitted and the beaker allowed to reflux under evaporators for 30 minutes, before finally being rinsed with ultra-pure H_2O. All future references to 'pure' and 'ultra-pure' reagents imply the levels of Pb contamination detailed in **Table Ba**.

The columns used for the chemical separation of U and Pb were made from heat-shrink PTFE tubing. An aluminium former was machined to the required internal column dimensions and design (see overleaf) and heated in a furnace at 370°C for 90 seconds. A length of PTFE tubing was placed carefully over the former, and the apparatus returned to the furnace until the tubing exceeded its crystalline melting point of 327°C and became transparent (usually around 3 minutes). At

this point, the former and tubing were removed from the furnace and quenched under cold, running water to facilitate easy removal of the column. Columns were initially cleaned in concentrated AnalaR® HNO_3 and heated to 60°C for 24 hours, before being washed in distilled, de-ionised water and transferred to concentrated AnalaR® HCl at 60°C for a further 24 hours. Finally, the columns were rinsed in pure H_2O and fitted with porous polyethylene frits (maximum pore size 95 μm) that had been ultrasonically agitated in acetone.

Two sizes of column were required;

- a design capable of holding 2.25 cm^3 of anion exchange resin, with a resin length to diameter ratio of 13, was manufactured from heat-shrink PTFE 1/4" tubing. The total column volume was 3.11 cm^3.

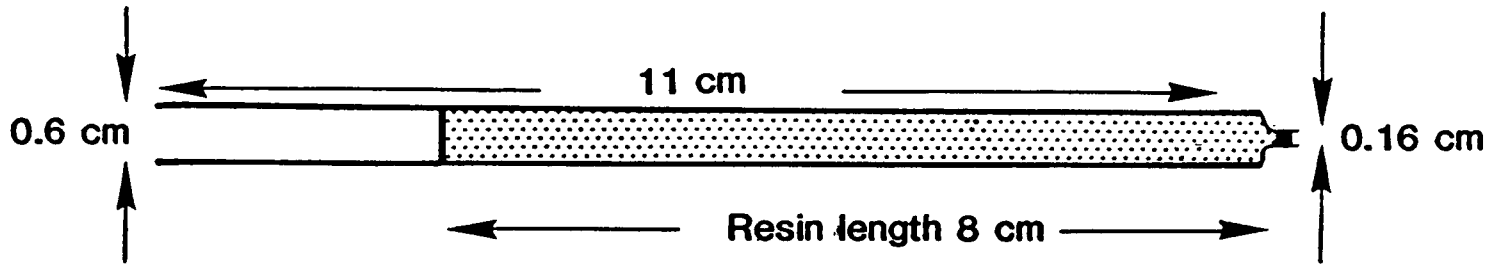

Only the portion of the column designed to hold the porous frit was allowed to fully shrink to the quoted post-heating internal diameter of 0.16 cm. This column type was used for U separation and for the first stage of the Pb separation procedure.

- a design capable of holding 0.3 cm^3 of resin, with a resin length to diameter ratio of 6 (the minimum for efficient fluid flow), was made from heat-shrink PTFE 1/2" tubing. The total column volume was 2.5 cm^3.

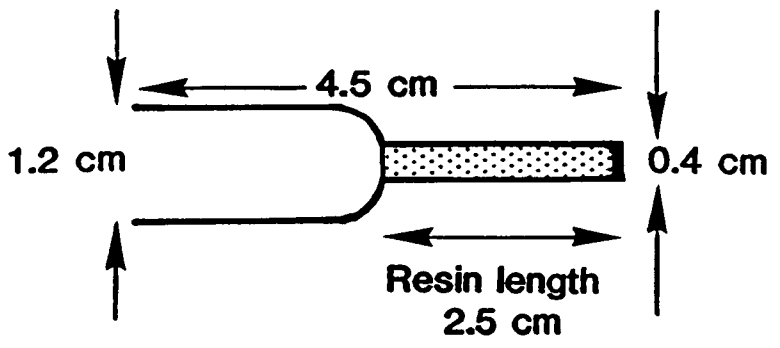

While the diameter of the solution well was only slightly smaller than the original diameter of 1.27 cm, the section for the resin was allowed to shrink to 0.4 cm. This column type was used for the second and third stages of the Pb separation procedure.

B.3: ANALYTICAL DETAILS

B.3.1: *SAMPLE PREPARATION AND DISSOLUTION*

Hand specimens were broken into smaller fragments, between 0.8 and 2.0 g in weight, using a cleaned bolster chisel and hammer on a cleaned steel plate. Weathered surfaces and visually altered material were physically removed from the small fragments. After each hand specimen had been broken, the hammer, steel plate and bolster chisel blade were first cleaned using a power drill fitted with wire brush attachment and then wiped with acetone on a tissue to avoid cross contamination. The outer surface of each fragment was ground away using a diamond-studded grinding wheel, lubricated with pure H_2O. The grinding wheel was cleaned with carborundum and pure H_2O after each common set of fragments.

A series of empty, cleaned PFA Teflon® 15 ml beakers were weighed and the beaker numbers and weights recorded. The sample fragments were washed in ultra-pure H_2O and dried under the evaporators. The beakers were then re-weighed containing the samples and the coarse sample weights calculated.

Dissolution of the carbonate fractions of the samples was accomplished using ultra-pure HCl. 3 ml were placed in each beaker, the screw-top refitted and the solution allowed to react until neutral. Ultra-pure 6M HCl was then added, 1 ml at a time, until the reaction had gone to completion and all of the carbonate fraction dissolved. Between each addition of 6M HCl, the screw-top was loosely fitted on the beaker to allow the generated CO_2 to escape without loss of sample solution. Dissolution of samples using various molarities of ultra-pure HBr, HNO_3 and perchloric acid was found to be more problematic and less effective than using HCl.

The solutions were allowed to settle for 24 hours before each supernate was transferred to a numbered 15 ml, non-rimmed centrifuge tube. The tubes were covered in Parafilm® and centrifuged at 3500 rpm for 15 minutes. Any settled residue was slightly disturbed and the solutions then centrifuged for a further 15 minutes at 3500 rpm. This centrifuging stage improved the efficiency of solution flow through the anion exchange resin by removing the majority of fine particulate materials. The clear supernates were very carefully transferred to a further set of cleaned, numbered 15 ml beakers using 1.5 ml PTFE Teflon® dropper pipettes and the residues from the centrifuge tubes were washed with ultra-pure water and returned to their original dissolution beakers. The centrifuge tubes were cleaned

out with acetone and tissues, rinsed with pure H_2O and stored in pure 0.1M HCl until needed again. Frequently, impure carbonate samples required centrifuging for longer than 15 minutes.

Dissolution beakers and their HCl-insoluble contents were evaporated down to dryness and weighed, allowing the weight of residue and therefore the weight of dissolved sample to be calculated. As required, these residues (predominantly silicates and non-identified organic materials) were also dissolved using 2.5 ml of pure concentrated HF. Samples were held overnight at 60°C in an aluminium heating block, allowed to cool and evaporated to dryness before being taken up in 2.0 ml of ultra-pure 6M HCl, evaporated to dryness again and finally converted to the bromide form by solution in 1 ml of ultra-pure 0.5M HBr. In this state, they could either be separately analysed or recombined with the corresponding HCl-soluble fraction.

If determination of elemental concentrations was required, a set of cleaned 7 ml PFA Teflon® beakers were spiked for either U and Pb or for Pb alone (as required) and the beaker numbers and spike weights noted. Isotopic compositions and concentrations for the U and Pb spikes in use at Oxford are detailed in **Appendix A**, along with the associated errors. The 15 ml beakers containing the centrifuged supernates were weighed, the weight of each sample solution calculated and an aliquot of approximately 25% pipetted to the spiked 7 ml beakers for isotope dilution (ID) chemistry. The 15 ml beakers containing the remaining 75% of sample solution for isotopic composition (IC) determination were then reweighed and the exact weight of the ID and IC solution aliquots calculated. These measurements could be easily translated into equivalent weights of HCl-soluble sample.

B.3.2: *CHEMICAL PROCEDURE FOR SEPARATION OF Pb*

IC sample solutions were evaporated down to dryness in the chloride form and converted to the bromide form by solution in 1.5 ml of ultra-pure 0.5M HBr. The ID samples were similarly converted to the bromide form in 1.0 ml of ultra-pure 0.5M HBr.

A set of the larger PTFE columns were prepared in the following manner for Pb separation. Analytical grade anion-exchange resin, AG® 1-X8, 100-200 mesh chloride form was used for Pb separations. PTFE columns were washed with 2 x 3 ml of pure 6M HCl, rinsed with 2 x 3 ml of pure H_2O and loaded with 2.25 cm^3 anion

exchange resin, suspended in pure H_2O. The resin was washed with 1 ml of ultra-pure 3M HCl, 2 x 1 ml of ultra-pure 6M HCl, 1 ml of ultra-pure 3M HCl and 2 x 1 ml of ultra-pure H_2O. The wash procedure was then repeated. Finally, the resin was cleaned with 2 x 1 ml of pure 0.25M HNO_3, rinsed with ultra-pure H_2O until neutral and equilibrated with 2 x 1 ml of ultra-pure 0.5M HBr.

IC sample solutions were loaded onto the large columns from clean PTFE Teflon® dropper pipettes and then washed with 5 x 1 ml of ultra-pure 0.5M HBr. The wash solutions were discarded. A new set of cleaned 7 ml PFA beakers were placed beneath the columns and the Pb samples eluted with 3 x 1 ml and 1 x 0.5 ml of ultra-pure 6M HCl. These solutions were evaporated down to dryness and reconverted to the bromide form by solution in 0.3 ml of ultra-pure 0.5M HBr. The large columns were washed out with acetone and pure H_2O to remove all resin and then reprepared as required. ID sample solutions spiked for Pb alone were treated exactly in the same fashion. For ID sample solutions spiked for Pb and U, all wash solutions were collected in a fresh set of clean, numbered 7 ml PFA beakers and these were set aside for subsequent U separation. In all other respects, the procedure was identical.

A set of the smaller PTFE columns were then prepared for the two-stage clean-up of Pb that had been separated using the larger columns. AG® 1-X8 anion exchange resin was again used. PTFE columns were washed with 2 x 2.5 ml of pure 6M HCl, rinsed with 2 x 2.5 ml of pure H_2O and loaded with 0.3 cm^3 anion exchange resin suspended in pure H_2O. The resin was washed with 0.5 ml of ultra-pure 3M HCl, 1 ml of ultra-pure 6M HCl, 0.5 ml of ultra-pure 3M HCl and 1 ml of ultra-pure H_2O. The resin wash procedure was then repeated. Finally, the resin was cleaned with 1 ml of pure 0.25M HNO_3, rinsed with ultra-pure H_2O until neutral and equilibrated with 0.5 ml of ultra-pure 0.5M HBr.

The IC sample solutions in the 7 ml PFA beakers were loaded onto the small columns using clean Teflon® dropper pipettes and washed with 5 x 0.2 ml of ultra-pure 0.5M HBr. The wash solutions were discarded. A new set of cleaned 7 ml PFA beakers were placed beneath the columns and the Pb samples eluted with 5 x 0.2 ml of ultra-pure 6M HCl. These solutions were evaporated down to dryness and reconverted to the bromide form by solution in 0.2 ml of ultra-pure 0.5M HBr. The small columns and resin were reconstituted for the second clean-up phase by washing the resin with 1 ml of ultra-pure H_2O, cleaning with 1 ml of pure 0.25M HNO_3, rinsing with ultra-pure H_2O until neutral and equilibrating with 0.5 ml of ultra-pure

0.5M HBr. At this point, the sample solutions were loaded onto the corresponding PTFE column used in the first stage and washed with 5 x 0.2 ml of ultra-pure 0.5M HBr. The wash solutions were discarded and the Pb samples eluted with 5 x 0.2 ml of ultra-pure 6M HCl into the corresponding 7 ml PFA beakers.

These solutions were evaporated down to incipient dryness, treated with 0.05 ml of 'Aqua Regia' solution and evaporated to hard dryness. The IC samples were then ready to load onto filaments for mass spectrometric analysis (see loading procedure, section **B.4.1**). To remove all of the old resin, the small PTFE columns were washed out with acetone and pure H_2O and reprepared as required.

Pb ID samples were prepared in exactly the same fashion.

B.3.3: *CHEMICAL PROCEDURE FOR SEPARATION OF U*

The separation of U from the ID wash solutions that had been set aside previously, was based on the method described by Arden & Gale (1974a). The bromide solutions were evaporated down to dryness and converted to the nitrate form by solution in 2 ml of concentrated pure HNO_3. Evaporation was repeated, the samples taken up in 1 ml of concentrated pure HNO_3, evaporated to dryness again and finally taken into solution with 1.5 ml of pure 5.5M HNO_3.

0.5 g of 40-60 mesh PTFE powder was weighed out separately for each PTFE column and combined with 0.15 ml of tri-*n*-butyl phosphate (TBP) solution. After mixing well with a PTFE Teflon® rod, the suspension was slurried into cleaned large columns with ultra-pure water. Powders were first packed down with the rod to remove any air bubbles and then the columns were prepared for U separation by washing with 2 x 1 ml of pure 5.5M HNO_3, adding ultra-pure H_2O until neutral and finally equilibrating with 5 x 0.5 ml of pure 5.5M HNO_3. Sample solutions were loaded onto the PTFE columns using PTFE Teflon® dropper pipettes and washed with 3 x 0.5 ml of pure 5.5M HNO_3. A fresh set of cleaned 7 ml PFA beakers was placed beneath the columns and the U eluted with 6 x 0.5 ml of ultra-pure H_2O. Samples were evaporated to dryness and taken up in 0.5 ml of pure 5.5M HNO_3.

After the same PTFE columns had been reconstituted with 5 x 0.5 ml of pure 5.5M HNO_3, the solutions were reloaded and the washing and elution steps repeated. Samples were collected in the corresponding 7 ml PFA beakers and evaporated to hard dryness. In this state, the samples were ready for loading onto filaments

prior to analysis.

The procedures described above require the use of a large number of beakers and it is essential to maintain clear records to keep track of which numbered beakers are in use at each stage and which samples they contain.

B.4: MASS SPECTROMETRY

Pb and U analyses were performed on a fully automated VG Isomass 54E mass spectrometer fitted with a single Faraday cup. The original specification had been upgraded by addition of an ultra-low noise Keithley 642 electrometer remote head. A Hewlett Packard 9845B computer was used to run the analytical software written by P.N.Taylor and modified by J.Russell and C.E.Jones.

B.4.1: *MASS SPECTROMETRY OF Pb*

Pb IC and ID samples were loaded onto outgassed single rhenium filaments for isotopic analysis. The entire loading procedure took place in a laminar flow cabinet to minimise contamination. The sample was taken up in 3 μl of ultra-pure 0.1M HNO_3 and allowed to dissolve into the nitrate form. 4 μl of ultra-pure 0.25M H_3PO_4 was loaded dropwise onto the centre of the filament from a fixed volume 1 μl pipette fitted with disposable tips and evaporated gently to half volume. 4 μl of silica gel, prepared from high purity silicon tetrachloride (Barnes et al., 1973) and washed in ultra-pure 5M HNO_3 to remove cation impurities (Tera & Wasserburg, 1975), was loaded on top of the H_3PO_4 and again evaporated gently to half volume. The sample was loaded into the silica gel/H_3PO_4 mixture and evaporated slowly to hard dryness, ready for analysis.

The filament loading blank was measured as 0.006 ng, identical to that reported by Abranches (1977) for the Oxford laboratory (0.006 ng). This loading blank contributes just 0.9% towards the total procedure blank of 0.70 ± 0.30 ng, itself negligible for Pb samples of ≥ 1 μg.

In the mass spectrometer, filament currents were slowly raised over 15 minutes to the target current of 2.45 A. A scan routine located and centred the relevant isotope beam and then the programme slowly raised the filament current, re-centering the beam after each turn-up sub-routine, until the desired intensity for

data collection was achieved. Data was collected using the Faraday cup. Each data block constituted the average of 15 sets of isotope ratios. ^{204}Pb, ^{206}Pb, ^{207}Pb and ^{208}Pb beams were each integrated over 5 seconds and corrected for a background noise contribution that was measured 30 times during each block. After each data block the filament current was adjusted to re-establish the optimum beam intensity, the beam refocused and additional data collected and statistically combined until, either the desired precision for the measured ratios was achieved, or the maximum filament current allowed (usually 3.6A) was exceeded. For ID samples, precision of 1% of the measured ratio was acceptable, while for IC samples, precision of greater than 0.18 ‰ was desired for all ratios. This procedure, and the reagent volumes indicated, achieved stable Pb ion emission in the mass spectrometer.

Nineteen analyses of the NBS 981 standard solution between 04/07/88 and 24/09/91 gave mass fractionation corrections (F) for $^{206}Pb/^{204}Pb$, $^{207}Pb/^{204}Pb$ and $^{208}Pb/^{204}Pb$ ratios of ± 0.127 (± 0.0014), ± 0.124 (± 0.0018) and ± 0.138 (± 0.0022)% per atomic mass unit, respectively (errors at 2σ level). Details of the analytical results and calculation of the mass fractionation correction, plus associated errors, are described in **Appendix A.3.1**. The average value for F of ± 0.130% ± 0.012 (2σ) amu^{-1} was adopted for Pb samples analysed during this study.

B.4.2: *MASS SPECTROMETRY OF U*

U ID analyses were also made using the VG Isomass 54E Faraday cup collector. It was not found necessary to use the Daly scintillation detection system. The loading procedure of Kakazu et al. (1981), itself adapted from that of Arden & Gale (1974a), was adopted and flat single rhenium filaments were used. 0.1 g of graphite (Aquadag) was mixed with 10 ml of ultra-pure H_2O and agitated so that a colloidal suspension was produced. 8 µl of this suspension was loaded across the entire upper surface of the rhenium filament and evaporated gently down to dryness, leaving a thin graphite film. The U sample was taken into solution with 3 µl of ultra-pure H_2O, loaded onto the filament and evaporated gently to dryness. For microgramme quantities of U on the filament, a C/U ratio of around 100 achieved an adequate metal/oxide ion ratio emission for successful analysis (Kakazu et al., 1981).

The filament loading blank was not measured directly, but since the quoted total U blank of 0.039 ± 0.01 ng (see **Appendix A.4.2**) contributes a maximum of just 0.36% towards the smallest U sample analysed, the loading blank and procedural

blank were considered negligible.

In the mass spectrometer, filament currents were gradually raised to the starting current of 3.9 A over a 15 minute period. After the relevant beams had been located, centred and increased to the required magnitude, ^{235}U, ^{238}U and two background counts were sequentially integrated ten times over 5 seconds to statistically generate the $^{235}U/^{238}U$ ratio. A precision of 1% of the measured ratio was deemed acceptable. Significant within-run fractionation was not found to be a problem.

Between 08/05/90 and 09/05/91, eight analyses of the NBS U-500 standard solution gave a mass fractionation correction (F) for the $^{235}U/^{238}U$ ratio of - 0.132% ± 0.011 (2σ) amu^{-1}. Details of the analytical results and calculation of the mass fractionation correction plus associated errors are to be found in **Appendix A.3.2**.

B.5: ANALYSIS OF STABLE ISOTOPES

Samples for carbon and oxygen stable isotopic analysis were prepared using the procedures described in Corfield et al. (1992). Carbonate material was drilled from fresh sample surfaces using an engraving tool, cleaned for 30 minutes in 10% H_2O_2 to remove any organic materials, rinsed in acetone and then dried for 30 minutes at 60°C.

The samples were analysed at Oxford by on-line reaction with purified orthophosphoric acid at a temperature of 90°C using a VG Isotech PRISM mass spectrometer. Results are all calibrated to the Peedee belemnite (PDB) standard. The reproducibility of replicate standards was always better than 0.1‰ for both $\delta^{13}C$ and $\delta^{18}O$ (Corfield et al., 1992).

REFERENCES

ABRANCHES, M.C.B., 1977. Uranium and lead abundances and isotopic compositions in ordinary chondritic meteorites. Unpublished D.Phil Thesis, Univ. Oxford, 212 pp.

ALLÈGRE, C.J. & ROUSSEAU, D., 1984. The growth of the continent through geologic time studied by Nd isotope analysis of shale. *Earth Plan. Sci. Lett.*, **67**, pp 19–34.

ALLEN, J.R.L., 1965. Fining–upward cycles in alluvial successions. *Geol. Journ.*, **4**, pp 229–246.

AMIEL, A.J., MILLER, D.S. & FRIEDMAN, G.M., 1973. Incorporation of uranium in modern corals. *Sedimentology*, **20**, pp 523–528.

ANDERSEN, T. & TAYLOR, P.N., 1988. Pb isotope geochemistry of the Fen carbonatite complex, southeast Norway: Age and petrogenetic implications. *Geochim. Cosmochim. Acta*, **52**, pp 209–215.

ANDERSON, R.F., 1982. Concentration, vertical flux and remineralisation of particulate uranium in sea water. *Geochim. Cosmochim. Acta*, **46**, pp 1293–1299.

ANDERSON, R.F., LEHURAY, A.P., FLEISHER, M.Q. & MURRAY, J.W., 1989. Uranium deposition in Saanich Inlet sediments, Vancouver Island. *Geochim. Cosmochim. Acta*, **53**, pp 2205–2213.

ARDEN, J.W. & GALE, N.H., 1974a. Separation of trace amounts of uranium and thorium and their determination by mass spectrometric isotope dilution. *Analyt. Chem.*, **46**, pp 687–691.

ARDEN, J.W. & GALE, N.H., 1974b. New electrochemical technique for the separation of lead at trace levels from natural silicates. *Analyt. Chem.*, **46**, pp 2–9.

ARMSTRONG, R.L., 1978. Pre–Cenozoic Phanerozoic time scale. In: *Contribution to the Geological Time Scale.* Cohee et al. (eds.). *Am. Ass. Pet. Geol., Studies in Geol.* **6**, pp 73–91.

ARNETH, J.D., SCHIDLOWSKI, M., SARBAS, B., GOERG, U. & AMSTUTZ, G.C., 1985. Graphite content and isotopic fractionation between calcite–graphite pairs in metasediments from the Mgama Hills, southern Kenya. *Geochim. Cosmochim. Acta*, **49**, pp 1553–1560.

ARONSON, J.L. & HOWER, J., 1976. Mechanism of burial metamorphism of argillaceous sediments 2: Radiogenic argon evidence. *Bull. Geol. Soc. Am.*, **87**, pp 738–744.

AUDEN, J.B., 1933. Vindhyan sedimentation in the Son Valley, Mirzapur District. *Mem. Geol. Surv. Ind.*, **62**, pp 141–250.

AWASTHI, A.K. & PRAKESH, B., 1981. Depositional environments of unfossiliferous sediments of the Jodhpur Group, western India. *Sed. Geol.*, **30**, pp 15–42.

AZAD, H.S. & BORCHARDT, J.A., 1970. Variations in phosphorus uptake by algae. *Environ. Sci. Tech.*, **4**, pp 737–743.

BACON, M.P. & ANDERSON, R.F., 1982. Distribution of thorium isotopes between dissolved and particulate forms in the deep sea. *Journ. Geophys. Res.*, **87**, pp 2045–2056.

BACON, M.P., BELASTOCK, R.A., TECOTZKY, M., TUREKIAN, K.K. & SPENCER, D.W., 1988. Lead–210 and polonium–210 in ocean water profiles of the continental shelf and slope of New England. *Cont. Shelf. Res.*, **8**, pp 841–853.

BALISTIERI, L.S. & MURRAY, J.W., 1982. The adsorption of Cu, Pb, Zn and Cd on goethite from major ion seawater. *Geochim. Cosmochim. Acta*, **46**, pp 1253–1265.

BALISTIERI, L.S. & MURRAY, J.W., 1983. Metal–solid interactions in the marine environment: Estimating apparent equilibrium binding constants. *Geochim. Cosmochim. Acta*, **47**, pp 1091–1098.

BALISTIERI, L.S. & MURRAY, J.W., 1986. The surface chemistry of sediments from the Panama Basin: The influence of Mn oxides on metal adsorption. *Geochim. Cosmochim. Acta*, **50**, pp 2235–2243.

BALISTRIERI, L.S., BREWER, P.G. & MURRAY, J.W., 1981. Scavenging residence time of trace metals and surface chemistry of sinking particles in the oceans *Deep Sea Res.*, **28**, pp 101–121.

BANERJEE, D.M., 1971a. Precambrian stromatolitic phosphorites of Udaipur, Rajasthan, India. *Bull. Geol. Soc. Am.*, **82**, pp 2319–2330.

BANERJEE, D.M., 1971b. Aravallian stromatolites from Udaipur, Rajasthan. *Journ. Geol. Soc. Ind.*, **12**, pp 249–355.

BANERJEE, D.M., 1983. Filamentous micro–organisms in late Precambrian phosphatic stromatolites from India. 7th I.S.S.O.L. Congress, Mainz 1983, pp 1–10.

BANERJEE, D.M., 1986. Proterozoic and Cambrian phosphorites – regional review: Indian subcontinent. In: *World Phosphorite Deposits I.* Cook, P.J. & Shergoed, J.H. (eds.). Cambridge Univ. Press.

BANERJEE, D.M., 1990. Carbon isotope variations in Cambrian–Proterozoic rocks: A case for secular global trend. In: *Precambrian Continental Crust and its Economic Resources.* Naqvi, S.M. (ed.). *Developments in Precamb. Geol.*, **8**, pp 453–470.

BANERJEE, D.M. & BHATTACHARYA, P., 1989. Petrofacies analysis of the clastic rocks in the Proterozoic Aravalli Basin, Udaipur district, south central Rajasthan. *Ind. Minerals*, **43**, pp 194–225.

BANERJEE, D.M. & JYOTSNA CHOPRA, 1986. Morphometric analysis of Proterozoic stromatolites from India – preliminary report on the testing of a new technique. *Precamb. Res.*, **33**, pp 265–282.

BANERJEE, D.M. & MITRA, S.K., 1977. Deformation and metamorphism in the Precambrian of Rajasthan. *Journ. Geol. Soc. Ind.*, **18**, pp 644–652.

BANERJEE, D.M., BASU, P.C. & SRIVASTAVA, N., 1980. Petrology, mineralogy, geochemistry and origin of the Precambrian Aravallian phosphorite deposits of Udaipur and Jhabua, India. *Econ. Geol.*, **75**, pp 1181–1199.

BANERJEE, D.M., DEB, M. & STRAUSS, H., 1992. Organic carbon isotopic composition of Proterozoic sedimentary rocks from India: Preliminary results. In: *Early Organic Evolution.* Schidlowski, M. et al. (eds.). Springer–Verlag, Berlin Heidelberg.

BANERJEE, D.M., SCHIDLOWSKI, M. & ARNETH, J.D., 1986. Genesis of Upper Proterozoic–Cambrian phosphorite deposits of India: Isotopic inferences from carbonate fluorapatite, carbonate and organic carbon. *Precamb. Res.*, **33**, pp 239–253.

BARMAN, G., 1980. An analysis of the Marwar Basin, western Rajasthan in the light of stromatolite study. *Geol. Surv. Ind., Misc. Pub.* **44**, pp 292–297.

BARNES, I.L., CARPENTER, B.S., GARNER, E.L., GRAMLICH, J.W., KUEHNER, E.C., MACHLAN, L.A., MAIENTHAL, E.J., MOODY, J.R., MOORE, L.J., MURPHY, T.J., PAULSEN, P.J., SAPPENFIELD, K.M. & SHIELDS, W.R., 1972. Isotopic abundance ratios and concentrations of selected elements in Apollo–14 samples. *Proc.Third Lunar Sci. Conf.* **2** (*Geochim. Cosmochim. Acta, Supp.* **3**), pp 1465–1472.

BARNES, I.L., MURPHY, T.J., GRAMLICH, J.W. & SHIELDS, W.R., 1973. Lead separation by anodic deposition and isotope ratio mass spectrometry of microgramme and smaller samples. *Analyt. Chem.*, **45**, pp 1881–1884.

BASSETT, M.G., COCKS, L.R.M., HOLLAND, C.H., RICKARDS, R.B. & WARREN, P.T., 1975. The type Wenlock series. *Inst. Geol. Sci. Rep.*, **75/12**, pp 1–19.

BASSETT, M.G., KALJO, D. & TELLER, L., 1989. The Baltic region. In: *A Global Standard for the Silurian System.* Holland, C.H. & Bassett, M.G. (eds.). National Museum of Wales, *Geol. Ser.* **9**, Cardiff, pp 158–170.

BATURIN, G.N., 1969. Uranium in the surface layer of sediments in the northwestern Indian Ocean. *Oceanology Acad. Sci., U.S.S.R.*, **9**, pp 828–833.

BATURIN, G.N. & KOCHENOV, A.V., 1973. Uranium in the interstitial waters of marine and oceanic sediments. *Geokhimya*, **10**, pp 1529–1536.

BATURIN, G.N., KOCHENOV, A.V. & SENIN YU, M., 1971. Uranium concentration in recent ocean sediments in zones of rising currents. *Geochem. Int.*, **8**, pp 281–286.

BELL, K., 1963. Uranium in carbonate rocks. Shorter Contributions to General Geology, *U.S. Geol. Surv. Prof. Paper* **474–A**, pp A27–A29.

BERGMAN, C.F., 1979. Ripple marks in the Silurian of Gotland, Sweden. *Geol. Fören. Stockholm Förhand.*, **101**, pp 217–222.

BERTRAND–SARFATI, J. & ERIKSSON, K.A., 1977. Columnar stromatolites from the Early Proterozoic Schmidtsdrif Formation, northern Cape Province, South Africa – Part 1: Systematic and diagnostic features. *Pal. Afr.*, **20**, pp 1–26.

BODDINGTON, T.D.M., 1987. Abra, a Middle Proterozoic mineralised body, Western Australia. *Aus. Inst. Min. Metal., Bull. and Proc.* **292**, pp 59–69.

BOFINGER, V.M., 1967. Geochronology of the east Kimberley area of Western Australia. Unpublished Ph.D. Thesis, Aus. National Univ.

BONHOMME, M.G., 1982. The use of Rb–Sr and K–Ar dating methods as a stratigraphic tool applied to sedimentary rocks and minerals. *Precamb. Res.*, **18**, pp 5–25.

BOYAJIAN, G.E. & LABARBERA, M., 1987. Biomechanical analysis of passive flow of stromatoporoids – morphologic, palaeoecologic and systematic implications. *Lethaia*, **20**, pp 223–229.

BREGER, I.A., 1974. The role of organic matter in the accumulation of uranium: The organic geochemistry of the coal–uranium association. In: *Formation of Uranium Ore Deposits.*, I.A.E.A., Vienna, pp 99–123.

BREWER, P.G., 1975. Minor elements in sea water. In: *Chemical Oceanography, Volume 1.* Riley, J.P. & Skirrow, G. (eds.). London, Academic Press, pp 415–96.

BROECKER, W.S. & PENG, T.H., 1982. Tracers in the sea. Lamont–Doherty Geol. Obs. Pub., New York.

BROECKER, W.S., THURBER, D.L., GODDARD, J., KU, T.L., MATTHEWS, R.K. & MESOLELLA, K.J., 1968. Milankovitch hypothesis supported by precise dating of coral reefs and deep–sea sediments. *Science*, **159**, pp 297–300.

BRULAND, K.W., 1983. Trace elements in sea water. In: *Chemical Oceanography, Volume 8.* Riley, J.P. & Chester, R. (eds.). Academic Press, London, pp 156–220.

BRULAND, K.W. & FRANKS, R.P., 1983. Mn, Ni, Zn and Cd in the western North Atlantic. In: *Trace Metals in Seawater*. Wong, C.S., Boyle, E., Bruland, K.W., Burton, J.D. & Goldberg, E.D. (eds.). New York, Plenum, pp 395–414.

BUHL, D., 1987. U–Pb and Rb–Sr altersbeshmungen and untersuchuchung zum strintium isotopenasntausch and granuliten stuindiens. In: *Field Guide of the Workshop on the Deep Continental Crust of S.India*. Ashwal, L.D. (ed.). Houston, *Lunar Planet. Inst. Tech. Rept.* **88–06**, p 252.

BUHL, D., GRAUERT, B. & RAITH, M., 1987. U–Pb zircon dating of Archaean rocks from the south Indian Craton: Results from amphibolite to granulite facies transition zone at Kabbal Quarry, south Karnataka. *Fortschritte der Mineralogie*, **61**, pp 43–45.

BUNTING, J.A., 1986. Geology of the eastern part of the Nabberu Basin, Western Australia. *W.Aus. Geol. Surv., Bull.* **131**.

BUNTING, J.A., DeLAETER, J.R. & LIBBY, W.G., 1980. Evidence for the age and cryptoexplosive origin of the Teague ring structure. *W.Aus. Geol. Surv., Ann. Rept. 1979*, pp 81–85.

BURKE, W.H., DENISON, R.E., HEATHERINGTON, E.A., KOEPNICK, R.B., NELSON, H.F. & OTTO, J.B., 1982. Variation of seawater $^{87}Sr/^{86}Sr$ throughout Phanerozoic time. *Geology*, **10**, pp 516–519.

BURST, J.F., 1958. Glauconite pellets, their mineral nature and applications to stratigraphic interpretations. *Bull. Am. Ass. Pet. Geol.*, **2**, pp 310–327.

ÇAGATAY, M.N., GEDIK, A. & SALTOGLU, T., 1990. Geochemistry of uranium in the late Pleistocene–Holocene sediments from the southern part of the Black Sea basin. *Geochim. Cosmochim. Acta*, **82**, pp 129–144.

CAMERON, E.M., 1982. Sulphate and sulphate reduction in early Precambrian oceans. *Nature*, **296**, pp 145–148.

CATANZARO, E.J., MURPHY, T.J., SHIELDS, W.R. & GARNER, E.L., 1968. Absolute isotopic abundance ratios of common, equal atom and radiogenic Pb isotopic standards. *Journ. Res. N.B.S.*, **72A**, p 261.

CHADWICK, B., VASUDEV, V.N., KRISHNA RAO, B. & HEGDE, G.V., 1990. The stratigraphy and structure of the Late Archaean Dharwar Supergroup and its basement in the area of the Honnali Dome, Karnataka. Dept. Mines and Geol., Bangalore, *Geol. Studies Spec. Vol.* **154**, 36 pp.

CHADWICK, B., VASUDEV, V.N., KRISHNA RAO, B. & HEGDE, G.V., 1991. The stratigraphy and structure of the Dharwar Supergroup adjacent to the Honnali Dome: Implications for Late Archaean basin development and regional structure in the western part of Karnataka. *Journ. Geol. Soc. Ind.*, **38**, pp 457–484.

CHADWICK, B., VASUDEV, V.N., KRISHNA RAO, B. & HEGDE, G.V., in press. The Dharwar Supergroup: Basin development and implications for Late Archaean tectonic setting in western Karnataka, southern India. 3rd Int. Arch. Symp. 1990, *Procs. Vol.*, Perth, Australia.

CHAUHAN, D.S., 1979. Phosphate–bearing stromatolites of the Precambrian Aravalli phosphorite deposits of Udaipur region, their environmental significance and genesis of phosphorite. *Precamb. Res.*, **8**, pp 95–126.

CHAUHAN, D.S., 1980. Aravalli stromatolites and biostratigraphy. *Geol. Surv. Ind., Misc. Pub.* **44**, pp 128–133.

CHERNS, L., 1982. Palaeokarst, tidal erosion surfaces and stromatolites in the Silurian Eke Formation of Gotland, Sweden. *Sedimentology*, **28**, pp 819–833.

CHERNYSHEV, I.V., SAFONOV, Y.G., RADHAKRISHNA, B.P., KRISHNA RAO, B., VASUDEV, V.N. & DEB, M., 1980. Study of lead isotopes for investigating the origin of endogenic deposits with special reference to some ore deposits from India. *Journ. Geol. Soc. Ind.*, **21**, pp 107–116.

CHESTER, R., 1990. Marine geochemistry. Unwin Hyman, London, 698 pp.

CHIN, R.J. & DeLAETER, J.R., 1981. The relationship of new Rb–Sr isotopic dates from the Rudall metamorphic complex to the geology of the Paterson Province. *W.Aus. Geol. Surv. Ann. Rept. 1980*, pp 80–87.

CHIN, R.J., WILLIAMS, I.R., WILLIAMS, S.J. & CROWE, R.W.A., 1980. Explanatory notes: Rudall, Western Australia. W.Aus. Geol. Surv., 1:250000 Geological Series.

CHOUDHARY, A.K., GOPALAN, K. & SASTRY, C.A., 1984. Present status of the geochronology of the Precambrian rocks of Rajasthan. *Tectonophys.*, **105**, pp 131–140.

CHOW, T.J., 1965. Radiogenic leads of the Canadian and Baltic Shield regions. In: *Symposium on Marine Geochemistry 1964*. Rhode Island Univ., *Narrangansett Marine Lab. Occ. Pub.* **3**, pp 631–634.

CHOW, T.J., 1968. Lead isotopes of the Red Sea region. *Earth Plan. Sci. Lett.*, **5**, pp 143–147.

CHOW, T.J. & PATTERSON, C.C., 1959. Lead isotopes in manganese nodules. *Geochim. Cosmochim. Acta*, **17**, pp 21–31.

CHOW, T.J. & PATTERSON, C.C., 1962a. The occurrence and significance of lead isotopes in pelagic sediments. *Geochim. Cosmochim. Acta*, **26**, pp 263–308.

CHUNG, G.S., 1988. The application of nuclear track mapping of uranium to the study of diagenesis in carbonate rocks. Unpublished Ph.D.Thesis, Univ. Miami, 256 pp.

CHUNG, G.S. & SWART, P.K., 1986. Uranium as a diagenetic indicator in carbonate systems. *Geol. Soc. Am., Prog. with Abstracts*, **18**, p 564, (abstract).

CHUNG, G.S. & SWART, P.K., 1990. The concentration of uranium in freshwater vadose and phreatic cements in a Holocene ooid clay: A method of identifying ancient water tables. *Journ. Sed. Pet.*, **60**, pp 735–746.

CHUNG, G.S., EVANS, C. & SWART, P.K., 1985. Uranium as an indicator of diagenesis and water flow in the Pleistocene Miami limestone. *Geol. Soc. Am., Prog. with Abstracts*, **17**, p 546, (abstract).

CLAUER, N., 1979. A new approach to Rb–Sr dating of sedimentary rocks. In: *Lectures in Isotope Geology*. Jäger, E. & Hunziker, J.C. (eds.). Springer–Verlag, Berlin, pp 30–51.

CLAUER, N., 1981. Rb–Sr and K–Ar dating of Precambrian clays and glauconies. *Precamb. Res.*, **15**, pp 331–352.

CLAUER, N., 1982. The Rb–Sr method applied to sediments: Certitudes and uncertainties. In: *Numerical Dating in Stratigraphy*. Odin, G.S. (ed.). Wiley, Chichester, UK, pp 245–276.

CLAYPOOL, G.E., HOLSER, W.T., KAPLAN, I.R., SAKAI, H. & ZAK, I., 1980. The age curves of sulfur and oxygen isotopes in marine sulfate and their mutual interpretation. *Chem. Geol.*, **28**, pp 199–260.

COATS, R.P. & PREISS, W.V., 1980. Stratigraphic and geochronological reinterpretation of Late Proterozoic glaciogenic sequences in the Kimberley region, Western Australia. *Precamb. Res.*, **13**, pp 181–208.

COBB, J.C. & KULP, J.L., 1961. Isotopic geochemistry of uranium and lead in the Swedish kolm and its associated shale. *Geochim. Cosmochim. Acta*, **24**, pp 226–249.

COCHRAN, J.K., 1982. The oceanic chemistry of the U– and Th–series nuclides. In: *Uranium Series Disequilibrium: Applications to Environmental Problems*. Ivanovich, M. & Harmon, R.S. (eds.). Clarendon Press, Oxford, pp 384–430.

COLLEY, S., THOMSON, J. & TOOLE, J., 1989. Uranium relocations and derivation of quasi–isochrons for a turbidite/pelagic sequence in the northeast Atlantic. *Geochim. Cosmochim. Acta*, **53**, pp 1223–1234.

COMPSTON, W. & ARRIENS, P.A., 1968. The Precambrian geochronology of Australia. *Can. Journ. Earth Sci.*, **5**, pp 561–583.

COMPSTON, W., FANNING, C.M. & WILLIAMS, I.S., 1991. Iron probe zircon ages for the British Ordovician and Silurian stratotypes. 6th Int. Symp. on Ordovician System, Sydney 1991, p 12, (abstract).

COMPSTON, W., WILLIAMS, I.S., McCULLOCH, M.T., FOSTER, J.J., ARRIENS, P.A. & TRENDALL, A.F., 1981. A revised age for the Hamersley Group. Geol. Soc. Aus., 5th Annual Convention, *Abstracts* **3**, p 40, (abstract).

CORFIELD, R.M., SIVETER, D.J., CARTLIDGE, J.E. & McKERROW, W.S., 1992. Carbon isotope excursion near the Wenlock-Ludlow (Silurian) boundary in the Anglo-Welsh area. *Geology*, **20**, pp 371-374.

COWIE, J.W. & BRASIER, M.D., 1989. The Precambrian–Cambrian boundary. *Oxford Monogr. Geol. Geophys.*, **12**, Clarendon.

CRAWFORD, A.R., 1969. India, Ceylon and Pakistan: New age data and comparison with Antartica. *Nature*, **223**, pp 380–381.

CRAWFORD, A.R., 1970. The Precambrian geochronology of Rajasthan and Bundelkhand, northern India. *Can. Journ. Earth Sci.*, **7**, pp 91–110.

CRAWFORD, A.R. & COMPSTON, W., 1970. The age of the Vindhyan System of Peninsular India. *Quart. Journ. Geol. Soc. Lond.*, **125**, pp 351–371.

CRAWFORD, A.R. & COMPSTON, W., 1973. The age of the Cuddapah and Kurnool Systems, southern India. *Journ. Geol. Soc. Aus.*, **129**, pp 453–464.

CUVELLIER, H., 1989. La datation des roches carbonatées par la methode Pb/Pb. Unpublished D.E.A. Thesis, Rennes, 20 pp.

DeLAETER, J.R. & BLOCKLEY, J.G., 1972. Granite ages within the Archaean Pilbara Block. *Spec. Pub. Geol. Soc. Aus.*, **19**, pp 363–370.

DEB, M., THORPE, R.I., CUMMING, G.L. & WAGNER, P.A., 1989. Age, source and stratigraphic implications of Pb isotope data for conformable, sediment–hosted, base metal deposits in the Proterozoic Aravalli–Delhi orogenic belt, northwestern India. *Precamb. Res.*, **43**, pp 1–22.

DEBENHAM, N.C. & AITKEN, M.J., 1984. Thermoluminescence dating of stalagtitic calcite. *Archaeometry*, **26**, pp 155–170.

DeDECKKER, P., 1988. Large Australian lakes during the last 20 million years: Sites for petroleum source rock or metal ore deposition, or both? In: *Lacustrine Source Rocks*. Fleet, A.J., Kelts, K. & Talbot, M.R. (eds.). *Geol. Soc. Spec. Pub.*, **40**, pp 45–58.

DEER, W.A., HOWIE, R.A. & ZUSSMAN, J., 1977. An introduction to the rock–forming minerals. Longman, 528 pp.

DEGENS, E.T., KHOO, R. & MICHAELIS, W., 1977. Uranium anomalies in Black Sea sediments. *Nature*, **269**, pp 566–569.

DeWOLF, C.P. & HALLIDAY, A.N., 1991. U–Pb dating of a remagnetised Palaeozoic limestone. *Geophys. Res. Lett.*, **18**, pp 1445–1448.

DEYNOUX, M., TROMPETTE, R., CLAUER, N. & SOUGY, J., 1978. Upper Precambrian and lowermost Palaeozoic correlations in west Africa and in the western part of central Africa. Probable diachronism of the late Precambrian tillite. *Geol. Rudsch.*, **67**, pp 615–630.

DISNAR, J.R., 1981. Etude expérimentale de la fixation de métaux par un matériau sédimenataire actuel d'origine algaire II. Fixation "in vitro" de UO_2^{2+}, Cu^{2+}, Ni^{2+}, Zn^{2+}, Pb^{2+}, Co^{2+}, Mn^{2+}, ainsi que de VO^{3-}, MoO_4^{2-} et GeO_3^{2-}. *Geochim. Cosmochim. Acta*, **45**, pp 363–379.

DISNAR, J.R. & TRICHET, J., 1983. Pyrolyse de complexes organo–métalliques formés entre un matériau organique actuel d'origine algaire et divers cations métalliques divalents. (UO_2^{2+}, Cu^{2+}, Pb^{2+}, Ni^{2+}, Mn^{2+}, Zn^{2+} et Co^{2+}). *Chem. Geol.*, **40**, pp 203–223.

DOE, B.R., 1970a. Lead isotopes. *Minerals, Rocks and Inorganic Materials*, **3**. Springer–Verlag, 137 pp.

DOE, B.R., 1970b. Evaluation of U–Th–Pb whole rock dating on Phanerozoic sedimentary rocks. *Eclogae Geol. Helv.*, **63**, pp 79–82.

DOE, B.R., HEDGE, C.E. & WHITE D.E., 1966. Preliminary investigation of the source of lead and strontium in deep geothermal brines underlying the Salton Sea geothermal area. *Econ. Geol.*, **61**, pp 462–483.

DONNER, J. & JUNGNER, H., 1981. Radiocarbon dating of marine shells from southeastern Australia as a means of dating relative sea–level changes. *Ann. Acad. Sci. Fennicae, Ser. A*, **III**, Geologica–Geographica, Helsinki.

DOW, D.B., GEMUTS, I., PLUMB, K.A. & DUNNET, D., 1964. The geology of the Ord River region, Western Australia. *Aus. Bureau Min. Res., Rec.* **1964/104** (unpublished).

DRISCOLL, C.T., FULLER, R.D. & SIMONE, D.M., 1988. Longitudinal variations in trace metal concentrations in a northern forested ecosystem. *Journ. Env. Qual.*, **17**, pp 101–107.

DRURY, S.A. & HOLT, R.W., 1980. The tectonic framework of the south India craton: A reconnaissance involving LANDSAT imagery. *Tectonophys.*, **65**, pp T1–T5.

DUINKER, J.C. & KRAMER, J.M., 1977. An experimental study on the speciation of dissolved Zn, Cd, Pb and Cu in River Rhine and North Sea water by difference pulse anodic stripping voltammetry. *Mar. Chem.*, **5**, pp 207–228.

DUNHAM, R.J., 1969. Early vadose silt in Townsend Mound (reef), New Mexico. In: *Depositional Environments in Carbonate Rocks*. Friedman, G.M. (ed.). *S.E.P.M. Spec. Pub.* **14**, pp 139–181.

DUTT, N.V.B.S., 1963. Stratigraphy and correlation of the Indravati Series (Purana Group) of Bastar District, Madhya Pradesh. *Journ. Geol. Soc. Ind.*, **4**, pp 35–48.

EGLINGTON, B.M. & HARMER, R.E., 1989. Geodate version 1.0 – A program for processing and regression of isotope data using IBM–compatible microcomputers. Div. Earth Mar. Atmos. Sci. and Tech., Pretoria, South Africa, 58 pp.

EMERSON, S. & DYMOND, J., 1984. Benthic organic cycles: Toward a balance of fluxes from particle settling and pore water gradients. In: *Global Ocean Flux Study*. National Academy Press, Washington D.C., pp 285–304.

EMILIANI, C. & SHACKLETON, N.J., 1974. The Brunhes epoch: Isotopic palaeotemperatures and geochronology. *Science*, **183**, pp 511–514.

ENGEL, A.E. & PATTERSON, C.C., 1957. Isotopic composition of lead in the Leadville limestone hydrothermal dolomite, and associated ore. *Bull. Geol. Soc. Am.*, **68**, p 1723.

EPSTEIN, A.G., EPSTEIN, G.B. & HARRIS, L.D., 1977. Conodont colour alteration–an index to organic metamorphism. *U.S. Geol. Surv. Prof. Paper*, **995**, pp 1–27.

EREL, Y., MORGAN, J.J. & PATTERSON, C.C., 1991. Natural levels of lead and cadmium in a remote mountain stream. *Geochim. Cosmochim. Acta*, **55**, pp 707–719.

EVANS, R.D. & GOODMAN, C., 1941. Radioactivity of rocks. *Bull. Geol. Soc. Am.*, **52**, pp 459–490.

EWERS, G.R. & FERGUSON, J., 1985. Unconformity–related uranium deposits – Turee Creek uranium prospect, Western Australia. *Aus. Bureau Min. Res., Ann. Rept.*, pp 35–37.

FAREEDDUDIN, JANARDHAN, A.S. & BASAVALINGU, B., 1988. Sedimentology, mineralogy and geochemistry of the Kalasapura conglomerate. *Geol. Soc. Ind. Mem.* **9**, pp 65–82.

FAURE, G., 1986. Principles of isotope geology (second edition). Wiley, 589 pp.

FILIPPOV, M.S., KOMLEV, L.V. & KUCHINA, G.N., 1961. Argon ages on rocks from the northwestern Ukrainian shield. Tr. 9th Sess. Komissii po Opredelediyu Absolutnogo Vozrasta Geologicheskikh Formatsyi, Moscow, pp 41–51, (in Russian).

FLODÉN, T., 1980. Seismic stratigraphy and bedrock geology of the central Baltic. *Stockholm Contrib. Geol.*, **35**, pp 1–240.

FLORENCE, T.M. & BATLEY, G.E., 1976. Trace metal species in sea water. *Talanta*, **23**, pp 179–186.

FRANK, J.R., CARPENTER, A.B. & OGLESBY, T.W., 1982. Cathodoluminescence and composition of calcite cement in the Taum Saul Limestone (upper Cambrian), southeast Missouri. *Journ. Sed. Pet.*, **52**, pp 631–638.

FRAREY, M.J., 1981. A provisional standard for correlating the Precambrian rocks of the Canadian Shield: Discussion. *Geol. Surv. Can. Paper* **81–1C**, pp 83–88.

FRIEND, C.R.L. & NUTMAN, A.P., 1991. S.H.R.I.M.P. U–Pb geochronolgy of the Closepet Granite and Peninsular Gneiss, Karnataka, south India. *Journ. Geol. Soc. Ind.*, **38**, pp 357–368.

FRYKMAN, P., 1984. Cement stratigraphy in Silurian bioherm, Gotland, Sweden. I.A.S., 5th European Meeting, Marseille 1984, pp 181–182.

FRYKMAN, P., 1985. Subaerial exposure and cement stratigraphy of a Silurian bioherm in the Klinteberg Beds, Gotland, Sweden. *Geol. Fören. Stockholm Förhand.*, **107**, pp 77–88.

FRYKMAN, P., 1986. Diagenesis of Silurian bioherms in the Klinteberg Formation, Gotland, Sweden. In: *Reef Diagenesis*. Schroeder, J.H. & Purser, B.H. (eds.). Springer–Verlag, Berlin Heidelberg, pp 399–423.

FRYKMAN, P., 1989. Carbonate ramp facies of the Klinteberg Formation, Wenlock–Ludlow transition on Gotland, Sweden. *Sveriges Geol. Unders.*, **C820**, pp 1–79.

GALE, N.H., 1985. Numerical calibration of the Palaeozoic time scale: Ordovician, Silurian and Devonian periods. In: *The Chronology of the Geological Record*. Snelling, N.J. (ed.). *Geol. Soc. Lond. Mem.* **10**, pp 81–88.

GALE, N.H. & MUSSETT, A.E., 1973. Episodic uranium–lead models and the interpretation of variations in the isotopic composition of lead in rocks. *Rev. Geophys. Space Phys.*, **11**, pp 27–86.

GALE, N.H., ARDEN, J.W. & ABRANCHES, M.C.B., 1980a. Uranium–lead in the Bruderheim L6 chondrite and the 500 Ma shock event in the L–Group parent body. *Earth Plan. Sci. Lett.*, **48**, pp 311–324.

GALLOWAY, J.J., 1957. Structure and classification of the Stromatoporoidea. *Bull. Am. Pal.*, **37**, pp 345–480.

GARNER, E.L., MACHLAN, L.A. & SHIELDS, W.R., 1971. Standard reference materials; boric acid isotopic and assay standard reference materials (Dec. 1969). *N.B.S. Spec. Pub.*, **260–17**, pp 65–74.

GEE, R.D., 1980. Summary of the Precambrian stratigraphy of Western Australia. *W.Aus. Geol. Surv., Ann. Rept.*, pp 85–90.

GEE, R.D., 1990. Nabberu Basin. In: *Geology and Mineral Resources of Western Australia. W.Aus. Geol. Surv., Mem.* **3**, pp 202–210.

GEE, R.D., DeLAETER, J.R. & DRAKE, J.R., 1976. Geology and geochronology of altered rhyolite from the lower part of the Bangemall Basin near Tangadee, Western Australia. *W.Aus. Geol. Surv., Ann. Rept. 1975*, pp 112–117.

GELLATLY, D.C., DERRICK, G.M. & PLUMB, K.A., 1975. The geology of the Lansdowne 1:250000 sheet area, Western Australia. *Aus. Bureau Min. Res., Rept.* **152**.

GOBEIL, C. & SILVERBERG, N., 1989. Early diagenesis of lead in Laurentian Trough sediments. *Geochim. Cosmochim. Acta*, **53**, pp 1889–1895.

GOELLNICHT, N.M., GROVES, I.M., GROVES, D.I., HO, S.E. & McNAUGHTON, N.J., 1988. A comparison between mesothermal gold deposits of the Yilgarbn Block and gold mineralisation at Telfer and Miralga Creek, Western Australia: Indirect evidence for a non–magmatic origin for greenstone–hosted gold deposits. In: *Advances in Understanding Precambrian Gold Deposits, Vol. II.* Ho, S.E. & Groves, D.I. (eds.). *Univ. W.Aus., Dept. Geol. and Extension Servive, Pub.* **12**, pp 23–40.

GOLDBERG, E.D., 1954. Marine geochemistry I. Chemical scavengers. *Journ. Geol.*, **62**, pp 249–265.

GOLDBERG, E.D. & GRIFFIN, J.J., 1964. Sedimentation rates and mineralogy in the south Atlantic. *Journ. Geophys. Res.*, **69**, pp 4293–4309.

GOLDBERG, E.D. & KOIDE, M., 1963. Rates of sediment accumulation in the Indian Ocean. In: *Earth Science and Meteoritics*. Geiss, J. & Goldberg, E.D. (eds.). North Holland, Amsterdam, pp 90–102.

GOLDICH, S.S., 1968. Geochronology in the Lake Superior region. *Can. Journ. Earth Sci.*, **5**, pp 715–724.

GOLDICH, S.S. & MUDREY, M.G., 1972. Dilatancy model for discordant U–Pb zircon ages. In: *Contributions to Recent Geochemistry and Analytical Chemistry (A.P. Vinogradov Vol.)*. Tugarinov, A.I. (ed.). Moscow, Nauka Pub. Office, pp 415–418.

GOLDICH, S.S., BAADSGAARD, H., EDWARDS, G. & WEAVER, C.E., 1959. Investigations in radioactivity – dating of sediments. *Bull. Am. Ass. Pet. Geol.*, **43**, pp 654–662.

GOLDSTEIN, S., O'NIONS, R.K. & HAMILTON, P.J., 1984. A Sm–Nd isotopic study of atmospheric dust and particulates from major river systems. *Earth Plan. Sci. Lett.*, **70**, pp 221–236.

GOODE, A.D.T. & HALL, W.D.M., 1981. The Middle Proterozoic eastern Bangemall Basin, Western Australia. *Precamb. Res.*, **16**, pp 11–29.

GOPALAN, K., TRIVEDI, J.R., BALASUBRAHMANYAN, M.N., RAY, S.K. & SASTRY, C.A., 1979. Rb–Sr chronology of the Khetri copper belt, Rajasthan. *Journ. Geol. Soc. Ind.*, **20**, pp 450–456.

GOROKHOV, I.M., 1964. Rb–Sr whole rock age determinations of the Korosten granites, the Dnieper migmatites and the metabasites. *Ukraine Geokhim.*, **8**, pp 744–753, (in Russian).

GOROKHOV, I.M., CLAUER, N., VARSHAVSKAYA, E.S., KUTYAVIN, E.P. & DRANNIK, A.S., 1981. Rb–Sr ages of Precambrian sediments from the Ovruch mountain range, northwest Ukraine. *Precamb. Res.*, **16**, pp 55–65.

GREW, E.S. & MANTON, W.I., 1984. Age of allanite from Kabbaldurga Quarry, Karnataka. *Journ. Geol. Soc. Ind.*, **25**, pp 193–195.

GREY, K., 1982. Aspects of Proterozoic biostratigraphy in Western Australia. *Precamb. Res.*, **18**, pp 347–365.

GREY, K., 1984. Stromatolitic limestone from the Duck Creek Dolomite, near Kennedy Creek (Turee Creek Sheet), and a reassessment of the occurrence of *Patomia* form indet. at the same locality. W.*Aus. Geol. Surv., Pal. Rept.* **8/84**, (unpublished).

GREY, K., 1985. Stromatolites in the Proterozoic Duck Creek Dolomite, Western Australia. In: *Professional Papers for 1983. W.Aus. Geol. Surv., Rept.* **14**, pp 94–103.

GREY, K. & THORNE, A.M., 1985. Biostratigraphic significance of stromatolites in upward–shallowing sequences of the Early Proterozoic Duck Creek Dolomite, Western Australia. *Precamb. Res.*, **29**, pp 183–206.

GRIFFIN, T.J. & GREY, K., 1990. Kimberley Basin. In: *Geology and Mineral Resources of Western Australia. W.Aus. Geol. Surv., Mem.* **3**, pp 293–301.

GRIFFIN, T.J. & MYERS, J.S., 1988a. Geological note – a Proterozoic terrain boundary in the King Leopold Orogen, Western Australia. *Aus. Journ. Earth Sci.*, **35**, pp 131–132.

GRIFFIN, T.J. & MYERS, J.S., 1988b. Reply to discussion – a Proterozoic terrain boundary in the King Leopold Orogen, Western Australia. *Aus. Journ. Earth Sci.*, **35**, p 132.

GRIFFIN, T.J., TYLER, I.M. & PLAYFORD, P.E., In press. Explanatory notes on the Lennard River 1:250 000 Geological Sheet SE/51–8, Western Australia. Geol. Surv. W.Aus.

GROTZINGER, J.P., 1988. Introdution to Precambrian reefs. In: *Reefs – Canada and Adjacent Areas*. Geldsetzer, H., James, N.P. & Tebbutt, G. (eds.). *Can. Soc. Petrol. Geol., Mem.* **13**, pp 9–12.

GROTZINGER, J.P., 1989. Facies and evolution of Precambrian carbonate depositional systems: Emergence of the modern platform archetype. In: *Controls on Carbonate Platform and Basin Development*. Crevello, P.D., Wilson, J.L.. Sarg, J.F. & Read, J.F. (eds.). *S.E.P.M. Spec. Pub.* **44**, pp 79–106.

GROVER, G. & READ, J.F., 1983. Palaeoaquifer and deep burial related cements defined by regional cathodoluminescence patterns, Middle Ordovician carbonates, Virginia. *Bull. Am. Ass. Pet. Geol.*, **67**, pp 1275–1303.

GUPTA, J.N., PANDEY, B.K., PRASAD, R.N., YADAV, G.S., RAMESH KUMAR, K. & RAO, S.S., 1988. Rb–Sr geochronology of some granitic rocks around Arbail and age of uraniferous arenite and quartz–pebble conglomerates of western Karnataka. *Mem. Geol. Soc. Ind.*, **9**, pp 101–108.

GUPTA, S.N., ARORA, Y.K., MATHUR, R.K., IQBALUDDIN, PRASAD, B., SAHAI, T.N. & SHARMA, S.B., 1980. Lithostratigraphic map of Aravalli region, southern Rajasthan and northeastern Gujarat. *Geol. Surv. Ind. Pub.*, Hyderabad.

GVIRTZMANN, G., FRIEDMAN, G.M. & MILLER, D.S., 1973. Control and distribution of uranium in coral reefs during diagenesis. *Journ. Sed. Pet.*, **43**, pp 983–997.

HAGLUND, D.S., FRIEDMAN, G.M. & MILLER, D.S., 1969. The effect of freshwater on the redistribution of uranium in carbonate sediments. *Journ. Sed. Pet.*, **39**, pp 1283–1296.

HAMELIN, B., GROUSSET, F. & SHOLKOVITZ, E.R., 1990. Pb isotopes in surficial pelagic sediments from the North Atlantic. *Geochim. Cosmochim. Acta*, **54**, pp 37–47.

HAMILTON, P.J., EVENSEN, N.M., O'NIONS, R.K., GLIKSON, A.Y. & HICKMAN, A.H., 1981. Sm–Nd dating of the North Star basalt, Warrawoona Group, Pilbara Block, Western Australia. *Spec. Pub. Geol. Soc. Aus.*, **7**, pp 187–192.

HANCOCK, J.M., 1991. Ammonite scales for the Cretaceous System. *Cret. Res.*, **12**, pp 259–292.

HANSEN, B.T. & KALSBEEK, F., 1989. Precise age for the Ammassalik intrusive complex. *Rapp. Grønl. Geol. Unders.*, **146**, pp 46–47.

HARLAND, W.B., 1978. Geochronologic scales. *Am. Ass. Pet. Geol., Studies in Geol.*, **6**, pp 9–32.

HARLAND, W.B., ARMSTRONG, R.L., COX, A.V., CRAIG, L.E., SMITH, A.G. & SMITH, D., 1989. A geologic time scale, 1989. Cambridge Univ. Press, 263 pp.

HARLAND, W.B., COX, A.V., LLEWELLYN, P.G., PICKTON, C.A.G., SMITH, A.G. & WALTERS, R., 1982. A geologic time scale. Cambridge Univ. Press, 131 pp.

HARLAND, W.B., SMITH, A.G. & WILCOCK, B. (eds.)., 1964. The Phanerozoic time scale. *Quart. Journ. Geol. Soc. Lond.*, **120s**, 458 pp.

HART, S.R. & TILTON, G.R., 1966. The isotope geochemistry of strontium and lead in Lake Superior sediments and water. In: *The Earth Beneath the Continents*. Am. Geophys. Union, *Geophys. Mon. Ser.* **10**, pp 127–137.

HEDE, J.E., 1921. Gottlands Silurstratigrafi. *Sveriges Geol. Unders.*, **C331**, pp 1–100.

HEDE, J.E., 1925a. Beskrivning av Gotlands Silurlager. In: *Gotlands Geologi, en Översikt.* Munthe, H., Hede, J.E. & von Post, L. (eds.). *Sveriges Geol. Unders.*, **C331**, pp 13–30.

HEDE, J.E., 1925b. Berggrunden (Silursystemet). In: *Beskrivning till Kartbladet Roehamn.* Munthe, H., Hede, J.E. & van Post, L. (eds.). *Sveriges Geol. Unders.*, **Aa156**, pp 14–51.

HEDE, J.E., 1927a. Berggrunden (Silursystemet). In: *Beskrivning till Kartbladet Klintehamn.* Munthe, H., Hede, J.E. & Lundqvist, G. (eds.). *Sveriges Geol. Unders.*, **Aa160**, pp 12–54.

HEDE, J.E., 1927b. Berggrunden (Silursystemet). In: *Beskrivning till Kartbladet Hemse.* Munthe, H., Hede, J.E. & van Post, L. (eds.). *Sveriges Geol. Unders.*, **Aa164**, pp 15–56.

HEDE, J.E., 1928. Berggrunden (Silursystemet). In: *Beskrivning till Kartbladet Slite.* Munthe, H., Hede, J.E. & Lundqvist, G. (eds.). *Sveriges Geol. Unders.*, **Aa169**, pp 13–65.

HEDE, J.E., 1929. Berggrunden (Silursystemet). In: *Beskrivning till Kartbladet Katthammarsvik.* Munthe, H., Hede, J.E. & Lundqvist, G. (eds.). *Sveriges Geol. Unders.*, **Aa170**, pp 14–57.

HEDE, J.E., 1933. Berggrunden (Silursystemet). In: *Beskrivning till Kartbladet Kappelshamn.* Munthe, H., Hede, J.E. & Lundqvist, G. (eds.). *Sveriges Geol. Unders.*, **Aa171**, pp 10–59.

HEDE, J.E., 1936. Berggrunden (Silursystemet). In: *Beskrivning till Kartbladet Fårö.* Munthe, H., Hede, J.E. & Lundqvist, G. (eds.). *Sveriges Geol. Unders.*, **Aa180**, pp 11–42.

HEDE, J.E., 1940. Berggrunden (Silursystemet). In: *Beskrivning till Kartbladen Visby och Lummelanda.* Lundqvist, G., Hede, J.E. & Sundius, N.E. (eds.). *Sveriges Geol. Unders.*, **Aa183**, pp 9–68.

HEDE, J.E., 1958. Silurian entries. In: *Lexique Stratigraphique International 1, Europe 2c, Suede–Sweden–Sverige*, 498 pp.

HEINRICHS, H. & MAYER, R., 1977. Distribution and cycling of major trace elements in two central European forest ecosystems. *Journ. Env. Qual.*, **6**, pp 402–407.

HERON, A.M., 1935. Synopsis of the pre–Vindhyan geology of Rajputana. *Trans. Nat. Inst. Sci. Ind.*, **1**, pp 17–33.

HERON, A.M., 1936. Geology of southeastern Mewar, Rajputana. *Mem. Geol. Surv. Ind.*, **68**, pp 1–120.

HERON, A.M., 1953. The geology of central Rajputana. *Mem. Geol. Surv. Ind.*, **79**, 389 pp.

HEUMANN, K.G., KUBASSEK, E., SCHWABENBAUER, W. & STADLER, I., 1979. Analytical method for the K–Ca age determination of geological samples. *Fresnius Z. Analyt. Chem.*, **297**, pp 35–43.

HICKMAN, A.H., 1980. Archaean geology of the Pilbara Block. 2nd Int. Arch. Symp. (Perth), Excursion Guide, Canberra, Geol. Soc. Aus., 55 pp.

HOEFS, J. & FREY, M., 1976. Isotopic composition of carbonaceous matter in a metamorphic profile from the Swiss Alps. *Geochim. Cosmochim. Acta*, **40**, pp 945–951.

HOFFMAN, P.F., 1975. Shoaling–upward shale to dolomite cycles in the Rocknest Formation (Lower Proterozoic), Northwest Territories, Canada. In: *Tidal Deposits*. Ginsburg, R.N. (ed.). Springer, New York, pp 257–265.

HOFFMAN, P.F. & BOWRING, S.A., 1984. Short–lived 1.9 Ga continental margin and its destruction, Wopmay Orogen, northwest Canada. *Geology*, **12**, pp 68–72.

HOFMANN, H.J. & SCHOPF, J.W., 1983. Early Proterozoic microfossils. In: *Earth's Earliest Biosphere: Its Origin and Evolution*. Schopf, J.W. (ed.). Princeton Univ. Press, pp 321–359.

HORWITZ, R.C., 1975. Provisional geological map at 1:250000 of the northeast margin of the Yilgarn Block. *Aus. C.S.I.R.O., Min. Res. Lab., Division of Mineralogy, Rept.* **FP10**.

HORWITZ, R.C., 1981. Large scale slumping in the Ashburton Trough of Western Australia. *Precamb. Res.*, **14**, pp 389–401.

HORWITZ, R.C., 1982. Geological history of the Early Proterozoic Paraburdoo Hinge Zone, Western Australia. *Precamb. Res.*, **19**, pp 191–200.

HSI, C.K.D. & LANGMUIR, D., 1985. Adsorption of uranyl onto ferric oxyhydroxides: Application of the surface complexation site–binding model. *Geochim. Cosmochim. Acta*, **49**, pp 1931–1941.

IKEYA, M., 1975. Dating a stalactite by electron paramagnetic resonance. *Nature*, **225**, pp 48–50.

IKEYA, M., 1978. Electron spin resonance as a method of dating. *Archaeometry*, **20**, pp 147–158.

IVANTISHIN, M.N., KHATUNTSEVA, A.Y., ZAIDIS, B.B. & DEMIDENKO, S.G., 1962. Absolute age of the Ovruch Series, the Perga and Osnian Granites, the gneisses and granites of the Volyn Group. Tr. 10th Sess. Komissii po Opredeleniyu Absolutnogo Vozrasta Geol. Formatsyi, Moscow, pp 112–118, (in Russian).

JAEGER, H., 1981. Comments on the graptolite chronology of Gotland. In: *Proceeding of Project Ecostratigraphy Plenary Meeting, Gotland, 1981*. Laufeld, S. (ed.). *Sveriges Geol. Unders., rapporter och meddelanden*, **25**, p 12.

JAHN, B.M., 1988. Pb/Pb dating of young marbles from Taiwan. *Nature*, **332**, pp 429–432.

JAHN, B.M. & CUVELLIER, H., 1989. Pb/Pb geochronology of carbonates and dating of sedimentary rocks. E.U.G. V, Geochronology Subsection OS06, (abstract).

JAHN, B.M., BERTRAND–SARFATI, J., MORIN, N. & MACÉ, J., 1990. Direct dating of stromatolitic carbonates from the Schmidtsdrif Formation (Transvaal Dolomite), South Africa, with implications on the age of the Ventersdorp Supergroup. *Geology*, **18**, pp 1211–1214.

JAHN, B.M., MARTINEAU, F. & CORNICHET, J., 1984. Chronological significance of Sr isotopic compositions in the crystalline limestones of the Central Range, Taiwan. *Journ. Geol. Soc. China, Mem.* **6**, pp 295–301.

JAIRAMAN, R. & BANERJEE, D.M., 1980. Preliminary studies of stromatolites from the Raipur area, Chattisgarh Basin. *Geol. Surv. Ind. Misc. Pub.* **44**, 57 pp.

JAMES, H.L., 1972. Subdivision of the Precambrian: An interim scheme to be used by the U.S. Geological Survey. *Bull. Am. Ass. Pet. Geol.*, **56**, pp 11026–11030.

JAMES, H.L., 1979. Precambrian subdivided. *Episodes*, **4**, p 34.

JAMES, N.P. & CHOQUETTE, P.W., 1983. Limestones – the seafloor diagenetic environment. *Geosci. Can.*, **10**, pp 159–179.

JEPPSSON, L., 1974. Aspects of late Silurian conodonts. *Fossils & Strata*, **6**, pp 1–54.

JEPPSSON, L., 1979. Conodont element function. *Lethaia*, **12**, pp 153–171.

JEPPSSON, L., 1982. Third European conodont symposium (ECOS III), guide to excursion. *Pub. Inst. Min. Pal. Quat. Geol., Univ. Lund*, **239**, pp 1–32.

JEPPSSON, L., 1983. Silurian conodont faunas of Gotland. *Fossils & Strata*, **15**, pp 121–144.

JEPPSSON, L. & LAUFELD, S., 1986. The Late Silurian Öved–Ramsåsa Group in Skåne, South Sweden. *Sveriges Geol. Unders.*, **58**, pp 1–45.

JICKELLS, T.D., DEUSER, W.G. & KNAPP, A.H., 1984. The sedimentation rates of trace elements in the Sargasso Sea measured by sediment trap. *Deep Sea Res.*, **31**, pp 1169–1178.

JONES, B.G., CARR, P.F. & WRIGHT, A.J., 1981. Silurian and early Devonian geochronology – a reappraisal with new evidence from the Bungonian Limestone. *Alcheringa*, **5**, pp 197–207.

JONES, B., LOCKHART, E.B. & SQUAIR, C., 1984. Phreatic and vadose cements in the Tertiary Bluff Formation of Grand Cayman Island, British West Indies. *Bull. Can. Pet. Geol.*, **32**, pp 382–397.

JONES, C.E., 1992. Strontium isotopes in Jurassic and Cretaceous seawater. Unpublished D. Phil. Thesis, Univ. Oxford, 307 pp.

KAHN, M.I. & WILLIAMS, D.F., 1981. Oxygen and carbon isotopic composition of living planktonic foraminifera from the northeast Pacific Ocean. *Paleo. Paleo. Paleo.*, **33**, pp 47–69.

KAKAZU, M.H., MORAES, N.M.P., IYER, S.S. & RODRIGUES, C., 1981. Reduction of oxide ions of uranium in single filament surface–ionisation mass spectrometry with application to rock samples. *Analyt. Chim. Acta*, **132**, pp 209–213.

KALDI, J. & GIDMAN, J., 1982. Early diagenetic dolomite cements: Examples from the Permian Lower Magnesian Limestone of England and the Pleistocene carbonates of the Bahamas. *Journ. Sed. Pet.*, **52**, pp 1073–1085.

KALSBEEK, F. & TAYLOR, P.N., 1989. Programme of geochronology and isotope geochemistry in the Ammassalik district, southeast Greenland: Outline and preliminary results. *Rapp. Grønl. Geol. Unders.*, **146**, pp 13–16.

KALSBEEK, F., TAYLOR, P.N. & HENRIKSEN, N., 1984. Age of rocks, structures and metamorphism in the Nagssugtoqidian mobile belt, west Greenland – field and Pb isotope evidence. *Can. Journ. Earth Sci.*, **21**, pp 1126–1131.

KAZMIERCZAK, J., 1976. Cyanophycean nature of stromatoporoids. *Nature*, **264**, pp 49–51.

KAZMIERCZAK, J. & KRUMBEIN, W.E., 1983. Identification of calcified coccoid cyanobacteria forming stromatoporoid colonies. *Lethaia*, **16**, pp 207–213.

KELLER, B.M., KAZAKOV, G.A., KRYLOV, I.N., NUZNOV, S.V. & SEMIKHATOV, M.A., 1960. New data on the stratigraphy of the Riphean Group (Upper Proterozoic). *Izvestia Akademii Nauka, SSSR, Ser. Geol.* **2**, pp 21–23.

KERSHAW, S., 1981. Stromatoporoid growth form and taxonomy in a Silurian biostrome, Gotland. *Journ. Pal.*, **5**, pp 1284–1295.

KERSHAW, S., 1984. Patterns of stromatoporoid growth in level–bottom environments. *Palaeontology*, **24**, pp 113–130.

KERSHAW, S., 1987. Stromatoporoid–coral intergrowths in a Silurian biostrome. *Lethaia*, **20**, pp 371–380.

KERSHAW, S., 1990. Stromatoporoid palaeobiology and taphonomy in a Silurian biostrome on Gotland, Sweden. *Palaeontology*, **33**, pp 681–705.

KHAN, E.A., 1971. Geological mapping in parts of Jodhpur and Nagaur Districts, Rajasthan. *Geol. Surv. Ind., Prog. Rept. 1969–1970* (unpublished).

KING, W., 1885. Sketch of the progress of the geological work in the Chattisgarh Division of the Central Provinces. *Rec. Geol. Surv. Ind.*, **18**.

KLINKHAMMER, G.P. & PALMER, M.R., 1991. Uranium in the oceans: Where it goes and why. *Geochim. Cosmochim. Acta*, **55**, pp 1799–1806.

KNIEWALD, G. & BRANICA, M., 1988. Role of uranium (V) in marine sedimentary environments: A geochemical possibility. *Mar. Chem.*, **24**, pp 1–12.

KNOLL, A.H. & BARGHOORN, E.S., 1976. A Gunflint–type microbiota from the Duck Creek Dolomite, Western Australia. *Origins of Life*, **7**, pp 417–423.

KNOLL, A.H., BARGHOORN, E.S. & AWRAMIK, S.M., 1978. New microorganisms from the Aphebian Gunflint Iron Formation, Ontario. *Journ. Pal.*, **52**, pp 976–992.

KOLODNY, Y. & KAPLAN, I.R., 1973. Deposition of uranium in the sediment and interstitial water of an anoxic fjord. In: *Proc. Symp. Hydrogeochem. Biogeochem. Part 1: Hydrogeochem.* Clarke Co., Washington D.C., pp 418–442.

KOMLEV, L.V. & GOROKHOV, I.M., 1962. Age of some Precambrian formations of Ukraine determined by the strontium method. Tr. 10th Sess. Komissii po Opredeleniyu Absolutnogo Vozrasta Geol. Formatsyi, Moscow, pp 93–101, (in Russian).

KORSCH, R.J. & KENNARD, J.M., 1991. Geological and geophysical studies in the Amadeus Basin, central Australia. *Aus. Bureau Min. Res., Bull.* **236**, 594 pp.

KOWALLIS, B.J., CHRISTIANSEN, E.H. & DEINO, A., 1989. Multi–characteristic correlation of Upper Cretaceous volcanic ash beds from southwestern Utah to central Colorado. *Utah Geol. and Min. Surv., Misc. Pub.* **89–5**, 22 pp.

KRAUSKOPF, K.B., 1956. Factors controlling the concentrations of thirteen rare metals in sea water. *Geochim. Cosmochim. Acta*, **12**, pp 61–84.

KREUZER, H., KARRE, W., KURSTEN, M., SCHNITZER, W.A., MURTI, K.S. & SRIVASTAVA, N.K., 1977. K–Ar dates of two glauconites from the Chandarpur Series (Chattisgarh, India): On the stratigraphic status of the late Precambrian basins in central India. *Geol. Jahrb.*, **28**, pp 23–36.

KUEHNER, E.C., ALVAREZ, R., PAULSEN, P.J. & MURPHY, T.J., 1972. Production and analysis of special high–purity acids purified by sub–boiling distillation. *Analyt. Chem.*, **44**, pp 2050–2056.

KUMAR, M.D. & REDDY, V.G., 1985. The thermodynamic metastability of Cr(III) and chromium speciation in natural waters. *Ind. Journ. Mar. Sci.*, **14**, pp 151–155.

KUMAR, S., 1976. Significance of stromatolites in the correlation of the Semri Series (Lower Vindhyan) of Son Valley and Chitrakoot area, U.P. *Journ. Pal. Soc. Ind.*, **19**, pp 24–27.

KUMAR, S., 1982. Geology of Vindhyanchal. In: *Geology of Vindhyanchal.* Valdiya, K.S., Bhatia, S.B. & Gaur, V.K. (eds.). New Delhi, pp 102–112.

KUNK, M.J., SUTTER, J., OBRADOVICH, J.D. & LANPHERE, M.A., 1985. Age of biostratigraphic horizons within the Ordovician and Silurian systems. In: *The Chronology of the Geological Record.* Snelling, N.J. (ed.). *Geol. Soc. Lond. Mem.* **10**, pp 89–92.

KWEIYANG INSTITUTE OF GEOCHEMISTRY, LABORATORY OF ISOTOPE GEOLOGY., 1977. On the Sinian geochronological scale of China based on isotopic ages for the Sinian strata in the Yenshan Region, North China. *Scientia Sinica*, **20**, pp 818–834.

LAHNER, I., 1939. Uran– und thoriumbestimmungen an kalken und dolomiten und die frage des radioaktiven gleichgewichtes in diesen gesteinen. *Akad. Wiss. Wien, Math. Naturwiss. Kl., Sitzungsber*, **148**, pp 149–162.

LAHOUD, J.A., MILLER, D.S. & FRIEDMAN, G.M., 1966. Relationship between depositional environment and uranium concentration of molluskan shells. *Journ. Sed. Pet.*, **36**, pp 541–547.

LANGLEY, K.M., 1978. Dating sediments by a K–Ar method. *Nature*, **276**, pp 56–57.

LANGMUIR, D., 1978. Uranium solution–mineral equilibria at low temperature with applications to sedimentary ore deposits. *Geochim. Cosmochim. Acta*, **42**, pp 547–569.

LARSSON, K., 1979. Silurian tentaculids from Gotland and Scania. *Fossils & Strata*, **11**, pp 1–180.

LAUFELD, S., 1974a. Silurian Chitinozoa from Gotland. *Fossils & Strata*, **5**, pp 1–130.

LAUFELD, S., 1974b. Reference localities for palaeontology and geology in the Silurian of Gotland. *Sveriges Geol. Unders.*, **C705**, pp 1–172.

LAUFELD, S. & BASSETT, M.G., 1981. Gotland: The anatomy of a Silurian carbonate platform. *Episodes*, **2**, pp 23–27.

LAUFELD, S. & JEPPSSON, L., 1976. Silicification and bentonites in the Silurian of Gotland. *Geol. Fören. Stockholm Förhand.*, **98**, pp 31–44.

LAUFELD, S., SUNDQUIST, B. & SJÖSTRÖM, H., 1978. Megapolygonal bedrock structures in the Silurian of Gotland. *Sveriges Geol. Unders.*, **C759**, pp 1–26.

LECKIE, J.O., APPLETON, A.R., BALL, N.B., HAYES, K.F. & HONEYMAN, B.D., 1984. Adsorptive removal of trace elements from fly–ash pond effluents onto iron oxyhydroxide. *Electric Power Res. Inst. Rept.*, **EPRI–RP–910–1**, Palo Alto, California.

LECOMPTE, M., 1956. Stromatoporoidea. In: *Treatise on Invertebrate Palaeontology – Coelenterata*. Moore, R.C. (ed.). *Geol. Soc. Am.*, pp F107–144.

LEGGO, P.J., COMPSTON, W. & TRENDALL, A.F., 1965. Radiometric ages of some Precambrian rocks from the Northwest Division of Western Australia. *Journ. Geol. Soc. Aus.*, **12**, pp 53–65.

LION, L.W., ALTMANN, R.S. & LECKIE, J.O., 1982. Trace metal adsorption characteristics of estuarine particulate matter: Evaluation of contribution of Fe/Mn oxide and organic surface coatings. *Environ. Sci. Technol.*, **16**, pp 660–666.

LIPSON, J., 1958. Potassium–argon dating of sedimentary rocks. *Bull. Geol. Soc. Am.*, **69**, pp 137–150.

LOHMANN, K.C. & MEYERS, W.J., 1977. Microdolomite inclusions in cloudy prismatic calcites – a proposed criterion for former high Mg calcites. *Journ. Sed. Pet.*, **42**, pp 1078–1088.

LOWE, D.R., 1980. Stromatolites 3400 Myr–old from the Archaean of Western Australia. *Nature*, **284**, pp 441–443.

LUDWIG, K.R., 1980. Calculation of uncertainties of U–Pb isotope data. *Earth Plan. Sci. Lett.*, **46**, pp 212–220.

LUDWIG, K.R., 1990. Isoplot – a plotting and regression program for radiogenic isotope data, for IBM–PC compatible computers. Version 2.11. *United States Geol. Surv., Open–File Rept.* **88–557**, 33 pp.

MacDOUGALL, J.D., GOPALAN, K., LUGMAIR, G.W. & ROY, A.B., 1983. The Banded Gneissic Complex of Rajasthan, India: Early crust from depleted mantle at 3.5 Ga? *EOS, Trans. Am. Geophys. Union*, **64**, p 351.

MacDOUGALL, J.D., WILLIS, R., LUGMAIR, G.W., ROY, A.B. & GOPALAN, K., 1984. The Aravalli sequence of Rajasthan, India: A Precambrian continental margin. Workshop on the Early Earth 1984, Lunar Planet. Inst., Houston, Texas, pp 55–56.

MacLEOD, W.N., De la HUNTY, L.E., JONES, W.R. & HALLIGAN, R., 1963. A preliminary report on the Hamersley Iron Province, Northwest Division. *W.Aus. Geol. Surv., Ann. Rept. 1962*, pp 44–54.

MARTIN, J–M. & WHITFIELD, M., 1983. The significance of the river input of chemical elements to the ocean. In: *Trace Metals in Seawater*. Wong, C.S., Boyle, E., Bruland, K.W., Burton, J.D. & Goldberg, E.D. (eds.). New York, Plenum, pp 265–96.

MARTINSSON, A., 1967. The succession and correlation of ostracode faunas in the Silurian of Gotland. *Geol. Fören. Stockholm Förhand.*, **89**, pp 350–386.

MATTINSON, J.M., 1972. Preparation of hydrofluoric, hydrochloric and nitric acids at ultra–low lead levels. *Analyt. Chem.*, **44**, pp 1715–1716.

McARTHUR, J.M., KENNEDY, W.J., GALE, A.S., THIRLWALL, M.F., CHEN, M., BURNETT, J., HANCOCK, J. & LORD, A.R., 1992. Strontium isotope stratigraphy in the Late Cretaceous: Intercontinental correlation of the Campanian–Maastrichtian boundary. *Terra Nova*, **4**, pp 385-393.

McKERROW, W.S., 1979. Ordovician and Silurian changes in sea level. *Journ. Geol. Soc. Lond.*, **136**, pp 137–145.

McKERROW, W.S., 1992. Time scale, April 1992, (in prep.).

McKERROW, W.S., LAMBERT, R.StJ. & CHAMBERLAIN, V.E., 1980. The Ordovician, Silurian and Devonian time scales. *Earth Plan. Sci. Lett.*, **51**, pp 1–8.

McKERROW, W.S., LAMBERT, R.StJ. & COCKS, L.R.M., 1985. The Ordovician, Silurian and Devonian periods. In: *The Chronology of the Geological Record*. Snelling, N.J. (ed.). *Geol. Soc. Mem.* **10**, pp 73–80.

MEUNIER, J.D., LANDAIS, P. & PAGEL, M., 1990. Experimental evidence of uraninite formation from diagenesis of uranium–rich organic matter. *Geochim. Cosmochim. Acta*, **54**, pp 809–817.

MO, T., SUTTLE, A.D. & SACKETT, W.M., 1973. Uranium concentrations in marine sediments. *Geochim. Cosmochim. Acta*, **37**, pp 35–51.

MOHANTY, S. & NAHA, K., 1986. Stratigraphic relations of the Precambrian rocks in the Salumbar area, southeast Rajasthan. *Journ. Geol. Soc. Ind.*, **27**, pp 479–493.

MÖLLER, M., RAJAGOPALIN, G. & GERMANN, K., 1976. A geochemical model for dolomitization. *Geol. Jahrb.*, **20**, pp 57–76.

MONTY, C.L.V., 1977. Evolving concepts on the nature and ecological significance of stromatolites. In: *Fossil Algae: Recent Results and Devlopments*. Flugel, E. (ed.). Springer–Verlag, Heidelberg, pp 15–35.

MOOK, W.G., 1980. The principles and applications of radiocarbon dating. Elsevier, Amsterdam.

MOORBATH, S., 1969. Evidence for the age of deposition of the Torridonian sediments of northwest Scotland. *Scott. Journ. Geol.*, **5**, pp 154–170.

MOORBATH, S. & TAYLOR, P.N., 1981. Isotopic evidence for continental growth in the Precambrian. In: *Precambrian Plate Tectonics*. Kröner, A. (ed.). Elsevier, Amsterdam, pp 491–525.

MOORBATH, S. & TAYLOR, P.N., 1985. Precambrian geochronology and the geological record. In: *The Geochronology of the Geological Record*. Snelling, N.J. (ed.). *Geol. Soc. Lond. Mem.* **10**, pp 10–28.

MOORBATH, S., TAYLOR, P.N., ORPEN, J.L., TRELOAR, P. & WILSON, J.F., 1987. First direct radiometric dating of Archaean stromatolitic limestone. *Nature*, **326**, pp 865–867.

MORI, K., 1969. Stromatoporoids from the Silurian of Gotland, Part 1. *Stockholm Contrib. Geol.*, **19**, pp 1–100.

MORI, K., 1970. Stromatoporoids from the Silurian of Gotland, Part 2. *Stockholm Contrib. Geol.*, **22**, pp 1–152.

MUFFLER, L.J.P. & DOE, B.R., 1968. Composition and mean age of detritus of the Colorado River delta in the Salton Trough, southeastern California. *Journ. Sed. Pet.*, **38**, pp 384–399.

MUHLING, P.C. & BRAKEL, A.T., 1985. Geology of the Bangemall Group – the evolution of an intracratonic Proterozoic basin. *W.Aus. Geol. Surv., Bull.* **128**.

MUKHOPADHYAY, D. & GHOSH, K.P., 1980. Deformation of early lineations in the Aravalli rocks, Fatehpur, Udaipur district, south Rajasthan, India. *Ind. Journ. Earth Sci.*, **7**, pp 64–75.

MUKTINATH & SANT, V.N., 1967. Occurrence of algal phosphorite in the Precambrian rocks of Rajasthan. *Curr. Sci.*, **36**, p 630.

MUKTINATH, SANT, V.N., DAS, N., CHAKRAVARTY, D.K., SAXENA, S.P., CHAKRAVARTY, B. & SINGH, G.B., 1969. Precambrian phosphorites near Udaipur. *Journ. Mines, Metals & Fuels*, **17**, pp 335–339.

MURCHISON, R.I., 1839. The Silurian system founded on geological Montgomery, Caermarthen, Brecon, Pembroke, Monmouth, Gloucester, Worcester and Stafford: With descriptions of the coal field and overlying formations. Murray, London, 2 vols., 768 pp.

MURTHY, P.S.N. & KRISHNA REDDY, K., 1984. 2900 My old stromatolite from Sandur greenstone belt of Karnataka Craton, India. *Journ. Geol. Soc. Ind.*, **25**, pp 263–265.

MURTI, K.S., 1987. Stratigraphy and sedimentation in the Chattisgarh Basin. *Geol. Soc. Ind. Mem.* **6**, pp 239–260.

MYERS, J.S. & HOCKING, R.M., 1988. Geological map of Western Australia – explanatory notes. Geol. Surv. W.Aus., 13 pp.

NAHA, K. & CHAUDHURI, A.K., 1968. Large–scale fold interference in a metamorphic migmatitic complex. *Tectonophys.*, **6**, pp 127–142.

NAHA, K. & HALYBURTON, R.V., 1974. Late stress systems deduced from conjugate folds and kink bands in the "main Raialo syncline", Udaipur district, Rajasthan, India. *Bull. Geol. Soc. Am.*, **85**, pp 251–256.

NAHA, K. & HALYBURTON, R.V., 1977a. Structural pattern and strain history of a superposed fold system in the Precambrian of central Rajasthan, India. I – Structural pattern in the "main Raialo syncline", central Rajasthan. *Precamb. Res.*, **4**, pp 39–84.

NAHA, K. & HALYBURTON, R.V., 1977b. Structural pattern and strain history of a superposed fold system in the Precambrian of central Rajasthan, India. II – Strain history. *Precamb. Res.*, **4**, pp 85–111.

NAHA, K., CHAUDHURI, A.K. & MUKHERJI, P., 1967. Evolution of the Banded Gneissic Complex of central Rajasthan, India. *Contrib. Min. Pet.*, **15**, pp 191–216.

NAHA,K., MUKHOPADHYAY, D.K., MOHANTY, R., MITRA, S.K. & BISWAL, T.K., 1984. Significance of contrast in the early stages of the structural history of the Delhi and pre–Delhi rock groups in the Proterozoic of Rajasthan, western India. *Tectonophys.*, **105**, pp 193–206.

NAND LAL, NAGPAUL, K.K. & SHARMA, K.K., 1976. Fission track ages and uranium concentration in garnets from Rajasthan, India. B*ull. Geol. Soc. Am.*, **87**, pp 687–690.

NAQVI, S.M., VISWANATHAN, S. & VISWANATHA, M.N., 1978. Geology and geochemistry of the Holenarsipur Schist Belt and its place in the evolutionary history of the Indian Peninsula. In: *Archaean Geochemistry*. Windley, B.F. & Naqvi, S.M. (eds.). Elsevier, Amsterdam, pp 102–136.

NG, A. & PATTERSON, C.C., 1982. Changes of lead and barium with time in California offshore basin sediments. *Geochim. Cosmochim. Acta*, **46**, pp 2307–2321.

NICHOLSON, H.A., 1896. A monograph of the British Stromatoporoids (Part I). *Pal. Soc. Lond.*, **14**, pp 159–202.

NOZAKI, Y., HORIBE, Y. & TSUBOTA, H., 1981. The water column distributions of thorium isotopes in the western North Pacific. *Earth Plan. Sci. Lett.*, **54**, pp 203–216.

O'NIONS, R.K., HAMILTON, P.J. & HOOKER, P.J., 1983. A Nd isotope investigation of sediments related to crustal development in the British Isles *Earth Plan. Sci. Lett.*, **63**, pp 229–240.

OBRADOVICH, J.D., 1988. A different perspective on glauconite as a geochronometer for geologic time scale studies. *Paleoceanogr.*, **3**, pp 757–770.

OBRADOVICH, J.D. & COBBAN, W.A., 1975. A time scale for the Late Cretaceous of the Western Interior of North America. In: *The Cretaceous System in the Western Interior of North America*. Caldwell, W.G.E. (ed.). *Geol. Ass. Can. Spec. Paper*, **13**, pp 31–54.

ODIN, G.S. (ed.)., 1982. Numerical dating in stratigraphy. Wiley, Chichester, 1040 pp.

ODIN, G.S., CURRY, D., GALE, N.H. & KENNEDY, W.J., 1982. The Phanerozoic time scale in 1981. In: *Numerical Dating in Stratigraphy*. Odin, G.S. (ed.). Wiley, Chichester, pp 957–960.

ODIN, G.S., HUNZIKER, J.C., JEPPSSON, L. & SPIELDANES, N., 1986a. Ages radiometriques K–Ar de biotites pyroclastiques sedimentées dans le Wenlock de Gotland (Suède). In: *Calibration of the PhanerozoicTime Scale*. Odin, G.S. (ed.). *Chem. Geol. (Isotope Geoscience Section)*, **59**, pp 117–125.

ODIN, G.S., HURFORD, J.A., MORGAN, D.J. & TOGHILL, P., 1986b. K–Ar biotite data for Ludlovian bentonites from Great Britain. In: *Calibration of the Phanerozoic Time Scale*. Odin, G.S. (ed.). *Chem. Geol. (Isotope Geoscience Section)*, **59**, pp 127–131.

ODIN, G.S., SPJELDNAES, N., JEPPSSON, L. & NIELSEN THORSHOJ, A., 1984. Field meeting in Scandanavia – time scale calibration. *Bulletin de liaison et informations, I.G.C.P. Project 196*, **3**, pp 6–23.

ORPEN, J.L. & WILSON, J.F., 1981. Stromatolites at c.3500 Myr and a greenstone–granite unconformity in the Zimbabwean Archaean. *Nature*, **291**, pp 218–220.

OVERSBY, V.M., 1976. Isotopic ages and geochemistry of Archaean acid igneous rocks from the Pilbara, Western Australia. *Geochim. Cosmochim. Acta*, **40**, pp 817–829.

PAGE, R.W., 1976. Reinterpretation of isotopic ages from the Halls Creek Mobile Zone, northwestern Australia. *Aus. Bureau Min. Res., Journ. Aus. Geol. and Geophys.*, **1**, pp 79–81.

PAGE, R.W., McCULLOCH, M.T. & BLACK, L.P., 1984. Isotopic record of major Precambrian events in Australia. *Procs. 27th Int. Geol. Congr., Moscow 1984*, **5**, pp 25–72.

PALIWAL, B.S., 1980. Systematics of the Precambrian stromatolites of Rajasthan: A review in light of tectonic deformation. *Geol. Surv. Ind., Misc. Pub.* **44**.

PARNELL, J. & SWAINBANK, I., 1990. Pb/Pb dating of hydrocarbon migration into a bitumen–bearing ore deposit, North Wales. *Geology*, **18**, pp 1028–1030.

PATTERSON, C.C., 1953. The isotopic composition of meteoric, basaltic and oceanic leads, and the age of the earth. Proc. Conf. on Nucl. Proc. in Geol. Settings, pp 36–40.

PAULSON, A.J., FEELY, R.A., CURL, H.C., CRECELIUS, E.A. & GEISELMAN, T., 1988. The impact of scavenging on trace metal budgets in Puget Sound. *Geochim. Cosmochim. Acta*, **52**, pp 1765–1779.

PERRY, E.A., 1974. Diagenesis and the K–Ar dating of clays and shales. *Bull. Geol. Soc. Am.*, **85**, pp 827–830.

PETTIJOHN, F.J., 1975. Sedimentary rocks (3rd edition). Harper & Row, New York, 628 pp.

PIDGEON, R.T., 1978. 3450 Myr–old volcanics in the Archaean layered greenstone succession of the Pilbara Block, Western Australia. *Earth Plan. Sci. Lett.*, **37**, pp 421–428.

PIDGEON, R.T. & HORWITZ, R.C., 1991. The origin of olistoliths in Proterozoic rocks of the Ashburton Trough, Western Australia, using zircon U–Pb isotopic characteristics. *Aus. Journ. Earth Sci.*, **38**, pp 55–63.

PINGITORE, N.E., 1976. Vadose and phreatic diagenesis, processes, products and their recognition in corals. *Journ. Sed. Pet.*, **42**, pp 985–1006.

PLUMB, K.A., ALLEN, R. & HANCOCK, S.L., 1985. Excursion guide – Proterozoic evolution of the Halls Creek Province, Western Australia. Conference on Tectonics and Geochemistry of Early to Middle Proterozoic Fold Belts, Darwin, N.T. 1985. *Aus. Bureau Min. Res., Rec.* **1985/25**, (unpublished).

PLUMB, K.A., DERRICK, G.M., NEEDHAM, R.S. & SHAW, R.D., 1981. The Proterozoic of northern Australia. In: *Precambrian of the Southern Hemisphere.* Hunter, D.R. (ed.). Elsevier, Amsterdam, pp 205–307.

PLUMMER, L.N., VACHER, H.L., MacKENZIE, F.T., BRICKER, O.P. & LAND, L.S., 1976. Hydrogeochemistry of Bermuda – a case history of groundwater diagenesis of biocalcarenites. *Bull. Geol. Soc. Am.*, **87**, pp 1301–1316.

POLEVAYA, N.I., TITOV, N.E., BELYAEV, V.S. & SPRINTSSON, V.D., 1958. Application of the Ca method in the absolute age determination of sylvite. *Geochemistry*, **8**, pp 897–906.

PRASAD, B., 1975. Lower Vindhyan formations of Rajasthan. *Rec. Geol. Surv. Ind.*, **106**, pp 31–53.

PREISS, W.V., JACKSON, M.J., PAGE, R.W. & COMPSTON, W., 1975. Regional geology, stromatolite biostratigraphy and isotopic data bearing on the age of a Precambrian sequence near Lake Carnegie, Western Australia. Geol. Soc. Aus., 1st Aus. Geol. Conv., Adelaide 1975, pp 92–93, (abstract).

PYE, K., 1982. Thermoluminescence dating of sand dunes. *Nature*, **299**, p 376.

RAJA RAO, C.S., 1976. Precambrian sequences of Rajasthan. *Misc. Pub. Geol. Surv. Ind.*, **23**, pp 497–516.

RAJA RAO, C.S., IQBALUDDIN & MATHUR, R.K., 1968. Algal structures from Aravalli beds near Dakan Kotra, Udaipur district, Rajasthan. *Curr. Sci.*, **37**, pp 560–561.

RAJA RAO, C.S. & MAHAJAN, V.D., 1965. Note on the stromatolites and probable correlation of the Bhagwanpura Limestone, Chittorgarh district, Rajasthan. *Curr. Sci.*, **34**, pp 82–83.

RAY, J.N., 1983. Superposed deformation in Delhi rocks near Patan, Sikar district, Rajasthan. *Journ. Geol. Soc. Ind.*, **24**, pp 229–236.

RICHARDS, J.R. & GEE, R.D., 1985. Galena lead isotopes from the eastern part of the Nabberu Basin, Western Australia. *Aus. Journ. Earth Sci.*, **32**, pp 47–54.

RICHARDS, J.R., BLOCKLEY, J.G., FLETCHER, I.R. & GEE, D,G., in prep. Galena Pb isotope data from the Capricorn Orogen.

RIDING, R., 1981. Composition, structure and environmental setting of Silurian bioherms and biostromes in northern Europe. *S.E.P.M., Spec. Pub.* **30**, pp 41–83.

RODAY, P.P., 1979. Structural patterns in the Ajabgarh rocks around Anakhor. *Journ. Geol. Soc. Ind.*, **20**, pp 441–449.

ROE, K.K. & BURNETT, W.C., 1985. Uranium geochemistry and the dating of Pacific island apatite. *Geochim. Cosmochim. Acta*, **49**, pp 1581-1592.

ROSHOLT, J.N., ZARTMAN, R.E. & NKOMO, I.T., 1973. Lead isotope systematics and uranium depletion in the Granite Mountains, Wyoming. *Bull. Geol. Soc. Am.*, **84**, pp 989–1002.

ROSS, R.J., NAESER, C.W., IZETT, G.A., OBRADOVICH, J.D., BASSETT, M.G., HUGHES, C.P., COCKS, L.R.M., DEAN, W.T., INGHAM, J.K., JENKINS, C.J., RICKARDS, R.B., SHELDON, P.R., TOGHILL, P., WHITTINGTON, H.B. & ZALZSIEWICZ, J., 1982. Fission–track dating of British Ordovician and Silurian stratotypes. *Geol. Mag.*, **119**, pp 135–153.

ROY, A. & BISWAS, S.K., 1979. Metamorphic history of the Sandur Schist Belt, Karnataka. *Journ. Geol. Soc. Ind.*, **20**, pp 179–187.

ROY, A. & BISWAS, S.K., 1983. Stratigraphy and structure of the Sandur Schist Belt, Karnataka. *Journ. Geol. Soc. Ind.*, **24**, pp 19–29.

ROY, A.B., 1973. Nature and evolution of subhorizontal crenulation cleavage in the type Aravalli rocks around Udaipur, Rajasthan. *Proc. Nat. Inst. Sci. Ind.*, **39**, pp 119–131.

ROY, A.B., 1987. Stratigraphic and tectonic framework of the Aravalli mountain range. *Mem. Geol. Soc. Ind.*, **7**, pp 3–31.

ROY, A.B. & DAS, A.R., 1985. A study of the time relations between movements, metamorphism and granite emplcement in the Middle Proterozoic Delhi Supergroup of Rajasthan. *Journ. Geol. Soc. Ind.*, **26**, pp 726–733.

ROY, A.B. & JAIN, A.K., 1974. Polyphase deformation in the Pb–Zn bearing Precambrian rocks of Zawarmala, Udaipur, southern Rajasthan. *Quart. Journ. Geol. Min. Met. Sci. Ind.*, **46**, pp 81–86.

ROY, A.B. & PALIWAL, B.S., 1981. Evolution of Lower Proterozoic epicontinental deposits: Stromatolite–bearing Aravalli rocks of Udaipur, Rajasthan, India. *Precamb. Res.*, **14**, pp 49–74.

ROY, A.B., GOLANI, P.R. & BEJARNIYA, B.R., 1985. The Ahar River Granite, its stratigraphic and structural relations with the Early Proterozoic rocks of southeast Rajasthan. *Journ. Geol. Soc. Ind.*, **26**, pp 315–325.

ROY, A.B., NAGORI, D.K., GOLANI, P.R., DHAKAR, S.P. & CHAUDHURI, R., 1980. Structural geometry of the rock–phosphate bearing Aravalli rocks around Jhamarkotra mines area, Udaipur district, Rajasthan. *Ind. Journ. Earth Sci.*, **7**, pp 191–202.

ROY, A.B., PALIWAL, B.S. & BEJARNIYA, B.R., 1984. The Aravalli rocks: An evolutionary model and metallogenic trends. *Ind. Journ. Earth Sci., C.E.I.S.M. Seminar Vol.*, pp 73–83.

ROY, A.B., PALIWAL, B.S. & GOEL, O.P., 1971. Superposed folding in the Aravalli rocks of the type area around Udaipur, Rajasthan. *Journ. Geol. Soc. Ind.*, **12**, pp 342–348.

ROY, A.B., SOMANI, M.K. & SHARMA, N.K., 1981. Aravalli, pre–Aravalli relationship: A study from the Bhinder region, south Rajasthan. *Ind. Journ. Earth Sci.*, **8**, pp 119–130.

RUSH, P.F. & CHAFETZ, H.S., 1991. Skeletal mineralogy of Devonian stromatoporoids. *Journ. Sed. Pet.*, **61**, pp 364–369.

RUSSELL, J., 1991. U–Pb systematics applied to the dating of carbonates and carbonate macrofossils. *Terra Abstracts*, **3**, (abstract).

RUSSELL, J., in prep. New Pb/Pb dates from Gotland, Sweden and their geological implications.

RUSSELL, J. & BANERJEE, D.M., in prep. Indian Proterozoic stromatolite geochronology: Further application of the Pb/Pb method.

RUSSELL, J. & CHADWICK, B., in prep. Pb/Pb dating of Precambrian marbles: Examples from the Late Archaean of Karnataka, Peninsular India.

RUSSELL, J. & GREY, K., in prep. Pb/Pb stromatolite geochronology in the Proterozoic of Western Australia.

RUSSELL, W.A. & PAPANASTASSIOU, D.A., 1978. Calcium isotope fractionation in ion exchange chromatography. *Analyt. Chem.*, **50**, pp 1151–1154.

RUSSELL, W.A., PAPANASTASSIOU, D.A. & TOMBRELLO, T.A., 1978. Ca isotopic fractionation on the earth and other solar system materials. *Geochim. Cosmochim. Acta*, **42**, pp 1075–1090.

SACKETT, W.M., MO, T., SPALDING, R.F. & EXNER, M.E., 1973. A re–evaluation of the marine chemistry of uranium. In: *Radioactive Contamination in the Marine Environment*. I.A.E.A.–SM–158/51, Vienna, pp 757–769.

SALOP, L.I., 1977. Precambrian of the Northern Hemisphere. Elsevier, Amsterdam, 378 pp.

SALOP, L.I., 1968. Precambrian stratigraphy and geochronology of Peninsular India. Dhanbad Publishers, India, 33 pp.

SANTSCHI, P.H., LI, Y.H. & BELL, J., 1979. Natural radionuclides in the water of Narragansett Bay. *Earth Plan. Sci. Lett.*, **45**, pp 201-213.

SCHAULE, B.K. & PATTERSON, C.C., 1981. Lead concentrations in the northeast Pacific: Evidence for global anthropogenic peturbations. *Earth Plan. Sci. Lett.*, **54**, pp 97–116.

SCHERBAK, N.P. (ed.)., 1978. Catalogue of isotopic ages for rocks of the Ukrainian shield. Naukova Dumka, Kiev, 223 pp, (in Russian).

SCHIDLOWSKI, M., HAYES, J.M. & KAPLAN, I.R., 1983. Isotopic inferences of ancient biochemistries: Carbon, sulfur, hydrogen and nitrogen. In: *Earth's Earliest Biosphere: Its Origin and Evolution.* Schopf, J.W. (ed.). University Press, Princeton, pp 149–187.

SCHIDLOWSKI, M., JUNGE, C.E. & PIETREK, H., 1977. Sulfur isotope variations in marine sulfate evaporites and the Phanerozoic oxygen budget. *Journ. Geophys. Res.*, **82**, pp 2557–2565.

SCHNITZER, W.A., 1971. Das Jungprakambrium Indians "Purana System". *Geol. Abs.*, **85**, p 44.

SCHOPF, J.W. (ed.)., 1983. Earth's earliest biosphere: Its origin and evolution. Princeton, Princeton Univ. Press, 543 pp.

SCHROEDER, J.H., MILLER, D.S. & FRIEDMAN, G.M., 1970. Uranium distributions in recent skeletal carbonates. *Journ. Sed. Pet.*, **40**, pp 672–681.

SCOFFIN, T.P., 1971. The conditions of growth of the Wenlock reefs of Shropshire, England. *Sedimentology*, **17**, pp 173–219.

SCOFFIN, T.P., 1987. An introduction to carbonate sediments and rocks. Blackie, Glasgow and London, 274 pp.

SCOTESE, C.R. & McKERROW, W.S., 1990. Revised world maps and introduction. In: *Palaeozoic Palaeogeography and Biogeography.* McKerrow, W.S. & Scotese, C.R. (eds.). *Geol. Soc. Mem.* **12**, pp 1–21.

SEMIKHATOV, M.A., 1976. Experience in stromatolite studies in the USSR. In: *Stromatolites.* Walter, M.R. (ed.). *Developments in Sedimentology* **20**, Elsevier, Amsterdam, pp 337–357.

SEMIKHATOV, M.A., 1978. Some Aphebian carbonate stromatolites of the Canadian Shield. In: *Lower Boundary of the Riphean and Stromatolites of the Aphebian.* Raaben, M.E. (ed.). *Trudy Geol. Inst. Akad. Nauk SSSR*, **312**, pp 111–147, (in Russian).

SEN, S., 1970. Some problems of Precambrian geology of central and south Aravalli Range, Rajasthan. *Journ. Geol. Soc. Ind.*, **11**, pp 217–231.

SEN, S., 1983. Stratigraphy of the crystalline Precambrian of central and north Rajasthan: A review. In: *Structure and Tectonics of the Precambrian Rocks.* Sinha–Roy, S. (ed.). *Recent Res. in Geol.*, **10**, Hindustan Pub. Corpn., Delhi, pp 26–39.

SETTLE, D.M. & PATTERSON, C.C., 1980. Lead in albacore: Guide to lead pollution in Americans. *Science*, **207**, pp 1167–1176.

SEYMOUR, D.B., THORNE, A.M. & BLIGHT, D.F., 1988. Explanatory notes. 1:250000 Geological Series, Wyloo, Western Australia. W.Aus. Geol. Surv., 2nd Edition.

SHARMA, K.K., 1978. Structural and geochronological data from Gangapur area, central Rajasthan and bearing on the Precambrian structural history of Rajasthan, India. In: Verma, V.K. & Verma, P.K. (eds.). *Recent Res. in Geol.*, **7**, Hindustan Pub. Corpn., Delhi, pp 118–131.

SHIRAHATA, H., ELIAS, R.W. & PATTERSON, C.C., 1980. Chronological variations in concentrations and isotopic compositions of anthropogenic atmospheric lead in sediments of a remote sub–alpine pond. *Geochim. Cosmochim. Acta*, **49**, pp 149–162.

SILVER, L.T., WOODHEAD, J.A. & WILLIAMS, I.S., 1982. Primary mineral distribution and secondary mobilisation of uranium and thorium in radioactive granites. In: *Uranium Exploration Methods*. Symp. Proc., O.E.C.D. Nucl. Energy Agency, Paris, pp 355–366.

SIMS, P.K., 1980. Subdivision of the Proterozoic and Archaean Eons: Recommendations and suggestions by the International Subcommission on Precambrian Stratigraphy. *Precamb. Res.*, **13**, pp 379–380.

SINGH, S.N. & PAL, O.P., 1970. Geology around Chitrakut area, district Banda, U.P. *Journ. Pal. Soc. Ind.*, **14**, pp 77–85.

SINGH, S.P., 1982. Palaeotectonics and sedimentation trend of the Delhi Supergroup around Rajgarh, northeast Rajasthan. *Journ. Ind. Ass. Sed.*, **3**, pp 29–44.

SINGHVI, A.K., SHARMA, P., SHARMA, Y.P., AGRAWAL, D.P., 1982. Thermoluminescence dating of sand dunes. *Nature*, **295**, pp 313–315.

SMITH, P.E. & FARQUHAR, R.M., 1989. Direct dating of Phanerozoic sediments by the ^{238}U–^{206}Pb method. *Nature*, **341**, pp 518–521.

SMITH, P.E., FARQUHAR, R.M. & HANCOCK, R.G., 1991. Direct radiometric age determination of carbonate diagenesis using U–Pb in secondary calcite. *Earth Plan. Sci. Lett.*, **105**, pp 474–491.

SONI, M.K., CHAKRABORTY, S. & JAIN, V.K., 1987. Vindhyan Supergroup – a review. *Geol. Soc. Ind. Mem.* **6**, pp 87–138.

SRIVASTAVA, N.K., 1977. Sedimentpetrological and geochemical studies of late Precambrian stromatolites of India. In: *Fossil Algae, Recent Results and Developments*. Flugel, E. (ed.). Springer–Verlag, Berlin–Heidelberg, New York, pp 107–112.

STACEY, J.S. & KRAMERS, J.D., 1975. Approximation of terrestrial lead isotope evolution by a two–stage model. *Earth Plan. Sci. Lett.*, **26**, pp 207–221.

STEARN, C.W., 1980. Classification of the Palaeozoic stromatoporoids. *Journ. Pal.*, **54**, pp 881–902.

STEARN, C.W. & MAH, A.J., 1987. Skeletal microstructure of Paleozoic stromatoporoids and its mineralogical implications. *Palaios*, **2**, pp 76–84.

STEIGER, R.H. & JÄGER, E., 1977. Subcommission on geochronology: Convention on the use of decay constants in geo– and cosmochronology. *Earth Plan. Sci. Lett.*, **36**, pp 359–362.

STERN, T.W., GOLDICH, S.S. & NEWELL, M.F., 1966. Effects of weathering on the U–Pb ages of zircon from the Morton Gneiss, Minnesota. *Earth Plan. Sci. Lett.*, **36**, pp 369–371.

STOCKWELL, H.C., 1964. Fourth report on structural provinces, orogenies and time classification of rocks of the Canadian Precambrian Shield. *Can. Geol. Surv. Paper* **64–17**, 21 pp.

STUCKLESS, J.S., BUNTING, J.A. & NKOMO, I.T., 1981. U–Th–Pb systematics of some granitoids from the northeastern Yilgarn Block, Western Australia and implications for uranium source rock potential. *Journ. Geol. Soc. Aus.*, **28**, pp 364–375.

SUGDEN, T.J., DEB, M. & WINDLEY, B.F., In press. The tectonic setting of mineralisation in the Proterozoic Aravalli–Delhi Orogenic belt, northwest India. In: *Developments in Precambrian Geology*. Naqvi, S.M. (ed.). Elsevier, Amsterdam.

SUNDQUIST, B., 1982a. Wackestone petrography and bipolar orientation of cephalopods as indicators of littoral sedimentation in the Ludlovian of Gotland. *Geol. Fören. Stockholm Förhand.*, **104**, pp 81–90.

SUNDQUIST, B., 1982b. Carbonate petrography of the Wenlockian Slite Beds at Haganäs, Gotland. *Sveriges Geol. Unders.*, **C796**, pp 1–79.

SWAMI NATH, J., RAMAKRISHNAN, M. & VISWANATH, M.N., 1976. Dharwar stratigraphic model and Karnataka Craton evolution. *Rec. Geol. Surv. Ind.*, **107**, pp 149–175.

SWART, P.K., 1988. The elucidation of dolomitisation events using nuclear track mapping. In: *Sedimentology and Geochemistry of Dolomites*. Shukla, V.J. & Baker, P.A. (eds.). *S.E.P.M. Spec. Pub.*, **43**, pp 13–19.

SWART, P.K. & HUBBARD, J.A.E.B., 1982. Uranium in scleractinian corals. *Coral Reefs*, **1**, pp 13–19.

TANAKA, S., INOUE, T. & IMAMURA, M., 1977. The ^{10}Be method of dating marine sediments – comparison with the palaeomagnetic method. *Earth Plan. Sci. Lett.*, **37**, pp 55–60.

TATSUMOTO, M. & SNAVELY, P.D., 1969. Isotopic composition of leads in rocks of the Coast Range, Oregon and Washington. *Journ. Geophys. Res.*, **74**, pp 1087–1100.

TATSUMOTO, M., KNIGHT, R.J. & ALLÈGRE, C.J., 1973. Time differences in the formation of meteorites as determined from the ratio of 207–lead to 206–lead. *Science*, **180**, pp 1279–1283.

TAYLOR, P.N. & KALSBEEK, F., 1990. Dating the metamorphism of Precambrian marbles: Examples from Proterozoic mobile belts in Greenland. *Chem. Geol. (Isotope Geoscience Section)*, **86**, pp 21–28.

TAYLOR, P.N., CHADWICK, B., FRIEND, C.R.L., RAMAKRISHNAN, M., MOORBATH, S. & VISWANATHA, M.N., 1988. New age data on the geological evolution of southern India. *Journ. Geol. Soc. Ind.*, **31**, pp 155–157.

TAYLOR, P.N., CHADWICK, B., MOORBATH, S., RAMAKRISHNAN, M. & VISWANATHA, M.N., 1984. Petrography, chemistry and isotopic ages of Peninsular Gneiss, Dharwar acid volcanic rocks and the Chitradurga Granite with special reference to the Late Archaean evolution of the Karnataka Craton, southern India. *Precamb. Res.*, **23**, pp 349–375.

TAYLOR, S.R. & McLENNAN, S.M., 1985. The continental crust: Its composition and evolution. Blackwell, Oxford, 312 pp.

TERA, F. & WASSERBURG, G.J., 1975. Precise isotopic analysis of lead in picomole and subpicomole quantities. *Analyt. Chem.*, **47**, pp 2214–2220.

THIRLWALL, M.F., 1988. Geochronology of Late Caledonian magmatism in northern Britain. *Journ. Geol. Soc. Lond.*, **145**, pp 951–967.

THODE, H.G. & MONSTER, J., 1965. Sulfur isotope geochemistry of petroleum, evaporites and ancient seas. In: *Fluids in Subsurface Environments.* Young, A. & Galley, J.E. (eds.). *Am. Ass. Pet. Geol., Mem.* **4**, pp 367–377.

THOMSON, J., COLLEY, S., HIGGS, N.C., HYDES, D.J., WILSON, T.R.S. & SØRENSEN, J., 1987. Geochemical oxidation fronts in northeast Atlantic distal turbidites and their effect in the sedimentary record. In: *Geology and Geochemistry of Abyssal Plains.* Weaver, P.P.E. & Thomson, J. (eds.). *Geol. Soc. Am. Spec. Pub.* **31**, pp 167–177.

THORNE, A.M., 1985. Upward–shallowing sequences in the Precambrian Duck Creek Dolomite, Western Australia. Prof. Papers for 1983, *W.Aus. Geol. Surv., Rept.* **14**, pp 81–93.

THORNE, A.M. & SEYMOUR, D.B., 1991. Geology of the Ashburton Basin. *Geol. Surv. W.Aus., Bull.* **139**, 141 pp.

THOROGOOD, E.J., 1991. Provenance of the pre–Devonian sediments of England and Wales: Sm–Nd isotopic evidence. Unpublished D.Phil Thesis, Univ. Oxford, 197 pp.

TILTON, G.R., 1960. Volume diffusion as a mechanism for discordant lead ages. *Journ. Geophys. Res.*, **65**, pp 2933–2945.

TITTERINGTON, D.M. & HALLIDAY, A.N., 1979. On the fitting of parallel isochrons and the method of maximum likelihood. *Chem. Geol.*, **26**, pp 183–195.

TODD, J.F., ELSINGER, R.J. & MOORE, W.S., 1988. The distribution of uranium, radium and thorium isotopes in two anoxic fjords: Framvaren (Norway) and Saanich Inlet (British Columbia). *Mar. Chem.*, **23**, pp 393–415.

TREFRY, J.H., METZ, S., TROCINE, R.P. & NELSON, T.A., 1985. A decline in lead transport by the Mississippi River. *Science*, **230**, pp 439–441.

TUCKER, M.E., 1986. Carbon isotope excursions in Precambrian–Cambrian boundary beds, Morocco. *Nature*, **319**, pp 48–50.

TUCKER, R.D., KROGH, T.E., ROSS, R.J. & WILLIAMS, S.H., 1990. Time scale calibration by high–precision U–Pb zircon dating of interstratified volcanic ashes in the Ordovician and Lower Silurian stratotypes of Britain. *Earth Plan. Sci. Lett.*, **100**, pp 51–58.

TUGARINOV, A.I., SHANIN, L.L., KAZAKOV, G.A. & ARAKELYANTS, M.M., 1965. On the glauconite ages of the Vindhyan System (India). *Geokhimya*, **6**, pp 652–660.

TYLER, A.M. & THORNE, A.M., 1990. The northern margin of the Capricorn Orogen, Western Australia – an example of an Early Proterozoic collision zone. *Journ. Struct. Geol.*, **12**, pp 485–502.

TYLER, G., 1981. Leaching of metals from the A–horizon of a spruce forest soil. *Water Air Soil Pollut.*, **15**, pp 353–369.

URBAN, N.R., EISENREICH, S.J., GRIGAL, D.F. & SCHURR, K.T., 1990. Mobility and diagenesis of Pb and ^{210}Pb in peat. *Geochim. Cosmochim. Acta*, **54**, pp 3329–3346.

VALLEY, J.W. & O'NEIL, J.R., 1981. $^{13}C/^{12}C$ interchange between calcite and graphite: A possible thermometer in Grenville marbles. *Geochim. Cosmochim. Acta*, **40**, pp 411–419.

VASUDEV, V.N., NAQVI, S.M., SHUKLA, M. & UDAY RAJ, B., 1989. Stromatolites from the chert–dolomites of Archaean Shimoga Schist Belt, Dharwar Craton, India. *Journ. Geol. Soc. Ind.*, **33**, pp 201–205.

VEEH, H.H., 1966. $^{230}Th/^{238}U$ and $^{234}U/^{238}U$ ages of Pleistocene high sea level stand. *Journ. Geophys. Res.*, **71**, pp 3379–3386.

VEIZER, J., HOLSER, W.T. & WILGUS, C,K., 1980. Correlation of $^{13}C/^{12}C$ and $^{34}S/^{32}S$ secular variations. *Geochim. Cosmochim. Acta*, **44**, pp 579–587.

VENKATASUBRAMANIAN, V.S., 1975. Studies in the geochronology of the Mysore Craton. *Geophys. Res. Bull.*, **13**, pp 239–246.

VENKATASUBRAMANIAN, V.S. & NARAYANASWAMY, R., 1974a. Rb–Sr whole rock isochron studies on granitic rocks from Chitradurga and north Mysore. *Journ. Geol. Soc. Ind.*, **15**, pp 77–81.

VENKATASUBRAMANIAN, V.S. & NARAYANASWAMY, R., 1974b. Primary and metamorphic Rb–Sr chronology in some areas of south Mysore. *Journ. Geol. Soc. Ind.*, **15**, pp 200–205.

VENKATASUBRAMANIAN, V.S. & NARAYANASWAMY, R., 1974c. The age of some gneissic pebbles in Kaldurga Conglomerate, Karnataka, south India. *Journ. Geol. Soc. Ind.*, **15**, pp 318–319.

VERMA, R.K., SAMADDER, A.K. & MURTI, K.S., 1977. Palaeomagnetic study of Gunderdehi Shale of Raipur Group from the Chattisgarh Basin in India. *Ind. Journ. Earth Sci.*, **4**, pp 183–191.

VINOGRADOV, A.P., TUGARINOV, A.I., FEDOROVA, V.A. & ZYKOV, S.I., 1957. The age of the Ukrainian Precambrian rocks III. *Geokhimya*, **7**, pp 559–565, (in Russian).

VINOGRADOV, A., TUGARINOV, A., ZHYKOV, C., STAPNIKOVA, N., BIBIKOVA, E. & KHORRE, K., 1964. Geochronology of the Indian Precambrian. 22nd Int. Geol. Congr., New Delhi, Part x, Arch. and Precambrian Geol., pp 553–567.

VOGT, J.H. & STUMPFL, E.F., 1987. Abra – a stratabound Pb–Cu–Ba mineralization in the Bangemall Basin, Western Australia. *Econ. Geol.*, **82**, pp 805–825.

WADIA, D.N., 1966. Geology of India. Macmillan, New York, 536 pp.

WALLACE, H.E., THOMSON, J., WILSON, T.R.S., WEAVER, P.P.E., HIGGS, N.C. & HYDES, D.J., 1988. Active diagenetic formation of metal–rich layers in northeast Atlantic sediments. *Geochim. Cosmochim. Acta*, **52**, pp 1557–1569.

WALTER, M.R., 1972. Stromatolites and the biostratigraphy of the Australian Precambrian and Cambrian. *Spec. Papers in Pal.*, **11**, Pal. Ass. Lond., 190 pp.

WALTER, M.R., 1977. Interpreting stromatolites. *Am. Sci.*, **65**, pp 563–571.

WALTER, M.R., BAULD, J. & BROCK, T.D., 1976. Microbiology and morphogenesis of columnar stromatolites (*Conophyton, Vacerilla*) from hot springs in Yellowstone National Park. In: *Stromatolites*. Walter, M.R. (ed.). *Developments in Sedimentology*, **20**, Elsevier, Amsterdam, pp 273–310.

WALTER, M.R., GOODE, A.D.T. & HALL, W.D.M., 1976. Microfossils from a newly discovered Precambrian stromatolite iron formation in Western Australia. *Nature*, **261**, pp 221–223.

WAMPLER, J.M. & KULP, J.L., 1962. Isotopic composition and concentration of lead in some carbonate rocks. *Bull. Geol. Soc. Am., Buddington Vol.*, pp 105–114.

WANGERSKY, P.J., 1986. Biological control of trace metal residence time and speciation: A review and synthesis. *Mar. Chem.*, **18**, pp 269–97.

WAPSTRA, A.H. & BOS, K., 1977. The 1977 atomic mass evaluation Part 1. Atomic Mass Table. *At. Data. Nucl. Data Tables*, **19**, pp 177–214.

WASSERBURG, G.J., 1963. Diffusion processes in lead–uranium systems. *Journ. Geophys. Res.*, **68**, pp 4823–4846.

WATTS, N.R., 1982. Early carbonate fabrics in Silurian reefs on Gotland, Sweden. *Am. Ass. Pet. Geol. Bull.*, **66**, pp 640–641.

WEDEPOHL, K.H., 1960. Spuren analytische untersuchungen an tiefseetonen aus dem Atlantik. *Geochim. Cosmochim. Acta*, **18**, pp 200–231.

WETHERILL, G.W., 1956. Discordant uranium–lead ages. *Trans. Am. Geophys. Union*, **37**, pp 320–326.

WETHERILL, G.W., 1963. Discordant uranium–lead ages– pt.2; discordant ages resulting from diffusion of lead and uranium. *Journ. Geophys. Res.*, **68**, pp 2957–2965.

WETHERILL, G.W., 1966. Radioactive decay constants and energies. In: *Handbook of Physical Constants*. Clarke, S.E. (ed.). *Geol. Soc. Am. Mem.* **97**, pp 514–519.

WHITE, W.M., DUPRÉ, B. & VIDAL, P., 1985. Isotope and trace element geochemistry of sediments from the Barbados Ridge–Demerera Plain region, Atlantic Ocean. *Geochim. Cosmochim. Acta*, **49**, pp 1875–1886.

WHITEHOUSE, M.J., 1989. Pb isotopic evidence for U–Th–Pb behaviour in a prograde amphibolite to granulite facies transition from the Lewisian Complex of northwest Scotland: Implications for Pb/Pb dating. *Geochim. Cosmochim. Acta*, **53**, pp 717–724.

WHITFIELD, M. & TURNER, D.R., 1982. Ultimate removal mechanisms of elements from the ocean – a comment. *Geochim. Cosmochim. Acta*, **46**, pp 1989–1992.

WHITFIELD, M. & TURNER, D.R., 1987. The role of particles in regulating the composition of sea water. In: *Aquatic Surface Chemistry: Chemical Processes at the Particle–Water Interface*. Stumm, W. (ed.). Wiley, New York, pp 457–493.

WILHELM, H.G. & ACKERMANN, W., 1972. Age determination of sylvite from the Upper Zechstein deposits of the Werra District by the K–Ca method. *Z. Naturforschung*, **27A**, pp 1256–1259.

WILLIAMS, I.R., 1990a. Bangemall Basin. In: *Geology and Mineral Resources of Western Australia. W.Aus. Geol. Surv., Mem.* **3**, pp 308–329.

WILLIAMS, I.R., 1990b. Savory Basin. In: *Geology and Mineral Resources of Western Australia. W.Aus. Geol. Surv., Mem.* **3**, pp 329–335.

WILLIAMS, I.R., 1990c. Yeneena Basin. In: *Geology and Mineral Resources of Western Australia. W.Aus. Geol. Surv., Mem.* **3**, pp 277–282.

WILLIAMS, I.R., 1992. Geology of the Savory Basin. *W.Aus. Geol. Surv., Bull.* **141**, 115 pp.

WILLIAMS, S.J., ELIAS, M. & DeLAETER, J.R., 1978. Geochronology and evolution of the eastern Gascoyne Province and adjacent Yilgarn Block. *W.Aus. Geol. Surv., Ann. Rept. 1977*, pp 50–56.

WINTERHALTER, B., FLODÉN, T., IGNATIUS, H., AXBERG, S. & NIEMISTÖ, L., 1982. Geology of the Baltic Sea. In: *The Baltic Sea*. Voipio, A. (ed.). *Elsevier Oceanog. Ser.* **30**, pp 1–121.

WOODRUFF, R., SAVIN, S.M. & DOUGLAS, R.E., 1981. Miocene stable isotope record: A detailed deep Pacific Ocean study and its paleoclimatic implications. *Science*, **212**, pp 665–668.

WYBORN, D., OWEN, N., COMPSTON, W. & McDOUGALL, I., 1982. The Laidlaw Volcanics: A late Silurian tie–point on the geological time scale. *Earth Plan. Sci. Lett.*, **59**, pp 99–100.

YORK, D., 1969. Least squares fitting of a straight line with correlated errors. *Earth Plan. Sci. Lett.*, **5**, pp 320–324.

ZELLER, E.J., WRAY, J.L. & DANIELS, F., 1957. Factors in age determination of carbonate sediments by thermoluminescence. *Bull. Am. Ass. Pet. Geol.*, **40**, pp 140–152.